

THE JOURNAL OF PHYSICAL CHEMISTRY

Volume 74, Number 15 July 23, 1970

Kinetics of the Hydrolysis of Aqueous Indium(III) and Gallium(III) Perchlorates Paul Hemmes, Larry D. Rich, David L. Cole, and Edward M. Eyring	2859
The Oxidation of Cysteine and Glutathione by Molybdenum(VI) J. F. Martin and J. T. Spence	2863
Surface and Bulk Reactions of Carbon Tetrachloride with Titanium Dioxide M. Primet, J. Basset, M. V. Mathieu, and M. Prettre	2868
Thermal Decomposition of Potassium Bicarbonate I. C. Hisatsune and T. Adl	2875
The Rate Constants of Hydrated Electron, Hydrogen Atom, and Hydroxyl Radical Reactions with Benzene, 1,3-Cyclohexadiene, 1,4-Cyclohexadiene, and Cyclohexene B. D. Michael and Edwin J. Hart	2878
Evidence for Very Early Ionic Events in the Radiolysis of Ethanol Shamsheer Khorana and William H. Hamill	2885
Electron Scavenging in the γ Radiolysis of Liquid Diethyl Ether Krishan M. Bansal and Stefan J. Rzed	2888
Effects of Ethene and Ethane on the Photochemical Production of Carbon Monoxide from Acetone A. S. Gordon and R. H. Knipe	2893
Mechanism of Photodissociation of Hydroquinone Derivatives Hikoichiro Yamada, Nobuaki Nakashima, and Hiroshi Tsubomura	2897
Studies on the Molecular Hydrogen Formation (G_{H_2}) in the Radiation Chemistry of Aqueous Solutions E. Peled and G. Czapski	2903
Combined Low-Energy Electron Diffraction and Mass Spectrometer Observations on Some Gas-Solid Reactions and Evidence for Place Exchange H. E. Farnsworth	2912
Thermodynamic Equilibria from Plasma Sources. III. Carbon-Hydrogen-Nitrogen Systems P. R. Griffiths, P. J. Schuhmann, and E. R. Lippincott	2916
Spectral Characterization of Activated Carbon R. A. Friedel and L. J. E. Hofer	2921
Electron Spin Resonance Study of 2,6-Di- <i>t</i> -butyl-4-methylphenol Oxidation on Alumina Isao Suzuki, Yoshio Ono, and Tominaga Keii	2923
Electron Paramagnetic Resonance of Free-Radical Intermediates in the System Titanous Ion-Hydrogen Peroxide Yasuhiro Shimizu, Takeshi Shiga, and Keiji Kuwata	2929
Radical Intermediates. IV. Electron Spin Resonance Studies on the Alkali Metal Nitrobenzenides in Nitrilic Solvents J. M. Gross and J. D. Barnes	2936
Magnetic Resonance Studies of Aromatic Hydrocarbons Adsorbed on Silica-Alumina. IV. Oxidation Strength of the Surface Electrophilic Sites G. M. Muha	2939
Stepped Isotherms on Inorganic Oxides S. A. Selim, R. Sh. Mikhail, and R. I. Razouk	2944
Some Aspects of Diffusion in Ternary Systems V. Vitagliano and R. Sartorio	2949
Diffusion in Mixed Solvents. I. Iodine in Ethanol-Water and <i>t</i> -Butyl Alcohol-Water Solutions Koichiro Nakanishi and Teruko Ozasa	2956
Cross-Phenomenological Coefficients. XIII. Electroosmotic Transport in Membranes R. P. Rastogi, M. L. Srivastava, and Sri Nath Singh	2960
On the Ratio of Osmotic to Tracer Permeability in a Homogeneous Liquid Membrane I. Robert Fenichel and Samuel B. Horowitz	2966

Gas Chromatographic Determination of Partition Coefficients of Some Unsaturated Hydrocarbons and Their Deuterated Isomers in Aqueous Silver Nitrate Solutions	S. P. Wasik and W. Tsang	2970
Activity Coefficients and Ion Pairs in the Systems Sodium Chloride–Sodium Bicarbonate–Water and Sodium Chloride–Sodium Carbonate–Water.	James N. Butler and Rima Huston	2976
The Vapor Pressure of Ice between $+10^{-2}$ and -10^{+2}°	Gabor Jancso, Jovan Pupezin, and W. Alexander Van Hook	2984
A Near-Infrared Spectroscopic Method for Investigating the Hydration of a Solute in Aqueous Solution	William C. McCabe and Harvey F. Fisher	2990
Crystal Lattice Effects in the Nuclear Quadruple Resonance Spectra of Some Hexachlorostannate(IV) Salts	T. B. Brill, Z Z. Hugus, Jr., and A. F. Schreiner	2999
Flash Photolysis of the Charge-Transfer Band of 1-Methylpyridinium, 1-Methylcollidinium, and 1-Methylquinolinium Iodides	R. F. Cozzens and Thomas A. Gover	3003
Photoconductive and Photovoltaic Effects in Dibenzothiophene and Its Molecular Complexes	Tapan K. Mukherjee	3006
The Effect of Pressure on the Density and Dielectric Constant of Polar Solvents	L. G. Schornack and C. A. Eckert	3014

NOTES

Locations of Cations in Alkaline Earth Hydrogen Y Zeolites	John W. Ward	3021
Interpretations of Nuclear Quadrupole Resonance Data in Some <i>trans</i> -Dichlorobis(ethylenediamine)cobalt(III) Salts	T. B. Brill and Z Z. Hugus, Jr.	3022
A Comparison of the Gibbs Energy and Entropy of Interfaces Water– <i>n</i> -Hexane and Water–Perfluorotributylamine.	R. G. Linford, R. J. Powell, and J. H. Hildebrand	3024

COMMUNICATIONS TO THE EDITOR

Electron Spin Resonance of β -Chloroalkyl Nitroxides. Angular Dependence of β -Chlorine Hyperfine Coupling	Edward G. Janzen, Bruce R. Knauer, Lewis T. Williams, and W. B. Harrison	3025
Water Structure Promotion by Large Organic Anions.	Siegfried Lindenbaum	3027

AUTHOR INDEX

- Adl, T., 2875
 Bansal, K. M., 2888
 Barnes, J. D., 2936
 Basset, J., 2868
 Brill, T. B., 2999, 3022
 Butler, J. N., 2976
 Cole, D. L., 2859
 Cozzens, R. F., 3003
 Czapski, G., 2903
 Eckert, C. A., 3014
 Eyring, E. M., 2859
 Farnsworth, H. E., 2912
 Fenichel, I. R., 2966
 Fisher, H. F., 2990
 Friedel, R. A., 2921
 Gordon, A. S., 2893
 Gover, T. A., 3003
 Griffiths, P. R., 2916
 Gross, J. M., 2936
 Hamill, W. H., 2885
 Harrison, W. B., 3025
 Hart, E. J., 2878
 Hemmes, P., 2859
 Hildebrand, J. H., 3024
 Hisatsune, I. C., 2875
 Hofer, L. J. E., 2921
 Horowitz, S. B., 2966
 Hugus, Z. Z., Jr., 2999, 3022
 Huston, R., 2976
 Jancso, G., 2984
 Janzen, E. G., 3025
 Keii, T., 2923
 Khorana, S., 2885
 Knauer, B. R., 3025
 Knipe, R. H., 2893
 Kuwata, K., 2929
 Lindenbaum, S., 3027
 Linford, R. J., 3024
 Lippincott, E. R., 2916
 Martin, J. F., 2863
 Mathieu, M. V., 2868
 McCabe, W. C., 2990
 Michael, B. D., 2878
 Mikhail, R. S., 2944
 Muha, G. M., 2939
 Mukherjee, T. K., 3006
 Nakanishi, K., 2956
 Nakashima, N., 2897
 Ono, Y., 2923
 Ozasa, T., 2956
 Peled, E., 2903
 Powell, R. J., 3024
 Prettre, M., 2868
 Primet, M., 2868
 Pupezin, J., 2984
 Rastogi, R. P., 2960
 Razouk, R. I., 2944
 Rich, L. D., 2859
 Rzd, S. J., 2888
 Sartorio, R., 2949
 Schornack, L. G., 3014
 Schreiner, A. F., 2999
 Schuhmann, P. J., 2916
 Selim, S. A., 2944
 Shiga, T., 2929
 Shimizu, Y., 2929
 Singh, S. N., 2960
 Spence, J. T., 2863
 Srivastava, M. L., 2960
 Suzuki, I., 2923
 Tsang, W., 2970
 Tsubomura, H., 2897
 Van Hook, W. A., 2984
 Vitagliano, V., 2949
 Ward, J. W., 3021
 Wasik, S. P., 2970
 Williams, L. T., 3025
 Yamada, H., 2897

THE JOURNAL OF PHYSICAL CHEMISTRY

Registered in U. S. Patent Office © Copyright, 1970, by the American Chemical Society

VOLUME 74, NUMBER 15 JULY 23, 1970

Kinetics of the Hydrolysis of Aqueous Indium(III) and Gallium(III) Perchlorates

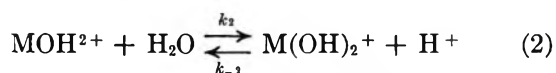
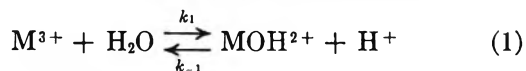
by Paul Hemmes, Larry D. Rich, David L. Cole, and Edward M. Eyring

Department of Chemistry, University of Utah, Salt Lake City, Utah 84112 (Received March 10, 1970)

The electric field jump relaxation method was used to determine rate constants in the hydrolysis equilibria of dilute indium(III) and gallium(III) perchlorates in acidic aqueous solutions having ionic strengths of $10^{-3} M$ or less. Assignment of the single, microsecond relaxation time observed for each sample solution to one of two possible hydrolysis steps was based on relaxation amplitude considerations. A strong correlation between specific rates and ionic radii is not observed. The ion recombinations $H^+ + InOH^{2+} \rightarrow$ and $H^+ + GaOH^{2+} \rightarrow$ are both nearly diffusion-controlled processes.

Introduction

The hydrolysis kinetics of metal ions may depend on several factors, notably the charge, radius, and electronic configuration of the metal ions. The determination of the influence of just one of these factors upon the rate of hydrolysis is difficult since one cannot readily vary a single parameter while holding all other factors constant. The dependence on ionic radius is best observed by comparing metals from a single group of the periodic table for which charge is constant and electronic configurations are similar. The influence of charge is best studied by examining multistep hydrolysis reactions



where contrary to what the above notation might suggest the reactant water molecule is understood to be in the first coordination sphere of the aquated metal ion M^{3+} undergoing hydrolysis. The major difference in reactions 1 and 2 is the charge of the proton acceptor.

To elucidate the kinetic effects of ionic radius and charge we have determined the hydrolysis rates of aqueous indium(III) and gallium(III) by the electric field jump (E-jump) relaxation method.¹ The principal

difficulty of such a study is the observation of only a single microsecond time scale relaxation where two would normally be anticipated for the coupled equilibria 1 and 2. This apparent discrepancy can be resolved by consideration of the amplitudes of the measured relaxations as shown below.

Experimental Section

G. F. Smith Co. reagent grade indium(III) perchlorate and gallium(III) perchlorate were each recrystallized from water-perchloric acid. Stock solutions were titrated with EDTA using as indicators Eriochrome Black T for indium² and Galloxyanine for gallium.³

Sample solutions for the E-jump experiments were prepared by adding, under a nitrogen atmosphere, small aliquots of the particular stock solution to $10^{-7} \text{ ohm}^{-1} \text{ cm}^{-1}$ water prepared by an electrophoretic ion exclusion technique.⁴ A Beckman 1019 pH meter with a 41263 glass and a 39071 calomel electrode was used to

(1) M. Eigen and L. DeMaeyer, "Technique of Organic Chemistry," Vol. VIII, Part II, S. L. Friess, E. S. Lewis, and A. Weissberger, Ed., Interscience, New York, N. Y., 1963, p 988 ff.

(2) F. J. Welcher, "The Analytical Uses of Ethylenediamine Tetraacetic Acid," Van Nostrand, Princeton, N. J., 1958, p 178.

(3) See ref 2, p 177.

(4) W. Haller and H. C. Duecker, *J. Res. Nat. Bur. Stand., Sect. A*, **64**, 527 (1960).

Table I: Calculated Molar Concentrations and Experimental Dissociation Field Effect Relaxation Times in Aqueous Solutions at 25°

$c_0,^a$ 10 ⁻³ M	pH ^b	[H ⁺], ^c 10 ⁻⁵ M	[M ³⁺], ^d 10 ⁻⁵ M	[MOH ²⁺], ^d 10 ⁻⁵ M	[M(OH) ₂], ^d 10 ⁻⁵ M	[M ₂ (OH) ₂ ⁴⁺], ^d 10 ⁻⁶ M	$\bar{\tau},^e$ μsec	n ^f
Indium(III) perchlorate *pK ₁ = 4.42, ^g *pK ₂ = 3.9, ^g *pβ ₂₂ = 5.21 ^g								
1.02	4.746	1.80	0.569	0.120	0.837	0.006	3.42 ± 0.13	6
3.04	4.426	3.79	0.565	0.567	1.88	0.137	2.00 ± 0.06	6
5.07	4.226	6.04	1.69	1.06	2.22	0.485	1.42 ± 0.17	6
7.10	4.125	7.66	2.99	1.48	2.44	0.939	1.04 ± 0.03	6
10.15	4.064	8.86	4.80	2.06	2.93	1.81	0.91 ± 0.05	6
Gallium(III) perchlorate *pK ₁ = 2.60, ^h *pK ₂ = 3.46 ^h								
0.505	4.584	2.62	0.0004	0.0354	0.469		2.95 ± 0.18	6
1.01	4.570	2.71	0.0008	0.0731	0.937		2.39 ± 0.26	6
2.53	4.188	6.54	0.104	0.400	2.12		1.57 ± 0.10	6
3.79	4.014	9.79	0.032	0.827	2.93		1.42 ± 0.24	5
5.05	3.898	12.8	0.069	1.35	3.64		1.11 ± 0.17	6

^a Total molar concentration of metal(III) perchlorate. ^b Glass electrode pH of the sample solution. ^c Molar concentration of hydrogen ion [H⁺] = 10^{-pH}/γ_{H⁺} where the activity coefficient is calculated from the Debye-Hückel limiting law. ^d Molar ionic concentration calculated from eq 3 through 9 of the text. ^e Average experimental dissociation field effect relaxation time with standard deviation calculated from the range. ^f Number of independent determinations of the relaxation time. ^g Acid dissociation constants for In³⁺(aq) and InOH²⁺(aq), respectively, reported by Biedermann, ref 6 of text. ^h Acid dissociation constants for Ga³⁺(aq) and GaOH²⁺(aq), respectively, reported by Fricke and Meyring, ref 7 of text.

measure the pH of each sample solution. Our E-jump apparatus has been described before in considerable detail.⁵

The experimental relaxation times, total metal(III) perchlorate concentrations c_0 , and measured values of pH are all shown in Table I. Also shown in Table I are calculated concentrations of the several types of ions present. These were obtained from the following set of equations

$$*K_1 = \frac{k_1}{k_{-1}} = \frac{[H^+][MOH^{2+}]}{[M^{3+}]} \quad (3)$$

$$*K_2 = \frac{k_2}{k_{-2}} = \frac{[H^+][M(OH)_2^+]}{[MOH^{2+}]} \quad (4)$$

$$*\beta_{22} = \frac{[H^+]^2[M_2(OH)_2^{4+}]}{[M^{3+}]^2} \quad (5)$$

$$c_0 = [M^{3+}] + [MOH^{2+}] + [M(OH)_2^+] + 2[M_2(OH)_2^{4+}] \quad (6)$$

$$\mu = \frac{1}{2}(9[M^{3+}] + 4[MOH^{2+}] + [M(OH)_2^+] + 16[M_2(OH)_2^{4+}] + [H^+] + 3c_0) \quad (7)$$

$$-\log \gamma_{H^+} = 0.509\sqrt{\mu} \quad (8)$$

$$[H^+] = 10^{-pH}/\gamma_{H^+} \quad (9)$$

The equilibrium constants used in these calculations (see Table I) were those reported by Biedermann⁶ for indium(III) hydrolysis and by Fricke and Meyring⁷ for gallium(III) hydrolysis.

As noted above, only one relaxation was observed where two could have been reasonably anticipated.

The problem is to determine which of the two relaxations is being observed or whether the observed relaxation is a composite of the two theoretically present. For a two-step hydrolysis process, eq 1 and 2, the two relaxation times are given by

$$\tau_{1,2}^{-1} = \frac{a_{11} + a_{22}}{2} \pm \frac{1}{2}\sqrt{(a_{11} + a_{22})^2 - 4(a_{11}a_{22} - a_{12}a_{21})} \quad (10)$$

where

$$a_{11} = k_{-1}(*K_1 + [H^+] + [MOH^{2+}]) = k_{-1}\theta \quad (11)$$

$$a_{12} = k_{-1}([H^+] - [MOH^{2+}]) \quad (12)$$

$$a_{21} = k_{-2}(*K_2 - [M(OH)_2^+]) \quad (13)$$

$$a_{22} = k_{-2}(*K_2 + [H^+] + [MOH^{2+}]) = k_{-2}\Phi \quad (14)$$

In general, the observed relaxations should not correspond to either reaction 1 or 2 alone. If, however, either a_{11} or a_{22} is at least ten times as large as the other, then the two relaxations will approximately correspond to the two separate reactions. We will show below that this latter possibility is true for both indium and gallium.

First let us treat our aqueous indium perchlorate kinetic data. Let us consider the ratio $a_{11}/a_{22} = k_{-1}\theta/k_{-2}\Phi$, since as we see from Table I $\theta/\Phi \cong 0.5 \pm$

(5) D. T. Rampton, L. P. Holmes, D. L. Cole, R. P. Jensen, and E. M. Eyring, *Rev. Sci. Instrum.*, **38**, 1637 (1967).

(6) G. Biedermann, *Ark. Kemi*, **9**, 277 (1956); *Recl. Trav. Chim. Pays-Bas*, **75**, 716 (1956).

(7) R. Fricke and K. Meyring, *Z. Anorg. Allg. Chem.*, **176**, 325 (1928).

0.1. For all our experiments, the ratio a_{11}/a_{22} will exceed 10 only for $k_{-1} \geq 20k_{-2}$. This last relationship is improbable since Debye's phenomenological theory⁸ of diffusion-controlled reactions would predict $k_{-2} > k_{-1}$. We may therefore exclude the case where $a_{11} \gg a_{22}$. Similarly for a_{11}/a_{22} to be 0.1 or less it is necessary that $k_{-2} \geq 5k_{-1}$. On the basis of the Debye equation, a ratio $k_{-2}/k_{-1} = 5$ is indeed possible. Thus the observed relaxations may be due to a limiting case of eq 10.

Returning now to a consideration of eq 10, we may determine the sign of the radical, in a zero-order approach, by neglecting the radical completely. We may then write

$$\tau_{\text{obsd}}^{-1} = \frac{a_{11} + a_{22}}{2} \quad (15)$$

where τ_{obsd} is our experimental relaxation time. We may write eq 15 as

$$\tau_{\text{obsd}}^{-1} = \frac{1}{2}(k_{-1}\theta + k_{-2}\Phi) \quad (16)$$

$$\frac{\tau_{\text{obsd}}^{-1}}{\theta} = \frac{k_{-1}}{2} + \frac{k_{-2}}{2} \frac{\Phi}{\theta} \quad (17)$$

A plot of the data in Table I in terms of $\tau_{\text{obsd}}^{-1}/\theta$ vs. Φ/θ yields a negative value for k_{-2} . (Note that in a preceding argument, the quotient θ/Φ was treated as a constant. In fact there is a small variation of this quotient that makes the plot suggested by eq 17 possible, although the variation in θ/Φ is not so great as to invalidate the earlier assumption of its constancy.) From the fact that τ_{obsd}^{-1} is less than $\frac{1}{2}(a_{11} + a_{22})$ it follows that the negative root in eq 10 is the one to be utilized. Hence we conclude that the observed relaxation time corresponds to the slow process.

We must now consider the reasons for observing only the slow relaxation time. Following the procedures outlined by Eigen and DeMaeyer,⁹ we have calculated relaxation amplitudes for two coupled hydrolysis reactions, eq 1 and 2, subjected to a jump in electric field intensity E . The resulting equations are

$$\frac{\partial y_1}{\partial E} = + \frac{\Delta D_1^*}{RT} \frac{(\tau_2^{-1} - \tau_1^{-1})}{a_{12}} \Gamma_1^{-1} \quad (18)$$

$$\frac{\partial y_2}{\partial E} = - \frac{\Delta D_2^*}{RT} \frac{(\tau_2^{-1} - \tau_1^{-1})}{a_{11} - \tau_2^{-1}} \Gamma_2^{-1} \quad (19)$$

Here y_i is the normal concentration variable $dy_i/dt = \tau_i^{-1}y_i$, the "polarization" D_i^* is the thermodynamically conjugate variable to the electric field intensity E

$$\Delta D_1^* = \Delta D_{12}^* - \left(\frac{a_{11} - \tau_1^{-1}}{a_{12}} - 1 \right) \Delta D_{23}^* \quad (20)$$

$$\Delta D_2^* = \Delta D_{12}^* - \left(\frac{a_{11} - \tau_2^{-1}}{a_{12}} - 1 \right) \Delta D_{23}^* \quad (21)$$

$\Delta D_{12}^*/RT = -(\partial \ln K_{12})/\partial |E|$ with $K_{12} \equiv {}^*K_1$ the equilibrium constant for the first hydrolysis reaction, $\Delta D_{23}^*/RT = -(\partial \ln K_{23})/\partial |E|$ with $K_{23} \equiv {}^*K_2$ the equilibrium constant for the second hydrolysis reaction, and

$$\Gamma_1 = \frac{1}{[H^+]} + \frac{1}{[MOH^{2+}]} + \frac{1}{[M^{3+}]} \quad (22)$$

$$\Gamma_2 = \frac{1}{[H^+]} + \frac{1}{[MOH^{2+}]} + \frac{1}{[M(OH)_2^+]} \quad (23)$$

In order that the amplitude of the process corresponding to τ_2^{-1} is very much larger than the amplitude of the fast process (τ_1^{-1}), $a_{11} - \tau_2^{-1}$ must be $\ll a_{12}$. This will always be true when $a_{11} \cong \tau_2^{-1}$. Since Γ_1^{-1} and Γ_2^{-1} are roughly the same and assuming that $\Delta D_1^* \geq \Delta D_2^*$, the only way that the slow process can be observed exclusive of the fast process is when $a_{11} - \tau_2^{-1} \ll a_{12}$. Since experimentally there is no evidence for a fast process, we can conclude that this inequality is fulfilled. Hence we are able to say that the observed reciprocal relaxation time is approximately equal to a_{11} . If we assume that $\tau_{\text{obsd}}^{-1} = a_{11}$, the results will be approximate since we neglect second-order terms from the radical in eq 10. We must now consider the error introduced by using the approximation $\tau_{\text{obsd}}^{-1} = a_{11}$. In line with the assumption about the ΔD_i^* 's it can be seen that if $|a_{11} - \tau_2^{-1}| \leq a_{12}/10$, then the amplitudes will differ by a factor of ten. The error introduced by assuming $a_{11} = \tau_{\text{obsd}}^{-1}$ will then be no greater than 10%. Since this is comparable to the experimental error, it seems that refinement of the data treatment would not be profitable.

In the case of gallium(III), the concentration term Γ_1^{-1} is very much less than Γ_2^{-1} . Hence only the slow process will be observable. This same conclusion can also be reached by means of the argument used for indium(III). Once again we can make the assignment $a_{11} \cong \tau_{\text{obsd}}^{-1}$. Once again for both indium(III) and gallium(III) we can therefore say that the rate process we observe corresponds to the first hydrolysis equilibrium, eq 1.

Results

A least-squares analysis of τ_{obsd}^{-1} vs. $[H^+] + [MOH^{2+}]$ using the indium(III) data of Table I yields a slope $k_{-1} = 9 \times 10^9 M^{-1} \text{sec}^{-1}$ and an intercept $k_1 = 1 \times 10^5 \text{sec}^{-1}$. The calculated equilibrium constant $k_1/k_{-1} = 10^{-5}$ is in fair agreement with Biedermann's value of ${}^*K_1 = 10^{-4.42}$. Since the ionic strength of our sample solutions ($\mu \leq 5 \times 10^{-4} M$) is much lower than Biedermann's ($\mu = 3.0 M$), this agreement is reasonable. It should be noted that the kinetic results are not very sensitive to the value of the equilibrium con-

(8) P. Debye, *Trans. Electrochem. Soc.*, **82**, 265 (1942).

(9) Reference 1, p 928 ff.

stant chosen, since the dominant term is $[H^+]$ which is measured rather than calculated from $*K_1$.

A similar least-squares analysis of the gallium(III) data of Table I in terms of the equation $\tau_{\text{obsd}}^{-1} = k_1 + k_{-1} ([H^+] + [MOH^{2+}])$ yields $k_{-1} = 4.4 \times 10^9 M^{-1} \text{sec}^{-1}$ and $k_1 = 2.7 \times 10^5 \text{sec}^{-1}$. The calculated equilibrium constant $k_1/k_{-1} = 10^{-4.2}$ is in poor agreement with the value given by Fricke and Meyring,⁷ $*K_1 = 10^{-2.6}$. These authors did not include, however, a dimerization step in their hydrolysis scheme and also worked at high ionic strength ($\mu = 3.0 M$). Since a dimerization is known to occur in aqueous gallium(III) perchlorate solutions (with a temperature jump equilibrium constant $*K_{22} = [Ga_2(OH)_2^{4+}] \cdot [GaOH^{2+}]^{-2} = 10^{1.67}$ at 25° and 0.5 M ionic strength),¹⁰ these factors may account for this serious discrepancy in the kinetic and thermodynamic values of $*K_1$. Clearly a major new equilibrium study of aqueous gallium(III) perchlorate at ionic strengths below 0.1 M should be undertaken.

Discussion

While we cannot directly deduce values of the rate constant k_{-2} for the faster process from the kinetic data of Table I, it is possible to get a crude estimate of k_{-2} from our values of k_{-1} and a rule suggested by Kustin and DeMaeyer.¹¹ According to this rule, the rate constant for a diffusion-controlled reaction between a proton and a cation in water will decrease by a factor of 0.3 to 0.5 for each positive charge added to the cation. Accepting the validity of this generalization k_{-2} for indium would be $(\sim 2-3) \times 10^{10} M^{-1} \text{sec}^{-1}$, and for gallium k_{-2} would be $(\sim 1-2) \times 10^{10} M^{-1} \text{sec}^{-1}$. These numbers are quite reasonable in respect to the values of the hydrolysis rates for single-step reactions of dipositive cations such as uranyl¹² and

cupric¹³ which are $1.7 \times 10^{10} M^{-1} \text{sec}^{-1}$ and $\sim 10^{10} M^{-1} \text{sec}^{-1}$, respectively.

In line with previous results, the values of k_1 for both indium(III) and gallium(III) fall in the range $(1-3) \times 10^5 \text{sec}^{-1}$. The values of k_{-1} are indicative of a diffusion-controlled reaction between MOH^{2+} and H^+ . The dependence of k_{-1} upon ionic radius is relatively slight.

The observation of the slow relaxation time in both cases is due to the near equality of the terms a_{11} and a_{22} and the fact that the concentration of free $[M^{+3}]$ is very much lower than that of either $[MOH^{2+}]$ or $[M(OH)_2^+]$. Indeed one could have qualitatively predicted such behavior on the basis of the well-known generalizations that if an equilibrium system lies very far to one side the extent of perturbation will be very small.¹⁴

The very weak dependence of k_{-1} and k_1 on ionic radius may lead to a useful generalization about the rates of uninvestigated hydrolysis reactions. However, these generalizations must break down in cases where the equilibrium constant for the hydrolysis reaction is very large as, for example, in the case of Ce(IV).¹⁵

Acknowledgment. This research was supported by the Directorate of Chemical Sciences, Air Force Office of Scientific Research under Grant AFOSR-69-1717.

- (10) J. D. Owen and E. M. Eyring, *J. Inorg. Nucl. Chem.*, in press.
- (11) L. DeMaeyer and K. Kustin, *Ann. Rev. Phys. Chem.*, **14**, 5 (1963).
- (12) D. L. Cole, E. M. Eyring, D. T. Rampton, A. Silzars, and R. P. Jensen, *J. Phys. Chem.*, **71**, 2771 (1967).
- (13) M. Eigen, K. Tamm, and K. Tjaden, unpublished data cited by Eigen, *et al.*, "Progress in Reaction Kinetics," Vol. 2, G. Porter, Ed., Pergamon Press, Oxford, England, 1964, Chapter 6.
- (14) Reference 1, p 935 ff.
- (15) F. B. Baker, T. W. Newton, and M. Kahn, *J. Phys. Chem.*, **64**, 109 (1960).

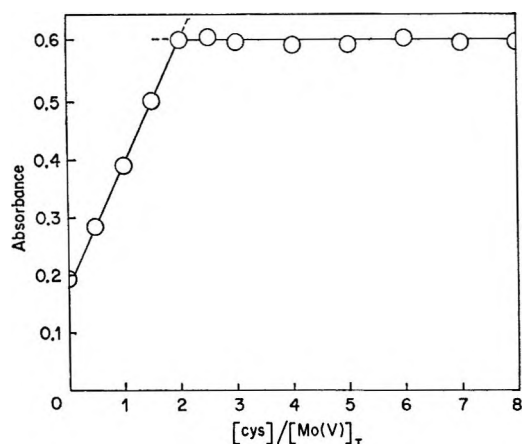


Figure 1. Molar ratio plot for Mo(V)_2 -cysteine complex. Absorbance at $303 \text{ m}\mu$ is plotted vs. ratio $[\text{cys}]/[\text{Mo(V)}]_T$. $[\text{Mo(V)}] = 7.50 \times 10^{-4} \text{ M}$.

It should be pointed out that the question regarding the structure of the complex is unresolved. If the above interpretation is correct, the 1:1 dioxobridged complex is not in equilibrium with the 1:2 species in solution at this pH.

Solutions of Mo(V)_2 and cysteine exhibit an esr signal at this pH. The signal is small, however, accounting for less than 1% of the total Mo(V) . The g values of the signal were determined to be $g_{\parallel} = 2.015$, $g_{\perp} = 1.958$, $\bar{g} = 1.978$ (Figure 2). The g value agrees reasonably well with that reported by Huang and Haight for the system.⁸ As with most Mo(V) -thiol systems, the g values are quite high, indicating considerable electron delocalization.

Solutions of glutathione and either MoOCl_5^{2-} (which is dimerized at this pH) or MoO_4^{2-} gave no spectral evidence of complex formation at pH 7.50 in phosphate buffer. A small amount of a monomeric Mo(V) complex (<1% of total Mo(V)) must be present, however, since a small esr signal was obtained with the glutathione solution with $g_{\parallel} = 2.010$, $g_{\perp} = 1.979$, and $\bar{g} = 1.987$ (Figure 2). As esr signal has been previously reported by Huang and Haight for this system under similar conditions; their reported parameters, however, differ from those found in this work. (They gave a value of $\bar{g} = 1.951$. It seems likely their value is an average of both the Mo(V) -glutathione signal and the Mo(V) -phosphate signal, $g = 1.921$, which is also present in small amount, and is also evident in their published spectrum.)⁸

Kinetics. When excess cysteine and MoO_4^{2-} are mixed at pH 7.50 in deaerated phosphate buffer, the absorbance at $305 \text{ m}\mu$, due to $\text{Mo(V)}_2\text{O}_3(\text{cys})_4^{4-}$ increases with time as the cysteine is oxidized to cystine and the MoO_4^{2-} reduced. Eventually, the absorbance becomes constant, and no further change occurs over several days, indicating the reaction does not proceed beyond a one-electron reduction of Mo(VI) (in the case of thioglycolic acid, an Mo(IV) species is formed).³

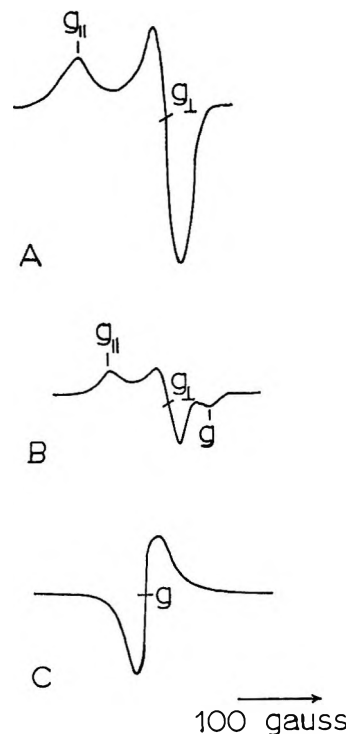


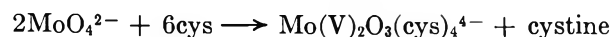
Figure 2. ESR spectra: A, $\text{Mo(V)}_2\text{O}_3(\text{cys})_4^{4-}$, $3.00 \times 10^{-2} \text{ M}$; $g_{\parallel} = 2.015$, $g_{\perp} = 1.959$, $\bar{g} = 1.978$; $SL = 100$; B, $[\text{Mo(V)}] = 3.00 \times 10^{-3} \text{ M}$, $[\text{GSH}] = 5.00 \times 10^{-1} \text{ M}$. $g_{\parallel} = 2.010$, $g_{\perp} = 1.979$, $\bar{g} = 1.987$, $g = 1.910$; $SL = 100$; C, $[\text{Mo(V)}] = 3.00 \times 10^{-3} \text{ M}$; $g = 1.921$; $SL = 250$; all spectra recorded in 1.00 M phosphate, pH 7.50, 77° . $MA = 4000$, attenuation = 5.90.

Since the molar ratio study indicated essentially all the Mo(V) is present as the 1:2 complex and as no other species absorb in this region, the increase in absorbance at $305 \text{ m}\mu$ was used to follow the kinetics.

Trial and error plots of the rate data, for runs with excess cysteine, indicated the reaction was first order in Mo(VI) . Straight lines were obtained up to $\sim 70\%$ reaction, and the slopes gave consistent rate constants for different initial Mo(VI) concentrations. The dependence of the rate on cysteine concentration was determined from a plot of $\log k$ vs. $\log [\text{cys}]$ ($\text{cys} = \text{cysteine}$). This plot gave a straight line with slope of 2.11, indicating the reaction is second order in cysteine. The rate of the reaction can therefore be expressed as

$$-\frac{d[\text{Mo(VI)}]}{dt} = k_3[\text{Mo(VI)}][\text{cys}]^2$$

Since the molar ratio studies indicated Mo(V) forms a strong 1:2 complex with cysteine, but apparently no complex with Mo(VI) , the stoichiometric reaction may be written



(9) P. C. H. Mitchell, *Quart. Rev.*, **20**, 103 (1966).

(10) P. C. H. Mitchell, *J. Chem. Soc. A*, 146 (1969).

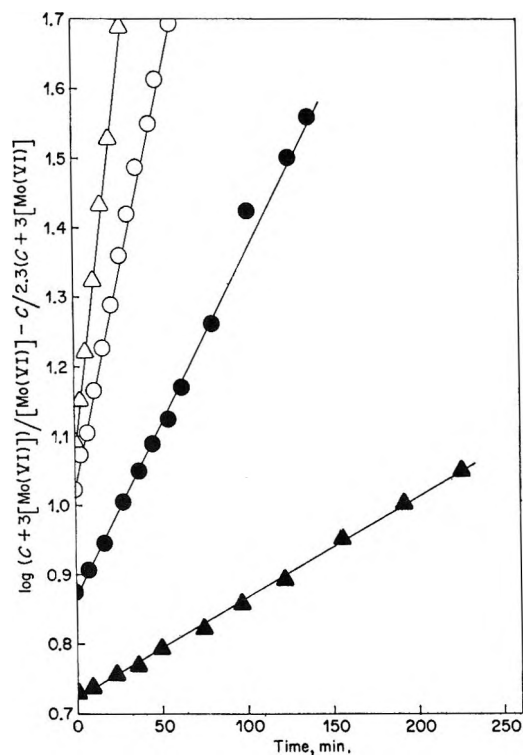


Figure 3. Third-order plots for the oxidation of cysteine by Mo(VI): $C = [\text{cys}]_0 - 3[\text{Mo(VI)}]_0$, Δ , $[\text{cys}]_0 = 3.00 \times 10^{-1} M$, $[\text{Mo(VI)}]_0 = 1.00 \times 10^{-2} M$; \circ , $[\text{cys}]_0 = 2.50 \times 10^{-1} M$, $[\text{Mo(VI)}]_0 = 1.00 \times 10^{-2} M$; \bullet , $[\text{cys}]_0 = 1.70 \times 10^{-1} M$, $[\text{Mo(VI)}]_0 = 1.00 \times 10^{-2} M$; \blacktriangle , $[\text{cys}]_0 = 1.10 \times 10^{-2} M$, $[\text{Mo(VI)}]_0 = 1.00 \times 10^{-2} M$; 1.00 M phosphate, pH 7.50, μ 1.71, 60°.

Although the cysteine was in excess in all runs, the excess is not sufficiently great to assume the cysteine concentration remains constant, since three cysteine molecules are required for each Mo(VI) reduced. When this was taken into account and the data was plotted using the appropriate integrated third-order equation, the plots were linear to >85% reaction (Figure 3) and rate constants were consistent. The values of these constants obtained from the third-order plots are found in Table I. The product, cystine, was found to have no effect on the rate (run 5).

Table I: Rate Constants for the Oxidation of L-Cysteine by Mo(VI)

Run	$[\text{Mo(VI)}]_0$, $M \times 10^2$	$[\text{cys}]_0$, $M \times 10$	$k_2 \times 10$ $M^{-2} \text{ min}^{-1}$
1	1.00	3.00	6.49
2	1.00	2.50	5.83
3	1.00	1.70	5.83
4	1.00	1.10	5.14
5	1.00	3.00	6.32 ^b

^a $k_3 = 5.99 \times 10^{-1} \pm 0.49 \pm 10^{-1} M^{-2} \text{ min}^{-1}$. ^b 1.00 $\times 10^{-2} M$ cystine added, all runs in 1.00 M phosphate buffer, pH 7.50, μ 1.71, 60°, each constant is the average of two or more runs.

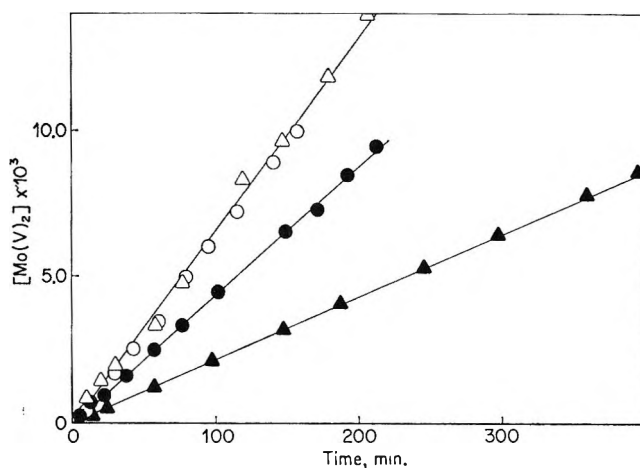


Figure 4. Zero-order plots for the oxidation of glutathione by Mo(VI): Δ , $[\text{GSH}]_0 = 5.00 \times 10^{-1} M$, $[\text{Mo(VI)}]_0 = 3.00 \times 10^{-2} M$; \circ , $[\text{GSH}]_0 = 5.00 \times 10^{-1} M$, $[\text{Mo(VI)}]_0 = 2.00 \times 10^{-1} M$; \bullet , $[\text{GSH}]_0 = 3.50 \times 10^{-1} M$, $[\text{Mo(VI)}]_0 = 2.00 \times 10^{-2} M$; \blacktriangle , $[\text{GSH}]_0 = 2.00 \times 10^{-1} M$, $[\text{Mo(VI)}]_0 = 2.00 \times 10^{-2} M$; 1.00 M phosphate buffer, pH 7.50, μ 1.71, 60°.

Solutions of Mo(V) have an absorbance maximum at 303 m μ in phosphate buffer at this pH with ϵ 5.20×10^3 . As indicated above, no change in the absorbance was observed when excess glutathione was added to solutions of Mo(V), so essentially all the Mo(V) is most likely present as a dimeric phosphate complex. When glutathione and MoO_4^{2-} are mixed in deaerated buffer at pH 7.50, the absorbance at 303 m μ increases with time as Mo(VI) is reduced to Mo(V) and glutathione oxidized to the disulfide. As with cysteine, the absorbance becomes constant after some time, indicating no further reduction beyond Mo(V) occurs. The rate of the reaction was followed by measuring the absorbance at 303 m μ .

In contrast to the reaction with cysteine, the rate was found to be independent of Mo(VI) concentration, when Mo(VI) concentration $\cong 10^{-2} M$. In the presence of excess glutathione, zero-order plots gave straight lines for 80–85% reaction (Figure 4). At the lowest ratio of glutathione:Mo(VI) (run 1) the concentration of glutathione actually decreases 20% by the end of the reaction. When the data for this run was plotted as first order to take this into account, only the last point (\sim 85% reaction) was found to fit the straight line better, and the rate constant was found to be almost the same as that obtained from the zero-order plots. Therefore, at high glutathione:Mo(VI) ratios, the small change in glutathione concentration can be neglected. The dependence on glutathione concentration was determined from a plot of $\log k$ vs. $\log [\text{GSH}]_0$, which gave a straight line with slope = 1.18. The reaction rate can therefore be expressed as $-d[\text{Mo(VI)}]/dt = k = k_1[\text{GSH}]$. The first-order rate constant, k_1 , was obtained from the pseudo-zero-order constant using the relationship, $k = k_1[\text{GSH}]$. These

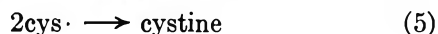
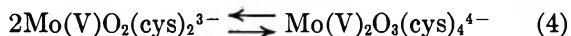
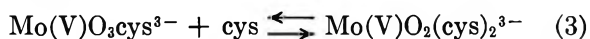
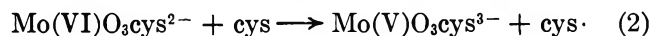
Table II: Rate Constants for the Oxidation of Glutathione by Mo(VI)

Run	[Mo(VI)] ₀ , M × 10 ²	[GSH] ₀ , M × 10	k ₁ × 10 ⁴ min ⁻¹	k ₂ × 10 M ⁻¹ min ⁻¹
1 ^a	2.00	1.00	2.54	
2	2.00	1.00	2.19	
3	2.00	2.50	2.30	
4	2.00	3.50	2.49	
5	2.00	5.00	2.62	
6	1.00	5.00	2.82	
7	3.00	5.00	2.60	
8	4.00	5.00	2.48	
9	1.00	5.00	2.65 ^b	
10	0.0200	0.0500		9.20
11	0.0400	0.0500		9.34

^a Runs 1-9, k₁ = 2.37 × 10⁻⁴ ± 0.38 × 10⁻⁴ min⁻¹. ^b 1.00 × 10⁻² M oxidized glutathione added. All runs in 1.00 M phosphate buffer, pH 7.50, μ 1.71, 60°. Each constant is the average of two or more runs.

constants are found in Table II. Again, as with cysteine, no effect on the rate by added product (oxidized glutathione) was found (run 9). When the Mo(VI) concentration was reduced to very low values (~10⁻⁴ M), considerable deviation in zero-order plots was observed, and it was found that the data were better treated by a first-order expression (Figure 5). Thus, the order of the reaction changed as the Mo(VI) concentration was reduced.

Mechanisms and Discussion. The results suggest the following mechanism for the oxidation of cysteine by Mo(VI)



In this mechanism, the reactive species is a 1:1 Mo(VI)-cysteine complex, which is present in very small amounts. This complex reacts with another cysteine in the rate-controlling step 2, while equilibria 3 and 4 and reaction 5 account for the formation of the products.

The rate of disappearance of Mo(VI) may be written

$$-d[\text{Mo(VI)}]/dt = k_1[\text{Mo(VI)}][\text{cys}] - k_{-1}[\text{Mo(VI)O}_3\text{cys}^{2-}]$$

applying the steady-state assumption to [Mo(VI)O₃cys²⁻] gives

$$-d[\text{Mo(VI)}]/dt = \frac{k_1 k_2 [\text{Mo(VI)}][\text{cys}]^2}{k_{-1} + k_2 [\text{cys}]}$$

If k₋₁ ≫ k₂[cys], this reduces to

$$-d[\text{Mo(VI)}]/dt = \frac{k_1 k_2}{k_{-1}} [\text{Mo(VI)}][\text{cys}]^2$$

This is identical with the experimental rate law.

The presence of a small esr signal in the reaction is accounted for by equilibrium 4, which is greatly in favor of the dimer.

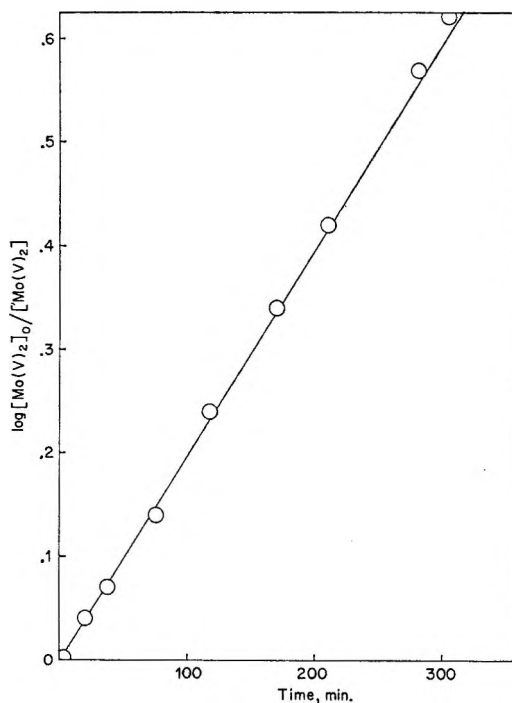
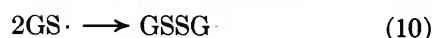
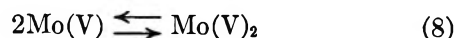
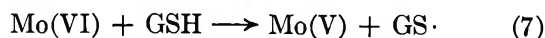


Figure 5. First-order plot for the oxidation of glutathione by Mo(VI). [GSH]₀ = 5.00 × 10⁻³ M, [Mo(VI)]₀ = 2.00 × 10⁻⁴ M. 1.00 M phosphate, pH 7.50, μ 1.71, 60°.

In the reaction of glutathione with Mo(VI), a different mechanism is necessary. Since at high Mo(VI) concentrations (~10⁻² M) the rate is independent of Mo(VI) concentration, the rate-controlling step must involve only glutathione. Glutathione is well known to exist in a number of possible cyclic forms in acid solution.¹¹ Nothing is known, however, about its structure in neutral or basic solution. To explain the results, an unreactive form (GSH'), possibly a cyclic thioether, is proposed to be in equilibrium with the reactive form (GSH).



(11) M. Calvin, "Glutathione-A Symposium," S. Colowick, A. Lazarow, E. Racker, D. R. Schwarz, E. Stahtman, and H. Waelsch, Ed., Academic Press, Inc., New York, N. Y., 1954, p 3.

In this mechanism, the rate-controlling step is reaction 1, which produces the reactive form GSH. The rate may be expressed

$$-d[\text{Mo(VI)}]/dt = k_2[\text{Mo(VI)}][\text{GSH}]$$

Applying the steady-state condition to GSH leads directly to

$$-d[\text{Mo(VI)}]/dt = \frac{k_1 k_2 [\text{Mo(VI)}][\text{GSH}']}{k_{-1} + k_2 [\text{Mo(VI)}]}$$

If $k_2[\text{Mo(VI)}] \gg k_{-1}$, which might be the case at high Mo(VI) concentration, this reduces to the first-order expression

$$-d[\text{Mo(VI)}]/dt = k_1[\text{GSH}']$$

This agrees with the experimental rate law at high Mo(VI) concentrations.

If $k_{-1} \gg k_2[\text{Mo(VI)}]$, which might be the case at low Mo(VI) concentrations, this reduces to the second-order expression

$$-d[\text{Mo(VI)}]/dt = \frac{k_1 k_2}{k_{-1}} [\text{Mo(VI)}][\text{GSH}']$$

This again agrees with the experimental results, since the order was found to change from first to second at low Mo(VI) concentrations.

Both monomeric and dimeric forms of Mo(V) exist undoubtedly as oxophosphate complexes; since their structures are unknown, they are indicated simply as Mo(V) and Mo(V)₂, respectively, in this mechanism.

The spectral results indicate no appreciable amount of a Mo(V)-GSH complex exists, but a small amount of an esr-active (monomeric) complex is present. This is accounted for by equilibrium 9 in the mechanism.

The results suggest glutathione exists primarily in a nonreactive state (GSH') at pH 7.50, possibly a cyclic thioether which does not complex nor react with Mo(VI). Work to determine the nature of this species is planned.

As was reported for the reaction of thioglycolic acid with Mo(VI),³ both cysteine and glutathione are oxidized by Mo(VI), which suggests the possibility of such a reaction in the molybdenum enzymes.

Experimental Section

Materials. Molybdenum(VI) solutions were prepared from B & A. Na₂MoO₄·H₂O, the purity of which was determined by the α-benzoinoxime method to be 99.8%.¹² Molybdenum(V) solutions were prepared by the quantitative reduction of Mo(V) solutions over Hg in 3 M HCl, or from (NH₄)₂MoOCl₅. Identical

results were obtained, indicating the same species of Mo(V) (a dimer) is present. The (NH₄)₂MoOCl₅ was prepared and its purity determined as described previously.^{3,13}

L-Cysteine and glutathione were obtained from Sigma Chemical Co., and their purity was determined by iodine titration. Prepurified He (99.995%, J. T. Baker and Co.) was used to deaerate solutions.

Analytical Methods. The concentration of Mo(V) was determined by removing samples of the reaction solution with a gas-tight syringe, diluting them under He with the proper amount of buffer, and measuring the absorbance. In the reactions with cysteine, the maximum absorbance at 305 mμ was used, while with glutathione, the maximum at 303 mμ was used. In both cases, using Mo(V) solutions of known concentration, it was determined that Beer's law was followed over the concentration range used.

Molar Ratio Determination. A series of solutions each containing Mo(V) at a concentration of 7.50 × 10⁻⁴ M and increasing amounts of L-cysteine were prepared by dilution of the appropriate stock solutions with deaerated buffer. Samples were transferred with a gas-tight syringe to stoppered cells under He, and the absorbance was measured in a Beckman DU spectrophotometer.

Kinetics. The kinetics were determined by following the total concentration of Mo(V) with time. The reactions were run in vessels that could be deaerated with He and kept under He pressure. Rate constants were obtained from the proper plots, using the method of least squares to obtain the best values of the slopes.

Esr Analysis. Samples for esr analysis were removed with a gas-tight syringe and frozen immediately in deaerated quartz esr tubes in liquid N₂. A solution of K₃Mo(CN)₆, prepared as described previously,^{3,14} was used to estimate the number of spins in the samples. The *g* values were obtained by comparison with the *g* values of 1,1-diphenyl-2-picrylhydrazyl. All esr spectra were obtained with a Varian V-4500-10 X-band spectrometer equipped with 100-kc field modulation.

Acknowledgment. This work was supported by the U. S. Public Health Service, Grant GM 08347, National Institute of General Medical Sciences and by Research Career Development Award 5-K3-GM22,643, to J. T. S.

(12) H. B. Knowles, *J. Res. Nat. Bur. Stand.*, **9**, 1 (1932).

(13) W. G. Palmer, "Experimental Inorganic Chemistry," Cambridge University Press, Cambridge, 1954, p 406.

(14) N. H. Furman and C. O. Miller, *Inorg. Syn.*, **3**, 160 (1950).

Surface and Bulk Reactions of Carbon Tetrachloride with Titanium Dioxide

by M. Primet, J. Basset, M. V. Mathieu, and M. Prettre

Institut de Recherches sur la Catalyse, Villeurbanne, France (Received December 12, 1969)

Two different reactions occur between CCl_4 and TiO_2 . At moderate temperature, the nature of the superficial reaction strongly depends on the hydration state of the solid. On a dry titanium dioxide, CCl_4 chemisorption on two bridges Ti-O-Ti gives a carbonyl complex detected by infrared spectroscopy. The reaction which follows from destruction of this complex proceeds by exchange of two superficial oxygen atoms for four chlorine atoms, with formation of gaseous CO_2 . Strongly oxidizing Ti^{4+} ions, with high electron accepting properties, are created through the elimination of superficial oxygen atoms. On hydrated titanium dioxide, these reactions are followed by the formation of HCl which generates hydronium ions. Results obtained on TiO_2 and γ alumina point out the high reactivity towards CCl_4 of superficial oxygen atoms, compared to hydroxyl groups. Reticular reaction, which starts at 150° , is a proof of the relatively high mobility of the oxygen in the anatase lattice.

Introduction

The oxidation of hydrocarbons is generally catalyzed by transition metals or their oxides. The catalytic activity of these oxides is mainly determined by the bond energy, *i.e.*, the mobility of oxygen in the surface layer.¹ Until now, different types of superficial reactions have been studied to obtain information on the reactivity of superficial oxygen atoms: homomolecular exchange $^{16}\text{O}_2(\text{g})$ $^{18}\text{O}_2(\text{g})$ ¹⁻³ and $^{18}\text{O}_2(\text{g})$ $\text{C}^{16}\text{O}_2(\text{g})$,⁴ heteromolecular exchange $^{18}\text{O}_2(\text{g})$ $^{16}\text{O}(\text{s})$, catalytic transfer of oxygen between CO and CO_2 ,⁵ reduction of solids by CO^6 or H_2 .⁷

From this standpoint, the study of carbon tetrachloride oxidation by mean of superficial oxygen atoms of a solid offers a double advantage. First this reaction characterizes the reactivity of superficial groups.⁸ Second, exchange of oxygen atoms or hydroxyl groups by chlorine atoms may confer to the solid interesting catalytic properties.^{9,10}

Gravimetric,¹¹ microcalorimetric,⁸ and kinetic¹² studies have shown different types of interactions and reactions between CCl_4 and γ alumina. At room temperature, CCl_4 reaction with a fraction of the surface produces carbonate and CO_2 . At 200° , reaction extends to the overall surface, its stoichiometry varies according to the hydroxyl group content. For a sample heated at 200° , CCl_4 exchanges one chlorine atom for one hydroxyl group; the obtained solid exhibits a weak Lewis acidity. For a sample heated above 300° , CCl_4 exchanges four chlorine atoms for two surface oxygen atoms; the study of redox character of such a solid by epr shows the existence of strongly oxidizing sites which have been identified as aluminum ions exposed through elimination of oxygen ions.¹³ Above 230° , the attack of CCl_4 spreads into the lattice; the sublimation of AlCl_3 thus formed is detected above 300° .

In the present work, we have studied the oxidation

of CCl_4 by TiO_2 in order to compare the oxidative character of TiO_2 with that of γ alumina. For this study we have mainly used infrared technique which is able to provide information on the reaction mechanism by identifying the intermediate superficial species.

Experimental Section

Materials. Titanium dioxide was supplied by the firm Degussa (Frankfurt am Main) as a crystalline and nonporous solid composed of anatase (85%) and rutile (15%). Before each experiment, samples are calcined under oxygen at 400° for 15 hr and desorbed under vacuum at 200° for 15 hr ($\text{TiO}_{2,(200)}$). The specific surface area of such material is $60 \text{ m}^2/\text{g}$, and about 50% of the surface is covered with hydroxyl groups ($6 \text{ OH}/100 \text{ \AA}^2$). In some experiments, samples are calcined under oxygen at 400° for 15 hr and desorbed under vacuum at the same temperature for 15 hr ($\text{TiO}_{2,(400)}$); the solid obtained is completely dehydroxylated.

- (1) G. K. Borekov, *Discuss. Faraday Soc.*, **41**, 263 (1966).
- (2) A. P. Dzizyak, G. K. Borekov, and L. A. Kasatkina, *Kinet. Katal.*, **3**, 81 (1962).
- (3) G. K. Borekov, A. P. Dzizyak, and L. A. Kasatkina, *ibid.*, **4**, 383 (1963).
- (4) T. Kiyoura, *Bull. Chem. Soc. Jap.*, **39**, 2135 (1966).
- (5) D. Y. Cha and G. Parravano, *J. Catal.*, **11**, 3, 228 (1968).
- (6) P. Pichat and G. Brau, *J. Chim. Phys.*, **66**, 724 (1969).
- (7) W. M. H. Sachtler and J. H. de Boer, *Proc. Intern. Congr. Catal.*, **3rd**, **1**, 252 (1964).
- (8) J. Basset, M. V. Mathieu, and M. Prettre, *J. Chim. Phys.*, **66**, 1264 (1969).
- (9) A. G. Goble and P. A. Lawrence, *Proc. Int. Congr. Catal.*, **3rd**, **1**, 320 (1964).
- (10) J. Basset, F. Figueras, M. V. Mathieu, and M. Prettre, *J. Catal.*, **16**, 53 (1970).
- (11) J. Basset, M. V. Mathieu, and M. Prettre, *Rev. Chim. Min.*, **5**, 879 (1968).
- (12) J. Basset, M. V. Mathieu, and M. Prettre, *J. Chim. Phys.*, **66**, 611 (1969).
- (13) J. Basset, C. Naccache, M. V. Mathieu, and M. Prettre, *ibid.*, **66**, 1522 (1969).

The γ alumina has been previously described;¹¹ before each experiment, this solid is calcined under vacuum at 500° for 15 hr; its specific surface area is 300 m²/g and its hydroxyl content 2 OH/100 Å².

The different reactants are dried by treatment with P₂O₅ and molecular sieves 5A (Union Carbide) previously calcined; they are degassed by repeated freezing and evacuation before use.

Apparatus and Procedure. Infrared spectra are recorded with a Perkin-Elmer 125 spectrometer. Two types of cell have been used: a classical cell which allows the experiment to be done under controlled atmosphere at different temperatures, the spectra being recorded after cooling of the sample to room temperature,¹⁴ and a high-temperature cell which allows the spectra to be recorded at the reaction temperature. Gravimetric, kinetic, and epr techniques have been described in previous papers.¹¹⁻¹³

Results

A. Infrared Spectrometry. (1) Reaction of CCl₄ with Titanium Dioxide. The infrared spectrum of TiO_{2,(200)} is characterized by $\nu(\text{OH})$ bands at 3715, 3660, and 3410 cm⁻¹.¹⁵ CCl₄ adsorption at room temperature modifies these bands and creates new species detectable by their bands in the region 4000-400 cm⁻¹ (Figure 1).

The $\nu(\text{OH})$ bands are replaced by a narrow one at 3540 cm⁻¹ and by a very broad one centered around 3470 cm⁻¹. The position and the narrowness of the 3540-cm⁻¹ band must be produced by a specific interaction between one hydroxyl group and one chlorine atom.

The presence of carbon dioxide is characterized by a weak band at 2350 cm⁻¹ (ν_3). A band at 1700 cm⁻¹ also appears; the same band is observed on alumina as well.

Gaseous or physisorbed CCl₄ is detected by its ν_3 vibration (790 cm⁻¹, 762 cm⁻¹) and by its combinations bands $\nu_1 + \nu_3$ (1250, 1230 cm⁻¹) and $2\nu_3$ (1550 cm⁻¹).

Heating the sample under CCl₄ at 100° does not produce marked modification of the spectrum except that the band at 1700 cm⁻¹ disappears and the intensity of the CO₂ band at 2350 cm⁻¹ increases. At 130°, the appearance of vibration rotation band of gaseous HCl, centered around 2890 cm⁻¹, is paralleled by the reduction of intensity of the $\nu(\text{OH})$ bands at 3540 and 3470 cm⁻¹. Simultaneously a narrow band is formed at 1590 cm⁻¹. We shall see later that the same band is created by reaction of anhydrous hydrogen chloride with a TiO_{2,(200)} surface. At 150°, the phenomena observed at 130° are more pronounced; consumption of hydroxyl groups, appearance of larger quantities of CO₂ and HCl and growth of the band at 1590 cm⁻¹. In addition two bands centered around 1400 and 1450 cm⁻¹ are produced by the fixation of CO₂ on superficial oxygen atoms. At 200°, the elimination of

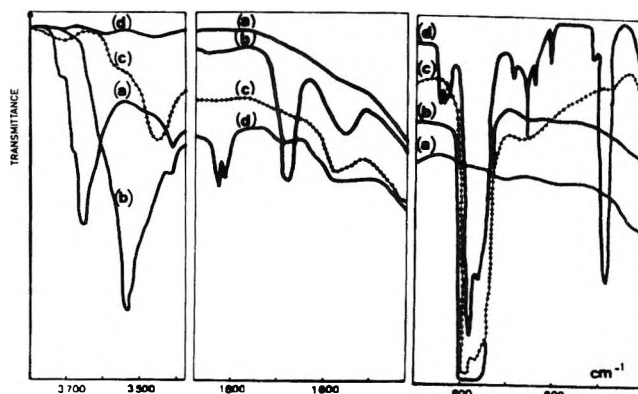


Figure 1. Infrared spectra of CCl₄ adsorbed in TiO_{2,(200)}: (a) initial solid, (b) after admission of 100 Torr of CCl₄ at room temperature, (c) after heating at 150° under CCl₄ for 8 hr, (d) after heating at 300° under CCl₄ for 10 hr.

hydroxyl groups is achieved. Simultaneously the intensity of HCl and CO₂ bands increases and the stretching bands ν_1 (1825 cm⁻¹) and ν_4 (849 cm⁻¹)¹⁶ of gaseous or physisorbed phosgene are observed. At this temperature there appears a band at 1700 cm⁻¹, attributed to chemisorbed phosgene. The intensity of ν_3 vibration of CO₂ increases, while the P and R combination bands of CO₂ appear at 3609 cm⁻¹ ($2\nu_2 + \nu_3$) and 3716 cm⁻¹ ($\nu_1 + \nu_3$) as well as the bands at 720, 665, 645, and 615 cm⁻¹. These bands are caused by transitions from excited states of ν_2 (667 cm⁻¹).¹⁷ Finally, we observe at 490 cm⁻¹, a narrow band ($\Delta\nu_{1/2} = 10$ cm⁻¹) which is attributed to ν_3 vibration of gaseous TiCl₄. At 300°, the intensity of the bands attributed to CO₂, HCl, and TiCl₄ considerably increases.

After evacuation at room temperature, the spectrum of the solid is characterized by bands of low intensity associated with adsorbed CCl₄ and TiCl₄. The desorption of these compounds is performed at 100° under vacuum. In order to explain the origin of the different bands observed during the reaction of CCl₄ with TiO₂, we have studied the reaction of HCl and COCl₂ with TiO₂ and the reaction of CCl₄ with γ alumina.

(2) *Reaction of HCl with Titanium Dioxide.* The spectra resulting from the adsorption of HCl on TiO₂ at different temperatures are shown in Figure 2. At room temperature, the stretching bands $\nu(\text{OH})$ of the initial solid are replaced by two maxima of absorption: the first at 3540 cm⁻¹ is very sharp; the second centered around 3330 cm⁻¹ is very broad. A narrow band at 1595 cm⁻¹ is probably due to the bending vibration $\delta(\text{OH})$ of molecular water which could be pro-

(14) M. V. Mathieu and P. Pichat, "La Catalyse au Laboratoire et dans l'Industrie," Masson et Cie, Paris, 1967, p 319.

(15) M. Primet, P. Pichat, and M. V. Mathieu, *C. R. Acad. Sci.*, **267B**, 799 (1968).

(16) A. H. Nielsen, T. G. Burke, P. J. H. Woltz, and E. A. Jones, *J. Chem. Phys.*, **20**, 596 (1952).

(17) J. Lecomte, "Handbuch der Physik, Licht und Materie," Vol. XXVI, Part II, Springer-Verlag, Berlin, 1958, p 660.

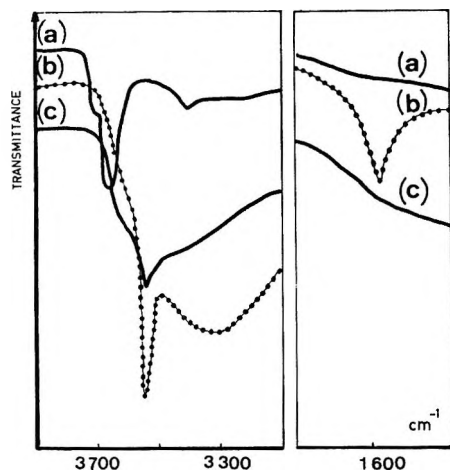


Figure 2. Infrared spectra of HCl adsorbed on $\text{TiO}_{2,(200)}$: (a) initial solid, (b) after admission of 100 Torr HCl at room temperature, (c) after heating at 300° under HCl for 9 hr and evacuation at 200° for 10 hr.

duced by the reaction of hydrogen chloride with superficial hydroxyl groups. Indeed, we have found the same band by chemisorption of water on TiO_2 chlorinated by CCl_4 .

Heating at 300° under HCl, followed by cooling at room temperature, does not noticeably modify the intensity of these bands, but makes the band a 3330 cm^{-1} narrower and higher in frequency (3470 cm^{-1}). Evacuation at 25° decreases the intensity of $\delta(\text{OH})$ and $\nu(\text{OH})$ bands. At 200° , molecular water has disappeared and only a few OH groups remain on the solid.

(3) *Reaction of CCl_4 with γ Alumina.* The spectrum of γ alumina which is characterized by $\nu(\text{OH})$ bands at 3795 , 3735 , and 3695 cm^{-1} is modified by the reaction of CCl_4 at room temperature, as was shown by Peri.¹⁸ The (OH) bands are replaced by a very broad absorption maximum connected with the formation of hydrogen bands between the adsorbate and the hydroxyl groups. Besides, we observe bands in the spectral region $1800\text{--}1200\text{ cm}^{-1}$ (Figure 3): adsorbed CCl_4 is detected by its combination bands at 1550 , 1250 , and 1230 cm^{-1} and is completely desorbed by evacuation under vacuum at 200° ; two bands at 1440 and 1360 cm^{-1} formed at room temperature are probably due to symmetric and antisymmetric stretching vibration of a monodentate carbonate. Heating at 200° makes them disappear and be replaced by a band at 1450 cm^{-1} caused by the antisymmetric stretching vibration of a carbonate ion; a broad band, centered around 1650 cm^{-1} is displaced higher in frequency on heating (1670 cm^{-1} at 70° and 1680 cm^{-1} at 160°) and disappears at 200° .

(4) *Reaction of COCl_2 with TiO_2 and γ Alumina.* Changes in the spectrum of a $\text{TiO}_{2,(400)}$, after adsorption of COCl_2 at room temperature, are shown in Figure 4. We find at 1825 cm^{-1} (ν_2) (high intensity) and

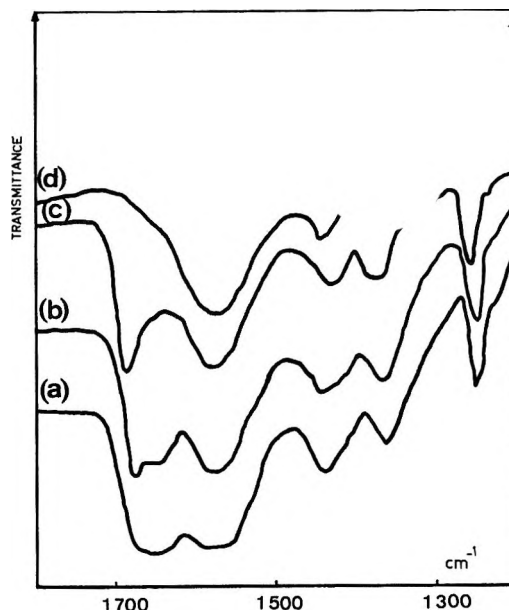


Figure 3. Infrared spectra of CCl_4 adsorbed on $\text{Al}_2\text{O}_{3,(600)}$: (a) initial solid after admission of 100 Torr CCl_4 at room temperature, (b) after heating at 70° under CCl_4 for 12 hr, (d) after heating at 200° under CCl_4 for 12 hr.

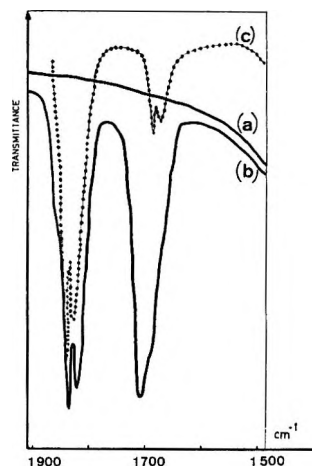


Figure 4. Infrared spectra of phosgene adsorbed on $\text{TiO}_{2,(200)}$: (a) initial solid, (b) after admission of 10 Torr of COCl_2 at room temperature, (c) gaseous phase.

1677 cm^{-1} ($2\nu_4$) (low intensity) the bands of gaseous COCl_2 and at 1820 cm^{-1} the fundamental band (ν_2) of physisorbed phosgene. We also observe an intense band at 1705 cm^{-1} . All of these bands are eliminated under vacuum at 25° .

γ alumina exhibits the same phenomena but the band situated at 1705 cm^{-1} associated with TiO_2 is displaced at 1690 cm^{-1} with γ alumina.

B. Gravimetric and Kinetic Results. Changes in weight registered during reaction of CCl_4 with $\text{TiO}_{2,(400)}$ at different temperatures are shown in Figure 5. Up to 130° , the initial increase in weight (part AB, curve 1)

(18) J. B. Peri and R. B. Hannan, *J. Phys. Chem.*, **64**, 1526 (1960).

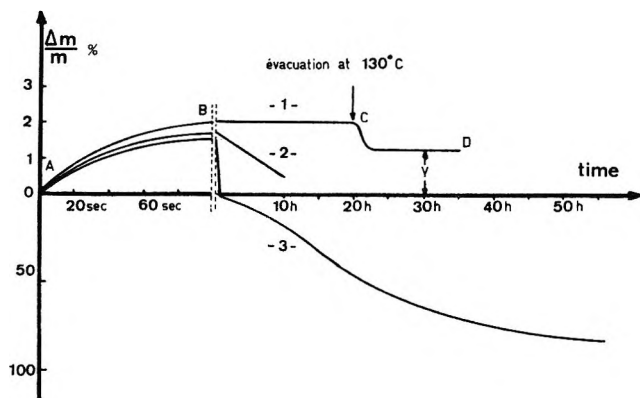


Figure 5. Changes in weight with time registered after CCl_4 admission on $\text{TiO}_{2(400)}$ at various temperatures: (1) 130° , (2) 150° , (3) 200° .

is followed by a plateau (part BC, curve 1). This phenomenon must be connected with the CCl_4 adsorption and its reaction with the superficial oxygen atoms of the solid. The evacuation at this temperature (part CD, curve 1) removes the weakly adsorbed species (CCl_4 and CO_2). Stoichiometry of the superficial reaction has been defined by the ratio of the chlorine content to the increase in weight (Y) observed in D. The obtained value (1.41) is in agreement with the calculated one (1.30) for the exchange of one oxygen atom for two chlorine atoms.

Above 150° , the initial increase in weight is followed by a loss in weight (Figure 5, curve 2) which arises from the formation of gaseous TiCl_4 . The attack of the lattice may be complete and the changes in weight with time obey a sigmoid law, characteristic of gas-solid reactions with germination.¹⁹ The activation energy, determined at the maximum rate between 200 and 270° has been found equal to 25 ± 2 kcal/mol.

Variations of chlorine content against reaction temperature are shown in Figure 6. In agreement with our infrared and gravimetric results, superficial reaction takes place at room temperature. Above approximately 150° , chlorine content is constant. Desorption between 200 and 400° of a $\text{TiO}_{2(400)}$ chlorinated at 130° brings about a small change in chlorine content, which implies that the remaining chlorine is firmly bound.

The rate of chlorination has been measured by the quantity of CO_2 produced per second. At 200° , two successive phenomena have been observed (Figure 7). The rate first obeys a decreasing exponential law; the plateau coincides with the formation of gaseous TiCl_4 .

Discussion

We can assume two different types of reaction between CCl_4 and TiO_2 to explain our gravimetric, kinetic, and infrared results. The first reaction, which takes place at a high rate, even at room temperature, is superficial. The second one, which is detected by

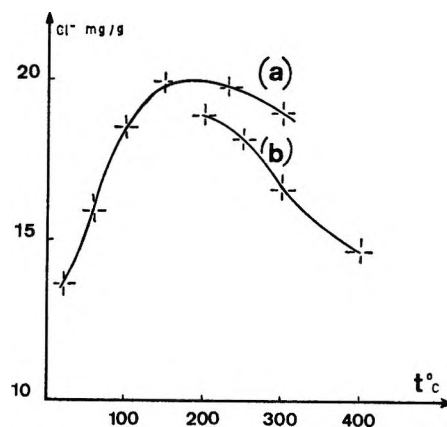


Figure 6. Thermal stability of superficial chlorine atoms: (a) effect of reaction temperature with $\text{TiO}_{2(400)}$ on the chlorine content after evacuation at the reaction temperature, (b) effect of desorption temperature on the chlorine content for a sample of $\text{TiO}_{2(400)}$ chlorinated at 130° .

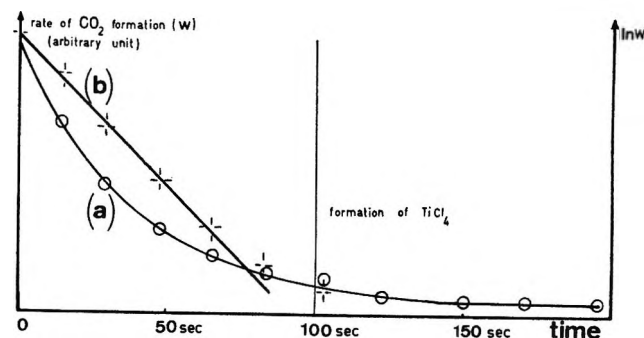


Figure 7. Kinetic data: (a) rate of CO_2 formation plotted vs. time during the reaction of CCl_4 with $\text{TiO}_{2(400)}$ at 200° , (b) plots of $L_n(W)$ vs. time.

the appearance of gaseous TiCl_4 at higher temperatures, concerns the attack of the lattice. We shall discuss these two kinds of reaction separately.

I. Reaction of CCl_4 with TiO_2 at Moderate Temperature

(A) *Nature of Superficial Reactions.* At room temperature, no hydrogen-containing product being detected, the CCl_4 reaction must occur with superficial oxygen atoms of TiO_2 . The exchange of one oxygen atom for two chlorine atoms which, we have demonstrated on a dry $\text{TiO}_{2(400)}$, takes place in accordance with the following equation



The mechanism of this reaction can be deduced from the infrared results obtained on alumina and titania. For these solids, CCl_4 chemisorption is connected with the formation of a band situated around 1700 cm^{-1} (1690 cm^{-1} for TiO_2 and 1680 cm^{-1} for γ alumina). Bands appear in the same region of the spectra

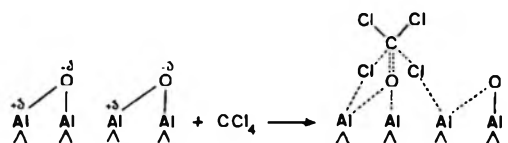
(19) B. Delmon, *Rev. Inst. Fr. Pétrole*, **13**, 472 (1963).

when phosgene is absorbed on titania (band at 1705 cm^{-1}) or γ alumina (band at 1690 cm^{-1}) at room temperature. These last bands cannot arise from the perturbation of the fundamental vibration $\nu(\text{C}=\text{O})$ of phosgene, which is shifted to 1820 cm^{-1} by adsorption. Furthermore they cannot be due to the increase in frequency of the $2\nu_4$ vibration of phosgene which is less intense. These 1680–1705- cm^{-1} bands, although relatively low in frequency, can be assigned to carbonyl groups.²⁰ Scott²¹ has shown that in carboxylates, the higher the frequency $\nu(\text{C}=\text{O})$, the lower the electronic density on the oxygen, corresponding to the electronic release of alkyl radical. Likewise fundamental vibration $\nu(\text{CO})$ of F_2CO is higher than that of Cl_2CO .¹⁶ Therefore a low frequency for a vibration $\nu(\text{C}=\text{O})$ is characteristic of an increase in electronic density on the oxygen.

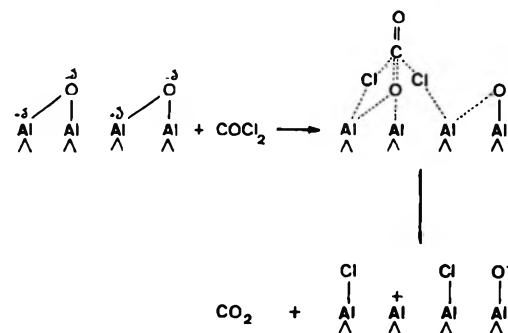
We have proposed below two models for the chemisorption and reaction of CCl_4 and COCl_2 on TiO_2 or Al_2O_3 . These models account for the formation of electron-deficient titanium atoms, which attract electrons of the $\text{C}=\text{O}$ band created by chemisorption. This explains the low frequencies observed for the $\nu(\text{C}=\text{O})$ vibrations of chemisorbed phosgenes or CCl_4 .

Schemes I and II. The complex I would account for the bands situated around 1700 cm^{-1} observed during the chemisorption of CCl_4 on alumina or titania; on titania it is formed at room temperature and destroyed at 70°, whereas on alumina its stability extends from 70 to 200°.

Scheme I



Scheme II

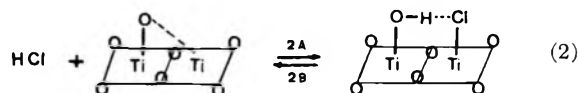


It is reasonable to suppose that, at room temperature, CCl_4 chemisorbs on Ti-O-Ti bridges and gives the complex I. The decomposition of this complex gives COCl_2 .

Since no band at 1820 cm^{-1} is detected at moderate temperature, chemisorption of phosgene according to complex II must be followed by a rapid reaction which produces gaseous CO_2 . The solid is then partially chlorinated and its chlorine content is about 4 Cl/100 \AA^2 .

The spectrum of adsorbed HCl , which exhibits a band at 3540 cm^{-1} , facilitates the assignment of the same band obtained by chlorination of TiO_2 with CCl_4 (3540 cm^{-1} , $\Delta\nu_{1/2} = 40 \text{ cm}^{-1}$). The most likely mechanism of HCl adsorption is a dissociative chemisorption^{11,21} on Ti-O-Ti groups according to reaction scheme III.

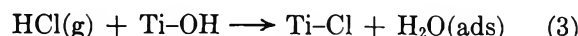
Scheme III



Scheme III. Therefore, superficial chlorine atoms, created by reaction 1, cause the formation of hydrogen bonds with OH groups which are fixed to well-defined crystalline sites. The position and the narrowness of 3540- cm^{-1} band are then explained by the constant distance between chlorine atoms and OH groups as shown on the above scheme.

If temperature is raised to 130°, the rupture of these hydrogen bonds, according to reaction 2B, causes the appearance of gaseous hydrogen chloride. In much the same way, the heating of a sample of HCl -chlorinated TiO_2 at 200° partially restores the Ti-O-Ti groups initially present on the solid.

The hydrogen chloride thus liberated can then react with OH groups, as was shown on alumina^{11,22} or silica²³



The Ti-O-Ti groups, created by the elimination of hydrogen chloride, can react again with CCl_4 according to reaction 1. Simultaneity of reaction 1, 2B, and 3 explains most of the experimental results observed when the reaction temperature is raised: disappearance of hydroxyl groups; formation of hydrogen chloride and molecular water; increase of chlorine content with reaction temperature.

The band at 1590 cm^{-1} has been designated as a bending vibration, the nature of which has to be determined. It should be noted that the band is situated near the bending vibration of gaseous molecular water.²⁴ However its frequency is very low if we refer to gener-

(20) L. J. Bellamy, "Advances in Infrared Group Frequencies," Methuen and Co., 1968, p 154.

(21) J. Scott and R. Goulden, *Nature*, **220**, 5168, 698 (1968).

(22) J. B. Peri, *J. Phys. Chem.*, **70**, 1482 (1966).

(23) M. Baverez, B. Hatier, M. Bastick, and J. Bastick, *Bull. Soc. Chim. Fr.*, 1298 (1964).

(24) W. S. Benedict, N. Gailar, and E. K. Plyler, *J. Chem. Phys.*, **24**, 1139 (1956).

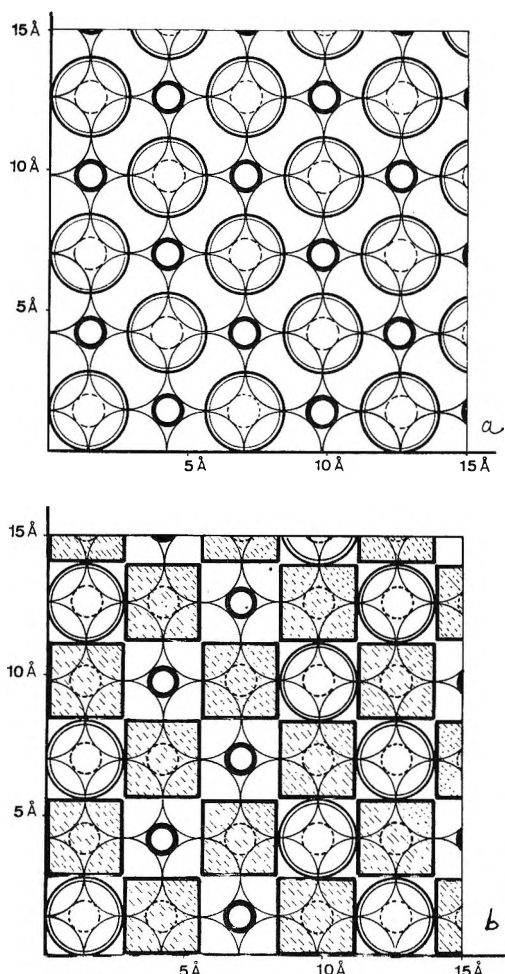


Figure 8. (a) Plane 001 of anatase surface wholly and regularly dehydroxylated: \odot , oxygen atom of the superficial layer; \circ , oxygen atom of the lower layer; \bullet , exposed titanium atom of the lower layer; \ominus , titanium atom of the lower layer covered by a superficial oxygen atom. (b) transformation of model (a) after complete chlorination: \odot , unreacted oxygen atom of the superficial layer; \circ , oxygen atom of the lower layer; \blacksquare , chlorine atom; \bullet , titanium atom exposed through the elimination of a superficial oxygen atom; \ominus , titanium atom of the lower layer covered by a superficial oxygen atom.

ally known values, especially to results of Peri on chlorinated aluminas by HCl.²² On these solids the hydrogen bands which are produced between molecular water and electronegative centers of the surface (chlorine or oxygen atoms) increase the force constant of the bending $\delta(\text{OH})$. On the contrary, on our solids the highly oxidizing sites demonstrated by epr could adsorb water molecules forming coordinate bonds which utilize electron pairs of oxygen atoms.

The frequency $\delta(\text{OH})$ of such a species could be as low as those already observed by Adams²⁵ and Baettie²⁶ in complexes of transition metals. But the adsorption of pyridine on TiO_2 chlorinated by CCl_4 is accompanied by the disappearance of the band at 1590 cm^{-1} and the formation of pyridinium ion which may be desorbed at 200° , whereas pyridinium ions detected on fluorinated aluminas persist until 500° .^{27,28}

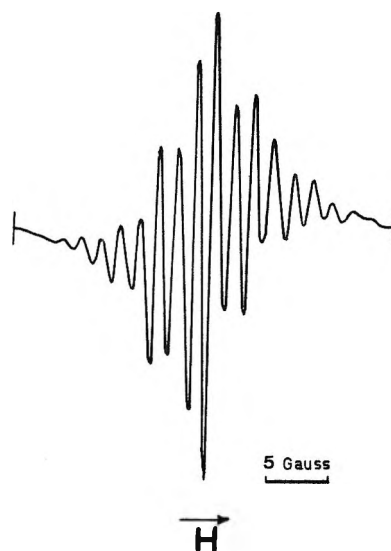
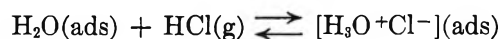


Figure 9. Epr spectrum of anthracene adsorbed on $\text{TiO}_2(400)$ chlorinated by CCl_4 at 130° and desorbed at the same temperature.

It seems logical to attribute the disappearance of pyridinium ion to the sublimation of pyridinium chloride which could be produced from the species $\text{Cl}^- \text{H}_3\text{O}^+$ arising from the solvation of the proton of hydrogen chloride according to the reaction



This hypothesis finds corroboration in the vibration frequency of hydronium ion in the compound $\text{H}_3\text{O}^+ \text{ClO}_4^-$ ²⁹ near 1590 cm^{-1} . On other chlorinated solids, a further study of formation conditions of the 1590-cm^{-1} band, and properties of the species responsible, should permit a distinction between the two hypotheses: chemisorption of water by coordinative ligand or formation of hydronium ions.

(B) *A Model for the Chlorinated Surface.* The surface of a wholly dehydroxylated titanium dioxide (face 001) holds six superficial oxygen atoms/ 100 \AA^2 . Complete exchange of these oxygens according to the proposed stoichiometry would give $12\text{ Cl}/100\text{ \AA}^2$. Whatever be the reaction temperature, maximum chlorine content is $6\text{ Cl}/100\text{ \AA}^2$, which proceeds from the exchange of half of the superficial oxygen atoms. Reaction of CCl_4 and COCl_2 in conformity with schemes I and II requires two Ti-O-Ti groups but only one oxygen is exchanged, so that the remaining oxygen cannot react.

(25) D. M. Adams, private communication.

(26) I. R. Baettie, T. R. Gilson, and G. A. Ozin, *J. Chem. Soc., A*, 4, 534 (1969).

(27) T. V. Antipina, O. V. Bulgarov, and A. V. Uvarov, *Proc. Int. Congr. Catal., 4th, Moscow*, Paper No. 79 (1968).

(28) T. R. Hugues, H. M. White, and R. J. White, *J. Catal.*, 13, 58 (1969).

(29) R. C. Taylor and G. L. Vidale, *J. Amer. Chem. Soc.*, 78, 5999 (1956).

We have represented in Figure 8a the 001 face^{15,30} of a wholly and regularly dehydroxylated anatase. The same face, after complete chlorination is shown in Figure 8b. This model accounts for the exchange of 50% of superficial oxygen atoms by twice their quantity of chlorine atoms. Besides, this model shows electron-poor Ti^{4+} ions, the presence of which has been confirmed by epr study.

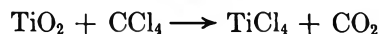
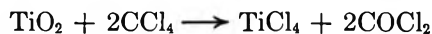
Anthracene is oxidized to its monopositive ion when chemisorbed on superficially chlorinated TiO_2 . The high resolution of the hyperfine structure (Figure 9) can be connected with the existence of strongly oxidizing sites which possess a high-electron attractive power such as we have previously observed on chlorinated aluminas.¹² These sites could stabilize hydronium ions which have been detected on chlorinated TiO_2 .

II. Reaction of CCl_4 with TiO_2 at 150° and Higher Temperatures

As was shown by gravimetric, kinetic, and infrared results, the first phenomenon observed above 150° when CCl_4 comes in contact with TiO_2 is a rapid superficial reaction. The attack of the lattice which proceeds afterwards is confirmed by three experimental facts: appearance of gaseous or physisorbed $TiCl_4$, loss in weight due to the sublimation of $TiCl_4$, and constant chlorine content of the solid above 150°.

This reticular reaction does not proceed according to the same mechanism as the superficial one. Besides, considering its high-activation energy (25 kcal/mol), it

cannot progress at low temperature with a reasonable rate. The stoichiometry of this gas-solid reaction, which produces $COCl_2$, CO_2 , and $TiCl_4$ would be



Considering the oxidizing properties of titanium dioxide, it is not surprising that reticular reaction occurs on this solid at a lower temperature than on alumina. On alumina, $AlCl_3$ formation begins around 230°, and its sublimation begins at 300°.¹¹

Conclusion

The mechanism of the surface chlorination of TiO_2 by CCl_4 has been specified by identification of carbonyl complexes detected by means infrared spectroscopy. Particular hydroxyl bands have been found which explain the formation of hydrogen chloride and the presence of hydronium ions. A model of the chlorinated surface has been proposed which accounts for the observed chlorine content and the presence of electron-deficient Ti^{4+} ions. Results obtained with TiO_2 and γ alumina point out the high reactivity towards CCl_4 , of superficial oxygen atoms, compared to hydroxyl groups. Reticular reaction which begins at 150° indicates the relatively high mobility of oxygen in the anatase lattice.

(30) H. P. Boehm, *Advan. Catal.*, **16**, 179 (1966).

Thermal Decomposition of Potassium Bicarbonate¹

by I. C. Hisatsune and T. Adl

Department of Chemistry, Whitmore Laboratory, The Pennsylvania State University, University Park, Pennsylvania 16802
(Received April 2, 1970)

The thermal decomposition reactions of potassium bicarbonate dispersed in the KBr pressed disk have been studied by observing the changes in the infrared spectrum of the disk with heating. In the temperature range of 140–220°, the principal reaction in a disk containing up to about 2 mg/g of solute was the decomposition of the cyclic bicarbonate dimer into two monomeric anions with a rate constant of $7.2 \times 10^2 \exp[-(14 \pm 2 \text{ kcal})/RT] \text{ sec}^{-1}$. Some carbonate ion was also produced during this reaction, and its yield increased with increasing initial concentration of the solute. At higher reaction temperatures, the formate ion was also produced at a rate second order in the bicarbonate monomer. The rate constant was $7.6 \times 10^{13} \exp[-(49 \pm 6 \text{ kcal})/RT] M^{-1} \text{ sec}^{-1}$ for the temperature range 420–500°, and the reaction stoichiometry suggested one formate ion produced from each bicarbonate monomer. The rate of carbonate production in the temperature range 450–550° appeared to be second order in the bicarbonate monomer with an Arrhenius activation energy of about 20 kcal/mol, but quantitative kinetic results could not be obtained for this reaction because of interference by the formate reaction.

Introduction

When potassium bicarbonate consisting of hydrogen-bonded cyclic dimer anions² is dispersed in a KBr pressed disk and heated at about 500°, monomeric bicarbonate ion³ as well as the carbonate ion is trapped in the matrix. Continued heating of the disk causes the monomer ion to decompose, and the formate ion appears as an unexpected reaction product.⁴ In the present study, these decomposition reactions of the bicarbonate monomer and dimer anions have been examined quantitatively by infrared spectroscopy.

Experimental Section

Fisher reagent grade potassium bicarbonate, without further purification, was our solute, and this was mixed with Harshaw Co. optical grade KBr powder to prepare the pressed disks. The technique of fabrication of these disks and their use in thermal decomposition studies have been described before.^{3,5} All kinetic data were obtained with a Perkin-Elmer Model 521 grating infrared spectrophotometer.

Results

A temperature range of 140–220° and solute concentrations from 0.4 to 2 mg/g of matrix were used to study the decomposition of the bicarbonate dimer into two monomer ions. Under these experimental conditions, the 880-cm⁻¹ CO₃²⁻ and the 1633-cm⁻¹ HCO₂⁻ infrared bands were usually absent during the reaction, and the optical density of a HCO₃⁻ monomer infrared band varied linearly with respect to a dimer infrared band. The 830- and 697-cm⁻¹ bands of the dimer⁶ were used to follow the kinetics since other fundamental absorption bands overlapped with those of the reaction products. The sharp monomer band³ at 1697 cm⁻¹ was not used generally since its optical density became too large as the reaction progressed. However, whether

an infrared band of the dimer or that of the monomer was used, the decomposition of the dimer was observed to be first order in the dimer. The rate constants from these kinetic runs are summarized as an Arrhenius plot in Figure 1, and the reaction activation energy and frequency factor are listed in Table I.

Table I: Arrhenius Parameters for Some Reactions of Potassium Bicarbonate in a KBr Matrix

Reaction	Temp range, °C	Frequency factor	Activation energy, kcal/mol
(HCO ₃ ⁻) ₂ → 2HCO ₃ ⁻	140–220	7.2 × 10 ² sec ⁻¹	14 ± 2
2HCO ₃ ⁻ →	420–500	7.6 × 10 ¹³ M ⁻¹ sec ⁻¹	49 ± 6
2HCO ₂ ⁻ + O ₂			
2HCO ₃ ⁻ → CO ₃ ²⁻ + H ₂ O + CO ₂	450–550	...	~20

Once the HCO₃⁻ ion was trapped in a KBr disk, it was relatively stable until the reaction temperature was increased appreciably. At about 450°, the infrared spectrum of the disk showed a gradual decay of the monomer bands and a concomitant growth of the HCO₂⁻ bands. During these changes the optical density of the 1633-cm⁻¹ formate band varied linearly

(1) This work was supported by PHS Grant EC-97 from the Environmental Control Administration and by Grant AFOSR-907-67 from the AFOSR(SRC)-OAR, USAF.

(2) I. Nitta, Y. Tomiie, and C. H. Koo, *Acta Crystallogr.*, **5**, 292 (1952).

(3) D. L. Bernitt, K. O. Hartman, and I. C. Hisatsune, *J. Chem. Phys.*, **42**, 3553 (1965).

(4) I. C. Hisatsune and K. O. Hartman, *Science*, **145**, 1455 (1964).

(5) I. C. Hisatsune, *Nippon Kagaku Zasshi*, **89**, 1143 (1968).

(6) K. Nakamoto, Y. A. Sarma, and H. Ogoshi, *J. Chem. Phys.*, **43**, 1177 (1965).

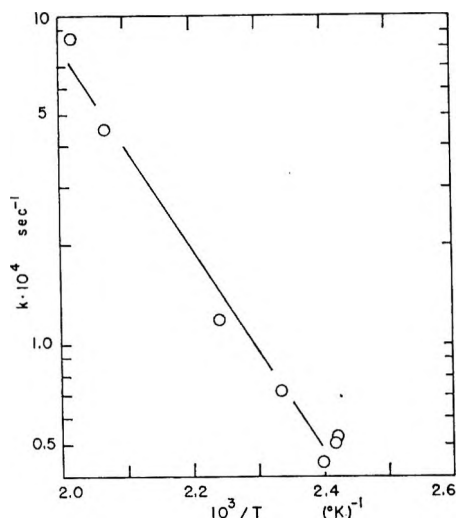


Figure 1. First-order rate constants for $(\text{HCO}_3^-)_2 \rightarrow 2\text{HCO}_3^-$ in a KBr matrix.

with respect to the optical densities of the bicarbonate bands. From nine such optical density correlation plots, it was found that the 1697-cm^{-1} HCO_3^- band was 1.65 ± 0.36 times more intense than the 1633-cm^{-1} HCO_2^- band whose molar extinction coefficient from independent calibration measurements was $1.81 \times 10^3 \text{ M}^{-1} \text{ cm}^{-1}$. Since the most reasonable reaction stoichiometry consistent with the experimental data was to take the mole ratio $\text{HCO}_3^-/\text{HCO}_2^-$ as one, the molar extinction coefficient of the 1697-cm^{-1} bicarbonate band was calculated to be $2.99 \times 10^3 \text{ M}^{-1} \text{ cm}^{-1}$. Using this value together with the known extinction coefficients for HCO_2^- and CO_3^{2-} infrared bands, we have determined the yield of ionic products in a series of decomposition reactions of the dimer. The results are summarized in Table II. In calculating the carbon

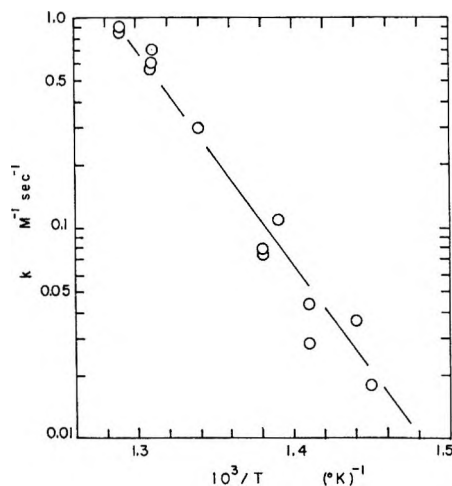


Figure 2. Second-order rate constants for $2\text{HCO}_3^- \rightarrow 2\text{HCO}_2^- + \text{O}_2$ in a KBr matrix.

concentration since CO_2 , the remaining carbon product in the formation of CO_3^{2-} , was only partially trapped in the KBr disks.

For the temperature range of $420\text{--}500^\circ$, the formate producing decomposition reaction of bicarbonate was second order in HCO_3^- , and the rate constants obtained from the infrared bands of the formate and the bicarbonate monomer were the same within experimental uncertainties. Figure 2 summarizes the experimental rate constants, and the Arrhenius parameters are given in Table I.

A number of kinetic runs on the formate production showed, near the end of the reaction, systematic deviations of the experimental points from the expected second-order behavior. In such runs, the formate production appeared to cease and the decay of the bicarbonate monomer was about an order of magnitude slower than during the formate growth stage. This slow-decay reaction was observed more often when the initial concentration of the monomer was low. Although it was not possible to differentiate clearly this slow-decay reaction from the faster formate reaction, it appeared that a product of the former reaction was carbonate and that the reaction was also second order in HCO_3^- . The rate constants were of the order of $10^{-2} \text{ M}^{-1} \text{ sec}^{-1}$ in the temperature range of $450\text{--}500^\circ$ and showed only a small temperature dependence corresponding to about 20-kcal/mol activation energy.

The decomposition of HCO_3^- was complicated, in addition, when the initial concentration of CO_3^{2-} was high. In such a disk, the HCO_3^- decay was generally slower and the CO_3^{2-} infrared band often showed some decay with reaction time. As summarized in Table II, a high initial concentration of bicarbonate dimer gave more CO_3^{2-} relative to HCO_3^- . Prolonged grinding of the solute and matrix salts also led to disks with higher concentrations of CO_3^{2-} . However, freeze-drying of the solute did not appear to have much effect

Table II: Decomposition Stoichiometry of Potassium Bicarbonate in a KBr Matrix

Initial mol. ^a (HCO_3^-) ₂	Final mol. ^a			Carbon balance ^b	Heating	
	HCO_3^-	HCO_2^-	CO_3^{2-}		Time, min	Temp, °C
1.3	1.6	0.41	0.35	1.0	9	488
2.5	2.8	1.3	0.76	1.1	9	488
4.9	5.5	0.73	2.1	1.1	35	450
5.2	7.7	0.94	1.6	1.1	5	488
5.2	7.0	0.24	2.7	1.2	25	450
6.3	7.1	0.73	1.9	0.92	35	450
6.4	7.1	0.55	2.2	0.94	35	450
8.5	4.1	0.41	8.0	1.2	30	300
66	12	6.9	84	1.4	25	505

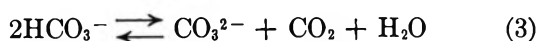
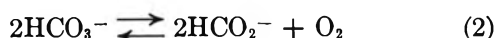
^a Units are in 10^{-7} mol. ^b Ratio of final mol of $(\text{HCO}_3^- + \text{HCO}_2^- + 2\text{CO}_3^{2-})$ to twice the initial mol of $(\text{HCO}_3^-)_2$.

balance in this table, the contribution of CO_3^{2-} to the reaction products was taken as twice the observed con-

on the HCO_3^- reaction. One disk prepared by the freeze-dry method with 0.22 mg/g of solute gave a formate yield of 85%, based on the actual initial HCO_3^- concentration, and a rate constant of $0.11 \text{ M}^{-1} \text{ sec}^{-1}$ at 450° . On the other hand, the decomposition at 488° of a disk prepared by grinding 0.21 mg/g solute gave a 79% yield of formate and a monomer decay rate constant of $0.71 \text{ M}^{-1} \text{ sec}^{-1}$.

Discussion

The following sequence of reactions, which may not necessarily be elementary, appears to account for the bicarbonate decompositions observed in this study.



Although the experimental activation energy given in Table I for reaction 1 is similar to the hydrogen-bond energies in carboxylic acid dimers,⁷ the small frequency factor and essentially the same activation energies observed in recombination reactions of anion free radicals⁸ suggest that the Arrhenius energy for reaction 1 may be the activation energy for the diffusion of HCO_3^- in a KBr pressed disk. The occurrence of the reverse step in reaction 1 is suggested by an observation³ that the HCO_3^- infrared bands all decrease and dimer spectrum is partially regenerated when the disk is allowed to stand at room temperature for a few weeks or when the disk is reground.

In reaction 2 an attempt was made to detect the formation of oxygen by decomposing the bicarbonate dimer in a KI matrix at 490° , but no iodate was produced. However, the reverse of this reaction was

observed in our earlier study⁹ of the decomposition of HCO_2^- . In that decomposition, HCO_3^- was always observed as a minor product, and DCO_2^- gave DCO_3^- which soon changed to HCO_3^- on heating. (This rapid hydrogen exchange reaction prevented us from examining the decomposition kinetics of DCO_3^- .) Also, when a heated formate disk was ground in an oxygen atmosphere and then reheated, slightly more HCO_3^- was formed than from a disk ground in air. Interestingly, the decomposition of the formate ion was also a second-order reaction, and its Arrhenius activation energy of $50.7 \pm 3.5 \text{ kcal/mol}$ is similar to the activation energy of reaction 2. However, the rate of bicarbonate decomposition is about three orders of magnitude faster than the rate of formate decay.

Reaction 3 is a familiar one, and it becomes dominant as the bicarbonate concentration is increased (Table II). Thus, in the decomposition of pure potassium bicarbonate or of bicarbonate/KBr mixture in a powdered form, only the carbonate ion is detected as the final ionic product. The kinetics of this reaction is uncertain, but our estimated reaction activation energy is comparable to a value reported recently¹⁰ for the decomposition of pure potassium bicarbonate. The activation energy for the decomposition of silver carbonate giving CO_2 is also about 20 kcal/mol .¹¹

(7) G. C. Pimentel and A. L. McClellan, "The Hydrogen Bond," W. H. Freeman, San Francisco, Calif., 1960.

(8) I. C. Hisatsune, T. Adl, E. C. Reahm, and R. J. Kempf, submitted for publication to *J. Phys. Chem.*

(9) K. O. Hartman and I. C. Hisatsune, *ibid.*, **70**, 1281 (1966).

(10) I. P. Ishkin and E. S. Dubil, *Zh. Prikl. Khim.* (Leningrad), **41**, 52 (1968).

(11) T. Wydeven and M. Leban, *Anal. Chem.*, **40**, 363 (1968).

The Rate Constants of Hydrated Electron, Hydrogen Atom, and Hydroxyl Radical Reactions with Benzene, 1,3-Cyclohexadiene, 1,4-Cyclohexadiene, and Cyclohexene¹

by B. D. Michael² and Edwin J. Hart

Chemistry Division, Argonne National Laboratory, Argonne, Illinois 60439 (Received October 2, 1969)

The hydrated electron, H atom, and OH radical rate constants of reaction with benzene, 1,3-cyclohexadiene (1,3-C₆H₈), 1,4-cyclohexadiene (1,4-C₆H₈), and cyclohexene (C₆H₁₀) in aqueous solutions were determined by pulse radiolysis. In the order, e_{aq}⁻, H, and OH, these rate constants in units of M⁻¹ sec⁻¹ are: C₆H₆, (1.2 ± 0.2) × 10⁷, (5.3 ± 1.0) × 10⁸, (7.6 ± 1.9) × 10⁹; 1,3-C₆H₈, (1.0 ± 0.15) × 10⁹, (9.8 ± 2.0) × 10⁹, (9.8 ± 2.5) × 10⁹; 1,4-C₆H₈, <7.5 × 10⁸, (4.7 ± 1.0) × 10⁹, (7.7 ± 1.9) × 10⁹; C₆H₁₀, <10⁸, (3.0 ± 0.6) × 10⁹, (8.8 ± 2.2) × 10⁹. The hydrated electron rate constants were determined at pH 11 by the decay of its absorption at 715 nm. The H atom and OH radical rate constants were determined by measuring the reactivity of the hydrocarbon relative to *p*-nitrobenzoic acid (PNBA) at pH 2.0 and with its ion (PNBA⁻) in neutral solution, respectively. The H-atom adduct of PNBA has a strong absorption band at 400 nm; the OH radical adduct of PNBA⁻ has its band centered at 415 nm. By measuring the attenuation of these bands as a function of hydrocarbon concentration, their relative rate constants were determined. Spectroscopic evidence was obtained that OH reacts with 1,3-C₆H₈ and 1,4-C₆H₈ partly by H-atom abstraction to give C₆H₇; the proportions abstracting were 30 and 45%, respectively.

Introduction

Benzene and its reduction products, 1,4-C₆H₈, 1,3-C₆H₈, and C₆H₁₀, form an interesting series of hydrocarbons that are very reactive with OH and H but of highly selective reactivity with e_{aq}⁻. Considerable progress has been made in recent years in working out the mechanism of O₂-free aqueous benzene radiolysis.³ Phenol and diphenyl are the principal identifiable stable products although hydrogenated dimeric products have been postulated because of a lack of material balance.³⁻⁷ Pulse radiolysis techniques have provided rate constants for the reactions of e_{aq}⁻, H, and OH with C₆H₆⁷⁻⁹ and have established the spectral and kinetic properties of the H and OH radical adducts, C₆H₇· and C₆H₆OH·, respectively.⁷⁻⁹ It has recently been shown that 1,4-C₆H₈, C₆H₁₀, and C₆H₁₂ as well as a group of dimeric products consisting of C₁₂H₁₄, C₁₂H₁₆, C₁₂H₁₈, C₁₂H₂₀, and C₁₂H₂₂, result from the radiolysis of C₆H₆ under 2400 psi H₂ pressure at pH 13;¹⁰ under these conditions H and OH are replaced in large measure by e_{aq}⁻. When e_{aq}⁻ is replaced by OH, yields of phenol and diphenyl increase.¹¹ In the present paper we report the rate constants of e_{aq}⁻, H, and OH with C₆H₆, 1,4-C₆H₈, 1,3-C₆H₈, and C₆H₁₀.

The e_{aq}⁻ rate constants were measured directly by the decay of its 715-nm absorption band. Since the H and OH adducts of C₆H₆ and its unsaturated reduction products have transient optical absorption spectra, direct measurement of their rate constants is theoretically possible. However, because these transient spectra lie at λ < 313 nm, photochemical decomposi-

tion by the intense analyzing light beam and the appearance of impurity spectra interfere with the measurements. Consequently, we developed a relative scavenging method which allowed indirect observation of the reactions at longer wavelengths using *p*-nitrobenzoic acid (PNBA) and *p*-nitrobenzoate ion (PNBA⁻) as the reference solutes. The rates of formation of the transients absorbing at 400 and 415 nm produced by the reactions H + PNBA and OH + PNBA⁻, respectively, are known.^{12,13} The diminution of these absorptions in the presence of competing concentrations

(1) Based on work performed under the auspices of the U. S. Atomic Energy Commission.

(2) Research Unit in Radiobiology, British Empire Cancer Campaign for Research, Mount Vernon Hospital, Northwood, Middlesex, England.

(3) H. Christensen, Aktiebolaget Atomenergi, Stockholm, AE-142, May 1964.

(4) P. V. Phung and M. Burton, *Radiat. Res.*, **7**, 199 (1957).

(5) E. V. Bareiko, L. I. Kartasheva, P. D. Novikov, and M. A. Proskurnin, "Proceedings of the First All-Union Conference on Radiation Chemistry," Moscow, 1957, p 81.

(6) J. H. Baxendale and D. Smithies, *J. Chem. Soc.*, 779 (1959).

(7) L. M. Dorfman, I. A. Taub, and R. E. Bühler, *J. Chem. Phys.*, **36**, 3051 (1962).

(8) M. Anbar and E. J. Hart, *J. Amer. Chem. Soc.*, **86**, 5633 (1964).

(9) M. C. Sauer, Jr., and B. Ward, *J. Phys. Chem.*, **71**, 3971 (1967).

(10) M. H. Studier and E. J. Hart, *J. Amer. Chem. Soc.*, **91**, 4068 (1969).

(11) M. Tsuda, *Bull. Chem. Soc. Jap.*, **36**, 1582 (1963).

(12) P. Neta and L. M. Dorfman, *J. Phys. Chem.*, **73**, 413 (1969).

(13) P. Neta and L. M. Dorfman, *Advances in Chemistry Series*, No. 81, American Chemical Society, Washington, D. C., 1968, p 222.

of the hydrocarbons was used to determine the absolute reaction rates of H and OH with these compounds.

Materials and Techniques

High-Pressure Irradiation Cell. Since the OH radical reacts rapidly with C_6H_6 and its reduction products, suppression of this reaction by CD_3OH and H_2 was resorted to in the measurement of e_{aq}^- and H-atom rate constants. In the special case of obtaining the absorption spectrum of the $C_6H_7\cdot$ radical, high-pressure H_2 was used in order to eliminate possible transient absorbing species due to OH reaction products. Figure 1 illustrates our optical high-pressure irradiation cell which has been designed for pressures up to 5000 psi. Some of its dimensions are shown. The main barrel is machined from a 2 in. \times 2 in. \times 3 $\frac{3}{32}$ in. stainless steel block. It has a centered oval hole $\frac{5}{8}$ in. wide and $\frac{3}{4}$ in. high made to accommodate the 2 in. \times $\frac{1}{2}$ in. diameter Suprasil optical absorption cell shown. The silica cell, with tapered joint removed, is placed inside the vessel and connected with the tapered male joint which is positioned through the top opening and seated in the cone of the optical cell. This vertical 1-in. long joint prevents loss of solution during subsequent shaking and analysis operations. The two circular Suprasil $\frac{1}{4}$ -in. thick \times 1-in. diameter end windows are held in place with two O-rings. The 1 $\frac{31}{32}$ in. polyethylene gaskets and end-plates seal the cell. Visible in the side of the irradiation cell is a rectangular cavity $\frac{9}{16}$ in. deep with a $\frac{1}{8}$ -in. thick wall. The 15-MeV electron beam enters the cell through this wall at right angles to the analyzing optical path. The filling, pressurizing, and equilibration techniques have already been described.¹⁰ Because of its compact design it is possible to run spectra in a Cary spectrophotometer and thereby determine the concentration of benzene and other permanent optically absorbing products.

Solutions. They were prepared in triply distilled deaerated water using the syringe technique.^{14,15} Standard saturated solutions were made of benzene (99.999%, Litton Chemical Co., Inc.), 1,3- C_6H_8 and 1,4- C_6H_8 (99%, Chemical Samples Co.) and C_6H_{10} (99.94%, Philips Petroleum Co.). These solutions were prepared by shaking a slight excess volume of the hydrocarbon liquid with H_2 -saturated water in a 100-ml syringe containing 20 ml of H_2 . After a few minutes shaking, the H_2 is expelled. Finally after 30-min standing the excess hydrocarbon is discharged. This method has the advantage that it does not concentrate the more soluble impurities that would result if a large excess of hydrocarbon were used. Furthermore, it enables most of the dissolved O_2 introduced with the hydrocarbon to be discharged with the H_2 . Since these solutes are very volatile, the aqueous solutions are stored in completely filled syringes and the solutions were usually irradiated in the absence of a gas phase. The concentrations of hydrocarbons were determined using an

F & M 5750 (Hewlett-Packard) gas chromatograph. The solutions were shaken with a known volume of H_2 in a syringe, and a small measured volume of gas was then introduced into the column.¹⁰ In the cases of benzene and 1,3- C_6H_8 the concentrations were also determined from their uv absorption spectra (on a Cary spectrophotometer). Both analytical methods were standardized using dilute solutions of the compounds prepared by the injection of alcoholic solutions of known concentrations into water-filled syringes.¹⁶ The concentrations of the saturated aqueous solutions were found to be C_6H_6 20.2 mM; 1,3- C_6H_8 10.2 mM; 1,4- C_6H_8 11.2 mM; C_6H_{10} 2.9 mM; all at 25°. In estimating our C_6H_6 concentrations by uv spectrophotometry we used $\epsilon(264) \text{ nm} = 180 \text{ M}^{-1} \text{ cm}^{-1}$. This value compares with a recently published one of 178.4.¹⁶ Most cited values are too low.¹⁶

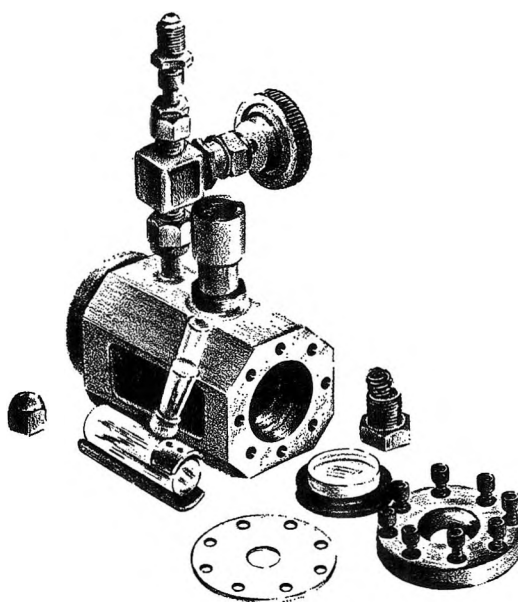


Figure 1. Stainless steel high-pressure cell for the pulse radiolysis of solutions equilibrated with hydrogen at 2000 psi pressure.

Pulse Radiolysis. Conventional pulse radiolysis apparatus was used. The effective level of scattered light in the ultraviolet measurements was kept below 1% by using an HTV-R166 solar-blind photomultiplier in the wavelength range 230–300 nm. The dose delivered in each pulse was monitored by charge collection, calibration being obtained using a standard Fricke dosimeter solution. The dose ranged from 0.1 to 1.6 krad/pulse and the pulse duration from 0.4 to 3.0 μsec .

(14) C. B. Senvar and E. J. Hart, *Proc. U. N. Int. Conf. Peaceful Uses At. Energy*, 2nd, 29, 19 (1958).

(15) E. J. Hart, S. Gordon, and J. K. Thomas, *J. Phys. Chem.*, 68, 1271 (1964).

(16) D. G. Marketos, *Anal. Chem.*, 41, 195 (1969).

Table I: Summary of e_{aq}^- , H, and OH Reaction Rates, $M^{-1} \text{sec}^{-1}$

	C_6H_6	1,3- C_6H_8	1,4- C_6H_8	C_6H_{10}
e_{aq}^-	$(1.2 \pm 0.2) \times 10^7$	$(1.0 \pm 0.15) \times 10^9$	$< 7.5 \times 10^6$	$< 10^6$
H	$(5.3 \pm 1.0) \times 10^8$	$(9.8 \pm 2.0) \times 10^9$	$(4.7 \pm 1.0) \times 10^9$	$(3.0 \pm 0.6) \times 10^9$
OH	$(7.6 \pm 1.9) \times 10^9$	$(9.8 \pm 2.5) \times 10^9$	$(7.7 \pm 1.9) \times 10^9$	$(8.8 \pm 2.2) \times 10^9$

Experimental Results

Our rate constants are summarized in Table I. The methods used in measuring are below.

Reactions of e_{aq}^- . Reactions of e_{aq}^- were studied by observing its pseudo-first-order disappearance at 715 nm in the presence of relatively high concentrations of the compounds.

First-order plots of the reaction with benzene at pH 13.0 are shown in Figure 2 and give the rate as $(1.2 \pm 0.2) \times 10^7 M^{-1} \text{sec}^{-1}$. Reaction rates with the other compounds were determined at pH 11.0 using CH_3OH as an OH scavenger to increase the natural lifetime of e_{aq}^- . Only in the case of 1,3- C_6H_8 was the electron reactivity found to be high. Its rate was determined not only from a first-order plot (Figure 2) at 0.85 mM 1,3- C_6H_8 but also at 10.2 mM concentration by comparing the equilibrium absorbance (A_{eq}) due to e_{aq}^- during a nearly rectangular 2.8- μsec electron pulse [$t_{1/2}(e_{aq}^-) \ll 2.8 \mu\text{sec}$] with a maximum absorbance (A_{max}) produced at the end of a similar pulse with no scavenger present. Under these conditions

$$k = \frac{A_{max}}{A_{eq}} \frac{1}{st}$$

k is the reaction rate constant in $M^{-1} \text{sec}^{-1}$, s is the solute concentration in M , and t is the half-intensity pulse length in seconds.

Small corrections were applied for pulse to pulse dose variation. In addition, the effect of second-order decay of e_{aq}^- during the pulse on the measured value of A_{max} was eliminated by an analytic correction. The rates obtained by both methods agree with each other and give $k_{(e_{aq}^- + 1,3-C_6H_8)} = (1.0 \pm 0.15) \times 10^9 M^{-1} \text{sec}^{-1}$.

1,4- C_6H_8 and C_6H_{10} show little or no reactivity with e_{aq}^- , and it is possible to determine only the upper limits as 7.5×10^6 and $1 \times 10^6 M^{-1} \text{sec}^{-1}$, respectively. In these cases low concentrations of reactive impurities were removed by preirradiation.¹⁷ These low values were obtained after an equilibrium e_{aq}^- decay curve was achieved.

Reactions of H Atoms. The H-atom rates were determined by a competition method using PNBA as a reference solute.¹² The reaction of H atoms with this compound gives the transient product shown in Figure 3 with an absorption maximum at 400 nm. This wavelength is convenient for measurement since none of the H-atom reaction products of the hydrocarbons studied absorbs appreciably in this region. Competi-

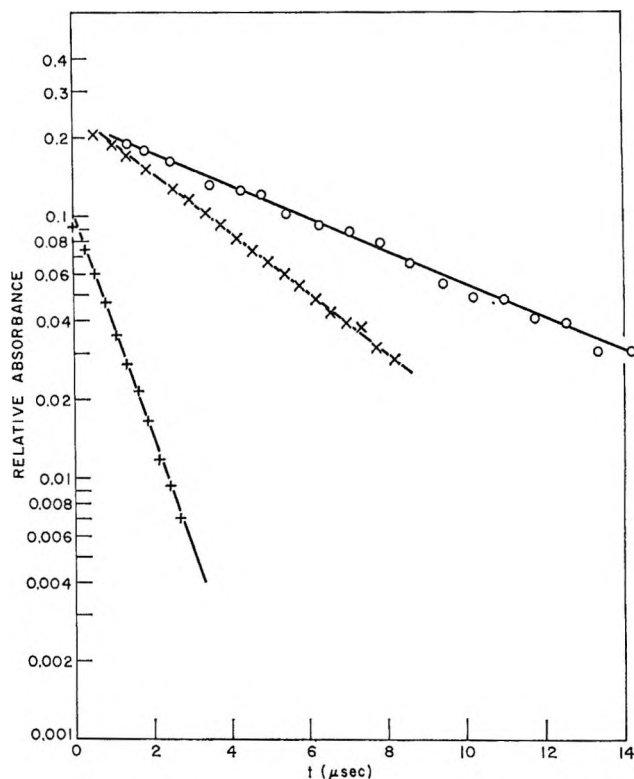


Figure 2. First-order decay of e_{aq}^- at 715 nm: O, 12.1 mM C_6H_6 , 100 rads/pulse, pH 13; X, 20.2 mM C_6H_6 , 1 krad/pulse, pH 13; +, 0.85 mM 1,3- C_6H_8 , 1 krad/pulse, pH 11.

tion plots of reciprocal relative absorbance against relative solute concentration are shown in Figure 4. The transient at 400 nm forms immediately after the electron pulse and decays with first-order kinetics with a half-life of 16 μsec . This decay affects the rate measurement, and corrections were required to obtain the relative rates from the competition plots (see Appendix). The relative absorbances shown in Figure 4 were measured 12 μsec after the electron pulse.

Our value for k_1 , the rate of reaction of H atoms with PNBA, of $(1.0 \pm 0.1) \times 10^9 M^{-1} \text{sec}^{-1}$ agrees with that obtained by Neta and Dorfman.¹² Since the rate of reaction of e_{aq}^- with PNBA⁻ was found to be $3.4 \times 10^{10} M^{-1} \text{sec}^{-1}$, the competition measurements were carried out at pH 2.0 to ensure complete conversion of e_{aq}^- into H atoms and to maintain PNBA well below its pK of 3.41.

(17) E. J. Hart and E. M. Fielden, *Advances in Chemistry Series*, No. 50, American Chemical Society, Washington, D. C., 1965, p 253.

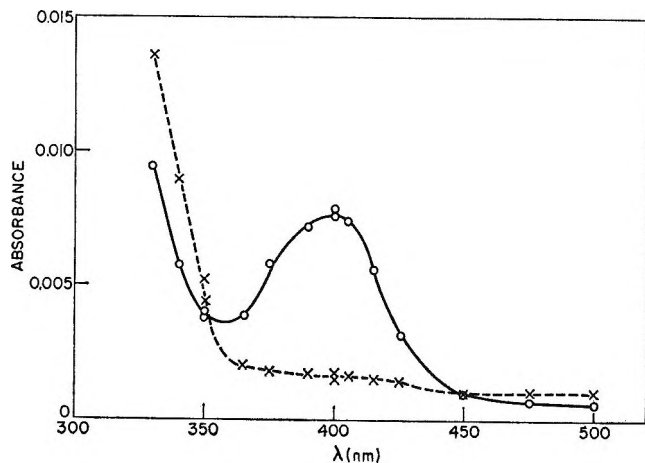


Figure 3. Transient absorption spectra of the H-atom adduct of 200 μM PNBA, 20 mM CD_3OH , pH 2, 135 rads/pulse: O, 10 μsec after pulse; X, 90 μsec after pulse.

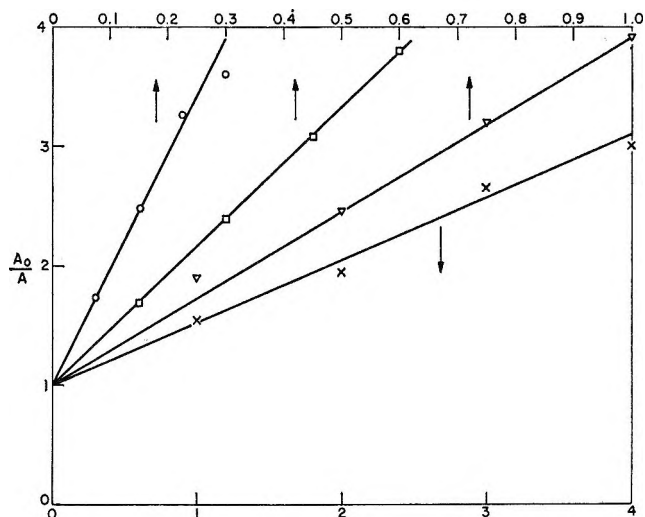


Figure 4. Competition plots for measurement of relative H-atom rates; 200 μM PNBA, 20 mM CD_3OH , pH 2.0, 200 rads/pulse. Ordinate: reciprocal relative absorbance at 400 nm; A_0 is the absorbance in the presence of PNBA only, A is the absorbance in the presence of added solute; abscissa: [solute]/[PNBA]: O, 1,3- C_6H_8 ; □, 1,4- C_6H_8 ; ∇, C_6H_{10} ; X, C_6H_6 .

Hydroxyl radicals react with PNBA to produce a transient species with an absorption maximum at 415 nm.¹³ In order to prevent any optical absorption formed by reaction of OH with PNBA from interfering with the H-atom measurements, all competition experiments were carried out with a sufficient concentration of CD_3OH present, 20 mM, to scavenge most of the OH radicals, but not to affect our H-atom rate constants by more than 0.8%. In view of the high ratio of the OH to H reaction rate constants (3×10^3) and low reactivity of the CD_2OH radicals with the aromatic nucleus, CD_3OH is highly suitable for removing OH and preserving H atoms.^{9,12}

A further possibility that the highly reactive nitro substituent¹³ might react with CD_2OH radicals to

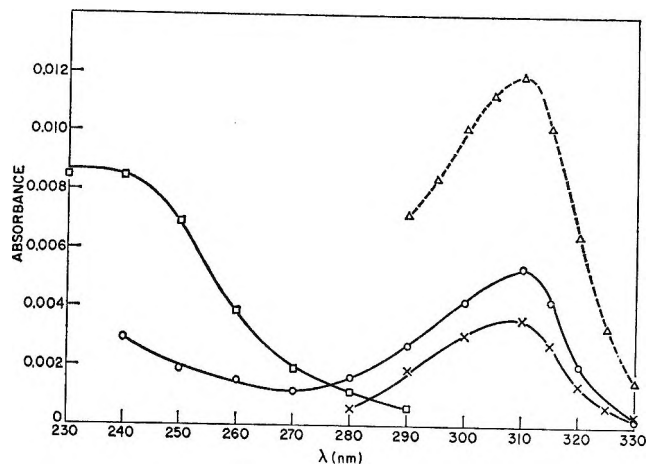


Figure 5. Transient absorption spectra of OH-hydrocarbon radicals immediately following a 0.4- μsec pulse of 135 rads in neutral solutions containing 100 μM of each compound and 1 mM N_2O : □, C_6H_{10} ; X, 1,3- C_6H_8 ; O, 1,4- C_6H_8 ; Δ, normalized spectrum of $\text{C}_6\text{H}_7\cdot$. The $\text{C}_6\text{H}_7\cdot$ radical spectrum was determined using the high-pressure hydrogen cell and has been normalized so that $G(\text{C}_6\text{H}_7\cdot) = G(\text{OH}) + G(e_{\text{aq}}^-) = 5.6$ to allow direct comparison with the OH transients.

produce an interfering absorption was examined. The pulse-induced absorption at 400 nm in a deaerated solution containing 100 μM PNBA and 50 mM CD_3OH at pH 2.75 was compared with that produced in a similar solution when saturated with N_2O . In the latter case, a reduction in absorbance by a factor of 3.7 was found. This agrees quantitatively with the expected H-atom adduct absorption at this wavelength.

We also observed the $\text{C}_6\text{H}_7\cdot$ absorption spectrum and measured its second-order decay in an essentially one radical system. Deaerated solutions containing 120 μM benzene at pH 4 were equilibrated with H_2 at 2000 psi pressure in the cell shown in Figure 1. Under these conditions e_{aq}^- and OH are rapidly converted into H atoms which then react with benzene to form the $\text{C}_6\text{H}_7\cdot$ radical. The absorption spectrum is shown in the top curve of Figure 5. Taking the total $G(\text{H})$ as 6.2 and allowing for a calculated 38% loss of H atoms by dimerization, we estimate the peak-molar extinction coefficient of $\text{C}_6\text{H}_7\cdot$ at 310 nm as $3300 \pm 200 \text{ M}^{-1} \text{ cm}^{-1}$. This is appreciably lower than a previously reported value of $5400 \pm 500 \text{ M}^{-1} \text{ cm}^{-1}$,⁹ but is similar to $\epsilon_{\text{max}} = 3700 \text{ M}^{-1} \text{ cm}^{-1}$ for the H-atom adduct of benzoic acid.¹⁹ A fraction of OH radicals reacted directly with benzene, and approximately 15% of the transient product was OHC_6H_6 . This OH adduct has an absorption band⁷ which is closely similar to that of $\text{C}_6\text{H}_7\cdot$ and will therefore have introduced little error into our spectrum.

The decay at 310 nm follows second-order kinetics, shown in Figure 6, for which $2k(\text{C}_6\text{H}_7\cdot + \text{C}_6\text{H}_7\cdot)$ is

(18) B. Cercek and M. Ebert, *Advances in Chemistry Series*, No. 81, American Chemical Society, Washington, D. C., 1968, p 210.

(19) R. Wander, P. Neta, and L. M. Dorfman, *J. Phys. Chem.*, **72**, 2946 (1968).

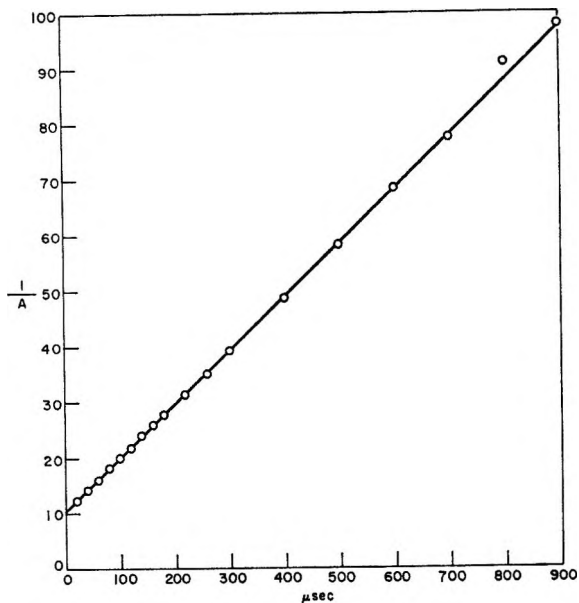


Figure 6. Second-order decay of the $C_6H_7\cdot$ radical at 310 nm. $120 \mu M C_6H_6$, pH 4.0, 2000 psi H_2 , 1.6 krad/pulse.

$(1.6 \pm 0.15) \times 10^9 M^{-1} sec^{-1}$. A previous value of $3.6 \times 10^9 M^{-1} sec^{-1}$ was obtained by Sauer and Ward⁹ for which a correction for a concurrent reaction with $\dot{C}H_2OH$ radicals was made. This difference in rate constant is mainly attributable to the higher value for ϵ_{311} of $5400 \pm 500 M^{-1} cm^{-1}$ obtained by these authors.

Reactions of OH Radicals. The OH rate constants were measured by competition with $PNBA^-$ at pH 7.0 in N_2O saturated solution. The OH adduct of $PNBA^-$ has a long-lived transient absorption band at 415 nm and is formed at a rate of $2.6 \times 10^9 M^{-1} sec^{-1}$.¹³ None of the other OH reaction products, either transient or permanent, absorbs appreciably at this wavelength. The results are shown in Figure 7. There appears to be little difference in the OH reactivities of the compounds. Our value of $7.6 \times 10^9 M^{-1} sec^{-1}$ for C_6H_6 agrees well with a recent published value of $7.8 \pm 1.1 M^{-1} sec^{-1}$.¹³

Transient Radical Spectra. The spectra of some of the transient radicals of $PNBA$, C_6H_6 , $1,4-C_6H_8$, $1,3-C_6H_8$ produced by H and OH radicals have been obtained. Those for $PNBA$ and C_6H_6 agree closely with published data. The spectra for $C_6H_7\cdot$ obtained with our high-pressure H_2 cell and the radicals formed from OH reaction with $1,4-C_6H_8$, $1,3-C_6H_8$, and C_6H_{10} are shown in Figure 5. Both of these compounds give transient absorptions which have peaks at 310 nm and are similar to that of the $C_6H_7\cdot$ radical.

Discussion

Rate Constants. Of the rate constants given in Table I, those of e_{aq}^- show the greatest variation. The enhanced e_{aq}^- activity of $1,3-C_6H_8$ contrasts sharply with the 1000-fold lower activity of the $1,4-C_6H_8$ isomer which is similar to that of C_6H_{10} . These differences in e_{aq}^- reactivity exist between conjugated 1,3-butadiene

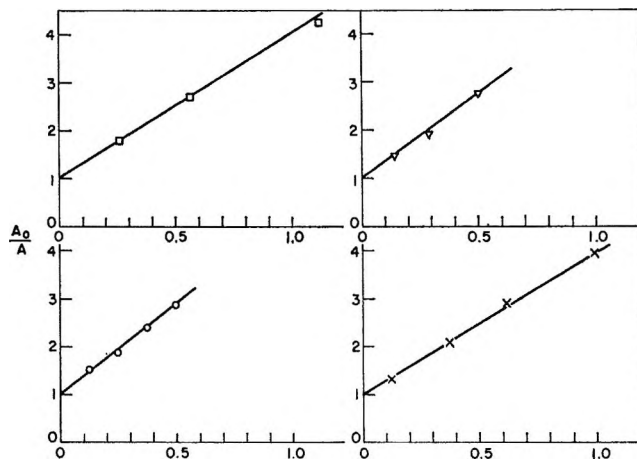


Figure 7. Competition plots for measurement of relative OH rates: $200 \mu M PNBA^-$, pH 7.0, N_2O -saturated solution, 135 rads/pulse. Ordinate: relative absorbance at 415 nm; abscissa: [solute]/[$PNBA^-$]: \circ , $1,3-C_6H_8$; \square , $1,4-C_6H_8$; ∇ , C_6H_{10} ; \times , C_6H_6 .

($k = 8 \times 10^9 M^{-1} sec^{-1}$)¹⁵ and ethylene ($k < 2.5 \times 10^6 M^{-1} sec^{-1}$).²⁰ Conjugated carbon-carbon double bonds are necessary in hydrocarbons for high e_{aq}^- reactivity. The lower reactivity of C_6H_6 is expected in view of its large resonance energy. Only when electron-withdrawing groups are added to the aromatic nucleus does it become highly reactive. Our value of $1.2 \times 10^7 M^{-1} sec^{-1}$ for $k(e_{aq}^- + C_6H_6)$ agrees satisfactorily with the previously reported $1.4 \times 10^7 M^{-1} sec^{-1}$.⁸ In contrast to the highly selective action of e_{aq}^- , except for the relatively low rate constant of H with C_6H_6 , the remainder of the H and OH reaction rates with C_6H_6 , $1,3-C_6H_8$, $1,4-C_6H_8$, and C_6H_{10} varies between the rather narrow limits of 3.0 and $9.8 \times 10^9 M^{-1} sec^{-1}$. There is, however, a bias in favor of higher OH radical and $1,3-C_6H_8$ reactivity. Of the rate constants given in Table I, those of OH and H with C_6H_6 have been published. We find excellent agreement with the Neta and Dorfman¹³ $k(OH + C_6H_6)$ value of $(7.8 \pm 1.1) \times 10^9$ and our $7.6 \times 10^9 M^{-1} sec^{-1}$. Less satisfactory is the difference between our $k(H + C_6H_6)$ value of 5.3×10^9 and the Sauer and Ward⁹ value of $1.1 \times 10^9 M^{-1} sec^{-1}$. We are unable to resolve this discrepancy.²¹ However, we find the transient $PNBA-H$ adduct with λ_{max} at 400 nm better suited to H-atom rate constant measurements than the $C_6H_7\cdot$ radical with λ_{max} at 310 nm. At 400 nm the instability of the irradiated solutions and the complications arising from transient radicals absorbing at 310 nm are avoided.

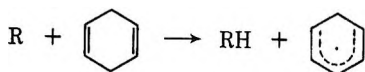
Transient Spectra—Cyclohexadienyl Radical. In the radiolysis of aqueous C_6H_6 solutions $C_6H_7\cdot$ forms with a yield and absorption spectrum similar to that of the hydroxycyclohexadienyl radical, $C_6H_6OH\cdot$. Since

(20) C. F. Cullis, J. M. Francis, and A. J. Swallow, *Proc. Roy. Soc., Ser. A*, **287**, 15 (1965).

(21) M. C. Sauer, Jr., private communication.

$g(\text{H}) \sim g(\text{OH})$ and because $k(\text{OH} + \text{C}_6\text{H}_6)/k(\text{H} + \text{C}_6\text{H}_6) \sim 20$ and $k(\text{H} + \text{H})/k(\text{OH} + \text{OH}) = 2$, $G(\text{C}_6\text{H}_7\cdot)$ is generally lower than $G(\text{C}_6\text{H}_5\text{OH}\cdot)$ at the electron dose rates normally used in pulse radiolysis. Consequently the spectrum of $\text{C}_6\text{H}_7\cdot$ is generally contaminated with absorption due to $\text{C}_6\text{H}_5\text{OH}\cdot$.⁷ And unless the H-atom and e_{aq}^- scavengers are used to remove these species, the $\text{C}_6\text{H}_5\text{OH}\cdot$ spectrum, too, is contaminated with that of $\text{C}_6\text{H}_7\cdot$. In order to obtain a $\text{C}_6\text{H}_7\cdot$ spectrum as free as possible from OH-scavenger effects and $\text{C}_6\text{H}_5\text{OH}\cdot$, 2000 psi H_2 (0.10 M) was used to convert OH into H, enhancing H-atom and lowering OH radical effects. At 0.10 mM C_6H_6 , we estimate our $\text{C}_6\text{H}_7\cdot$ spectrum contains 15% $\text{C}_6\text{H}_5\text{OH}\cdot$, an amount that should have a relatively small effect on the extinction coefficient as well as on its second-order decay constant. From our data we conclude that the properties of $\text{C}_6\text{H}_7\cdot$ are λ_{max} at 310 nm; $\epsilon_{310} = 3300 \pm 200 M^{-1} \text{cm}^{-1}$; a second-order decay constant, $2k = (1.6 \pm 0.15) \times 10^9 M^{-1} \text{sec}^{-1}$.

The spectrum of the $\text{C}_6\text{H}_7\cdot$ radical has also been obtained by a completely different reaction, namely, the oxidation of 1,4- C_6H_8 by OH radicals. Below 100° alkyl radicals generate $\text{C}_6\text{H}_7\cdot$ by the established gas phase reaction²²



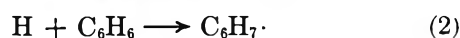
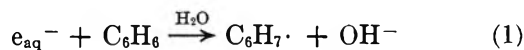
We find that the OH radical extracts H from both 1,3- and 1,4- C_6H_8 , since $\text{C}_6\text{H}_7\cdot$ forms in each case. (See Figure 5.) However, this is not an exclusive reaction since the expected amount of $\text{C}_6\text{H}_7\cdot$ is not obtained. In these cases the OH reacts partly by H abstraction and partly by addition. From these data the relative proportions of H abstraction to OH addition are 45% with 1,4- C_6H_8 and 30% with 1,3- C_6H_8 . Because of the high H-atom rate constants of these hydrocarbons, the H atom appears to add exclusively.

Cyclohexene, too, forms a transient absorption upon reaction with OH, but with $\lambda_{\text{max}} \leq 240$ nm. It was not possible to determine the extent to which each of the four possible modes of the reaction contributed to this absorption; however, to explain the absorbance obtained at 230–240 nm the extinction coefficient of one of the products must be greater than $2400 M^{-1} \text{cm}^{-1}$. We tentatively assign the absorption to the allylic isomer of $\text{C}_6\text{H}_9\cdot$. We exclude $\text{C}_6\text{H}_{10}\text{OH}\cdot$ as a major contributor although isomers of this radical have an absorption maximum at 230 nm in aqueous solution,²³ because their extinction coefficients are only about half the value we observe at this wavelength. Similarly we exclude nonallylic $\text{C}_6\text{H}_9\cdot$ since this radical would be expected to display a β -alkyl radical type of absorption spectrum. In aqueous solution β -alkyl²¹ and β -carboxyalkyl²⁴ radicals have absorption maxima ≤ 240 nm; however, their peak extinction coefficients are

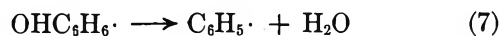
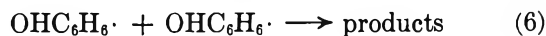
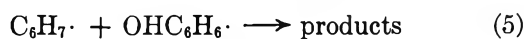
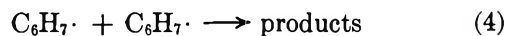
$\sim 1000 M^{-1} \text{cm}^{-1}$. Support for the view that the delocalized allyl radical would have a higher extinction coefficient than the alkyl radical comes from studies on irradiated polyethylene²⁵ where the following absorption maxima were reported: alkyl, $\epsilon_{215} = 1600 M^{-1} \text{cm}^{-1}$; allyl, $\epsilon_{258} = 6800 M^{-1} \text{cm}^{-1}$; dienyl, $\epsilon_{258} = 18,000 M^{-1} \text{cm}^{-1}$.

Products of C_6H_6 Radiolysis. It is clear from the extensive studies made on the deaerated aqueous C_6H_6 system that the radiolysis products are indeed complex.³ Phenol, diphenyl, and a group of hydrogenated diphenyl derivatives are the common products reported. When e_{aq}^- is converted to OH by N_2O , the proportion of phenol and diphenyl rises in the expected manner.¹¹ And when the OH and H atoms are converted to e_{aq}^- , then the reduced products, 1,4- C_6H_8 , C_6H_{10} , C_6H_{12} , and the group of dimeric products ranging from $\text{C}_{12}\text{H}_{14}$ to $\text{C}_{12}\text{H}_{22}$ appear.¹⁰ In acid H_2 solutions where OH and e_{aq}^- are converted to H atoms, the reduction proceeds at a lower rate but the nature of the monomeric products changes. Now 1,3- C_6H_8 is the dominant C_6H_8 isomer and the proportion of dimeric products increases appreciably.

The present results with emphasis primarily on the reduction products of C_6H_6 indicate the types of compounds to be looked for in the radiolysis of C_6H_6 .^{3-7,11,12} Generally accepted now are the primary reactions



followed by



These reactions and their rate constants have all been established by pulse radiolysis techniques. When any appreciable concentration of C_6H_6 is present, e_{aq}^- , H, and OH react exclusively with benzene. At low pH, H-atom reactions are dominant. In neutral and alkaline solutions e_{aq}^- reactions become important. The radicals $\text{C}_6\text{H}_7\cdot$ and $\text{OHC}_6\text{H}_6\cdot$ form phenol and diphenyl through reactions 4, 5, and 6. However, in many studies in which phenol and diphenyl only were reported,³⁻⁷ a lack of material balance is found. Reduced dimers are suggested as the missing products. In view

(22) D. G. L. James and R. D. Stuart, *Trans. Faraday Soc.*, **64**, 2752 (1968).

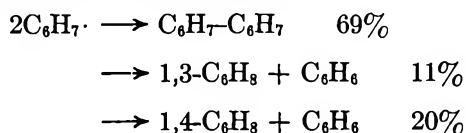
(23) M. Simic, P. Neta, and E. Hayon, *J. Phys. Chem.*, **73**, 3754 (1969).

(24) P. Neta, M. Simic, and E. Hayon, *ibid.*, in press.

(25) D. C. Waterman and M. Dole, *ibid.*, in press.

of the nearly equal yields of $(\text{H} + e_{\text{aq}}^-)$ and OH and the similar rates of reactions 4, 5, and 6, 1,4- C_6H_8 should form in neutral and alkaline solutions, whereas 1,4- and 1,3- C_6H_8 should be present in acid solutions. Dimerization products of $\text{C}_6\text{H}_7^\cdot$, $\text{C}_6\text{H}_6\text{OH}^\cdot$, and $\text{C}_6\text{H}_5^\cdot$ should also be found.

Previous work¹⁰ indicates that $\text{C}_6\text{H}_7^\cdot$ disproportionates in aqueous solution to produce about 25% C_6H_8 and 75% dimers. This is close to the fraction reported in the gas phase²⁰ where

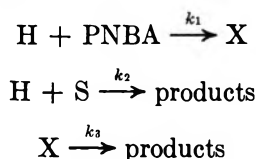


According to this distribution, some 1,4- C_6H_8 should be found in neutral and alkaline solutions. The absence of 1,3- C_6H_8 in our previous work¹⁰ is probably due to its high e_{aq}^- rate constant which is 100-fold greater than that of C_6H_6 and >1000-fold higher than that of 1,4- C_6H_8 . This large divergence in e_{aq}^- rate constant between 1,3- and 1,4- C_6H_8 explains the absence of the former in metal- NH_3 reductions of C_6H_6 .

Acknowledgments. We wish to thank Mr. E. E. Klocek for the design of the optical high-pressure cell, Miss P. Walsh and Mr. R. M. Clarke for technical assistance, and the accelerator crew, particularly Mr. B. Naderer, for their cooperation.

Appendix

Kinetic Treatment of H-Atom Competition Results. The competing reactions of H atoms with a solute, S, and with PNBA to form an absorbing product, X, which subsequently undergoes a first-order decay, follow the reaction scheme



The solution for H-atom concentration [H] is

$$[\text{H}] = [\text{H}]_0 e^{-(k_1[\text{PNBA}] + k_2[\text{S}])t}$$

where $[\text{H}]_0$ is the initial concentration of H atoms formed during the pulse and t is the time after the pulse.

The solution for [X] is

$$[\text{X}] = \frac{[\text{H}]_0 e^{-k_3 t} (1 - e^{-(k_1[\text{PNBA}] + k_2[\text{S}] - k_3)t}) k_1 [\text{PNBA}]}{k_1 [\text{PNBA}] + k_2 [\text{S}] - k_3}$$

The reciprocal relative concentration of X is given by

$$\frac{[\text{X}]_0}{[\text{X}]} = F \left[1 - \frac{k_2 [\text{S}]}{k_1 [\text{PNBA}] - k_3} \right] \quad (1)$$

where $[\text{X}] = [\text{X}]_0$ when $[\text{S}] = 0$, thus

$$F = \frac{1 - e^{-(k_1[\text{PNBA}] - k_3)t}}{1 - e^{-(k_1[\text{PNBA}] + k_2[\text{S}] - k_3)t}}$$

The expression in brackets in eq 1 leads to a linear competition plot of $[\text{X}]_0/[\text{X}]$ vs. $[\text{S}]/[\text{PNBA}]$ of slope $[\text{PNBA}]k_2/[\text{PNBA}]k_1 - k_3$ if F is close to unity. However, under the experimental conditions used ($k_1[\text{PNBA}] = 2 \times 10^5 \text{ sec}^{-1}$, $k_3 = 4.1 \times 10^4 \text{ sec}^{-1}$ and $t = 12 \mu\text{sec}$), F varies from 1.000 for $k_2[\text{S}] = 0$ to 0.851 for $k_2[\text{S}] = 5.6 \times 10^5$.

Under these experimental conditions, a theoretical plot of $[\text{X}]_0/[\text{X}]$ vs. $k_2[\text{S}]$ may be drawn. The dependence of F on $k_2[\text{S}]$ introduces a slight curvature, although this was not observed experimentally in Figure 4 because of random errors. The best fitting straight line on the theoretical plot for the range of values of $[\text{X}]_0/[\text{X}]$ used experimentally passes through the points $[\text{X}]_0/[\text{X}] = 2.5$ where $k_2[\text{S}] = 3.05 \times 10^5 \text{ sec}^{-1}$. Accordingly, values of $([\text{S}]/\text{PNBA})_{\text{exp}}$ have been determined from the best fitting straight lines in Figure 4 such that $A_0/A = 2.5$. For each solute k_2 , the H-atom rate constant is calculated from the equation

$$k_2 = \frac{3.05 \times 10^5}{[\text{PNBA}]} \left(\frac{[\text{PNBA}]}{[\text{S}]} \right)_{\text{exp}}$$

Evidence for Very Early Ionic Events in the Radiolysis of Ethanol

by Shamsheer Khorana and William H. Hamill

Department of Chemistry and the Radiation Laboratory,¹ University of Notre Dame, Notre Dame, Indiana 46556
(Received January 30, 1970)

Very early ionic events in polar systems, *e.g.*, $<10^{-11}$ sec, precede dipole relaxation and they are expected to resemble in part those which occur in alkanes. Reactions or reaction efficiencies which are markedly enhanced in alkanes provide suitable tests. Benzene, as an additive, traps electrons efficiently in alkanes but reacts slowly with solvated electrons, e_s^- , with $k(e_s^- + C_6H_6) \cong 10^7 M^{-1} \text{sec}^{-1}$. In contrast H_s^+ reacts very fast with e_s^- and not measurably with the dry electron, e^- . Preceding solvation, H_2O^+ or $C_2H_5OH^+$ will oxidize, or be scavenged by, Cl_s^- , while $H_3O_s^+$ is a much weaker oxidant. Ethanol solutions have been chosen for study because $G(e_s^-) \cong 1$ and $G(e^-)$ should be large. Addition of 0.1 *M* alkyl halide RX was used to scavenge all e_s^- and some e^- and the yield was measured as $G(\text{RH})$. Added CaCl_2 increased $G(\text{RH})$ and is attributed to hole scavenging followed by $e^- \rightarrow e_s^-$. Addition of acid decreased $G(\text{RH})$ to a limit of $\sim 50\%$, with $G^\circ(e_s^-) = 1.0$, but further addition of benzene decreased $G(\text{RH})$ considerably. Addition of benzene to neutral 0.1 *M* RX decreased $G(\text{RH})$ with $G^\circ(e^-) = 1.1$.

Introduction

There is a considerable amount of work which supports the hypothesis that the geminate dry charge pair, H_2O^+ and e^- , can be trapped in aqueous systems with suitable solutes at $\lesssim 0.1 M$.² This hypothesis is supported by quantitative correlations for aqueous systems of both recent and earlier studies.^{3,4} It is also supported by the recent striking experiments of Hunt and coworkers⁵ who have presented evidence from pulse radiolysis with 24 psec resolution that electrons react with high concentrations of appropriate solutes before becoming hydrated. Effective solutes were NaNO_3 , CdCl_2 , H_2O_2 , and acetone, but H_{aq}^+ was not effective.

Ethanol as solvent offers significant advantages for studies of charge trapping. Since $G(e_s^-)$ is only ~ 1 there should be a large yield of scavengable dry electrons, possibly ~ 3 . Ion solvation energies and the rate constants $k(e_s^- + S)$ are nearly the same as for water,^{6,7} while the energetic primary positive ion is also degraded by protonation. It will be assumed hereafter that $k(e_{\text{aq}}^- + S) = k(e_s^- + S)_{\text{ethanol}}$. The differences in chemistry are not relevant to charge trapping, while the improved solubility for organic compounds is critical for the high solute concentrations required.

The primary objective of this work is to provide qualitative evidence for trapping the dry electron and the dry hole. Since hole trapping by anions increases the yield of solvated electrons,⁴ the two experimental procedures will be similar since $\Delta G(e_s^-)$ due to anions measures $\Delta G(\text{holes})$. Benzene and phenol appear to be the most appropriate of the known traps for dry electrons because their rate constants for scavenging e_{aq}^- are $\sim 10^7 M^{-1} \text{sec}^{-1}$, and this very small value facilitates distinguishing between e^- and e_s^- .⁴ The anions of both benzene and phenol abstract protons from alcohols^{4,8} but it does not appear to be feasible to measure the ultimate products of the dienyl radicals.

Instead, alkyl halides have been used as reference solutes in competition with H^+ or aromatic compounds. Alkyl halides react efficiently both with e^- and e_s^- by dissociative electron attachment. In ethanol as solvent the alkyl radical can be expected to yield alkane almost quantitatively and the change in yield of alkane measures the change in $G(\text{electrons})$ due to trapping holes or electrons.

The rate of reaction between the H atom and ethanol to form H_2 under the conditions of this work greatly exceeds the rate of reaction between the H atom and 0.1 *M* propyl chloride to form HCl .⁶ Consequently $G(\text{C}_3\text{H}_8)$ is expected to be a valid measure of dissociative electron attachment. The ratio of the corresponding rates of H atoms with ethanol and 0.1 *M* alkyl bromide is $\sim 20^6$ and the contribution to $G(\text{C}_5\text{H}_{10})$ is not important.

The effect produced by addition of CaCl_2 will be attributed exclusively to hole trapping by Cl^- . The small difference between the first and second ionization potentials of Ca (6.1 and 11.9 eV) and the large single ion solvation energy of Ca^{2+} (~ 18 eV) exclude electron

(1) The Radiation Laboratory of the University of Notre Dame is operated under contract with the U. S. Atomic Energy Commission. This is AEC Document No. COO-38-717.

(2) W. H. Hamill, *J. Phys. Chem.*, **73**, 1341 (1969).

(3) P. L. T. Bevan and W. H. Hamill, *Trans. Faraday Soc.*, in press.

(4) T. Sawai and W. H. Hamill, *J. Phys. Chem.*, **74**, in press.

(5) M. J. Bronskill, R. J. Wolff, and J. W. Hunt, *J. Chem. Phys.*, in press. This and other related work was presented at the "Symposium on Very Early Effects" at the International Meeting on Primary Radiation Effects in Chemistry and Biology, Buenos Aires, March 9-14, 1970.

(6) M. Anbar and P. Neta, *Int. J. Appl. Radiat. Isotop.*, **18**, 433 (1967).

(7) L. M. Dorfman and M. S. Matheson, chapter on pulse radiolysis in "Progress in Reaction Kinetics," Vol. 3, G. Porter, Ed., Pergamon Press, New York, N. Y., 1965, p 237.

(8) T. Shida and W. H. Hamill, *J. Amer. Chem. Soc.*, **88**, 3639 (1966).

trapping by Ca_s^{2+} . It will be assumed tentatively that H_s^+ traps only e_s^- , for which there is some basis,² and HCl will be used at constant concentration of Cl^- .

It will be assumed tentatively that the relative probabilities for trapping e^- by alkyl halide and benzene is given by $\kappa_2[\text{RX}]/\kappa_1[\text{C}_6\text{H}_6]$, where the κ 's are cross sections. For competition between RX and H^+ for e_s^- the relative probabilities become $\kappa_2[\text{RX}]/\kappa_1[\text{H}^+]$ but the κ 's will be read, in context, as rate constants. An additional rate process for "first-order" recombination of e_s^- or solvation of e^- , as appropriate, will be represented by κ_3 . The expression A is quite

$$\Delta G(\text{RH}) = \frac{G^\circ(\text{precursor})\kappa_1[\text{S}]}{\kappa_1[\text{S}] + \kappa_2[\text{RX}] + \kappa_3} \quad (\text{A})$$

similar to expressions used previously for trapping dry electrons.^{3,4} It should be observed that the usual plot of $1/\Delta G$ vs. $1/[\text{S}]$ will give an intercept $1/G^\circ$ but the slope will be $(\kappa_2[\text{RX}] + \kappa_3)/G^\circ\kappa_1$ and $[\text{RX}] > 0$ in all systems.

Experimental Section

n-Propyl chloride and *c*-pentyl bromide, Eastman White Label grade, and phenol, Mallinckrodt AR grade, were used as received. Benzene, Fisher's certified grade, was recrystallized 3 times.

All solutions contained 0.1 *M* *n*-propyl chloride or *c*-pentyl bromide in 95% ethanol of USP grade. The only reaction products of interest were propane or *c*-pentane which were analyzed using a Carbowax-1500 packed gel column at 70°. All solutions were purged with nitrogen and ⁶⁰Co γ irradiated to 5×10^{19} eV/g at ambient temperature.

Results

Both benzene and phenol depress $G(\text{C}_3\text{H}_8)$ and at 0.7, 0.9, and 1.0 *M* of either the effects are substantially equal. Benzene was used for all other experiments. It can be seen from Table I that ~ 0.9 *M* benzene depressed the yield of propane (expressed in arbitrary units) by $\sim 50\%$, even though a considerable part of this product must have been formed by e_s^- . This component is not susceptible to appreciable interference by benzene in competition with propyl chloride since $k(e_{\text{aq}}^- + \text{C}_3\text{H}_7\text{Cl}) \cong 10^9 \text{ M}^{-1} \text{ sec}^{-1}$ while $k(e_{\text{aq}}^- + \text{C}_6\text{H}_6) = 1.4 \times 10^7$.⁶ Equation A can be fitted to the 5 most concentrated solutions with $G^\circ \cong 70$ (in arbitrary units); *i.e.*, $\sim 70\%$ of the precursors of propane are scavengable by benzene.

The hydrogen ion reacts $\sim 10^2$ faster with e_{aq}^- than does propyl chloride and acid should therefore suppress strongly the component of propane with e_s^- as precursor. The results in Table I show the expected decrease followed, however, by a marked increase. The latter might be a consequence of hole trapping by Cl^- and this possibility was tested by adding CaCl_2 . As Table I shows, the yield of propane was increased

Table I: The Effects of C_6H_6 , H^+ , and Cl^- on the Yield of C_3H_8 from 0.1 *M* 1- $\text{C}_3\text{H}_7\text{Cl}$ in Ethanol

Solute	[Solute], <i>M</i>	Yield C_3H_8 , arbitrary units	Solute	[Solute], <i>M</i>	Yield C_3H_8 , arbitrary units	
None		100	None		100	
C_6H_6	0.05	82.3	HCl	0.2	69	
	0.10	73		0.4	57	
	0.20	70		0.6	69	
	0.30	69		0.8	72	
	0.50	59		1.0	75	
	0.70	52				
	0.90	49				
	1.00	46				
None		100	Cl^- H^+, Cl^-	1.0	144	
CaCl_2	0.1	107		0.05, 1.0	114	
	0.2	114		0.1, 1.0	96	
	0.4	134		0.2, 1.0	81	
	0.6	139		0.6, 1.0	76	
	0.8	130		0.8, 1.0	76	
	1.0	145		1.0, 1.0	75	
				1.0, 1.0	30	

considerably. The effect of H^+ was then examined in solutions containing both HCl and CaCl_2 , keeping $[\text{Cl}^-]$ constant (Table I). The yield of propane decreased and leveled off at 52% of the value in neutral solution. That is, only 48% of the precursor of propane was scavengable. These results are fairly well described by eq A with $G^\circ = 70$, in arbitrary units. Since $\kappa_3 = 0$ in this system the ratio $\kappa_1(e_s^- + \text{H}^+)/\kappa_2(e_s^- + \text{C}_3\text{H}_7\text{Cl}) = 42$ can be evaluated. The corresponding ratio in water is ~ 40 . The limiting yield at high acid concentrations was further reduced to 20% of the initial value by addition of 1 *M* benzene, the $\Delta G(\text{C}_3\text{H}_8)$ being slightly less than that for 1 *M* benzene in neutral solution.

The results for cyclopentyl bromide, which proved to be more satisfactory than isopropyl chloride for analytical reasons, are in good qualitative agreement with the earlier data and quantitatively somewhat more precise. These data will be presented in the format of competition kinetics using eq A. The observed 100-eV yield of *c*-pentane in neutral 0.1 *M* *c*- $\text{C}_5\text{H}_9\text{Br}$ was 1.32 but $\Delta G = 1.40 - G(c\text{-C}_5\text{H}_{10})$ fits eq A better for acidic solutions and has been used in Figure 1. The intercept gives $G^\circ = 1.02$ or 73% of the precursor of C_5H_{10} is scavengable by H^+ , about the same as the result using propyl chloride. From the slope, 0.48, one finds $\kappa_1(e_s^- + \text{H}^+)/\kappa_2(e_s^- + \text{C}_5\text{H}_9\text{Br}) = 2.1$ provided $\kappa_3 = 0$. For aqueous butyl bromide the corresponding ratio of rate constants is 2.0.⁶

The dependence of the yield of *c*-pentane from 0.1 *M* *c*-pentyl bromide on the concentration of benzene appears in Figure 2 for a best fit $\Delta G(\text{C}_5\text{H}_{10}) = 1.45 - G(\text{C}_5\text{H}_{10})$. From the intercept we find $G^\circ = 1.10$ for the precursor. From the slope $(\kappa_2[\text{C}_5\text{H}_9\text{Br}] + \kappa_3)/\kappa_1$

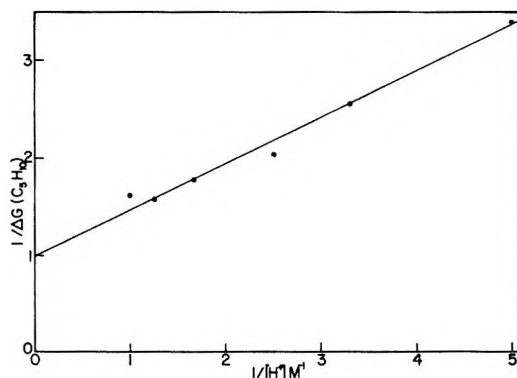


Figure 1. The dependence of $G(c\text{-C}_5\text{H}_{10})$ from $c\text{-C}_5\text{H}_9\text{Br}$ in ethanol as a function of the concentration of HCl at constant $[\text{Cl}^-]$.

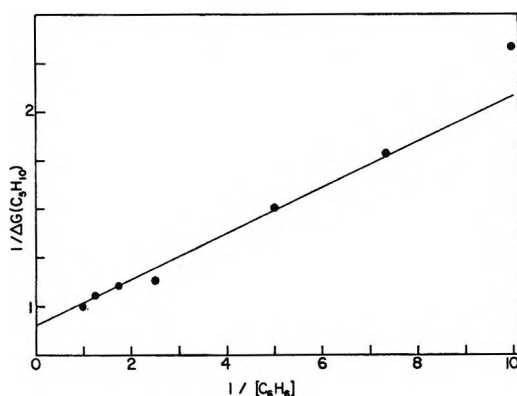


Figure 2. The dependence of $G(c\text{-C}_5\text{H}_{10})$ from $c\text{-C}_5\text{H}_9\text{Br}$ in ethanol as a function of the concentration of C_6H_6 , with $[\text{Cl}^-] = 1\text{ M}$.

$= 0.12$. The corresponding result for propyl chloride (both halides 0.1 M) and benzene is 0.36 .

Discussion

There appear to be two principal precursors of alkane from alkyl halide in the solutions examined, benzene being nearly specific for one, acid for the other.

It has been shown that benzene traps mobile electrons in methanol at 77°K , the product observed being C_6H_7 . It is not produced by scavenging H atoms but is produced from C_6H_6^- by proton abstraction from the solvent.⁸ It was shown that acid had no effect on the yield of C_6H_7 and very little on the yield of $\text{C}_6\text{H}_6\text{OH}$ from phenol.⁴ The facts reported here follow the same pattern, and they cannot be accommodated by the conventional description of ionic processes in polar media.

Alkyl chlorides and bromides in 0.1 M cyclohexane solution appear to generate alkyl radicals exclusively by electron capture, as shown by the recent work of Warman, *et al.*⁹ This applies equally for reactions of benzyl acetate with electrons in ethanol.¹⁰ If substantially all RH from RX arises from dissociative electron attachment, then there appear to be two kinds

of electrons. One of these is characterized by reacting efficiently with H_2^+ and RX and is the solvated electron, e_s^- . The residual yield of RH which remains at high-acid concentrations can be attributed to another population of electrons which still reacts with RX and which can be scavenged by benzene. They behave the same as electrons in alkane liquids or glassy solids and are considered to be dry electrons, e^- .

In the absence of benzene, 0.1 M *c*-pentyl bromide produced 1.45 *c*-pentane per 100 eV . The extrapolated yield of *c*-pentane precursors susceptible to scavenging by benzene was $G^\circ = 1.10$. Since the rate constant for scavenging e_s^- by the halide is $\sim 10^3$ larger than that for benzene it is concluded that benzene scavenges e^- . Since e^- is presumably the precursor of e_s^- it might be expected that in the limit of high benzene concentration $G(c\text{-C}_5\text{H}_{10})$ would approach zero, or $G^\circ = 1.45$, rather than 1.10 . Since the extrapolated value was appreciably smaller it may be that the trial function (A) is inadequate, although it has been satisfactory for a considerable number of aqueous systems.^{3,4} Alternatively, there may be a small yield of solvated electrons produced as such from an excited state below the ionization potential of ethanol, *e.g.*, Rydberg states.

The interpretation of results for systems containing benzene would be complicated if alkyl radicals were scavenged by benzene, rather than abstracting H from ethanol. This appears to be very unlikely. The thermal decomposition of biacetyl peroxide in toluene solution produces C_2H_6 , CH_4 , and CO_2 with $(2\text{C}_2\text{H}_6 + \text{CH}_4)/\text{CO}_2 = 0.98$, the alkanes having only CH_3 for precursor.¹¹ The rate constant for H abstraction by CH_3 is about the same for toluene and ethanol.¹² Since $[\text{C}_2\text{H}_5\text{OH}]/[\text{C}_6\text{H}_6] > 17$ in the present work, addition of radicals to benzene is not to be expected. Neither was there analytical evidence of such products.

The lifetime τ of e^- in a liquid alkane is limited by the rate of recombination, κ_r . In a polar medium it depends also on the rate of solvation and $\tau = (\kappa_r + \kappa_s)^{-1}$. A rather rough estimate of the relative rates is provided by $G_{e^-}/G_{e_s^-} = \kappa_r/\kappa_s$, about 3 in ethanol and 0.5 in water. That is, τ is about $1/3$ as great in water as in an alkane, in qualitative agreement with the higher concentrations required to scavenge e^- in water. To trap 50% of the dry electrons in water requires $\sim 0.4\text{ M}$ phenol.⁴ If the thermalized dry electron reacts upon encounter with a molecule of phenol, then on the average e^- sweeps out a volume occupied by $\sim 0.4 \times 55$ or $\sim 22\text{ H}_2\text{O}$, or its mean path is $\sim 70\text{ \AA}$ in length. At

(9) J. M. Warman, K. D. Asmus, and R. H. Schuler, *J. Phys. Chem.*, **73**, 931 (1969).

(10) J. A. Ward and W. H. Hamill, *J. Amer. Chem. Soc.*, **87**, 1853 (1965).

(11) A. Rembaum and M. Szwarc, *ibid.*, **77**, 3486 (1955).

(12) A. F. Trotman-Dickenson and E. W. R. Steacie, *J. Chem. Phys.*, **19**, 329 (1951).

thermal velocity this corresponds to $\tau \cong 7 \times 10^{-14}$ sec. This recombination time approximates the value deduced initially by Samuel and Magee,¹³ whose theory describes the behavior of dry electrons. The dielectric relaxation time at constant charge has been shown by Mozumder to be 4×10^{-13} sec, but the microscopic relaxation time may be less.¹⁴

Theard and Burton¹⁵ observed large effects of halides in methanolic solutions, with $\Delta G(\text{glycol}) \cong -\Delta G(\text{CH}_2\text{O}) \cong -2.5$ at $[\text{Cl}^-] = 1.5 M$. Hole trapping is

considerable at this concentration and the effect may be due to neutralization of CH_3OH^+ prior to proton transfer which would decrease $G(\text{CH}_2\text{OH})$, and therefore $G(\text{glycol})$. The increase in $G(\text{CH}_2\text{O})$ may be due to the reaction $\text{CH}_2\text{OH} + \text{X}_2^- \rightarrow \text{CH}_2\text{O} + \text{H}^+ + 2\text{X}^-$, thereby accounting for the somewhat symmetric ΔG 's of these two products.

(13) A. H. Samuel and J. L. Magee, *J. Chem. Phys.*, **21**, 1080 (1953).

(14) A. Mozumder, *ibid.*, **50**, 3153, 3162 (1969).

(15) L. M. Theard and M. Burton, *J. Phys. Chem.*, **67**, 53 (1963).

Electron Scavenging in the γ Radiolysis of Liquid Diethyl Ether¹

by Krishan M. Bansal and Stefan J. Rzad

Radiation Research Laboratories, Mellon Institute, Carnegie-Mellon University, Pittsburgh, Pennsylvania 15213
(Received March 30, 1970)

The concentration dependence of electron capture in the γ radiolysis of diethyl ether–methyl bromide solutions can be quantitatively accounted for by the empirical model previously proposed for hydrocarbons and extended to alcohols. The free and geminate ion pair yields are estimated as 0.15 and 3.8, respectively. Competition experiments allowed the determination of the reactivities of SF_6 and N_2O towards electrons in the ether. From the study of the decrease in hydrogen yield upon addition of these electron scavengers, it is concluded that only 40% of the ion-neutralization processes yield hydrogen.

Introduction

The γ radiolysis of diethyl ether has, so far, received very little attention.^{2,3} Our interest in the study of diethyl ether radiolysis originates from the fact that its dielectric constant (4.3) lies in the range between those of hydrocarbons (~ 2.0) and alcohols ($\epsilon_{\text{CH}_3\text{OH}}$ 32.6, $\epsilon_{\text{C}_2\text{H}_5\text{OH}}$ 24.3). While several studies involving the use of electron scavengers in the radiolysis of hydrocarbons and alcohols^{4,5} have been carried out, no such information is available for ethers. The present investigation was undertaken to understand the electron capture processes in diethyl ether by using (¹⁴C) methyl bromide (electron scavenger) as a probe. Furthermore, the effect of various electron scavengers (CH_3Br , N_2O and SF_6) on the hydrogen yield (a major radiolysis product) was also studied to obtain information concerning the importance of ion–electron neutralization processes leading to hydrogen formation.

Experimental Section

Sulfur hexafluoride, ¹⁴C methyl bromide, and nitrous oxide were purified by a method described elsewhere.⁶ Matheson CF_3Br was distilled at -78° and stored. Spectrograde diethyl ether from Eastman Organic Chemicals Co. was first outgassed at liquid nitrogen temperature. After that $1/3$ of the volume of ether was

pumped away at room temperature to remove dissolved carbon dioxide. The next $1/3$ fraction was distilled and stored into a glass reservoir on the vacuum line. This diethyl ether was used throughout the experiments since the same yields of methyl radicals were obtained whether or not the ether was dried over sodium and no impurities (*e.g.*, ethanol) could be detected by gas chromatography using a 2.5-m column packed with 10% di-2-ethylhexylsebacate on diatoport WAW (60–80 mesh) or a 10-m column packed with 25% silicone grease on Chromosorb P.

A known amount of ether (usually 1.2 cm³) was distilled into the irradiation cell and was degassed again by the freeze–pump–thaw cycles. The desired amount of the solute, as determined by pressure–volume measurements, was then distilled into the

(1) Supported in part by the U. S. Atomic Energy Commission.

(2) G. E. Adams, J. H. Baxendale, and R. D. Sedgwick, *J. Phys. Chem.*, **63**, 854 (1959).

(3) M. K. M. Ng and G. R. Freeman, *J. Amer. Chem. Soc.*, **87**, 1635 (1965).

(4) J. M. Warman, K.-D. Asmus, and R. H. Schuler, *Advances in Chemistry Series*, No. 82, American Chemical Society, Washington, D. C., 1968, p 25, and references cited therein.

(5) J. Teply, *Radiat. Res. Rev.*, **1**, 361 (1969), and references cited therein.

(6) J. M. Warman and S. J. Rzad, *J. Chem. Phys.*, **52**, 485 (1970).

irradiation cell containing the outgassed ether. The cell was sealed off in such a way that the vapor volume was approximately 0.2 cm³. For solutions containing less than 10⁻⁴ M methyl bromide an approximate amount of methyl bromide was added initially and the actual concentration was determined from the methyl bromide activity as measured during the analysis. The concentration of the solute in diethyl ether was calculated on the assumption of the complete solubility of CH₃Br, N₂O, SF₆, and CF₃Br in the ether.

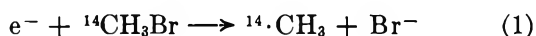
The radio-gas chromatographic method of analysis used has been described before.^{6,7}

The volume of diethyl ether used for samples for which the analysis of noncondensable gases (H₂, CH₄, and CO) at liquid nitrogen temperature was carried out was usually 5.2 cm³. The vapor volume after sealing off the sample tube was approximately 0.5 cm³. After irradiation, the total amount of the products volatile at liquid nitrogen temperature was measured in a Toepler-McLeod apparatus and subsequently analyzed by mass spectrometry.

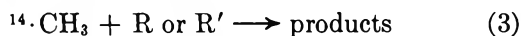
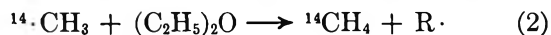
The samples were irradiated in a tubular ⁶⁰Co γ -ray source at a dose rate in the ether of 6.6 \times 10¹⁶ eV/cm³ min or 3.4 \times 10¹⁷ eV/cm³ min.

Results and Discussion

A. Diethyl Ether-Methyl Bromide Solutions. In the radiolysis of hydrocarbons or alcohols containing methyl bromide, it was shown that the methyl radicals are produced as a result of dissociative electron capture from methyl bromide (reaction 1).⁸⁻¹⁰ These methyl radicals



can either abstract a hydrogen atom from the solvent (reaction 2) or react with other radicals R or R' (reaction 3). The radio-gas chromatographic analysis of



the products from the radiolysis of diethyl ether-methyl bromide solutions showed that reaction 3 amounts to about 1% of the total methyl radicals produced by reaction 1. Therefore, the yield of (¹⁴C) methyl radicals¹¹ (or methane with a suitable correction for the occurrence of reaction 3) will give the yield of the scavenged electrons. The dependence of the methyl radicals yield on the concentration of methyl bromide was studied over the concentration range from 7 \times 10⁻⁶ to 0.3 M and the results are reported in Figure 1. Over this entire concentration range the yield of methyl radicals changed from approximately 0.08 to 2.9 (Figure 1). Analysis sensitivity required higher doses to be given to samples containing higher concentrations of methyl bromide. Indeed the higher the concentration of the latter the more it has to be diluted with inactive methyl bromide for practical reasons.

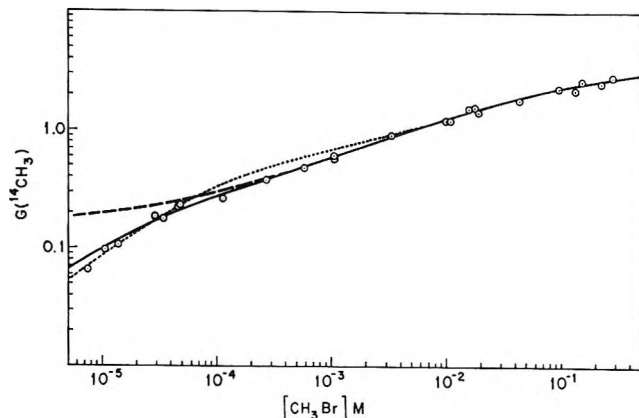


Figure 1. Yield of methyl radicals as a function of methyl bromide concentration in diethyl ether. Solid line calculated using eq II with $G_{fi}^0 = 0.15$, $G_{gi}^0 = 3.8$, $\alpha = 18 \text{ M}^{-1}$, $\delta = 5.1 \times 10^4 \text{ M}^{-1}$. The dashed and dotted lines are calculated as described in the text.

The doses which correspond to the data presented in Figure 1 are in the range of 1.3 \times 10¹⁷ to 1 \times 10¹⁹ eV/cm³. Since no dose effect on the methyl radical formation is observed, the intercomparison of the different data is warranted.

It was shown that in the case of hydrocarbons, the concentration dependence of methyl radical yield could be described by the empirical eq I^{8,10,12}

$$G(e^-) = G_{fi} + G_{gi} \frac{\sqrt{\alpha S}}{1 + \sqrt{\alpha S}} \quad (I)$$

where G_{fi} and G_{gi} represent the yield of the free and geminate electrons, respectively, S is the concentration of the scavenger, and α is a parameter which represents the reactivity of the solute towards the electrons relative to their recombination with the positive ions.

In the present study of the radiolysis of diethyl ether-methyl bromide solutions, it was observed that eq I, together with suitable parameters ($G_{fi} = 0.15$, $G_{gi} = 3.8$, $\alpha = 18$) is a good description of the experimental data (Figure 1) at scavenger concentrations above 3 \times 10⁻⁴ M. Below this concentration, the experimental points fall below the calculated values (dashed line in Figure 1). A similar behavior for methyl radical production was found in the radiolysis of solutions of methyl bromide in methanol and ethanol in which case eq II was found to describe the data quite well.⁹

(7) S. J. Rząd and R. H. Schuler, *J. Phys. Chem.*, **72**, 228 (1968).

(8) S. J. Rząd and J. M. Warman, *J. Chem. Phys.*, **49**, 2861 (1968).

(9) S. J. Rząd and J. H. Fendler, *ibid.*, **52**, 5395 (1970).

(10) J. M. Warman, K.-D. Asmus, and R. H. Schuler, *J. Phys. Chem.*, **73**, 931 (1969).

(11) Throughout the text methyl radical yield refers only to the (¹⁴C) methyl radicals.

(12) K.-D. Asmus, J. M. Warman, and R. H. Schuler, *J. Phys. Chem.*, **74**, 246 (1970).

$$G(e_s^-) = G_{fi}^s \frac{\delta S}{1 + \delta S} + G_{gi}^s \frac{\sqrt{\alpha S}}{1 + \sqrt{\alpha S}} \quad (\text{II})$$

In this equation, $\delta = k/k_d$, where k_d represents the first-order rate constant for the decay of the solvated electron and k is the second-order rate constant for its scavenging by the solute. G_{fi}^s and G_{gi}^s represent the solvated free and geminate electrons, respectively. The solid curve drawn through the points in Figure 1 represents the best fit of eq II with the following parameters: $G_{fi}^s = 0.15$; $G_{gi}^s = 3.8$; $\alpha = 18 M^{-1}$ and $\delta = 5.1 \times 10^4 M^{-1}$. Although in alcohols the pulse radiolysis studies have shown the existence of solvated electrons,¹³ no such direct evidence for their existence in diethyl ether at room temperature is available. However, from the observation of the solvated electrons in pulse-irradiated diethyl ether at -110° ($\tau_{1/2} = 2 \mu\text{sec}$)¹⁴ and the similarities in electron scavenging curves for diethyl ether and alcohols,⁹ it appears that the electrons may also be solvated in diethyl ether at room temperature and the lack of their observation in the pulse-radiolysis study¹⁴ might be due to the time-scale limitations of the technique used. Assuming that these electrons are solvated one can obtain the value of their first-order decay rate constant (k_d) from the parameter δ provided the value of the rate constant k is known. The rate constant k is expected to have a value between $3 \times 10^{11} M^{-1} \text{sec}^{-1}$,¹⁵ reported for electron scavenging by biphenyl in cyclohexane and $1.4 \times 10^{10} M^{-1} \text{sec}^{-1}$ reported for electron scavenging by methyl bromide in methanol and ethanol.⁹ Using a value of $3 \times 10^{11} M^{-1} \text{sec}^{-1}$, an estimate of the value of $k_d = 5.9 \times 10^6 \text{sec}^{-1}$ is obtained. This corresponds to $\tau_{1/2}$ of 0.1 μsec for solvated free electrons in diethyl ether. Assuming no rise time of the equipment and using $k_d = 5.9 \times 10^6 \text{sec}^{-1}$, the fraction of solvated free electrons remaining at the end of a 0.4 and 0.1- μsec pulse¹⁶ is 0.38 and 0.17, respectively. Since $G_{fi}^s = 0.15$, these values correspond to yields of $G = 0.06$ and 0.03, respectively. On the other hand, a value of $1.4 \times 10^{10} M^{-1} \text{sec}^{-1}$ would lead to the following parameters: $k_d = 2.8 \times 10^8 \text{sec}^{-1}$, $\tau_{1/2} = 2.5 \mu\text{sec}$, and fractions of 0.95 and 0.87 remaining at the end of a 0.4 and 1- μsec pulse, respectively. These fractions correspond to $G = 0.14$ and 0.13. The lack of observation of any optical absorption for solvated electron in pulse-irradiated diethyl ether at room temperature¹⁴ would be more consistent with a half-life of $\tau_{1/2} = 0.1 \mu\text{sec}$ indicating that the rate constant for electron scavenging in diethyl ether is similar to that in cyclohexane. It should be pointed out here that a value of $\sim 3 \times 10^{11} M^{-1} \text{sec}^{-1}$ for electron scavenging by methyl bromide in diethyl ether is not unreasonable in view of the following. A value of $3 \times 10^{11} M^{-1} \text{sec}^{-1}$ is a lower limit¹⁵ in cyclohexane and, bearing in mind the recent measurement of a high electronic mobility in cyclohexane¹⁷ ($0.35 \text{cm}^2 \text{V}^{-1} \text{sec}^{-1}$), may actually be higher

by at least one order of magnitude. On the other hand, in polar media such as alcohols^{9,18} and water¹⁸ the rate constant of reaction of the solvated electron with a solute is of the order of magnitude of the diffusion-controlled rate constant as calculated by the Debye equation when using for the solvated electron a mobility comparable to that of a negative ion.¹⁹ Diethyl ether with a dielectric constant of 4.3 is closer to hydrocarbons and one would expect that the electron be less solvated (bound) in this medium than in more polar liquids. This in turn would give a higher mobility to the solvated electron leading to a higher rate constant for its scavenging. The departure of the yields from the dashed line (Figure 1) at low methyl bromide concentrations could result from small amounts of impurity present in diethyl ether. For example, if the rate of electron scavenging by methyl bromide and the impurity were similar ($3 \times 10^{11} M^{-1} \text{sec}^{-1}$), the concentration of the latter would be $2 \times 10^{-5} M$. Such a concentration should have been detected by gas chromatography. However, a definite proof of the existence of the solvated electron in diethyl ether will eventually come from nanosecond pulse-radiolysis experiments.

The yield of G_{fi}^s obtained in the present study agrees well with the value of 0.19 obtained by conductivity measurements in pure diethyl ether²⁰ but disagrees with that obtained by Schmidt and Allen²¹ ($G_{fi} = 0.35$) using the Clearing Field technique. By using this latter value of $G_{fi}^s = 0.35$, the best fit of equation II to the experimental data at high solute concentrations ($>10^{-3} M$), is obtained with $G_{fi}^s = 4.0$ and $\alpha = 9.3 M^{-1}$. These parameters together with a value of $\delta = 1.6 \times 10^4 M^{-1}$ also give a good fit to the experimental data at low solute concentrations ($<10^{-4} M$); however, the fit in the solute concentration range 10^{-4} to $10^{-3} M$ is poor (dotted line in Figure 1). The present study shows that the total ion-pair yield is $G_i = G_{fi}^s + G_{gi}^s = 3.95$ which agrees reasonably well with the value of 4.2 calculated on the basis of gas phase W value of 23.6 eV for diethyl ether.²²

B. Competition Studies between Methyl Bromide and Other Solutes in Diethyl Ether. Studies involving the

(13) For example, I. A. Taub, D. A. Harter, M. C. Sauer, Jr., and L. M. Dorfman, *J. Chem. Phys.*, **41**, 979 (1964).

(14) S. Arai and M. C. Sauer, Jr., *ibid.*, **44**, 2297 (1966).

(15) S. J. Rząd, P. P. Infelta, J. M. Warman, and R. H. Schuler, *ibid.*, **50**, 5034 (1969).

(16) This fraction can be calculated using eq 17 of ref 9.

(17) W. F. Schmidt and A. O. Allen, *J. Chem. Phys.*, **52**, 4788 (1970).

(18) See, for example, J. K. Thomas, *Radiat. Res. Rev.*, **1**, 183 (1968).

(19) *E.g.*, the diffusion of the solvated electron in water has been measured to be $4.75 \times 10^{-5} \text{cm}^2 \text{sec}^{-1}$, K. H. Schmidt and W. L. Buck, *Science*, **151**, 70 (1966).

(20) G. R. Freeman and J. M. Fayadh, *J. Chem. Phys.*, **43**, 86 (1965).

(21) W. F. Schmidt and A. O. Allen, *J. Phys. Chem.*, **72**, 3730 (1968).

(22) P. Adler and H. K. Bothe, *Z. Naturforsch. A*, **20**, 1700 (1965).

competitive electron capture by two solutes in diethyl ether were also carried out. The scavenger combinations used were methyl bromide-nitrous oxide and methyl bromide-sulfur hexafluoride. The results are presented in Table I. Assuming ideal behavior, one

Table I: $^{14}\text{CH}_3$ Yields from Competitive Studies between Methyl Bromide and Other Solute in Diethyl Ether^a

Solute, $M \times 10^3$	$[\text{CH}_3\text{Br}]$, $M \times 10^3$	$G_{\text{obsd}}(\text{CH}_3)$	$G_{\text{calcd}}(\text{CH}_3)^b$
N ₂ O solute, $\alpha = 16$			
0.89	1.49	0.46	0.52
2.24	1.69	0.42	0.43
2.27	1.69	0.39	0.43
2.50	5.35	0.79	0.84
4.98	5.35	0.54	0.70
5.09	5.60	0.67	0.72
8.80	5.35	0.55	0.57
2.30	9.30	1.03	1.10
4.80	9.00	1.05	0.96
10.8	9.00	0.80	0.76
21.4	9.40	0.71	0.58
31.7	9.40	0.58	0.47
30.0	9.90	0.53	0.51
21.0	10.36	0.69	0.63
36.0	83.0	1.81	1.74
75.9	84.5	1.36	1.42
80.0	84.6	1.31	1.39
116.0	81.7	1.28	1.16
SF ₆ solute, $\alpha = 42$			
2.28	9.0	0.93	0.90
4.98	9.0	0.73	0.70
11.0	9.0	0.54	0.48
21.5	9.0	0.41	0.32
12.7	74.3	1.79	1.69
20.4	76.8	1.57	1.51
39.3	76.8	1.06	1.18
78.7	76.6	0.73	0.82

^a The dose was 3.4×10^{18} eV/cm³ but for solutions containing $[\text{CH}_3\text{Br}] > 0.01 M$ it was 1×10^{19} eV/cm³. ^b Calculated using eq III, the values of α and the following parameters: $G_{\text{H}_2}^{\text{e}}$ = 0.15, $G_{\text{e}_1}^{\text{e}}$ = 3.8, $\alpha_{\text{CH}_3\text{Br}} = 18 M^{-1}$.

can use eq III which gives the yield of electrons scavenged by a solute at concentration S_1 , in the presence of a second solute at concentration S_2 . The various symbols

$$G(e_{\cdot}^-)_{S_1} = \left[G_{\text{H}_2}^{\text{e}} \frac{\delta_1 S_1 + \delta_2 S_2}{1 + (\delta_1 S_1 + \delta_2 S_2)} + G_{\text{e}_1}^{\text{e}} \frac{(\alpha_1 S_1 + \alpha_2 S_2)^{1/2}}{1 + (\alpha_1 S_1 + \alpha_2 S_2)^{1/2}} \right] \frac{\alpha_1 S_1}{\alpha_1 S_1 + \alpha_2 S_2} \quad (\text{III})$$

in this equation have the same meaning as in case of eq II and the subscripts 1 and 2 refer to methyl bromide and the second solute, respectively. At methyl bromide concentrations above $3 \times 10^{-4} M$, the decay of the solvated electron is negligible and, therefore, eq III will reduce to a form which has only one unknown

parameter α_2 . For this reason, the methyl bromide concentration used in competition experiments was always greater than $10^{-3} M$. The best fit of eq III to the experimental data, neglecting the solvated electron decay, allowed the determination of $\alpha_{\text{N}_2\text{O}} = 16$ and $\alpha_{\text{SF}_6} = 42$. The values of $G_{\text{calcd}}(\text{CH}_3)$ are presented in the last column of Table I and the agreement with $G_{\text{obsd}}(\text{CH}_3)$ is fairly good.

C. Hydrogen, Methane, and Carbon Monoxide Yields. The hydrogen yield changed from 3.35 to 3.20 as the total dose absorbed was increased from 1.7×10^{18} to 1.2×10^{19} eV/cm³. The extrapolated $G(\text{H}_2)$ value to zero dose was found to be 3.4, which is slightly lower than the value of 3.7 found by Ng and Freeman.³ Over this dose range studied, the yields of methane and carbon monoxide ($G(\text{CH}_4) = 0.37$, $G(\text{CO}) = 0.08$) remained unchanged with dose.

Effect of Electron Scavengers. The dependence of the yield of hydrogen on the concentration of various electron scavengers (CH_3Br , N_2O , SF_6) was studied and the results are presented in Table II. Furthermore, it

Table II: Hydrogen Yields from the Radiolysis of Diethyl Ether-Scavenger Solutions^a

$[S]$, mM	$G(\text{H}_2)_{\text{obsd}}$	$G(\text{H}_2)_{\text{calcd}}^b$
Scavenger, N ₂ O		
0.30	3.47	3.30
2.76	3.06	3.14
9.41	2.92	2.98
35.5	2.74	2.75
106	2.61	2.54
289	2.40	2.36
Scavenger, CH ₃ Br		
0.36	3.40	3.29
3.08	3.03	3.11
9.90	2.86	2.95
32.5	2.70	2.74
35.5	2.65	2.72
114	2.50	2.50
115	2.54	2.50
336	2.39	2.32
Scavenger, SF ₆		
115	2.51	2.36
335	2.30	2.20

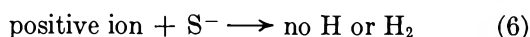
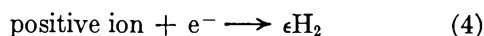
^a The dose was 3.4×10^{18} eV/cm³. ^b Calculated using eq IV and the following parameters: $G(\text{H}_2)_0 = 3.4$, $G_{\text{e}_1}^{\text{e}} = 3.8$, $\alpha_{\text{N}_2\text{O}} = 16$, $\alpha_{\text{CH}_3\text{Br}} = 18$, $\alpha_{\text{SF}_6} = 42$, $\epsilon = 0.4$.

was also observed that the addition of $0.11 M \text{CF}_3\text{Br}$ reduced the hydrogen yield to 2.60.

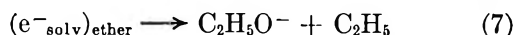
The yields of methane and carbon monoxide remained unaffected by the addition of electron scavengers (N_2O , SF_6 , CF_3Br) indicating that excited states pro-

duced directly in the ether are the precursors for their formation.

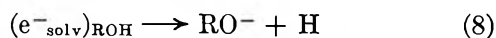
The various electron scavengers are expected to affect the hydrogen yield by interfering with the positive ion electron neutralization processes. The overall hydrogen production by ionic processes can then be represented by the following general scheme



where the positive ion can be a primary or a secondary positive ion and ϵ is the efficiency for production of hydrogen upon neutralization. It was assumed that the solvated free electrons decay according to reaction 7 and hence do not contribute to any hydrogen produc-



tion. This reaction is analogous to the decay of the solvated free electrons in alcohols.²³



According to this general scheme, the yield of hydrogen at any electron scavenger concentration S is given by eq IV, where $G(\text{H}_2)_0$ ($= 3.4$) is the hydrogen yield in the

$$G(\text{H}_2) = G(\text{H}_2)_0 - \epsilon \left[G_{\text{gi}} \frac{\sqrt{\alpha S}}{1 + \sqrt{\alpha S}} \right] \quad (\text{IV})$$

absence of the scavenger. The best fit of eq IV to the experimental data was obtained with $\epsilon = 0.4$. The calculated values of the hydrogen yields are given in the last column of Table II. The overall agreement with the observed values is fairly good. From the above it follows that a yield of hydrogen of 1.52 ($G(\text{H}_2)_{\text{ion}} = G_{\text{gi}} \times \epsilon$) comes from ionic precursors and 1.88 ($G(\text{H}_2)_{\text{non ionic}} = G(\text{H}_2)_{\text{total}} - G(\text{H}_2)_{\text{ion}}$) from nonionic processes.

D. Nitrogen Yield from Diethyl Ether-N₂O Solutions. The yields of nitrogen from the radiolysis of diethyl ether-N₂O solutions are shown in Table III together with the yields of electrons scavenged by N₂O ($G(e_s^-)$) calculated by using eq II. As previously noted in hydrocarbons,^{24,25} the yield of nitrogen is in excess of the yield of scavenged electrons at any N₂O concentra-

Table III: Nitrogen Yield from the Radiolysis of Diethyl Ether-N₂O Solutions^a

[N ₂ O], mM	G(N ₂)	G(e _s ⁻) ^b	G(N ₂)/ G(e ⁻)
0.30	0.60	0.38	1.58
2.76	1.20	0.81	1.48
9.41	1.75	1.21	1.45
35.5	2.59	1.78	1.46
106	3.25	2.30	1.41
289	4.04	2.74	1.47

^a The dose was 5×10^{18} eV/cm³. ^b Calculated using eq II with the following parameters: $G_{\text{ri}}^a = 0.15$, $G_{\text{gi}}^a = 3.8$, $\alpha_{\text{N}_2\text{O}} = 16$, $\delta = 4.4 \times 10^4 M^{-1}$.

tion used. Electron scavenging parameters obtained for nitrous oxide in methanol and ethanol⁹ seem to indicate that the yield of nitrogen observed in these alcohols²⁶⁻²⁸ is also greater than the yield of the scavenged electrons. In the case of cyclohexane-nitrous oxide solutions, this excess nitrogen yield can be quantitatively accounted for if one assumes that a secondary reaction of the anion to produce nitrogen competes with the neutralization process.⁴ Such an explanation also describes the excess nitrogen yield in benzene-nitrous oxide solutions.²⁵ In the present study of diethyl ether-N₂O solutions, a constant ratio $G(\text{N}_2)/G(e_s^-)$ of 1.46 is observed over the entire concentration range studied (Table III) indicating that the mechanism used for hydrocarbons does not apply to diethyl ether. As yet there is not enough information available as to make further speculation about the reaction mechanism worthwhile.

Acknowledgment. The authors wish to express their appreciation to Dr. R. H. Schuler for helpful discussions.

(23) G. R. Freeman in "Actions Chimiques et Biologiques des Radiations," Vol. 14, M. Haissinsky, Ed., Masson et Cie Editeurs, 1969, and references cited therein.

(24) M. G. Robinson and G. R. Freeman *J. Chem. Phys.*, **48**, 983 (1968).

(25) R. R. Hentz and W. V. Sherman, *J. Phys. Chem.*, **73**, 2676 (1969).

(26) W. V. Sherman, *ibid.*, **71**, 4245 (1967).

(27) J. C. Russell and G. R. Freeman, *ibid.*, **72**, 816 (1968).

(28) K. N. Jha and G. R. Freeman, *J. Chem. Phys.*, **48**, 5480 (1968)

Effects of Ethene and Ethane on the Photochemical Production of Carbon Monoxide from Acetone

by A. S. Gordon and R. H. Knipe

Research Department, Chemistry Division, Code 6059, Naval Weapons Center, China Lake, California 93555
(Received March 2, 1970)

The effect of ethane and ethene on the photolysis of acetone has been studied from 30 to 350°. Ethane increases the rate of CO production at lower temperatures, becoming inert at about 150°. Ethene is an inhibitor, its effectiveness decreasing with increasing temperature. At about 150° it becomes inert, but then at higher temperature it increases the rate of formation of CO. Evidence is presented that the high-temperature photochemical reaction between acetone and ethene is a radical chain reaction, the chain length increasing with temperature. The reaction has been studied extensively at 350°. A mechanism is proposed which is in accord with the observations.

Introduction

The effect of various gases on the photochemical production of CO from acetone has been reported by Caldwell and Hoare.¹ They report an increase in yield which depends on the pressure and nature of the added gas, and the temperature.

In this paper we would like to report an extension of the above study in which we concentrated on ethane and ethene as diluents because the "chemical" effects of quenching could be compared with the "collisional" effects. A new effect of ethene has been studied in some detail.

Materials and Apparatus

Eastman Kodak spectroscopic grade acetone was used without purification since gas chromatographic analysis showed that no appreciable impurity was present. It was freed of air by the conventional freeze-pump-warm cycle. Phillips ethene had only a few hundredths of 1% ethane and methane impurities; Phillips ethane had no discernible impurity by our gas chromatographic analysis.

The reactants were photolyzed in a heated cylindrical quartz vessel, 2-cm in diameter and 4-cm long with flat end windows. A similar vessel filled with quartz shell tubing, with the long axes of the pieces of tubing parallel to the long axis of the reaction vessel, was used in experiments to evaluate the effect of surface.

A medium-pressure mercury lamp (Hanovia) was the radiation source. It was used unfiltered or with a lime glass filter which sharply cut all the radiation below 2900 Å, with ~35% transmission at 3130 Å, and 100% at 3600 Å. The intensity was varied with stainless screen filters.

The reaction products were quantitatively transferred onto a 3/16 in. × 6 ft 1.5% squalane on pelletex gas chromatograph column, temperature programmed from liquid N₂ to 100°. The low-boiling products separated

on a pelletex column were trapped on a 3/16 in. × 8 ft Sieve 5A column, temperature programmed from liquid N₂ to 110°. The CO analyses in the presence of ethane have been shown to be about 10% low due to entrapment in the solid during chromatographic analysis. A correction is not applied because the experimental scatter of the results is of the same order of magnitude.

Results and Discussion

In Figures 1 and 2, the ratio of the rates of CO formation from a constant concentration ($2.36 \times 10^{-3} M$) of pure acetone vapor in the presence of $2.37 \times 10^{-2} M$ of ethane or ethene is plotted as a function of temperature. To emphasize the dual effect of ethene (Figure 2), the ratios plotted for the low-temperature range, $R_{CO_{\text{pure}}}/R_{CO_{\text{mix}}}$, are the inverse of the ratios plotted for the high-temperature range.

At low temperature the effect of ethane (Figure 1) is to increase the rate of CO production; the effect decreases with increase in temperature until about 150°, where the effect disappears. Since we did not survey the effect of pressure of ethane at any one temperature, our results cannot be compared in detail with those of Hoare and Caldwell.¹ Our results, in qualitative agreement with theirs, show that the effect of diluent decreases with increase in temperature.

The photo rate of production of CO from acetone in the presence of ethene relative to that from pure acetone is plotted in Figure 2. At low temperatures (30 to 125°) ethene is seen to be an effective quencher. Actually, its quenching effect is greater than indicated by the ratio, since the ratio indicates the overall effect, which is, in part, an increase in rate of formation of CO because ethene also behaves as a third body. The

(1) J. Caldwell and D. E. Hoare, *J. Amer. Chem. Soc.*, **84**, 3987 (1962).

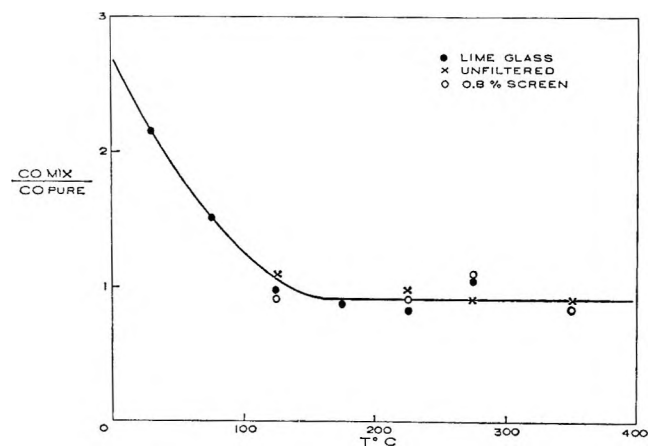


Figure 1. Ratio of rates of formation of CO from acetone (CO_{pure}) and a 10 ethane-1 acetone mixture (CO_{mix}) as a function of temperature.

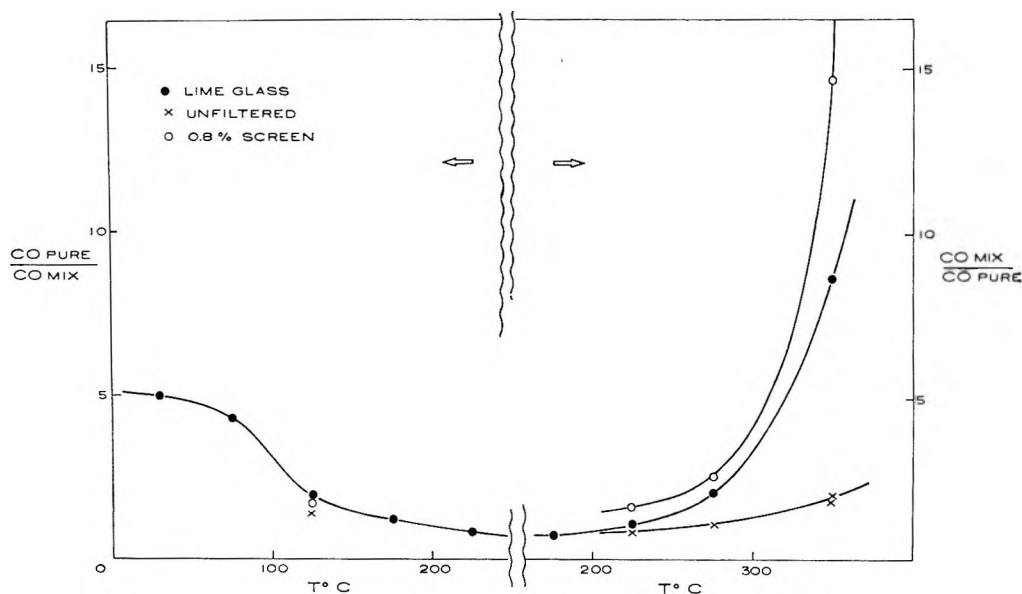


Figure 2. Ratio of rates of formation of CO from acetone (CO_{pure}) and a 10 ethene-1 acetone mixture (CO_{mix}) as a function of temperature.

effect of ethene, as that for ethane, decreases with temperature until about 125–150°, where there is no apparent effect. With increasing temperature a new phenomenon appears; the photo rate of CO production in the presence of ethene increases relative to the rate for pure acetone. When a lime glass filter is used, the effect of ethene on acetone photolysis is amplified so that at 350° the rate of CO production is eight times that for pure acetone at the same pressure as the acetone partial pressure in the mix; with unfiltered radiation the rate from the ethene-acetone mix is twice the pure acetone rate. Although this might argue for a wavelength effect, absorption spectra of the mixes showed no significant excess absorption at any wavelength in the presence of ethene in the temperature range of this study. The apparent inconsistency was resolved when it was recognized that the insertion of the lime glass

filter reduced the total actinic flux in addition to eliminating the shorter wavelengths. The hypothesis was tested by replacing the lime glass filter with a neutral density filter of stainless steel screen which transmitted 35% of the radiation. This increased the rate of CO production from twice that of pure acetone to over three times that for pure acetone under the same conditions. When a second stainless steel screen was inserted, giving an 85% overall reduction of intensity, the rate climbed to over five times the pure acetone rate under the same conditions, and for a screen with a transmission of 0.8% the ratio climbs to about sixteen. The results are characteristic of a chain reaction; the lower the flux the lower the steady-state radical concentration and the longer the chain length, since the chains are terminated by radical-radical reactions and carried by radical concentration to the first power.

The effect of temperature was not studied above 350° because ketene is a product of acetone photolysis at higher temperatures increasing markedly with temperature. This reactive product would be an added complication.

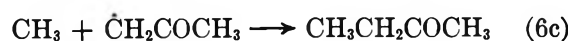
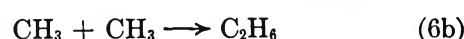
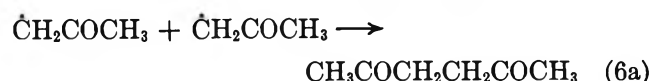
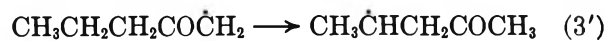
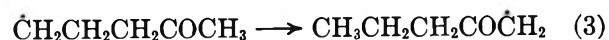
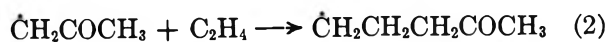
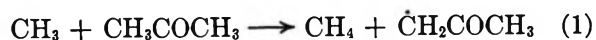
Since the quantum yield of CO from an acetone-ethene mix can be many times unity at 350°, a study of the effects of concentration, intensity, and surface was made at this temperature. The rate of CO produced was found to be moderately retarded by surface and independent of ethene concentration over a tenfold range (see Table I). The effect of light intensity and acetone concentration could be correlated with the amount of light absorbed as monitored by the rate of CO production from pure acetone at a pressure equal to the partial pressure of acetone in the acetone-ethene mix under the same experimental conditions.

Table I: Effect of Some Olefins on the Relative Quantum Yield of CO from Acetone Photolysis at 350°

$[\text{CO}]_{\text{mix}}/[\text{CO}]_{\text{pure}}$	$[\text{Acetone}]/\sqrt{R_{\text{CO pure}}}$ mol ^{1/2} sec ^{1/2}	$[\text{Acetone}]$, $M \times 10^{-3}$	Reaction mixt, ethene-acetone	Time, sec	Surface/vol	Rel intens
1.3	1.5	0.26	1	120	1.6	100
1.9	3.4	1.03	1	60	1.6	100
1.8	3.2	1.03	10	60	1.6	100
2.1	3.9	0.26	1	960	1.6	14
2.5	5.7	2.32	1	60	1.6	100
2.5	6.2	2.32	1	60	7.6	100
3.4	8.9	1.03	1	480	1.6	14
3.0	8.6	1.03	10	240	1.6	14
2.8	8.6	0.26	1	1800	1.6	L.G. ^a
5.6	14.3	2.32	1	30	1.6	14
5.3	14.1	2.32	1	60	1.6	14
4.6	14.3	2.32	1	240	1.6	14
5.2	17.8	1.03	1	600	1.6	L.G. ^a
7.3	28	2.32	1	300	1.6	L.G. ^a
6.5	29	1.03	10	420	1.6	1
8.7	33	1.03	10	420	1.6	1
6.0	32	1.03	10	1800	1.6	1
4.1	35	1.03	10	900	7.6	1
13	52	2.32	1	120	1.6	1
14	49	2.32	1	120	1.6	1
11	53	2.32	1	480	1.6	1
12	54	2.32	1	900	1.6	1
10	53	2.32	1	1800	1.6	1
7.7	57	2.32	1	900	7.6	1
15.7	50	2.32	10	90	1.6	L.G. ^a
15.3	52	2.32	10	90	1.6	L.G. ^a
13.5	50	2.32	0.1 propene- 10 ethene- 1 acetone	90	1.6	L.G. ^a
13.6	52	2.32	0.1 propene- 10 ethene- 1 acetone	90	1.6	L.G. ^a
			Propene-acetone			
1.9	52	2.32	1	120	1.6	1
1.4	54	2.32	1	960	1.6	1
1.3	54	2.32	5	960	1.6	1
9.2	57	2.32	9 He- 1 ethene- 1 acetone	300	7.6	1
12	45	2.32	1 CF ₃ CHCH ₂ - 1 acetone	960	1.6	1

^a L.G. = Lime glass filter.

The ratio of rates of CO production from the acetone-ethene mix to that from the same pressure of pure acetone, $\text{CO}_{\text{mix}}/\text{CO}_{\text{pure}}$, could be varied from a value slightly greater than 1 to a value of 16, depending on the partial pressure of the acetone in the mix and the light flux. A simple mechanism which is consonant with the observations may be formulated



Assume that reactions 3, 3', 4, and 5 are very rapid relative to reaction 2 (*i.e.*, $(\dot{\text{C}}\text{H}_2\text{COCH}_3) \gg (\dot{\text{C}}\text{H}_2\text{CH}_2\text{CH}_2\text{COCH}_3)$)

CH_2COCH_3) or its isomers). Then $R_{\text{CO mix}} = R_{\text{CO pure}} + k_2(\dot{\text{C}}\text{H}_2\text{COCH}_3)(\text{C}_2\text{H}_4)$ and dividing by $R_{\text{CO pure}}$

$$\frac{R_{\text{CO mix}}}{R_{\text{CO pure}}} = 1 + k_2(\dot{\text{C}}\text{H}_2\text{COCH}_3)(\text{C}_2\text{H}_4)/R_{\text{CO pure}}$$

where R = rate. At steady state

$$R_{(\text{CH}_3)} = 2R_{\text{CO pure}} = 2k_{6a}(\dot{\text{C}}\text{H}_2\text{COCH}_3)^2 + k_{6b}(\text{CH}_3)^2 + 2k_{6c}(\text{CH}_3)(\dot{\text{C}}\text{H}_2\text{COCH}_3)$$

where the factors of 2 multiplying the k 's take into account that two radicals are destroyed for each product molecule produced and

$$k_1(\text{CH}_3)(\text{CH}_3\text{COCH}_3) = k_2(\dot{\text{C}}\text{H}_2\text{COCH}_3)(\text{C}_2\text{H}_4) + 2k_{6a}(\dot{\text{C}}\text{H}_2\text{COCH}_3)^2 + k_{6c}(\text{CH}_3)(\dot{\text{C}}\text{H}_2\text{COCH}_3)$$

For long chains the propagation reactions 1 and 2 dominate those reactions which quench the acetyl radical 6a and 6c, so that

$$\frac{R_{\text{CO mix}}}{R_{\text{CO pure}}} = 1 + \frac{k_1(\text{CH}_3\text{COCH}_3)}{R_{\text{CO pure}}^{1/2} \left\{ k_{6b} + k_{6c} \frac{k_1(\text{CH}_3\text{COCH}_3)}{k_2(\text{C}_2\text{H}_4)} + k_{6a} \left[\frac{k_1(\text{CH}_3\text{COCH}_3)}{k_2(\text{C}_2\text{H}_4)} \right]^2 \right\}^{1/2}}$$

Our experiments at 350° show that (C_2H_4) concentration has no appreciable effect on the ratio $R_{\text{CO mix}}/R_{\text{CO pure}}$ over the range of C_2H_4 concentrations studied. To rationalize this observation with the mechanism, $k_2(\text{C}_2\text{H}_4)$ must be larger than $k_1(\text{CH}_3\text{COCH}_3)$. Thus

$$\frac{R_{\text{CO mix}}}{R_{\text{CO pure}}} \simeq 1 + \frac{k_1(\text{CH}_3\text{COCH}_3)}{R_{\text{CO pure}}^{1/2} k_{6a}^{1/2}}$$

As may be seen in Figure 3, the experimental points fall on a reasonably good straight line when plotted as a function of $R_{\text{CO mix}}/R_{\text{CO pure}}$ vs. $(\text{CH}_3\text{COCH}_3)/R_{\text{CO pure}}^{1/2}$. Since a range of almost 16-fold is encompassed by the experiments, the proposed mechanism is given some substantiation. The slope of the line in Figure 3, $k_1/k_{6a}^{1/2}$ is $0.3 \text{ l.}^{1/2} \text{ mol}^{-1/2} \text{ sec}^{-1/2}$, easily within the combined errors of this and other work² where $k_1/k_{6a}^{1/2}$ has been measured by a different technique in a lower temperature range. It should be noted that for values of $R_{\text{CO mix}}/R_{\text{CO pure}} \simeq 1$, the chain length is short. In this region, the assumption regarding the dominance of propagation over quenching is not valid. However, since the value 1 is a lower bound for $R_{\text{CO mix}}/R_{\text{CO pure}}$, deviations from the linear relationship indicated in Figure 3 due to this cause would not be detectable within the precision of the experimental values.

Endrenzi and LeRoy,³ in an analysis of the products of the same complicated system of acetone and ethene in a lower temperature range, come to the conclusion that the Arrhenius factors for addition of methyl and acetyl radicals to ethene are the same, even though the acetyl radical has some resonance energy. Our

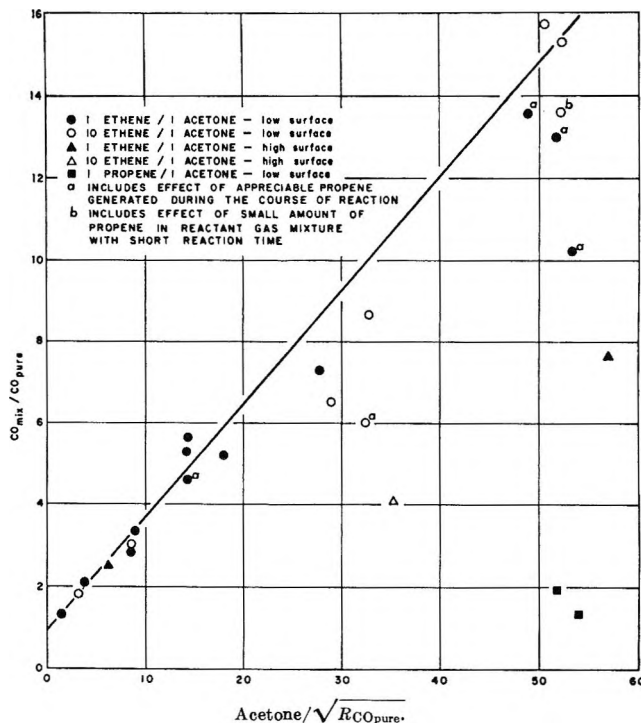


Figure 3. Effect of $[\text{acetone}]/[\text{rate CO formation in pure acetone}]^{1/2}$ on the relative rate of CO formation in acetone-olefin mixes at 350°.

experiments at 350° do not permit quantitative evaluation of the reaction of acetyl and ethene. Our only interpretation is that the acetyl radical adds rapidly to ethene and that the sequence of isomerization reactions and radical decompositions to form a molecule of CO and a methyl radical is so fast that all the intermediate radicals are held at relatively low steady-state concentration.

The simple mechanism proposed above assumes that methyl radical is the only alkyl radical in the chain. Actually, it has been shown⁴ that methyl radical in the presence of ethene at 350° sets up long chains in which n -propyl, and probably n -pentyl, and n -hexyl radicals are present in addition to methyl radicals. We assume all the alkyl radicals abstract H from acetone with the same specific rate constant. Work on methyl and n -propyl abstraction³ indicates that the energy of activation for abstraction of H is greater for methyl than for propyl radical while the A factor is less for propyl. The factors compensate to some extent, and at 350°, specific rate constants are probably the same within a factor of 5, with that for methyl being the larger.

The parallel reaction chain initiated by the addition of methyl radicals to ethene introduces considerable

(2) H. Shaw and S. Toby, *J. Phys. Chem.*, **72**, 2337 (1968); E. Whittle and E. W. R. Steacie, *J. Chem. Phys.*, **21**, 993 (1953).

(3) L. Endrenzi and D. J. LeRoy, *J. Phys. Chem.*, **71**, 1334 (1967).

(4) A. S. Gordon and J. R. McNesby, *J. Chem. Phys.*, **31**, 853 (1959).

complexity into the interpretation of the hydrocarbon products. However, propene has been observed to be a major product of the reaction as would be predicted by both chain mechanisms. The CO-producing mechanism predicts that

$$R_{\text{propene}} = R_{\text{CO}_{\text{mix}}} - R_{\text{CO}_{\text{pure}}}$$

We observe the propene rate to be at least tenfold the rate from the above relation, showing that the chain initiated by methyl adding to ethene is at least ninefold faster than the chain producing CO. This implies that methyl and other alkyl radicals are important chain carriers in the reaction and thus the proposed mechanism represents a considerable simplification.

It may be noted that some of the points in Figure 3 are considerably below the line. Propene has three easily abstractible hydrogens and can act as a chain quencher. The hypothesis was tested in three ways. (1) The same mixture was run for different lengths of time. As time increased the points fell further below the line. (2) Propene-acetone mixes (1:1 and 5:1) were run under conditions where ethene-acetone mixes would give $\text{CO}_{\text{mix}}/\text{CO}_{\text{pure}}$ ratios up to 14. The ratios were less than 2, independent of the mix ratio,

confirming that propene is a strong chain inhibitor in the system. (3) Ethene-acetone mixes containing a small amount of propene were run at short times under conditions where high $\text{CO}_{\text{mix}}/\text{CO}_{\text{pure}}$ ratios are found. A significant decrease in CO yield was observed.

The easily abstractible H atoms in propene were blocked by using 1,1,1-trifluoropropene in place of the propene. As may be seen by reference to Table I, a 1:1 mix produced a $\text{CO}_{\text{mix}}/\text{CO}_{\text{pure}}$ ratio very close to that for ethene-acetone. In addition, a 1,1,1-trifluorobutene was observed with a rate roughly equal to $R_{\text{CO}_{\text{mix}}} - R_{\text{CO}_{\text{pure}}}$. On the basis of the mechanism, the butene should be $\text{CF}_3\text{CH}_2\text{CH}=\text{CH}_2$, but isomeric identification was not attempted. Since propene has such a large effect on the $R_{\text{CO}_{\text{pure}}}/R_{\text{CO}_{\text{mix}}}$ ratio, the experimental values at even the shortest times are somewhat low and the slope of the experimental line is less than the true slope.

Most of the studies were made in a reaction vessel with a surface/volume = 1.6. In order to ascertain the effect of surface, some studies were made in a reaction with a $s/v = 7.6$. As may be noted in Table I and Figure 3, the bulk of such reactions show that the surface lowers the $\text{CO}_{\text{mix}}/\text{CO}_{\text{pure}}$ ratio, probably by acting as a radical trap.

Mechanism of Photodissociation of Hydroquinone Derivatives

by Hikoichiro Yamada, Nobuaki Nakashima, and Hiroshi Tsubomura

*Department of Chemistry, Faculty of Engineering Science, Osaka University, Toyonaka, Osaka, Japan
(Received January 21, 1970)*

The mechanism of the photodissociation of hydroquinone and some of its derivatives irradiated in the near-ultraviolet region in the matrix of ethanol at 77°K was studied by use of the electronic absorption spectra of these radicals. The dependences of the rates of radical formation on the light intensity and the effect of intermittent irradiation on the radical yield were investigated, and it was concluded that the side-chain photolysis of these compounds occurs through the biphotonic, two-step process *via* the lowest triplet state of the parent molecule. It was also concluded that these reactions may occur unimolecularly. A new procedure was proposed for the treatment of the intermittent irradiation data.

It is well known that the near-ultraviolet irradiation of benzene derivatives in rigid matrices produces two types of unstable species. One is the radical due to the fission at the β bond of the side chain,¹⁻³ and another is the cation due to the ejection of an electron into the matrix.⁴⁻⁸ One of the present authors has pointed out⁹ that these types of photochemical products from various aromatics are related with their ionization potentials, namely the photoionization is predominant for aromatics having low ionization potentials such as

tetramethyl-*p*-phenylenediamine, while photodissociation is predominant for aromatics having rather high ionization potentials such as anisole.

- (1) G. Porter and E. Strachan, *Trans. Faraday Soc.*, **54**, 1595 (1958).
- (2) E. J. Land, G. Porter, and E. Strachan, *ibid.*, **57**, 1885 (1961).
- (3) B. Brocklehurst, W. A. Gibbons, F. T. Lang, G. Porter, and M. I. Savadatti, *ibid.*, **62**, 1793 (1966).
- (4) G. N. Lewis and D. Lipkin, *J. Amer. Chem. Soc.*, **64**, 2301 (1942).
- (5) G. N. Lewis and J. Bigeleisen, *ibid.*, **65**, 520 (1943).

The photoionization of aromatics by the near-ultraviolet irradiation was studied by many authors since the work of Lewis,^{4,5} and it has been established that the photoionization generally occurs by two-step excitation with the lowest triplet state as the intermediate.⁶⁻⁸ The sensitized decomposition of aliphatic hydrocarbons and alcohols has also been studied by esr technique, and it has been concluded that it occurs by the energy transfer from higher triplet states of the solute (sensitizer) molecule excited by stepwise absorptions of two photons to the solvent molecule.¹⁰⁻¹² On the other hand, the details of the mechanism of the photodissociation of substituted benzenes is mostly unknown, although it has been shown that the dissociations of toluene² and triphenylmethane¹³ at 77°K require more than one photon when near-ultraviolet light is used, and in case of triphenylmethane the intermediate state may be its triplet state.¹³

The purpose of the present work is to elucidate the mechanism of side-chain photolysis of benzene derivatives. For this purpose, we have investigated the light-intensity dependence of the rates of radical formations from hydroquinone derivatives and the effect of intermittent irradiation on the radical yield. We have concluded that the side-chain photolyses of these compounds occur through the biphotonic, two-step process *via* the triplet state.

Experimental Section

Commercial materials of hydroquinone, hydroquinone monomethyl ether (MeOC₆H₄OH), hydroquinone dimethyl ether (MeOC₆H₄OMe), and hydroquinone dibenzyl ether (C₆H₅CH₂OC₆H₄OCH₂C₆H₅) were purified by recrystallization from ethanol followed by vacuum sublimations. Ethanol was used as rigid matrices throughout this work. It was purified by distillations. The matrix is transparent in the region from 250 to 800 m μ at 77°K. Each of the ethanol solutions was put into a quartz cylindrical cell, 15 mm in diameter, connected to a glass vacuum line through graded seal, and degassed by a series of freeze-pump-thaw cycles. Concentrations of samples were in the region of 1×10^{-2} to 4×10^{-4} M. The cell was immersed in liquid nitrogen contained in a partially unsilvered quartz Dewar. The irradiations were carried out with a 250-W high-pressure mercury lamp of Ushio Electric Co. The light intensity at the cell was changed quantitatively either by changing the distance between the cell and the lamp from 12 to 50 cm or by using various neutral filters made of wire mesh. In the former case, the light intensity incident upon the sample was calculated, taking account of the refractions by the Dewar and liquid nitrogen. The amount of the radical produced was determined by measuring the absorbance at the peak of one of the electronic absorption bands of the radical in the visible region. Elec-

tronic absorption spectra were measured with a Cary spectrophotometer Model 15.

The intermittent irradiation was carried out by using a rotating sector placed between the lamp and the sample and driven by various synchronous motors. The period of the irradiation was changed by the slit width of the rotating sector. The interval between irradiating periods was changed by the motor speed.

The T-T' spectrum and the phosphorescence spectrum of hydroquinone-monomethyl ether were measured with a Nalumi spectrometer (RM23) and Fuji Neopan SSS film (ASA 200) or recorded with an RCA 1P28 photomultiplier and Yokogawa LER 12 recorder. In the former case, the density on the film was measured with a Nalumi microphotometer NLM-7.¹⁴ The spectrum as shown in Figure 4 is not corrected for spectral sensitivity. Filters used were Toshiba UV-D25 glass filter (transparent from 250 to 380 m μ), an aqueous solution of nickel sulfate (NiSO₄·6H₂O (30 g)-H₂O (100 ml)), and an aqueous solution of nickel sulfate and cobalt sulfate (Ni·SO₄·6H₂O (13.8 g) + CoSO₄·7H₂O (4.2 g)-H₂O(100 ml)), which were put in 1-cm quartz cells.

Results and Discussion

Assignments of the Radical Spectra. The ultraviolet and visible spectrum of *p*-hydroxyphenoxyl radical (\cdot OC₆H₄OH) in viscous paraffin was detected by Porter, *et al.*, using the flash photolysis technique.¹⁵ Spectra of *p*-hydroxyphenoxyl radical and *p*-methoxyphenoxyl radical (\cdot OC₆H₄OMe) in ethanol were measured and assigned unambiguously by the low-temperature matrix technique in our laboratory.^{16,17}

In the present work, therefore, there was no problem to assign the spectra obtained by the photolyses of hydroquinone and hydroquinone-monomethyl ether in ethanol matrices at 77°K to \cdot OC₆H₄OH and \cdot OC₆H₄OMe, respectively. By the photolysis of hydroquinone-dibenzyl ether in ethanol at 77°K, the spectrum shown in Figure 1 was obtained. The peak at 318 m μ is

(6) J. Jousset-Dubien and R. Lesclaux, *Compt. Rend.*, **258**, 4260 (1964).

(7) K. D. Cadogan and A. C. Albrecht, *J. Chem. Phys.*, **43**, 2550 (1965).

(8) Y. Nakato, N. Yamamoto, and H. Tsubomura, *Bull. Chem. Soc. Jap.*, **40**, 2480 (1967).

(9) H. Tsubomura, *ibid.*, **42**, 3604 (1969).

(10) B. Smaller, *Nature*, **195**, 593 (1962).

(11) Kh. S. Bagdasar'yan, V. I. Muromtsev, and Z. A. Sinitsyna, *Dokl. Akad. Nauk SSSR*, **152**, 349 (1963).

(12) S. Siegel and K. Eisenthal, *J. Chem. Phys.*, **42**, 2494 (1965).

(13) Yu. I. Kozlov and D. N. Shigorin, *Dokl. Akad. Nauk SSSR*, **161**, 871 (1965).

(14) The details of the method of measuring the T-T' spectrum will be published.

(15) E. J. Land and G. Porter, *Trans. Faraday Soc.*, **59**, 2016 (1963).

(16) H. Tsubomura, K. Kimura, H. Yamada, and M. Kato, *Tetrahedron Lett.*, **47**, 4217 (1965).

(17) K. Kimura, K. Yoshinaga, and H. Tsubomura, *J. Phys. Chem.*, **71**, 4485 (1967).

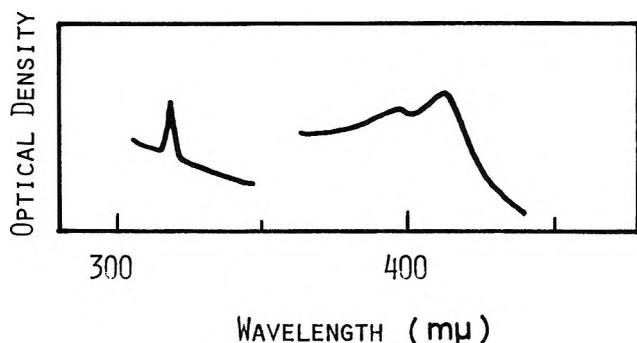


Figure 1. Electronic absorption spectrum of the species formed by near-ultraviolet irradiation of hydroquinone-dibenzyl ether in ethanol solution at 77°K.

assigned to the spectrum of benzyl radical, and the spectrum around 400 $m\mu$ may be assigned to that of the radical, $C_6H_5CH_2O-C_6H_4O\cdot$, from its resemblance with those of similar radicals.

Relation between Radical Yield and Intensity of Irradiation. If the aromatic molecules excited to the lowest singlet or the lowest triplet level change into the radical, the initial rate of formation of the radical should be proportional to the intensity of the absorbed light. On the other hand, if the radical is formed only from much higher levels derived by the stepwise absorptions of two photons, the initial rate of the radical formation should be proportional to the square of the light intensity. We can, therefore, decide the mechanism of photodissociation by studying the relation between the rate of radical formation and the intensity of exciting light.

For the ultraviolet irradiation experiments in low-temperature matrices, it frequently happens that the concentration of the molecules in the triplet state becomes so large that it cannot be neglected in comparison with that of the molecules in the ground state. If this occurs, the analysis of the observed results should be made by taking account of the steady-state concentration of the triplet molecules, leading to a considerable complexity of the procedure.¹⁸ Therefore, we first of all proved that the intensity of the phosphorescence of hydroquinone-monomethyl ether was proportional to the intensity of the exciting light. (As for the light intensity measurements, see Experimental Section.) This result confirmed that the concentration of the triplet molecules was negligible in our experimental condition. It seems reasonable to assume that the same situation will hold for other compounds studied in the present work.

The amounts of the radical formed [R] were then plotted as functions of time at various light intensities. As an example, some of the results obtained are shown in Figure 2. The initial slopes, that is, the initial rates of radical formation, were determined from the curves in the figure and were plotted against the light intensity (I) on a log-log section paper. If the points

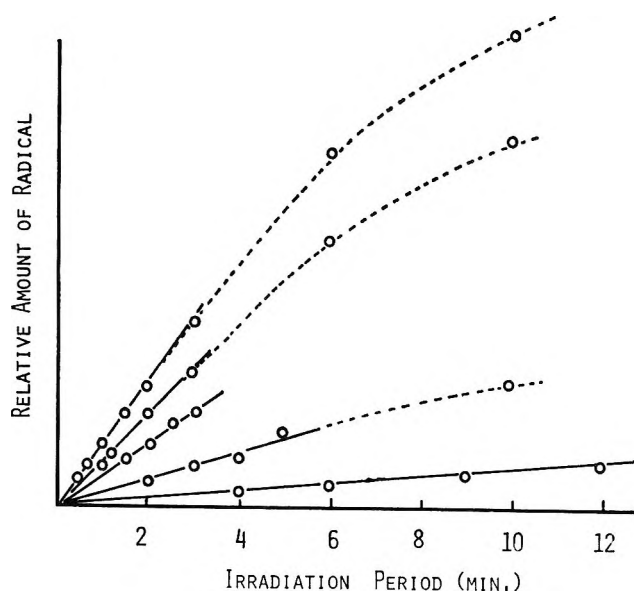


Figure 2. Relations between amounts of radical formed and period of irradiation at various light intensities, from which initial rates of radical formations were determined; hydroquinone-monomethyl ether ($1.5 \times 10^{-3} M$) in ethanol at 77°K, using aqueous $NiSO_4$ filter.

lie on a straight line whose slope is 2, the following equation should hold

$$(d[R]/dt)_{t=0} = \text{constant} \times I^2 \quad (1)$$

In that case, it should be concluded that the radical is formed by two-step excitation. On the other hand, if the radical is formed by one-step excitation, the experimental points should lie on a straight line whose slope is equal to 1.

In the case of hydroquinone-monomethyl ether without filter (case 1 in Table I), the plot of initial rates against the light intensities was not straight as shown in Figure 3a. In the case of using an aqueous nickel sulfate filter (case 2), the plot of the initial rates lay on a nearly straight line, and its slope was *ca.* 1.7. It was observed that the electronic absorption bands due to the radical were bleached by irradiation in the region of these bands. In view of this fact, the quantitative results obtained above may be explained by assuming that the radical is formed by the two-photon excitation of the parent molecule and some part of the radicals are decomposed by absorbing one photon in the region of its visible absorption bands. Thus the following equation is derived where a and b are con-

$$d[R]/dt = aI^2 - bI[R] \quad (2)$$

stants. By integrating (2) and introducing the initial condition $[R] = 0$ at $t = 0$, a general expression for [R] is obtained

$$[R] = (a/b)I\{1 - \exp(-bIt)\} \quad (3)$$

(18) J. P. Ray and T. D. S. Hamilton, *Nature*, **206**, 1040 (1965).

Table I: Dependences of the Initial Rates of Radical Formation on Intensities of Irradiation Lights

	Concentration of hydroquinone-monomethyl ether, M	Filter	Region of irradiation, $m\mu$	Slope
1	4.0×10^{-3}	None		Not straight Cf. Figure 3a
2	1.5×10^{-3}	Aqueous NiSO_4	200-350 and 420-570	1.6
3	1.5×10^{-3}	Aqueous $\text{NiSO}_4 + \text{CoSO}_4$ and UV-D25	290-330	2.0 Cf. Figure 3b
	Concentration of hydroquinone, M			
4	5.0×10^{-3}	Glass filter	300	1.0
5	1.5×10^{-3}	Aqueous NiSO_4	200-350 and 420-570	1.6

Curves in Figure 2 are found to conform well with this equation, if a and b are evaluated suitably.

By use of a combination of aqueous nickel sulfate and aqueous cobalt sulfate filters, the photodecomposition of the radical was found to be wholly prevented (case 3). The initial rates obtained in this case were plotted against light intensities as shown in Figure 3b. The experimental points lie on a straight line, whose slope turned out to be 2.0. From these results, it can be concluded that $(d[R]/dt)_{t=0}$ is proportional to I^2 ; in other words, the radical is formed by the biphotonic excitation.

In the case of irradiation of hydroquinone without filter, the initial rates fitted on a straight line whose slope was almost 1. Using an aqueous nickel sulfate filter, the slope became 1.7. It is, therefore, concluded that the photolysis of this compound also takes place by the biphotonic excitation.

In the case of hydroquinone-dimethyl ether, the quantum yield of radical formation was so small that it was impossible to obtain the rate of formation at weak exciting light intensity. It was, therefore, difficult to derive accurate relationship between light intensity and the initial rate of formation. However, the results obtained show that the dissociation is much more likely to be biphotonic than monophotonic.

We have confirmed, for the case of hydroquinone-monomethyl ether, that the initial rate of radical formation has been found to be constant at constant light intensity even if the concentration of the parent compound is changed from 4×10^{-4} to $4 \times 10^{-3} M$. One might point out that the proportionality of the initial rates of radical formation to I^2 found by us can be explained also by the assumption that the radicals are formed from singlet levels caused by the T-T annihilation process. If this would be true, the radical yield should depend on the rate of T-T annihilation and therefore on the concentration of triplet molecules.

The concentration of triplet molecules is a function of path length in the sample cell, and the slope should be steeper as the concentration of the parent molecules becomes higher. At a constant light intensity for excitation, the concentration of triplet molecule in the side of the light source becomes higher, and the amount of T-T annihilation product should be larger as a whole, the higher the concentration of the parent molecules. Based on the above result, the bimolecular reaction such as T-T annihilation can be excluded.

It is, therefore, concluded that the fission of the side chain of hydroquinone and its derivatives needs biphotonic stepwise excitation of a parent molecule.

The T-T' Spectrum of Hydroquinone-Monomethyl Ether. As described in the previous section, it is concluded that the photochemical formation of the radicals from hydroquinone and its derivatives in the low-temperature matrices is caused by two-step excitation. By analogy with the mechanism of photoionization, it is then easily conceivable that the most probable intermediate for such a two-step excitation is the lowest triplet state of substituted benzenes which have long lifetimes, mostly of the order of a few seconds at 77°K. As far as the authors are aware, there has been no report on the phosphorescence lifetimes of hydroquinone and its derivatives. We have, therefore, determined the phosphorescence lifetime of hydroquinone-monomethyl ether, and the result is 3.0 sec in ethanol solution at 77°K. Therefore, the concentration of the molecules in the triplet state should be sufficiently large during the irradiation so that the second-step excitation should occur to an appreciable degree.

We have also measured the T-T' absorption spectrum, that is, transitions from the lowest triplet state to higher triplet states, of hydroquinone-monomethyl ether in an ethanol matrix at 77°K as shown in Figure 4. The lifetime was also determined from the decay of

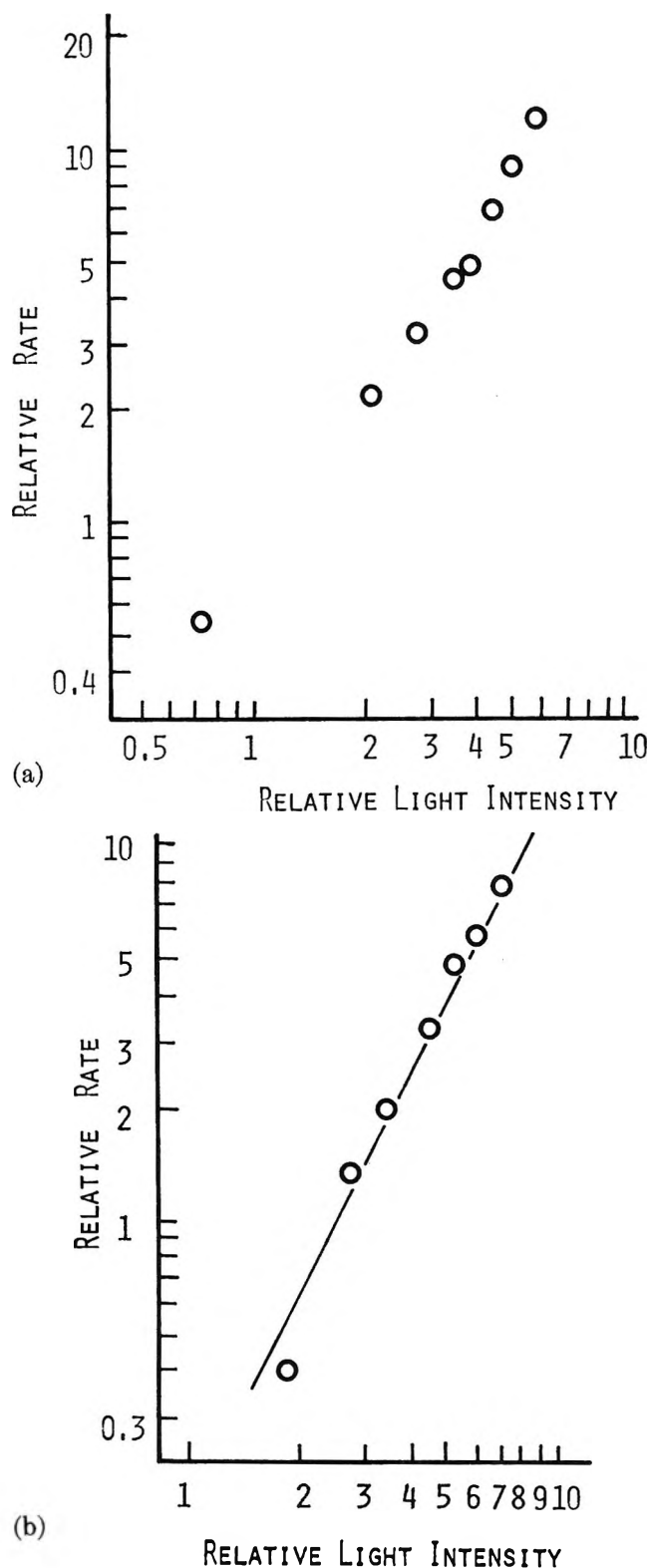


Figure 3. Plots of initial rates of radical formation against irradiation intensities; ethanol solutions of hydroquinone-monomethyl ether at 77°K: (a) $4.0 \times 10^{-3} M$, irradiated without filter; (b) $1.5 \times 10^{-3} M$, irradiated using aqueous NiSO_4 and CoSO_4 filter and Toshiba UV-D25 glass filter; the slope is 2.0.

absorption bands at each 10-m μ interval to be 2.9 ± 0.2 sec. This value agrees well with the phosphorescence

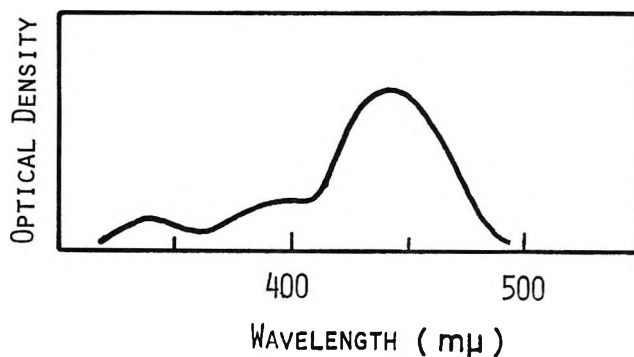


Figure 4. T-T' absorption spectrum of hydroquinone-monomethylether in ethanol at 77°K, excited through Toshiba UV-D25 glass filter.

lifetime and confirms the fact that the absorption bands are due to T-T' transition.

Generally speaking, a good way to prove the above-mentioned two-step excitation mechanism is to examine the effect of strong illumination in the region of the T-T' absorption bands (which alone has no photochemical effect on the parent molecule) on the yield of radical production of the sample irradiated in the near-ultraviolet region.^{6,13} In the present case, a part of the T-T' absorption spectrum lies in the same wavelength region as that of its radical, and unfortunately, the radical decomposes rapidly by the light in this region of wavelength. Therefore, such a cross-illumination technique is unapplicable for the present case.

Radical Formation by the Intermittent Irradiation. To obtain more definite information on the nature of the intermediate, we carried out the following experiment in which the radical yields were compared in the cases of continuous and intermittent irradiation. If the radical is produced by the two-step excitation as concluded above, the amount of radical formed should be proportional to the amount of light energy absorbed by the intermediate. This, in turn, should be proportional to the number of intermediates during the irradiation. The concentration $[C]$ of the intermediate formed in the period of irradiation with intensity I is given by the following equation, subject to $[C] = 0$ at $t = 0$

$$d[C]/dt = kI - [C]/\tau \quad (4)$$

where τ is the lifetime of the intermediate. Rigorously speaking, the first term should not be expressed as kI , k being a constant, but should depend on the concentration of the parent compound which may change considerably by the irradiation. In the present experimental condition, however, the concentrations of the triplet intermediate and final radical product are negligibly small compared with that of the parent compound, and hence, k may be taken as a constant throughout. Integrating eq 4, we have

$$[C] = kI\{1 - \exp(-t/\tau)\} \quad (5)$$

This equation means that it needs a period of time of the order of τ for the concentration of the intermediate to reach almost an equilibrium value. It is, therefore, easily understood that the amount of radical formed by an intermittent irradiation is different from that by continuous irradiation, even if the total period of irradiation is made the same for both cases. For the case of intermittent irradiation, the sample was irradiated for a period T (0.1 to 2.0 sec) and the light was shut off for a period (10 to 20 sec) which is sufficiently larger than τ so that no accumulation of the triplet molecules takes place. If such an intermittent irradiation was carried out for m times, the total period of irradiation is mT . We define $[R_{\text{int}}]$ as the yield of radical formed by such an intermittent irradiation, and $[R]$ as that by a continuous irradiation for the same total period mT . For the case where the rate of decomposition of radical is negligibly small compared to the rate of formation of radical, we have

$$d[R]/dt = k'I[C] \quad (6)$$

where $[C]$ is given by eq 5. Substituting $[C]$ expressed in eq 5 into eq 6 and integrating the latter, with the condition that $[R] = 0$ at $t = 0$, leads to the following equations

$$[R_{\text{int}}] = \tau^2 m k k' I^2 \{ T/\tau + \exp(-T/\tau) - 1 \} \quad (7)$$

$$[R] = \tau^2 k k' I^2 \{ mT/\tau + \exp(-mT/\tau) - 1 \} \quad (8)$$

From these equations, the general expression for the ratio $[R]/[R_{\text{int}}]$ is obtained. The dependences of

$$[R]/[R_{\text{int}}] = \frac{mT/\tau + \exp(-mT/\tau) - 1}{m\{T/\tau + \exp(-T/\tau) - 1\}} \quad (9)$$

$[R]/[R_{\text{int}}]$ on T/τ at various m values are shown in Figure 5, by use of which τ can be determined from experimental values of $[R]/[R_{\text{int}}]$ at given values of m and T . This method of the intermittent irradiation described here is superior to the method proposed by Bagdasar'yan, *et al.*,¹⁹ in that the former is based on more appropriate assumptions.

In the case of hydroquinone-monomethyl ether, the value of τ is obtained to be 2.8 ± 0.2 sec. This value, within the limit of experimental security, agrees with the value of the lifetime of its phosphorescence which was measured with the same sample as that used in this work (3.0 sec). This result should be considered as a verification of two-photon process for the radical formation *via* the intermediate of the lowest triplet state of the parent molecule.

In the preceding discussions, it has been tacitly assumed that the photodissociation is undergone unimolecularly. Vinogradova, *et al.*,²⁰ on the other hand, proposed that the dissociation of toluene in the matrix is caused by the energy transfer from the higher triplet state of toluene to the solvent molecule followed by the dissociation of the latter and hydrogen abstraction from

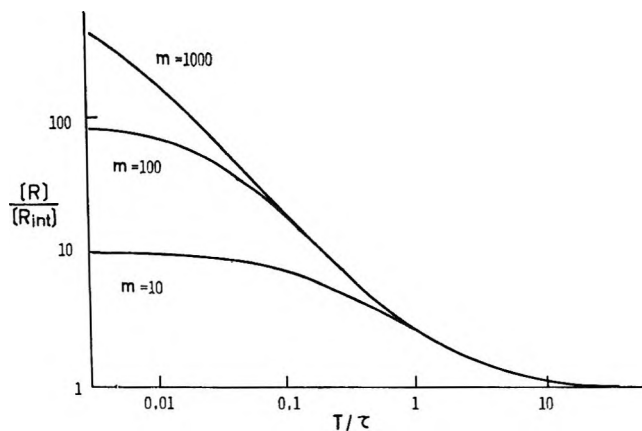
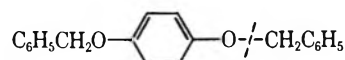


Figure 5. Dependences of $[R]/[R_{\text{int}}]$ on T/τ at three m values.

toluene. Rice, *et al.*,²¹ reported that photodissociation of xylene occurs in the argon matrix and concluded that its reaction is unimolecular.

To settle the question whether the photodissociation of substituted benzenes is caused by bimolecular or unimolecular process, we have studied the photodissociation of hydroquinone-dibenzyl ether in an ethanol matrix at 77°K . As the result, the characteristic absorption band of benzyl radical was obtained at $318\text{ m}\mu$, in addition to a spectrum which is similar to those of other phenoxy-type radicals (Figure 1). The initial rates of formations of these radicals were proportional to the square of the light intensity. This result shows that the photodissociation is from a higher triplet state and one of the O-C bonds of hydroquinone-dibenzyl ether is dissociated from the parent compound as shown below because the attack of a hydrogen atom or



any fragment radical from the solvent molecule on this compound should never lead to the result obtained. Hence, it may be concluded that the photolyses in this work are unimolecular reactions.

The dissociation energy of the OH bond of hydroquinone derivatives may be estimated to be of the order of 4.0 to 4.5 eV, based on that of water, 5.2 eV²² and taking account of the resonance stabilization of the radical. The lowest excited singlet states (S) of these compounds have the energy of *ca.* 4.0 eV. Thus it is hard to conclude whether the O-H bond photodissociation directly from the S state is energetically forbidden. The present results definitely indicate that the photodissociation from the S state does not occur and takes

(19) Kh. S. Bagdasar'yan, Z. A. Sinitsyna, and V. I. Muromtsev, *Dokl. Akad. Nauk SSSR*, **153**, 374 (1963).

(20) V. G. Vinogradova, B. N. Sheimov, N. V. Fok, and V. V. Voevodskii, *ibid.*, **154**, 188 (1964).

(21) P. M. Johnson and S. A. Rice, *Chem. Phys. Lett.*, **1**, 309 (1968).

(22) L. Pauling, "The Nature of the Chemical Bond," 3rd ed, Cornell University Press, Ithaca, N. Y., 1960, p 85.

place only from much higher energy levels. The higher excited triplet state which is concluded by us to undergo dissociation may be estimated to have a range of energy of 7.3 to 6.0 eV (3.3 eV for the lowest triplet state and 2.7 to 4.0 eV for the second transition in our experimental condition), which is much higher than its

dissociation energy, but is short of its ionization energy, *ca.* 8 eV estimated from anisole's 8.20 eV.²³ The mechanism concluded in the present paper, therefore, seems reasonable from the energetic point of view.

(23) K. Watanabe, *J. Chem. Phys.*, **26**, 542 (1957).

Studies on the Molecular Hydrogen Formation (G_{H_2}) in the Radiation Chemistry of Aqueous Solutions

by E. Peled and G. Czapski

Department of Physical Chemistry, The Hebrew University, Jerusalem, Israel (Received November 17, 1969)

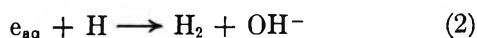
G_{H_2} in the γ radiolysis of air-free 0.01, 0.1, and 1 *M* solutions of various cations and anions were measured. The rate constants of most of these ions with e_{aq} at different ionic strength were directly determined by the pulse radiolysis technique. The effect of ionic strength on spurs reactions and on scavenging efficiency was studied. Difficulties previously observed, concerning the lack of correlation between $k_{e_{aq}+s}[S]$ and the scavenging efficiency of G_{H_2} were shown to be mainly due to ionic strength effects on $k_{e_{aq}+s}$. Hence it is concluded that e_{aq} is the main precursor of G_{H_2} through the reactions: $e_{aq} + H$ and $e_{aq} + e_{aq}$. It is suggested that $G^{\circ}_{H_2}$ and G°_H (which were proposed by Schwarz to be formed directly) result from spurs which are characterized by initially higher radical concentrations.

The irradiation of many aqueous systems has shown that hydrogen, with a yield of about 0.45, is formed as a molecular product.¹ When the concentration of some of the solutes in such systems is increased, a decrease in the molecular yield may be observed. This behavior is attributed to partial scavenging of the precursors of the molecular hydrogen by the solutes. It is generally accepted that molecular hydrogen is formed in the spurs following the recombination of its precursors.¹ The detailed mechanism of the formation of H_2 raises several questions. (1) Which are the precursors? (2) Which are the exact spur recombination reactions responsible for the molecular yield? (3) Is the entire molecular yield due only to spur recombination reactions, and is its total scavenging possible?

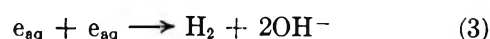
During the very early stages of the study of radiation chemistry of aqueous solutions, it was assumed that OH and H radicals were formed in spurs so that the origin of molecular H_2 was attributed to the following reaction¹



Later, however, it was shown that most of the reducing species are e_{aq} rather than H atoms and other reactions were assumed.



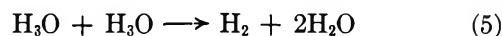
and



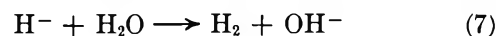
In addition, H atoms are formed at least partially in the spurs through



Sworski² suggested the existence of a short-lived H_3O in the spurs, rather than H or e_{aq} and this species is the precursor of H_2 . Accordingly, H_2 would be formed by the reaction



Other suggested sources for H_2 were excited water molecules³ or hydride ions⁴



(1) (a) J. W. T. Spinks and R. J. Woods, "An Introduction to Radiation Chemistry," Wiley, New York, N. Y., 1964; (b) A. O. Allen, "The Radiation Chemistry of Water and Aqueous Solutions," Van Nostrand, Princeton, N. J., 1961.

(2) T. J. Sworski, *Advance in Chemistry Series*, No. 50, American Chemical Society, Washington, D. C., 1965.

(3) M. Anbar, S. Guttmann, and G. Stein, *J. Chem. Phys.*, **34**, 703 (1961).

(4) M. Faragi and J. Desalos, *Int. J. Radiat. Phys. Chem.*, **1**, 335 (1969).

Hayon⁵ suggested that reaction 3 is the main source of H_2 , with some possible additional contribution from reactions 1 and 2. His conclusion was based on the plot of $G(H_2)$ as a function of $[S]^{1/3}$ which exhibits a break in the straight line. Furthermore, Hayon and Moreau⁶ claimed a good agreement between $k_{e_{aq^+s}}$ and the reduction of G_{H_2} at low scavenger concentrations while better correlation was found for the rate constants k_{H+S} at high solute concentrations.

According to Faragi and Desalos,⁴ there is no correlation between $k_{e_{aq^+s}}$ and the efficiency of the decrease of G_{H_2} . In order to bring a little more light to the mechanism of formation of molecular hydrogen and to determine the source of G_{H_2} , we have taken up once again the study of the effect of certain scavengers on G_{H_2} .

Experimental Section

Materials. All solutions were prepared with triple-distilled water. Materials were all of analytical grade and were used without further purification.

Dosimetry. A Fricke dosimeter served to determine the dose rates, taking $G(Fe^{3+}) = 15.5$. The absorbed dose in concentrated solutions was corrected according to the relative electron density of the solutions.

$G(H_2)$ Determination. Irradiations were carried out in a ^{137}Cs γ source. The dose rates were either 200 or 80 rads/min. Total doses amounted to 25,000–80,000 rads. All solutions were argon-saturated, and irradiated in 10-cm³ syringes. Gas products were determined by gas chromatography, the detailed method of which was described earlier.⁷ All the $G(H_2)$ yields were found to be linear with dose, and the G values are averages of 4–10 measurements.

Determination of $k_{e_{aq^+s}}$. The rate constants of e_{aq} with different scavengers as a function of ionic strength (μ), were determined by pulse radiolysis.

A Varian V-7715 linear accelerator gave 5-MeV electron pulses, with 200 mA current. The pulse length was 0.1–0.15 μ sec.

The irradiation cell, made of Spectrosil, was 4 cm long. The analyzing light was from a 150-W xenon arc passing three times through the cell. Details of the experimental assembly are given elsewhere.⁸

Results and Discussion

Molecular hydrogen yields were measured in irradiated 0.01, 0.1, and 1 M aqueous solutions of various solutes. The $G(H_2)$ values were corrected according to the electron density of the solutions.

Br^- (10^{-3} M) was added to all solutions in order to protect the molecular hydrogen from attack of OH radicals. When silver salts were used, 10^{-3} M NO_2^- was added instead of bromide.

Effect of Cations on G_{H_2} . Table I⁹ and Figure 1 show the effect of various cations (which contained 10^{-3} M NO_3^- or 10^{-3} M NO_2^-) on G_{H_2} . We found that the

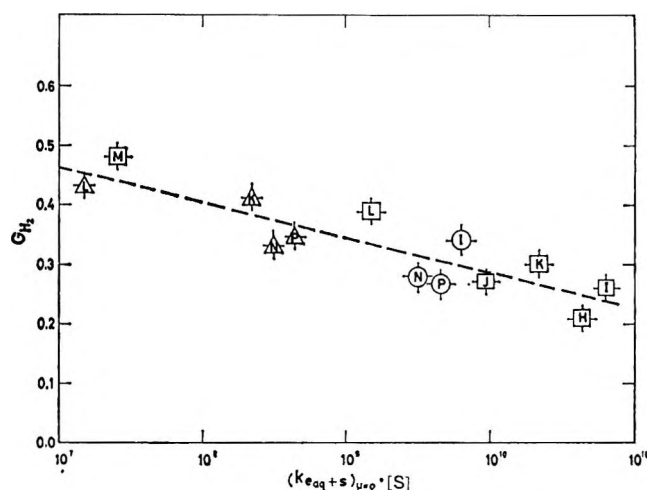


Figure 1. G_{H_2} as a function of $k_{e_{aq^+s}}[S]$ for cationic scavengers. Values of $k_{e_{aq^+s}}$ are taken for $\mu = 0$, from Table I: H, $CuSO_4$; L, $CdSO_4$; J, $Co(ClO_4)_2$; K, $NiSO_4$; L, $ZnSO_4$; M, $MnSO_4$; N, $AgClO_4$; P, $Cu(ClO_4)_2$; \square , 1 M; \circ , 0.1 M; \triangle , 0.01 M.

Table I: G_{H_2} as a Function of Different Cations

Solutes, M	G_{H_2}	$(k_{e_{aq^+s}})_{\mu=0}$, ^a $M^{-1} \text{ sec}^{-1}$	k_{H+S} , ^b $M^{-1} \text{ sec}^{-1}$	pH
1.0 $CuSO_4$	0.21	4.5×10^{10}	6×10^8	3.4
1.0 $CdSO_4$	0.26	6.4×10^{10}	$<10^5$	4.4
1.0 $Co(ClO_4)_2$	0.27	9.5×10^9		4.0
1.0 $NiSO_4$	0.30	2.2×10^{10}	$<10^5$	3.7
1.0 $ZnSO_4$	0.39	1.5×10^9 ^b	$<10^5$	4.3
1.0 $MnSO_4$	0.48	$(4-8) \times 10^7$ ^b	2.5×10^7	3.7
0.1 $Cu(ClO_4)_2$	0.27	4.5×10^{10}	6×10^8	4
0.1 $CdSO_4$	0.34	6.4×10^{10}	$<10^5$	4.5
0.01 $AgClO_4$	0.33	3.2×10^{10}	1.15×10^{10}	4
0.01 $CuSO_4$	0.35	4.5×10^{10}	6×10^8	4
0.01 $NiSO_4$	0.41	2.2×10^{10}	$<10^5$	4
0.01 $ZnSO_4$	0.435	1.5×10^9 ^b	$<10^5$	4.5
0.01 $Cu(ClO_4)_2$	0.35	4.5×10^{10}	6×10^8	4
1.0 $ZnSO_4$ ^c	0.75	1.5×10^9 ^b	$<10^5$	4.3
1.0 $MnSO_4$ ^c	0.70	$(4-8) \times 10^7$ ^b	2.5×10^7	3.7

^a Measured values. ^b Reference 9. ^c These solutions did not contain 10^{-3} M NO_3^- or 10^{-3} M NO_2^- .

addition of 10^{-3} M NO_3^- or 10^{-3} M NO_2^- to the irradiated solutions of Zn^{2+} , Mn^{2+} , Ni^{2+} , and Co^{2+} lowered the G_{H_2} values in comparison to solutions which did not contain NO_3^- or NO_2^- . (The role of either NO_2^- or NO_3^- is to react with M^{+10} to prevent any other reactions of M^+ which may yield H_2 .) For

(5) E. Hayon, *Nature*, **194**, 737 (1962).

(6) E. Hayon and M. Moreau, *J. Phys. Chem.*, **69**, 4058 (1965).

(7) G. Czapski and E. Peled, *Isr. J. Chem.*, **6**, 421 (1968).

(8) Internal report of Accelerator Laboratory, Hebrew University, Jerusalem, Israel.

(9) M. Anbar and P. Neta, *Int. J. Appl. Radiat. Isotop.*, **18**, 493 (1967).

(10) D. Meyerstein and W. A. Mulac, *J. Phys. Chem.*, **72**, 784 (1968).

example, in irradiated solutions of 1 M Zn²⁺ or 1 M Mn²⁺ $G_{H_2} \approx 0.7$ was measured, while the addition of 10⁻³ M NO₃⁻ to the same solutions gave $G_{H_2} = 0.39$ and 0.48, respectively. The addition of 10⁻³ M NO₃⁻ to Cu²⁺ or Cd²⁺ solutions did not affect the H₂ yield.

It can be seen that cations which are characterized by similar rate constants with e_{aq} either increase G_{H_2} as in the case of Mn²⁺, or reduce the value of G_{H_2} with different efficiencies. Thus for example Cu²⁺ is more efficient than Cd²⁺ in reducing G_{H_2} , although it reacts slower with e_{aq} .

These anomalies may be due to several reasons: the small efficiency of Cd²⁺, Co²⁺, Zn²⁺, and of Ni²⁺ in reducing G_{H_2} , and the increase of G_{H_2} by Mn²⁺ (and Zn²⁺ in the absence of NO₃⁻) may well result from the reactions either of the reduced form of the metal ion M⁺ or of the neutral atoms in the spurs and/or in the bulk. There is also the possibility that the monovalent ions form back e_{aq} (as was shown to occur for water decomposition by U³⁺¹¹), which would lead to a decrease of efficiency in reducing G_{H_2} . Metal atoms may form again, e_{aq} and/or H, or lead to the direct formation of H₂ through reaction with water: $M^0 + 2H_2O \rightarrow H_2 + 2OH^- + M^{2+}$ which will result in an increased H₂ yield. (This reaction is probably the way Raney nickel reacts.) These possible reactions fit in with the lack of deposition of metal in irradiated solutions which contain ions like Zn²⁺, etc., even though these ions are reduced by e_{aq} .

As can be seen in Table I and Figure 1, all these cations (except Mn²⁺) decrease G_{H_2} in the presence of M⁺ scavengers. Meyerstein¹² reported similar effects of these cations. Faragi and Desalos⁴ reported the same results for Cd²⁺ and Cu²⁺ solutions but higher values of G_{H_2} for Ni²⁺, Co²⁺, and Zn²⁺ solutions. This seems to result from the absence of M⁺ scavengers (such as NO₂⁻ or NO₃⁻) in their experiments.

Even in the presence of 10⁻³ M NO₃⁻, Ni²⁺, Co²⁺, Cd²⁺, and Zn²⁺ reduce G_{H_2} less efficiently than Cu²⁺ or Ag⁺ (at similar values of $k_{e_{aq}+s}[S]$). The higher yields in solutions of Cd²⁺, Zn²⁺, Ni²⁺, and Co²⁺ can be rationalized by the following scheme: M⁰ is formed in the reactions $2M^+ \rightarrow M^{2+} + M^0$ and by $M^+ + e_{aq} \rightarrow M^0$. The addition of 10⁻³ M NO₂⁻ or NO₃⁻ competes with these reactions in the bulk but not necessarily in the spurs, while in the case of Ag⁺ and Cu²⁺, neither M⁰ nor M⁺ yield H₂ or H. Thus, for these cations one can not expect full correlation between $k_{e_{aq}+s}$ and the efficiency in reducing G_{H_2} .

Another possible reason for the high H₂ yield in Mn²⁺ solutions is that its reactivity towards OH radicals in the spurs may lead to reduction in the back reaction $e_{aq} + OH$ and thus leave more e_{aq} in the spurs which may form more H₂.

The Efficiency in Reducing G_{H_2} by Different Solutes. The G_{H_2} values given in Table I and in Table II are plotted as a function of $\log(k_{e_{aq}+s}[S])$ in Figures 1-3.

Table II: Scavenging Effects of Anions and Neutral Molecules on G_{H_2}

Solutes, ^a M	G_{H_2} , ^c	$(k_{e_{aq}+s})_{\mu=0}$, ^c M ⁻¹ sec ⁻¹	k_{h+s} , ^d M ⁻¹ sec ⁻¹
1.0 Na ₂ Cr ₂ O ₇	0.026	6.0×10^{10}	1.8×10^{10}
1.0 Na ₂ CrO ₄	0.044	1.8×10^{10}	1×10^{10}
1.0 NaNO ₃	0.094	1.05×10^{10}	1×10^7
1.0 NaBrO ₃	0.12	3.4×10^9	2×10^7
1.0 Na ₂ S ₂ O ₃	0.23	6×10^8 ^d	
1.0 H ₂ O ₂	0.19 ^b	1.2×10^{10} ^d	$(5-9) \times 10^7$
1.0 Acrylamide	0.12 ^b	$(1.8-3.3) \times 10^{10}$ ^d	
0.1 Na ₂ Cr ₂ O ₇	0.16	6.0×10^{10}	1.8×10^{10}
0.1 Na ₂ CrO ₄	0.193	1.8×10^{10}	1×10^{10}
0.1 NaNO ₃	0.26	1.05×10^{10}	1×10^7
0.1 KIO ₃	0.275	8.5×10^9	5.9×10^7
0.1 NaBrO ₃	0.315	3.4×10^9	2×10^7
0.1 H ₂ O ₂	0.31 ^b	1.2×10^{10} ^d	$(5-9) \times 10^7$
0.1 Acrylamide	0.23 ^b	$(1.8-3.3) \times 10^{10}$ ^d	
0.01 Na ₂ Cr ₂ O ₇	0.294	6.0×10^{10}	1.8×10^{10}
0.01 NaCrO ₄	0.317	1.8×10^{10}	1×10^{10}
0.01 NaNO ₃	0.357	1.05×10^{10}	1×10^7
0.01 KIO ₃	0.37	8.5×10^9	5.9×10^7
0.01 NaBrO ₃	0.39	3.4×10^9	2×10^7
0.01 Na ₃ Fe(CN) ₆	0.356	3×10^9 ^d	4×10^9
0.01 H ₂ O ₂	0.38 ^b	1.2×10^{10} ^d	$(5-9) \times 10^7$
0.01 Acrylamide	0.33 ^b	$(1.8-3.3) \times 10^{10}$ ^d	

^a Neutral pH. ^b Interpolated values, ref 6. ^c Measured values (this work). ^d Reference 9.

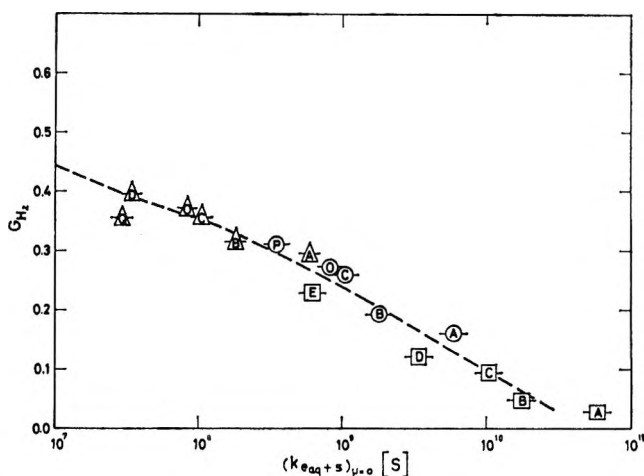


Figure 2. G_{H_2} as a function of $k_{e_{aq}+s}[S]$ for anionic scavengers. Values of $k_{e_{aq}+s}$ are taken for $\mu = 0$, from Table II: A, Na₂Cr₂O₇; B, Na₂CrO₄; C, NaNO₃; D, NaBrO₃; E, Na₂S₂O₃; O, KIO₃; Q, Na₃Fe(CN)₆; -E, 1 M; -Q, 0.1 M; -A, 0.01 M.

It appears from these figures that for neutral molecules, cations and anions, in each group, there is a correlation between the rate constant of e_{aq} with the solute, and efficiency in the reduction of G_{H_2} . However, when all three groups are compared, a big difference is found (see Figure 4) between positive ions, negative ions, and

(11) D. C. Walker, *Can. J. Chem.*, **44**, 2226 (1966).

(12) D. Meyerstein, Ph.D. Thesis.

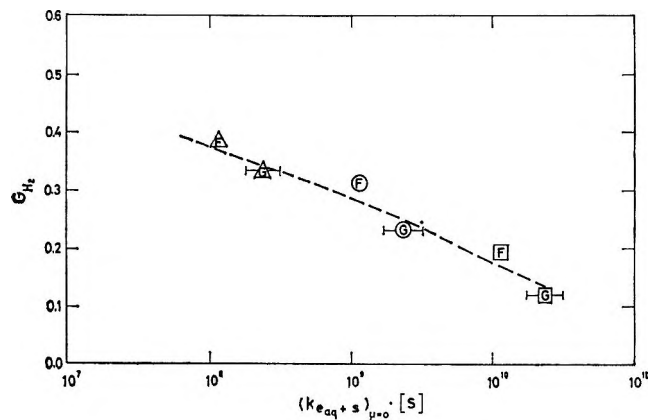


Figure 3. G_{H_2} as a function of $k_{e_{aq}+s}$ for uncharged scavengers. $k_{e_{aq}+s}$ are taken from Table II: G, acrylamide; F, H_2O_2 ; \square , 1 M; \circ , 0.1 M; Δ , 0.01 M.

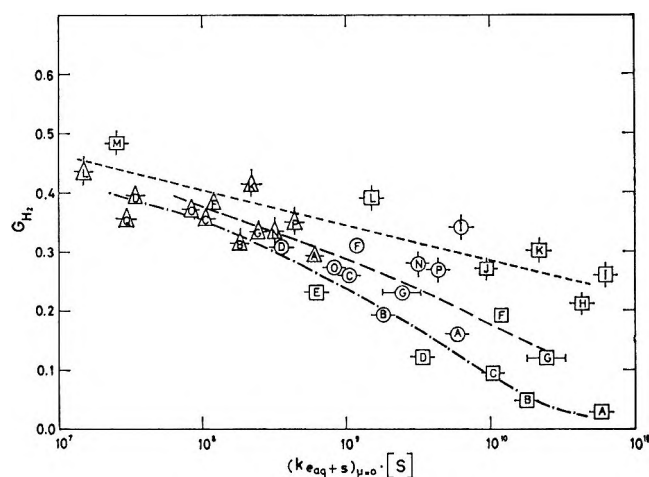


Figure 4. G_{H_2} as a function of the product $k_{e_{aq}+s}$ for $\mu = 0$, for all kind of scavengers. The notation of the scavengers is the same as for Figures 1-3 (upper line, cations; middle line, neutral molecules; lower line, anions).

neutral molecules. The efficiency decreases according to the order: anions, neutral molecules, and then cations. For example, Co^{2+} , H_2O_2 , and NO_3^- have rate constants of about $10^{10} M^{-1} sec^{-1}$ when reacting with e_{aq} . In 1 M solutions of NO_3^- , H_2O_2 , and Co^{2+} , the values of G_{H_2} recorded are 0.094, 0.19, and 0.27, respectively. This behavior will be discussed later.

Ion Pair Formation. At first glance, it could be assumed that the relative inefficiency of $CuSO_4$, $CdSO_4$, $NiSO_4$, and of $CoSO_4$ to reduce G_{H_2} when compared to other solutes possessing the same reactivity characteristics with e_{aq} , results from ion-pair production of these cations with SO_4^{2-} . The association constant of all these cations is about 2.5×10^{-2} .¹³ Thus in 1 M solutions, there would be only about 6% dissociation. Hence, if the reactive species involves only the free ion,¹⁴ this would explain the inefficiency of the solutes at high concentrations. To test this possibility, we compared G_{H_2} yields of 0.1 M $Cu(ClO_4)_2$ and 0.1 M

$CdSO_4$ solutions with, and without the addition of 0.8 M Na_2SO_4 (Table III). The results showed that adding 0.8 M Na_2SO_4 to the solutions did not affect the scavenging efficiency while the free metal ion concentration decreased from 0.1 M Cu^{2+} or 0.02 M Cd^{2+} to 4×10^{-4} M in these solutions. This means that the scavenging efficiency of the ion pair ($Cu^{2+}SO_4^{2-}$) and ($Cd^{2+}SO_4^{2-}$) is about the same as that of the free ions.

Table III: Effect of Association of Cations to Ionic Pair on G_{H_2}

Solutes, M	Added inert salt, M	G_{H_2}
0.1 $CdSO_4$...	0.34 ± 0.01
0.1 $CdSO_4$	0.8 Na_2SO_4	0.33 ± 0.01^a
0.1 $Cu(ClO_4)_2$...	0.27 ± 0.01
0.1 $Cu(ClO_4)_2$	0.8 Na_2SO_4	0.27 ± 0.005^a

^a These values are corrected to the increase in dose due to increase in electron density.

Effects of Ionic Strength. The line of reasoning followed till now does not explain the difference in G_{H_2} reducing efficiency between the cations and the neutral molecules and the anions.

A possible reason for the different efficiency of these groups in scavenging G_{H_2} may be due to the effect of ionic strength on the rate of the reaction of e_{aq} with these scavengers.

The Dependence of Rate Constants of Ionic Reactions on the Ionic Strength

The rate constant of a reaction between ions of charge Z_A and Z_B is found to follow the equation

$$\log \frac{k}{k_0} = \frac{Z_A Z_B \sqrt{\mu}}{1 + \alpha \sqrt{\mu}} \quad (I)$$

(where k and k_0 are the values of the rate constant at a given ionic strength and zero ionic strength, respectively.)

Where solutions at higher ionic strength are concerned, this equation should be modified as follows¹⁵

$$\log \frac{k}{k_0} = \frac{Z_A Z_B \sqrt{\mu}}{1 + \alpha \sqrt{\mu}} - 0.2\mu \quad (II)$$

These equations are based on the assumption that $\tau_{1/2}$ of the reaction is long, compared to the relaxation time of the ionic atmosphere of the reacting species. In other words, the ionic atmosphere is built up around the reacting species before the reaction starts.

(13) C. W. Davies, "Ion Association," Butterworths, Washington, D. C., 1962.

(14) H. A. Schwarz, *J. Amer. Chem. Soc.*, **77**, 4960 (1955).

(15) C. W. Davies, *J. Chem. Soc.*, 2093 (1938).

Logan¹⁶ was able to show that in such reactions, when only one of the reacting species has an ionic atmosphere, the effect of ionic strength can vary but does not disappear.

The change of $k_{e_{aq}+I_3^-}$ as a function of μ has been shown to depend on $\tau_{1/2}$ of e_{aq} .¹⁷ When $\tau_{1/2}$ becomes small when compared to the relaxation time of the ionic atmosphere around e_{aq} , the rate constant was found experimentally to be only about 60% of the rate constant observed when conditions of full relaxation were achieved.¹⁷

It would be of interest to find out the relaxation times of e_{aq} under different experimental conditions, and thus be able to estimate the ionic strength effect in spur scavenging and spur recombination reactions.

The relaxation time of the ionic atmosphere of monovalent electrolytes in aqueous solutions is given by¹⁸

$$\tau_{relax} = \frac{7.1 \times 10^{-9}}{\mu(\Lambda^+ + \Lambda^-)} \text{ (sec)} \quad (III)$$

where Λ are the equivalent conductance of the monovalent cation and anion, and μ is the ionic strength.

The half-life time of the reaction $e_{aq} + e_{aq} \rightarrow H_2$ in the spur in the absence of solutes is given by

$$\tau_{1/2}(e_{aq} + e_{aq}) = \frac{1}{2k_{e_{aq}+e_{aq}}[e_{aq}]}$$

Dividing τ_{relax} by $\tau_{1/2}(e_{aq} + e_{aq})$ yields

$$\frac{\tau_{relax}}{\tau_{1/2}(e_{aq} + e_{aq})} = \frac{(7.1 \times 10^{-9})2k(e_{aq} + e_{aq})[e_{aq}]}{\mu(\Lambda^+ + \Lambda^-)} \quad (IV)$$

The main charged species initially present in a spur are e_{aq} and H^+ . Assuming $[e_{aq}] \sim [H^+]$, the initial ionic strength in the spur is approximately the concentration of e_{aq} . So, eq IV reduces to

$$\frac{\tau_{relax}}{\tau_{1/2}(e_{aq} + e_{aq})} = \frac{(7.1 \times 10^{-9})2k(e_{aq} + e_{aq})}{\Lambda_{H^+} + \Lambda_{e_{aq}^-}} \quad (V)$$

This, $\tau_{relax}/\tau_{1/2}(e_{aq} + e_{aq})$ does not depend on the initial concentration of e_{aq} .

Taking $\Lambda_{H^+} = 350$ and $\Lambda_{e_{aq}^-} = 170$ ¹⁹ we obtain

$$\frac{\tau_{relax}}{\tau_{1/2}(e_{aq} + e_{aq})} = 0.14$$

This argument demonstrates that in the absence of any solutes, most of the e_{aq} have their ionic atmosphere built up before their recombination.

In the presence of ionic scavengers, the ionic atmosphere around the scavengers themselves is obviously relaxed a long time before the spurs are formed. At low concentration of such ionic scavengers, where only a small decrease of G_{H_2} is observed, $\tau_{1/2}$ of the electron in the spur is only slightly decreased: the previous arguments presented above for the absence of scavengers are even more valid.

In concentrated solutions exceeding 0.1 M, where $k_{e_{aq}+s}[S] > 10^{10}$, G_{H_2} is appreciably reduced, a situation can be reached where τ_{relax} is close to the value of $\tau_{1/2}$ for e_{aq} . In these concentrated solutions, a part of the e_{aq} may react before there is a complete relaxation of the ionic atmosphere.

Logan¹⁶ analyzed the extreme case, where no relaxation of the ionic atmosphere around e_{aq} is achieved. Making use of his theory and taking the diffusion coefficients $D_{e_{aq}} = 4.7 \times 10^{-5} \text{ cm}^2 \text{ sec}^{-1}$ ²⁰ and $D_{scavenger} \simeq 1 \times 10^{-5} \text{ cm}^2 \text{ sec}^{-1}$ ²¹ it can be shown that in this case a correction of less than 30% should be made for $k_{e_{aq}+s}$ as compared to a case of relaxed ionic atmosphere around e_{aq} .

In any case, even at the most extreme ionic strength and lowest $\tau_{1/2}(e_{aq} + s)$, the use of eq II will lead to an error of less than 30%, but under our experimental conditions the error was *much lower*, as a partial buildup of the ionic atmosphere is achieved around e_{aq} prior to its decay.

The use of eq III-V is justified: τ_{relax} , found experimentally in the reaction of $e_{aq} + I_3^-$,¹⁷ is in reasonable agreement with the value calculated from eq III. The arguments thus favor an attempt to correct the effect of μ on the scavenging of G_{H_2} , by the various scavengers, even for concentrated solutions where only partial relaxation of the ionic atmosphere around e_{aq} is achieved.

Equation II can be used for the calculation of $k_{e_{aq}+s}$ at different ionic strengths. However, in concentrated solutions eq II can lead to a considerable error, due in part to specific salt effects, so we decided to measure directly $k_{e_{aq}+s}$ as a function of the ionic strength for the scavengers used in the present work.

Measurements of $k_{e_{aq}+s}$ at Different μ . We have measured $k_{e_{aq}+s}$ as a function of ionic strength in the range $\mu = 0.01$ –3.0, for 10 different anion and cation scavengers of G_{H_2} . These rate constants were determined by pulse radiolysis, using solutions containing $10^{-3} M$ ethanol.

The e_{aq} decay was followed at 5500 Å. As in these experiments $[S] \gg [e_{aq}]$, a first-order decay of e_{aq} was observed.

From the decay plots, the pseudo-first-order rate constant was determined at each concentration of $[S]$, and an average of 4–5 determinations were recorded. This procedure was repeated in turn for each scavenger, at different ionic strengths and at 3–4 different initial

(16) S. R. Logan, *Trans. Faraday Soc.*, **63**, 3004 (1967).

(17) F. S. Dainton and S. R. Logan, *Proc. Roy. Soc., Sect. A*, **287**, 281 (1965).

(18) S. R. Logan, *Trans. Faraday Soc.*, **62**, 3423 (1966).

(19) M. S. Matheson, *Advances in Chemistry Series*, No. 50, American Chemical Society, Washington, D. C., 1965, p 45.

(20) K. H. Schmidt and W. L. Buck, *Science*, **151**, 70 (1966).

(21) S. W. Benson, "The Foundations of Chemical Kinetics," McGraw-Hill, New York, N. Y., 1960, p 498.

Table IV: The Effect of Inert Salts on $k_{e_{aq}+s}$

Solutes, <i>M</i>	$(k_{e_{aq}+s})_{\mu=0}$, ^b $M^{-1} \text{ sec}^{-1}$	$(k_{e_{aq}+s})_{p,\mu}$, $M^{-1} \text{ sec}^{-1}$	
		Measured ^c	Calcd ^d
1.0 Na ₂ Cr ₂ O ₇	6.0×10^{10}	5.0×10^{10} (1 <i>M</i> Na ₂ SO ₄)	<i>e</i>
1.0 Na ₂ CrO ₄	1.8×10^{10}	2.6×10^{10} (1 <i>M</i> Na ₂ SO ₄)	<i>e</i>
1.0 NaNO ₃	1.05×10^{10}	1.6×10^{10} (1 <i>M</i> NaClO ₄)	<i>e</i>
1.0 NaBrO ₃	3.4×10^9	6.15×10^9 (1 <i>M</i> NaClO ₄)	<i>e</i>
1.0 Na ₂ S ₂ O ₃	9×10^8	1.35×10^9 (1 <i>M</i> Na ₂ SO ₄)	<i>e</i>
1.0 CuSO ₄	4.5×10^{10}	9.1×10^9 (1 <i>M</i> Na ₂ SO ₄)	<i>e</i>
1.0 CdSO ₄	6.4×10^{10}	9.6×10^9 (1 <i>M</i> Na ₂ SO ₄)	<i>e</i>
1.0 Co(ClO ₄) ₂	9.5×10^9	3.7×10^9 (3 <i>M</i> NaClO ₄)	<i>e</i>
1.0 NiSO ₄	2.2×10^{10}	1.9×10^9 (1 <i>M</i> Na ₂ SO ₄)	<i>e</i>
0.1 Na ₂ Cr ₂ O ₇	6.0×10^{10}	7×10^{10} (0.1 <i>M</i> Na ₂ SO ₄)	1.7×10^{11}
0.1 Na ₂ CrO ₄	1.8×10^{10}	2.7×10^{10} (0.1 <i>M</i> Na ₂ SO ₄)	8×10^{10}
0.1 NaNO ₃	1.05×10^{10}	1.30×10^{10} (0.1 <i>M</i> NaClO ₄)	1.7×10^{10}
0.1 AgClO ₄	3.3×10^{10} ^a		2.0×10^{10}
0.1 KIO ₃	8.5×10^9	1.2×10^{10} (0.1 <i>M</i> NaClO ₄)	1.48×10^{10}
0.1 NaBrO ₃	3.4×10^9	5×10^9 (0.1 <i>M</i> NaClO ₄)	6.1×10^9
0.1 Cu(ClO ₄) ₂	4.5×10^{10}	1.7×10^{10} (0.3 <i>M</i> NaClO ₄)	1.5×10^{10}
0.1 CdSO ₄	6.4×10^{10}	1.9×10^{10} (0.1 <i>M</i> Na ₂ SO ₄)	2.2×10^{10}
0.01 Na ₂ Cr ₂ O ₇	6.0×10^{10}	7.5×10^{10} (0.3 <i>M</i> NaClO ₄)	1.08×10^{11}
0.01 AgClO ₄	3.3×10^{10} ^a		2.6×10^{10}
0.01 Na ₂ CrO ₄	1.8×10^{10}		3.6×10^{10}
0.01 NaNO ₃	1.05×10^{10}		1.2×10^{10}
0.01 NiSO ₄	2.2×10^{10}		1.2×10^{10}
0.01 ZnSO ₄	1.5×10^9		8×10^8
0.01 Cu(ClO ₄) ₂	4.4×10^{10}	2.7×10^{10} (0.03 <i>M</i> NaClO ₄)	2.5×10^{10}
0.01 KIO ₃	8.5×10^9		1.16×10^{10}
0.01 NaBrO ₃	3.4×10^9	4.1×10^9 (0.01 <i>M</i> NaClO ₄)	4.5×10^9
0.01 Na ₃ Fe(CN) ₆ ^a	3×10^9		1.1×10^{10}

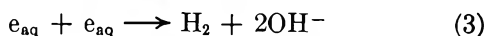
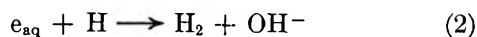
^a Reference 9. ^b Measured values. ^c Measured values in the presence of the inert salt written in brackets. ^d These values were calculated using $(k_{e_{aq}+s})_{\mu=0}$ from column 2 and eq II (see text). ^e Correction at these high μ is omitted as eq II does not necessarily hold for such high μ . ^f $(k_{e_{aq}+s})_{p,\mu}$ means rate constant of the reaction $e_{aq}+s$ in proper μ .

scavenger concentrations, differing from one another by at least a factor of 4. $k_{e_{aq}+s}$ was thus calculated at every ionic strength from these results, not omitting to correct for the self-decay of e_{aq} . (These corrections amounted to 3–10%.)

Results are presented in Table IV where $k_{e_{aq}+s}$ is also calculated at different ionic strengths, with the aid of eq II, where $\alpha = 2$ for Co²⁺, Ni²⁺, Cd²⁺, Cu²⁺, and Cr₂O₇²⁻, and $\alpha = 1$ for the other ions. ($\alpha = 2$ was taken for those ions whose ionic radii are about 5–6 Å and $\alpha = 1$ for those ions whose ionic radii are about 3–4 Å.)²² For these calculations the values of $k_{e_{aq}+s}$ at $\mu = 0$ were taken from our measurements.

Effects of Ionic Strength on G_{H_2} . As it is assumed that e_{aq} is the main precursor of G_{H_2} in the spurs, it can be expected that the ionic strength affects G_{H_2} .

Using calculations for the diffusion model, Schwarz²³ was able to show that G_{H_2} in neutral solutions originates from three main sources, whose contributions are similar. Two of these sources are given by the reactions



while a third source, described as $G_{H_2}^0$, is formed

“directly.” The rate of reaction 3 would depend on the ionic strength, and increasing the ionic strength would tend to increase the rate of this reaction. On the other hand, H atoms are also formed in a spur reaction



and the rate of this reaction would be slowed down with increased ionic strength.

When inert salts, such as Na₂SO₄ or MgSO₄, are added to a neutral solution of 10^{-3} *M* NO₂⁻ + 10^{-3} *M* Br⁻, G_{H_2} is found to be independent of the ionic strength—as shown in Table V.

Mahlman obtained similar results²⁴ and found $G_{H_2} = 0.46$ – 0.47 in irradiated 10^{-3} *M* Br⁻ solutions, and $G_{H_2} = 0.47$ in 10^{-3} *M* Br⁻ solutions containing 0.6 *M* and 1 *M* Na₂SO₄.

The fact that G_{H_2} is independent of μ is not too surprising. During the first half-life of the spur, the intrinsic ionic strength is about 0.1, while in concentrated

(22) I. M. Klotz, “Chemical Thermodynamics,” Prentice-Hall, Englewood Cliffs, N. J., 1950, p 331.

(23) (a) H. A. Schwarz, submitted to *J. Phys. Chem.* (b) H. A. Schwarz, in the Summary of Proceedings of the Fifth Informal Conference on the Rad. Chem. of Water, Notre Dame, October 1966, p 53.

(24) H. A. Mahlman, *J. Chem. Phys.*, **28**, 1256 (1958).

Table V: Effect of Inert Salts on G_{H_2} in the Absence of H_2 Scavenger

Added solute ^a	$G_{H_2}^b$	μ
...	0.43 ± 0.01	0.001
0.1 M Na ₂ SO ₄	0.45 ± 0.01	0.3
0.8 M Na ₂ SO ₄	0.43 ± 0.01	2.4
1 M MgSO ₄	0.43 ± 0.01	2.4

^a All solutions contained 10^{-3} M Br⁻ + 10^{-3} M NO₂⁻ (or 10^{-3} M NO₃⁻). ^b These values were corrected to the increase in electron density in the solutions.

solutions $\mu < 3$. Thus $k_{e_{aq}+e_{aq}}$ or $k_{e_{aq}+H^+}$ in the region $\mu = 0.1-3$ are modified by a factor of less than 1.25; G_{H_2} would not reveal such a change.

During the latter life of the spur, when it is already expanded, the intrinsic ionic strength is reduced to a value as low as 0.01²⁵ (and later, μ decreases even more, but the formation of G_{H_2} in the spur is over). In such a case, in the absence or in the presence of added salts, the difference in rate constants may be as high as 1.6. However, the overall effect is expected to be small as about one-third of G_{H_2} is formed "directly"²³ as $G^{\circ}_{H_2}$, and is independent of μ . As to the remaining contribution to G_{H_2} , there will be less H atoms formed at high μ and of course a smaller contribution of the reaction $e_{aq} + H$ is expected. This will be compensated by a slightly faster rate of $e_{aq} + e_{aq}$. This line of reasoning is consistent with the results of Mahlman²⁴ and with our experiments.

The Effect of μ on the Scavenger Efficiency of G_{H_2} . G_{H_2} was measured at given concentrations of different scavengers at different ionic strengths. The results are given in Table VI. It can be seen that the effect is very small, almost within the accuracy of the measurements. Nevertheless, the direction of the effect is that by increasing μ the efficiency of anionic scavengers increases. The small magnitude of the ionic strength effect in these experiments is not surprising due to the intrinsic value of μ in the spur, as discussed in the previous paragraph.

In Figure 4 it can be seen that plotting G_{H_2} as a function of $k_{e_{aq}+s}[S]$ results in large deviations for anions, cations, and neutral molecules, especially at high concentrations. The reason for these deviations might be due to μ effects.

The values of $k_{e_{aq}+s}$ used in Figure 4 and in ref 4 and 6 are the values measured at very low μ . As shown in Table IV, $k_{e_{aq}+s}$ changes in some cases up to one order of magnitude between dilute and concentrated solutions. This change has to be taken into account.

We have replotted Figure 4, where $k_{e_{aq}+s}$ was taken for each solute at the correct μ (Figure 5). This figure shows that (when applying this correction) G_{H_2} for all solutes falls more or less on single Unified Curve (moving the anions to the right and the cations to the

Table VI: Effects of Inert Salts on Scavenging Efficiency of Different Anions on G_{H_2}

Solute, M	Added inert salt, M	$G_{H_2}^a$
0.1 Na ₂ CrO ₄	...	0.193 ± 0.002
	0.8 Na ₂ SO ₄	0.193 ± 0.002
0.1 NaBrO ₃	...	0.315 ± 0.005
	0.5 Na ₂ SO ₄	0.295 ± 0.005
0.1 NaNO ₃	...	0.26 ± 0.01
	0.8 Na ₂ SO ₄	0.25 ± 0.01
0.01 NaNO ₃	...	0.357 ± 0.009
	0.1 Na ₂ SO ₄	0.346 ± 0.015
	0.3 NaClO ₄	0.350 ± 0.002
	0.8 Na ₂ SO ₄	0.33 ± 0.01
0.01 Na ₂ CrO ₄	...	0.317 ± 0.008
	0.1 Na ₂ SO ₄	0.30 ± 0.012
	0.8 Na ₂ SO ₄	0.297 ± 0.009
0.01 Na ₂ Cr ₂ O ₇ ²⁻	...	0.294 ± 0.005
	0.1 Na ₂ SO ₄	0.288 ± 0.015
	0.3 NaClO ₄	0.275 ± 0.012
0.01 Na ₃ Fe(CN) ₆	...	0.356 ± 0.014
	0.2 Na ₂ SO ₄	0.337 ± 0.007
0.01 NaIO ₃	...	0.37 ± 0.018
	0.1 Na ₂ SO ₄	0.35 ± 0.01
0.01 NaBrO ₃	...	0.39 ± 0.02
	0.1 Na ₂ SO ₄	0.38 ± 0.02

^a These values were corrected to the increase in electron density due to the addition of the inert salt.

left in Figure 4). Even in spur reactions the use of $k_{e_{aq}+s}$ taken at the proper ionic strength is justified. If $\tau_{1/2}$ of e_{aq} is short, the correction necessary for $k_{e_{aq}+s}$ due to incomplete relaxation is rather small, as demonstrated and discussed earlier. One must keep in mind that some scatter in Figure 5 will occur due to the different reactivities of S with OH, and the possible reactions in the spur of the products of S with either OH or e_{aq} , and reactions of M⁰ and M⁺ in the case of some cations.

The effect of ionic strength on G_{H_2} in presence of scavengers shows clearly that the precursor of G_{H_2} is negatively charged. The anomalies in dependence of G_{H_2} on $k_{e_{aq}+s}[S]$ ^{4,6} are shown to be due to a faulty selection of $k_{e_{aq}+s}$. When $k_{e_{aq}+s}$ was selected to correspond to the actual μ of the experiments, a unified curve was found.

The present data constitute strong evidence that e_{aq} is the main precursor of G_{H_2} . Hamill²⁶ recently proposed that the precursor of the molecular hydrogen is the nonhydrated electron, which yields H atoms in geminate pairs of "(H, H, OH, OH)." The dry electron is assumed to react at thermal energies with various e_{aq} scavengers such as N₂O, acetone, and Lewis acids, but not with H⁺. The good agreement between reducing

(25) G. Stein and M. Tomkiewicz, U. S. Atomic Energy Commission Report No. NYO-3242-30, 1969.

(26) W. H. Hamill, *J. Phys. Chem.*, **73**, 1341 (1969).

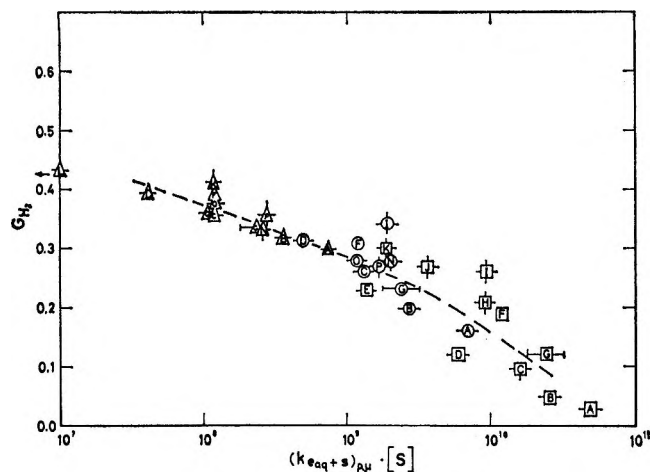


Figure 5. G_{H_2} as a function of the product $k_{e_{aq}+s}[S]$ corrected for μ , for all kinds of scavengers. Values for $(k_{e_{aq}+s})_{p,\mu}$ are taken from Table IV. The notation of the scavengers is the same as for Figures 1-3.

efficiency of G_{H_2} and $(k_{e_{aq}+s})_{p,\mu}[S]$ for many cations/anions and neutral molecules from 0.01 M to 1 M solutions (Figure 5), shows that either these solutes (at the above concentrations) do not, or only slightly react with the dry electron (before its hydration), or that their reactivities towards e_{aq} are in correlation with their reactivities towards the dry electron.

The role and possible existence of a dry electron might be important in the mechanism of water decomposition by irradiation. Nevertheless, it seems to us that one cannot avoid the assumption that e_{aq} is finally formed in spurs and is the precursor of G_{H_2} .

Precursors of G_{H_2} . Hayon replotted results of G_{H_2} as a function of $[S]^{1/2}$ for NO_3^- and H_2O_2 .⁵ Each plot yields two straight lines with different slopes (Figure 6). In both systems each of these two lines extrapolates back to similar intercepts, a fact which induced Hayon to assume two different modes of H_2 formation. The part of H_2 which is easy to scavenge was attributed to the reaction $e_{aq} + e_{aq}$ while the more difficult scavengeable part was assumed to be formed from H atoms. This hypothesis is based on the fact that NO_3^- and H_2O_2 react much faster with e_{aq} than with H atoms. We replotted other results of $G(H_2)$ as a function of $[S]^{1/2}$ ($S = Cr_2O_7^{2-}, NO_2^-$) (Figure 6) from a latter work of Hayon and Moreau.⁶ The plots are identical with those plotted by Hayon for H_2O_2 and NO_3^- ,⁵ even though the rates of $Cr_2O_7^{2-}$ and NO_2^- with e_{aq} and H are similar. Thus, one may safely conclude that the two straight lines in this kind of plot do not have any correlation with $k_{h+s}/k_{e_{aq}+s}$. Moreover, it should be remembered that: (a) straight lines should not result theoretically when $G(H_2)$ is plotted as a function of $[S]^{1/2}$,²⁷ (b) in this kind of plot no corrections of $k_{e_{aq}+s}$ to changes of μ were made. Thus we may also conclude that the present results do not constitute any proof that there are two different modes of formation of H_2 .

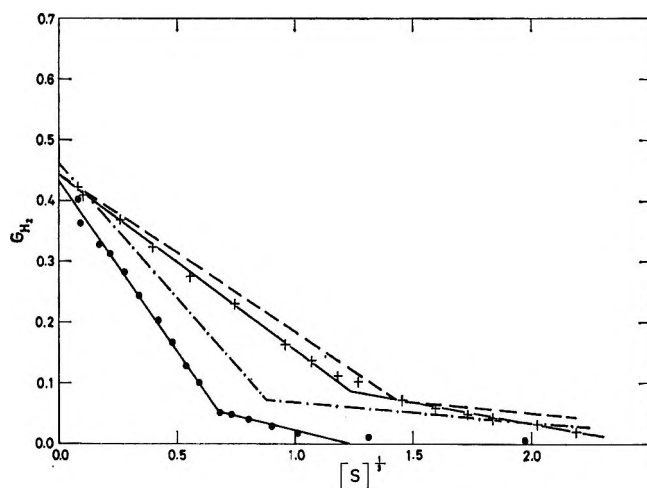


Figure 6. Dependence of G_{H_2} on $[concentration]^{1/2}$ $Cr_2O_7^{2-}$ (\bullet , ref 6); NO_2^- ($+$, ref 6); H_2O_2 (---, ref 5); NO_3^- [$activity]^{1/2}$ (-·-·-, ref 5).

Other sources for the formation of H_2 were put forward, such as H^- ,⁴ H_3O^+ ,² and H_2O^* .³ There is no evidence to support H_2O^* or H^- . Recent experiments carried out by Bronskill, Wolff, and Hunt²⁸ seem to rule out H_3O^+ as after 35 psec a full yield of e_{aq} was observed.

We believe that a possible source for the "independent yield" of G_{H_2} (as suggested by Schwarz)²³ could still be e_{aq} . The fact that 1 M of good electron scavengers such as $Cr_2O_7^{2-}$ decreases G_{H_2} to about 5% shows that $G^{\circ}_{H_2}$ is not a primary yield and can be efficiently scavenged. (The assumption here is that even in such concentrated solutions, direct effects—other than of the absorbed dose for which correction was made—are minor.)

All diffusion model computations assumed a distribution of spurs with different numbers of radicals present, but with identical initial concentrations. It is reasonable to assume also a distribution of the initial concentrations of the radicals in all kinds of spurs, so that a fraction of the spurs would possess a much higher initial concentration of radicals. In these spurs, it would be much more difficult for solutes to scavenge the precursors of G_{H_2} , $G^{\circ}_{H_2}$ and G°_H may originate in these condensed spurs.

This possible source of $G^{\circ}_{H_2}$ could clarify several points. It could explain the break of G_{H_2} plotted against $[S]^{1/2}$, shown by Hayon⁵ and Mahlman²⁹ (Figure 6), as being the general picture of this phenomenon; *i.e.*, the real difficulty of scavenging the last remnant of G_{H_2} .

Another difficulty is the interpretation of the isotopic effects on G_{H_2} . The isotopic separation factor of G_{H_2} was found to be 2.2 independent of pH, in the range

(27) G. Czapski, *Discuss. Faraday Soc.*, **36**, 321 (1963).

(28) M. J. Bronskill, R. K. Wolff, and J. W. Hunt, *J. Phys. Chem.*, **73**, 1175 (1969).

(29) H. A. Mahlman, *J. Chem. Phys.*, **32**, 601 (1960).

1.1–14.³⁰ If reactions 1–3 are the source of G_{H_2} , it could be expected that the isotopic effect would change with pH due to the different contributions of reaction 4.³⁰ The isotopic separation factor of reaction 1 is 2.6 at pH >6 and 3.5 at pH 1, of reaction 2 1.5 at pH 10 and 1.9 at pH 4, and for reaction 3 4.7 independent of pH. Schwarz²³ showed that if we assume $G^{\circ}_{H_2} = 0.15$ ($\sim 30\%$ of G_{H_2}), with an isotopic separation factor of 1.8 which is pH independent, G_{H_2} would not show any appreciable change in the isotopic effect in this pH range. As we are suggesting that $G^{\circ}_{H_2}$ is formed from the condensed spurs, mainly through reaction 2 (which has an isotopic effect of 1.6³⁰), this would explain the pH independence of the isotopic effect. (The pH effect on condensed spurs is in all probability small, as H^+ and other electron scavengers are inefficient in these spurs). Other results obtained, concerning the isotope effect of $G^{\circ}_{H_2}$, measured in 1 M NO_3^- , were: $G_{H_2} = 0.09$ and the isotopic effect was found to be 1.5 ± 0.2 .³¹ In this system, where most of G_H is scavenged, the residual G_{H_2} , probably comes from the condensed spurs, or in the main part from reaction 2.

The isotopic effect observed is in good agreement with the condensed spur model and with $G^{\circ}_{H_2}$ as suggested by Schwarz.²³

We think that in the condensed spurs, the contribution to G_{H_2} of the reaction $e_{aq} + H$ in all probability

dominates the reaction $e_{aq} + e_{aq}$, as compared with the usual spurs, since in these spurs more H atoms are formed, and $k_2 > k_3$. (Thus, the isotopic effect of $G_{H_2}^{\circ}$ should be about 1.6, like that of reaction 2.) It is conceivable that such spurs may well be the source of $G^{\circ}_{H_2}$,²³ as well as of G°_H and, following the same train of thought, $G^{\circ}_{H_2O_2}$ could be expected as well.

Conclusions

(1) The evidence showing that e_{aq} is the precursor of G_{H_2} is quite sound. (2) Agreement is good between the efficiency of G_{H_2} scavengers and the product $k_{e_{aq}+s}[S]$ corresponding to the correct ionic strength. (3) It is suggested that G_{H_2} originates from recombinations of e_{aq} and H in the spurs, in reactions 1–3; some G_{H_2} may even originate in condensed spurs and thus might be " $G^{\circ}_{H_2}$." (4) As it is known that almost the entire G_{H_2} can be scavenged by electron and H atom scavengers (for example, $Cr_2O_7^{2-}$), this would seem to prove that almost all precursors of G_{H_2} may also be scavenged and that there is not direct formation of G_{H_2} .

Acknowledgment. We are grateful to Dr. H. A. Schwarz for many fruitful discussions and suggestions, and to Mr. J. Ogdan for technical assistance.

(30) M. Anbar and D. Meyerstein, *Trans. Faraday Soc.*, **62**, 2121 (1966).

(31) S. Alfassi, M. Anbar, and D. Meyerstein, unpublished results.

Combined Low-Energy Electron Diffraction and Mass Spectrometer

Observations on Some Gas-Solid Reactions and

Evidence for Place Exchange^{1a,b}

by H. E. Farnsworth

Brown University, Providence, Rhode Island 02912 (Received March 9, 1970)

Combined LEED and MS observations were used to obtain information on lattice structure and reaction products when an atomically clean Ni (100) crystal was exposed to gases such as O₂ and CO. Measurements of changes in work function and of diffraction spot intensity, as a function of electron energy, were obtained to determine if place exchange or simple adsorption occurred. It was concluded that place exchange occurred when Ni (100) was exposed to O₂ at 22°. Two different place exchange structures occurred on Mo (100) when the oxygen-contaminated surface was heated at two different temperatures. Adsorption, without place exchange, occurred at 22° for CO, CO₂, and NO on Ni (100) and for O₂, and CO on Re (0001).

Introduction

The combination of low-energy electron diffraction (LEED)² and mass spectrometer (MS) equipments permits one to obtain information on both surface structures and desorbed reaction products. However, it requires that contamination of the reaction product from sources other than the crystal surface be minimized.

Experimental Section

The above requirement is satisfied in our equipment by an arrangement in which gas desorbed from the crystal face by heat treatment is transferred preferentially through a fused-silica tube to the ionization chamber of the quadrupole mass spectrometer,^{3a} as shown in Figure 1.

The LEED system is the rapid-scan electrical detection type.^{3b} A narrow beam of electrons strikes the crystal at normal incidence and the elastically diffracted electrons are measured by means of a movable Faraday cage. In addition to obtaining spot patterns by a rapid scan, involving simultaneous rotations of the crystal and the Faraday collector, the intensity *vs.* voltage (*I vs. V*) curve for any selected spot or beam may be obtained over a wide range of voltage in a few minutes. This curve, showing variation of spot intensity with primary voltage or wave length for normal incidence, contains significant information. Because the low-energy electrons penetrate only a few monolayers, with the effect of the surface monolayer predominating, the shape of the *I vs. V* curve may be strongly affected by an adsorbed monolayer. In this paper we shall consider some of the factors which influence the shape of this curve.

Changes in work function are obtained by measuring the crystal current as a function of retarding crystal

potential for different surface conditions and observing the change in the cut-off voltage.

Results and Discussion

Spurious results due to small amounts of surface contaminants must be avoided. As an example, the influence of small amounts of surface contamination on CO adsorption on Ni (100) is shown in Figure 2. The upper curve shows the development of the CO-peak intensity with exposure for a clean surface. The lower curve was taken after slight bulk contamination (less than 1 monolayer) had diffused to the surface by heating the crystal. This result indicates the great sensitivity of surface reactions to minute amounts of contaminant and the precautions that must be observed in obtaining a clean surface.

We shall consider first the interactions of CO and O₂ with Ni crystal surfaces. In Figure 3, the upper frame contains a copy of the reciprocal lattice spot pattern for CO on Ni (100). The large solid circles are from the nickel lattice and the small solid circles are from the CO lattice on the surface. A model which will produce this pattern is shown below. The open circles represent the nickel atoms and the solid circles represent the CO molecules.

(1) (a) This paper was presented at the "Diffraction and Structure," symposium of the Division of Physical Chemistry, American Chemical Society National Meeting, New York, Sept 1969. (b) This work was supported by the National Science Foundation, the Advanced Research Projects Agency, and the Department of the Air Force, Wright-Patterson Air Force Base.

(2) H. E. Farnsworth, *Advan. Catal.*, **15**, 31 (1964); "The Solid Gas Interface," Vol. I, E. Alison Flood, Ed., Marcel Dekker, New York, N. Y., 1967, Chapter 13; "Experimental Methods in Catalytic Research," R. B. Anderson, Ed., Academic Press, New York, N. Y., 1968, pp 265-285; J. W. May, *Ind. Eng. Chem.*, **57**, 18 (1965).

(3) (a) M. Onchi and H. E. Farnsworth, *Surface Sci.*, **11**, 203 (1968); (b) R. L. Park and H. E. Farnsworth, *Rev. Sci. Instrum.*, **35**, 1592 (1964).

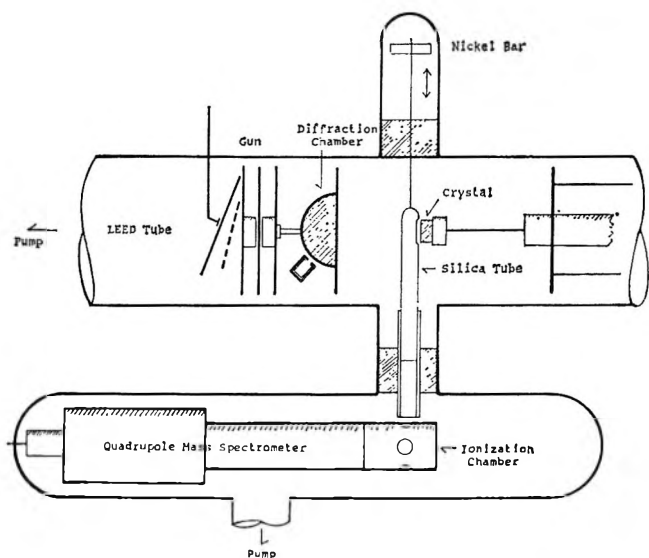


Figure 1. Combined LEED and mass spectrometer system (courtesy of *Surface Sci.*).

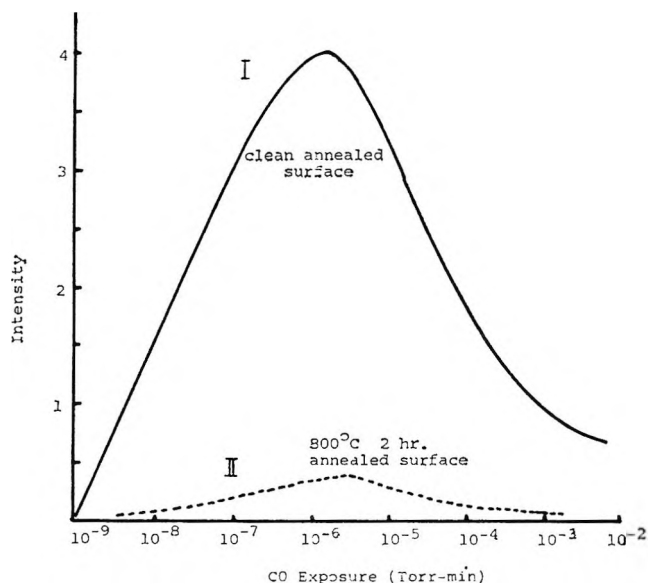


Figure 2. Development of 34-eV peak in $(\frac{1}{2} \frac{1}{2})$ beam by CO exposure (courtesy of *Surface Sci.*).

Figure 4 shows the I vs. V curve for one of the spots due to CO after exposure at room temperature. A slight heating of this surface *in vacuo* intensified the pattern, thus suggesting that the CO lattice had been improved. When this surface was exposed to O_2 , a similar but weaker curve was obtained, thus indicating that structureless oxygen had partially covered the CO lattice. After slight heating of this surface *in vacuo*, a new intensity curve was obtained which was the same as that for oxygen on a clean Ni (100) surface. Mass spectrometer tests showed that during the slight heating the adsorbed oxygen had combined with adsorbed CO to form CO_2 which desorbed with an excess of oxygen remaining on the crystal surface.

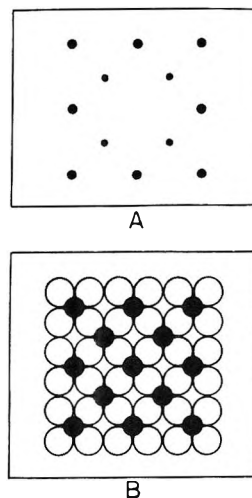


Figure 3. A, Copy of reciprocal lattice spot pattern from a Ni (100) crystal face after exposure of the clean surface to CO at 10^{-8} Torr min (60 eV). Large solid circles are from the nickel lattice. Small solid circles are from the adsorbed CO lattice. B, Model of Ni atoms positions (large open circles) and CO molecule positions (small solid circles) which account for the pattern in Figure 2A.

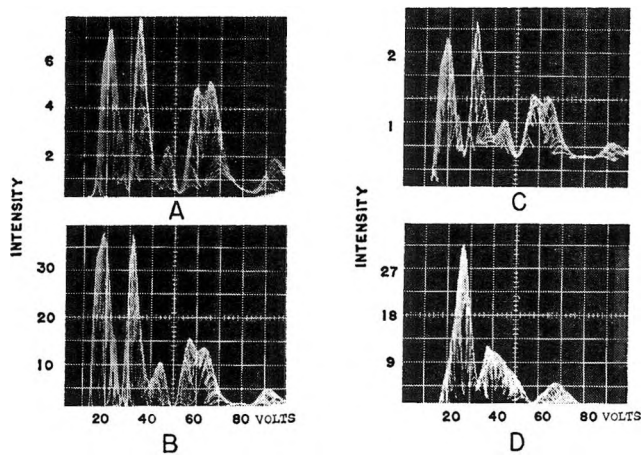


Figure 4. Intensity vs. voltage curves for $(\frac{1}{2} \frac{1}{2})$ beam from Ni (100) (courtesy of *J. Chem. Phys.*): A, after exposure of clean Ni (100) to CO at 22°; B, after heating crystal to 300° and cooling to 22°; C, after the CO covered surface had been exposed to O_2 at 22°; D, after heating the CO + O_2 surface to 250° and cooling to 22°.

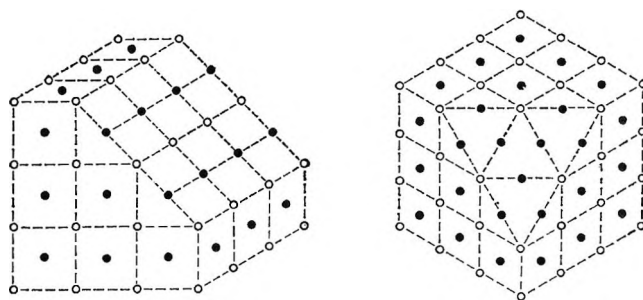


Figure 5. Ni_3O lattice showing (100), (110), and (111) faces. Open circles indicate O atoms. Solid circles indicate Ni atoms (courtesy of *Appl. Phys. Lett.*).

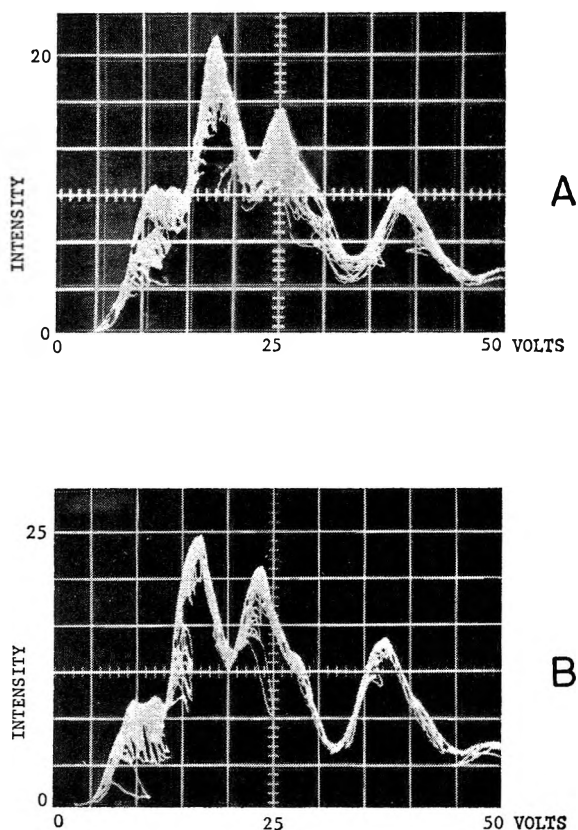


Figure 6. A, $(0 \frac{1}{2})$ beam after 1×10^{-2} Torr min CO exposure of a clean Re (0001) surface at 22° and subsequent vacuum heating at 425° for 10 min (courtesy of *Surface Sci.*); B, $(0 \frac{1}{2})$ beam after 1×10^{-7} Torr min O_2 exposure of a clean Re (0001) surface at 22° and subsequent vacuum heating at 425° for 10 min (courtesy of *Surface Sci.*).

It is important to note that the spot patterns for CO and O_2 on Ni (100) are the same in this case, but the I vs. V curves are entirely different. Because of the large binding energy of oxygen and the work function decrease associated with the formation of this structure, the mechanism of place exchange between oxygen and nickel atoms has been suggested.⁴ In fact, this result, combined with those for Ni (110) and Ni (111), leads to the interpretation of a place exchange structure of Ni_3O in which the interatomic spacing is essentially the same as that for pure nickel (Figure 5).⁵

In contrast with the results on the intensity curves for CO and O_2 on nickel, we have found that CO and O_2 adsorbed on Re (0001) not only have the same spot patterns but also similar I vs. V curves. Figure 6 shows the I vs. V curves from double-spaced structures for these two cases. These results suggest that in the case of Re, CO and O_2 are both adsorbed on the surface and that multiple scattering, as discussed by McRae,⁶ results in similar intensity curves. In the case of Ni, there is place exchange between oxygen and Ni atoms instead of adsorption on the surface, thus altering the multiple scattering conditions.

To test further the validity of this hypothesis, we

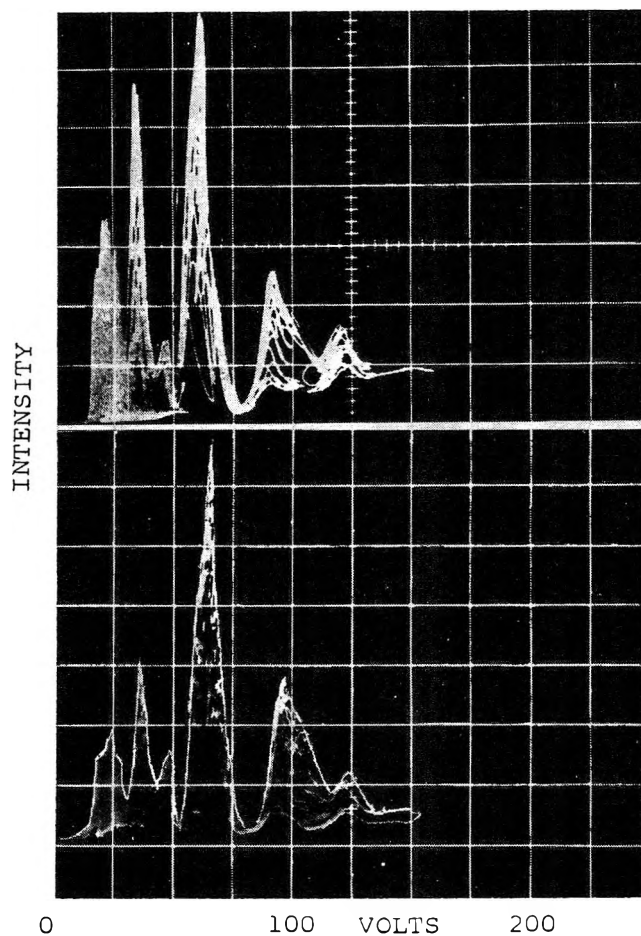


Figure 7. A, $(\frac{1}{2} \frac{1}{2})$ beam after 1×10^{-6} Torr min NO exposure of a clean Ni (100) surface at 22° ; B, $(\frac{1}{2} \frac{1}{2})$ beam after 2.5×10^{-5} Torr min CO_2 exposure of a clean Ni (100) surface at 22° .

have made observations with other gas-solid combinations. Figure 7 shows I vs. V curves from similar multiple-spaced structures for NO and CO_2 on Ni (100). It is seen that here also the curves are very similar, except for a displacement of the NO curve toward lower voltages. Figure 8 contains curves for CO_2 and CO. Here there is considerable similarity also, except for the double peak between 50 and 75 eV in the CO curve.

From these results, it appears that although place exchange occurred with oxygen and Ni (100), this was not the case with CO, CO_2 , and NO, while with Re (0001), no place exchange occurred with either O_2 or CO.

Because there have been differences of opinion concerning the concept of place exchange⁷ (or reconstruction), details of another case are considered, namely, the oxygen-molybdenum reaction, which also supports

(4) H. E. Farnsworth and H. H. Madden, Jr., *Bull. Amer. Phys. Soc.*, **5**, 349 (1960); *J. Appl. Phys.*, **32**, 1933 (1961).

(5) H. E. Farnsworth, *Appl. Phys. Lett.*, **2**, 199 (1963).

(6) E. G. McRae, *Surface Sci.*, **11**, 492 (1968).

(7) E. Bauer, *ibid.*, **15**, 152 (1966).

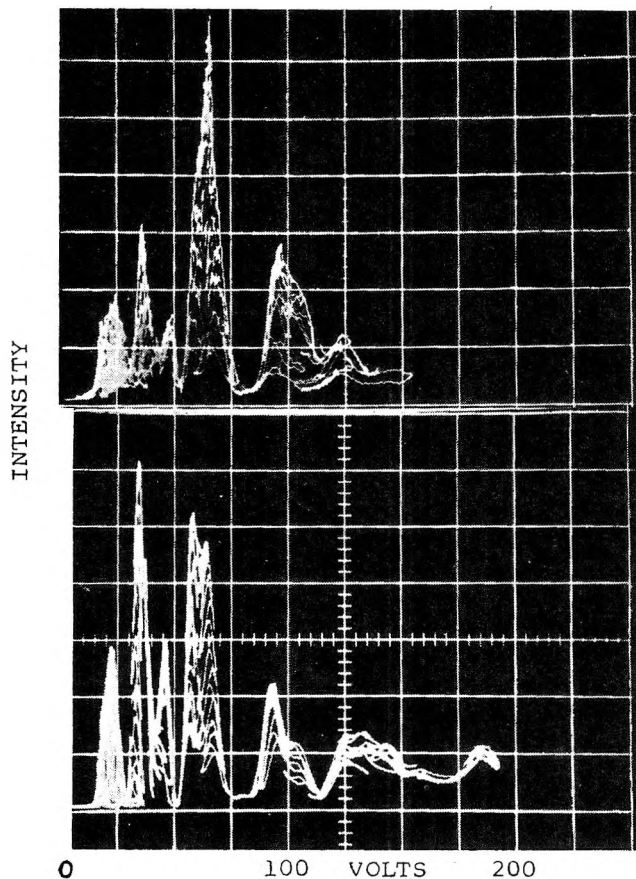


Figure 8. A, $(\frac{1}{2} \frac{1}{2})$ beam after 2.5×10^{-5} Torr min CO_2 exposure of a clean Ni (100) surface at 22° ; B, $(\frac{1}{2} \frac{1}{2})$ beam after 1×10^{-7} Torr min CO exposure of a clean Ni (100) surface at 22° .

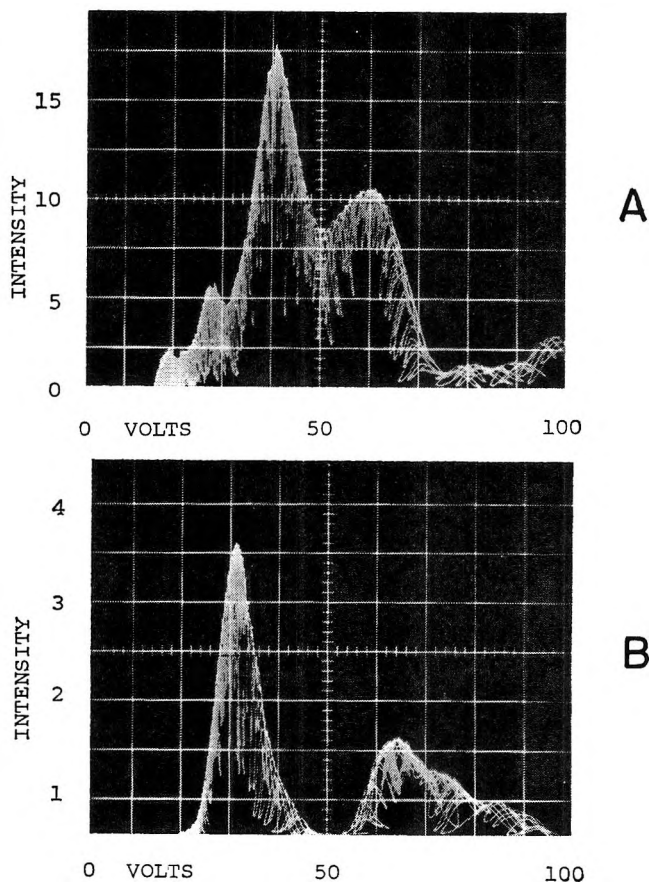


Figure 10. A, (10) beam from a clean Mo (001) surface (courtesy of *Surface Sci.*); B, (10) beam after 6×10^{-6} Torr sec O_2 exposure of a clean Mo (001) surface at 22° .

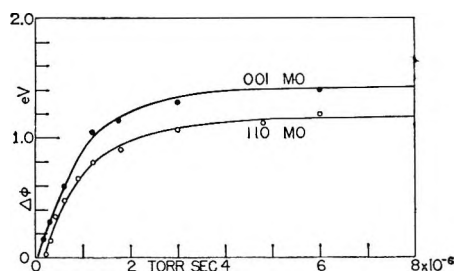


Figure 9. Work function changes as functions of oxygen exposure (courtesy of *Surface Sci.*).

this concept. Exposure of a Mo (100) surface, at room temperature, to O_2 in the 10^{-9} to 10^{-7} Torr range did not produce new diffraction beams characteristic of multiple spacing, that is, the spot patterns were identical. However, the work function and the I vs. V curve of the integral-order beams were changed appreciably. Figure 9 shows the change in work function with increasing oxygen exposure for both Mo (100) and Mo (110) surfaces. Limiting values were obtained after a total exposure of 6×10^{-6} Torr sec with no appreciable changes for additional exposures to 6×10^{-3} Torr sec. Figure 10 shows I vs. V curves for the (10)

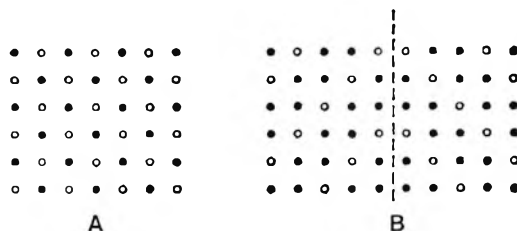


Figure 11. Place exchange models of molybdenum and oxygen atom positions in the surface plane of Mo (001). Open circles represent molybdenum atoms. Solid circles represent oxygen atoms: A, one-half monolayer of oxygen atoms. B, two-thirds monolayer of oxygen atoms.

beam from clean and O_2 exposed Mo (100) surfaces. The increased work function plus absence of fractional orders indicates that a surface monolayer of oxygen was formed with a unit mesh having the same dimensions as that of the underlying molybdenum. Further exposure caused a decrease of diffracted intensity, suggesting the formation of a second amorphous layer. Heating the oxygen-covered (100) surface at 500° produced intense half-order $(\frac{1}{2} \frac{1}{2})$ beams, suggesting the presence of a $cc(2 \times 2)$ (one-half monolayer) structure, and further heating at between 500 and 1000° caused these $(\frac{1}{2} \frac{1}{2})$ beams to disappear and the

appearance of strong ($1/3$ $1/3$) beams (one-third monolayer structure).

Both of the structures which produced these two sets of beams are believed to be exchange structures for the following reasons. (1) The work functions for the two structures were the same or less than that of a clean surface, whereas exposures at room temperature produced work functions greater than the clean-surface value. (2) Adsorption at room temperature produced no fractional-order beams, but the I vs. V curves of the integral order beams were altered, thus showing that oxygen was adsorbed on the surface in the same lattice as that of the molybdenum substrate. (3) Because of the activation energies involved, it appears probable that the $1/2$ and $1/3$ monolayer structures were formed with atomic oxygen while the monolayer formed at room temperature was in the form of molecular oxygen.

It appears unreasonable to expect only $1/2$ monolayer of oxygen atoms above the Mo surface in its most dense form when a complete monolayer of molecular oxygen forms at room temperature.

Models for the $1/2$ and $1/3$ monolayers are shown in Figures 11a and 11b, respectively. Place exchange structures for the Mo (110) surface were observed after oxygen exposures at room temperature.

In conclusion, it has been shown that a surface reaction between two constituents on a solid surface may be monitored by an LEED and MS system to obtain the lattice structures before and after the reaction and also the nature of the reaction product. Evidence is presented to support the view that place exchange can occur between adsorbed oxygen and the metal substrate for both Ni and Mo in a manner which results in multiple-spaced structures.

Thermodynamic Equilibria from Plasma Sources.

III. Carbon-Hydrogen-Nitrogen Systems¹

by P. R. Griffiths, P. J. Schuhmann, and E. R. Lippincott

Department of Chemistry, University of Maryland, College Park, Maryland (Received August 20, 1969)

Some organic nitrogen compounds have been subjected to a radiofrequency electrodeless discharge, and the products analyzed. Although the exact composition can be explained only by invoking kinetic factors, the approximate product distribution as the species emerge from the plasma may be computed by assuming a high-temperature limited thermodynamic equilibrium. The final distribution of the hydrocarbons corresponds to a temperature of about 1300°K, while that of the major nitrogenous compounds corresponds to a higher temperature, owing to the high activation energy needed to break the triple bond of the cyano radical which is formed in the plasma.

Introduction

In the first two papers in this series,^{2a,b} it was shown that the distribution of the reaction products formed when organic oxygen compounds^{2a} or hydrocarbons^{2b} are subjected to a radiofrequency electrodeless discharge is approximately that corresponding to a limited chemical equilibrium for temperatures between about 1400 and 1000°K. The mechanism postulated involves the complete breakdown of the reactant molecules into atomic, radical, and ionic fragments in the center of the plasma, with the subsequent recombination of these highly reactive fragments as the mixture flows through the reaction tube, the product distribution corresponding to that at thermodynamic equilibrium at the translational temperature of the gaseous

species. When the kinetic and electronic energy of the molecules is sufficiently low that the activation energy of the reactions involved cannot be overcome, the equilibrium becomes frozen at this temperature. There is an apparent range of as much as 400°K over which this process can occur.

The method used to calculate the distribution of species at equilibrium was that of the minimization of the total free energy of the system as described by White, Johnson, and Dantzig³ and used by Dayhoff,

(1) This research has been sponsored in part by the National Aeronautics and Space Administration.

(2) (a) C. K. Wiefenbach, P. R. Griffiths, P. J. Schuhmann, and E. R. Lippincott, *J. Phys. Chem.*, **73**, 2526 (1969); (b) P. R. Griffiths, P. J. Schuhmann, and E. R. Lippincott, *ibid.*, **73**, 2532 (1969).

et al., in a series of computations on model^{4,5} or actual^{6,7} planetary atmospheres.

The results described in the two previous papers in this series^{2a,b} show that the approximation used by Dayhoff, *et al.*,^{4,5} in excluding graphite as a possible product was experimentally justified, that the high molecular weight product is largely composed of polynuclear aromatic hydrocarbons, and that the product distribution after the gas had been subjected to the discharge does indeed approach that computed for a limited high-temperature equilibrium.

One of the objects of Dayhoff's early work⁴⁻⁷ was to compute the concentration of biologically important molecules in prebiotic atmosphere. In this respect, the effect of discharges on C-H-N systems is more relevant than the previous systems studied,^{2a,b} since as early as 1953, Miller^{8,9} showed that one of the effects of spark discharges on C-H-N-O systems was the synthesis of some of the natural amino acids. Since then, several other workers have shown the same type of result with other techniques.¹⁰⁻¹³ It is the purpose of this paper to describe both qualitatively and quantitatively the product distribution after the action of a radiofrequency discharge on a series of organic nitrogen compounds in the *absence* of oxygen. The capability of a limited high-temperature thermodynamic equilibrium to predict the composition of the product will be discussed, while in a later paper it will be shown that amino acids and other biologically important molecules can be prepared using these products as intermediates.

Experimental Section

The apparatus and experimental methods have been described in some detail in the earlier papers in the series.^{2a,b} Pure compounds were again used as starting materials in order to completely specify the elemental composition of the reactant gas, and the compounds used are shown in Table I. A 3000-W, 10-MHz

the first was used to separate the light components of the mixture using a 3 ft by 1/8 in. column of Linde 5B molecular sieve and temperature programming between 60 and 400°. A thermal conductivity detector was used in the estimation of H₂ and N₂, while a flame ionization detector was used to determine CH₄, C₂H₆, C₂H₄, and C₂H₂. The components of the second sample were separated in a different GC in order to determine the heavier and more polar molecules present; of these HCN was determined quantitatively while the majority of the minor components, which never comprised more than 0.1% of the gas mixture, could be qualitatively identified. Initially the column was packed with Porapak Q, but later it was found that by coating this with 2% FFAP (free fatty acid polymer) retention times were reduced and peaks were sharpened up considerably. In both cases, temperature programming between 100 and 250° was used.

For the quantitative determination of H₂, N₂, CH₄, C₂H₆, C₂H₄, and C₂H₂, calibration was carried out using a precision gas mixture supplied by Matheson. To determine the sensitivity of the flame ionization detector to HCN, a sample of HCN was prepared by dropping concentrated H₂SO₄ onto NaCN, drying and distilling the product: chromatography showed less than 2% impurity.

Results and Discussion

a. Formation of a Solid Product. A similar effect was found to that described in the second paper of this series^{2b} as to the variation of the pressure at which the transition from a glow to flame plasma takes place. For compounds where the ratio of carbon to hydrogen is large (CH₃CN and C₂H₃CN) it was found that this transition took place at about 12 Torr, whereas for hydrogen-rich mixtures and CH₃NH₂ the transition never occurred; for the intermediate case of C₂H₅NH₂ and (CH₃)₂NH, the transition took place at a pressure of about 30 Torr, which was the maximum pressure used in these experiments. It was previously suggested^{2b} that the appearance of the flame plasma was caused by incandescent solid particles which were

Table I: Starting Compositions

Compound	Source	% C	% H	% N
Acetonitrile	Baker Analyzed	33.3	50.0	16.7
Acrylonitrile	Matheson Coleman and Bell redistilled	42.9	42.9	14.3
Monomethylamine	Air Products	14.3	71.4	14.3
Dimethylamine	Air Products	20	70	10
Monoethylamine	Matheson	20	70	10

oscillator was used to produce the discharge, and after the reactions had been stopped, the gaseous products were collected by filling the apparatus with 300 Torr of helium to facilitate separation of the products by gas chromatography (GLC). Two samples were collected;

(3) W. B. White, S. M. Johnson, and G. B. Dantzig, *J. Chem. Phys.*, **28**, 751 (1958).

(4) M. O. Dayhoff, E. R. Lippincott, and R. V. Eck, *Science*, **146**, 1461 (1964).

(5) R. V. Eck, E. R. Lippincott, M. O. Dayhoff, and Y. T. Pratt, *ibid.*, **153**, 628 (1966).

(6) E. R. Lippincott, R. V. Eck, M. O. Dayhoff, and C. Sagan, *Astrophys. J., Suppl. Ser.*, **147**, 753 (1967).

(7) C. Sagan, E. R. Lippincott, M. O. Dayhoff, and R. V. Eck, *Nature*, **213**, 273 (1967).

(8) S. L. Miller, *Science*, **117**, 528 (1953).

(9) S. L. Miller, *J. Amer. Chem. Soc.*, **77**, 2351 (1955).

(10) P. H. Abelson, *Science*, **124**, 935 (1956).

(11) J. Oro and S. S. Kamat, *Nature*, **190**, 442 (1961).

(12) K. Harada and S. W. Fox, *ibid.*, **201**, 235 (1964).

(13) R. A. Sanchez, J. P. Ferris, and L. E. Oregel, *Science*, **154**, 784 (1966).

Table II: The Effect of Adding H₂ and N₂ to CH₃CN in the Reactant Gas

Percentages of the starting materials			Atom percentages in the gas mixture			Weight percentages in the solid deposit		
CH ₃ CN	H ₂	N ₂	C	H	N	C	H	N
100	0	0	33.3	50.0	16.7	87.40	3.27	6.38
64.2	0	35.8	28.1	42.2	29.8	87.04	3.18	6.20
73.1	26.9	0	29.7	55.4	14.9	86.80	3.55	6.68

subsequently deposited on the walls of the reaction tube. In this work, it was verified that when CH₃CN and C₂H₃CN are used as starting materials, a large amount of solid was deposited on the walls of the tube: when CH₃NH₂ was used, no deposition occurred. In the intermediate case of C₂H₅NH₂ and (CH₃)₂NH, a slight discoloration of the walls occurred, indicating that this composition falls on the asphalt threshold.^{2b,4,5}

When computations were made for a series of C-H-N compositions over a large part of the ternary diagram, it was found that the extent of the computed asphalt region was strongly temperature dependent, and Figure 1 shows the position of the threshold, above which the concentration of asphalt is greater than 0.1%, for temperatures of 1000, 1400, and 2000°K. Also marked on the graph are the points representing the composition of the compounds used in this study as starting materials. It is seen that at 1400°K, the computed threshold passes through the composition corresponding to (CH₃)₂NH and C₂H₅NH₂.

A series of experiments were carried out in which CH₃CN was passed through the reaction tube after being mixed with nitrogen or hydrogen, so that the elemental composition of the reactant gas changed. The elemental analyses of the solid deposits are shown in Table II. Each of the analyses is very nearly the same, indicating that a similar product is formed each time, having the approximate composition of 66 atom % carbon, 4 atom % nitrogen, and 30 atom % hydrogen. In the earlier experiments using hydrocarbons^{2a} and C-H-O systems,^{2a} it was suggested that about 70% of the deposit was comprised of asphaltic hydrocarbons and the other 30% of aliphatic hydrocarbons which were probably formed as intermediates in the synthesis of the aromatic molecules. This conclusion was made by a comparison of the experimental results with calculations involving a model compound "asphalt" which has been extensively discussed.^{1,2,4-7,14} The free energy of formation of asphalt was estimated using the group contribution method,¹⁵ and a similar method may be used to calculate the free energy of formation of an asphaltic molecule with one nitrogen atom present. Several guesses were made as to the chemical nature of this nitrogen atom, including the substitution of a hydrogen atom by a —C≡N group and a —NH₂ group and the substitution of an aromatic CH group by a pyridine-type nitrogen atom. In no case was the resulting molecule computed to be present

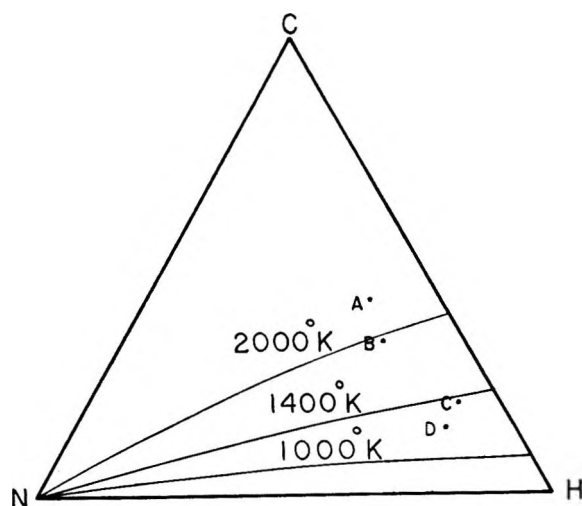


Figure 1. The computed asphalt thresholds at 1000, 1400, and 2000°K. The compositions of acrylonitrile, A, acetonitrile, B, monoethylamine and dimethylamine, C, and monomethylamine, D, are also shown.

at a concentration above 0.1% that of the parent molecule. From this it may be concluded that the nitrogen in the solid is present in a molecule which is either thermodynamically unstable at high temperatures, or a completely different type of compound is present in addition to the molecules which were found with the hydrocarbon system.^{2b}

It was noticed that the hydrogen concentration was greater in the solid product containing nitrogen than in the previous work when no nitrogen was present.^{2b} This led to the postulation that nitrogen was present in a separate compound, the formula of which is

Table III: Experimentally Measured Percentages of the Major Gaseous Products

Starting material	H ₂	N ₂	HCN	CH ₄	C ₂ H ₂	C ₂ H ₄	C ₂ H ₆
CH ₃ CN	40.8	3.6	47.2	1.4	6.1	0.43	0.06
C ₂ H ₃ CN	39.3	4.4	48.0	1.0	6.8	0.33	0.07
CH ₃ NH ₂	69.2	3.0	24.6	2.0	0.9	0.11	0.15
(CH ₃) ₂ NH	58.2	2.4	28.6	3.2	6.6	0.84	0.17
C ₂ H ₅ NH ₂	64.1	0.7	26.8	2.7	4.7	0.72	0.17

(14) H. C. Urey and J. S. Lewis, *Science*, **152**, 102 (1966).

(15) D. W. van Krevelin and H. A. G. Chermin, *Chem. Eng. Sci.*, **1**, 66 (1951).

Table IV: Computed Percentages of the Major Gaseous Products

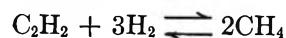
Temp, °K	(a) Starting Material, CH ₃ CN						
	H ₂	N ₂	HCN	CH ₄	C ₂ H ₂	C ₂ H ₄	C ₂ H ₆
1000	48.2	33.1	0.83	13.7	0.0034	0.021	7.8 × 10 ⁻⁴
1200	58.9	30.1	1.4	3.9	0.49	0.093	2.3 × 10 ⁻⁴
1400	46.7	25.7	8.2	0.78	12.8	0.14	3.4 × 10 ⁻⁶
Temp, °K	(b) Starting Material, C ₂ H ₅ NH ₂ -(CH ₃) ₂ NH						
	H ₂	N ₂	HCN	CH ₄	C ₂ H ₂	C ₂ H ₄	C ₂ H ₆
1000	61.7	15.9	0.060	20.5	0.0036	0.029	1.4 × 10 ⁻³
1200	76.0	13.9	0.96	6.0	0.53	0.13	4.3 × 10 ⁻⁴
1400	67.5	10.9	5.2	1.3	12.4	0.19	6.9 × 10 ⁻⁶
Temp, °K	(c) Starting Material, CH ₃ NH ₂						
	H ₂	N ₂	HCN	CH ₄	C ₂ H ₂	C ₂ H ₄	C ₂ H ₆
1000	59.8	20.4	0.65	18.8	0.0034	0.026	1.2 × 10 ⁻³
1200	73.3	18.0	1.1	5.4	0.50	0.11	3.6 × 10 ⁻⁴
1400	67.7	14.6	5.4	1.2	10.0	0.15	5.6 × 10 ⁻⁶

generally given as (HCN)_n, caused by the polymerization of HCN. Since the composition of this polymer is not well known,¹⁶ and many workers have cited different ways that HCN can polymerize,¹⁷⁻¹⁹ its free energy of formation could not easily be estimated in order to test its stability between 1000 and 1500°K. However, if the percentages of hydrogen and carbon equal to that measured for nitrogen are subtracted from the overall composition of the deposit, it is found that the resulting composition, 71 atom % carbon, 29 atom % hydrogen, corresponds exactly to that measured for the deposit formed with the hydrocarbons.^{2b} It is therefore suggested that a third type high molecular weight product is formed by the polymerization of HCN, which is shown in the next section to be present in high concentration. This conclusion has important implications in subsequent work on the formation of biologically important molecules.

b. Gaseous Products. Results of the analyses of the gaseous products are shown in Table III; these are the average of at least three runs, and are reproducible to ±10%. Unlike the results described in the previous papers,^{2a,b} the concentrations of the major products do not obviously correspond to equilibrium over a small temperature range. Computations were made for the compositions of CH₃CN, C₂H₅NH₂, and CH₃NH₂ at temperatures of 1000, 1200, and 1400°K, and the concentrations of the compounds which have been determined experimentally are shown in Table IV. A comparison of these two tables shows that the concentration of methane and acetylene correspond to equilibria occurring at about 1300°K for all three compounds, while the measured concentration of ethylene and ethane is always above the computed concentration. This is precisely the same result that was found for hydrocarbon and C-H-O^{2a} systems.

For these systems it was known that the C₂ radical is present in the plasma, and that the most stable

molecule at high-temperature equilibrium is acetylene. As the temperature is reduced, methane becomes thermodynamically favored, and the reaction may be represented as



The rupture of the C≡C bond necessary for this reaction to occur must take place in a series of steps involving radical hydrogenation prior to bond fission, which explains why both C₂H₄ and C₂H₆ are present above their equilibrium concentration.

For the C-H-N systems investigated in this work, the major discrepancy between the computed and the experimental results involves the relative concentrations of N₂ and HCN; the former is apparently formed at too low a concentration, while HCN is present at a much higher concentration than expected. For C-H-N systems at high temperature, one of the most stable components thermodynamically is the C≡N radical, while HCN is the most stable molecule. Only at temperatures below 1600°K does molecular nitrogen become thermodynamically favored over HCN. However at these lower temperatures, the activation energy required for the rupture of the C≡N band is difficult to overcome, especially because the formation of amines through hydrogenation reactions is not favored thermodynamically.

Of the minor compounds, acetonitrile and acrylonitrile are the only two detected that contain nitrogen, and both of these were present at a concentration of less than 0.01%. No trace of cyanoacetylene was seen in the chromatograms, although this molecule has

(16) T. Volker, *Angew. Chem.*, **72**, 379 (1960).

(17) R. M. Kliss and C. M. Mathews, *Proc. Nat. Acad. Sci. U. S.*, **48**, 1300 (1962).

(18) J. Oro, *Nature*, **191**, 1193 (1961).

(19) J. Oro and A. P. Kimball, *Arch. Biochem. Biophys.*, **96**, 293 (1963).

been suggested by Sanchez, *et al.*,¹³ to be an important product of the action of an electrical discharge on mixtures of methane and nitrogen. Hydrocarbons with more than two carbon atoms show a very similar pattern on gas chromatography to that found in the previous study on hydrocarbons.^{2b} Computations bear out the fact that at the high temperatures in the plasma, nitriles, especially unsaturated nitriles, are the dominant species. Aliphatic amines are computed to be present at very low concentration, even at temperatures below 1000°K, and no trace of any amine has been seen in any of the chromatograms.

Conclusion

At the present time, there are insufficient data for the construction of a kinetic model to estimate the concentrations of radicals produced by the rapid heating of an organic vapor to the plasma state, and for the consideration of the relaxation processes whereby these species react as they emerge from the plasma. It has been shown in the two earlier papers in this series^{2a,b} that this composition can be simply estimated to a first approximation by calculating the equilibrium concentration of all the possible species at temperatures between 1100 and 1400°K. It was also shown, for species which are stable at high temperatures, that the kinetics involved in adjusting the composition of the mixture as the temperature is reduced may lead to anomalous concentrations for some species. A similar, but somewhat more pronounced, result has been found for the C-H-N systems described above. Both the appearance of a solid deposit when reactant molecules with a high carbon:hydrogen ratio are used and a comparison between the experimentally determined and computed concentrations for most of the major products suggests that the reactions dominated by the tendency to reach thermodynamic equilibrium start slowing down at approximately 1600°K. By the time the temperature approaches

1300°K, the energy of the species emerging from the plasma is too low for the activation energies involved in further reactions to be overcome, and the product distribution remains essentially constant as the temperature drops.

Since the cyano radical is an important constituent of the plasma at high temperatures, HCN is present at higher concentrations than is calculated for the product distribution corresponding to equilibrium at 1300°K. This has the important result that (HCN)_x is a major component of the solid deposited on the walls of the reaction tube. In addition, the fact that HCN is present in the gas phase at relatively high concentration, after the rapid relaxation from a high-temperature equilibrium mixture, means that it could be formed in large quantities in prebiological atmospheres through the action of exciting radiation and discharges even though it would not be expected to be present in such large quantities through equilibrium calculations.

One result of these calculations has been to show that it is possible to estimate the product distribution after the action of a discharge on an organic mixture through equilibrium calculations where the only necessary data are the free energies of formation of any molecule or radical under consideration over a range of temperature. In this way it has been shown that the molecular distribution has been fairly well approximated for three different systems by assuming that equilibrium reactions cease to occur at significant rates below about 1300°K. Deviations from these equilibrium compositions have been explained qualitatively through kinetic effects, assuming that the activation energy needed for the fission of a strong bond cannot be overcome owing to the rapid relaxation of the reacting gas to lower temperature. However, the necessity of setting up complex models to simulate these results on a kinetic basis, with many unknown rate constants, has been obviated.

Spectral Characterization of Activated Carbon

by R. A. Friedel

U. S. Bureau of Mines, Pittsburgh, Pennsylvania

and L. J. E. Hofer¹

Mellon Institute of Carnegie-Mellon University, Pittsburgh, Pennsylvania (Received February 2, 1970)

The infrared absorption spectrum of activated carbon has been observed for the first time. The method of sample preparation which involves very intense grinding is described in detail. The spectrum shows definite bands at 1735 cm^{-1} , 1590 cm^{-1} , and 1215 cm^{-1} . These are interpreted, respectively, in terms of a carbonyl, aromatic structures or unconjugated chelated carbonyl, and C—O groups. The technique opens up the possibility for direct study both of the various functional groups on activated carbon itself and of various adsorbed species on activated carbon.

Infrared characterization of activated carbon is important for: (1) providing information on structure, such as the functional groups contained in the carbon, possibly mineral constituents, etc., (2) providing basic spectra of the activated carbon for comparison with spectra of the same carbon containing adsorbed material. Spectral studies of specific sorbates can provide much information on the molecular forces involved. No absorption spectra of activated carbon have appeared in the literature, presumably because of the difficulties involved in obtaining spectra. Coals and carbons are strong absorbers of visible radiation, but in nearly all cases transmission of infrared energy occurs. Usable coal sections several microns thick can be prepared rather easily;^{2a,b} however, for particulate samples such as carbons and cokes the thin section technique is, of course, not applicable. Even if sectioning were successful, the specimen would be full of holes and therefore unusable for spectral measurements. A successful approach involves the preparation of halide pellets (potassium bromide has been used in this work) in which finely divided carbonaceous samples are uniformly distributed.^{2b-4} Difficulties are least with carbon blacks which are finely divided, but chars and activated carbons are very hard and are difficult to grind. This publication describes the preparation of halide pellets of activated carbon suitable for spectral characterization, the techniques necessary for scanning spectra, and the type of spectrum obtained. Mattson and coworkers have reported spectra of sorbates on activated carbons by means of the attenuated total reflectance (ATR) technique.⁵⁻⁷

For obtaining absorption spectra the preparation of KBr pellets of chars and activated carbons requires reducing the sample to a very finely divided form by grinding it for many hours in a ball mill. The ball mill used is a power-driven vibrator (frequency 3500 strokes/min, amplitude 5 mm) driving a stainless steel vial (i.d. 9 mm, inner length 15 mm with four $\frac{1}{8}$ -in.

stainless steel balls). Total grinding time used is about 24 hr. It is important that the sample be no more than a few milligrams in order to ensure thorough grinding. If a large amount of sample is used in a small vial the sample serves as a cushion and thorough grinding is prevented. A standard KBr pellet is then prepared at a concentration of about 0.5 wt %.⁸ The spectrometers used in this work were Perkin-Elmer Models 21 and 521.

The absorption of carbonaceous materials may be so intense due to electronic absorption⁹ that the sample is completely opaque to visible and near-infrared light. This is not necessarily detrimental as transparency may exist for most carbonaceous materials in the infrared region of interest, particularly at lower frequencies. The spectral position of the initial transmittance, the so-called energy gap,^{9,10} differs for different carbons and coals. For Pittsburgh CAL activated carbon the energy gap is about 2300 cm^{-1} , or 0.3 eV.

If the first scan of the spectrum in the infrared shows complete or nearly complete absorption (Figure 1, spectrum a), one then rescans the spectrum with scale expansion or with a calibrated screen in the reference beam in order to produce a large magnification of the

(1) Head, Adsorption Fellowship, sponsored by Pittsburgh Activated Carbon Division, a subsidiary of Calgon Corp.

(2) (a) R. A. Friedel and M. G. Pelipetz, *J. Opt. Soc. Amer.*, **43**, 1051 (1953); (b) R. A. Friedel and J. A. Queiser, *Anal. Chem.*, **28**, 22 (1956).

(3) V. A. Garten and D. E. Weiss, *Aust. J. Chem.*, **10**, 295 (1957).

(4) R. A. Friedel, Proceedings of the Fourth Carbon Conference, University of Buffalo, Pergamon Press, New York, N. Y., 1960, p 321.

(5) J. S. Mattson, H. B. Mark, Jr., M. D. Malbin, W. J. Weber, and J. C. Crittenden, *J. Colloid Interface Sci.*, **31**, 116 (1969).

(6) J. S. Mattson and H. B. Mark, Jr., *ibid.*, **31**, 131 (1969).

(7) J. S. Mattson and H. B. Mark, Jr., *Anal. Chem.*, **41**, 355 (1969).

(8) R. A. Friedel, R. A. Durie, and Y. Shewchyk, *Carbon (Oxford)*, **5**, 559 (1968).

(9) R. A. Friedel, *Fuel*, **38**, 541 (1959).

(10) R. A. Friedel, *Brennst.-Chem.*, **44**, 23 (1963).

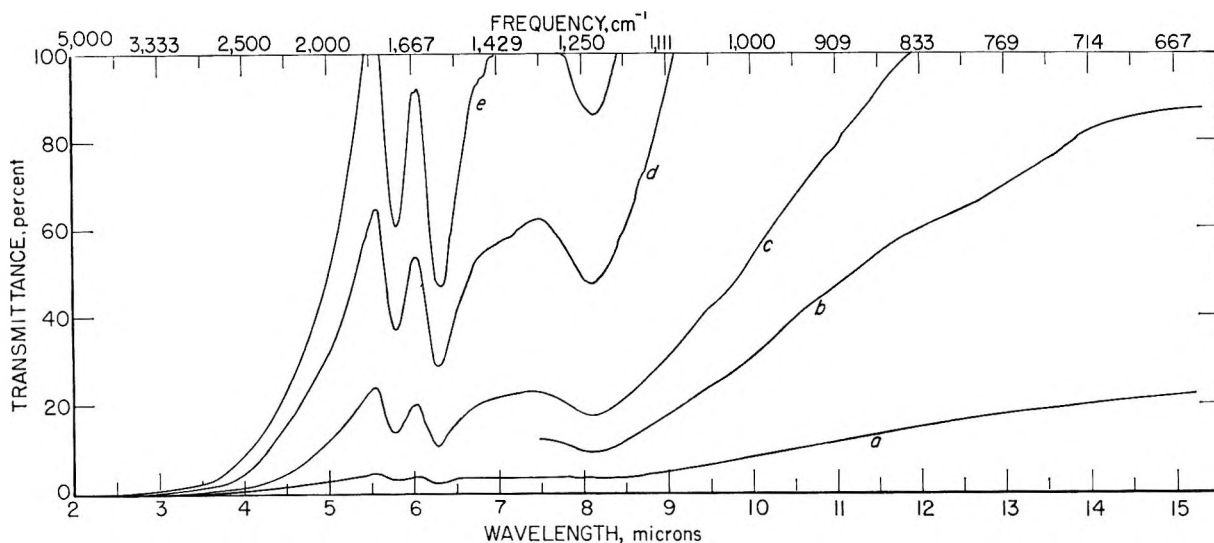


Figure 1. Infrared spectra of Pittsburgh activated carbon, type CAL. Spectrum a: KBr pellet, 0.540 mm thick and 12.7 mm in diameter, containing 0.5 wt % carbon in 200 mg of KBr; spectra b, c, d, e: scale expansions of spectrum a, at 3 \times , 5.5 \times , 14 \times , and 21 \times , respectively.

transmitted energy. Wider slits and slower spectral scanning speeds must be used. If too great magnification is used, it is possible to reach a point where the apparent transmittance may consist of an appreciable amount of instrumental scattered energy; the usual check for scattered energy must be made. In a spectrum of Pittsburgh CAL activated carbon (Figure 1) some functional groups are observable, such as (1) the band at 1735 cm^{-1} attributable to carbonyl groups, probably unconjugated ketone structures; (2) the band at 1590 cm^{-1} , the well-known carbonaceous band which is variously attributed to aromatic structures and to unconjugated, chelated carbonyl groups;^{2,8,11} and (3) the band at 1215 cm^{-1} which is probably associated with a carbon-oxygen absorption and/or phenoxy absorption. The bottom curve on the spectrum is the original scan under ordinary instrument conditions, with no amplification of transmitted energy. The other curves are all amplifications of the transmitted energy. The actual transmittance values for all the curves are calculated from the parameters of the scale-expansion or the calibrated screens. A spectrum of activated carbon obtained at low noise level by the

method described makes it possible to carry out spectral investigations of systems consisting of carbon and added materials. With this usable spectrum studies of sorbed species on activated carbon become possible.

A point of difference appears between Mattson's ATR results and the present results—little or no structure appears for the untreated, activated carbon by the ATR technique, whereas our absorption spectra demonstrate the presence of three distinct absorption bands. These bands are expected from the appearance of similar bands in spectra of coals and carbon blacks.^{2,12} We believe it is significant that the absorption technique appears to be more sensitive for observing the broad bands of activated carbons than the ATR technique. The fact that the absorption technique involves Mattson's "diffuse reflectance"⁵⁻⁷ is not necessarily a disadvantage since measurement of any spectrum, even of gases, suffers some loss of energy due to scatter, as the ATR method also does.

(11) J. K. Brown, *J. Chem. Soc. (London)*, 744 (1955).

(12) V. A. Garten and D. E. Weiss in "Proceedings of the Third Conference on Carbon," S. Mrozowski, Ed., Pergamon Press, New York, N. Y., 1959, p 295.

Electron Spin Resonance Study of 2,6-Di-*t*-butyl-4-methylphenol

Oxidation on Alumina

by Isao Suzuki, Yoshio Ono, and Tominaga Keiichi

Department of Chemical Engineering, Faculty of Engineering, Tokyo Institute of Technology, Meguro-ku, Tokyo, Japan
(Received January 14, 1970)

Three kinds of esr spectra have been obtained from 2,6-di-*t*-butyl-4-methylphenol on alumina catalyst under an oxygen atmosphere. A quadruplet spectrum (1:3:3:1) with splitting of 12 G appeared initially and was converted into a singlet with $\Delta H_{pp} = 13.3$ G at room temperature. Above 80°, the latter spectrum faded and a new singlet spectrum with $\Delta H_{pp} = 8$ G gradually appeared. These spectra were assigned to 2,6-di-*t*-butyl-4-methylphenoxy radical, 2,6-di-*t*-butyl-4-aldehydephenoxy radical, and galvinoxyl radical, respectively. These intermediates are the same ones confirmed in the liquid-phase oxidation. It is concluded that this catalytic oxidation occurs with a similar reaction path as the liquid-phase oxidation. Examining the poisoning effects of HCl and NH₃ on the radical formation with the catalyst, it is suggested that the active sites for the oxidation are basic ones. The final product (nonradical) of the oxidation was confirmed as a quinone by ir spectroscopy.

Introduction

Sterically hindered phenols such as 2,6-di-*t*-butyl-4-methylphenol are useful as antioxidants in the autoxidation of hydrocarbons. The oxidation of the phenols and their roles as inhibitors have been studied in the light of radical mechanisms. The liquid phase oxidation of the hindered phenols has been extensively investigated by the electron spin resonance (esr) method. Becconsall, *et al.*,^{1,2} have shown that the radicals formed during the oxidation of the phenols with lead dioxide in cyclohexane are mainly of two types: (a) primary radicals, *i.e.*, phenoxy radicals, formed by the abstraction of the phenolic hydrogen atom from the parent phenols; (b) secondary radicals, *i.e.*, more highly oxidized radicals formed from the primary radicals by the oxidation of their *para* substituents. Buchachenko, *et al.*,³ and Pokhodenko, *et al.*,^{4,5} reported a different oxidation path indicating that the phenoxy radical primarily formed was converted to the benzyl radical with hydrogen transfer from the *p*-methyl group to oxygen. Both subsequent dimerization of the benzyl radical and oxidation of the dimer result in the final product, stilbenquinone, *via* radicals.

In heterogeneous systems, similar esr studies on the oxidation have been carried out. Some typical esr spectra have been found with diphenylamine adsorbed on the catalysts like vanadium pentoxide, cupric oxide, cuprous oxide, and alumina under air.⁶ These findings indicate that it may be possible to use the catalysts as adsorbents for the hindered phenols in their heterogeneous oxidations.

The aim of the present work is to examine the intermediates of the oxidation of 2,6-di-*t*-butyl-4-methylphenol on alumina catalyst and to elucidate the mechanism of the oxidation.

Experimental Section

Materials. Alumina catalyst was prepared as follows. Aluminum isopropoxide was purified by distillation under reduced pressure and was hydrolyzed. The aluminum hydroxide thus obtained was dried at 120° for 2 hr and was activated by calcination at 550° for 2 hr. Silica gel was similarly prepared from ethyl orthosilicate. Silica-alumina catalyst was prepared by hydrolysis of the mixture of aluminum isopropoxide and ethyl orthosilicate. The ratio of the two components of the mixture was adjusted so that the alumina content of the silica-alumina was 17%. The specific surface areas of alumina, silica gel, and silica-alumina, measured by the BET method with nitrogen, were 244, 280, and 283 m²/g, respectively. Commercial grades of 2,6-di-*t*-butyl-4-methylphenol (DBMP), 3,3'-5,5'-tetra-*t*-butyl-4,4'-dihydroxydiphenylmethane (DHDH) and 2,4,6-tri-methylphenol (TMP), supplied from Tokyo Kasei Kogyo Co., were purified by repeated recrystallizations. From DBMP, 1,2-bis(3,5-di-*t*-butyl-4-hydroxyphenyl)ethane (DHDE) and 3,5-di-*t*-butyl-4-hydroxybenzaldehyde (HBA) were prepared by the methods of Cook⁷ and Coppinger,⁸ respectively.

(1) J. K. Becconsall, S. Clough, and G. Scott, *Proc. Chem. Soc.*, 308 (1959).

(2) J. K. Becconsall, S. Clough, and G. Scott, *Trans. Faraday Soc.*, 56, 459 (1960).

(3) A. L. Buchachenko and M. B. Neimann, *Dokl. Akad. Nauk SSSR*, 139, 916 (1961).

(4) V. D. Pokhodenko, L. N. Ganyuk, and A. I. Brodskii, *ibid.*, 145, 815 (1962).

(5) A. I. Brodskii, V. D. Pokhodenko, and L. N. Ganyuk, *Zh. Strukt. Khim.* 4, 210 (1963).

(6) K. Hirota, Y. Kageyama, and K. Kuwata, *Bull. Chem. Soc. Jap.*, 36, 875 (1963).

(7) C. D. Cook, *J. Org. Chem.*, 18, 261 (1953).

Cylinder oxygen was obtained from Suzuki Shokan Co. Before use, the oxygen was passed through a trap of liquid nitrogen to remove its moisture and was kept in a glass globe.

Apparatus and Procedure. The esr sample cell was a quartz tube of 8-mm outer diameter. Its upper part had a neck and a stopcock. A small amount of DBMP was packed into a small glass bulb, degassed, and sealed *in situ*. The alumina catalyst (200 mg) was put into the bottom of the cell and the glass bulb was placed on the neck. The catalyst was evacuated at 500° for 2 hr, which is the standard pretreatment of the catalyst in this experiment. After the catalyst had been cooled, the glass bulb was broken by a breaker so that the DBMP was spread over the alumina catalyst. The cell was then placed in a thermostat maintained at 100° for 30 min in order to assure further contact of the DBMP with the alumina catalyst. A given pressure of oxygen was introduced to the cell, and the DBMP-treated alumina was exposed to the oxygen for various durations. The esr measurements were carried out at room temperature after evacuation of the oxygen to prevent distortion due to it. The esr spectra were measured with a Japan Electron Optics X-band spectrometer (JES 3110-X), using 100-kHz field modulation. The line shapes measured were essentially independent of the modulation widths ranging from 1.0 to 4.0 G. Therefore, we used the modulation width of 4.0 G. The g value was determined using 1,1-diphenyl-2-picrylhydrazyl (DPPH, $g = 2.0036$). Absolute measurement of the number of spins was carried out by double integration using a benzene solution of DPPH as a standard. Infrared and visible spectra were recorded on Shimadzu Model IR-27A and UV-50M spectrometers, respectively.

Results and Discussion

Radical Formation on the Catalyst Surface. Remarkable esr absorption spectra were observed from the alumina-DBMP-oxygen system. Since no esr signal appeared unless oxygen was introduced to the system of alumina-DBMP, oxygen is required to form the radicals. On the other hand, no esr signal was observed from the system of DBMP-oxygen without alumina, leading to the conclusion that alumina is necessary to form the radicals. The shape and the intensity of the spectrum varied with the contact time as illustrated in Figure 1. The spectrum observed initially was a quadruplet with splitting of 12 G, and the intensity ratio of four peaks was roughly 1:3:3:1, as shown in (1) in Figure 1. A new singlet spectrum with $\Delta H_{pp} = 13.3$ G was observed upon longer exposure to oxygen, where ΔH_{pp} means peak to peak width. The g values of the quadruplet and the singlet were both 2.004. The spectra 2, 3, and 4 in Figure 1 were obtained at contact times of 10 min, 150 min, and 33 hr, respectively. As seen from these spectra in Figure 1,

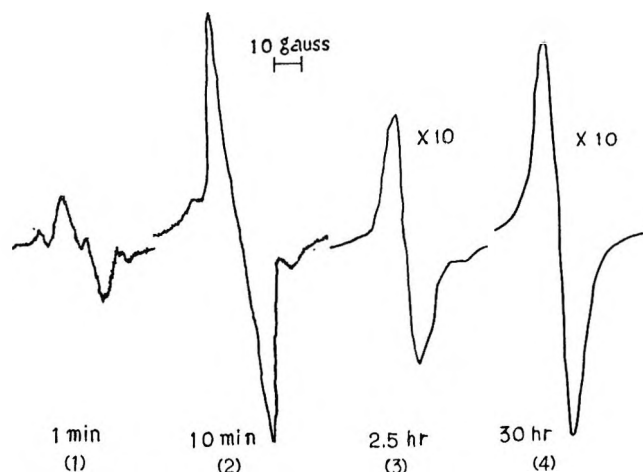


Figure 1. The esr spectra from DBMP on the alumina (measured *in vacuo*) after the various exposures to oxygen (15.3 Torr).

the shoulders in (2) and (3) become smaller as contact time increases, whereas the singlet peak becomes larger. Lastly, the shoulders disappeared completely as shown in 4 in the figure. Since the separation between the shoulders is similar to that between the outside peaks of the quadruplet spectrum, it is considered that the singlet spectrum is superimposed on the quadruplet spectrum in the spectra 2 and 3 in Figure 1. Hereafter, the radicals corresponding to the quadruplet spectrum and the singlet spectrum are called A radical and B radical, respectively. From the changes in the spectra as mentioned above, we arrive at the conclusion that A radical forms initially and converts into B radical in the presence of oxygen. Since the change in the spectra was stopped when the oxygen was evacuated from the system, it can be said that the conversion from A radical to B radical is an oxidation process. The singlet spectrum corresponding to B radical is rather stable under oxygen at room temperature. However, it changes at temperatures above 80°. That is, when exposing the DBMP-alumina to oxygen of the pressure of 100 Torr at room temperature, the intensity of the singlet spectrum corresponding to B radical increases and attains a plateau value within several days but ΔH_{pp} is constant. As soon as the temperature of the system under oxygen is raised to 100°, the width, ΔH_{pp} , decreases to a stationary value of 8 G, which shows that B radical changes to another one. The intensity, on the other hand, increases slightly initially and then decreases monotonically, as shown in Figure 2. The spectrum finally obtained is a singlet with $\Delta H_{pp} = 8$ G and g value of 2.004 (Figure 3). The corresponding radical is hereafter called C radical. In the course of the conversion from B radical to C radical, the overlap of the two spectra has been observed.

(8) G. M. Coppinger and T. W. Campbell, *J. Amer. Chem. Soc.*, **75**, 734 (1953).

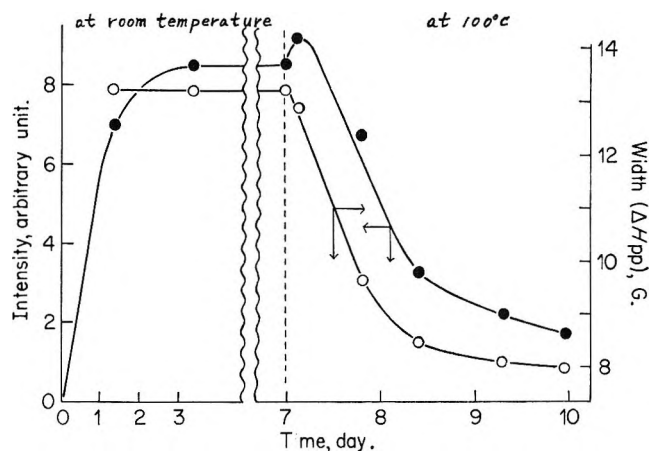


Figure 2. Changes in intensity (●) and in width (ΔH_{pp}) (○) of the esr signal obtained from DBMP on the alumina after the exposure to 100 Torr of oxygen with time.

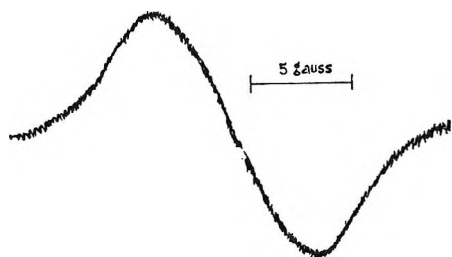


Figure 3. The final esr spectrum obtained from DBMP on the alumina by heating at 100° under oxygen.

The maximum amount of the radicals formed was estimated as follows. After the alumina catalyst (200 mg) was immersed in 1 cm^3 of the cyclohexane solution of DBMP ($1 \times 10^{-3} \text{ M}$) for 1 day at room temperature, the cyclohexane was removed thoroughly by evacuation. Oxygen (100 Torr) was admitted to the alumina, keeping the temperature of the system at 100° . The intensity of the esr signal increased and reached a maximum after 7 hr. The total amount of radicals at the maximum was $1 \sim 3 \times 10^{-7} \text{ mol}$ which corresponded to $10 \sim 30\%$ of the DBMP added to the alumina. This fairly large amount of the radicals thus produced on the surface of the alumina suggests strongly that the radicals are main intermediates of the oxidation of the DBMP. The nature of these three radicals, A, B, C, will be discussed in the following paragraphs.

Identification of A Radical. A radical can be identified with 2,6-di-*t*-butyl-4-methylphenoxy radical (called 4-methylphenoxy radical hereafter) on the surface in the following way. The esr spectrum of this radical in cyclohexane is a quadruplet (1:3:3:1) with coupling constant = 10.8 G, each components of which splits into three lines (1:2:1) with a coupling constant of 1.8 G.^{1,2} The spectrum of A radical ((1) in Figure 1) is the quadruplet with the intensity ratio, 1:3:3:1, without further splitting. On the surface, the esr

spectra of the radicals are usually so broadened that small hyperfine splittings are masked. Hence it is reasonable that the spectrum of A radical be regarded as that of 4-methylphenoxy radical. The same explanation can be applied to the identification of the phenoxy radical from TMP on the alumina. Figure 4 shows the esr spectrum obtained from TMP on the surface of the alumina after the exposure to oxygen.

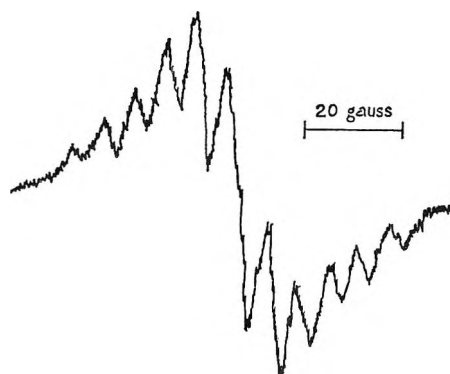


Figure 4. The esr spectrum from TMP on the alumina after the exposure to oxygen.

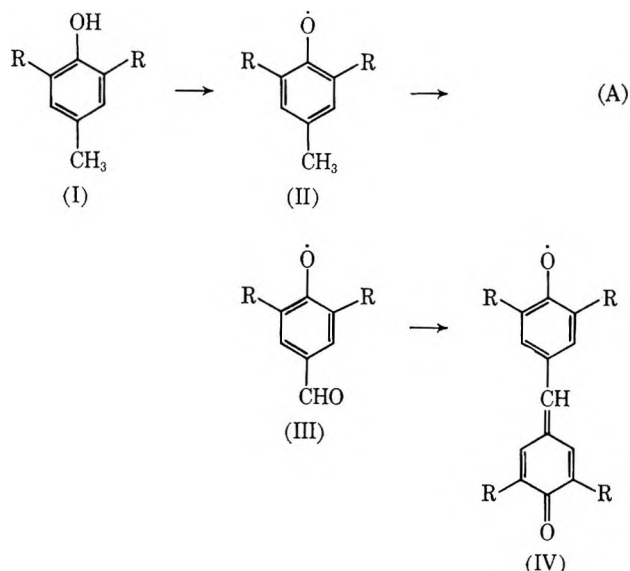
Identification of B Radical and C Radical. It is well known that cation radicals are formed from polyaromatic hydrocarbons on solid acids such as silica-alumina, alumina, and zeolites as well as in concentrated sulfuric acid.⁹ However, no esr signal could be observed from DBMP in concentrated sulfuric acid. It is, therefore, unlikely that DBMP forms its cation radical on the surface of the alumina. The difficulty of cation-radical formation from DBMP may be expected from higher ionization potentials of phenols.¹⁰ On the other hand, the experimental fact that the phenoxy radical is easily formed from DBMP in the oxidation process can be understood on the basis of lower redox potentials of phenol-phenoxy systems.¹¹ Identification of B and C radicals on the surface of the alumina can be made from considerations of the reaction path of the liquid-phase oxidation of DBMP. As concluded above, DBMP is initially oxidized to 4-methylphenoxy radical on the surface of the alumina. The experimental evidence showed that 4-methylphenoxy radical was successively oxidized into B radical.

Becconell, *et al.*,^{1,2} have suggested the following reaction paths on the basis of esr spectral data obtained in the oxidation of DBMP with lead dioxide in cyclohexane.

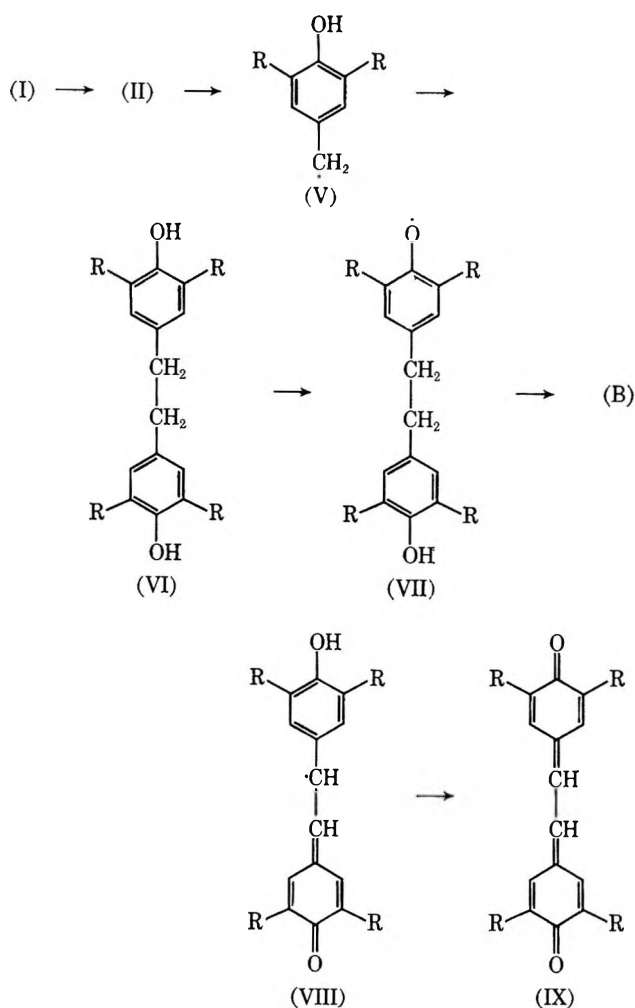
(9) W. K. Hall, *J. Catal.*, **1**, 53 (1962); D. M. Brouwer, *ibid.*, **1**, 372 (1962); H. Imai, Y. Ono, and T. Keii, *J. Phys. Chem.*, **69**, 1082 (1965); J. T. Richardson, *J. Catal.*, **9**, 172 (1967).

(10) G. F. Crable and G. L. Kearns, *J. Phys. Chem.*, **66**, 436 (1962).

(11) H. Mauser and B. Nickel, *Angew. Chem.*, **77**, 378 (1965).



R is a *t*-butyl group. On the other hand, Buchachenko, *et al.*,³ and Pokhodenko, *et al.*,⁴ have proposed a different path of the oxidation. That is, 4-methylphenoxy radical II is converted to 3,5-di-*t*-butyl-4-hydroxybenzyl radical V (called benzyl radical hereafter), instead of the conversion to 2,6-di-*t*-butyl-4-aldehydephenoxy radical III (called 4-aldehydephenoxy radical).



Provided that the oxidation path of DBMP on the alumina surface is similar to that in the solution investigated by these authors, one of the two reaction paths may be responsible for the present case. Then, B radical must be 4-aldehydephenoxy radical III in path A or either the benzyl V or the phenoxy radical VII in path B. On the basis of the following experiment, it has been concluded that B radical is 4-aldehydephenoxy radical III in path A. When HBA was adsorbed on the alumina in the same manner as with DBMP and the system was kept under 20 Torr of oxygen at room temperature, a singlet esr spectrum of $\Delta H_{pp} = 13$ G, g value = 2.004, was observed. The hydrogen of the hydroxy group of DBMP or TMP on the alumina is easily eliminated by oxidation to form the phenoxy radical as described above. Therefore, the spectrum observed here must be attributed to 4-aldehydephenoxy radical III. The value of ΔH_{pp} of B radical (13.3 G) agrees with that of 4-aldehydephenoxy radical III (13 G), which suggest that B radical is 4-aldehydephenoxy radical III in path A. If B radical is the benzyl radical V in path B, it must dimerize to form nonradical compound DHDE (VI), followed by the formation of its phenoxy radical VII in the presence of oxygen. This mechanism can be discounted by the following observation. The temperature of the DBMP-alumina was raised to 70° in the absence of oxygen after the intensity of the esr signal corresponding to B radical attained a plateau value at room temperature in the presence of oxygen. As seen from Figure 5, the intensity of the esr signal decreased while ΔH_{pp} remained unchanged. Changes neither in intensity nor in ΔH_{pp} were observed in the system when 100 Torr of oxygen was readmitted. On the other hand, a singlet spectrum ($\Delta H_{pp} = 14.3$ G) was observed from DHDE on the alumina at room temperature after the exposure to oxygen. Here, this esr spectrum should be that of its phenoxy radical VII, and the phenoxy radical VII cannot be formed from DBMP on the surface of the alumina. It is thus concluded that B radical is identical with 4-aldehydephenoxy radical III in path A, in which A radical is involved as 4-methylphenoxy radical II. Accordingly, it is suggested that C radical is galvinoxyl radical IV in path A. As mentioned above, the spectrum of C radical is the singlet with ΔH_{pp} of 8 G and g value of 2.004. The same esr spectrum can be obtained from DHDM on the alumina after the exposure to oxygen. Figure 6 shows the esr spectra obtained from DHDM adsorbed on the alumina in the same manner as with DBMP after the exposure to 5 Torr of oxygen at room temperature. The primary esr spectrum ((1) in Figure 6) is a triplet with splitting of 8 G, and the corresponding radical can be identified with its phenoxy radical by comparing with the spectrum of the radical in the solution.¹² This triplet spectrum is

(12) J. Pannell, *Chem. Ind.*, 1797 (1962).

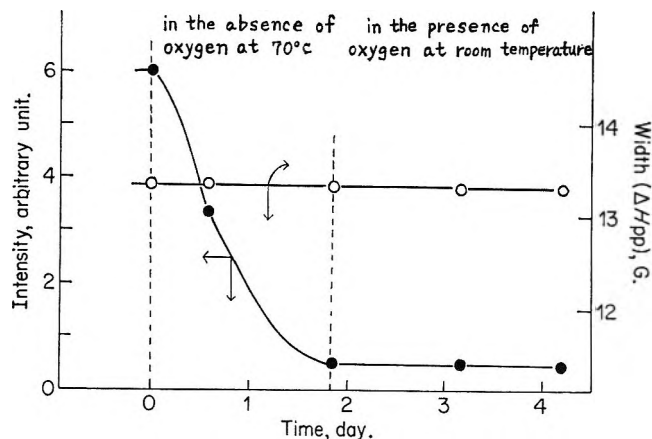


Figure 5. Changes in intensity (●) and in width ΔH_{pp} (○) of the esr signal from DBMP on the alumina with time.

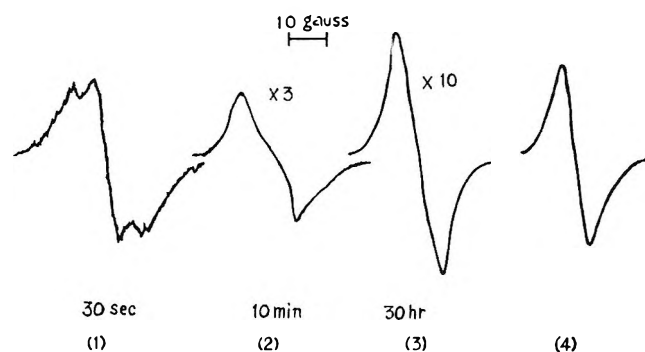


Figure 6. The esr spectra obtained from DHDM on the alumina (1)–(3) after the exposure to 5 Torr of oxygen and (4) after heating at 100° under oxygen.

converted gradually into a singlet spectrum ($\Delta H_{pp} = 14.3$ G). When the temperature of the system is kept at 100° under oxygen, ΔH_{pp} of the singlet spectrum decreases gradually. The final esr spectrum obtained is a singlet ($\Delta H_{pp} = 8$ G) with a g value of 2.004, (4) in Figure 6, which agrees with that of C radical. The same spectrum could be obtained in the following way. Galvinoxyl radical IV is obtained finally in the oxidation of DBMP or DHDM with lead dioxide.^{1,2,12} The alumina was immersed in the cyclohexane solution containing galvinoxyl radical IV, and the cyclohexane was removed thoroughly by evacuation. From this alumina, the singlet esr spectrum with ΔH_{pp} of 8 G was obtained. From these results, it is concluded that C radical is identified with galvinoxyl radical IV.

Final Oxidation Product. The mixture of the alumina (20 g) and DBMP (0.5 g) was heated at 100° for 1 hr in the absence of oxygen and kept at the same temperature in air for 3 days. The alumina was washed with cyclohexane, followed by extraction of the oxidation products with hot ethanol. A small amount of oily residue was obtained from the ethanol. Its infrared spectrum is shown by a solid line in Figure 7 with that of DBMP (dotted line). The absorption at 1610

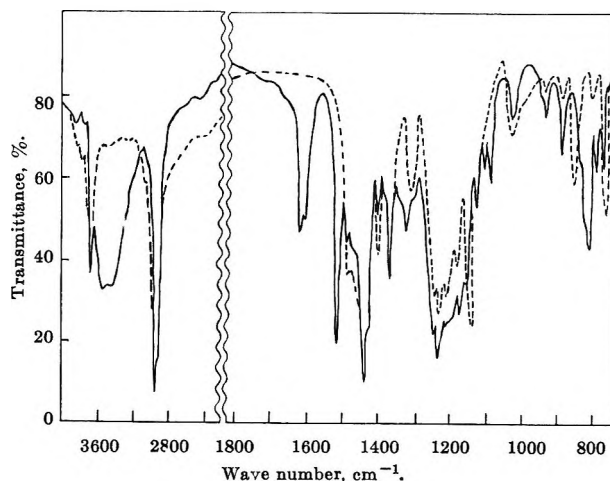


Figure 7. The infrared spectra of the oxidation products (—) from DBMP on the alumina and DBMP (---).

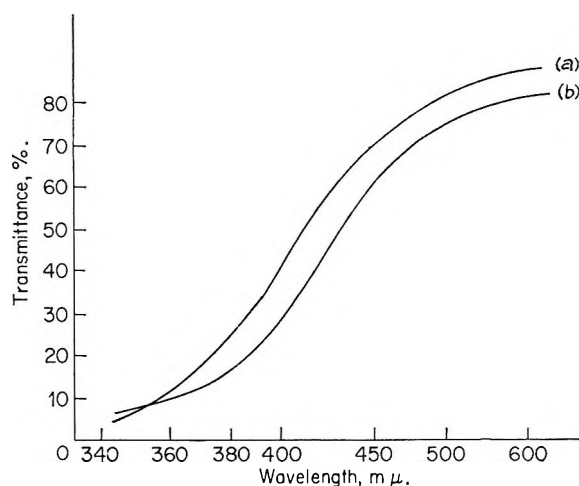
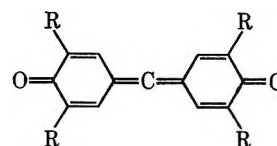


Figure 8. The visible spectra of the oxidation products from DBMP (a) and from DHDM (b) on the alumina.

cm^{-1} is well assignable to stretching of C=O in quinones which have two C=O groups in two benzene rings.¹³ The infrared spectrum of the oxidation products prepared similarly from DHDM on the alumina shows the same spectrum as that from DBMP. Also, visible absorption spectra of both oxidation products are shown in Figure 8 which appear to be very similar to each other. On the basis of the absorption spectra of both oxidation products, it can be considered that the final oxidation product from DBMP on the alumina catalyst is the quinoid species



Active Surface Site for DBMP Oxidation. ESR spectra were also obtained from DBMP on the silica-alumina

(13) J. M. Gordon and J. W. Forbes, *Appl. Spectrosc.*, 15, 19 (1961).

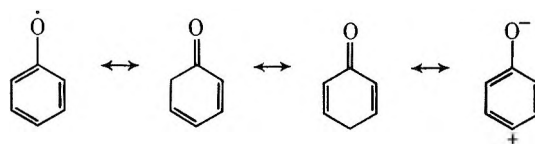
catalyst after the exposure to oxygen at room temperature. They are almost identical with those on the alumina and then the formations of 4-methylphenoxy radical II and 4-aldehydophenoxy radical III are proved. However, the amount of radicals on the silica-alumina was about $1/20$ th of that on the alumina. On the silica gel, no esr signal could be observed from DBMP after the exposure to oxygen. Since the specific surface areas of the three catalysts are almost equal, the differences must be attributed to the nature of the catalyst surfaces. Using the aluminas preliminarily treated with ammonia or hydrogen chloride, the total amounts of the radicals formed after the overnight exposure to 100 Torr of oxygen have been measured. Pretreatment conditions of the alumina catalyst and the ratio of the esr intensity of the radicals relative to

that obtained on the nonpretreated alumina are summarized in Table I. The amount of radicals obtained on the HCl-pretreated alumina (A-1, A-2) is enormously depressed while that on the NH_3 -pretreated alumina (B-1, B-2) is decreased only to one-half. It is suggested that the activity of the catalyst may be explained in terms of the basicity. Gersmann, *et al.*,¹⁴ have reported that the rate of autoxidation of DBMP in the solution of binary mixture of *t*-butyl alcohol and 1,2-dimethoxyethane, containing potassium *t*-butoxide, is much larger than that in alkaline ethanol. The difference was explained by the basicity of the solution: DBMP is completely ionized in the former solution whereas DBMP dissociated to the extent of only 20% in the alkaline ethanol. The following resonance can be written for phenoxy radical.¹⁵

Table I: The Pretreatment Condition and the Relative Intensity of the ESR Signal Obtained from DBMP on the Aluminas

Name	Pretreatment condition	Relative esr intensity
Alumina	Nontreatment	100
Alumina A-1	HCl, 300 Torr ^a (RT ^b)	0
Alumina A-2	HCl, 300 Torr (70°)	5
Alumina B-1	NH_3 , 300 Torr (RT)	45
Alumina B-2	NH_3 , 300 Torr (70°)	52

^a Exposed to 300 Torr of HCl (or NH_3) for 10 min at room temperature. ^b And evacuated for 30 min at room temperature (RT) or 70°.



In basic environments, DBMP may easily form its phenoxy radical. The present authors have observed the esr spectrum of 4-methylphenoxy radical II by the oxidation of DBMP with air in the benzene-ethanol containing sodium hydroxide, which suggests that DBMP is oxidized easily in a basic environment.

(14) H. Gersmann and F. Bickel, *J. Chem. Soc.*, 2356 (1962).

(15) E. Müller, K. Ley, and W. Keidaisch, *Chem. Ber.*, **87**, 1605 (1954).

Electron Paramagnetic Resonance Spectroscopy of Free-Radical Intermediates in the System Titanous Ion-Hydrogen Peroxide

by Yasuhiro Shimizu, Takeshi Shiga,¹ and Keiji Kuwata

Department of Chemistry, Faculty of Science, Osaka University, Toyonaka, Osaka, Japan (Received September 22, 1969)

The reaction of titanous chloride with hydrogen peroxide in acid solution was investigated by esr spectroscopy with a fast-flow technique and fast-quenching method. The g factors of the two signals (S_1 and S_2) observed in this system were not affected by the presence of extra anions, cations, or chelating reagents. This fact suggests that the free-radical species strongly coordinate with Ti(IV) ion or $Ti^{4+}(H_2O_2)_n$ complex ion and have no ability to form complexes with other metal ions, and that the unpaired electron is localized on the free-radical ligand and has low density on the Ti atom in the complex. Spectra similar to those of the Ti(III)-H₂O₂ system were observed for the uv-irradiated solution of $Ti^{4+}(H_2O_2)_n$ complex at room temperature, and the relative intensities of S_1 and S_2 depended on the ratio of concentrations of Ti(IV) ion and H₂O₂. The observed spectra in the solid phase mostly resembled that of the HO₂· radical in view of the anisotropy of the g factor. The variation in g factor and hyperfine splitting (hfs) constant from those of free HO₂· was calculated using Stone's method with extended Hückel MO theory. As a result S_1 and S_2 were assigned to HO₂· radicals coordinated with Ti(IV) or $Ti^{4+}(H_2O_2)_n$ and slightly perturbed by the coordination.

The fast-flow technique in esr spectroscopy has made possible the observation of many kinds of short-lived free radicals in the reaction of H₂O₂ with TiCl₃ in the presence of organic substrates.

When solutions of TiCl₃ and H₂O₂ were mixed in an esr cavity, Dixon and Norman² observed a narrow singlet spectrum, line width 1 G, which was attributed to the ·OH radical. Since their study, several investigations have been made of this reaction, and two narrow lines with a spacing of a few gauss in the esr spectrum have been reported.³⁻¹⁰

Piette, *et al.*,³ showed that the intensity ratio of the low-field peak to the high-field peak was variable, and they assigned the low-field peak S_1 to an HO₂· radical and the high-field peak S_2 to an ·OH radical. Many other investigators⁴⁻¹¹ have researched this system and related systems.

From these investigations the conclusion that the signals observed are due to complexes of an ·OH radical or an HO₂· radical with Ti(IV) ion or Ti(IV) complex ions has been reasonably substantiated, but mutually conflicting proposals for the structure of the complex have been made. The assignment of the signals seems to be unestablished so far.

In the present study, the authors conclude that the two peaks S_1 and S_2 in the esr spectra are due to complexes of HO₂· radicals with Ti(IV) ions and/or $Ti^{4+}(H_2O_2)_n$ complex ions of different composition. This conclusion is based on fast-flow and fast-quenching experiments, photolysis of a related system, and theoretical consideration of the g factor of HO₂· radicals in these complexes.

Experimental Section

Observation of Radicals in the Fast-Flow System. The

mixing chamber of the flow system, which was constructed according to Dixon and Norman's description,² was connected to a capillary cell for an esr cavity of TE₀₁₁ mode. Aqueous solutions of Ti(III) and H₂O₂ were prepared with distilled water or ion-free water and freed of oxygen by bubbling nitrogen through the solution in a container with a magnetic stirrer for 20-30 min. The design for the driving of reactant solutions into mixing cell and esr cavity has been described elsewhere.¹²

The effects of the addition of extra anion, cation or chelating reagent on g factors and intensities of the peaks were examined by adding these reagents to the reactants before mixing. The concentration of the additive was 0.1-0.5 M in the 1.3×10^{-2} M TiCl₃ solution and/or in the 1.5×10^{-1} M H₂O₂ solution, each being acidified to pH 2.0. The additional ions can bring

(1) Medical School Osaka University, Osaka, Japan.

(2) W. T. Dixon and R. O. C. Norman, *Nature*, **196**, 891 (1962); *J. Chem. Soc. (London)*, 3119 (1963).

(3) L. H. Piette and G. Bulow, Preprint, Petroleum Division, American Chemical Society, April 1964.

(4) (a) F. Sicilio, R. E. Florin, and L. A. Wall, *J. Phys. Chem.*, **70**, 47 (1966); (b) Y. S. Chiang, J. Craddock, D. Mickewich, and J. Turkevich, *ibid.*, **70**, 3509 (1966).

(5) H. Fischer, *Ber. Bunsenges. Phys. Chem.*, **71**, 685 (1967).

(6) J. Stauff and H. J. Huster, *Z. Phys. Chem. (Frankfurt am Main)*, **55**, 39 (1967).

(7) A. R. Metcalfe and W. A. Waters, *J. Chem. Soc., B*, 340 (1967).

(8) K. Takakura and B. Rånby, *J. Phys. Chem.*, **72**, 164 (1968).

(9) M. S. Bains, J. C. Arthur, Jr., and O. Hinojosa, *ibid.*, **72**, 2250 (1968).

(10) K. Ohno, J. Sohma, and G. Komatsu, Preprint, 7th Symposium on Electron Spin Resonance, Sapporo, Japan, 1968.

(11) (a) M. Setaka, Y. Kirino, T. Ozawa, and T. Kwan, *J. Catal.*, in press; (b) G. Czapski, H. Levanon, and A. Srauni, *Israel J. Chem.*, in press.

(12) T. Shiga, *J. Phys. Chem.*, **69**, 3805 (1965).

about reduction of the H_2O_2 , but titration showed that the consumption of H_2O_2 by these ions was negligible in acid solution except for the cases of SCN^- and NO_2^- . The reactivity of radicals in the system toward alcohol was also examined in the presence of additional metal ions.

To obtain the esr signals S_1 or S_2 from the solid phase, the solutions which contain radicals corresponding to S_1 or S_2 alone were rapidly injected into the liquid nitrogen and radical species were quickly quenched after the mixing.

In this quenching experiment the distance between the mixing chamber and the outlet of the capillary tubing was adjusted so that the time between mixing and quenching was the same as that of the esr measurement.

The ultraviolet irradiation of the flowing solution of Ti^{4+} - H_2O_2 complex in acid medium was carried out at room temperature, using a 1-kW high-pressure mercury arc lamp, the light of which was focused on a quartz cell in a resonant cavity by a quartz lens.

Photolysis in the Solid Phase. The frozen solution of Ti^{4+} - H_2O_2 complex was irradiated at 77°K with uv light at various concentration ratios of $\text{Ti}(\text{IV})$ to H_2O_2 .

Observation of O^- , O_2^- , O_3^- , $\cdot\text{OH}$, and $\text{HO}_2\cdot$ in the Solid Phase. Spectra were taken also of O^- ,^{13,14} O_2^- ,¹⁵⁻¹⁷ O_3^- ,¹⁸ $\cdot\text{OH}$,¹⁹ and $\text{HO}_2\cdot$.^{16,20-22} radicals by similar procedures.

The esr spectra were recorded using a Varian V-4500 spectrometer equipped with 100-kHz field modulation and partly using an X-band spectrometer with 455-kHz field modulation. The microwave frequency was approximately 9.45 GHz. The line separation and g factor observed in the flow system were determined with reference to that of an NO radical²³ in solution contained in a capillary tube attached to the outside of a flow cell. At 77°K, the g factor was measured by direct comparison with polycrystalline DPPH, for which $g = 2.0036$ at room temperature. The spin Hamiltonian in frozen solid solution was determined by comparison of the observed spectrum with the computed spectrum. The spectrum computation included an anisotropic g tensor and an isotropic hyperfine interaction with Gaussian line shape. This method is a modification of the original method of Kneubühl.²⁴

Calculation of g Factor of the $\text{HO}_2\cdot$ Radical

Writing the n th molecular orbital ϕ_n as a linear combination of atomic orbitals, $\phi_n = \sum_k \chi_k^{(n)}$, where $\chi_k^{(n)}$ is an (un-normalized) atomic orbital on atom k , Stone²⁵ has derived the following expression for the g factor of a radical

$$g_{zz} = 2.00232 + \frac{\sum_k \langle \chi_k^{(p)} | l_{kz} | \chi_k^{(n)} \rangle \sum_{k'} \zeta_{k'} \langle \chi_{k'}^{(n)} | l_{k'z} | \chi_{k'}^{(p)} \rangle}{\epsilon_p - \epsilon_n} \quad (1)$$

Here l_{kz} is the z component of angular momentum about atom k , ζ_k is the spin-orbit coupling constant for atom k , ϵ_p is the energy of the odd electron orbital, and ϵ_n is the energy of the n th molecular orbital in the molecule.

The n th extended Hückel molecular orbital ϕ_n is given as a linear combination of Slater atomic orbitals which are not orthogonal to each other, $\phi_n = \sum_k c_k^{(n)} \chi_k$,

where $c_k^{(n)}$ is the coefficient of the atomic orbital χ_k .²⁶

In the calculation of the g factor of a radical using Stone's theory, it is necessary to use molecular orbitals whose basis functions are orthonormal, so that the extended Hückel MO was transformed to the wave function ϕ'_n , which gave the same electron distribution on an atom, *viz.*

$$\phi'_n = \sum_k (\text{sign}) \sqrt{P_{kk}^{(n)}} \chi'_k \quad (2)$$

where χ'_k is a new atomic wave function which is orthogonal to all the others and $P_{kk}^{(n)}$ is the charge density on atom k of the n th orbital. This last quantity is given by

$$P_{kk}^{(n)} = \sum_q C_k^{(n)} C_q^{(n)} S_{kq} \quad (3)$$

In the extended Hückel MO calculations, the H_{ii} are taken to be the valence state ionization potentials, and the H_{ij} are calculated from $H_{ij} = 0.5K(H_{ii} + H_{jj})S_{ij}$ where $H_{ii}(\text{H}, 1s) = -13.6$ eV, $H_{ii}(\text{O}, 2s) = -35.30$ eV, $H_{ii}(\text{O}, 2p) = -17.76$ eV, and $K = 1.75$.²⁶

According to the discussion of the probable geometry of $\text{HO}_2\cdot$ radicals,^{27,28} we used $r(\text{OH}) = 0.958$ Å,

(13) M. J. Blandamer, L. Shields, and M. C. R. Symons, *J. Chem. Soc.*, 4352 (1964).

(14) J. R. Brailsford, J. R. Morton, and L. E. Vannott, *J. Chem. Phys.*, **49**, 2237 (1968).

(15) P. H. Kasai, *ibid.*, **43**, 3322 (1965).

(16) T. Ichikawa, M. Iwasaki, and K. Kuwata, *ibid.*, **44**, 2979 (1966).

(17) H. R. Zeller and W. Känzig, *Helv. Phys. Acta*, **40**, 845 (1967).

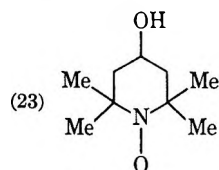
(18) T. Anderson, J. R. Byberg, and K. J. Olsen, *J. Phys. Chem.*, **71**, 4129 (1967).

(19) C. L. Aseltine and Y. W. Kim, *J. Phys. Chem. Solids*, **29**, 531 (1968).

(20) G. Czapski and B. H. Bielski, *J. Phys. Chem.*, **67**, 2180 (1963).

(21) F. J. Adrian, E. L. Cochran, and V. A. Bowers, *J. Chem. Phys.*, **47**, 5441 (1967).

(22) S. J. Wyard, R. C. Smith, and F. J. Adrian, *ibid.*, **49**, 2780 (1968).



$$g = 2.00657, a_N = 16.9 \text{ G}$$

(24) F. K. Kneubühl, *J. Chem. Phys.*, **33**, 1074 (1960).

(25) A. J. Stone, *Mol. Phys.*, **6**, 509 (1963).

(26) R. Hoffmann, *J. Chem. Phys.*, **39**, 1397 (1963).

(27) G. J. Minkoff, *Discuss. Faraday Soc.*, **2**, 151 (1947).

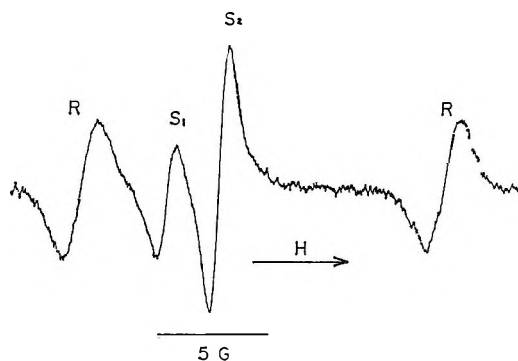


Figure 1. ESR spectrum of the free radicals observed in the TiCl₃-H₂O₂ system: [H₂O₂] = 1.5 × 10⁻¹ M, [TiCl₃] = 1.3 × 10⁻² M, and pH 2.0.

$r(\text{OO}) = 1.3 \text{ \AA}$, and $\angle \text{HOO} = 108^\circ$ for the ground state of $^2\text{A}''$, as in Boyd's paper.²⁸ The overlap integrals S_{ij} were calculated using Mulliken's table²⁹ for this molecular geometry.

Results

The Fast-Flow System of Ti(III)-H₂O₂. By mixing Ti(III) solution with H₂O₂ solution two singlets, S₁ at lower field and S₂ at higher field, can be observed with the intensity ratio of S₁ to S₂ dependent on the concentrations of Ti(III) and H₂O₂, as pointed out by earlier investigators.^{3,4a,8} Figure 1 shows the spectrum obtained by mixing the 1.3 × 10⁻² M TiCl₃ solution with the 1.5 × 10⁻¹ M H₂O₂ solution. The g factors of S₁ and S₂ were 2.01425 and 2.01276, respectively.

The effects of the presence of extra anions, cations, or chelating agents on the g factors of peaks S₁ and S₂ are summarized in Table I.

Table I: Effect of Presence of the Extra Anions, Cations, or Chelating Reagents on g Factors of Radical Species

	$g(\text{S}_1)$	$g(\text{S}_2)$
Mg ²⁺	2.01425	2.01281
Ca ²⁺	2.01430	2.01273
Sr ²⁺	2.01427	2.01279
Ba ²⁺	2.01425	2.01278
Zn ²⁺	2.01422	2.01266
Cd ²⁺	2.01429	2.01277
Hg ²⁺	2.01430	2.01265
Cl ⁻	2.01422	2.01275
SO ₄ ²⁻	2.01424	2.01269
NO ₃ ⁻	2.01428	2.01277
C ₆ H ₅ (OH)(NO ₂) ₂	2.01427	2.01271
EDTA	2.01428	...
Pyridine	2.01427	2.01268
SCN ⁻
NO ₂ ⁻

In the cases of EDTA, SCN⁻, and NO₂⁻, neither S₁ nor S₂ was observed, except at low concentration of EDTA, where S₁ appeared and its g factor was unchanged.

With the addition of Co(II) or Ni(II) ion to the system, S₂ only was observed, and its g factor was not affected. Cu(II) ion remarkably affected the intensity of both peaks; [Cu(II)] = 1 × 10⁻³ M, both peaks were absent. When 2.5 vol % of methanol was added to this system, however, an alcohol radical produced by the abstraction of a hydrogen atom from alcohol was formed. Table II shows the effect of such metal ions on the intensities of S₁, S₂, and on the reactivity of radicals in the system with methanol.

Table II: Effects of Metal Ions on the Intensity of the Signals and on the Reactivity of the System

Concn, mol/l.	Relative intensity		Reactivity	
	S ₁	S ₂		
II _a -II _b	5 × 10 ⁻¹	+	++	+
Co ²⁺	1 × 10 ⁻²	+	++	+
	1 × 10 ⁻¹	-	+	-
Ni ²⁺	1 × 10 ⁻²	+	++	+
	1 × 10 ⁻¹	-	++	-
Cu ²⁺	1 × 10 ⁻⁴	+	+	+
	1 × 10 ⁻³	-	-	+
Al ³⁺	1 × 10 ⁻²	+	++	+
	5 × 10 ⁻¹	-	-	+

Photolysis of Ti⁴⁺-(H₂O₂) Solution. The flowing aqueous solution of Ti⁴⁺(H₂O₂)_{*n*} complex was irradiated in an esr cavity with uv light and showed the same spectra as observed in the fast-flow system of Ti(III) and H₂O₂, whereas the Ti⁴⁺(H₂O₂)_{*n*} complex itself did not give a detectable signal without uv light irradiation.

The relative intensity of the two peaks varied with change in the concentration ratio of H₂O₂ to Ti(IV). At small values of concentrated (H₂O₂)/concentrated (Ti(IV)) two well-resolved peaks were observed with peak S₂ being enhanced to a greater extent than peak S₁. A typical spectrum observed in the system of 8.8 × 10⁻² M H₂O₂ and 5.6 × 10⁻² M Ti(IV) is shown in Figure 2a. With increase in the concentration ratio, however, the intensity of peak S₁ increased and that of peak S₂ decreased. Finally, in the case of 4.4 × 10⁻¹ M H₂O₂ and 1.2 × 10⁻² M Ti(IV), peak S₁ became predominant with only a trace of peak S₂, as seen in Figure 2b.

Esr Spectra of the Free Radicals in the Solid Phase. By fast quenching of the radical species corresponding to S₁ and S₂ in the Ti(III)-H₂O₂ system at 77°K, a spectrum of asymmetric lines (Figure 3) was observed. This spectrum has a shoulder on the low-field side, which is characteristic of the g anisotropy of nearly axial symmetry. The parameters in the spin Hamiltonian determined by comparison of the observed spectra with the computer-simulated ones are given in Table III and Figure 4.

(28) M. E. Boyd, *J. Chem. Phys.*, **37**, 1317 (1962).

(29) R. S. Mulliken, C. A. Rieke, D. Orloff, and H. Orloff, *ibid.*, **17**, 1248 (1949).

Table III: Principal Values of the g Tensor and Proton Hyperfine Coupling Constant for Free HO_2 , S_1 , and S_2 , Evaluated by Simulation. Calculated g Tensor and Spin Density ρ_0 on the Central Oxygen Atom of HO_2 .

		$\cdot\text{O}_2\text{H}$	S_1	S_2	Error in the determination by simulation
Observed	g_{zz}	2.0035	2.0035	2.0035	0.0005
	g_{yy}	2.0090	2.0090	2.0090	
	g_{xx}	2.0355	2.0300	2.0240	
	a_{H}	13 G	7 G	5 G	1 G
Calculated	$H_{\text{rr}}(\text{O}, 2p_x)^\dagger$	-16.56 eV	-15.90 eV	-15.71 eV	
	g_{zz}^a	2.00232	2.00232	2.00232	
	g_{yy}	2.00280	2.00264	2.00260	
	g_{xx}	2.03441	2.02711	2.02468	
	ρ_0	0.3114	0.2301	0.2102	

^a The x axis was taken to be along the 0-0 axis, and the z axis was perpendicular to the molecular plane. [†] The coulomb integral of the terminal oxygen atom.

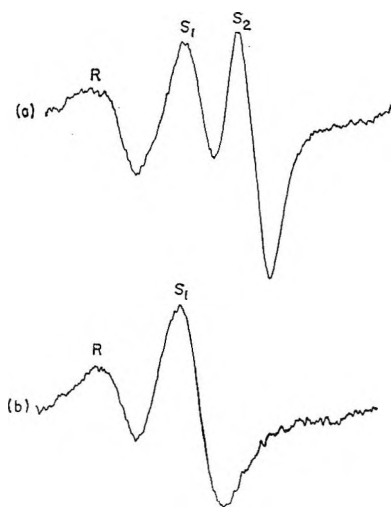


Figure 2. ESR spectra observed in the photolysis of the flow system of $\text{Ti}^{3+}(\text{H}_2\text{O}_2)_n$: (a) $[\text{H}_2\text{O}_2] = 8.8 \times 10^{-2} \text{ M}$, $[\text{TiCl}_4] = 5.6 \times 10^{-2} \text{ M}$, pH 1.5; (b) $[\text{H}_2\text{O}_2] = 4.4 \times 10^{-1} \text{ M}$, $[\text{TiCl}_4] = 1.2 \times 10^{-2} \text{ M}$, pH 1.5.

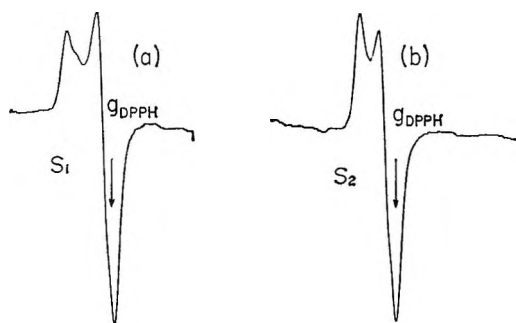


Figure 3. ESR spectra of S_1 and S_2 at 77°K in the solid phase after mixing of TiCl_3 with H_2O_2 : (a) $[\text{H}_2\text{O}_2] = 8.8 \times 10^{-2} \text{ M}$, $[\text{TiCl}_3] = 2.6 \times 10^{-2} \text{ M}$, pH 2.0; (b) $[\text{H}_2\text{O}_2] = 4.4 \times 10^{-1} \text{ M}$, $[\text{TiCl}_3] = 1.3 \times 10^{-1} \text{ M}$, pH 2.0.

Figure 5 shows the spectra obtained by uv irradiation of the frozen solution at various H_2O_2 -Ti(IV) concentration ratios.

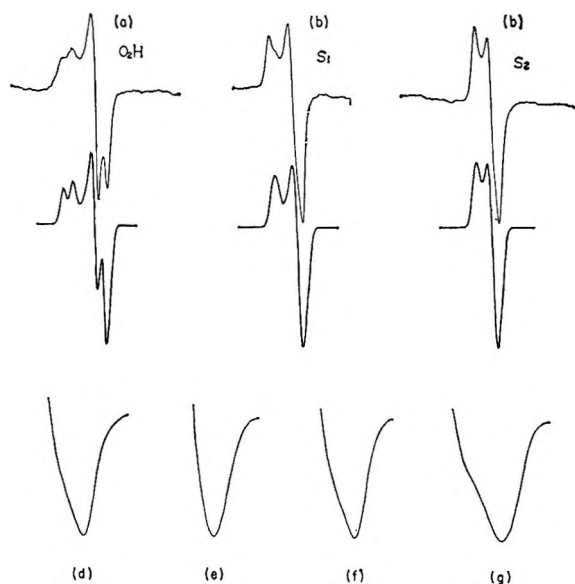


Figure 4. Comparison of observed spectra for free $\text{HO}_2\cdot$, S_1 , and S_2 with computer-simulated spectra using the values of g factor and hyperfine coupling constant of Table III. Observed spectra in upper row, and simulated spectra in middle row: (a) free $\text{HO}_2\cdot$; (b) S_1 ; (c) S_2 . The lower row shows the partially expanded spectra of S_1 with varying a_{H} ; (d) observed S_1 ; (e) $a_{\text{H}} = 0$; (f) $a_{\text{H}} = 7 \text{ G}$; (g) $a_{\text{H}} = 11 \text{ G}$ with the same g tensor and line width.

The observed spectra of $\cdot\text{OH}$, $\text{HO}_2\cdot$, and O_2^- in the solid phase at 77°K are shown in Figure 6.

Discussion

In esr studies of the system of TiCl_3 - H_2O_2 using fast-flow techniques, two peaks have been reported. There is a slight discrepancy between the values of g factors of the two peaks measured by many investigators for this system. For example, our values for the two peaks differ slightly from the apparently very accurate values of Fischer.⁵ The mutual differences between the g factors of the two peaks, however, are usually almost the same in each case. Thus these discrepancies seem-

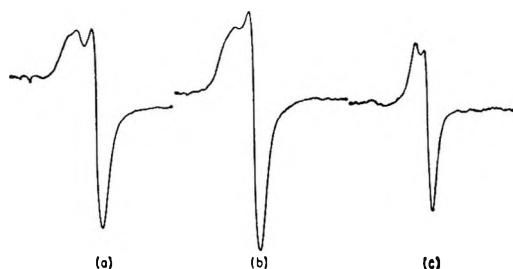


Figure 5. ESR spectra obtained by uv irradiation of a solid aqueous solution of $\text{Ti}^{4+}(\text{H}_2\text{O}_2)_n$ complex: (a) $[\text{H}_2\text{O}_2] = 9.7 \times 10^{-3} \text{ M}$, $[\text{TiCl}_4] = 1.2 \times 10^{-4} \text{ M}$; (b) $[\text{H}_2\text{O}_2] = 9.7 \times 10^{-3} \text{ M}$, $[\text{TiCl}_4] = 8.8 \times 10^{-3} \text{ M}$; (c) $[\text{H}_2\text{O}_2] = 9.7 \times 10^{-3} \text{ M}$, $[\text{TiCl}_4] = 2.4 \times 10^{-2} \text{ M}$.

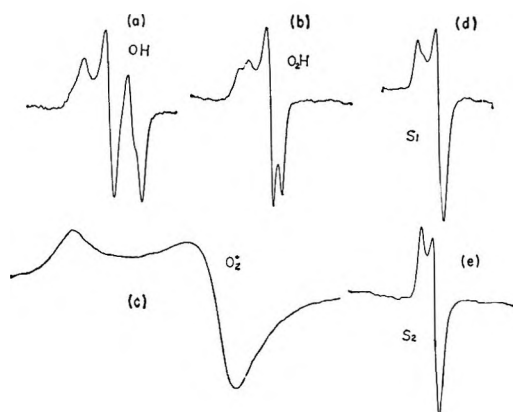


Figure 6. ESR spectra of $\cdot\text{OH}$, $\text{HO}_2\cdot$, $\text{O}_2\cdot^-$, and S_1 and S_2 at 77°K in the same scale: (a) $\cdot\text{OH}$ radical formed by uv irradiation of 0.03% H_2O_2 ; (b) $\text{HO}_2\cdot$ radical in the mixture $\text{H}_2\text{O}_2\text{-H}_2\text{O}$; (c) $\text{O}_2\cdot^-$ radical in NaO_2 powder; (d) S_1 ; (e) S_2 .

ingly originate from the method of determination of the g factor.

The marked enhancement of the intensity of both peaks in the presence of Ti(IV) ion or the yellowish $\text{Ti}^{4+}(\text{H}_2\text{O}_2)_n$ complex ion may suggest that the radical species are associated with Ti(IV) ion or $\text{Ti}^{4+}(\text{H}_2\text{O}_2)_n$ complex ion,⁵ and these radical species in question are probably the decomposition products of H_2O_2 , because similar spectra have been observed in the systems FeCl_2 or $\text{Ce}(\text{SO}_4)_2$ and H_2O_2 with TiCl_4 .^{8,9,11b}

The Effects of the Presence of Additional Ions or Chelating Reagents. The metal ions of group IIa and IIb, which have a strong tendency towards oxygenation, showed little scavenging effect in the intensity of the esr signals and had no effect on their g factors, as seen in Table II. This fact suggests that the radical species formed by the reaction of H_2O_2 with TiCl_3 strongly coordinate to Ti(IV) ion or $\text{Ti}^{4+}(\text{H}_2\text{O}_2)_n$ complex ion and have no ability to make additional complexes with other metal ions.

The facts that the presence of extra anions or chelating reagents did not affect the g factors is strong evidence for the low spin density at the central Ti atom in the complex ion. If the unpaired electron localizes on the central Ti atom, the change in ligand field split-

ting caused by the substitution of the ligand intensely affects the g factor, because the g factor of the central metal atom depends on the ligand field splitting.

The hyperfine coupling constant of Ti, however, is not as sensitive as the g factor to the type of complex, or ligand field splitting, because it is mainly due to the s - d electron exchange interaction in the Ti atom.

Fischer⁵ reported that both peaks S_1 and S_2 have three weak equidistant satellite lines on each side of the main peak; these satellite lines were attributed to the hyperfine interaction of $^{49}\text{Ti}(I = 7/2)$ and $^{47}\text{Ti}(I = 5/2)$ nuclei with an unpaired electron, on the basis of the intensity ratios of the satellite lines to the main peaks. He proposed 0.9 G for S_1 and 0.85 G for S_2 as the hyperfine coupling constants.

In many titanous complexes, isotropic hyperfine splitting of this kind is in the range 10 to 20 G.^{30,31} Taking the hyperfine coupling constant given for S_1 and S_2 by Fischer,⁵ the contribution of the 3d orbital of Ti to the bond between a Ti(IV) ion and a radical ligand was approximated to be 5–10%. This is consistent with our postulated localization of the spin density at the radical ligand.

In the presence of EDTA, NO_2^- , or SCN^- in TiCl_3 solution, the two signals S_1 and S_2 disappeared; this suggests that these substrates coordinate strongly with the Ti coordination sphere and that the titanium ion can no longer coordinate with the radical formed in the reaction of Ti(III) with H_2O_2 . At low concentration of EDTA, however, only the radical species S_1 was formed, and when a substrate such as an alcohol was added into this system, the free radical formed by the abstraction of a hydrogen atom from the alcohol was observed just as in the absence of EDTA.

The reaction of TiCl_3 with H_2O_2 in the presence of Co(II) or Ni(II) ion resulted in peak S_2 only, but no reactivity of the intermediate species to the organic substrates was found. In the presence of Cu(II) or Al(III) ion, S_1 and S_2 were not observed, but these systems showed the reactivity towards alcohol. These facts seemingly lead to the conclusion that the species giving peaks S_1 and S_2 are not the primary free $\cdot\text{OH}$ or $\text{HO}_2\cdot$ radicals which actually react with organic substrate.

The signal intensities of both peaks were rather sensitive to the concentrations of transition metals but not sensitive to the concentrations of alkaline earth metals. Thus the radical species giving peaks S_1 and S_2 may be the unstable intermediates of the oxidation-reduction process. For example, copper(II) ion oxidizes H_2O_2 in acid solution very poorly but is an effective oxidant for organic radicals under the same conditions.³²

(30) "Landolt-Bornstein, Neue Series," Vol. 2, Part 2, Springer-Verlag, Berlin, 1966, p 4-1-4-5.

(31) E. T. Kaiser and L. Kevan, Ed., "Radical Ions," John Wiley & Sons, Inc., New York, N. Y., 1968, p 579.

Radicals Observed in the Photolysis of $Ti^{4+}(H_2O_2)_n$. UV irradiation of the flowing solution of $Ti^{4+}(H_2O_2)_n$ complex at room temperature allows observation of two resolved narrow peaks, similar to those found in the $Ti(III)-H_2O_2$ system. The dependence of the relative intensity of the two peaks on the ratio of concentrations of $Ti(IV)$ and H_2O_2 should be noted here. At the highest ratio of H_2O_2 to $Ti(IV)$, only the intense signal of S_1 was observed. Upon decreasing the ratio of H_2O_2 to $Ti(IV)$, however, the intensity of S_1 decreased and the intensity of S_2 increased as seen in Figure 2. Accordingly, the variable affecting the intensity ratio of S_1 to S_2 seems to be the ratio concentrated ($Ti(IV)$)/concentrated (H_2O_2) even in the reaction of $Ti(III)$ with H_2O_2 .

The uv-irradiated solution of $Ti(IV)$ ion alone did not give any esr signal, so that H_2O_2 in the complex was decomposed and formed the free radicals. Czapski and coworkers^{20,33} have carried out the pulse radiolysis of aqueous H_2O_2 solutions and report that $HO_2\cdot$ and O_2^- are at equilibrium with a pK of 4.5. In the strongly acid solutions used in our experiments, the radical species $HO_2\cdot$ should be predominant.

The facts described above may indicate that the radical species giving S_1 and S_2 are the $HO_2\cdot$ radicals which associate with $Ti(IV)$ complexes of a different type.

g Factors of the Peaks S_1 and S_2 . As seen in Figure 6, the spectra of S_1 and S_2 in the solid phase most closely resemble those of the $HO_2\cdot$ radical among the transient free radicals in the decomposition of H_2O_2 , in view of the anisotropy in the g factor. It should be noted that $O^{13,14}$ showed a very large g anisotropy, whereas the O_3^- radical¹⁸ had a nearly isotropic g factor, and both species could not be the origin of S_1 and S_2 .

Dixon and Norman³⁴ reasonably explained that the spectrum of an $\cdot OH$ radical which was formed from the reaction of $Ti(III)$ with H_2O_2 should be a singlet in the aqueous solution at room temperature if it were observed, because of the rapid proton exchange of the $\cdot OH$ radical with the solvent.

This proton exchange effect, however, is eliminated in the solid state at low temperature, and the proton hyperfine splitting of tens of gauss¹⁹ would be expected to be in the present system if the radical species of S_1 and S_2 were actually $\cdot OH$ radicals.

If the radical species corresponding to S_1 and S_2 are assumed to be due to the $HO_2\cdot$ radical, the unpaired electron mainly localizes on the ligand radical, so that the ligand radical is in a state not very different from the free state, and the apparent effect of the coordination with the $Ti(IV)$ ion on the g factor could be treated as a small perturbation to the electronic state of the ligand through a small change in the coulomb integral of the atom with which coordination occurs. This treatment of the small perturbation is applicable

to the solvent effect³⁵ or the coordination effect³⁶ on g factors of the free radicals in the solution.

The variations in the g factor and in the hyperfine coupling constant for the species corresponding to S_1 and S_2 from those for a free $HO_2\cdot$ radical were calculated in this way.

First, as a test of the applicability of the extended Hückel MO approximation in determination of the g factor and unpaired electron distribution in this molecule, a calculation of the g factor and unpaired electron density for the free $HO_2\cdot$ radical was made. When $H_{1t}(O, 2p_z)$ of the terminal oxygen atom was taken as -16.56 eV, about 30% of the unpaired electron was found to reside on the central oxygen for free $HO_2\cdot$. This is consistent with the suggestion of Adrian, *et al.*,²¹ that $HO_2\cdot$ is a π radical having about 29% of the unpaired electron on the central oxygen atom. The energy difference between the unpaired electron orbital and the next lower orbital, which is the most influential parameter in the calculation of the g factor, was chosen as 0.946 eV in this calculation. This value does not differ much from Boyd's value²⁸ based on an SCF MO treatment.

The calculated value of g_{xx} was in fair agreement with the observed one. The other principal values, g_{zz} and g_{yy} , were slightly different from the observed ones, but close to that of a free electron. In this calculation the value of g_{xx} was fairly large compared to that of a free electron and very sensitive to the perturbation in the spin-orbit interaction between the unpaired π electron and the lone-pair electron, whereas g_{yy} and g_{zz} had values close to that of a free electron and were not sensitive to the perturbation.

According to the result noted above, if the radicals producing S_1 and S_2 are coordinated $HO_2\cdot$ radicals, the changing parameters in the spin Hamiltonian are g_{xx} and the hyperfine coupling tensor A . Between them g_{xx} is the more important parameter in determining the shape of the esr spectrum.

A computer-simulated spectrum for the free $HO_2\cdot$ radical with an appropriate isotropic hyperfine coupling constant and appropriate anisotropic g tensor, assuming a Gaussian line shape with a natural line width of 6.5 G (as ΔH_{msl}), fits the observed spectrum well, as seen in Figure 4a. The g tensor determined by this simulation was very close to that obtained by Wyard, *et al.*,²² using a more accurate method including an anisotropic hyperfine coupling tensor.

In determination of g_{xx} and the hyperfine coupling tensor A for S_1 and S_2 by spectrum simulation, no trial

(32) R. O. C. Norman and P. R. West, *J. Chem. Soc., B*, 389 (1969).

(33) G. Czapski and L. M. Dorfman, *J. Phys. Chem.*, **68**, 1169 (1964).

(34) The second article of ref 2.

(35) T. Kawamura, S. Matsunami, T. Yonezawa, and K. Fukui, *Bull. Chem. Soc. Jap.*, **38**, 1935 (1965).

(36) K. Kuwata and Y. Shimizu, *ibid.*, **42**, 864 (1969).

using different values of g_{xx} and line width, in the absence of hyperfine splitting, was able to reproduce the spectra of S₁ and S₂. Only with the inclusion of appropriate values for isotropic proton hyperfine splitting could the computed spectra be fit fairly well to the observed spectra of S₁ and S₂ as shown in Figure 4.

Using the principal values of g factors thus determined, the mean values \bar{g}_1 and \bar{g}_2 were calculated to be 2.0142 for S₁ and 2.0122 for S₂, while in aqueous solution at room temperature the isotropic g factors observed were 2.01425 for S₁ and 2.01276 for S₂. The good accordance of the mean values of \bar{g}_1 and \bar{g}_2 in the frozen state with the isotropic ones in the solution may show the reliability of the present determination of g_{xx} .

The hyperfine coupling constant and g_{xx} were found to decrease in the order free HO₂·, S₁, S₂. This fact seemingly correlates with the following consideration on the changes in g tensor and hyperfine coupling constant of the HO₂· radical, and will give information about the nature of the species which produce S₁ and S₂.

The extended Hückel MO treatment shows that change in the coulomb integral $H_{ii}(0,2p_z)$ of the terminal oxygen atom of the HO₂· radical causes change in the g tensor and in the unpaired electron density on the central oxygen, as shown in Table III. The hfs of the HO₂· radical originates from the s-p exchange interaction between a 1s electron of the H atom and a 2p unpaired electron on the neighboring oxygen atom, so that the hfs constant depends on the unpaired

electron density on the central oxygen atom. In the present calculation both the unpaired electron density on the central oxygen atom and the calculated g_{xx} decreased as the coulomb integral $H_{ii}(O, 2p_z)$ of the terminal oxygen atom increased.

Thus the present authors propose as the mechanism of change in the esr parameters of the HO₂· radical that the coordination of a metal ion to the terminal oxygen atom of an HO₂· radical increases the $H_{ii}(O, 2p_z)$ of the terminal oxygen atom. The apparent effects of the coordination of the HO₂· radical on its esr parameters are the decrease in g_{xx} and a small decrease in the hf coupling constant.

In photolysis of an acid solution of Ti⁴⁺(H₂O)_{*n*} complex with uv light at 77°K, a spectrum (Figure 5a) mainly due to free HO₂· radical was observed at higher concentration ratios of H₂O₂ to Ti(IV). As the ratio of H₂O₂ to Ti(IV) decreased, free HO₂· decreased, and the other signal S₁ was superposed on the spectrum of free HO₂·, as shown in Figure 5b. At extremely small ratios of H₂O₂ to Ti(IV), only S₂ was observed as shown in Figure 5c. These results seem to support the assignments of S₁ and S₂ to complexes of the HO₂· radical which coordinates with Ti⁴⁺(H₂O)_{*n*} complexes of different type.

Acknowledgment. The authors wish to express their thanks to Professor Kozo Hirota and Professor Ichiro Tyuma for their encouragement throughout this work.

Radical Intermediates. IV. Electron Spin Resonance Studies on the Alkali Metal Nitrobenzenides in Nitrilic Solvents

by J. M. Gross

Marconi-Elliott Computer Systems Limited, Borehamwood, Hertfordshire, England

and J. D. Barnes

The Chemistry Department, Sir John Cass College, London, E.C.3, England (Received December 23, 1969)

Alkali metal derivatives of the nitrobenzene radical anion have been prepared as stable solid salts. The spectra of the sodium salt in the nitriles is interpreted in terms of the existence of solvent shared ion pairs, while solutions of the potassium, rubidium, and cesium salts appear to contain ion pairs and free ions in equilibrium.

Since the first report of the electrochemical preparation of nitrobenzene radical anions by Geske and Maki,¹ acetonitrile and similar solvents have been increasingly used in the preparation of radicals for study by esr. It has been generally assumed that ion pairing does not take place in such solvents, but recently indirect evidence has been forthcoming to suggest that this assumption is not justified.²⁻⁴

As part of a general investigation of ionic solvation, utilizing the strong environmental dependence of the esr spectra of aromatic radical anions, we have developed a method for preparing such species as stable solid salts. The advantages of this method of preparation have been reviewed in a previous communication⁵ in which we indicated that significant amounts of ion pairs were present in solutions of nitrobenzenides in solvents such as acetone and acetonitrile, even at radical concentrations around 10^{-4} M. We now wish to report more detailed studies on such ion pairs in nitrilic solvents.

Experimental Section

The preparation and handling of solid alkali metal nitrobenzenides under high vacuum has been described previously.⁵ The solvents, which were Hopkin and Williams general purpose grade reagents, were refluxed for 48 hr *in vacuo* over calcium hydride and then distilled into glass bulbs on a high-vacuum line fitted with polytetrafluoroethylene glass greaseless stopcocks.

Spectra were recorded on a Decca X3 spectrometer using 100-kHz field modulation. The magnetic field was calibrated using a proton resonance magnetometer, and the coupling constants have an estimated accuracy of ± 0.03 G. The temperature within the cavity was maintained within $\pm 2^\circ$ of the required value by means of a Decca temperature controller.

Computer simulated spectra were obtained from an IBM 7094 computer using a program with facilities for reproducing most types of line width effects, and

were used to check for the presence of line width alternation.

Results

It was not possible to prepare stable paramagnetic solutions of lithium nitrobenzenide in the nitriles. Nitrilic solutions of the other alkali metal salts were somewhat less stable than alcoholic or ethereal solutions,⁶ but showed quite strong, well-resolved esr spectra.

The spectrum of sodium nitrobenzenide in all three nitriles was typical of that of an ion pair, showing a pronounced alkali metal splitting and no evidence of line width alternation at any accessible temperature. A typical spectrum is shown in Figure 1. Both the nitrogen and alkali metal splittings varied linearly with temperature as shown in Figures 2 and 3.

Hyperfine splittings are not quoted for solutions of the potassium, rubidium, or cesium salts in the nitriles since these varied by as much as 10% as the concentration of the solution was altered. No alkali metal splittings were evident in the spectra of such solutions, but pronounced line width alternation was frequently observed, the lines associated with the nitrogen spin quantum numbers $M_N = \pm 1$ being broader than the remaining lines. A typical spectrum is shown in Figure 4. Both the extent of the line width alternation and the line widths themselves were dependent upon the cation, the extent of alternation decreasing and the line widths increasing as the cationic radius increased. In a similar fashion, the extent of alternation decreased

(1) D. H. Geske and A. H. Maki, *J. Amer. Chem. Soc.*, **82**, 2671 (1960).

(2) T. Kitagawa, T. Layloff, and R. N. Adams, *Anal. Chem.*, **36**, 925 (1964).

(3) J. Q. Chambers and R. N. Adams, *Mol. Phys.*, **414** (1965).

(4) J. Oakes and H. C. R. Symons, *Chem. Commun.*, 194 (1968).

(5) J. M. Gross, J. D. Barnes, and G. N. Pillans, *J. Chem. Soc.*, **A**, 109 (1969).

(6) J. M. Gross and J. D. Barnes, *ibid.*, 2437 (1969).

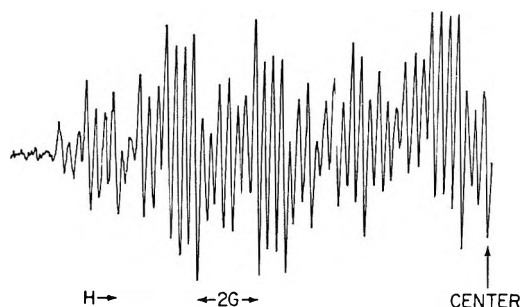


Figure 1. The esr spectrum of sodium nitrobenzenide in *n*-butyronitrile at room temperature. Only the low-field half of the spectrum is shown.

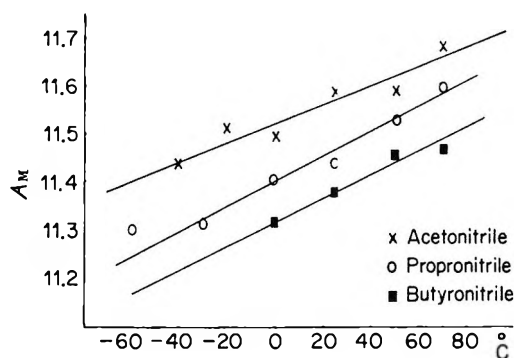


Figure 2. Temperature variation of the nitrogen splittings of sodium nitrobenzenide in nitriles.

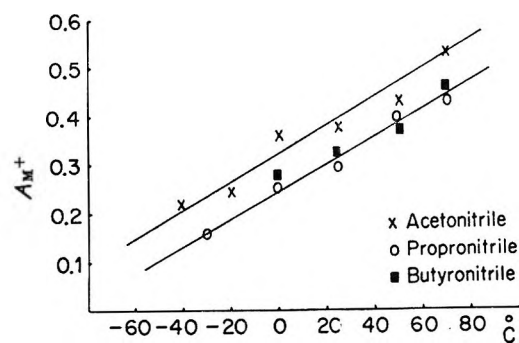


Figure 3. Temperature variation of the sodium metal hyperfine splitting in nitriles.

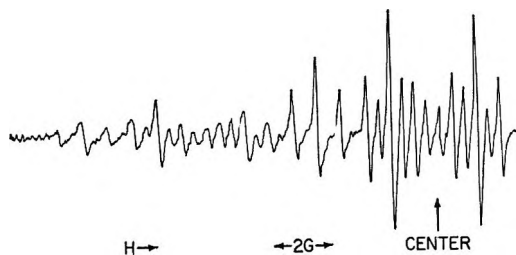


Figure 4. The esr spectrum of potassium nitrobenzenide in acetonitrile at room temperature; only the low-field half of the spectrum is shown.

and the line widths increased as the radical concentration increased. The possibility that the line widths might be determined by exchange between the nitro-

benzenide anion and neutral nitrobenzene can probably be discounted since no effect was observed on the addition of excess neutral nitrobenzene to solutions of nitrobenzenide ion pairs in ethers or to the free ions in alcohols.

Discussion

In a recent communication it has been emphasized that the structures of alkali metal nitrobenzenide ion pairs are largely determined by the properties of the solvent.⁶ Thus in alcohols, which are good anion solvators, association was proposed between an essentially unsolvated cation and an anion specifically solvated by one or two alcohol molecules attached to the oxygen atoms of the nitro group by hydrogen bonding. In ethers, which are reasonably good cation solvators, the association involves an essentially unsolvated anion, the cation being solvated for lithium and sodium and unsolvated for potassium, rubidium, and cesium. In no case was there evidence that the ion pairs were in equilibrium with another species at any attainable temperature.

The lack of any line width effects in the spectrum of sodium nitrobenzenide in the nitriles indicates that no dynamic equilibria occur in these solvents. The sodium metal splitting of around 0.3–0.4 G for the nitriles at room temperature represents a spin population in the cation 3s orbital of about 0.1%. This is of the order of the values obtained for the solvent shared ion pairs formed by lithium and sodium nitrobenzenides in ethers. The spin populations of the relevant cation s orbitals for potassium, rubidium, and cesium nitrobenzenides, which form contact ion pairs in the ethers, are around two or three times this value.⁶ It therefore seems probable that the structures of the sodium nitrobenzenide ion pairs in nitriles and in ethers are analogous, *i.e.*, the association involves an anion solvated only in the sense of bulk solvation, the cation being specifically solvated.

The decrease of both the nitrogen and metal splittings with increasing size of the nitrile may be explained on this basis. Thus, the decrease in dielectric constant with increasing size of the nitrile⁷ should cause a decrease in the bulk solvation of the anion, leading to a decrease in A_N . The size of the cation–solvent complex should increase with increasing size of the nitrile, thus reducing the perturbation of the anion by the cation and causing a decrease in both A_N and A_M^+ . However, the attenuation of the electrostatic attraction between the cation and anion by the solvent should decrease with decreasing dielectric constant of the solvent, thus causing an increase in both A_N and A_M^+ . The latter two effects work in opposition and in fact appear to cancel for *n*-propionitrile and *n*-butyronitrile, which show very closely similar sodium splittings.

(7) H. Schlundt, *J. Phys. Chem.*, **5**, 157 (1901).

Support for such a structure from other sources is difficult to obtain as there appear to have been few studies of the solvent character of nitriles. However, Kay, *et al.*,⁸ have measured the Walden product of sodium ions in acetonitrile, and the Stokes radius calculated from their data is 3.12 Å. This is similar to the values obtained by Szwarc⁹ for sodium ions in 1,2-dimethoxyethane (3.20 Å) and in tetrahydrofuran (3.95 Å) and is substantially larger than the crystallographic radius (0.95 Å). Though Stokes radii calculated on the simple model are somewhat suspect for ions with radii below about 5 Å,¹⁰ these values provide a reasonable qualitative indication that the degree of cationic solvation in ethers is similar to that in nitriles.

The line width alternation observed in the spectra of the potassium, rubidium, and cesium salts in the nitriles indicates the presence of a rapid equilibrium between two species with different nitrogen splittings, but equal or closely similar g values. The fact that both the alternation and the apparent nitrogen splitting are strongly concentration dependent suggests that the exchange is most probably between an ion pair and a free ion. However, in the absence of detailed measurements of the concentration dependence the possibility that the exchange is between two different types of ion pairs, one of which contains many associated solvent molecules and has no metal splitting, cannot be definitely excluded. The trends in the degree of alternation and in the widths of the lines associated with the nitrogen spin quantum number $M_N = 0$ indicate that the rate of exchange increases in the order $K^+ < Rb^+ < Cs^+$.

The similarity in the cation solvating properties of the ethers and the nitriles, as measured by Stokes

radii,^{8,9} suggests that the structures of the ion pairs formed in these solvents should be similar.

One would therefore expect the potassium, rubidium, and cesium nitrobenzenide ion pairs in nitriles to be essentially of the contact ion pair type.⁶ If this is so, it becomes necessary to explain not only the above order of increase in the rates of exchange, but also the fact that the solvent shared ion pair (as exemplified by the sodium salt) does not undergo exchange. A possible explanation for both these phenomena is that the mobility of the solvated cation in acetonitrile increases from sodium to cesium⁸ and the same is presumably also true for the other nitriles. Thus, if the cation and anion become momentarily separated, the high dielectric constant of the nitrile will greatly attenuate their mutual electrostatic attraction, thereby encouraging the formation of the free ions. The rate of this process will depend on the mobility of the cation. Comparable equilibria do not occur in ethereal solutions, presumably because of the much lower dielectric constants of these solvents.

Acknowledgment. We are indebted to Dr. K. D. Sales of Queen Mary College, London, for esr measurements which were performed as part of the University of London Intercollegiate Research Service, and to the Center for Computing and Automation of Imperial College, London, for computing facilities. We acknowledge financial support from Sir John College to J. D. B.

(8) R. L. Kay, B. J. Hales, and C. P. Cunningham, *J. Phys. Chem.*, **71**, 3925 (1967).

(9) P. Chang, R. V. Slaters, and M. Szwarc, *ibid.*, **70**, 3180 (1966).

(10) R. A. Robinson and R. H. Stokes, "Electrolyte Solutions," Butterworths, London, 1959 pp 124-125.

Magnetic Resonance Studies of Aromatic Hydrocarbons Adsorbed on Silica-Alumina. IV. Oxidation Strength of the Surface Electrophilic Sites

by G. M. Muha

University College, Rutgers, The State University of New Jersey, New Brunswick, New Jersey 08903
(Received February 24, 1970)

An attempt has been made to characterize the oxidizing ability of a silica-alumina catalyst by establishing the theoretical relationship between the experimentally measured electron spin resonance signal intensity and the half-wave oxidation potential for a series of polynuclear aromatic hydrocarbons. To explain the observed dependence, the presence of dipositive ions and carbonium ions along with the distribution in the oxidizing strengths of the surface electrophilic site must be taken into account. The interaction between the different species present is considered by assuming that a chemical equilibrium exists on the surface. The upper limit for the electrode potential of the surface electrophilic sites is estimated to be *ca.* 1.7 V relative to the standard hydrogen electrode.

The acidic nature of the silica-alumina surface is well known, the principal evidence being derived from spectroscopic studies of adsorbed hydrocarbon molecules¹ as well as the determination of the kinetic mechanism of hydrocarbon reactions.² When aromatic hydrocarbons are used, the reaction products include radical cations as well as other oxidation products. Thus the silica-alumina surface exhibits, in addition to acidic properties, the ability to serve as an oxidizing agent. The formal relationship between the electrophilic sites responsible for oxidation and the acidic sites responsible for the acidic behavior is not yet known.³

In this paper we report the results of a study designed to characterize the oxidizing strength of the electrophilic sites. The approach used generally parallels that used to study the acid strength and acid-strength distribution⁴ of the acidic sites through the use of chemical indicators.¹ The present work differs in that an electron spin resonance (esr) spectrometer is used to determine the concentration of the paramagnetic radical cation present. This concentration, proportional to the esr intensity, is measured for a series of aromatic hydrocarbons of known electrode potentials and the resulting intensity distribution is characterized by standard thermodynamic theory based on the Nernst equation.

Chemical equilibrium between all the species present on the surface is necessarily assumed. The other species present in addition to radical cations are neutral molecules, dipositive ions, and carbonium ions. The presence of these other species is of course not observed by the esr technique, the evidence for their inclusion in the equilibria being derived from other spectroscopic studies. For example, on this catalyst in addition to adsorbed (electrically) neutral molecules and radical cations, anthracene also forms carbonium ions and dipositive ions⁵ while tetracene forms dipositive ions.^{6,7} Perylene seems anomalous in its behavior in that only

neutral molecules and radical cations are observed on the surface.^{5,8}

As will be seen below, to explain the results of the present experiments, proper account must be taken of the effect of the interaction between all species present on the various chemical equilibria involved. Such a requirement, although taken for granted in a homogeneous system, might not be immediately suspected in a heterogeneous system in which different parts of the catalyst surface may exhibit quite different chemical properties. The fact that some form of interaction among the hydrocarbon species present serves to determine the concentration of the radical cation, whether properly described in terms of a chemical equilibrium or not, is considered one of the principal results of this work.

Experimental Section

The sample preparation and other experimental procedures were the same as those described previously⁹ with three exceptions. First, to preclude the possibility of photochemical decomposition, all steps in the sample preparation and the recording of the esr spectrum were

(1) H. P. Leftin and M. C. Hobson, Jr., *Advan. Catal.*, **14**, 115 (1963).

(2) Cf. H. H. Voge in "Catalysis," Vol. 6, P. P. Emmett, Ed., Reinhold, New York, N. Y., 1958, p 407.

(3) B. D. Flockhart and R. C. Pink, *J. Catal.*, **8**, 293 (1967).

(4) Cf. J. E. Germain, "Catalytic Conversion of Hydrocarbons," Academic Press, New York, N. Y., 1969, p 42 ff.

(5) W. K. Hall, *J. Catal.*, **1**, 53 (1962).

(6) In the spectrum of tetracene adsorbed on silica-alumina [A. Terenin, V. Barachevsky, E. Kotov, and V. Kolmogorov, *Spectrochim. Acta*, **19**, 1797 (1963)] three well resolved bands were observed but not assigned. These bands correspond almost exactly to those observed in the spectrum of tetracene dipositive ion⁷ and thus we assume that they correspond to the same species.

(7) W. I. Aalbersberg, G. J. Hoitink, E. L. Mackor, and W. P. Weijland, *J. Chem. Soc.*, 3055 (1959).

(8) R. P. Porter and W. K. Hall, *J. Catal.*, **5**, 366 (1966).

(9) G. M. Muha, *J. Phys. Chem.*, **71**, 633 (1967).

performed in a laboratory totally darkened except for two 40-W photographic safelights. Second, to minimize errors in the integrated intensity measurements, 8-mm i.d. quartz sample tubes were used. With this larger diameter tube, it was possible to ensure that the entire sample was in the *active* volume of the microwave cavity. Third, for each sample, the concentration was chosen such that the number of moles of hydrocarbon per gram of catalyst was held constant. Further, the number of moles was chosen to be twice the concentration of the perylene radical cation (per gram of catalyst). The reason for this choice is explained below.

A variety of solvents were used in the present work. No measurable effects on the esr intensity attributable to the solvent were observed. At least six samples were prepared for each hydrocarbon. The results for the measured integrated intensity agreed to within $\pm 11\%$ in the worst case. This value may be taken as an estimate of the reproducibility of the method. For each sample prepared, spectra were obtained at intervals for a period of 3 hr. The esr intensity for a given sample remained sensibly constant over this time interval.

Results

The experimental results (Table I) are given in terms of the intensity ratio (F) defined as the ratio of the integrated esr intensity observed for a given hydrocarbon to the value observed for the perylene radical cation. The variable is particularly convenient for use in the calculations which follow. Also given in Table I

Table I: Half-Wave Oxidation Potentials, Basicity Constants, and Integrated Esr Intensities

Compound	$E_{1/2}^a$	$\text{Log } K_b$	Integrated intensity ^b $\times 10^2$
Pentacene	0.40 ^c		7.5
Tetracene	0.54	5.8	41
9,10-Dimethyl-anthracene	0.57 ^d		78
Perylene	0.63 ^e	4.4	100
Anthracene	0.84	3.8	22
Pyrene	0.86	2.1	16
1,2-Benzanthracene	0.92	2.3	17
Chrysene	1.05	-0.17	7.0
Fluoranthrene	1.18		9.7
Phenanthrene	1.23	-3.5	13
Naphthalene	1.31	-4.0	7.0

^a Measured relative to $\text{Ag} - 0.1 \text{N Ag}^+$ in acetonitrile; see ref 10. ^b Relative value, perylene = 1.0. In absolute value, the perylene signal corresponds to 9×10^{17} spins/g of catalyst; however this value may be a factor of 2 too high due to a contribution from the counterion and may include a contribution from paramagnetic impurities in the catalyst. ^c Value obtained by interpolation using the Huckel coefficients. ^d E. S. Pysh and N. C. Yang, *J. Amer. Chem. Soc.*, **85**, 2124 (1963). ^e Reference 7.

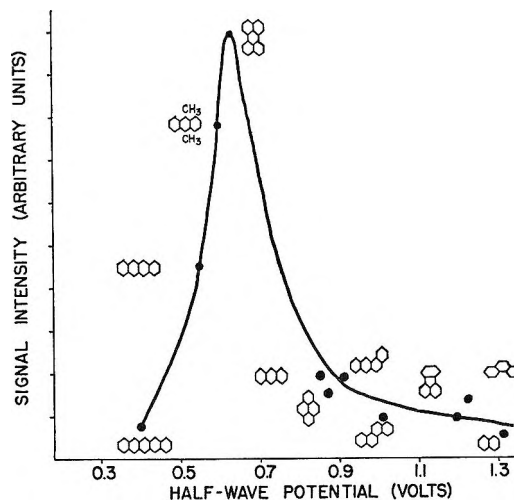


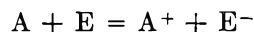
Figure 1. Dependence of the integrated esr signal intensity on the polarographic half-wave oxidation potential for the series of aromatic hydrocarbons given in Table I. The potentials are referenced to $\text{Ag} - 0.1 \text{N Ag}^+$ in acetonitrile.

are the half-wave oxidation potentials¹⁰ and the basicity constants (K_b)¹¹ for the aromatic series studied.

The results are also given in Figure 1, which displays the observed intensity as a function of the half-wave potential. Our purpose in this section is to develop a method to calculate a theoretical curve for comparison with the experimental result. To accomplish this, it is necessary to make the usual assumption concerning the equivalence of the half-wave potential and the standard electrode potential for a reversible reaction.¹² Also since a means of introducing activity corrections is not available, we assume all activity coefficients are unity. Since the same molar concentration is used throughout and the chemical compounds are somewhat similar, this assumption is probably justified as a first approximation.

To proceed, we first demonstrate that the assumption of a simple oxidation-reduction (redox) reaction in which all the electrophilic sites have the same oxidizing strength cannot explain the shape of the experimental curve.

Consider the simplest form of a redox reaction on this surface, the oxidation of an aromatic hydrocarbon (A) to a paramagnetic radical cation (A^+) by an electrophilic site (E)



If all the E sites have the same electrode potential, the equilibrium constant (K) for this reaction is given by

$$\log K = 16.95(\epsilon_E^0 - \epsilon_A^0)$$

(10) H. Lund, *Acta Chem. Scand.*, **11**, 1323 (1957); values are measured relative to $\text{Ag} - 0.1 \text{N Ag}^+$ in acetonitrile.

(11) E. L. Mackor, A. Hofstra, and J. H. van der Waals, *Trans. Faraday Soc.*, **54**, 66 (1958).

(12) M. E. Peover, *Trans. Faraday Soc.*, **60**, 417 (1964).

where the subscripts on the electrode potentials (ε^0) refer to the surface site and the hydrocarbon as in the preceding equation. The value of ε_E^0 is unknown but an estimate can be obtained by choosing a value so as to give the correct value of F for one of the experimental points.

Either naphthalene or perylene are suitable choices for this "scaling" procedure. Of the aromatic molecules studied, naphthalene is the most acidic and has the highest half-wave potential. Hence complications due to carbonium ion or dipositive ion side reactions are expected to be minimal. Similarly, a spectroscopic study⁸ of adsorbed perylene shows only the presence of neutral molecules and radical cations; thus difficulties due to side reactions are not expected.

The relationship between F and K can be obtained from the usual stoichiometric conditions implied by equilibrium. In this manner we find that, in the case of naphthalene, a value of $\log K$ of -2.56 is required to obtain the experimental value given in Table I. Thus ε_E^0 is 1.16 V and the values of F for the remaining hydrocarbons can be calculated. The results are shown as curve B in Figure 2. Clearly the theoretical fit to the experimental curve is unacceptable.

To demonstrate that the poor result is not due to the somewhat arbitrary choice of naphthalene as a reference point or because of the unsuspected presence of an additive constant in the values for the electrode potentials,^{13,14} we repeat the calculation for perylene in a different form.

Because of the choice of the initial hydrocarbon concentration (see preceding section), the equilibrium constant for the reaction involving perylene (K_p) can be written

$$K_p = E^-/E$$

Hence the initial concentration of the electrophilic site (E_i) is given by

$$E_i = N(1 + K_p)^{-1}$$

where N is the concentration of perylene radical cations (moles/cm²). Algebraic manipulation then allows the value of the equilibrium constant for any of the other hydrocarbons to be expressed in terms of the value for perylene

$$\log (K/K_p) = 16.95(\varepsilon_p^0 - \varepsilon_A^0)$$

The esr intensity ratio is then given by

$$F = 2(K/K_p)(1 + K/K_p)^{-1}$$

Results obtained from calculations using this expression are shown as curve C in Figure 2. Again, comparison with experiment is unsatisfactory.

As seen in this figure, the principal difficulty with the results shown as B and C is due to the slope of the theoretical curve. In the region above 0.7 V, the slope is too large in magnitude; in the region below 0.7 V the

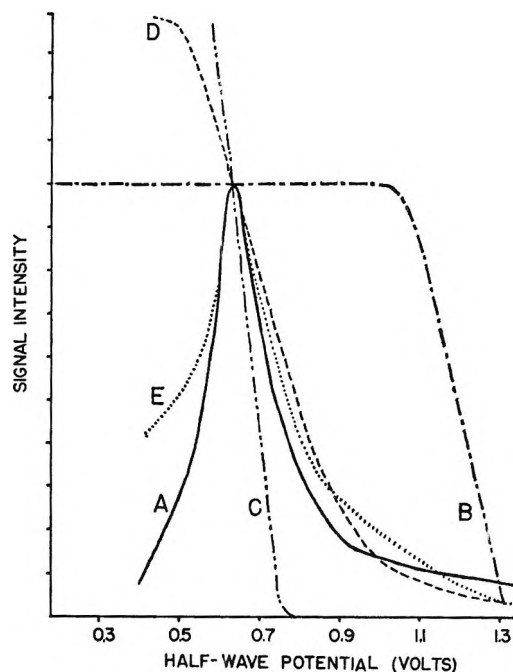


Figure 2. Fit of the calculated curve to the experimental curve for the various effects considered: A, experimental curve; B, data scaled to the naphthalene result; C, data scaled to perylene; D, distribution in the strength of oxidizing sites included; E, effect of dipositive ion formation.

slope is too small in magnitude and has the wrong algebraic sign. This difficulty can be corrected by removing two assumptions implicit in the above calculation: First, that all of the E sites have the same value of ε_E^0 and second, that only a simple redox reaction need be considered. These assumptions affect different regions of the curve to a varying degree. Hence, in the following, it is convenient to consider the regions above and below 0.7 V separately.

Consider first the region above 0.7 V. In this region the basicity constant is too low and the second-electron potential too high for the corresponding side reactions to affect the curve to the required degree. (Numerical estimates of these effects are given below.) Also, direct calculation shows that the choice of any other aromatic hydrocarbon for scaling gives the same poor fit of the experimental curve. Rather the basic difficulty with the calculated slope arises from the assumption that all the E sites have the same oxidizing ability, for then the resulting value of ε_E^0 is such as to make the difference in the electrode potentials quite large. The slope of the curve, which in this region depends exponentially on the difference in electrode potentials, is consequently numerically too large. However, ε_E^0

(13) Such a situation might develop if the assumed equivalence of the electrode potential and the half-wave potential was not true. However, even if untrue, experimental studies¹⁴ indicate that the difference between the values is constant for all of the aromatic hydrocarbons used in this work. Such a result is all that is required for the present argument.

(14) G. J. Hoijtink and J. van Schooten, *Rec. Trav. Chim. Pays-Bas*, 71, 1089 (1952).

cannot be chosen too small for then the calculated curve will not fit the experimental data for those hydrocarbons with high values of ϵ_A^0 .

This difficulty can be circumvented by assuming that a distribution exists in the oxidizing strength of the electrophilic sites, a behavior which parallels that already noted for the acidic properties of this catalyst. At present, the form of this distribution is unknown. Hence we may as well assume a functional dependence that is both reasonable as well as mathematically convenient. Thus we chose a Boltzmann distribution

$$\log E_i' = \log E_i - 16.95k(\epsilon_p^0 - \epsilon_A^0)$$

where k is a constant chosen to scale the theoretical results to the experimental curve.

By means of this scaling procedure, we find the required value of k is 0.87. The value of F can now be calculated from the expression

$$\log [F/(2 - F)] = 16.95(1 - k)(\epsilon_p^0 - \epsilon_A^0)$$

The results are shown as curve D in Figure 2. Clearly the improvement in the region above 0.7 V is noteworthy.

To improve the agreement in the region below 0.7 V, it is necessary to take into account the effect of carbonium ion and dipositive ion formation on the redox equilibrium. Consider the effect of carbonium ion formation first. The simplest procedure is to treat this effect as a side reaction¹⁵ on the redox equilibrium, equivalent to the complexing of the reduced species (*i.e.*, A) by hydrogen ions.¹⁶

In this fashion, direct calculation shows that the equilibrium constant is simply multiplied by a coefficient α where

$$\alpha^{-1} = 1 + K_b(\text{H}^+)$$

and (H^+) is the concentration of hydrogen ions on the surface that are not complexed. This concentration is not known; however, as a first approximation we can use the total number of acidic surface hydrogens present as measured by deuterium exchange.¹⁷ This value, $3 \times 10^{13} \text{ cm}^{-2}$, or on a volume basis, $2.7 \times 10^{-4} \text{ mol cm}^{-3}$, then gives for anthracene a value of $F = 0.23$ compared to the experimental result of 0.22. The agreement is probably fortuitous for this same calculation, when applied to tetracene, gives a value of 0.02 which is to be compared to the experimental result of 0.41. For the remaining hydrocarbons with values of ϵ_A^0 greater than 0.9 V, this mechanism is predicted to have a negligible effect on the esr intensity.

The value chosen for the hydrogen ion concentration is such that the above calculation gives the largest estimate possible for the effect.¹⁸ Thus it seems more proper to accept the introduction of the mechanism as giving the proper order of magnitude correction rather than relying on the actual numbers obtained. However, not explained by this mechanism is the experi-

mental observation that perylene does not form a carbonium ion on this catalyst.⁸ We return to this question below.

The introduction of a side reaction involving an oxidation step to dipositive ions also serves to improve the fit of the calculated curve to the experimental results.¹⁹ To estimate the magnitude of the effect, consider the reaction $\text{A}^+ + \text{E} = \text{A}^{2+} + \text{E}^-$ with an equilibrium constant K_d

$$\log K_d = 16.95(\epsilon_B^0 + \epsilon_A^0 - 2\epsilon_2^0)$$

where ϵ_2^0 is the electrode potential corresponding to the removal of two electrons from A. Further, define g as the ratio of the dipositive to monopositive ion concentration. Then

$$g = K_d(E/E^-)$$

and it is possible to derive an expression for F for an equilibrium involving A, A^+ , and A^{2+} . The result is somewhat complicated for now the ratio E^-/E is not given by K_p .

Unfortunately, values for ϵ_2^0 are not yet available; hence we again resort to an estimate. Since ϵ_2^0 cannot be less than ϵ_A^0 , we adopt this latter value for use in the calculation of F . Also, to reduce computation labor, it is convenient to assume that the ratio (E/E^-) is unchanged from the perylene result. The nature of these combined approximations is such that the value of F calculated represents the largest correction possible based on the dipositive ion effect.

The results of the calculation using these approximations is shown as curve E in Figure 2. The carbonium ion effect is not included in this calculation but the assumed distribution in the strength of the electrophilic sites is included. Clearly the result is a quite reasonable fit of the experimental data. Note the relatively minor importance of this mechanism in the region above 0.7 V.

Discussion

The most important result demonstrated by the above calculation is that the shape of the experimental curve can be explained, and even approximately reproduced numerically, by assuming a chemical equilibrium exists on the surface which relates the concentrations of the various species known to be present.

(15) A. Ringbom, "Complexation in Analytical Chemistry," Interscience, New York, N. Y., 1963, p 38.

(16) H. A. Laitinen, "Chemical Analysis," McGraw-Hill, New York, N. Y., 1960, p 290.

(17) W. K. Hall, H. P. Leftin, F. J. Cheselske, and D. E. O'Reilly, *J. Catal.*, **2**, 506 (1963).

(18) This statement is essentially unchanged if a distribution in the activity of the surface hydrogen ion is introduced into the calculation.

(19) We assume that the dipositive ion is diamagnetic. The possibility that a triplet spin system is formed was excluded by a search (at 77°K) for the triplet esr lines. The results were negative for all the hydrocarbon systems reported here.

In the presentation above each side reaction was treated independently. When treated together, and coupled with a judicious choice of the various parameters k , (H^+) , and ϵ_2^0 , essentially an exact fit of the experimental curve can be obtained. However, the presentation of the results of such a calculation are not warranted at this time for the theoretical significance is obscured by the uncertainties introduced into the procedure by the inherent uncertainties in the values of ϵ_A^0 and K_b as well as the neglect of other side reactions (e.g., ion-pair formation^{20,21}) and perhaps other factors not yet suspected.

Extensive numerical calculation shows that the single most important factor in determining the shape of the experimental curve is the functional dependence assumed for the distribution function describing the oxidizing strength of the E sites. The exponential dependence, used above because of its mathematical convenience, overestimates the role of the low-potential sites and hence minimizes the importance of the dipositive ion mechanism, and to a lesser extent, the effect of carbonium ion formation. An alternative distribution providing excellent results uses an exponential dependence in the region 1.3 to 0.7 V with a constant value to lower potentials. However, the justification for the use of any particular form of a distribution function must await the results of experiments specifically designed to measure this dependence.

With any assumed form for the distribution function, it appears that the upper limit on the oxidizing strength will be ca. 1.7 V vs. the standard hydrogen electrode,²² a value comparable to that of permanganate in strong acid solution. In view of the hypotheses concerning the role of adsorbed oxygen in determining the oxidizing properties of this type of catalyst,²³ it is interesting to compare this value to that of the oxygen couple in acidic solution (1.2 V vs. NHE).

The fact that a distribution in the oxidation strength is observed presumably arises because of some features of the catalyst structure similar to that postulated for the acidic sites.²⁴ In this connection, a point that we find particularly interesting is the nature of the "counterion" in dipositive ion formation. The equilibria considered above simply assume that the counterion ion is a pair of reduced E sites. However, these surface sites are presumably immobile and hence unusual effect might be expected in the esr spectrum. Such is the case with both tetracene and 9,10-dimethylantracene;²⁵ further work on this question is in progress.

Also in this connection, a question arises concerning the use of the Nernst equation in these calculations. The assumption of a chemical equilibrium involving several species implies that each is aware of the presence of the other (in a thermodynamic sense), a difficult feat if the counterions are imbedded in a dielectric surface. Nevertheless, the results given above indicate that the use of equilibrium constants to describe the interactions

is justified at least as an excellent first approximation. Hence, the species involved must exhibit an appreciable degree of mobility so that the concentrations in one region are related to those in other regions.²⁶ The mobility of these ions, as inferred from hyperfine effects in the esr spectrum²⁷ has been the subject of previous papers in this series.^{9,20,28}

It is difficult to devise a suitable experiment to test the thermodynamic reversibility of the surface reactions involved. One approach presently being pursued in our laboratory involves the development of an electrochemical series for radical cation formation.²⁹ Preliminary results indicate reversible behavior at least at low-hydrocarbon concentration levels.²⁵

In introducing the effect of carbonium ion formation of the radical cation equilibrium, it was implicitly assumed that the acid surface sites are distinct from the electrophilic sites. Such an assumption seems justified.^{9,20,28} However, not ruled out experimentally is the possibility of some form of interaction between the acidic and redox sites, perhaps involving a chemical equilibrium. In a restricted sense, a model involving such a behavior has been suggested.³⁰ The inclusion of such an effect in the above calculation would be straightforward. However, at the present time, not enough information is available concerning the details of the proposed model to permit estimates of the magnitude of the expected effect. Clearly more information, based on a variety of independent experimental techniques, is needed.

The question concerning the interrelation of the acidic and electrophilic sites is of great interest in view of the results reported in solution studies of radical cation formation.⁷ There it was observed that acid protons are required in addition to an oxidizing agent to prepare aromatic radical cations.³¹ Thus the present

(20) G. M. Muha, *J. Phys. Chem.*, **74**, 787 (1970).

(21) W. B. Schaap, *J. Amer. Chem. Soc.*, **82**, 1837 (1960).

(22) The conversion of the potential measured relative to the silver electrode in acetonitrile can be effected by using the conversion date of R. C. Larson, R. I. Iwamoto, and R. N. Adams, *Anal. Chim. Acta*, **25**, 371 (1961).

(23) J. K. Fogo, *J. Phys. Chem.*, **65**, 1919 (1961); F. R. Dollish and W. K. Hall, *ibid.*, **71**, 1005 (1967).

(24) Reference 4, p 38.

(25) G. M. Muha, unpublished results.

(26) Clearly the regions need not be so large as to result in a homogeneous surface, cf. F. F. Vol'kenshtein, "The Electronic Theory of Catalysis on Semiconductors," Macmillan, New York, N. Y., 1963, p 144.

(27) As a part of the present work, hyperfine effects have been observed in the spectra of all compounds used (Table I) with the exception of phenanthrene and chrysene. These two compounds have the largest anisotropic g -tensor components of the hydrocarbons listed. [See A. J. Stone, *Mol. Phys.*, **7**, 311 (1964).] Therefore they would be expected to exhibit the largest line width effects and the poorest resolution.

(28) G. M. Muha, *J. Phys. Chem.*, **71**, 640 (1967).

(29) M. E. Peover in "Electroanalytical Chemistry," Vol. 11, A. J. Bard, Ed., Marcel Dekker, Inc., New York, N. Y., 1967, p 47.

(30) A. E. Hirschler, *J. Catal.*, **5**, 196 (1966).

seemingly contradictory behavior of perylene on this catalyst,³² especially in view of the relatively rapid deuterium exchange of the perylene radical cation²⁸ (presumably involving a carbonium ion intermediate), is not understood. The behavior may represent a real effect involving a coupled reaction²⁹ or perhaps a kinetic effect.

Finally, we note that the above treatment does not include a consideration of the surface electric field in determining the reaction products.³³ At present the relative importance of this effect is unknown.

Acknowledgment. Some of the initial experimental work on this problem was done at the Esso Research

and Engineering Co. The author is grateful to this company for releasing the data from that phase of the work for publication and to the Rutgers Research Council for support of the remaining aspects of the work.

(31) In aprotic solvents, radical cations can be generated, but ultraviolet irradiation is required. See ref 7.

(32) In one study of perylene adsorbed on this catalyst [D. M. Brouwer, *J. Catal.*, **1**, 372 (1962)] one band observed in the optical spectrum was assigned to the perylene carbonium ion. Later work offered strong arguments against this assignment. See the discussion given in ref 8.

(33) G. J. Hoijtink in "The Mechanism of Heterogeneous Catalysis," J. H. DeBoer, Ed., Elsevier, Amsterdam, 1959, p 90.

Stepped Isotherms on Inorganic Oxides

by S. A. Selim, R. Sh. Mikhail, and R. I. Razouk

Department of Chemistry, Faculty of Science, Ain Shams University, Cairo, Egypt (Received December 1, 1969)

The adsorption of both cyclohexane on magnesium hydroxide and water vapor on chromia gel show distinct steps in their isotherms at 35°. By determining the monolayer capacity on the surface by means of nitrogen adsorption, it became evident that the step in the cyclohexane isotherm is obtained during the formation of the first layer (submonolayer), while for the water vapor the step is obtained on top of the first layer. Both steps could be interpreted as being due to two-dimensional condensation on the surface. Subcritical two-dimensional condensation of cyclohexane on magnesium hydroxide was found to be due to reorientation of the molecules on the surface to become vertically oriented and thus increasing their lateral interaction. On the other hand, the polar water molecules might have stronger adsorbate-adsorbent interaction, and therefore no condensation could take place in the first layer. Strong lateral interactions between the water molecules in the second layer allowed the condensation step to show itself on top of the first layer. From this investigation it seems that two-dimensional condensation could possibly take place on heterogeneous surfaces. This might be achieved if the lateral interaction between the adsorbate molecules in one and the same layer is stronger than the adsorbate-adsorbent interaction or than the interaction with the preceding layer.

Introduction

Extensive studies were carried out on the adsorption on graphitized carbon blacks either from the gas phase or from solution. The uniform, medium energy and nonpolar surface of graphitized carbon blacks permits the interpretation of adsorption data, in a manner not possible with heterogeneous surfaces such as inorganic oxides.

One consequence of such studies is that adsorption isotherms often show steps corresponding to the completion of successive layers.¹

For the occurrence of such stepwise isotherms, Pierce and Ewing² have shown that beside the surface homogeneity, there must be strong lateral interactions between adsorbed molecules, and that the temperature, and more correctly the reduced temperature,³ should

be low enough to inhibit thermal agitation of the adsorbed molecules.

The low temperature requirement was disproved by Zettlemoyer, *et al.*,⁴ who showed that the geometry and chemical nature of the adsorbate are more essential requirements than the low temperature.

The purpose of this article is to report that stepped isotherms can indeed be found for the adsorption on some inorganic oxides which definitely possess hetero-

(1) T. L. Hill, *J. Chem. Phys.*, **15**, 767 (1947); T. L. Hill, *ibid.*, **17**, 762 (1949); G. D. Halsey, Jr., *ibid.*, **16**, 931 (1948); M. N. Polley, W. D. Schaeffer, and W. R. Smith, *J. Phys. Chem.*, **57**, 469 (1953).

(2) C. Pierce and B. Ewing, *J. Amer. Chem. Soc.*, **84**, 4070 (1962).

(3) B. W. Davis and C. Pierce, *J. Phys. Chem.*, **70**, 1051 (1966).

(4) D. R. Bassett, E. A. Boucher, and A. C. Zettlemoyer, *ibid.*, **71**, 2787 (1967).

geneous surfaces. Thus, during an extensive study of the adsorption characteristics of single and mixed hydrous oxides of chromium and magnesium, very few specific adsorption isotherms of cyclohexane and water vapors at 35° showed a definite step-wise nature. Two specific cases will be discussed in the present investigation, namely the adsorption of cyclohexane on thermally treated magnesium hydroxide and the adsorption of water vapor on thermally treated chromium hydroxide gel.

Few workers appear to have studied the complete adsorption-desorption cycle. Polley, Schaeffer, and Smith⁵ observed hysteresis at $p/p_c > 0.75$, and in view of the nonporous nature of their solids they attributed this either to interparticulate condensation or to slow pressure equilibrium. Bonnetain, Duval, and Letort⁶ reported stepped isotherms for methane on natural graphite and other nonporous solids, which exhibit hysteresis extending down to the lowest pressures measured and which is almost identical with that reported by Greenhalgh and Redman.⁷ For porous solids, the hysteresis phenomenon is complicated by capillary condensation effects, and the solids used in the present investigation are porous in nature. Full adsorption-desorption isotherms are presented.

Experimental Section

Magnesium hydroxide (M) was precipitated from stoichiometric amounts of the nitrate with ammonia. Half the amount of ammonia was added to the salt solution and stirring continued for 4 hr after which the second half of the ammonia solution was added. After precipitation some excess of 20% ammonia solution was added to ensure the complete precipitation of the hydroxide. It was thoroughly washed and dried under vacuum at room temperature in presence of P_2O_5 to constant weight. The resulting product contained 31.77% water as compared with a theoretical value of 30.89% corresponding to the formula $Mg(OH)_2$. The product proved to be crystalline to X-rays.

Chromium hydroxide (C) was similarly precipitated from the nitrate (2 M) and ammonia (6 M) at room temperature by a method similar to that of Burwell, *et al.*,⁸ using more concentrated solutions. It was thoroughly washed with 1% ammonia and dried in a similar manner to the magnesium hydroxide. Its water content was 33.84% and proved to be amorphous to X-rays. The theoretical water content corresponding to the formula $Cr(OH)_3$ is 26.21%. Dehydration products were obtained for the above two preparations by heating at temperatures ranging from 160 to 740° for 3 hr in presence of air. The products obtained from magnesium hydroxide will be designated samples M and from chromium hydroxide samples C. The temperature of dehydration appears beside this letter; thus *e.g.*, sample M160 indicates magnesium hydroxide heated at 160° for 3 hr in air.

Cyclohexane (Carlo Erba), methanol (BDH), and nitrogen were purified by standard methods. The water used was redistilled.

Apparatus and Technique. Adsorption isotherms of cyclohexane and methanol at 35° and of nitrogen at 195° were determined with the aid of a conventional volumetric gas adsorption apparatus. For organic vapors, mercury cutouts were used in place of the conventionally used stopcocks. Dissolved gases in the vapors were removed by subjecting the liquid to several freeze-thaw cycles under high vacuum. The procedure adopted was to outgas the sample for 10 hr (10^{-5} mm) at the temperature of the experiment before carrying out any adsorption run. The adsorption of water vapor was carried out by a gravimetric apparatus using quartz springs of sensitivities ranging between 30 and 40 cm/g.

Results and Discussion

I. Adsorption of Cyclohexane on Thermally Treated $Mg(OH)_2$. The adsorption isotherms of cyclohexane on the parent $Mg(OH)_2$ as well as on some of its thermally treated products are shown in Figure 1. The isotherms on the parent material as well as those heated at 160 and 320° show definite steps at relative pressures of 0.185, 0.180, and 0.205, respectively. These steps disappeared for samples obtained at higher temperatures and the isotherms became of the normal Type II of Brunauer's classification. At temperatures above 320° transformation of the hydroxide to the oxide takes place. Measurements at very low pressures indicate the absence of any steps which might be present previous to those reported above. The adsorption isotherms showed no early convexity to the pressure axis as previously noted for other systems published in the literature. The relatively high pressure at which condensation takes place in the present investigation will be signified later on.

For the adsorption of cyclohexane on the parent magnesium hydroxide, it has already been indicated that in the low-pressure region no steps could be traced. This early region of the adsorption isotherm is shown in Figure 2. The full adsorption-desorption isotherms on this sample are shown in Figure 1, where there is a vertical step on the adsorption branch at a relative pressure of 0.18. Upon desorption, a wide open hysteresis loop is obtained which is persistent to the lowest relative pressure measured. Scanning of the main hysteresis loop was performed, and desorption was started at many points around the step region. The

(5) M. H. Polley, W. D. Schaeffer, and W. R. Smith, *J. Phys. Chem.*, **57**, 469 (1953).

(6) L. Bonnetain, Y. Duval, and M. Letort, *C. R. Acad. Sci.*, **234**, 1363 (1952).

(7) E. Greenhalgh and E. Redman, *J. Phys. Chem.*, **71**, 1151 (1967).

(8) R. L. Burwell, Jr., and S. H. Taylor, *J. Amer. Chem. Soc.*, **58**, 697 (1936).

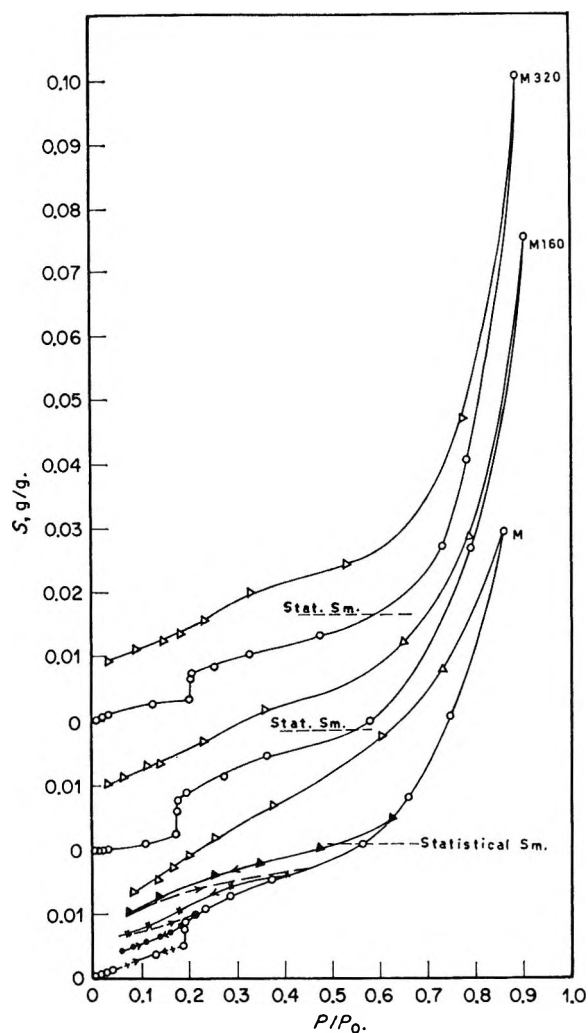


Figure 1. Adsorption-desorption isotherms of cyclohexane on $\text{Mg}(\text{OH})_2$ and its decomposition products M160 and M320: —○—○—, main ascending curve; —△—△—, main descending curve; ---, ascending scanning curves; —●—●—, —+—+—, —×—×—, —▲—▲—, descending scanning curves.

descending as well as the ascending scanning curves are typically shown in Figure 1 for sample M. The scanning behavior shows clearly that prior to the step formation, the adsorption is perfectly reversible showing no hysteresis effects. If, on the other hand, a descending scanning curve is started at any point along or beyond the step, strong hysteresis is obtained which gives an open loop persisting to the lowest pressures measured. Reversing the path to get an ascending scanning curve shows also hysteresis behavior between the ascending and descending curves. Evidently, the vertical step is smoothed out during desorption.

Measurement of the specific surface area by nitrogen adsorption using the BET equation led to a computed statistical monolayer capacity for cyclohexane on the surface to be 0.0208 g/g (an area of 49.1 m^2/g). This is shown as a dashed line in Figure 1. The statistical monolayer capacity (S_m) was evaluated assuming the molecules to reorient themselves to acquire a vertical

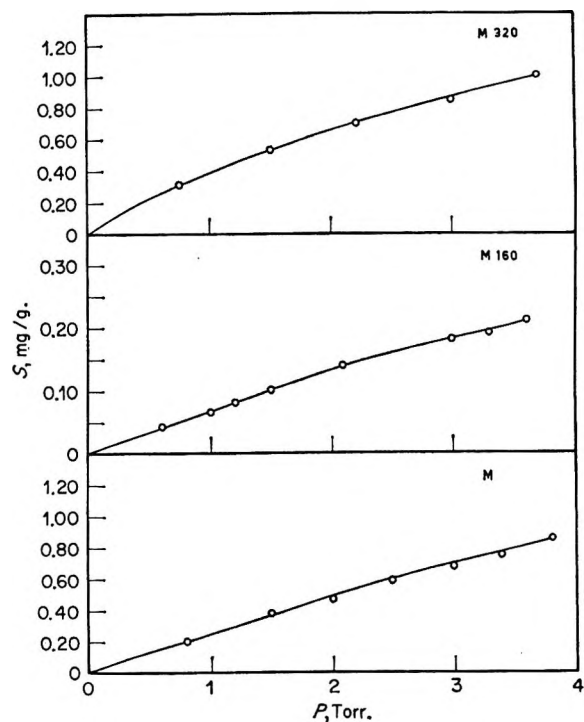


Figure 2. Low-pressure region of the isotherms of samples M, M160, and M320.

position on the surface. Some independent evidence for this mode of orientation will be discussed shortly.

The nearly vertical step at a definite vapor pressure might indicate a first-order two-dimensional phase transition on the surface, despite its heterogeneity. This corresponds to the formation of a two-dimensional condensed phase in equilibrium with a two-dimensional gaseous phase. de Boer and Broekhoff⁹ developed an analytical treatment for the two-dimensional van der Waals equation in its reduced form, through which it was possible to evaluate the monolayer capacity (S_m). Applying their method of analysis to the present data led to a computed monolayer capacity for cyclohexane on the surface to be 0.0208 g/g, in remarkable agreement with that computed from the nitrogen area assuming vertical orientation of cyclohexane on the surface.

Cyclohexane, however, should not condense two dimensionally at the temperature of the experiment (308°K) since the two-dimensional critical temperature (286.3°K) evaluated from a_2 and b_2 van der Waals values is lower than the temperature of the experiment. Only if the cyclohexane molecules take certain positions during the progress of the adsorption, a subcritical two-dimensional vapor would be formed which would condense, its two-dimensional critical temperature then being equal to or greater than 308°K. There are many cases where the two-dimensional critical

(9) J. H. de Boer and J. C. P. Broekhoff, *Proc. Kon. Ned. Akad. Wetensch., Ser. B*, **70**, 317 (1967).

Table I: Some Characteristics of Cyclohexane Adsorption on M, M160, and M320

Sample	S_g , g/g	S_c , g/g	k_1^a	Statistical S_m , g/g		Specific surface, m ² /g	b_2 (cyclohexane), cm ² /molecule
				From N ₂	From 2-dim cond step		
M	0.0050	0.009	6.9	0.0208	0.0208	49.1	33.37×10^{-16}
M160	0.0030	0.008	6.9	0.0185	0.0185	43.7	33.28×10^{-16}
M320	0.0032	0.008	7.1	0.0165	0.0165	39.0	32.37×10^{-16}

^a Computed by using S_c which is more reliable than S_g . (S_c and S_g represent the coexisting values of the amounts adsorbed in equilibrium with each other; S_c the upper end of the step and S_g the lower end).

temperature is higher than half the three-dimensional one, when the molecules are taking special positions on the surface.¹⁰

Following the same analytical treatment of de Boer and Broeckhoff,⁹ the actual two-dimensional critical temperature (T_{cr})₂ was found to be equal to 314.5°K, which is above the temperature of the experiment (308°K). Also, if the van der Waals a_2 constant is assumed to be less affected during the process of erection than the b_2 constant, then the acting b_2 value could be evaluated. This was found to be equal to 33.37×10^{-16} cm² molecule⁻¹, a value which could reasonably be assigned to an actual area occupied by a cyclohexane molecule vertically oriented to the surface.

In order to confirm the presence of this sub-two-dimensional condensation step during the adsorption of cyclohexane on magnesium hydroxide surface, two additional samples of the same hydroxide were investigated, one being heated at 160° and the other at 320°. Heating at such relatively low temperatures did not convert the hydroxide to the oxide, but it affected slightly the surface area through the destruction of some of the narrow pores. (Details will be published separately.) Still the same vertical rise was noticed to occur at almost the same pressure as the original hydroxide. Apparently the pore structure bears no direct influence on this two-dimensional mechanism.

The statistical monolayer capacity (S_m) of cyclohexane was computed by knowing the specific surface from nitrogen adsorption as compared to that computed from the condensation step. Some characteristics of the parent magnesium hydroxide and of samples M160 and M320 are summarized in Table I. The symbols and notations in Table I are those used by de Boer, *et al.*⁹

It is of particular interest to emphasize that a good agreement is obtained between the specific surface measured by nitrogen and that computed from the condensation step of cyclohexane by using a sectional area of 33.3 Å² per molecule. This is taken as evidence that condensation is due to a reorientation of the adsorbed molecules to acquire a vertical position on the surface, thus increasing their lateral interaction. By acquiring such orientation the interaction between the adsorbed molecules themselves is stronger than

the interaction between the adsorbed layer and the solid.

When the same magnesium hydroxide is heated at higher temperatures, namely at 510 and 740°, it is converted to the oxide, and their cyclohexane adsorption isotherms do not show any stepwise nature. The main point of interest in this connection is that their surface areas as determined by nitrogen agrees excellently with the surface areas determined from cyclohexane, when the latter molecule is considered to lie flat on the surface occupying an area of 39 Å². Apparently, therefore, no condensation could take place, because no reorientation of the cyclohexane molecules on the surface could take place which could possibly lead to an increase in their lateral interaction.

Stepped isotherms noted in the literature on homogeneous surfaces¹¹ show their first step at extremely low pressures with the initial part being convex to the pressure axis. In terms of the concept of active sites on the surface, this implies the presence of very few such sites which are first saturated with the adsorbate molecules and in doing so the surface is rendered homogeneous and condensation takes place. The stronger these sites are (small k_2 in van der Waals equation) the more the liability towards two-dimensional condensation to take place at lower pressures. As the adsorption becomes weaker and k_2 increases, the pressure at which condensation takes place is shifted to higher values. For adsorption on heterogeneous surfaces, the saturation of a bigger number of active sites on the surface could either result in a complete disappearance of the condensation step and smoothing of the isotherms, or, under the best suitable conditions to a delay in the appearance of the condensation step. Under favorable conditions, the adsorbed molecules could increase their lateral interaction to become stronger than the

(10) J. H. de Boer, "The Dynamical Character of Adsorption," The Clarendon Press, Oxford, 1963, Chapter VII, Sections 105 and 106.

(11) See, for example: J. H. de Boer, B. G. Linsen, and Th. J. Osinga, *J. Catal.*, **4**, 643 (1965); A. A. Isirikyan and A. V. Kiselev, *J. Phys. Chem.*, **65**, 601 (1965); J. H. de Boer, J. C. P. Broeckhoff, B. G. Linsen, and A. L. Meijer, *J. Catal.*, **7**, 135 (1967); J. H. Singleton and G. D. Halsey, *J. Phys. Chem.*, **58**, 1011 (1954); D. R. Bassett, E. A. Boucher, and A. C. Zettlemoyer, *ibid.*, **71**, 2787, 90 (1967); B. W. Davis and C. Pierce, *ibid.*, **70**, 1051 (1966).

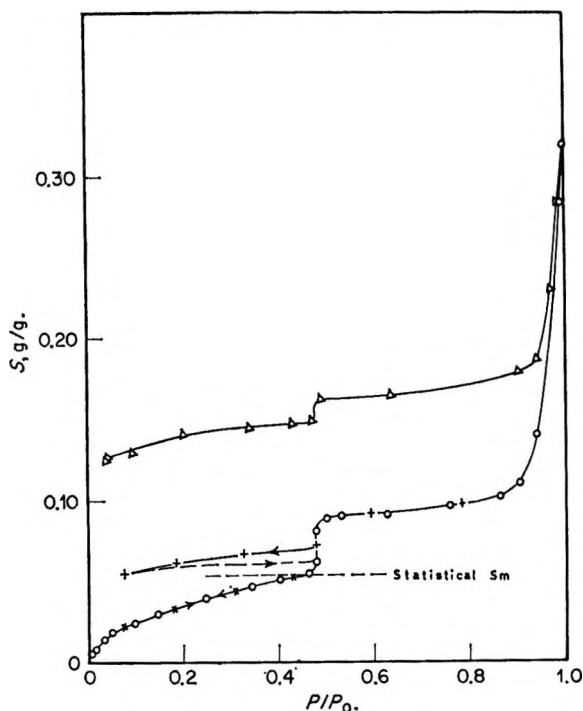


Figure 3. Adsorption-desorption isotherms of water vapor on chromia gel C320: —○—○—, main ascending curve; —△—△—, main descending curve; —×—×—, —+—+—, descending scanning curves; - - - -, ascending scanning curve.

interaction between the adsorbed layer and the solid. This could happen through specific reorientations on the surface.

It seems therefore that surface homogeneity is not a requirement for two-dimensional condensation to take place. More essential requirements than surface homogeneity is that there must be strong lateral interactions between adsorbed molecules. The temperature must be such that thermal agitation of the adsorbed molecules does not erase the discontinuities between the filling of the adsorbate layers.

Another interesting case of such stepped isotherms will be presented in this paper, and the results will add further support to these conclusions.

II. Adsorption of Water Vapor on Thermally Treated Chromia gel. For chromia gel heated at 320°, the adsorption isotherm of water vapor at 35° showed a definite step to occur at a relative pressure range 0.48–0.50. The isotherm is shown in Figure 3. Scanning of the main hysteresis loop was performed around the step region, and the ascending and descending scanning curves are also shown in Figure 3. These curves are self explanatory and clearly indicate the irreversibility in the formation of the step. Evidently, along the desorption branches of the isotherms, there is a decrease in the height of the vertical step, and this decrease seems to be a function of the relative pressure at which scanning starts. The higher the pressure the bigger the change in the height of the vertical step.

From the adsorption of nitrogen on this sample, an estimation of the surface area could be made, and it is noticed that this step occurs beyond a statistical monolayer coverage on the surface. The step which occurs beyond and on top of the first-layer formation could be also interpreted in terms of two-dimensional condensation. The two-dimensional critical temperature for water, which is 323.5°K, is well above the temperature of the experiment (308°K), thus facilitating such a process to take place when the experimental conditions are favorable. The absence of condensation in the first layer became evident through the inspection of the shape of the early region of the isotherm measured at low pressures.

From the beginning and the end of the condensation step of the second layer, a computed S_m value could be evaluated⁹ to be 0.0541 g/g, which is very close to that obtained from nitrogen adsorption, which is 0.0534 g/g (corresponding to an area of 187.8 m²/g). From the S_m value calculated from the condensation step and the surface area obtained from nitrogen adsorption, an acting b_2 value was calculated to be 10.4 Å², which is almost the same value computed on the basis of a close packing model on the surface, *viz.* 10.5 Å².

The significance of such results is that it adds strong support to the previously reached conclusion that strong lateral interaction between the adsorbed molecules is a main requirement for two-dimensional condensation to take place. If the surface is homogeneous in the energetic sense, the adsorption isotherm often shows steps corresponding to the filling of successive layers. The surface of chromia gel is more likely to be heterogeneous in the energetic sense. It seems that for the formation of the first layer on the surface, the adsorbent-adsorbate interaction is stronger than the lateral interactions between the adsorbate molecules, which are mainly responsible for the two-dimensional condensation. This is a normal situation of wide occurrence especially when dealing with heterogeneous surfaces and a polar molecule like water and this inhibits the formation of a step in the first layer. When the surface becomes covered by the adsorbate, then the active forces dominating in the second layer will be those between the adsorbate molecules themselves, *i.e.*, adsorbate-adsorbate interactions. For polar molecules like water strong lateral interaction could be achieved, but what seems to be more important is the relative magnitude of the forces of lateral interactions between the adsorbate molecules in one and the same layer and the forces of interaction between the adsorbate molecules with the solid surface or with the molecules of the preceding layer.

It is of general interest to mention in this connection that a decrease in the heat of adsorption with surface coverage is usually ascribed both to surface heterogeneity and to repulsion of adsorbed molecules. However, attraction is generally observed between them,

and the effect of this attraction is directly opposite to that of surface heterogeneity: heterogeneity leads to a decrease in the heat of adsorption while adsorbate-adsorbate attraction causes its increase. The adsorption properties depend on the geometry and chem-

istry of the surfaces. In particular instances, when the effect of this attraction balances or overcomes the effect due to the heterogeneity of the surface, the surface behaves more or less like an energetically homogeneous surface.

Some Aspects of Diffusion in Ternary Systems¹

by V. Vitagliano and R. Sartorio

Istituto Chimico dell'Università di Napoli, Naples, Italy (Received December 17, 1969)

Diffusion equations of three model ternary systems are discussed: (1) ideal ternary solution: solvent (0) + A + B; (2) ideal ternary solution with a chemical equilibrium: $0 + A + B \rightleftharpoons AB (= Z)$; (3) ternary solution with a salting out effect of component A (or B) on component B (or A). Laity^{2,3} and Dunlop⁴ equations are chosen to describe the flow process, $X_k = \sum_i R_{ki} c_i (v_k - v_i)$ (I). If no interactions exist between the flows (*i.e.*, the thermodynamic frictional coefficients relating the solute flows are zero and the only nonzero frictional coefficients are those relating solvent and solutes flows) the thermodynamic flow equations reduce to $X_i = R_{i0} c_0 (v_i - v_0)$ (II), where the index 0 refers to the solvent. It is shown that when eq II describes the flow process, the cross-diffusion coefficients D_{12} and D_{21} of the extended Fick's equations, $J_i = -\sum D_{ik} \times (\partial c_k / \partial x)$, are not zero and they may even reach orders of magnitude equal to those of the main terms D_{11} and D_{22} . They are generally negative for ideal solutions and for solutions with positive interactions between solutes, such as a chemical reaction (systems 1 and 2). They are positive when repulsive interactions (salting out effects) are present between the solutes (system 3). Numerical and graphical examples are given.

Diffusion in multicomponent systems has been the subject of increasing interest in recent years. The theoretical hydrodynamic and thermodynamic background describing this transport process has been already fully discussed and papers from several authors are readily available in the literature.⁵⁻¹⁰

We think it might be of some interest to write out explicitly the expressions for diffusion in some model systems and show the numerical values that transport coefficients can assume.

It is known that diffusion in ternary systems may be described by an extended Fick's law of the type

$$J_1 = -D_{11} \frac{\partial c_1}{\partial x} - D_{12} \frac{\partial c_2}{\partial x} \quad (1a)$$

$$J_2 = -D_{21} \frac{\partial c_1}{\partial x} - D_{22} \frac{\partial c_2}{\partial x} \quad (1b)$$

where the D_{ik} are the four experimentally measurable diffusion coefficients and indices 1 and 2 (and 0) refer to components 1 and 2 (and to the solvent).

Generally if $D_{12} = D_{21} = 0$ one speaks of noninteracting flows. Actually a definition of "noninteracting flows" applies better to phenomenological transport equations in terms of thermodynamic flows and forces. Assuming that interactions among flows should imply

the existence of some relative friction between species whose flows interact, we think that the best way to define diffusion with no interacting flows is through the use of the phenomenological equations proposed by Laity^{2,3} and by Dunlop⁴

$$-\frac{\partial \mu_k}{\partial x} = X_k = \sum_{i=1}^{n-1} R_{ki} c_i (v_k - v_i) \quad (2)$$

where μ_i = chemical potential of component i , c_i = concentration of component i , R_{ki} = frictional coefficient relating components i and k , v_i = velocity

(1) This work has been carried out with the financial support of the Italian C. N. R.

(2) R. W. Laity *J. Phys. Chem.*, **63**, 80 (1959).

(3) R. W. Laity, *J. Chem. Phys.*, **30**, 682 (1959).

(4) P. J. Dunlop, *J. Phys. Chem.*, **68**, 26 (1964).

(5) D. G. Miller, *Chem. Rev.*, **60**, 15 (1960).

(6) D. G. Miller, *J. Phys. Chem.*, **63**, 570 (1959).

(7) D. G. Miller, *ibid.*, **71**, 616 (1967).

(8) D. G. Miller, *ibid.*, **71**, 3588 (1967).

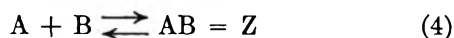
(9) T. K. Kett and D. K. Anderson, *ibid.*, **73**, 1262 (1969).

(10) An extensive literature on this subject can be found in the "Annual Reports on Mass Transport," published by *Ind. Eng. Chem.*; for example, A. Gomezplata and T. M. Regan, *Ind. Eng. Chem.*, **60**, No. 2, 53 (1969); K. B. Bischoff and D. M. Himmelblau, *ibid.*, **60**, No. 1, 66 (1969); K. B. Bischoff and D. M. Himmelblau, *ibid.*, **58**, No. 12, 32 (1966).

of component i measured with respect to any reference frame.¹¹ Interaction at least with the solvent must obviously exist, so we define a system with no interacting flows as one in which $R_{ki} = 0$ if both i and k do not refer to the solvent (i and $k \neq 0$). This assumption implies that there are no frictional effects between components i and k ; (eq 3 is given below¹¹).

We shall show that on this assumption experimental cross-diffusion coefficients may be measured whose values may be of the same order of magnitude as the main terms.

Three model systems will be discussed: (1) ideal ternary solution (solvent + A + B); (2) ideal ternary solution with a chemical equilibrium



(solvent + A + B + Z); (3) a ternary system where the A (or B) component promotes a salting out effect on the B (or A) component. The first two systems show negative values of the D_{12} and D_{21} cross coefficients, the third one shows positive values.

In the following, index 1 refers to the stoichiometric component A irrespective of its actual form in solution and index 2 refers to the component B. Capital letters (A, B, or Z) refer to the actual species existing in solution. The index 0 always refers to the solvent.

Thermodynamic Background

Systems 1 and 2. The various chemical potentials of an ideal system are

$$\begin{aligned} \mu_A &= \mu_A^\circ + RT \ln N_A \\ \mu_B &= \mu_B^\circ + RT \ln N_B \\ \mu_Z &= \mu_Z^\circ + RT \ln N_Z \\ \mu_0 &= \mu_0^\circ + RT \ln N_0 \end{aligned} \quad (5)$$

where the N_i are the mole fractions of the various species. From the equilibrium eq 4 we have

$$\mu_Z = \mu_A + \mu_B \quad (6)$$

also the equilibrium constant K relates the mole fractions of the solutes

$$N_Z = KN_A N_B \quad (7)$$

Therefore the stoichiometric mole fractions will be

$$\begin{aligned} y_0 &= N_0 / (1 + KN_A N_B) \\ y_1 &= (N_A + KN_A N_B) / (1 + KN_A N_B) \\ y_2 &= (N_B + KN_A N_B) / (1 + KN_A N_B) \end{aligned} \quad (8)$$

The stoichiometric chemical potentials of the three components remain μ_0 , μ_A , and μ_B , N_0 , N_A , and N_B being the activities

$$\begin{aligned} a_0 &= N_0 = f_0 y_0 \\ a_1 &= N_A = f_1 y_1 \\ a_2 &= N_B = f_2 y_2 \end{aligned} \quad (9)$$

where the f_i are the rational activity coefficients. To change from mole fractions to concentrations, the following expressions can be used

$$c_0 V_0 + c_1 V_1 + c_2 V_2 = 1 \quad (10)$$

where the V_i are the molar volumes (constant because of the ideality of the solution, $V_1 \equiv V_A$, $V_2 \equiv V_B$, $V_1 + V_2 \equiv V_Z$)

$$c_Z = \frac{1}{2} \left(c_1 + c_2 + \frac{1}{KV} \right) - \sqrt{(c_1 + c_2 + 1/KV)^2 - 4c_1 c_2} \quad (11)$$

V being the total volume

$$V = N_0 V_0 + N_A V_1 + N_B V_2 + N_Z (V_1 + V_2) \quad (12)$$

System 3. We assume the following expressions for the activity coefficients of components 1 and 2

$$\begin{aligned} \ln f_1 &= S y_1 y_2^2 / y_0^3 \\ \ln f_2 &= S y_1^2 y_2 / y_0^3 \end{aligned} \quad (13)$$

where, of course, $y_1 \equiv N_A$, $y_2 \equiv N_B$, and $y_0 \equiv N_0$. The $S > 0$ coefficient accounts for the salting out effect. Equations 13 obey the Gibbs-Duhem expression, the total free energy of mixing being

$$\frac{\Delta F}{RT} = y_0 \ln y_0 + y_1 \ln y_1 + y_2 \ln y_2 + \frac{1}{2} S \frac{y_1^2 y_2^2}{y_0^3} \quad (13a)$$

This model system exhibits a phase separation (see Figure 1).

The Flow Equations. For systems 1 and 2 eq 2 may be written

$$\begin{aligned} -\frac{\partial \ln N_A}{\partial x} &= R_{A0} c_0 (v_A - v_0) = \\ R_{A0} \left(\frac{c_0}{c_A} J_A - J_0 \right) &= X_A \equiv X_1 \end{aligned} \quad (14a)$$

$$\begin{aligned} -\frac{\partial \ln N_B}{\partial x} &= R_{B0} c_0 (v_B - v_0) = \\ R_{B0} \left(\frac{c_0}{c_B} J_B - J_0 \right) &= X_B \equiv X_2 \end{aligned} \quad (14b)$$

$$\begin{aligned} -\frac{\partial \ln N_Z}{\partial x} &= R_{Z0} c_0 (v_Z - v_0) = \\ R_{Z0} \left(\frac{c_0}{c_Z} J_Z - J_0 \right) &= X_Z \equiv X_1 + X_2 \end{aligned} \quad (14c)$$

where the cross-frictional terms R_{AB} , R_{AZ} , and R_{BZ} are absent in accordance with our definition of non-

(11) The flow process described by eq 2 is independent of reference frames because only relative velocities ($v_k - v_i$) appear in eq 2. The Onsager reciprocal relations hold among the frictional coefficients of eq 2; $R_{ik} = R_{ki}$ (3).

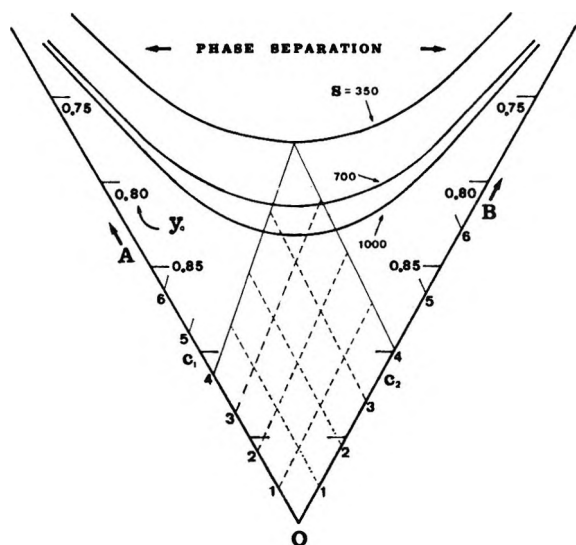


Figure 1. Phase diagram of a ternary system with activity coefficients and free energy of mixing given by eq 13 and 13a.

interacting flows. The stoichiometric flows of components 1 and 2 are

$$\begin{aligned} J_1 &= J_A + J_Z \\ J_2 &= J_B + J_Z \end{aligned} \quad (15)$$

and since

$$\begin{aligned} c_1 &= c_A + c_Z \\ c_2 &= c_B + c_Z \end{aligned} \quad (16)$$

eq 14 becomes

$$\begin{aligned} c_1(v_1 - v_0) &= \frac{1}{c_0} \left[\frac{c_A}{R_{A0}} + \frac{c_Z}{R_{Z0}} \right] X_A + \frac{c_Z}{c_0 R_{Z0}} X_B = (J_1)_s \\ c_2(v_2 - v_0) &= \frac{c_Z}{c_0 R_{Z0}} X_A + \\ &\quad \frac{1}{c_0} \left[\frac{c_B}{R_{B0}} + \frac{c_Z}{R_{Z0}} \right] X_B = (J_2)_s \end{aligned} \quad (17)$$

where the flows are measured with respect to a solvent fixed reference, $(J_0)_s = 0$. Equations 17 are in the form of thermodynamic flow equations. The entropy production is given by

$$T\sigma = -(J_1)_s X_A - (J_2)_s X_B \quad (18)$$

and the Onsager reciprocal relations hold between the cross coefficients

$$L_{12} = \frac{c_Z}{c_0 R_{Z0}} = L_{21} \quad (19)$$

Equations 17 may be written in the form of eq 2 by solving for X_A as a function of $(v_1 - v_0)$ and $(v_1 - v_2)$, and for X_B as a function of $(v_2 - v_0)$ and $(v_2 - v_1)$

$$\begin{aligned} X_A &= R_{10}c_0(v_1 - v_0) + R_{12}c_2(v_1 - v_2) = X_1 \\ X_B &= R_{21}c_1(v_2 - v_1) + R_{20}c_0(v_2 - v_0) = X_2 \end{aligned} \quad (20)$$

where

$$\begin{aligned} R_{10} &= \frac{1}{Hc_0} \left[\frac{c_B}{c_2 R_{B0}} + \frac{c_Z}{c_2 R_{Z0}} - \frac{c_Z}{c_1 R_{Z0}} \right] \\ R_{20} &= \frac{1}{Hc_0} \left[\frac{c_A}{c_1 R_{A0}} + \frac{c_Z}{c_1 R_{Z0}} - \frac{c_Z}{c_2 R_{Z0}} \right] \\ R_{12} &= \frac{c_Z}{Hc_1 c_2 R_{Z0}} = R_{21} \end{aligned} \quad (21)$$

$$H = \frac{1}{c_0 c_1 c_2} \left[\frac{c_A c_B}{R_{A0} R_{B0}} + \frac{c_A c_Z}{R_{A0} R_{Z0}} + \frac{c_B c_Z}{R_{B0} R_{Z0}} \right] \quad (22)$$

Equations 20 and 21 show that the equilibrium 4 gives rise to apparent interactions between the flows ($R_{12} \neq 0$) if they are measured as stoichiometric flows of components 1 and 2. In the limit where $K = 0$, eq 21 reduce to

$$\begin{aligned} R_{10} &= R_{A0} \\ R_{20} &= R_{B0} \\ R_{12} &= R_{21} = 0 \end{aligned} \quad (23)$$

in the opposite limit, where $K \rightarrow \infty$, eq 21 become¹²

$$\begin{aligned} c_1 &> c_2 \\ R_{10} &= R_{A0} \\ R_{20} &= R_{Z0} - R_{A0} \\ R_{12} &= c_0 R_{A0} / (c_1 - c_2) \end{aligned} \quad (24a)$$

$$\begin{aligned} c_2 &> c_1 \\ R_{10} &= R_{Z0} - R_{B0} \\ R_{20} &= R_{B0} \\ R_{12} &= c_0 R_{B0} / (c_2 - c_1) \end{aligned} \quad (24b)$$

System 3. System 3 needs no further comments; eq 14a and 14b hold for it, since $K = 0$ eq 23 are obtained.

(12) If $c_1 = c_2 = c$ we obtain

$$\begin{aligned} R_{10} &= R_{Z0} R_{A0} / \left[R_{Z0} + \frac{c_Z}{c} (R_{A0} + R_{B0} - R_{Z0}) \right] \\ R_{20} &= R_{Z0} R_{B0} / \left[R_{Z0} + \frac{c_Z}{c} (R_{A0} + R_{B0} - R_{Z0}) \right] \\ R_{12} &= \frac{c_0 R_{A0} R_{Z0} c_Z}{(c - c_Z) [c R_{Z0} + c_Z (R_{A0} + R_{B0} - R_{Z0})]} \end{aligned} \quad (25)$$

as K goes to infinity $R_{12} \rightarrow \infty$. It must be pointed out that in the absence of free A and B the only physically meaningful driving force is X_Z which is formally written $(X_A + X_B)$, and eq 20 with the aid of 25 then becomes

$$X_Z = R_{Z0} c_0 (v - v_0) \quad (26)$$

As we expect, the only measurable coefficient is R_{Z0} which refers to the only existing species, *i.e.*, Z; the cross coefficient R_{12} disappears in (26).

The Diffusion Coefficients

The flow eq 1 are measured with respect to a volume fixed frame

$$\sum_{i=1}^n V_i J_i = 0 \quad (27)$$

they are related to the thermodynamic forces by equations¹³

$$\begin{aligned} X_A &= X_1 = A_{11}J_1 + A_{12}J_2 \\ X_B &= X_2 = A_{21}J_1 + A_{22}J_2 \end{aligned} \quad (28)$$

where¹⁴

$$A_{ii} = \frac{c_k}{c_i} R_{ik} + \left[\frac{c_0}{c_i} + \frac{V_i}{V_0} \right] \quad (29)$$

$$A_{ik} = \frac{V_k}{V_0} R_{i0} - R_{ik} \quad (30)$$

On the other hand, the driving forces can be written as

$$X_i = - \sum_{k=1}^2 \mu_{ik} \frac{\partial c_k}{\partial x} \quad i = 1, 2 \quad (31)$$

where

$$\mu_{ik} = \frac{\partial \ln a_i}{\partial c_k} \quad (32)$$

a_i being the activities, eq 9 and 13. Solving eq 28 with the aid of eq 31, the Fick's eq 1 are obtained with the following values for the four diffusion coefficients

$$D_{ii} = (\mu_{ki}A_{ik} - \mu_{ii}A_{kk})/A \quad (33)$$

$$\begin{aligned} D_{ik} &= (\mu_{kk}A_{ik} - \mu_{ik}A_{kk})/A \\ A &= A_{ik}A_{ki} - A_{ii}A_{kk} \end{aligned} \quad (34)$$

System 1. If Z is absent, *i.e.*, $K = 0$, the diffusion coefficients are¹⁴

$$D_{ii} = \frac{c_i c_k V_k (V_0 - V_i)}{c_0 V_0 R_{k0} R_{i0} (c_i + c_k + c_0)} + \frac{1 - c_i V_i}{c_0 V_0 R_{i0} (c_i + c_k + c_0)} [1 + (V_0 - V_k) c_k] \quad (35)$$

$$D_{ik} = - \frac{c_i}{c_0 V_0 (c_i + c_k + c_0) R_{i0}} \left[(V_0 c_i + 1 - V_i c_i) \times \frac{V_k R_{i0}}{R_{k0}} + (V_0 - V_k) (1 - V_i c_i) \right] \quad (36)$$

It is interesting to discuss briefly eq 35 and 36, which show that even in the absence of interactions between components A and B ($K = 0$) the cross coefficients D_{ik} are not zero. In the limit of $C_k \rightarrow 0$, eq 35 reduces to the value of the diffusion coefficient of component i in a binary solution;¹⁵ surprisingly the D_{ik} coefficient does not disappear

$$\lim_{c_k \rightarrow 0} D_{ik} = - \frac{c_i}{c_0 + c_i} \left[\left(\frac{c_i}{c_0} + 1 \right) \frac{V_k}{R_{k0}} + \frac{V_0 - V_k}{R_{i0}} \right] \quad (37)$$

on the other hand¹⁶

$$\lim_{c_k \rightarrow 0} D_{ki} = 0 \quad (38)$$

While the main coefficients are always positive, the sign of the cross coefficients depends on the sign of the second factor in the right side of eq 36. A rearrangement of that equation gives the following inequality (relation 39).

Table I: Diffusion Coefficients in a Ternary Ideal Solution with No Interaction between the Solute Flows and Constant Frictional Coefficients, $V_0 = 0.020$, $V_A = 0.040$, $V_B = 0.070$, $R_{A0} = 0.004$, $R_{B0} = 0.006$

c_i	D_{11}	D_{12}	D_{21}	D_{22}
$c_2 = 0.0$				
0.0	5.000	0.000	0.000	3.3333
1.0	5.1020	0.0120	0.000	3.4722
2.0	5.2083	0.0136	0.000	3.6232
3.0	5.3191	0.0024	0.000	3.7879
4.0	5.4348	-0.0242	0.000	3.9682
$c_2 = 1.0$				
0.0	5.3763	0.000	-0.1449	3.5088
1.0	5.5036	0.0137	-0.1546	3.6583
2.0	5.6376	0.0155	-0.1655	3.8216
3.0	5.7789	0.0028	-0.1776	4.0006
4.0	5.9282	-0.0279	-0.1911	4.1976
$c_2 = 2.0$				
0.0	5.8140	0.000	-0.3170	3.7037
1.0	5.9783	0.0157	-0.3400	3.8655
2.0	6.1439	0.0179	-0.3657	4.0429
3.0	6.3256	0.0032	-0.3947	4.2385
4.0	6.5203	-0.0325	-0.4274	4.4553
$c_2 = 3.0$				
0.0	6.3291	0.000	-0.5242	3.9216
1.0	6.5317	0.0182	-0.5655	4.0974
2.0	6.7501	0.0209	-0.6121	4.2914
3.0	6.9866	0.0038	-0.6650	4.5066
4.0	7.2439	-0.0385	-0.7256	4.7468
$c_2 = 4.0$				
0.0	6.9444	0.000	-0.7778	4.1667
1.0	7.2046	0.0214	-0.8446	4.3590
2.0	7.4890	0.0247	-0.9210	4.5724
3.0	7.8018	0.0045	-1.0090	4.8108
4.0	8.1481	-0.0463	-1.1111	5.0794

(13) Reference 10 eq 16 and 17.

(14) The R_{i0} and R_{ik} are the stoichiometric frictional coefficients defined by eq 21, 22, and 23.

(15) Reference 10 eq 40.

(16) L. Sundelöf, *Ark. Kemi*, 20, 369 (1963).

(17) These values are arbitrary; they have been chosen to give diffusion coefficients in the range of unity, that is the order of magnitude of experimental diffusion coefficients if measured in $\text{cm}^2 \text{sec}^{-1} \times 10^6$.

$$D_{ik} \begin{cases} < 0 \\ = 0 \\ > 0 \end{cases} \text{ if } \left[\frac{V_0 c_i}{1 - V_i c_i} + 1 \right] \frac{R_{i0}}{R_{k0}} + V_0/V_k - 1 \begin{cases} > 0 \\ = 0 \\ < 0 \end{cases} \quad (39)$$

At higher values of c_i the D_{ik} coefficients are always negative, but if

$$\frac{R_{i0}}{R_{k0}} + \frac{V_0}{V_k} - 1 < 0 \quad (40)$$

there will be one value of c_i , independent of c_k , for which $D_{ik} = 0$

$$c_i = \frac{R_{k0}}{R_{i0}} \left[\frac{1 - V_i c_i}{V_0} \right] \left[1 - \frac{R_{i0}}{R_{k0}} - \frac{V_0}{V_k} \right] \quad (41)$$

At lower c_i values the D_{ik} will be positive (see Figure 2).

Numerical Examples

Some numerical examples may help to clarify the implications of the expressions obtained so far. All data will refer to a model system with the following values of the molar volumes and frictional coefficients: $V_0 = 20$ cm/mol, $V_A \equiv V_1 = 40$, $V_B \equiv V_2 = 70$,

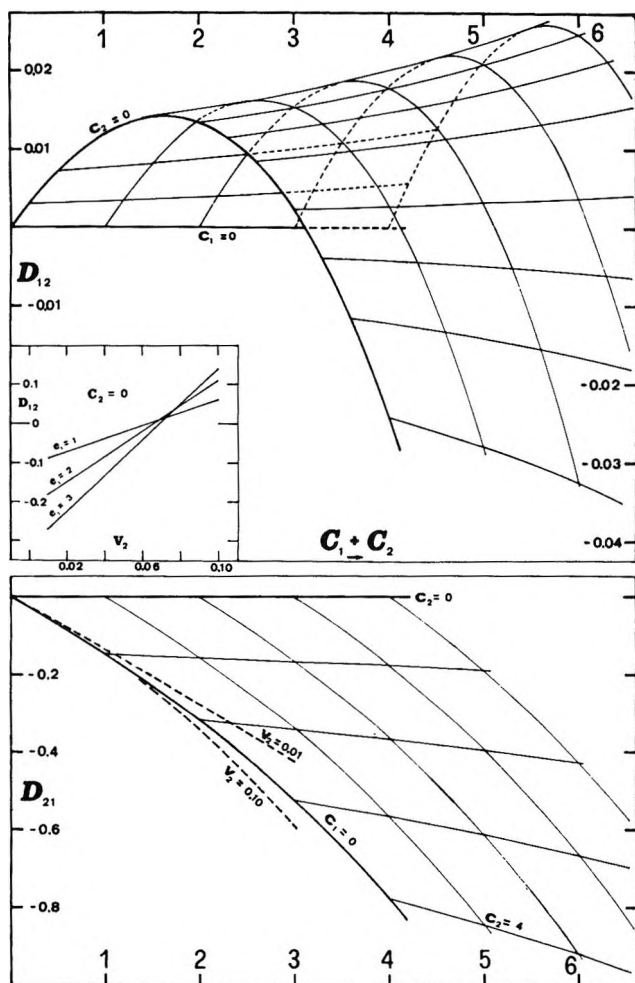


Figure 2. Cross diffusion coefficients in an ideal ternary system (see data of Table I) as a function of the two solutes concentrations.

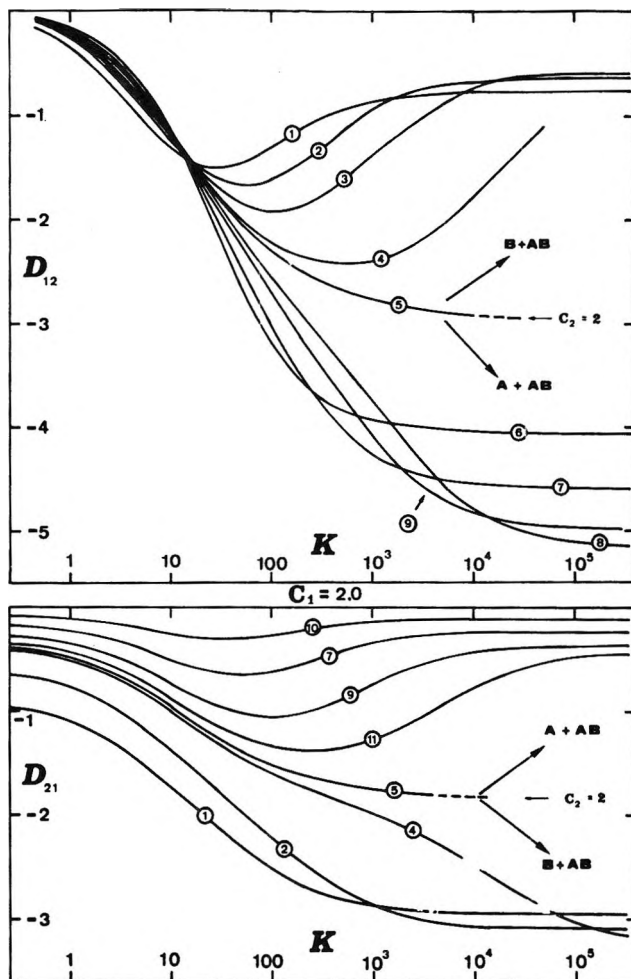


Figure 3. Cross diffusion coefficients in a ternary system with a chemical reaction ($A + B = Z$) between the solutes as a function of the equilibrium constant K (eq 7). The component 2 concentrations are: (1) $c_2 = 4.0$; (2) $c_2 = 3.0$; (3) $c_2 = 2.5$; (4) $c_2 = 2.1$; (5) $c_2 = 2.0$; (6) $c_2 = 0.2$; (7) $c_2 = 1.0$; (8) $c_2 = 1.7$; (9) $c_2 = 1.5$; (10) $c_2 = 0.5$; (11) $c_2 = 1.8$.

$R_{A0} = 0.004$, $R_{B0} = 0.006$, $R_{Z0} = 0.050$.¹⁷ Concentrations are in moles per liter. Computations have been made with the help of an IBM 1620 computer.

The four diffusion coefficients tabulated as functions of c_i and c_k in the concentration range 0 to 4 M are given in Table I for $K = 0$. Figure 2 shows the D_{12} and D_{21} coefficients as a function of c_1 and c_2 in a Zimm-like-plot graph.

The values of the diffusion coefficients when all of A or of B react to give Z ($K \rightarrow \infty$) are given in Table II).

The behavior of the diffusion coefficients and of the frictional coefficients in the region of equilibrium 4 is shown in Figures 3, 4, and 5. Figure 3 shows the behavior of D_{12} and D_{21} at $c_1 = 2$ M as a function of K for different c_2 values. Figures 4 and 5 show similar plots for R_{10} and $R_{12} (= R_{21})$, eq 21.

Finally, the behavior of a system with a salting out effect according to eq 13 is shown in Table III,

Table II: Diffusion Coefficients in a Ternary System Containing Component A and B which React Completely to Form a Compound Z ($K \rightarrow \infty$, eq 7), $V_0 = 0.020$, $V_A = 0.040$, $V_B = 0.070$, $R_{A0} = 0.004$, $R_{B0} = 0.006$, $R_{Z0} = 0.050$

c_1	D_{11}	D_{12}	D_{21}	D_{22}	
$c_2 \rightarrow 0$					
0.0 ^a	$D_Z = 0.4000$
1.0	5.102	-4.272	0.000	0.4167	
2.0	5.208	-3.932	0.000	0.4348	
3.0	5.319	-3.578	0.000	0.4546	
4.0	5.435	-3.212	0.000	0.4762	
$c_2 = 1.0$					
0.0	0.4301	0.000	-2.810	3.509	$D_Z = 0.4301$
1.0 ^a	
2.0	5.542	-4.590	-0.2312	0.6686	
3.0	5.689	-4.200	-0.2482	0.6820	
4.0	5.846	-3.792	-0.2672	0.6960	
$c_2 = 2.0$					
0.0	0.4651	0.000	-0.2674	3.704	$D_Z = 0.4651$
1.0	0.7256	-0.2758	-2.935	3.721	
2.0 ^a	
3.0	6.113	-5.000	-0.5330	0.9886	
4.0	6.324	-4.546	-0.5779	0.9946	
$c_2 = 3.0$					
0.0	0.5063	0.000	-2.524	3.922	$D_Z = 0.5063$
1.0	0.7785	-0.3202	-2.789	3.967	
2.0	1.108	-0.6429	-3.100	3.999	
3.0 ^a	
4.0	6.884	-5.549	-0.9432	1.410	
$c_2 = 4.0$					
0.0	0.5556	0.000	-2.356	4.167	$D_Z = 0.5556$
1.0	0.8400	-0.3764	-2.625	4.248	
2.0	1.190	-0.7627	-2.944	4.319	
3.0	1.624	-1.154	-3.326	4.376	
4.0 ^a	

^a In solution only the species Z is present.

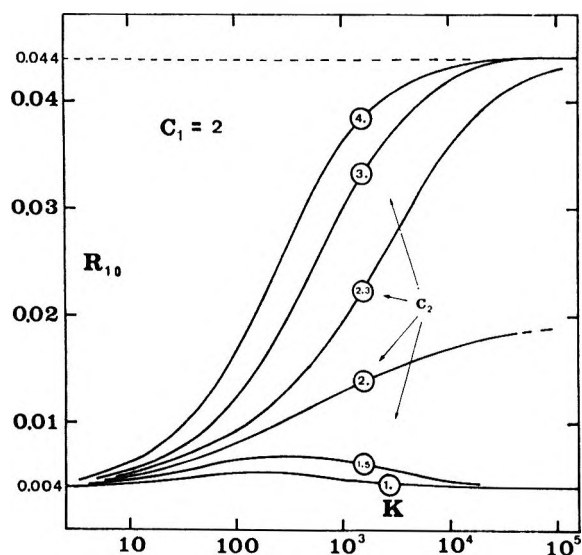


Figure 4. Main frictional coefficient R_{10} (eq 21) as a function of the equilibrium constant K (eq 7) at fixed $c_1 = 2.0$ concentration and varying c_2 concentration. The c_2 values are given on each curve.

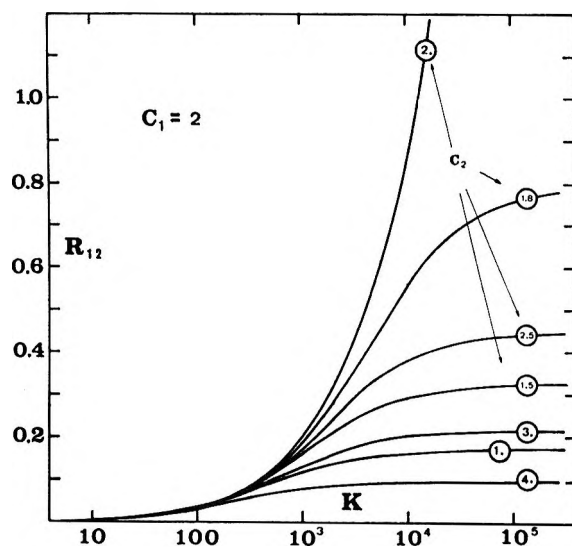


Figure 5. Cross-frictional coefficient R_{12} (eq 21) as a function of the equilibrium constant K (eq 7) at fixed $c_1 = 2.0$ concentration and varying c_2 concentration. The c_2 values are given on each curve.

in which we have collected the four diffusion coefficients as functions of the S parameter for some systems at different concentrations, including systems at the critical mixing composition (see Figure 1).

Table III: Diffusion Coefficients in a Ternary Solution with Salting Out Effect on Components A and B According to Eq 13, $V_0 = 0.020$, $V_A = 0.040$, $V_B = 0.070$, $R_{A0} = 0.004$, $R_{B0} = 0.006$

S	D_{11}	D_{12}	D_{21}	D_{22}	$ D_{ik} $
$c_1 = 2.0$					
$c_2 = 4.0$					
20	7.574	0.222	-0.764	4.664	
50	7.700	0.519	-0.528	4.803	
100	7.912	1.014	-0.136	5.033	
200	8.335	2.003	0.650	5.494	
300	8.758	2.992	1.435	5.954	
340	8.927	3.387	1.749	6.138	
350	8.969	3.486	1.828	6.184	
360	9.011	3.585	1.906	6.230	
$c_1 = 4.0$					
$c_2 = 4.0$					
20	8.682	1.241	-0.552	5.412	+47.9
50	9.484	3.173	0.287	5.912	+47.0
100	10.821	6.392	1.685	6.745	+62.0
200	13.49	12.83	4.482	8.411	+57.0
300	16.17	19.27	7.278	10.077	+23.0
340	17.24	21.84	8.397	10.744	+1.4
350	17.50	22.49	8.676	10.91	-0.4 ^a
360	17.77	23.13	8.96	11.08	-1.0 ^b
$c_1 = 3.0$					
$c_2 = 3.0$					
500	9.660	6.210	2.422	6.300	+45.8
1000	12.33	12.42	5.508	8.092	+31.3
1440	14.68	17.88	8.224	9.670	-0.5 ^a

^a Approximate critical mixing composition. ^b Unstable system, composition corresponding to a two-phase region.

Conclusions

From the expressions obtained in the previous pages and from inspection of the numerical results we may suggest the following conclusions.

(1) In an ideal ternary system with constant frictional coefficients and without interaction between the solute flows, the experimental cross-diffusion coefficients are not zero. They are likely to be negative and they may even be of the same order of magnitude of the main terms. If relation 40 holds, the D_{ik} term may become positive on dilution of component i , and it goes to zero from the positive side as c_i goes to zero (see Figure 2).

(2) The appearance of a chemical equilibrium between species A and B, with the existence of a third species $Z = AB$, increases the negative values of the cross-diffusion coefficients which may probably reach values close to those of the main terms.¹⁸

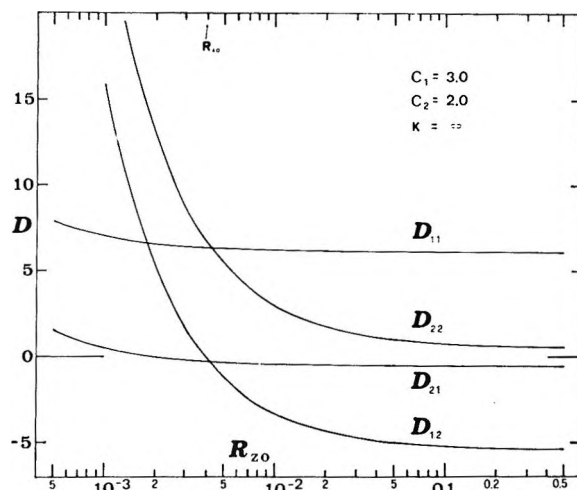


Figure 6. The four D_{ik} diffusion coefficients in a system containing A + AB as a function of the R_{z0} frictional coefficient at constant $R_{A0} = 0.004$.

(3) Repulsive interactions between species A and B, promoting a salting out, have an opposite effect on the cross-diffusion terms; these shift to positive values and may become even greater than the main terms. As may be expected,¹⁶ in the region of critical mixing

$$D_{11}D_{22} = D_{12}D_{21} \quad (42)$$

For a three-component system eq 42 corresponds in fact to the relation $D = 0$ at a critical point of a binary mixture.

Acknowledgments. The authors wish to thank Dr. H. Schönert for reading the paper and for discussions and useful suggestions.

Appendix

Some explicit expressions are given here to be used in the text equations

$$N_A = \frac{K(y_1 - y_2) - 1 + \sqrt{F_1}}{2K(1 - y_2)} \quad (43)$$

$$F_1 = [K(y_1 - y_2) - 1]^2 + 4Ky_1(1 - y_2) \quad (43a)$$

$$\mu_{11} = \frac{\partial \ln N_A}{\partial \ln y_1} \frac{\partial \ln y_1}{\partial c_1} + \frac{\partial \ln N_A}{\partial \ln y_2} \frac{\partial \ln y_2}{\partial c_1} \quad (44)$$

$$\mu_{12} = \frac{\partial \ln N_A}{\partial \ln y_1} \frac{\partial \ln y_1}{\partial c_2} + \frac{\partial \ln N_A}{\partial \ln y_2} \frac{\partial \ln y_2}{\partial c_2} \quad (44a)$$

$$\frac{\partial \ln N_A}{\partial \ln y_1} = \frac{1 + [(y_1 - y_2)K - 2y_2 + 1](\sqrt{F_1})^{-1}}{2(1 - y_2)} (y_1/N_A) \quad (45)$$

(18) The signs of the cross-diffusion coefficients do depend, of course, on the relative values of the three frictional coefficients. In the case that R_{z0} is lower than R_{A0} or R_{B0} the D_{ik} may become positive as shown in Figure 6. This case appears to be physically unreasonable and it looks like a simple algebraic speculation.

$$\frac{\partial \ln N_A}{\partial \ln y_2} = \frac{[K(y_1 - y_2) - 1 + \sqrt{F_1}] - K(1 - y_2) \times \{1 + [K(y_1 - y_2) + 2y_1 - 1](\sqrt{F_1})^{-1}\} (y_2/N_A)}{2K(1 - y_2)^2} \quad (45a)$$

$$\frac{\partial \ln y_1}{\partial \ln c_2} = - \left(1 - \frac{V_2}{V_0}\right) / (c_1 + c_2 + c_0) = T_1 \quad (46)$$

$$\frac{\partial \ln y_1}{\partial \ln c_1} = T_1 + 1/c_1 \quad (46a)$$

Expressions for N_B , μ_{21} , and μ_{22} , and for the derivatives can be obtained by interchanging indices A and B, 1 and 2. From eq 13 we have

$$\frac{\partial \ln a_i}{\partial \ln y_i} = i + S \frac{y_i y_k^2 (y_0 + 3y_i)}{y_0^4} \quad (47)$$

$$\frac{\partial \ln a_i}{\partial \ln y_k} = S \frac{y_i y_k^2 (2y_0 + 3y_k)}{y_0^4} \quad (47a)$$

Equations 47 and 47a substitute the $(\partial \ln N / \partial \ln y)$ in eq 44 and 44a to compute the μ_{ik} .

Diffusion in Mixed Solvents. I. Iodine in Ethanol-Water and *t*-Butyl Alcohol-Water Solutions

by Koichiro Nakanishi and Teruko Ozasa

Department of Industrial Chemistry, Kyoto University, Kyoto, Japan (Received February 16, 1970)

The diffusion coefficients of iodine diluted in ethanol-water and *t*-butyl alcohol-water solutions at 25.00° have been measured by the capillary-cell method. It is found that the diffusion coefficients do not vary linearly with the molar composition of mixed solvents and that the product $D_{i1}^0 \eta / T$ (D_{i1}^0 is the diffusion coefficient of iodine, η is the viscosity of solvent, T is the temperature) has a pronounced maximum at lower mole fraction (~ 0.05 – 0.1) of each alcohol. This fact is interpreted in terms of the structural anomaly in alcohol-water solutions.

Introduction

Although the liquid-phase diffusion in binary systems has received much attention in the past decades, very little work has been carried out in ternary systems. This is due to our incomplete understanding of the structure and properties of multicomponent liquid mixtures that is pertinent to the interpretation of experimental data and also to the relative difficulty in making precise determinations of diffusion coefficients. There are only a few reports on diffusion in ternary systems. In their pioneering works, Dunlop, Fujita, and Gosting¹ have measured the diffusion coefficients of two electrolytes or nonelectrolytes in water. Later, Toor, *et al.*,^{2–4} and Anderson, *et al.*,⁵ have studied the diffusivity in ternary systems of nonelectrolyte solutions such as alcohol mixtures.

The present study is confined to establishing the limiting values of the mutual diffusion coefficient of a single solute in mixed solvents where the concentration of diffusant is practically equal to zero. This quantity, denoted as D_{i1}^0 hereafter, is not identified with any

binary diffusion coefficients. However, since the fluxes are uncoupled at infinite dilution, D_{i1}^0 can be treated as a pseudobinary coefficient and our aim is to investigate how D_{i1}^0 depends on the molar compositions in mixed solvents.

Although this case of ternary diffusion has been studied experimentally by Toor, *et al.*,⁴ Wilke, *et al.*,⁶ Himmelblau, *et al.*,⁷ and Perkins, *et al.*,⁸ their experimental work and theoretical analysis are confined almost exclusively to the cases of nonassociating solutions

(1) For quick reference, see, for example, D. D. Fitts, "Non-Equilibrium Thermodynamics," McGraw-Hill, New York, N. Y., 1962, Chapter 10.

(2) J. K. Burchard and H. L. Toor, *J. Phys. Chem.*, **66**, 2015 (1962).

(3) F. O. Shuck and H. L. Toor, *ibid.*, **67**, 540 (1963).

(4) H. T. Cullinan, Jr., and H. L. Toor, *ibid.*, **69**, 3941 (1965).

(5) T. K. Kett and D. K. Anderson, *ibid.*, **73**, 1268 (1969).

(6) J. T. Holmes, C. R. Wilke, and D. R. Olander, *AIChE J.*, **8**, 646 (1962).

(7) Y. P. Tang and D. M. Himmelblau, *ibid.*, **11**, 54 (1965).

(8) L. R. Perkins and C. J. Geankoplis, *Chem. Eng. Sci.*, **24**, 1035 (1969).

with small nonideality. Wilke, *et al.*,⁶ have shown that the product $D_{11}^0 \eta/T$, where η is the viscosity of mixed solvents and T is the temperature in °K, can be assumed to vary linearly with the mole fraction of one component in a mixed solvent, x , though in one of their experiments, toluene in cyclohexane-*n*-decane, the data show a slight deviation from this linear relation. On the other hand, Himmelblau, *et al.*,⁷ have attempted to correlate their data with complex empirical equations. They reported that, among many correlations examined, an equation, in which the additivity of $D_{11}^0 \eta^{1/2}$ with regard to the mole fraction is assumed, was successful for reproducing the existing data including those with CO₂ in ethanol-water solutions. According to our opinion, such oversimplification may conceal important experimental information which might be incorporated in the data. Recently, Cullinan and Cusik⁹ have developed a predictive theory based on a linear additivity of the friction activation energy for mixed solvents. However, the application of this theory is limited to the nonassociated liquid mixtures. It is thus obvious that for the diffusion in mixed solvents, especially when they are highly nonideal and associated, there is at present no predictive theory or even extensive experimental evidence.

With this situation in mind, we have attempted to study the diffusion of a single dilute solute in various types of binary mixed solvents. In the present paper, we will report the data for the diffusion coefficients of iodine in ethanol-water and in *t*-butyl alcohol-water solutions at 25.00°. This choice of systems needs justification. First, we adopted iodine as the solute, as it is a very complex molecule which shows various types of specific interactions with many organic liquids.^{10,11} Moreover, we can utilize a rather detailed study made with pure solvents by Stokes, *et al.*¹² On the other hand, the complex structural anomalies in alcohol-water systems are well recognized,¹³⁻¹⁵ though our present knowledge is far from quantitative. It was believed that the most complicated systems should be studied in order to know the extent of anomalies involved. The ethanol-water solutions have the advantage of possessing abundant data for various properties which are helpful in interpreting the diffusion data. Another system, *t*-butyl alcohol-water solutions, was chosen because *t*-butyl alcohol dissolves into the water structure rather interstitially, while there occurs a substitutional dissolution in the cases of methanol and ethanol.¹³

Experimental Section

Solvents and Iodine. All solvents except water were of CP grade and were used without further purification. The water was deionized by an ion-exchange column. No other ions than hydrogen ions are added in the solution. Iodine was purified by sublimation.

Apparatus. The open-end capillary cell method

developed by Wang¹⁶ was used for the measurements of diffusion coefficients both in pure and mixed solvents. The principles and technique have been described in a monograph.¹⁷ The capillaries used in this study are made of glass tubings which are carefully selected by checking the uniformity in their diameter. It is of 60-70 mm length and the inner diameter is about 2 mm. The volume of capillaries is determined from the density and weight of carbon tetrachloride which occupies the cell at room temperature. It is between 2.06 and 2.16 ml for a set of capillaries which is used for one run.

The viscosity of solutions was determined with an Ostwald-type viscosimeter which was tightly fixed to a specially designed holder. The flow time for water was about 120 sec and reproducible within $\pm 0.1\%$. These measurements were performed in a thermostat which was controlled to $25.00 \pm 0.01^\circ$.

Procedure. The diffusion coefficient of iodine was determined by measuring the initial and final (averaged) concentrations of iodine in the capillaries which were immersed into about 2 l. of the solvent. In accordance with the suggestion by recent investigators,^{18,19} no stirring was taken place during the diffusion in order to avoid possible " Δl effect."

The diffusion coefficient D_{11}^0 may be calculated from

$$\frac{C_{av}}{C_0} = \sum_{n=0}^{\infty} \frac{8}{\pi^2(2n+1)^2} \exp\left[-\pi^2(2n+1)^2 \frac{D_{11}^0 t}{4L^2}\right] \quad (1)$$

where C_{av} is the average concentration of iodine in the capillary at the end of diffusion time, in arbitrary units; C_0 is the initial concentration, the same unit as C_{av} ; t is the time of diffusion, in seconds, and L is the length of the capillaries in centimeters.

In the present experiments, D_{11}^0 was between 2.5 and 0.4×10^{-5} cm²/sec, and t was 2 or 5 days. Since the infinite series in eq 1 converges rapidly, only the first three terms were necessary to calculate D_{11}^0 . Therefore we determined D_{11}^0 by a successive calculation involving the Newton-Raphson method. The analyses of iodine concentrations were performed by titration with a microburet graduated to 0.01 ml. A standard

(9) H. T. Cullinan, Jr., and M. R. Cusik, *AIChE J.*, **13**, 1171 (1967).

(10) J. H. Hildebrand and R. L. Scott, "Regular Solutions," Prentice-Hall, Englewood Cliff, N. J., 1962.

(11) E. M. Voigt, *J. Phys. Chem.*, **72**, 3300 (1968).

(12) R. H. Stokes, P. J. Dunlop, and J. R. Hall, *Trans. Faraday Soc.*, **47**, 886 (1953).

(13) F. Franks and D. J. G. Ives, *Quart. Rev. Chem. Soc.*, **20**, 1 (1966).

(14) F. Franks, Ed., "Physico-Chemical Processes in Mixed Aqueous Solvents," Heinemann, London, 1967.

(15) K. Nakanishi, *Bull. Chem. Soc. Jap.*, **33**, 793 (1960).

(16) J. H. Wang, *J. Amer. Chem. Soc.*, **76**, 4763 (1954).

(17) R. A. Robinson and R. H. Stokes, "Electrolyte Solutions," Butterworth, London, 1955, Chapter 10.

(18) P. M. Witherspoon and D. N. Saraf, *J. Phys. Chem.*, **69**, 3752 (1965).

(19) C. M. Gary-Bobo and H. W. Weber, *ibid.*, **73**, 1155 (1969).

solution of 0.005 *N* sodium thiosulfate was used for analysis of iodine in alcohol. The solubility of iodine in water and dilute aqueous solutions of alcohol was very small ($\sim 5 \times 10^{-4}$ *M*). For these cases, the concentration of the standard solution was 1/400 to 1/800 *N*. Even under such conditions, the titration could be done without much difficulty.

Results and Discussion

Diffusion Coefficient of I_2 in CCl_4 . In order to check the validity of the present measurement, we have done a control experiment in which the diffusion coefficient of I_2 in carbon tetrachloride is determined at 25.00°. As shown in Table I, the result is satisfactorily compared with literature values.^{12,20}

Table I: Diffusion Coefficient of Iodine in Carbon Tetrachloride at 25.00°

Author	Method	Diffusion coeff $D_{11}^0 \times 10^6$, cm ² /sec
See ref 12	Diaphragm	1.500
See ref 20	Capillary-cell	1.447
This work	Capillary-cell	1.474 ± 0.025

Diffusion Coefficients of I_2 in $EtOH-H_2O$ Solutions
The diffusion coefficients of I_2 in aqueous solutions of ethanol, together with those in pure solvents, have been measured at 25.00°. They are listed in Table II.^{21,22} The figures in the table represent average values over

Table II: Diffusion Coefficients of Iodine Dilute in Ethanol-Water Solutions at 25.00°

Mole fraction of ethanol, x_{EtOH}	Diffusion coeff $D_{11}^0 \times 10^6$, cm ² /sec	Initial concn of iodine, ^a C_{I_2} , <i>M</i>	Viscosity of solution, ^b η , cP	$D_{11}^0/T \times 10^{10}$
0.0000	2.25 ± 0.22	0.0003	0.8903	6.72
0.1000	1.59 ± 0.12	0.0012	1.910	10.20
0.1499	1.15 ± 0.08	0.0033	2.215	8.57
0.1999	0.92 ± 0.05	0.0098	2.335	7.18
0.3001	0.95 ± 0.15	0.0012	2.370	7.56
	0.93 ± 0.05	0.0197		7.38
0.5003	1.06 ± 0.03	0.0012	1.985	7.09
	1.04 ± 0.01	0.0197		6.94
0.6004	1.05 ± 0.01	0.0197	1.770	6.20
0.7505	1.07 ± 0.02	0.0197	1.475	5.29
1.0000	1.35 ± 0.03	0.0197	1.096	4.96

^a The final average concentration was 60–75% lower than the value listed in this column. ^b Interpolated from the literature values.^{21,22}

several runs. An estimated error limit for D_{11}^0 is also included. The concentration range of I_2 is not the same for all the solutions; since the solubilities of I_2 in water and dilute alcohol solutions are very small, we had to

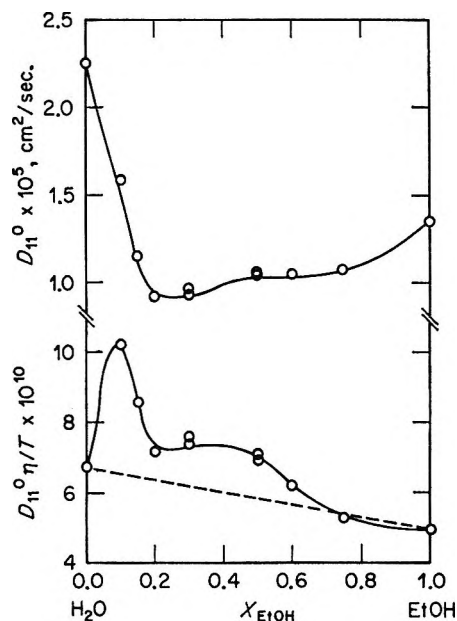


Figure 1. Diffusion coefficients D_{11}^0 of iodine and the product $D_{11}^0 \eta/T$ in ethanol-water solutions at 25.00°.

use a more dilute solution of I_2 as the mole fraction of alcohol in aqueous solutions becomes smaller. As Table II indicates, the concentrations of I_2 are always small enough to assume the present experimental conditions to be practically at infinite dilution. The duplicate data for $x_{EtOH} = 0.3$ and 0.5 indicate that the D_{11}^0 values are practically independent of the concentration of I_2 in such dilute solutions. Therefore, the data represent the limiting values of the main diffusion coefficient for I_2 at its infinite dilution.

Using the values of viscosity coefficients available in the literature,^{21,22} we have calculated the product $D_{11}^0 \eta/T$ for each composition. The D_{11}^0 vs. x and $D_{11}^0 \eta/T$ vs. x plots are shown in Figure 1. While the D_{11}^0 vs. x plot deviates negatively from the linear relation, the $D_{11}^0 \eta/T$ vs. x plot has a pronounced maximum near $x_{EtOH} = 0.1$. The overall uncertainty in $D_{11}^0 \eta/T$ values were estimated to be less than $\pm 10\%$, while the experimental $D_{11}^0 \eta/T$ values for $x_{EtOH} = 0.1-0.5$ are 40–60% higher than those expected from the linear relation. Thus, we believe that the maximum mentioned above is experimentally well established.

Diffusion Coefficients of I_2 in $t-BuOH-H_2O$ Solutions. The results of diffusion and viscosity measurements are summarized in Tables III and IV. Although the viscosity data for $t-BuOH-H_2O$ solutions are available in the literature,²² we have redetermined them and used for the calculation of $D_{11}^0 \eta/T$ values shown in Table

(20) E. W. Haycock, B. J. Alder, and J. H. Hildebrand, *J. Chem. Phys.*, 21, 1601 (1953).

(21) L. Korson, W. Drost-Hansen, and F. J. Millero, *J. Phys. Chem.*, 73, 34 (1969).

(22) N. A. Lange, Ed., "Handbook of Chemistry," 10th ed, McGraw Hill, New York, N. Y., 1967.

Table III: Viscosity Coefficients of *t*-Butyl Alcohol–Water Solutions at 25.00°

Mole fraction of <i>t</i> -Butyl alcohol, x_{BuOH}	Viscosity coeff, η , cP	Mole fraction of <i>t</i> -Butyl alcohol, x_{BuOH}	Viscosity coeff, η , cP
0.0000	0.8903 ^a	0.4313	5.285
0.0206	1.337	0.4315	5.316
0.0447	2.015	0.4939	5.199
0.0745	2.780	0.5965	4.912
0.1121	3.550	0.6961	4.646
0.1574	4.288	0.7888	4.392
0.2199	4.888	0.7907	4.397
0.3035	5.292	0.8932	4.308
0.4285	5.484	1.0000	4.352 ^b

^a Literature value from ref 21. ^b Extrapolated value from the data obtained at higher temperatures.

Table IV: Diffusion Coefficients of Iodine Dilute in *t*-Butyl Alcohol–Water Solutions at 25.00°

Mole fraction of <i>t</i> -Butyl alcohol, x_{BuOH}	Diffusion coeff $D_{11}^0 \times 10^5$, cm ² /sec	Initial concn of iodine, ^a C_{I_2} , M	Viscosity of solution, ^b η , cP	$D_{11}^0/T \times 10^{10}$
0.0000	2.25 ± 0.22	0.0003	0.8903	6.72
0.0499	1.37 ± 0.12	0.0012	2.125	9.76
0.1023	0.82 ± 0.20	0.0012	3.325	9.14
0.1500	0.59 ± 0.05	0.0016	4.225	8.36
0.2001	0.45 ± 0.08	0.0020	4.765	7.19
0.3000	0.39 ± 0.02	0.0197	5.305	6.94
0.5009	0.42 ± 0.01	0.0020	5.200	7.32
	0.45 ± 0.01	0.0197		7.85
0.7225	0.49 ± 0.03	0.0197	4.550	7.55
1.0000	0.51 ± 0.01	0.0197	4.352	7.42

^a See the footnote of Table II. ^b Interpolated from the data in Table III.

IV. The present data did not agree perfectly with the literature values in the alcohol-rich region. The D_{11}^0 vs. x and $D_{11}^0\eta/T$ vs. x plots are shown in Figure 2. The diffusion coefficient of I_2 in *t*-BuOH–H₂O solutions does not vary linearly with x_{BuOH} . It appears that a shallow minimum of D_{11}^0 exists near $x_{\text{BuOH}} = 0.3$. Again, the $D_{11}^0\eta/T$ vs. x curve has a pronounced maximum in the region near $x_{\text{BuOH}} = 0.05$.

Interpretation of Maximum in $D_{11}^0\eta/T$. The most significant fact revealed by the present data is a large positive deviation of $D_{11}^0\eta/T$ value from linearity occurred in the regions where the mole fraction of alcohol is less than 0.2. While the viscosity of solution in this region increases rapidly with the mole fraction of alcohols, the value of D_{11}^0 decreases appreciably. The present data indicate that the decrease in the diffusion coefficient is not so large as that expected from the increase in solution viscosity.

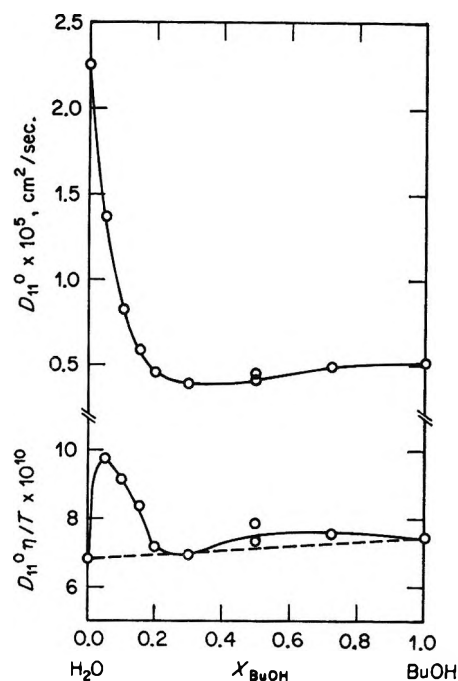


Figure 2. Diffusion coefficients D_{11}^0 of iodine and the product $D_{11}^0\eta/T$ in *t*-butyl alcohol–water solutions at 25.00°.

The diffusion coefficient in aqueous solutions of ethanol have been reported previously for CO₂ by Tang, *et al.*,⁷ and for acetic acid by Perkins, *et al.*⁸ It is found from the analysis of their data that the value of $D_{11}^0\eta/T$ for CO₂ increases rapidly with x_{EtOH} in the region of interest and reaches to a maximum value near $x_{\text{EtOH}} \cong 0.6$, but that the value of $D_{11}^0\eta/T$ for acetic acid takes a maximum near $x \cong 0.15$. These facts, together with our findings, suggest that, for aqueous alcohol solutions, the values of D_{11}^0 are strongly dependent on the structural characteristics of the mixtures used, insofar as the same unit diffusing species is involved.

Thus it can be concluded that the phenomena of having a maximum in $D_{11}^0\eta/T$ will be due to the structural characteristics of aqueous alcohol solutions.^{13,14} This interpretation is supported by the facts that, in the same composition range, these solutions exhibit peculiar anomalies for such properties as the partial molar volume,¹⁵ ultrasonic absorption,²³ gas solubilities,²⁴ etc. Then, our data seem to indicate that the promotion of water structure by alcohol molecule results in an enlargement of open cavities which is favorable for the translational motion of iodine molecule. For *t*-BuOH solutions, this structural promotion is limited to more dilute solutions.¹⁴ Moreover, it is believed¹³ that the *t*-BuOH molecule dissolves rather interstitially into water structure. These facts suggested that, in *t*-BuOH solution, the position of the peak in $D_{11}^0\eta/T$ will shift to lower alcohol fraction and the

(23) M. J. Blandamer, D. E. Clarke, N. J. Hidden, and M. C. R. Symons, *Trans Faraday Soc.*, **64**, 2691 (1968).

(24) A. Ben-Naim and S. Bear, *ibid.*, **60**, 1736 (1964).

height of the peak will decrease in comparison with those in ethanol solution. Although the present data can define the shape and position of the peaks rather poorly, we may conclude that the above predictions are virtually correct.

Although we have ascribed the unusual character of the $D_{11}^0\eta/T$ curve to the diffusivity, it is possible to relate this anomaly to the viscosity data.¹⁴ Our present knowledge of associated alcohol-water solutions is highly speculative and further experimental investigations must be necessary. For example, according to the above interpretation, the peak height in the value of $D_{11}^0\eta/T$ should increase with decreasing temperature. Also, the peak may disappear in aqueous solutions of any organic liquids which do not behave as a structural promoter (*e.g.*, acetone, dioxane, etc.). No such data are available at present.

In addition to the anomaly in the low alcohol concentration range, the value of $D_{11}^0\eta/T$ seems to exhibit another broad peak (or shoulder) at $x_{\text{EtOH}} = 0.5$ for ethanol solution and at $x_{\text{BtOH}} = 0.6$ for *t*-butyl alcohol solution. Although it is hard to explain the existence

of such broad peaks, it should be noted that recent precise measurements²⁵ on the enthalpy of mixing H^M in ethanol-water solutions have defined the presence of anomalous shoulder in the H^M vs. x curve in the alcohol-rich region.

The relationship of D_{11}^0 vs. x in a mixed solvent system may depend to some extent upon the solute chosen as diffusing species. In the cases of nonassociated solutions, Cullinan, *et al.*,⁹ have developed a theoretical approach, in which this dependence is taken into account by a thermodynamic parameter. Although we have only limited information at present, our present view is such that the structural characteristics plays a predominant role in determining the diffusivity in aqueous solutions.

Acknowledgments. The authors thank Professor N. Watanabe for his encouragement and Mr. M. Harima for performing preliminary experiments.

(25) J. A. Boyne and A. G. Williamson, *J. Chem. Eng. Data*, **12**, 318 (1967).

Cross-Phenomenological Coefficients. XIII.

Electroosmotic Transport in Membranes

by R. P. Rastogi, M. L. Srivastava, and Sri Nath Singh

Department of Chemistry, University of Gorakhpur, Gorakhpur (U. P.), India (Received September 2, 1969)

Directional characteristics of electroosmotic transport in Pyrex and quartz membranes have been investigated. No asymmetry in hydrodynamic transport is observed in either membrane. Electroosmotic studies show that Pyrex sinter is isotropic whereas quartz membrane is anisotropic. The nonlinear equation of electroosmotic transport suggested earlier by Rastogi, *et al.*, is found to satisfy the data for flows in both the forward and back directions.

Introduction

Recent experimental studies^{1,2} of the electroosmotic transport in Pyrex and quartz membranes show that the volume flux J is related to thermodynamic forces as follows

$$J = L_{11} \frac{\Delta P}{T} + L_{12} \frac{\Delta \phi}{T} + L_{112} \frac{\Delta P}{T} \cdot \frac{\Delta \phi}{T} + \frac{1}{2} L_{122} \left(\frac{\Delta \phi}{T} \right)^2 + \frac{1}{2} L_{1112} \left(\frac{\Delta P}{T} \right)^2 \left(\frac{\Delta \phi}{T} \right) + \frac{1}{2} L_{1122} \left(\frac{\Delta \phi}{T} \right)^2 \left(\frac{\Delta P}{T} \right) \quad (1)$$

where ΔP and $\Delta \phi$ represent the pressure difference and the potential difference on the two sides of the membranes. T is the temperature and L_{11} , L_{12} , L_{112} , L_{122} , L_{1112} , and L_{1122} are the phenomenological coefficients. Since J and the forces $\Delta P/T$ and $\Delta \phi/T$ are vectors, the appearance of second-order terms in eq 1 seems paradoxical unless the phenomenological coefficients are tensors of different ranks. Such terms can occur

(1) R. P. Rastogi, K. Singh, and M. L. Srivastava, *J. Phys. Chem.*, **73**, 46 (1969).

(2) R. P. Rastogi, K. Singh, and S. N. Singh, *ibid.*, **73**, 1593 (1969).

otherwise if the membrane is anisotropic. Experimental studies yielding information about the tensorial character of the phenomenological coefficients would be highly desirable to clarify the irreversible thermodynamics and transport properties of both isotropic and anisotropic membranes. It may be noted that this aspect has considerable biological interest³ since membrane anisotropy has been invoked for explaining the phenomenon of active transport.⁴⁻⁵ In the present paper the directional characteristics of electroosmotic transport for both Pyrex and quartz membranes have been investigated. The former is found to be isotropic while the latter behaves as an anisotropic membrane.

Experimental Section

(A) *Materials.* Acetone, methanol, and ethyl methyl ketone (AR Grade) were used as permeants. Acetone and methanol were purified as described earlier,^{1,2} whereas ethyl methyl ketone was distilled twice and used without any further purification. The purity of the sample was checked from density measurements. The densities of acetone, methanol, and methyl ethyl ketone at 30° were found to be 0.77882 g/ml, 0.7823 g/ml, and 0.79448 g/ml, respectively (lit.⁷ 0.77931 g/ml, 0.78250 g/ml, and 0.79452 g/ml, respectively).

(B) *Membrane.* Pyrex sinter (porosity G₄) and the quartz plug prepared by using finely powdered quartz (mesh 120) as described earlier² were used. The thickness of the former was 0.3 cm, whereas the latter was 1.10 cm thick. The average pore radii of the capillary channels in the two cases^{1,8} were of the order of 10⁻⁴ cm and 10⁻³ cm, respectively.

(C) *Experimental Procedure.* The electroosmotic flow through membranes was measured as described earlier.⁹ Measurements were repeated by reversing the direction of the flow. Solvodynamic permeability of the two membranes was also measured for both forward and reverse flow.

Streaming current measurements were made with a dc electrometer amplifier (Type 810 A supplied by Trombay Electronic Instrument Co.) which could measure very low current of the order of 10⁻¹² to 10⁻⁶ A. In order to have ΔP of higher magnitude a mercury pressure head as described earlier¹ was used. Streaming potentials in both the cases were measured in a manner described earlier.¹ The measurements were repeated for both forward and reverse directions of flow. The experiments were carried out in an air thermostat maintained at (35 ± 0.1) or (40 ± 0.1)°.

Results

Results are plotted in Figures 1-7. The uncertainty in electroosmotic flow measurements was ± 2% whereas that for streaming current and streaming potential measurements was ± 4% and 5%, respectively.

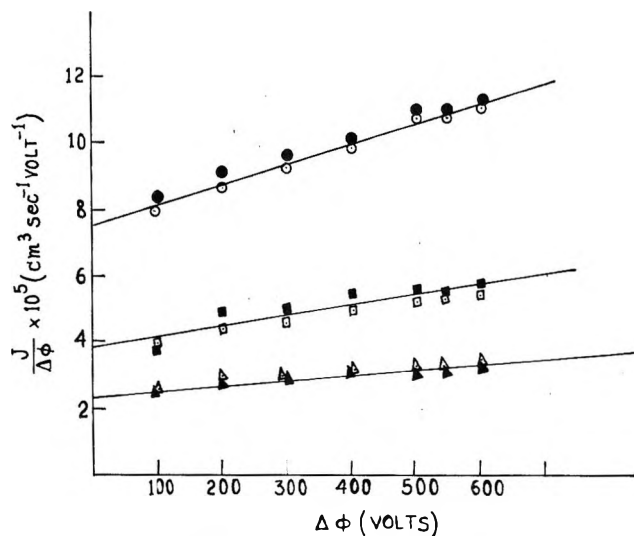


Figure 1. Estimation of L_{12}/T and L_{122}/T^2 : ○, ●, Pyrex-acetone; □, ■, Pyrex-methanol; and △, ▲, Pyrex-ethyl methyl ketone system.

Discussion

The magnitude of solvodynamic flow for both the membranes (Pyrex sinter and quartz plug) has been found to be independent of the direction of flow, and proportional to the pressure difference. This shows that L_{11} is scalar.

The relation between the electroosmotic flow J and the potential difference $\Delta\phi$ is found to be nonlinear for both the membranes. The transport equation

$$\bar{J} = L_{12} \left(\frac{\Delta\phi}{T} \right) + \frac{1}{2} L_{122} \left(\frac{\Delta\phi}{T} \right)^2 \quad (2)$$

satisfies the experimental data. The least-square values of L_{12}/T and L_{122}/T^2 obtained from the intercept and slope of Figures 1 and 2 are recorded in Tables I and II for both types of membranes and for all the three liquids studied. The experimental data were also analyzed by ignoring terms containing even powers of forces and retaining terms up to the fifth power of forces in eq 1 when $\Delta P = 0$, so that

$$J = L_{12} \frac{\Delta\phi}{T} + \frac{1}{6} L_{1222} \left(\frac{\Delta\phi}{T} \right)^3 + \frac{1}{24} L_{122222} \left(\frac{\Delta\phi}{T} \right)^5 \quad (3)$$

or (eq 4)

(3) W. D. Stein, "The Movement of Molecules Across Cell Membranes," Academic Press, New York, N. Y., 1967.

(4) S. I. Rapport, *J. Theor. Biol.*, **19**, 247 (1968).

(5) A. Eissing and S. R. Caplan, *Biophys. J.*, **8**, 1434 (1968).

(6) A. Katchalsky, "Neuro Sciences," G. C. Quarton, T. Melmechuk, and F. O. Schmitt, Ed., The Rockefeller University Press, New York, N. Y., 1967.

(7) Timmermans, "Physico Chemical Constants of Pure Organic Compounds," Elsevier, New York, N. Y., 1950.

(8) R. P. Rastogi, K. Singh, and S. N. Singh, *Ind. J. Chem.*, **6**, 466 (1968).

(9) R. P. Rastogi and K. M. Jha, *Trans. Faraday Soc.*, **62**, 585 (1966).

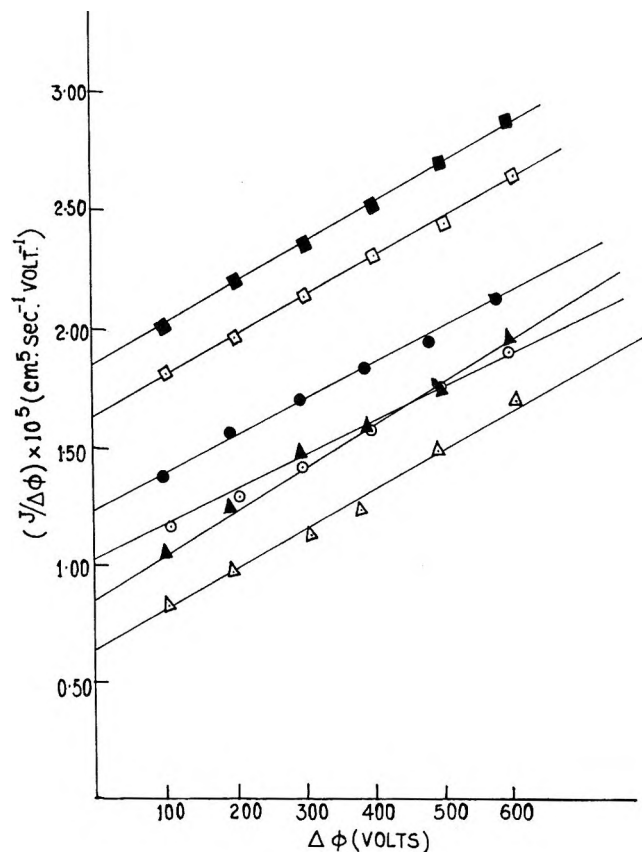


Figure 2. Estimation of L_{12}/T and L_{122}/T_2 : \circ , \bullet , quartz-acetone; \square , \blacksquare , quartz-methanol; and \triangle , \blacktriangle , quartz-ethyl methyl ketone system.

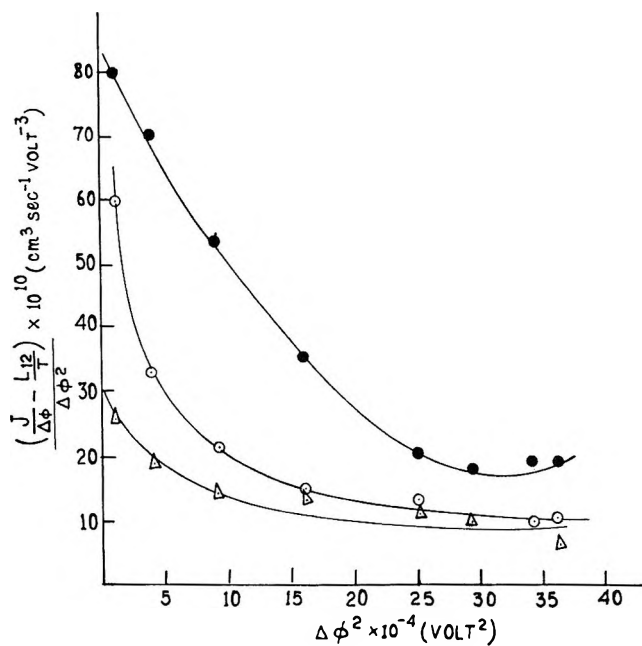


Figure 3. Test of eq 4: \circ , Pyrex-acetone; \bullet , Pyrex-methanol; and \triangle , Pyrex-ethyl methyl ketone system.

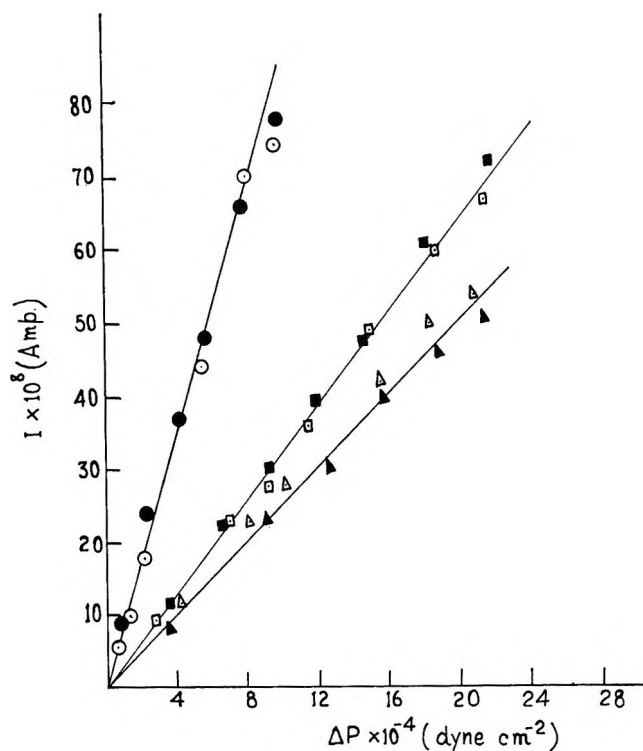


Figure 4. Directional dependence of streaming current, I , on applied pressure difference ΔP : \circ , \bullet , Pyrex-acetone; \square , \blacksquare , Pyrex-methanol; and \triangle , \blacktriangle , Pyrex-ethyl methyl ketone.

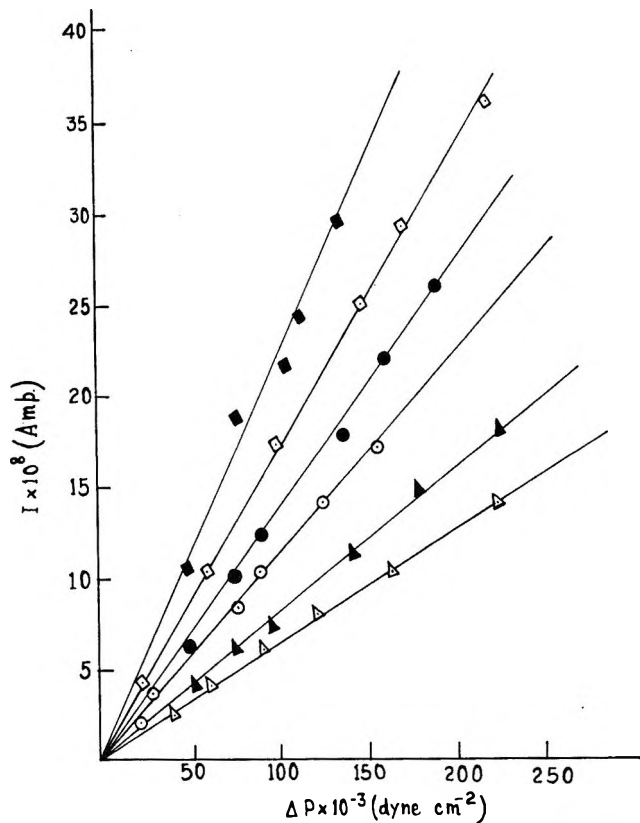


Figure 5. Directional dependence of streaming current, I , on applied pressure difference, ΔP : \circ , \bullet , quartz-acetone; \square , \blacksquare , quartz-methanol; and \triangle , \blacktriangle , quartz-ethyl methyl ketone.

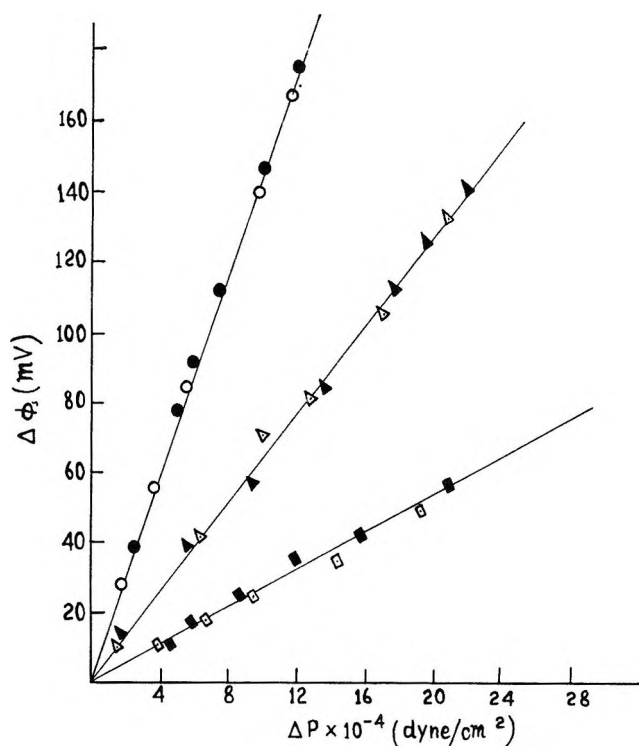


Figure 6. Directional dependence of streaming potential on pressure difference: \circ \bullet , Pyrex-acetone; \square \blacksquare , Pyrex-methanol and \triangle \blacktriangle , Pyrex-ethyl methyl ketone.

$$\left(\frac{J}{\Delta\phi} - \frac{L_{12}}{T} \right) / \Delta\phi^2 = \frac{1}{6} \frac{L_{1222}}{T^3} + \frac{1}{24} \frac{L_{122222}}{T^5} \Delta\phi^2 \quad (4)$$

It follows that a plot of $(J/\Delta\phi - L_{12}/T)/\Delta\phi^2$ against $\Delta\phi^2$ would give a straight line, if the above equation satisfies the data. Such a plot (Figure 3) does not yield a straight line showing that eq 4 does not satisfy the data. This further confirms that inclusion of terms containing even powers of forces is necessary to satisfy the data.

Table I (results for Pyrex sinter) shows that L_{12}/T and L_{122}/T^2 for both the directions of flow are the same within the limit of experimental error. However, for quartz plugs, Table II indicates that L_{12}/T differs appreciably on reversal of the direction of flow and the deviation is much beyond the limit of experimental error. This leads to the conclusion that Pyrex sinter is isotropic whereas the quartz membrane is anisotropic. L_{12} would be a tensor of zero rank. From Tables I and II it is also apparent that L_{122}/T^2 remains unaltered within experimental error, even on reversing the direction of the flow. Since J is a vector and the even powers of forces would be scalar, L_{122} is a second-rank tensor.

The thermodynamic consistency of the data was checked by streaming current and streaming potential measurements which are plotted in Figures 4–7 for both types of the membranes. These show that the streaming current, I , and streaming potential, $\Delta\phi_s$,

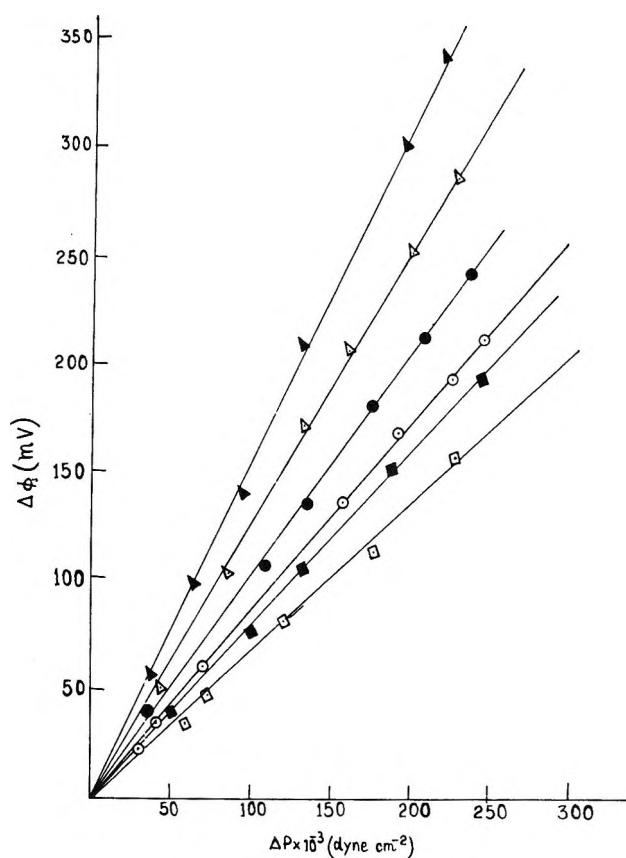


Figure 7. Directional dependence of streaming potential, $\Delta\phi$, on pressure difference ΔP : \circ \bullet , quartz-acetone; \square \blacksquare , quartz-methanol and \triangle \blacktriangle , quartz-ethyl methyl ketone.

vary linearly with pressure difference, ΔP , thus

$$\vec{I} = L_{21} \left(\frac{\vec{\Delta P}}{T} \right) \quad (5)$$

where L_{21} is the cross-phenomenological coefficient. Nonlinearity is not observed up to ΔP equal to 17 cm. The least-square values of L_{21}/T and (L_{21}/L_{22}) are recorded in Tables I and II for both the membranes and for all the three liquids studied. The results recorded in Tables I and II show that L_{21} has directional dependence similar to L_{12} for both the membranes.

An examination of Tables I and II reveals that Onsager's reciprocal relation is verified for all three liquids and for both the forward and reverse directions of flow in the case of both membranes, so that $L_{12} = L_{21}$.

Summarizing, we have the following relationship between the phenomenological coefficients in the two directions for the two membranes. (The arrow indicates the direction of the flow in Table III.)

The membranes will have a three dimensional network of capillaries and the volume flow J or current I normal to a particular plane would be made up of relative contributions along any three axes, which in turn would depend on $\partial X_i/\partial x$, $\partial X_i/\partial y$, and $\partial X_i/\partial z$ also, where X_i is any thermodynamic force. Thus for the relationship, $J = LX$, we should write

Table I: Phenomenological Coefficients for Isotropic Membrane (Pyrex)

Liquid	Membrane	Direction of flow →				← Direction of flow			
		(L_{11}/T) $\times 10^5$, $\text{cm}^3 \text{sec}^{-1}$ V^{-1}	(L_{21}/T) $\times 10^5$, $\text{cm}^3 \text{sec}^{-1}$ V^{-1}	(L_{12}/T^2) $\times 10^8$, $\text{cm}^3 \text{sec}^{-1}$ V^{-2}	(L_{21}/L_{22}) $\times 10^7$, $\text{cm}^3 \text{sec}^{-1}$ ohm^{-1}	(L_{11}/T) $\times 10^5$, $\text{cm}^3 \text{sec}^{-1}$ V^{-1}	(L_{21}/T) $\times 10^5$, $\text{cm}^3 \text{sec}^{-1}$ V^{-1}	(L_{12}/T^2) $\times 10^8$, $\text{cm}^3 \text{sec}^{-1}$ V^{-2}	(L_{21}/L_{22}) $\times 10^7$, $\text{cm}^3 \text{sec}^{-1}$ ohm^{-1}
Acetone	I	9.5	9.0	6.6	...	9.0	9.1	5.5	...
	II	9.4	9.1	5.7	...	8.9	8.8	5.4	...
	III	7.7	7.6	6.3	15.4	7.4	8.2	6.2	14.6
Methanol	IV	3.8	4.0	2.7	...	4.1	4.2	2.7	...
	V	4.0	3.4	2.7	2.4	3.8	3.3	3.0	2.5
	VI	5.3	5.2	3.9	...	5.1	5.5	4.3	...
Ethyl methyl ketone	VII	2.4	2.4	1.3	6.2	2.4	2.6	1.4	6.4
	VIII	2.6	2.8	1.4	8.4	2.6	2.6	1.4	8.1

^a The temperature is $(35 \pm 0.1)^\circ$.

Table II: Phenomenological Coefficients for Anisotropic Membrane (Quartz)

Liquid	Membrane	Direction of flow →				← Direction of flow			
		(L_{11}/T) $\times 10^5$, $\text{cm}^3 \text{sec}^{-1}$ V^{-1}	(L_{21}/T) $\times 10^5$, $\text{cm}^3 \text{sec}^{-1}$ V^{-1}	(L_{12}/T^2) $\times 10^8$, $\text{cm}^3 \text{sec}^{-1}$ V^{-2}	(L_{21}/L_{22}) $\times 10^7$, $\text{cm}^3 \text{sec}^{-1}$ ohm^{-1}	(L_{11}/T) $\times 10^5$, $\text{cm}^3 \text{sec}^{-1}$ V^{-1}	(L_{21}/T) $\times 10^5$, $\text{cm}^3 \text{sec}^{-1}$ V^{-1}	(L_{12}/T^2) $\times 10^8$, $\text{cm}^3 \text{sec}^{-1}$ V^{-2}	(L_{21}/L_{22}) $\times 10^7$, $\text{cm}^3 \text{sec}^{-1}$ ohm^{-1}
Ethyl methyl Ketone	I	0.61	0.64	1.83	1.30	0.79	0.83	1.81	1.49
	II	0.72	0.68	0.76	0.80
	III	0.74	0.70	0.82	0.84
Acetone	IV	0.64	0.61	0.70	0.72
	V	1.06	1.12	...	0.91	1.36	1.42	...	1.06
	VI	1.04	1.08	2.90	...	1.28	1.34	2.87	...
Methanol	VII	1.05	1.10	1.32	1.38
	VIII	1.63	1.70	1.77	0.70	1.84	1.96	1.80	0.83
	IX	1.66	1.72	1.87	1.92
	X	1.66	1.68	1.86	1.94

^a The temperature is $(40 \pm 0.1)^\circ$.

$$J_x = \left[k_{11} \frac{\partial X}{\partial x} + k_{12} \frac{\partial X}{\partial y} + k_{13} \frac{\partial X}{\partial z} \right]$$

$$J_y = \left[k_{21} \frac{\partial X}{\partial x} + k_{22} \frac{\partial X}{\partial y} + k_{23} \frac{\partial X}{\partial z} \right]$$

$$J_z = \left[k_{31} \frac{\partial X}{\partial x} + k_{32} \frac{\partial X}{\partial y} + k_{33} \frac{\partial X}{\partial z} \right]$$

Obviously, L would be tensor. L_{11} , L_{12} , and L_{21} , and L_{22} would be tensors of zero rank. The tensor corresponding to L_{12} and L_{21} on reversal of direction may or may

not be equal in magnitude whereas L_{11} has the same value in both the directions. The difference in character essentially arises on account of difference in the hydrodynamic flow and electroosmotic flow as indicated below

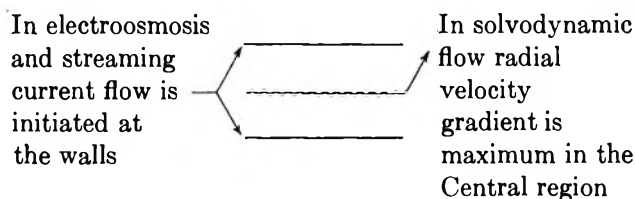


Table III: Directional Dependence of Phenomenological Coefficients

Pyrex sinter	Quartz plug
$\overrightarrow{L_{11}} = \overleftarrow{L_{11}}$	$\overrightarrow{L_{11}} = \overleftarrow{L_{11}}$
$\overrightarrow{L_{12}} = \overleftarrow{L_{12}}$	$\overrightarrow{L_{12}} \neq \overleftarrow{L_{12}}$
$\overrightarrow{L_{21}} = \overleftarrow{L_{21}}$	$\overrightarrow{L_{21}} \neq \overleftarrow{L_{21}}$
$\overrightarrow{L_{122}} = \overleftarrow{L_{122}}$	$\overrightarrow{L_{122}} = \overleftarrow{L_{122}}$
$(\overrightarrow{L_{21}/L_{22}}) = (\overleftarrow{L_{21}/L_{22}})$	$(\overrightarrow{L_{21}/L_{21}}) \neq (\overleftarrow{L_{21}/L_{22}})$

It is obvious that surface characteristics at the capillary entrance and exit would affect the electroosmotic flow rather than the solvodynamic flow.

From classical theory of electroosmosis and streaming current we know that

$$L_{12} = L_{21} = \frac{Dr^2\zeta}{4\eta l} \quad (6)$$

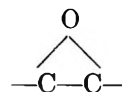
where D is the dielectric constant, ζ is the ζ potential, η

is the viscosity, and l is the length of the pore. Since D and ζ have tensorial character, it follows that L_{12} and L_{21} can have tensorial character.

It is difficult to understand how L_{122} is a vector. However, this could be possible if L_{122} is a function of the gradient of ζ potential or the dielectric constant which are actually much different at the interface as compared to the values for the bulk liquid. This point could be further clarified if a more realistic theory of electrical double layer were available.

The asymmetry in the behavior of electroosmosis and streaming current for quartz plug probably arises on account of difference in molecular character of the surface particularly at the capillary entrance on the two sides of the membrane. Quartz, a polymeric form of SiO_2 , is known to have a three-dimensional network in which every oxygen atom is common to two tetrahedral (SiO_4) groups. The structure is largely based on formation of large anions arranged about small cations. Regular arrangement is distorted to some extent so that spirals of $-\text{O}-\text{Si}-\text{O}-\text{Si}-$ chain lie around trigonal screw axis of symmetry. Such a structure cannot lead to asymmetry. It should be noted that Araldite was used for fixing the quartz membrane. The asymmetry of the membrane might be due to nonuniform coating of Araldite on quartz particles. This would make the

membrane inhomogeneous and asymmetric. Araldite contains epoxy resin¹⁰ having the group



There would be negative charge on the oxygen atom and thus the character of the surface would be similar to quartz although potential may not be the same at all the points in the quartz membrane.

On the other hand, the isotropic character of Pyrex sinter is not unexpected, particularly in view of the absence of symmetry in the atomic network¹¹ which will be statistically the same in all the directions. However, the random network theory has been questioned by later workers who believe that Pyrex glasses are inhomogeneous systems comprising both ordered (crystallite) and disordered (vitreous) zones. Since the Pyrex sinter is isotropic, the coefficients of first- and third-order terms would be tensors of zero rank whereas coefficients of second-order terms would be tensors of second rank in accordance with Curie's principle.

Acknowledgment. Help rendered by Dr. R. D. Shukla in streaming potential measurements is gratefully acknowledged. This work forms part of the CSIR sponsored research program.

(10) B. Golding, "Polymers and Resins," Van Nostrand-Reinhold, Princeton, N. J., p 355.

(11) W. H. Zachariasen, *J. Chem. Phys.*, **3**, 162 (1935).

On the Ratio of Osmotic to Tracer Permeability in a Homogeneous Liquid Membrane

by I. Robert Fenichel and Samuel B. Horowitz

Laboratory of Cellular Biophysics, Albert Einstein Medical Center, Philadelphia, Pennsylvania 19141
(Received December 3, 1969)

An analysis is made of the osmotic and tracer water permeabilities of a membrane consisting of a homogeneous liquid, which is free of pores and in which osmotic flow is a random walk diffusional process. The permeability ratio P_f/P_d is found not to reduce to unity but to be given by a more complicated expression, which diffusional theory indicates may considerably exceed unity. The limited data available for liquid systems support the expectation. The use of $P_f > P_d$ as a criterion for the presence of aqueous pores in a biological membrane, in the absence of detailed structural knowledge, is therefore not warranted. The property shown by an "unstirred layer," of affecting osmotic net flow less than tracer flow, is shown to be a special case of this general behavior of liquid systems.

Measurement of the ratio of the osmotic permeability coefficient, P_f , to the tracer water permeability coefficient, P_d , has been an important method of inferring structural information about cellular membranes and artificial thin lipid membranes.¹⁻⁷ If the ratio P_f/P_d exceeds unity, and if this is not due to the presence of unstirred layers,^{6,8} it is generally inferred that the membrane contains aqueous pores through which laminar flow of water may occur; conversely, if P_f/P_d is unity, it is inferred that aqueous pores are absent.

This method of attempting to infer structural characteristics of a membrane requires that P_f/P_d cannot exceed unity in a homogeneous liquid membrane which is devoid of pores and in which osmotic flow occurs by a random walk process, water molecules dissolving in and diffusing through the membrane. We propose to show that this requirement is not fulfilled. A liquid membrane will in general have a P_f/P_d ratio greater than unity, and this ratio may be quite large. Therefore, the observation that $P_f > P_d$ in a given membrane, in the absence of detailed knowledge of its composition and structure, does not permit the inference that aqueous pores are present. The present treatment, however, does provide equations whereby one may test, using bulk liquid systems, the applicability of a liquid model to thin membranes in which $P_f > P_d$.

Theory

We consider a liquid membrane consisting of a single phase composed of a nonelectrolytic membrane component and water. One side is bathed by water and the other by a dilute aqueous solution of an impermeant solute at concentration c_s' . The membrane component is not dispersible in the bathing media under the conditions of the experiment. We take the chemical potential of water to be continuous across each membrane-solution interface. Designating the values within

the membrane at the interfaces as $\mu_1(0)$ and $\mu_1(h)$, and in the corresponding solutions as μ_1^0 and μ_1' , we have $\mu_1(0) = \mu_1^0$ and $\mu_1(h) = \mu_1'$. We assume the unstirred layer to be of negligible importance, so that μ_1' has the value of the bulk solution: $\mu_1' = \mu_1^0 - gRT\bar{V}_1^0 c_s'$, where \bar{V}_1^0 is the partial molar volume of water and g is the osmotic coefficient of the solute.

We then have $\Delta\mu_1 \equiv \mu_1(h) - \mu_1(0) = -gRT\bar{V}_1^0 c_s'$. In a binary liquid mixture at constant temperature and pressure, the relative composition is determined by the chemical potential of one component. Since there is a gradient of chemical potential of water across the membrane, there will also be a gradient of water concentration, c_1 , and correspondingly a gradient of concentration of membrane material, c_2 . These gradients are defined by the relations

$$dc_1 = \left(\frac{\partial c_1}{\partial \mu_1}\right)_{T,P} d\mu_1 \quad (1)$$

$$\bar{V}_1 dc_1 + \bar{V}_2 dc_2 = 0 \quad (2)$$

$$c_1 d\mu_1 + c_2 d\mu_2 = 0 \quad (3)$$

The osmotic diffusion of water across the membrane then consists of the steady-state mutual diffusion of water and membrane material in a binary concentra-

(1) V. Koefoed-Johnsen and H. H. Ussing, *Acta Physiol. Scand.*, **28**, 60 (1953).

(2) D. M. Prescott and E. Zeuthen, *ibid.*, **28**, 77 (1953).

(3) C. V. Paganelli and A. K. Solomon, *J. Gen. Physiol.*, **41**, 259 (1957).

(4) T. Hanai, D. A. Haydon, and J. Taylor, *ibid.*, **48**, 59 (1965).

(5) C. Huang and T. E. Thompson, *J. Mol. Biol.*, **15**, 539 (1966).

(6) A. Cass and A. Finkelstein, *J. Gen. Physiol.*, **50**, 1765 (1967).

(7) T. E. Andreoli, V. W. Dennis, and A. M. Weigl, *ibid.*, **53**, 133 (1969).

(8) J. Dainty, *Advan. Botan. Res.*, **1**, 279 (1963).

tion gradient. Fick's law gives for the flux of water, j_1^* , relative to a volume-fixed coordinate system⁹

$$j_1^* = -D_{12} \frac{dc_1}{dy} \quad (4)$$

where D_{12} is the mutual diffusion coefficient and y the diffusion coordinate. However, the flux is normally measured relative to the membrane, and when there is a net flux of water across the membrane, as in osmotic flow, the membrane does not constitute a volume-fixed framework. The flux of water relative to the membrane, j_1 , is given by⁹

$$j_1 = -\frac{D_{12} dc_1}{\phi_2 dy} \quad (5)$$

where ϕ_2 is the volume fraction of membrane material and is equal to $c_2 \bar{V}_2$.

In the steady state, j_1 is constant through the membrane. For a small osmotic gradient, D_{12} , \bar{V}_1 , and \bar{V}_2 will be sensibly constant, and eq 5 can be integrated simply. Using eq 2, we get

$$j_1 = \frac{D_{12}}{\bar{V}_1 h} \ln \left[1 + \frac{\Delta\phi_2}{\phi_2(0)} \right] \quad (6)$$

where $\Delta\phi_2 \equiv \phi_2(h) - \phi_2(0)$. We take the gradient to be small enough so that $\Delta\phi_2 \ll \phi_2(0)$; we may then linearize eq 6 and drop the positional notation from $\phi_2(0)$. Using also $\Delta\phi_2 = -\Delta\phi_1 = -\bar{V}_1 \Delta c_1$, we get

$$j_1 = -\frac{D_{12}}{\phi_2 h} \Delta c_1 \quad (7)$$

Integrating eq 1, we get

$$\Delta c_1 = \left(\frac{\partial c_1}{\partial \mu_1} \right) \Delta \mu_1 \equiv B_{11} \Delta \mu_1 \quad (8)$$

$\partial c_1 / \partial \mu_1$ also being sensibly constant in the range of μ_1 . Finally, using $\Delta \mu_1 = -gRT \bar{V}_1^0 c_s'$, we obtain

$$j_1 = \frac{gRT D_{12} B_{11} \bar{V}_1^0}{\phi_2 h} c_s' \equiv P_t g c_s' \quad (9)$$

where, as in ref 6, P_t is defined so as to exclude g .

The steady-state flux of tracer water in the absence of net flow, with tracer introduced at concentration c_1^* on one side, is given by

$$j_1^* = -\frac{D_1^* K}{h} c_1^* = -\frac{D_1^* c_1 \bar{V}_1^0}{h} c_1^* \equiv -P_d c_1^* \quad (10)$$

where D_1^* is the tracer diffusion coefficient of water in the membrane and K is the concentration distribution coefficient of water between membrane and solution. The ratio P_t/P_d is given by

$$\frac{P_t}{P_d} = \frac{RT D_{12} B_{11}}{\phi_2 D_1^* c_1} = \frac{RT D_{12}}{\phi_2 D_1^*} \left(\frac{\partial \ln c_1}{\partial \mu_1} \right)_{T,P} \quad (11)$$

where we have again used the condition of a small osmotic gradient to set $B_{11} = c_1 (\partial \ln c_1 / \partial \mu_1)$.

Using the mole fractions of water and membrane material, x_1 and x_2 , and the mole fraction activity coefficient of water, γ_1 , eq 11 can be rewritten

$$\frac{P_t}{P_d} = \frac{D_{12}}{x_2 D_1^*} \left[1 + \frac{\partial \ln \gamma_1}{\partial \ln x_1} \right]^{-1} \equiv \frac{D_{12} A_{11}}{x_2 D_1^*} \quad (12)$$

Discussion

The right-hand side of eq 12 will in general differ from unity. The expectation that $P_t > P_d$ is indicated more explicitly by Bearman's¹⁰ frictional analysis of liquid diffusion. Using his expressions for the diffusion coefficients in terms of frictional coefficients, one obtains the frictional equivalent of eq 12

$$\frac{P_t}{P_d} = 1 + \frac{x_1 \zeta_{11}}{x_2 \zeta_{12}} \quad (13)$$

where ζ_{11} and ζ_{12} are, respectively, water-water and water-membrane material frictional coefficients, and both are expected to be positive.

For membranes having mole fractions of water approaching unity, we have $D_{12}/D_1^* \rightarrow D_2^*/D_1^*$ where D_2^* is the tracer diffusion coefficient of the membrane material;¹⁰ also $A_{11} \rightarrow 1$. Then

$$\frac{P_t}{P_d} = \frac{D_2^*}{x_2 D_1^*} \quad (14)$$

and P_t/P_d increases without limit as the membrane approaches pure water, subject to the condition of derivation that the osmotic gradient remains small compared to ϕ_2 .

For $x_1 = 0$, eq 13 indicates that P_t and P_d will be equal; but they will also both be zero. For membranes of low but nonvanishing water content, one would expect that the limiting ratio of unity would be approached; but how rapidly this occurs cannot be predicted because the relationship between D_{12} , D_1^* , x_2 , and A_{11} cannot be accurately obtained from theory. Bearman¹⁰ has obtained a relationship for a class of liquid mixtures which he designates as "regular," although they may not correspond exactly to those with ideal entropies of mixing.¹¹ For these, the tracer diffusion coefficients are related by

$$\frac{D_1^*}{D_2^*} = \frac{\bar{V}_2}{\bar{V}_1} \quad (15)$$

An additional characteristic is that $D_1^* \eta$ is independent of composition, η being the mixture viscosity. Bearman obtains

$$D_{12} = (x_2 D_1^* + x_1 D_2^*) \left(1 + \frac{\partial \ln \gamma_1}{\partial \ln x_1} \right) \quad (16)$$

(9) J. Crank, "The Mathematics of Diffusion," Clarendon Press, Oxford, 1956, pp 220, 224.

(10) R. J. Bearman, *J. Phys. Chem.*, **65**, 1961 (1961).

(11) J. H. Hildebrand and R. L. Scott, "The Solubility of Nonelectrolytes," Reinhold, New York, N. Y., 1950, p 46.

which gives, using eq 15

$$\frac{P_t}{P_d} = 1 + \frac{x_1 D_2^*}{x_2 D_1^*} = \frac{1}{\phi_2} \quad (17)$$

In practice, however, neither eq 15 nor eq 16 provides an adequate representation of diffusional data,¹²⁻¹⁴ even in some cases where the mixture obeys Raoult's law throughout,¹⁵ and it is necessary to make specific measurements of a given system in order to estimate P_t/P_d .

The only system which has been studied completely, both as a liquid membrane and in bulk, is the tributyl phosphate (TBP)-water system.¹⁶⁻¹⁸ At saturation $x_2 = 0.488$,¹⁷ the density of the phase is 0.976 g/ml, and taking $\bar{V}_1 = 18 \text{ cm}^3/\text{mol}$, we obtain $\phi_2 = 0.934$. From Figure 4 of ref 18 we obtain $A_{11} = 1.33$ at saturation. Michaeli and Kedem¹⁸ give $D_{12} = 3.2 \times 10^{-6}$ and $D_1^* = 4.5 \times 10^{-6} \text{ cm}^2/\text{sec}$, and inserting these values in eq 12 we obtain $P_t/P_d = 1.9$. The value of P_t/P_d obtained directly from permeability measurements on the saturated TBP membrane is 1.8,¹⁶ in good agreement with the calculated value. Were the system behaving as a regular solution, a value of 1.1 would be expected from eq 17.

The available data on liquid diffusion indicate that even greater deviations from regularity may be expected in other systems. For an equimolar acetone-water mixture at 25°, for example, we have¹³ $D_{12} = 0.85 \times 10^{-5}$, $D_1^* = 2.2 \times 10^{-5} \text{ cm}^2/\text{sec}$, and $A_{11} = 7.1$, giving $P_t/P_d = 5.5$; this corresponds to an equivalent pore radius of 8 Å.¹⁹ In this case, ϕ_2 is about 0.8, so that eq 17 would give $P_t/P_d = 1.25$. Although the acetone-water system is fully miscible and therefore not readily studied as a liquid membrane, one would anticipate that the homologous, partially miscible system diethyl ketone-water would also have a large permeability ratio.

The Unstirred Layer. In the above-mentioned systems, P_t/P_d exceeds unity primarily because of non-regularity rather than the reference-frame correction. A striking example of the latter is provided by the behavior of unstirred layers. Dainty⁸ recognized that an unstirred layer in series with a membrane would be less of a barrier to osmotic flow of water than to tracer movement, and this difference has been experimentally substantiated.⁶ Two factors are generally considered to play a role in this effect: convective stirring within the layer due to concentration gradients, which reduces the effective unstirred thickness; and an inherently more rapid flux during osmotic flow. Although Dainty provided equations to calculate the latter effect, its mechanism has never been made clear. We can see now that the effect derives from the reference-frame correction embodied in eq 5, which is required when diffusion is measured relative to stationary solute rather than to a volume-fixed framework. When the membrane is impermeable to the solute in the unstirred

layer, the solute is stationary relative to the membrane; the net flux of water in an osmotic experiment is measured relative to stationary solute, and must therefore, within the unstirred layer, be described by eq 5 rather than eq 4, ϕ_2 here being the volume fraction of solute. The unstirred layer constitutes, in fact, a liquid "membrane" in series with the experimental membrane, and its osmotic and tracer permeabilities are given by the expressions in eq 9 and 10. It is readily shown that the apparent osmotic permeability, P_t' , is related to the membrane and unstirred layer permeabilities P_t^m and P_t^u by the relation

$$\frac{1}{P_t'} = \frac{1}{P_t^m} + \frac{1}{P_t^u} \quad (18)$$

exactly in parallel to the relation among the tracer permeabilities (8). The value of P_t/P_d for the unstirred layer is given by eq 12: for a 0.3 M sucrose layer, $D_{12}/D_1^* \approx 0.2$,¹² $x_2 \approx 0.0057$, $A_{11} \approx 1$,²⁰ and therefore $P_t/P_d \approx 35$. This would appear to account amply for the unstirred layer effect; convective stirring may of course occur also, further increasing the apparent effect. (It can be seen that the present analysis is not applicable if the membrane is permeable to the solute, since the water flux in the unstirred layer is no longer being measured relative to stationary solute. As might be expected and as we will show elsewhere, the unstirred layer becomes an increasingly important barrier as the solute permeability increases; this can have a significant effect on the measurement of reflection coefficients and the estimation of equivalent pore radii.)

Thin Lipid Membranes and Cellular Membranes. Cass and Finkelstein⁶ have made a careful measurement of P_t/P_d in a thin lipid membrane system. They found the ratio to be unity, and inferred that no aqueous pores are present in the membrane. As we have mentioned above, the observation that $P_t/P_d = 1$ signified more than simply the absence of pores; we have also $x_2 \approx 1$ and $\partial \ln \gamma_1 / \partial \ln x_1 \approx 0$. Consistent with this are the observations by Hanai and Haydon²¹ and Finkelstein and Cass²² that P_d can be estimated

- (12) R. R. Irani and A. W. Adamson, *J. Phys. Chem.*, **64**, 199 (1960).
- (13) D. W. McCall and D. C. Douglass, *ibid.*, **71**, 987 (1967).
- (14) T. Loflin and E. McLaughlin, *ibid.*, **73**, 186 (1969).
- (15) C. H. Byers and C. J. King, *ibid.*, **70**, 2499 (1966).
- (16) G. Thau, R. Block, and O. Kedem, *Desalination*, **1**, 129 (1966).
- (17) C. J. Hardy, D. Fairhurst, H. A. C. McKay, and A. M. Willson, *Trans. Faraday Soc.*, **60**, 1626 (1964).
- (18) G. Michaeli and O. Kedem, "Water Transport in Hyperfiltration Membranes," Office of Saline Water, U. S. Department of the Interior, Report No. 401, 1968, p 35.
- (19) O. Kedem and A. Katchalsky, *J. Gen. Physiol.*, **45**, 143 (1961).
- (20) G. Scatchard, W. J. Hamer, and S. E. Wood, *J. Amer. Chem. Soc.*, **60**, 3061 (1938).
- (21) T. Hanai and D. A. Haydon, *J. Theoret. Biol.*, **11**, 370 (1966).
- (22) A. Finkelstein and A. Cass, *J. Gen. Physiol.*, **52**, 1455 (1968).

reasonably well from the solubility and diffusion of water in liquid hydrocarbons,^{23,24} for which $x_1 \approx 10^{-3}$. (Schatzberg²⁴ actually calculated a diffusion coefficient from a measurement of P_f rather than P_d , so that the appropriate comparison should be with P_f of the thin membrane; in this case, the distinction is trivial.)

By the same token, however, the present analysis shows that P_f/P_d is not a necessary condition for the absence of pores: thus, while Cass and Finkelstein⁶ may be correct in surmising that P_f/P_d exceeded unity in other studies of unmodified membranes^{4,5} only because of unstirred layers, the decision as to whether any of these is not behaving like a liquid does not, at this point, rest with the value of P_f/P_d . In this connection, it is interesting to note that Cass and Finkelstein, in their 1967 paper,⁶ added the proviso that the activity coefficient of water be constant throughout the membrane to the assertion that P_f/P_d is unity in a liquid membrane; interpreted in the present context that γ_1 is independent of composition, it can be seen that the proviso makes the original assertion more nearly correct.

With the possible exception of some membranes studied by Huang and Thompson,⁵ none of the unmodified membranes appear likely to have P_f/P_d ratios large enough that the presence of aqueous pores becomes a serious question. In the case of membranes modified by polyene antibiotics,^{7,22} however, the question is quite important. While reliable measurements of P_f/P_d in modified membranes have not been obtained, their sieving behavior^{7,22} suggests that the ratio may significantly exceed unity. The present

analysis indicates that a decision as to whether these membranes contain structural pores or remain liquid may be profitably pursued by studying, using eq 12, the thermodynamic and diffusional behavior of bulk systems of the type of a hexadecane-cholesterol-antibiotic mixture. As with the unmodified membrane,^{21,22} one would anticipate reproducing the behavior of P_f and P_d using a bulk liquid system only if a liquid model of the modified membrane is correct. Even if an accurate measurement of P_f/P_d in modified membranes is unattainable, there are sufficient additional points of comparison—such as sieving and its power dependence⁷—to establish with considerable certainty whether a liquid state model of the antibiotic effect is appropriate.

Much the same difficulty in measuring P_f/P_d occurs with cellular membranes. The careful study by Sha'afi, *et al.*,²⁵ seems to have established a ratio of 2.4 for human red cells. We need only point out here that their assumption, following the work of Thau, *et al.*,¹⁶ that 2.1 represents the upper limit for liquid membranes need not be correct.

Acknowledgment. This work was supported in part by grants from the U. S. Public Health Service (GM-14886) and the National Science Foundation (GB-8032).

(23) P. Schatzberg, *J. Phys. Chem.*, **67**, 776 (1963).

(24) P. Schatzberg, *J. Polymer Sci.*, **10**, 87 (1965).

(25) R. I. Sha'afi, G. T. Rich, V. W. Sidel, W. Bossert, and A. K. Solomon, *J. Gen. Physiol.*, **50**, 1377 (1967).

Gas Chromatographic Determination of Partition Coefficients of Some Unsaturated Hydrocarbons and Their Deuterated Isomers in Aqueous Silver Nitrate Solutions

by S. P. Wasik and W. Tsang

National Bureau of Standards, Washington, D. C. 20234 (Received January 26, 1970)

Experiments using aqueous solutions of silver nitrate as a gas chromatographic liquid phase have been carried out. Stability constants for the reaction, $(\text{Ag}^+)_{\text{aq}} + (\text{Hydrocarbon})_{\text{aq}} \rightleftharpoons (\text{Ag}^+\cdot\text{Hydrocarbon})_{\text{aq}}$, where $(\text{Hydrocarbon})_{\text{aq}}$ are various light olefins, aromatics, or some of their deuterated isomers have been determined. For the olefins these values are in quantitative agreement with those obtained from conventional static techniques. In the case of ethylene $\Delta H = -23$ kJ/mol and $\Delta S = -38$ J/mol deg. The isotope effect for the solubility of benzene- d_6 (compared to the lightest isomer) in water is 1.05. Aqueous silver nitrate columns should also have interesting analytical applications, particularly in the field of isotopic separations. They appear to be more efficient than the conventional ethylene glycol-silver nitrate columns.

Introduction

This investigation is concerned with the gas chromatographic properties of aqueous silver nitrate solutions. The greater degree of ionization of silver nitrate in water makes such columns more efficient than the more standard solvent phase of silver nitrate in ethylene glycol. Thus the many unique separations¹⁻⁴ effected with the latter solvent can be carried out under less severe (near room temperature, 6-12-ft columns) conditions. Furthermore, the gas chromatographic results can now be directly compared with those from static experiments. This provides a test of the reliability of this method as a means of studying reactions in aqueous solutions. Finally, with respect to the silver complexing reaction, thermal and isotope effects can be measured. For such determinations the gas chromatographic method has unique advantages due to the ease of carrying out such experiments at varying temperatures and the handling of small and/or impure samples. It is noteworthy that enthalpies and entropies as well as the extent of the deuterium isotope effect for such processes have not been determined using standard procedures.

Silver nitrate in inert organic solvents has long been used as a substrate in gas chromatography.¹ Due to the formation of silver-olefin complexes such columns are of special interest in olefin analysis. Muhs and Weiss² and Cvetanovic and coworkers^{3a,b} have made exhaustive chromatographic investigations of the silver nitrate-ethylene glycol system. The former authors derived stability constants for a large number of compounds, while the latter determined the enthalpies and entropies of the complex-forming reaction for several of the smaller olefins. They also found an isotope effect for the corresponding deuterated compounds and were

able to make satisfactory separations of the various isotopic isomers from each other.

There is a large volume of stability constant data for silver-olefin complexes in aqueous solution as determined by classical methods.⁵ Direct comparison with the earlier gas chromatographic experiments, however, cannot be made since silver nitrate in a medium such as ethylene glycol behaves as a weak salt and is not completely ionized.

Volatile substrates are, in general, unsuitable for gas chromatography since they may affect the sensitivity of the detector and make uncertain the amount of liquid loading. The former is not a problem in this study since a hydrogen flame detector was used and it is completely insensitive to the presence of water. The latter can be minimized by presaturating the helium carrier gas. The ideal situation is of course to have exactly the same amount of water coming in as leaving. This is not easily achieved with the usual techniques. Nevertheless, even with a variation of 5% in inlet and outlet water vapor concentration, at room temperature and usual flow rates (23° and 50 cm³/min) the total change of liquid loading will be less than 0.004 g/hr. Thus with a liquid loading of 5-15 g one can anticipate at steady state at least several weeks of steady opera-

(1) B. W. Bradford, D. Harvey, and D. E. Chalkley, *J. Inst. Petrol.*, London, **41**, 80 (1955).

(2) M. A. Muhs and F. T. Weiss, *J. Amer. Chem. Soc.*, **84**, 4697 (1962).

(3) (a) R. J. Cvetanovic, F. J. Duncan, and W. E. Falconer, *Can. J. Chem.*, **41**, 2095 (1963); (b) R. J. Cvetanovic, F. J. Duncan, W. E. Falconer, and R. S. Irwin, *J. Amer. Chem. Soc.*, **87**, 1827 (1965).

(4) J. G. Atkinson, A. A. Russell, and R. S. Stuart, *Can. J. Chem.*, **45**, 1963 (1967).

(5) L. G. Sillen and A. E. Martell, "Stability Constants," Special Publication No. 17, The Chemical Society, London, 1964.

tion. The situation will be more favorable at lower temperatures and less favorable at higher temperatures. Finally, and most important to the present study, the actual substance that is responsible for the retention of the hydrocarbons used in this work is the silver ion. It is involatile and the water may almost be regarded as an inert matrix. As a result, the concentration of water on the packing will have slight effect on the measured retention times. Thus, the limits set above can be relaxed considerably for this type of experiment.

There have been several previous gas chromatographic studies in which water was used as the stationary phase.⁶⁻⁸ Due to its extraordinary solvent properties, rather unusual separations were obtained. In all these cases the volatility of the water did not appear to be an insurmountable problem. There have not been any studies in which aqueous solutions of a strong electrolyte were used as the stationary phase.

Experimental Section

A sketch of the experimental setup is given in Figure 1. Water is introduced into the carrier gas stream by bubbling helium through an aqueous AgNO_3 solution of the same concentration as that in the column. The side arm in the saturator permits the replenishment of the evaporated water. In principle, the presence of the salt in the saturation should stabilize the concentration of water present on the packing. If pure water is used, the failure to saturate or to supersaturate the helium stream will ultimately result in a column that is either empty or filled with water. With the presence of the salt, if the departure from equilibrium is small there will be instead an adjustment of the water concentration to a level that is consistent with its partial pressure in the carrier gas stream. In other words, the salt acts as a buffer maintaining constant water content. As noted earlier, these factors are not of prime importance for experiments at or below room temperature (range of present experiments), but they must be considered as the vapor pressure of the solvent increases. Furthermore, since at steady state there will be a gradient in salt concentration along the column (due to the pressure drop), thermal measurements may be more difficult.

The packings were made by mixing the desired amounts of silver nitrate and Chromosorb P(AW) (15-30 g) with an excess of water. The mixture was heated to about 70° while constantly shaken until only the desired amount of water (by weight) was left. It was then poured into $1/4$ -in. o.d. stainless steel columns. They ranged in length from 5 to 12 ft and contained from 5 to 12 g of water. The silver nitrate concentrations were approximately 0, 0.21, 0.4, 0.98, 1.8, and 3.5 M. It is estimated that these concentrations are accurate to $\pm 2-5\%$. The columns with high silver nitrate concentration were somewhat unstable. The 3.5 M column has a half-life of about a month. All

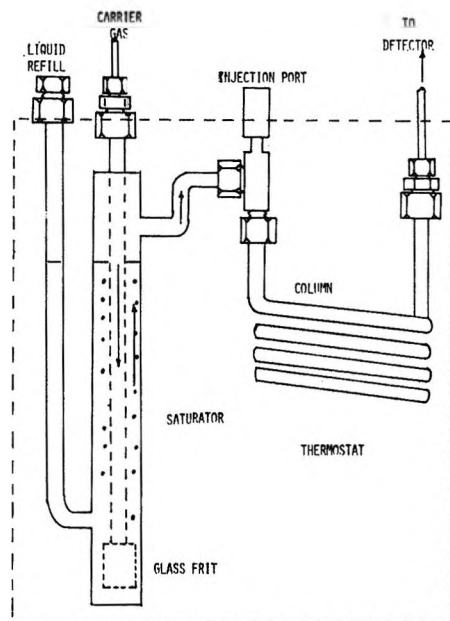


Figure 1. Experimental apparatus.

thermodynamic measurements were made within 1 or 2 days after packing and were therefore not affected by this problem. Ethylene, propylene, the four C_4 olefins, benzene, toluene, and xylenes were used as the solutes. They were injected onto the column with 10- or 100- μl syringes. The effluent was monitored by a GC-5 Beckman hydrogen flame detector. Helium was used as the carrier gas. Retention times, from many runs, over the period of several days were accurate to $\pm 0.5\%$.

Results and Discussion

I. Chromatographic Separations. A typical chromatogram for the separation of the olefins is given in Figure 2. The novel feature is the elution of *trans*-butene-2, isobutene, and propylene before ethylene. Column efficiencies for a given quantity of silver nitrate decrease with increasing water loading and temperature. For the 3.5 M AgNO_3 columns at 0° , the efficiencies are about 100-200 theoretical plates per foot. Figures 3, 4, and 5 illustrate the isotopic separations that may be effected with a 12-ft 3.5 M AgNO_3 column at 0° . The chromatograms of the olefin separations are comparable to that published by Cvetanovic and coworkers.^{3a,b} Their separations were carried out on a 40-ft AgNO_3 -ethylene glycol column at -14° and required a much longer retention time. This is apparently the first report of a separation of C_6D_6 from C_6H_6 with a silver nitrate column. Previously,^{9,10} these

- (6) L. H. Phifer and H. K. Plumer, *Anal. Chem.*, **38**, 1652 (1966).
- (7) R. E. Pecsar and J. J. Martin, *ibid.*, **38**, 1661 (1966).
- (8) B. Karger and A. Hartkopf, *ibid.*, **40**, 215 (1968).
- (9) M. Possanzini, A. Pela, A. Liberti, and G. P. Cartoni, *J. Chromatogr.*, **38**, 492 (1968).
- (10) A. Liberti, G. P. Cartoni, and F. Bruner, "Gas Chromatography," A. Goldup, Ed., Institute of Petroleum, London, 1965, p 301.

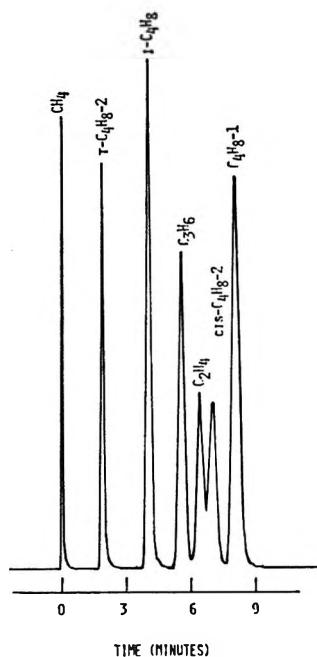


Figure 2. Separation of olefins on a 12-ft aqueous 3.5 M AgNO_3 column at 23° . Helium carrier gas $\sim 60 \text{ cm}^3/\text{min}$.

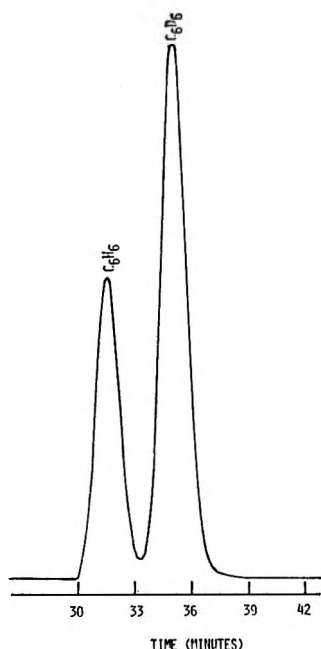


Figure 3. Separation of deuterated and normal benzene on 12-ft 3.5 M AgNO_3 column at 0° . Helium carrier gas $\sim 60 \text{ cm}^3/\text{min}$.

compounds have been separated *via* adsorption chromatography on graphitized carbon black, etched glass, and Porapak, and by liquid partition chromatography using squalane. In all cases the isotope effect was much smaller than that found here. Thus, longer columns were required.

These results illustrate the analytical possibilities of using aqueous columns. In the present case use has been made of the strong ionizing properties of

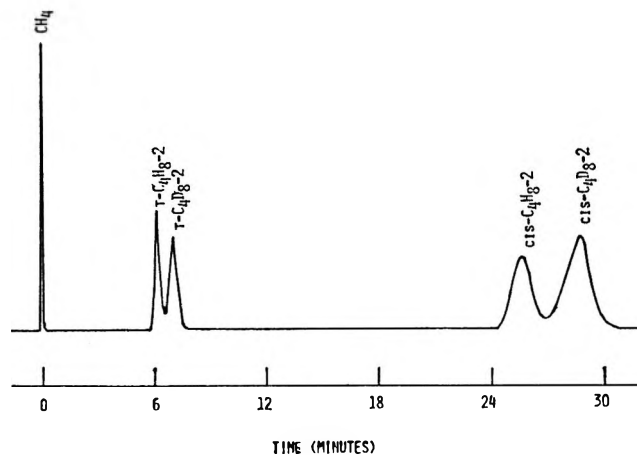


Figure 4. Separation of deuterated 2-butenes from isomers on 12-ft 3.5 M AgNO_3 column at 0° . Helium carrier gas $\sim 60 \text{ cm}^3/\text{min}$.

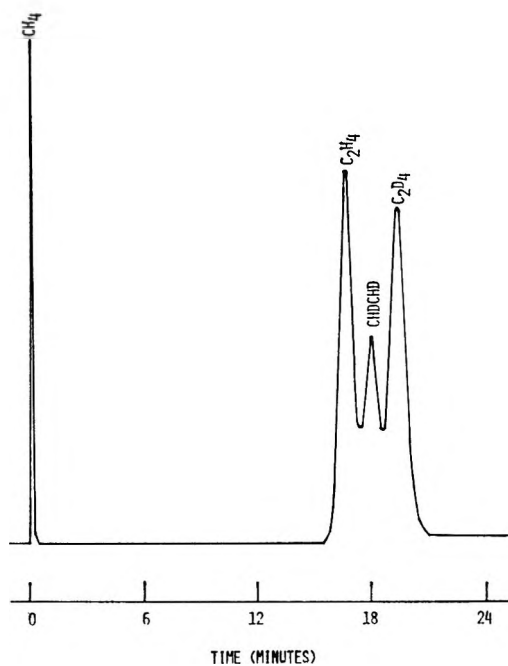


Figure 5. Separation of C_2H_4 , CHDCHD, and C_2D_4 isomers on 12-ft 3.5 M AgNO_3 column at 0° . Helium carrier gas $\sim 60 \text{ cm}^3/\text{min}$.

water, thus increasing the silver ion activity. It is clear that whenever metal ions are to be used in gas chromatography water is probably the preferred solvent. Furthermore, the enormous volume of data in the literature on chemical complexation in volatile solvents can be quantitatively used for the design of columns. These will be capable of making extremely specific separations since chemical interactions are now involved and effects due to volatility will be minimized. This of course assumes that equilibrium constants derived from standard techniques can be carried over to gas chromatography. This will be demonstrated to be the case in the subsequent section.

Table I: Partition Coefficients (Concn, Liquid Phase/Concn, Gas Phase), K_{obsd} , at Various Concentrations of $AgNO_3$ in Water as a Function of Temperature

	Pure water		0.21 M $AgNO_3$		0.40 M $AgNO_3$		0.98 M $AgNO_3$		1.8 M $AgNO_3$		3.5 M $AgNO_3$		
	0.0°	13.0°	0°	13.2°	15°	22.7°	15.0°	20.0°	25.0°	13.2°	23.2°	13.2°	23.2°
	$-\Delta H, \text{ kJ/mol}$		$-\Delta H, \text{ kJ/mol}$		$-\Delta H, \text{ kJ/mol}$		$-\Delta H, \text{ kJ/mol}$		$-\Delta H, \text{ kJ/mol}$		$-\Delta H, \text{ kJ/mol}$		
Ethylene													
Propylene													
Isobutene													
Butene-1													
cis-Butene-2													
trans-Butene-2													
Benzene	14.3	7.0	4.6	1.59	2.6	1.59	5.1	3.5	2.6	5.0	4.8	12.3	7.8
Toluene	23.2	9.2	20.0	9.2	5.8	3.9	6.0	4.3	6.0	4.3	134.2	63.8	39.7
p-Xylene	27.0	11.4	6.4	4.3	6.5	9.7					175		
o-Xylene	35.5	15.0	8.2	4.3							270		
Benzene- d_6	15.0	7.4	4.5	3.5							145.7	68.8	42.9

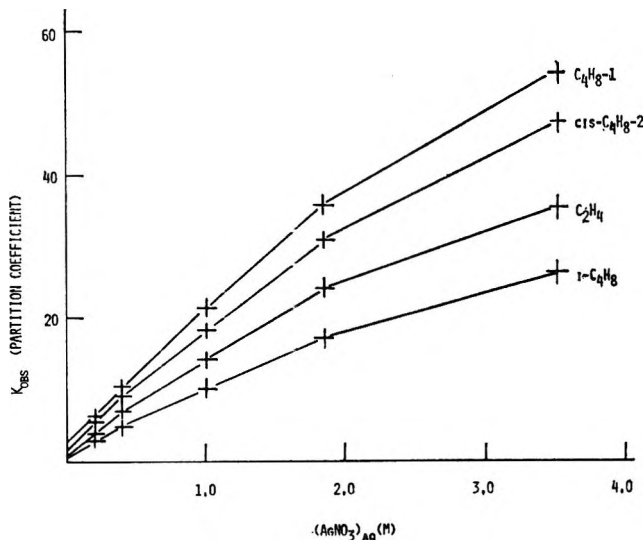


Figure 6. Variation of partition coefficients with $AgNO_3$ concentration at 13°.

II. Data Analysis. Quantitative results, expressed in terms of partition coefficients, K_{obsd} (concentration of sample in liquid phase/concentration of sample in gas phase), are summarized in Table I. They are derived from the well-known relation¹¹

$$K_{obsd} = \frac{3}{2} \left[\frac{(v_i/p_o)^2 - 1}{(v_i/p_o)^3 - 1} \right] \frac{F t_r T_c}{V_L T_f} \quad (1)$$

where p_i = inlet pressure, p_o = outlet pressure, F = flow rate, t_r = retention time (in this study, the time between the elution of methane and the peak of interest), T_c = column temperature, T_f = temperature of the flow meter, and V_L = volume occupied by the liquid phase. The dependence of the partition coefficient on silver nitrate concentration for various olefins is shown in Figure 6. It is similar to that found by Muhs and Weiss² in their studies using ethylene glycol as a solvent. They attribute the departure from linearity at high silver nitrate concentrations to a salting out effect. Also included in Table I are the heat quantities (from $\ln K_{obsd}$ vs. $1/T$ plots and represents the enthalpy for solute going into $AgNO_3$ solutions). For the olefins, these are much larger than usually encountered in chromatographic studies and are a reflection of the involvement of chemical interactions in the solution process. There is a noticeable increase in the negative heat of solution with decreasing silver nitrate concentration. This may be due to the incomplete ionization of silver nitrate at higher concentrations and/or a temperature dependence of the salting out effect.

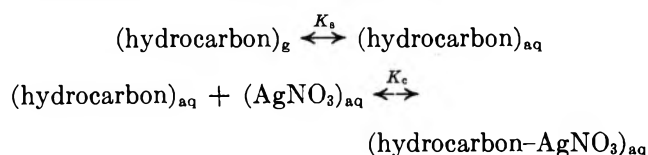
It was not possible to calculate partition coefficients from retention data of the olefins in the absence of silver nitrate due to their low solubility in water. From

(11) H. Purnell, "Gas Chromatography," Wiley, New York, N. Y., 1962.

literature values¹² it is estimated that for accurate determinations impractically long columns, several hundred meters, must be used.

For the aromatic compounds direct gas chromatographic determinations have been carried out. Of some interest is the presence of a rather significant isotope effect for the solubility of benzene in water. This has apparently never been reported before and demonstrates the special advantage of the gas chromatographic method since more conventional techniques will require vastly larger quantities of the deuterated benzene isomer.

The partition coefficients are directly related to the equilibrium constants for the various processes that occur in the chromatographic column. The procedure and relevant equations have been given by Muhs and Weiss.² This involves the assumption that during the course of the experiment two equilibria



are set up and lead to the relationship

$$H(\text{partition coefficient}) = K_s + K_s K_c (\text{AgNO}_3)_{aq} \quad (2)$$

Thus in the absence of silver nitrate the partition coefficient is equal to the solubility constant (as defined here it is essentially the inverse of the Henry's law constant). In the present study, as noted earlier, K_s for the olefins that are considered here cannot be directly determined. Furthermore, the experimental scatter is sufficiently large so as to render meaningless any attempt to determine K_s by extrapolating data such as given in Figure 6 to zero AgNO_3 concentration. Literature values must then be used.¹²⁻¹⁵ The available data are summarized in Table II.¹⁶⁻¹⁸ Unfortunately, data on this subject are extraordinarily scarce. Except for ethylene, the solubilities of small olefins have apparently never been studied over a range of temperatures. Also included in Table II are solubility data for the aromatic compounds.

Calculated values of the equilibrium constant of the complexing reaction at the temperature for which solubility data are available are given in Table III. For the aromatic compounds complexing constants are determined using the gas chromatographic values for the solubility constant. With regard to ethylene, the data in Table III yield an enthalpy and entropy for the complex-forming reaction of $\Delta H = -23$ kJ/mol and $\Delta S = -38$ J/mol deg. As noted earlier, the lack of solubility data prevents similar determinations for the other olefins. However, a rough estimate can be made if it is assumed that the excess energy of solution for these compounds is the same as that for ethylene. On this basis the enthalpies and entropies of reaction

Table II: Data on the Solubility of Olefins and Aromatics, K_s (in Terms of Partition Coefficients: Conc'n in Liquid Phase/Concn in Gas Phase)

	Temp, °C			
	0	13	23	25
Ethylene	0.20 ¹³	0.14 ¹³	0.11 ¹³	0.107 ^{12,13}
Propylene				0.125 ¹²
Isobutene				0.112 ¹²
Butene-1				0.105 ¹²
<i>cis</i> -Butene-2				0.106 ¹⁶
<i>trans</i> -Butene-2				0.109 ¹⁵
Benzene	16.6	8.4	4.9	4.48 ¹⁴
Toluene	19.2	8.8	5.0	4.52 ¹⁴
				3.87 ¹²
<i>p</i> -Xylene	20.0	9.0	4.6	4.05 ¹²
				4.15 ¹⁴
<i>o</i> -Xylene				4.62 ¹²
				5.39 ¹²

Table III: Summary of Experimental Results on Complexing Constants (M^{-1}), K_c , and Literature Values

	Temp, °C				Lit values, 25
	0	13.2	23.2 ^a	25 ^a	
Ethylene	203	127	92	85	85 ¹⁷
Propylene			85	79	87 ¹⁷
Isobutene			55	51	71 ¹⁸
1-Butene			120	110	118 ¹⁸
<i>cis</i> -Butene-2			90	83	62 ¹⁸
<i>trans</i> -Butene-2			29	27	25 ¹⁸
Benzene	1.86	1.45	1.58		2.41 ¹⁶
Toluene	0.43	0.52	1.19		2.95 ¹⁶

^a Values for olefins at 25° have been extrapolated assuming temperature dependence similar to that of ethylene.

turn out to be very similar to those given here for ethylene. Complexing constants for the aromatic compounds are more than an order of magnitude smaller than for the olefins. For reasons that will be dealt with subsequently, the quality of these data is probably inadequate for an accurate determination of enthalpies and entropies of reaction. Also included in Table III are the results from static experiments.¹⁶⁻¹⁸

Data on isotope effects, expressed as the ratio of retention time of the deuterated species with respect to

(12) C. McAuliffe, presented before the Division of Petroleum Chemistry, 148th National Meeting of the American Chemical Society, Chicago, Ill., Aug 1964.

(13) T. J. Morrison and F. Biller, *J. Chem. Soc.*, 3019 (1952).

(14) R. J. Bohon and W. F. Clauson, *J. Amer. Chem. Soc.*, **73**, 1572 (1951).

(15) F. Irrmann, *Chem.-Ing.-Tech.*, **37**, 789 (1965).

(16) L. J. Andrews and R. M. Keefer, *J. Amer. Chem. Soc.*, **71**, 3644 (1949).

(17) K. N. Trueblood and H. J. Lucas, *ibid.*, **74**, 1338 (1952).

(18) F. R. Hepner, K. N. Trueblood, and H. J. Lucas, *ibid.*, **74**, 1333 (1952).

Table IV: Data on Isotope Effects in 3.5 M AgNO₃

	Temp. °C	Present work	Cvetanovic, <i>et al.</i> , ^{3a,b,4} (in ethylene glycol)
C ₂ D ₄ -C ₂ H ₄	0	1.168 ^a	1.14 (1.161)
	23.2	1.142	1.113 (1.129)
CHDCHD- C ₂ H ₄	0	1.086	1.07 (1.085)
<i>cis</i> -C ₄ D ₈ -2-	0	1.119	1.08 (1.133)
<i>cis</i> -C ₄ H ₈ -2			
<i>trans</i> -C ₄ D ₈ -2-	0	1.144	1.09 (1.157)
<i>trans</i> -C ₄ H ₈ -2			
C ₆ D ₆ -C ₆ H ₆	0	1.086 (1.032) ^b	
	13.2	1.079 (1.027)	
	23.2	1.080 (1.028)	

^a Values are from ratio of retention times. ^b Values in parentheses have been corrected for isotope effect on solubility. They represent $K_c(\text{deuterated compound})/K_c(\text{light compound})$.

its light isomer, are summarized in Table IV. Also included are the results of Cvetanovic and coworkers from studies in ethylene glycol.⁴ In their studies they were able to determine the isotope effect for the solubility of the olefins in ethylene glycol. Thus, the isotope effect appropriate to the complexing reaction can be calculated. These numbers are the values in parentheses. In the present study a similar correction could not be applied due to the low solubility of the olefins in water. There is, however, extremely good correspondence between the corrected ethylene glycol values and the uncorrected results of the present investigation. This suggests that there is almost no isotope effect for the solution of the smaller olefins in water. With regard to benzene a complete set of data is available. As could have been expected from the relatively weak silver-benzene complex, the isotope effect for this reaction is small. Indeed, it is even smaller than that for the solubility of benzene in water.

III. Comparisons and Limitations. From an examination of the data summarized in Tables II, III, and IV it can be seen, in general, that there is satisfactory agreement between gas chromatographic and static determinations. For the olefins the agreement with respect to the stability constants can be regarded as quantitative. In the case of aromatic compounds the larger discrepancies between literature and experimental values are undoubtedly due to the fact that the contribution to the retention time of these compounds arises largely from insolubility in water rather than from the complex-forming reaction (as is the case of the olefins). See eq 2. Thus, small errors in the two measured quantities will result in large errors in the stability constant. One source of such error is the neglect of the salting out effect at the 0.214 M AgNO₃ concentration.

Another source of error is the possibility of surface effects. Conder, Locke, and Purnell¹⁹ have recently

published a series of papers on the importance of surface effects in gas-liquid partition chromatography. This has also been mentioned by Karger⁸ in his study of the separation of high molecular weight hydrocarbons by a water column. These considerations are not applicable to the aqueous silver nitrate columns when used with the olefins since surface effects are probably vastly smaller than the contribution to the retention time from the complexing reaction. For the aromatic compounds, even a small manifestation of this effect can cause serious errors. The increasing divergence of the solubility of the aromatics from the literature values for the xylenes as compared to the very good agreement for benzene and toluene may be caused by this sort of phenomenon. On the other hand, a factor that is of special importance here is the very heavy loading of the columns (up to 52% by weight). This will minimize surface effects not only by increasing the total volume but by decreasing the surface area. Water, with its high surface tension, should be particularly effective in this regard.

Finally, some comment should also be made on the correspondence between solubility determinations from static determinations and gas chromatography. In the former the values are appropriate to a particular pressure (1 atm for the olefins and saturation vapor pressure for the aromatics), while the latter are in principle at least for infinite dilution. Thus, in general, exact agreement for the two cases is not expected, although it appears to be a good approximation in the present case. (See, for example, the benzene results.) This may be due that even at the higher pressures the concentration of solute still obeys Henry's law.

IV. Conclusions. Bearing in mind the considerations outlined above, the general trends in the present study do establish the validity of the gas chromatographic method for the determination of physicochemical parameters involving volatile stationary liquid phases. The usefulness and reliability of this method for the generation of thermodynamic data involving nonvolatile solvents is fairly well established.²⁰ Unfortunately, since most solution chemistry is carried out in solvents of some volatility (water, acetone, methanol, etc.) the systems that have been studied chromatographically are of restricted interest to other fields of chemistry. The present study demonstrates that there are no additional problems when a volatile solvent is used. It is clear that the gas chromatographic method is applicable to a much larger variety of problems than has hitherto been thought possible.

With regard to complex formation by silver ions in water all of the past studies on this subject have been carried out at a single temperature. It is interesting

(19) J. R. Conder, D. C. Locke, and J. H. Purnell, *J. Phys. Chem.*, **73**, 700, 708 (1969).

(20) J. H. Purnell in "Gas Chromatography," A. B. Littlewood, Ed., Institute of Petroleum, London, 1966.

to note, however, that the thermal quantities (ΔH and ΔS) for the ethylene silver complex forming reaction are in the same range as those found by Denning, Hartley, and Venanzi²¹ on the formation of (allyl NR_3)⁺ PtCl_3^- complexes where R is either an H atom or an ethyl group. In comparison with the results of Cveta-
 novic and coworkers^{3a,b,4} using ethylene glycol, the thermal parameters and the stability constants in water are all larger. One rather surprising feature of the present study is that in contrast to the situation in ethylene gly-

col and in conformity with static experiments, the substitution of alkyl groups adjacent (compare propylene and 1-butene to ethylene) to the double bond does not cause any large decrease in stability constants. Thus, the earlier gas chromatographic results would seem to be due to the medium, ethylene glycol, rather than any specific property of the complexing reaction.

(21) R. G. Denning, F. R. Hartley, and L. M. Venanzi, *J. Chem. Soc.*, 324 (1967).

Activity Coefficients and Ion Pairs in the Systems Sodium

Chloride-Sodium Bicarbonate-Water and Sodium

Chloride-Sodium Carbonate-Water¹

by James N. Butler and Rima Huston

Tyco Laboratories, Inc., Bear Hill, Waltham, Massachusetts 02154 (Received January 6, 1970)

The mean activity coefficient of NaCl in electrolytes containing NaHCO_3 and Na_2CO_3 has been measured by the potentiometric method, employing both sodium amalgam electrodes and sodium-selective glass electrodes in cells without liquid junction. Harned's rule is obeyed over the ionic strength range from 0.5 to 3.0 with a coefficient $\alpha_{12} = 0.047 \pm 0.003$, independent of ionic strength or whether the anion is CO_3^{2-} or HCO_3^- . These results, as well as the equilibrium constants for protonation equilibria, are discussed in terms of a model where Na^+ forms ion pairs with the carbonate anions. Association constants (at $I = 1.0$) $\log K_1' = 0.96 \pm 0.13$ (for the formation of NaCO_3^-) and $\log K_1'' = -0.30 \pm 0.13$ (for the formation of NaHCO_3) are derived. Constants obtained at other ionic strengths and corrections to $I = 0$ are given. The relation of ion pairing to the salt effect on the carbonate protonation equilibria is discussed. Systematic deviations of several millivolts observed in the glass electrode data at pH 8 to 9 and ionic strengths below 1 indicate that caution must be exercised in interpreting such measurements.

Introduction

Despite the critical importance of bicarbonate and carbonate ions in natural water systems, little is known about the activity coefficients and ion-pairing equilibria of these species in the presence of alkali metal cations. One indirect study has been made² of the activity coefficients of NaHCO_3 and Na_2CO_3 alone in aqueous solutions, but no direct measurements have been made of multicomponent activity coefficients, either of NaCl in the presence of carbonate species, or of carbonates in the presence of substantial concentrations of NaCl.

On the other hand, a large body of data has been collected on the protonation equilibria of carbonates,^{3,4} mostly in media where extrapolation to infinite dilution is possible. Attempts^{4,5} have been made to obtain quantitative information about ion-pairing equilibria

from such data, but these rest on a number of *ad hoc* assumptions regarding single-ion activities and the

(1) Presented at the Symposium on Metal Ions in the Aqueous Environment, 158th National Meeting of the American Chemical Society (Division of Water, Air, and Waste Chemistry), New York, N. Y., Sept 1969.

(2) A. C. Walker, U. B. Bray, and J. W. Johnson, *J. Amer. Chem. Soc.*, **49**, 1235 (1927).

(3) (a) L. G. Sillén and A. E. Martell, "Stability Constants of Metal-Ion Complexes," The Chemical Society, London, Special Publication No. 17, 1964; (b) C. Culberson, D. R. Kester, and R. M. Pytkowicz, *Science*, **157**, 59 (1967); A. Distèche and S. Distèche, *J. Electrochem. Soc.*, **114**, 330 (1967); C. Culberson and R. M. Pytkowicz, *Limnol. Oceanogr.*, **13**, 403 (1968).

(4) F. S. Nakayama, private communication (submitted to *J. Phys. Chem.*).

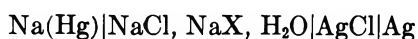
(5) R. M. Garrels, M. E. Thompson, and R. Siever, *Amer. J. Sci.*, **259**, 24 (1961).

constancy of liquid-junction potentials, and for that reason are difficult to relate to thermodynamic data.⁶

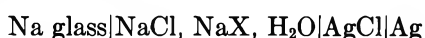
This paper describes several experiments designed to obtain the thermodynamic mean activity coefficient of NaCl in the presence of NaHCO₃ or Na₂CO₃, and attempts to relate these results to a model involving ion pairing between Na⁺ and HCO₃⁻ or CO₃²⁻.

Experimental Section

Activity coefficients of NaCl were obtained as described previously from potential measurements of the cell⁷⁻⁹



(where X represents HCO₃ or ¹/₂CO₃²⁻); or from measurements of the cell¹⁰



Two different types of sodium-selective glass electrodes were used. Electrode B was a Beckman No. 39278 sodium ion electrode (glass composition^{11,12} probably LAS-10-23), and electrode C was a Corning No. 476210 sodium ion electrode (glass composition NAS-11-18).

Solutions were prepared by weight from Fisher Certified reagent grade chemicals and triple-distilled water. NaCl contained less than 0.01% bromide, less than 0.002% iodide, and less than 0.0002% materials reducible by sodium amalgam. NaHCO₃ and Na₂CO₃ contained less than 0.003% chloride, less than 0.01% bromide or iodide, and less than 0.005% reducible metals. Solutions were analyzed for chloride by potentiometric titration with standard AgNO₃, for carbonate by potentiometric pH titration with standard HCl, and for bicarbonate by titration with standard NaOH. Gran¹³ plots of these titration curves indicated negligible material other than chloride reacting with the silver ion, and less than 0.2% excess base in the carbonate.⁶ For the amalgam electrode measurements, 0.001 *m* NaOH was added to the NaCl stock solution to minimize hydrogen evolution. The pH of each mixed solution was measured separately, and was in every case high enough to avoid interference with the sodium response of the glass electrode.

Results

Representative potential measurements obtained with the amalgam electrode cell are given in Tables I and II. The values (ΔE) given are the difference in potential between a cell containing the mixed electrolyte and a cell containing the NaCl stock solution. The amalgam composition was the same, since both cells were fed from the same amalgam reservoir and were measured simultaneously. The Ag-AgCl electrodes were matched to better than ± 0.01 mV. Activity coefficients of NaCl in the mixed electrolyte (γ_{12}) were calculated from the equation

$$E = E^0 + \frac{RT}{T} \ln \{m_{\text{Na}}m_{\text{Cl}}(\gamma_{12})^2\} \quad (1)$$

with E^0 evaluated from the known composition and activity coefficients of the NaCl stock solution.¹⁴ Correction of γ_{12} to round ionic strength was made by assuming Harned's rule¹⁵

$$\log \gamma_{12} = \log \gamma_{10} - \alpha_{12}I(1 - X_1) \quad (2)$$

where γ_{10} is the mean activity coefficient of NaCl alone at ionic strength I , and α_{12} is estimated from the uncorrected data. A second iteration did not change the value of α_{12} obtained from the corrected data.

Table I: Activity Coefficient Measurements in NaCl-NaHCO₃ Electrolytes at 25°; [Cell: Ag|AgCl|NaCl, NaHCO₃, H₂O|Na(Hg)]^a

Total ionic strength, I	X_1	pH	ΔE , mV	$-\log \gamma_{12}$ (exptl)	$-\log \gamma_{12}$ (cor) ^b
0.5031	1.0000	11.02	0	0.1672	0.1668
0.5073	0.7486	8.83	8.50	0.1791	0.1784
			8.25	0.1770	0.1763
0.5133	0.5055	8.18	18.15	0.1782	0.1767
			18.30	0.1795	0.1780
0.5215	0.1793	8.21	48.00	0.2092	0.2064 ?
			48.30	0.2117	0.2089 ?
0.5240	0.0761	8.22	68.50	0.1974	0.1941
			68.00	0.1932	0.1899
1.0981	1.0000	9.0	0	0.1838	0.1824
1.0400	0.4122	8.6	27.20	0.2102	0.2087
			27.28	0.2109	0.2094
1.0115	0.1135	8.4	62.50	0.2225	0.2219
			62.70	0.2234	0.2228
1.0049	0.0444	8.2	87.10	0.2255	0.2252
			87.30	0.2272	0.2269

^a Component 1 is NaCl, component 2 is NaHCO₃; $I = m_1 + m_2$, $X_1 = m_1/I$ (protonation equilibria *not* included in calculating ionic strength); pH of 0.5 *m* NaHCO₃ stock solution was 9.0; pH of 1.0 *m* NaHCO₃ stock solution was 8.12. ^b γ_{12} corrected to round ionic strength (0.50 or 1.00) in last column.

(6) J. N. Butler and R. Huston, "The Use of Amalgam Electrodes to Measure Activity Coefficients of Multicomponent Electrolyte Solutions," Interim Report No. 2, Office of Saline Water, Research and Development Progress Report No. 486, 1969, Interim Report No. 3, in preparation, 1970.

(7) J. N. Butler, P. T. Hsu, and J. C. Synnott, *J. Phys. Chem.*, **71**, 910 (1967).

(8) J. N. Butler, "The Use of Amalgam Electrodes to Measure Activity Coefficients of Multicomponent Electrolyte Solutions," Interim Report No. 1, Office of Saline Water, Research and Development Progress Report No. 388, 1968.

(9) J. N. Butler and R. Huston, *J. Phys. Chem.*, **71**, 4479 (1967).

(10) R. Huston and J. N. Butler, *Anal. Chem.*, **41**, 1695 (1969).

(11) G. A. Rechnitz, *Chem. Eng. News*, **45**, 146 (1967).

(12) G. L. Gardner and G. H. Nancollas, *Anal. Chem.*, **41**, 202 (1969).

(13) G. Gran, *Analyst* (London), **77**, 661 (1952).

(14) R. A. Robinson and R. H. Stokes, "Electrolyte Solutions," Butterworths, London, 1965.

(15) H. S. Harned and B. B. Owen, "The Physical Chemistry of Electrolyte Solutions," Reinhold, New York, N. Y., 1958.

Table II: Activity Coefficient Measurements in NaCl-Na₂CO₃ Electrolytes at 25°: [Cell: Ag|AgCl|NaCl, Na₂CO₃, H₂O|Na(Hg)]

Total ionic strength ^a	X ₁	pH ^b	ΔE, mV	-log γ ₁₂ (exptl)	-log γ ₁₂ (cor)
0.5685	1.0000	8.3	0	0.1707	0.1669
0.5575	0.9096	10.24	3.57	0.1707	0.1671
			3.70	0.1718	0.1682
0.5062	0.4868	10.89	26.98	0.1817	0.1812
			26.65	0.1789	0.1784
0.4699	0.1880	11.07	56.50	0.1794	0.1821
			56.10	0.1761	0.1788
0.4585	0.0944	10.99	77.30	0.1893	0.1932
			76.97	0.1865	0.1904
1.0315	1.0000	9.04	0	0.1832	0.1824
1.0092	0.5069	10.1	25.50	0.2085	0.2081
			25.40	0.2076	0.2072
0.9923	0.1357	10.8	66.10	0.2265	0.2269
			65.80	0.2240	0.2244
0.9883	0.0483	10.9	94.28	0.2301	0.2308
			93.95	0.2273	0.2280
3.0487	1.0000	10.90	0	0.1448	0.1465
3.0247	0.7459	10.98	14.70	0.1845	0.1851
			14.00	0.1786	0.1792
2.9973	0.4831	11.15	31.80	0.2112	0.2112
			31.71	0.2104	0.2104
2.9762	0.2621	11.00	54.40	0.2475	0.2475
			54.30	0.2466	0.2466
2.9523	0.0532	11.35	100.92	0.2715	0.2719
			100.65	0.2692	0.2696
1.0315 ^c	1.0000	9.04	0	0.1832	...
1.9883 ^c	0.5051	10.3	15.15	0.2441	...
			14.90	0.2420	...
2.6857 ^c	0.1444	11.0	45.64	0.2764	...
			45.88	0.2744	...
2.8762 ^c	0.0458	11.2	74.50	0.2797	...
			74.34	0.2784	...

^a $I = m_1 + 3m_2$, $X_1 = m_1/I$ (protonation equilibria *not* included in calculating ionic strength). ^b pH of 0.33 *m* Na₂CO₃ = 11.06; pH of 1.0 *m* Na₂CO₃ = 11.42. ^c These four solutions were at constant total molality rather than constant ionic strength.

Within experimental error, Harned's rule was obeyed for the amalgam electrode measurements in all solutions tested. Values of α_{12} obtained by a least-squares fit to the corrected γ_{12} data in Tables I and II are given in Table III. For all solutions tested at ionic strengths from 0.5 to 3.0, whether the second component was NaHCO₃ or Na₂CO₃, the Harned rule coefficient fell in the range 0.045 to 0.050. This is an unexpectedly simple result.

The glass electrode measurements in general confirmed the amalgam electrode results, but were less precise and apparently also less accurate. In particular, systematic deviations of the glass electrode measurements (Figure 1) occurred at low fractions of NaCl in a direction which would imply that the activity of sodium ion in the vicinity of the glass surface was considerably enhanced over that in the bulk. (These were not observed with the amalgam electrode cell.)

Table III: Harned Rule Coefficients

I ^a	pH	α_{12}
NaCl-NaHCO ₃		
0.50	8.2-9.2	0.050 ± 0.009
1.00	8.2-8.6	0.045 ± 0.003
NaCl-Na ₂ CO ₃		
0.50	10.2-11.1	0.048 ± 0.016
1.00	10.5-10.9	0.049 ± 0.003
3.00	10.9-11.4	0.044 ± 0.003

^a Note: I is formal ionic strength, held constant for the series; for NaCl-NaHCO₃, $I = m_1 + m_2$; for NaCl-Na₂CO₃, $I = m_1 + 3m_2$. The effect of protonation equilibria on ionic strength is *not* included. Errors on α_{12} are 95% confidence limits obtained by the method of least squares, allowing the intercept to vary.

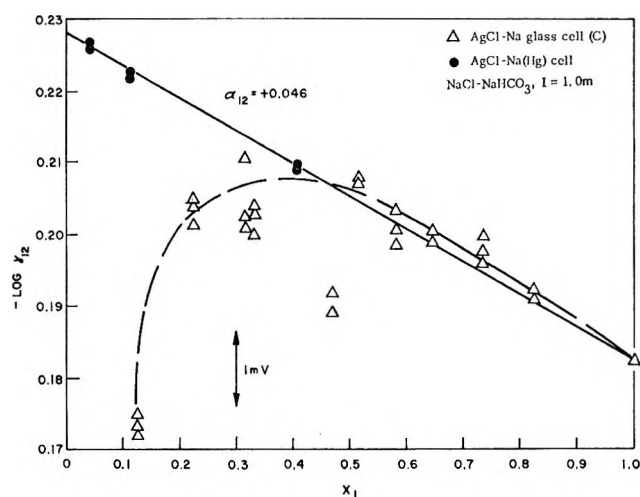


Figure 1. Activity coefficients of NaCl in NaCl-NaHCO₃ electrolytes at ionic strength 1.0 *m*. Note deviations of glass electrode data and agreement of amalgam electrode data with Harned's rule.

The most pronounced deviations of this type were found in dilute NaCl-NaHCO₃ electrolytes; they were noticeable but less pronounced in NaCl-Na₂CO₃ electrolytes at low concentrations and were negligible at high concentrations (Figure 2). Differences between glass electrodes B and C were noticeable, particularly in the dilute NaCl-NaHCO₃ electrolytes. There may also be an aging effect. Full data from these experiments are available.⁶

These differences appear to result from a specific but as yet unexplained effect on the glass electrode. Although the solutions used in the amalgam electrode experiments were somewhat more basic than those used in the glass electrode experiments (because of the addition of approximately 0.001 *m* NaOH to the NaCl stock solution), the effect of this on ionic strength is negligible, corresponding to less than 0.002 mV error. The amalgam electrode experiments were also carried

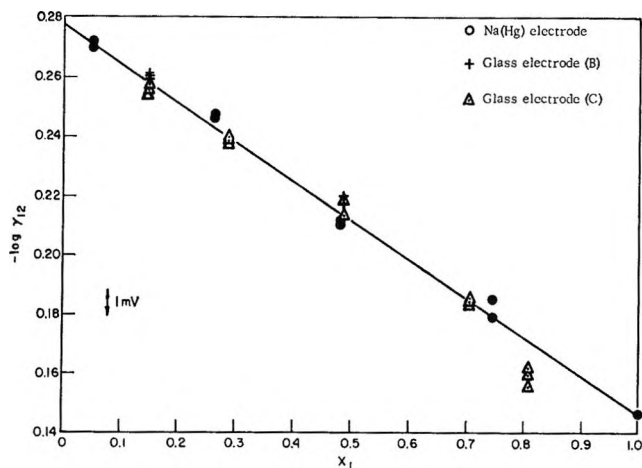


Figure 2. Activity coefficients of NaCl in NaCl-Na₂CO₃ electrolytes at ionic strength 3.0 *m*. Note agreement between glass electrode and amalgam electrode data.

out in closed vessels using solutions saturated with hydrogen, but any concentration changes due to removal of carbon dioxide by the hydrogen were estimated to have a negligible effect (<0.05 mV) on the observed potentials.

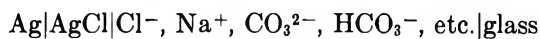
Since the same set of Ag-AgCl electrodes was used for all experiments this electrode cannot be the cause of the observed differences. No effect of hydrogen-saturated solutions compared to oxygen or carbon dioxide-saturated solutions is known to occur; in the presence of 1 *m* chloride, formation of Ag₂O requires pH values higher than 13 and formation of Ag₂CO₃ is not expected to occur at all.^{3a}

Amalgam electrode dissolution in solutions of pH 8.5 to 9 might have caused an excess concentration of Na⁺ to build up in the vicinity of the electrode and thus caused deviations from Harned's rule toward larger γ_{12} values at low NaCl fractions. Surprisingly, deviations in this direction were observed with the glass electrode but *not* with the amalgam electrode.

Thus the deviations of the glass electrode measurements cannot be explained by any simple experimental effect. The deviations are apparently reproducible within 1 mV using different glass electrodes and making measurements at different times on different solutions, and may possibly be attributed to a specific adsorption of sodium ion on the glass surface which is somehow aided by the presence of bicarbonate ion in solution. Thus, the use of sodium-selective glass electrodes in carbonate-containing solutions should be tempered with some caution, since deviations of several millivolts from the thermodynamic values may be obtained.

We also carried out a few measurements of the protonation equilibria in NaCl media of ionic strength 1.0 and 3.0. In these experiments, we kept the NaCl concentration high compared to the total carbonate concentration and used a cell without liquid junction. Since

the solutions contain a fixed concentration of chloride already, the reference electrode was Ag-AgCl. The indicator electrode was a conventional glass pH electrode (Beckman 39301). The potential of the cell



may be written in the form

$$E = E^0 + \frac{RT}{F} \ln \{ [\text{H}^+][\text{Cl}^-](\gamma_{21})^2 \} \quad (3)$$

where we have explicitly expressed the fact that γ_{21} , the mean activity coefficient of HCl in the medium (NaCl), is to be used.

These activity coefficient values in HCl-NaCl electrolytes have been measured by Harned and co-workers,¹⁶ and may be represented by Harned's rule with the coefficient $\alpha_{21} = +0.0315$ at $I = 1$ and $\alpha_{21} = +0.0300$ at $I = 3$ (here component 1 is NaCl and component 2 is HCl). The mean activity coefficients of pure HCl (γ_{20}) used to obtain γ_{21} from these coefficients (α_{21}) were obtained from the tables of Robinson and Stokes.¹³ The results were $\gamma_{21} = 0.7499$ at $I = 1.054$ *m* and $\gamma_{21} = 1.063$ at $I = 3.098$ *m*. Using these values, together with the known chloride concentration ($[\text{Cl}^-] = I$), we could relate E and $[\text{H}^+]$ quantitatively.

The glass electrode was calibrated to obtain E^0 by using a borax-NaCl buffer (0.01038 *m* Na₂B₄O₇ and 0.01925 *m* NaCl) of ionic strength 0.030. It was known to have¹⁷

$$p(a_{\text{H}}\gamma_{\text{Cl}}) = -\log \{ (\gamma_{21})^2 [\text{H}^+] \} = 9.239 \quad (4)$$

at 25° and $[\text{Cl}^-] = 0.01925$. E^0 was calculated from eq 3.

In the titration of NaHCO₃ with NaOH, the equation¹⁸

$$K_1 = \frac{1}{[\text{H}^+]} \left(\frac{1 - \phi}{\phi + K_{12}[\text{H}^+](\phi + 1)} \right) \quad (5)$$

where

$$\phi = \frac{CV - (V + V_0)[\text{OH}^-]}{C_0V_0}$$

and $\log K_{12} = 6.0$ (ref 19) which gives a value of K_1 for each point. For the titration of Na₂CO₃ with HCl, the equation

$$K_1 = \frac{1}{[\text{H}^+]} \left(\frac{\phi}{1 - \phi + K_{12}[\text{H}^+](2 - \phi)} \right) \quad (6)$$

where

(16) H. S. Harned, *J. Phys. Chem.*, **63**, 1299 (1959).

(17) R. G. Bates, "Determination of pH, Theory and Practice," Wiley, New York, N. Y., 1964, p 413.

(18) J. N. Butler, "Ionic Equilibrium," Addison-Wesley, Reading, Mass., 1964.

(19) M. Frydman, G. Nilsson, T. Rengemo, and L. G. Sillén, *Acta Chem. Scand.*, **12**, 878 (1958).

Table IV: Acid-Base Equilibrium of Carbonate in NaCl

Ionic strength ^a	Initial solution		Titrant	log K_1^b	
	NaHCO ₃ , <i>m</i>	Na ₂ CO ₃ , <i>m</i>			
1.056-1.069	0.0243	0.0021	1.00 M NaOH	9.75 ± 0.05	
1.055-1.031	0.0010	0.0130	1.00 M HCl	9.68 ± 0.10	
3.098-2.925	0.0005	0.0470	1.00 M HCl	9.63 ± 0.02	
Estimate from pH of Standard Buffers ^c					
			pH	log γ_H	
0.04	0.01	0.01	10.112	-0.074	10.038
0.10	0.025	0.025	10.018	-0.099	9.918
0.20	0.05	0.05	9.933	-0.115	9.817

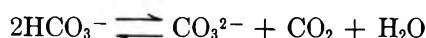
^a Primarily NaCl. A change of about 3% occurs during titration because of dilution and shifts in equilibria. The values given are the initial and final ionic strengths calculated in the course of determining K_1 . ^b Equilibrium constant for the reaction $H^+ + CO_3^{2-} \rightleftharpoons HCO_3^-$ (IUPAC notation). Standard state, unit molality in NaCl of ionic strength 1.06 or 3.00. Neglecting the minor component of the initial solution causes errors of about 0.2 logarithmic unit in K_1 for the first two titrations. ^c Data from ref 15, pp 712 and 716: $\log K_1 = \text{pH} + \log \gamma_H + \log (1 - K_1 K_{12} [H^+]^2) - \log (1 + 2K_{12} [H^+])$. γ_H was assumed equal to γ_{\pm} for HCl.

$$\phi = \frac{CV + (V + V_0)[OH^-]}{C_0 V_0}$$

gives a value of K_1 for each point. The results of such calculations are summarized in Table IV. (No equilibrium constants can be obtained from the titration of Na₂CO₃ with NaOH, and a sealed system is necessary to prevent errors from CO₂ loss in the titration of NaHCO₃ with HCl.) The composition of the starting solution was obtained by acidimetric titration because of the possibility of gaining or losing CO₂. Some values of K_1 at lower ionic strengths were calculated from the pH of standard buffers¹⁵ and are also included in Table IV.

Discussion

The first question to be considered is what effect the carbonate protonation equilibria may have on the measured values of activity coefficient for NaCl in the presence of carbonate or bicarbonate. Shifts in these equilibria under the conditions of our experiments could result from loss or gain of CO₂. This would not affect the concentrations of either Na⁺ or Cl⁻, but the total ionic strength would be affected because of the transformation of two singly charged ions into a doubly charged ion (or the reverse)



Loss of Δm mol/kg of CO₂ would increase the ionic strength of the solution by an amount Δm . Our observations on the relatively dilute carbonate and bicarbonate solutions used to determine K_1 indicated that during the normal course of laboratory manipulations, without taking special precautions to seal the solution against the atmosphere, NaHCO₃ solutions lost about 0.001 *m* CO₂ and Na₂CO₃ solutions gained about 0.001 *m* CO₂. The partial pressure of CO₂ above a bicarbonate solution with pH 8.5 is approximately 1

Torr, and that above a carbonate solution with pH 10.5 is approximately 0.001 Torr.^{3a} This gain and loss is thus reasonable when one considers that the normal partial pressure of atmospheric CO₂ falls well within this range.

What would then be the expected magnitude of the effect of CO₂ gain or loss on γ_{12} for NaCl in the mixed electrolytes we have been studying? At ionic strengths near 1.0, a change of 0.1 *m* in ionic strength produces a change of about 0.001 in log γ_{12} , corresponding to less than 0.1 mV in the measured cell potential. At ionic strengths near 3.0, a shift in *I* of 0.1 *m* produces a change in log γ_{12} corresponding to about 0.3 mV. The expected exchange of CO₂ with the vapor phase is considerably less than 0.1 *m*, and thus these effects are much smaller than the experimental errors and have an entirely negligible effect on the measured activity coefficients.

The second question to be considered is a possible explanation of the relatively large and highly consistent values of the Harned rule coefficient, α_{12} , which were obtained in our experiments. The addition of carbonate or bicarbonate to NaCl at constant ionic strength decreases the activity of NaCl by an amount corresponding to as much as 10 mV in potential, and a natural explanation may be sought in a model where ion pairs such as NaHCO₃ and NaCO₃⁻ are formed. A simple criterion for the self-consistency of such a model is whether the formation constants of these complexes are relatively independent of composition at constant ionic strength and whether the variation of the formation constants with ionic strength is consistent with expectations based on charge type. A final criterion lies in the agreement of calculations based on formation constants obtained from activity coefficient measurements with observations of the effect of different ionic media on the carbonate protonation equilibria.

Previous estimates of ion-pairing equilibrium constants^{5,20} have depended on rather uncertain values of activity coefficients for alkali carbonates and bicarbonates,² pH measurements in cells with liquid junction, and nonthermodynamic assumptions for single-ion activity coefficients.²¹ In our analysis we have attempted to be as explicit as possible about any nonthermodynamic assumptions introduced. We have been guided in our analysis by the discussion of the NaCl-Na₂SO₄ system in a recent paper by Pytkowicz and Kester,²² who showed that for weak association between Na⁺ and SO₄²⁻ a relationship approximating Harned's rule (with positive α_{12}) was obtained from a simple ion-pairing model.

For the NaCl (component 1)-Na₂CO₃ (component 2)-NaHCO₃ (component 3) system we have made the following assumptions. (1) The species present in the solution in appreciable concentrations were Na⁺, Cl⁻, CO₃²⁻, HCO₃⁻, NaCO₃⁻, and NaHCO₃ (a neutral ion pair). (2) The mean activity of NaCl changes *only* as a result of ion-pair formation, provided the total ionic strength is held constant. This may be expressed as

$$[\text{Na}^+][\text{Cl}^-]\gamma_{\text{Na}}\gamma_{\text{Cl}} = (m_1 + 2m_2 + m_3)m_1(\gamma_{12})^2 \quad (7)$$

where $(m_1 + 2m_2 + m_3)$ is the total concentration of sodium ion and $[\text{Na}^+]$ is the equilibrium concentration of free sodium ion. Since no ion pairs are formed by chloride, $[\text{Cl}^-] = m_1$, and we may define the mean activity of free Na⁺ and Cl⁻ ions to be $\gamma_1' = (\gamma_{\text{Na}}\gamma_{\text{Cl}})^{1/2}$

$$[\text{Na}^+](\gamma_1')^2 = (m_1 + 2m_2 + m_3)(\gamma_{12})^2 \quad (8)$$

Thus γ_1' is assumed to be equal to the mean activity coefficient of NaCl at ionic strength I' . This ionic strength is calculated not on a formal basis but on the basis of the equilibrium concentrations of the various ionic species

$$I' = 1/2\{[\text{Na}^+] + [\text{Cl}^-] + [\text{HCO}_3^-] + 4[\text{CO}_3^{2-}] + [\text{NaCO}_3^-]\} \quad (9)$$

These equilibrium concentrations, in turn, are obtained from the ion-pairing and protonation equilibria

$$[\text{HCO}_3^-] = K_1[\text{H}^+][\text{CO}_3^{2-}] \quad (10)$$

$$[\text{NaCO}_3^-] = K_1'[\text{Na}^+][\text{CO}_3^{2-}] \quad (11)$$

$$[\text{NaHCO}_3] = K_1''[\text{Na}^+][\text{HCO}_3^-] \quad (12)$$

together with the mass balances on the three components

$$[\text{Cl}^-] = m_1 \quad (13)$$

$$[\text{Na}^+] + [\text{NaHCO}_3] + [\text{NaCO}_3^-] = m_1 + 2m_2 + m_3 \quad (14)$$

$$[\text{HCO}_3^-] + [\text{CO}_3^{2-}] + [\text{NaHCO}_3] + [\text{NaCO}_3^-] = m_2 + m_3 \quad (15)$$

An iterative procedure was used to obtain the best values for the ion-pairing constants at each ionic strength. K_1 was taken from Table IV ($\log K_1 = 9.63$ at $I = 3$, 9.75 at $I = 1$, 9.8 at $I = 0.5$). For the first iteration, we assumed $\log K_1' = +0.5$ and $\log K_1'' = -0.5$, values obtained in a less rigorous treatment.⁶

From each experimental value of γ_{12} , a refined value of K_1' (NaCl-Na₂CO₃ electrolytes) or K_1'' (NaCl-NaHCO₃) electrolytes was obtained by the following procedure: assuming $I' = I$, γ_1 was obtained from data for pure NaCl solutions, and using the experimental γ_{12} , $[\text{Na}^+]$ was calculated by eq 8. The remainder of the concentrations were calculated using eq 10 to 15, and a revised value of I' was calculated from eq 9. This procedure was repeated until two successive values of I' agreed to within 0.001, at which point either K_1' or K_1'' was calculated from eq 11 or eq 12. The computer programs and details of the numerical results are given in full elsewhere.⁶

The average values of K_1' and K_1'' obtained at each ionic strength were then used as starting values for second and third approximations by the above procedure. The fourth approximation gave values of the constants which differed by less than 0.001 logarithmic unit, and these are given in Table V, together with their statistical 95% confidence limits.

The curve of $\log \gamma_{12}$ vs. X_1 calculated from these constants is nearly straight, even in the case where ion pairing is strongest: NaCl-Na₂CO₃ at $I = 3$. In Figure 3, the comparison is made with Harned's rule, which seems to be a slightly better fit to the experimental data. An additional curve, calculated assuming $I' = I$, shows what a large effect the formation of ion pairs has on the ionic strength of the medium. Although the ion-pairing model seems to give a slightly poorer fit than Harned's rule, it has the advantage of being easily extended to systems of many components, in a "chemical model." Such models are often invoked, and the approach described here provides a self-consistent and minimal set of empirical assumptions.

Note that the ion-pairing model does *not* explain the deviations (Figure 1) to smaller values of $-\log \gamma_{12}$ at low values of X_1 . For NaCl-NaHCO₃ electrolytes, the calculated curves are almost straight and give about as good a fit to the data as does Harned's rule. Although pH has little effect (in the range near 11.0) on the NaCl-Na₂CO₃ calculations, it has a much stronger effect on the NaCl-NaHCO₃ calculations. At pH 8.2 to 8.6 approximately 2 to 10% of HCO₃⁻ is present as CO₃²⁻ and since the ion pairs of Na⁺ with CO₃²⁻ are an

(20) R. M. Garrels and M. E. Thompson, *Amer. J. Sci.*, **260**, 57, (1962).

(21) R. G. Bates, "Ion-Selective Electrodes," R. A. Durst, Ed., National Bureau of Standards, Washington, D. C., Special Publication No. 314, 1969, Chapter 6.

(22) R. M. Pytkowicz and D. R. Kester, *Amer. J. Sci.*, **267**, 217 (1969).

Table V: Ion-Pairing Constants^a

Ionic strength or reference	$\log K_1'$		$\log K_1''$	
	Measured	Cor to $I = 0$	Measured	Cor to $I = 0$
3.0	0.37 ± 0.06	0.97 ± 0.23
1.0	0.27 ± 0.07	0.96 ± 0.13	-0.67 ± 0.10	-0.30 ± 0.13
0.5	0.14 ± 0.16	0.77 ± 0.18	-0.41 ± 0.19	-0.08 ± 0.20
Reference 5		1.27		-0.26
Reference 4 (<0.01)		0.55		$+0.16 \pm 0.06$

^a K_1' is the formation constant for NaCO_3^- and K_1'' is the formation constant for NaHCO_3 at the ionic strengths given. Errors on the measured values are 95% confidence limits based on the mean-square deviation of values corresponding to each experimental point in Tables I and II. Corrections to $I = 0$ were made with estimated activity coefficients⁶ and the confidence limits have been increased to reflect the estimated error in these values.

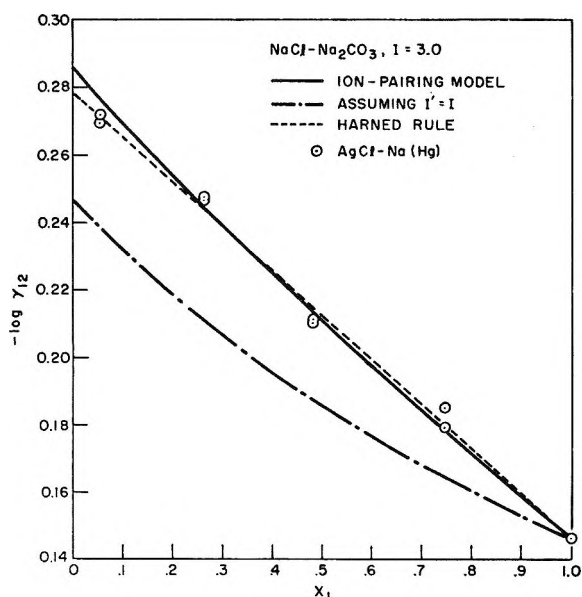


Figure 3. Application of ion-pairing model to $\text{NaCl-Na}_2\text{CO}_3$ electrolytes at ionic strength 3.0 m . Parameters used in calculations: $\alpha_{12} = 0.044$ for Harned's rule; $\log K_1' = +0.37$, $\log K_1'' = -0.67$, $\log K_1 = 9.63$, $\text{pH } 11.2$ for the ion-pairing model.

order of magnitude stronger than those with HCO_3^- , a relatively small change in pH can cause a relatively large change in $[\text{Na}^+]$ and hence in γ_{12} .

The first test of self-consistency—that the constants be independent of composition at constant ionic strength—is satisfied quite well for this system. The second test—that the variation of the constants with ionic strength be consistent with the charge type of the ions involved—may be examined only very approximately at these high ionic strengths, since no rigorous theory exists by which the dependence of these particular combinations of activity coefficients on ionic strength may be determined apart from the experiments we have just performed.

Examination of various approximations for activity coefficients (e.g., γ_{\pm} for NaCl , values for the carbonate and bicarbonate ions calculated by Walker, *et al.*,² the

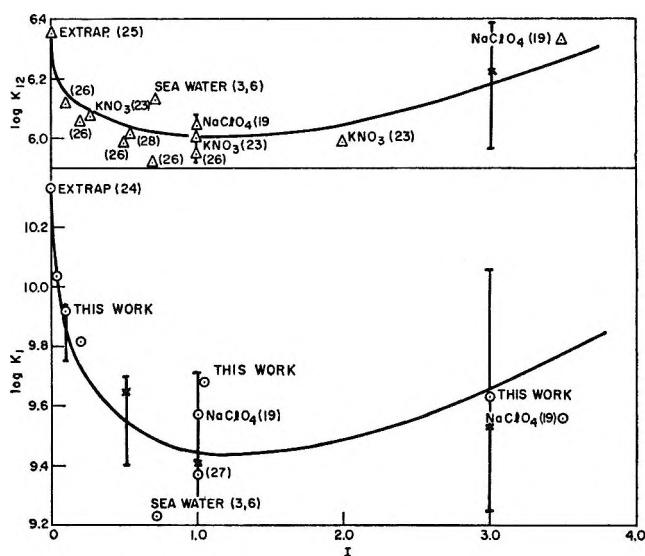


Figure 4. Ionic strength effect on protonation equilibrium constants. The medium is NaCl unless otherwise specified, and references are given in parentheses. Curves were calculated from estimated activity coefficients⁶ and the ion-pairing constants of Table V.

MacInnes assumption $\gamma_K = \gamma_{\text{Cl}}$ employed by Garrels^{5,20}) led us to estimates for the ion-pairing constants at $I = 0$ reported in Table V. Details are given elsewhere.⁶

As we have mentioned above, further evidence for ion pairing between Na^+ and CO_3^{2-} or HCO_3^- may be obtained from the variation of the acid-base equilibrium constants with ionic strength. Some representative values (ref 23–28) are plotted along with data from Table IV in Figure 4. The ionic medium and reference

(23) R. Näsänen, P. Meriläinen, and K. Leppänen, *Acta Chem. Scand.*, **15**, 913 (1961).

(24) H. S. Harned and S. R. Scholes, *J. Amer. Chem. Soc.*, **63**, 1706 (1941).

(25) H. S. Harned and R. Davis, *ibid.*, **66**, 651 (1944).

(26) H. S. Harned and F. T. Bonner, *ibid.*, **65**, 2030 (1943).

(27) S. Bruckenstein and D. C. Nelson, *J. Chem. Eng. Data*, **6**, 605 (1961).

(28) D. Dyrssen and L. G. Sillén, *Tellus*, **19**, 1 (1967).

is noted next to each point. Qualitatively, the association constant of HCO_3^- or CO_3^{2-} with H^+ (K_{12} or K_1) decreases in the presence of added salt in the direction predicted by assuming that the cation of the added salt is competing with H^+ for the carbonate ligand. The differences are small for K_{12} but much larger for K_1 .

However, the effect of increased ionic strength on the activity coefficients also causes the concentration equilibrium constants K_1 and K_{12} to shift in the observed direction. Separation of these two effects may be made by one of two alternatives: either the ion-pairing effect is known from other experiments, or the activity coefficient effect is known from other experiments. Both involve nonthermodynamic assumptions. Most workers^{3b-5} have calculated activity coefficients of the species involved and have obtained estimates of ion pairing from the ionic-strength effect on the protonation equilibria. We have approached from the other direction and have obtained an estimate of the ion-pairing effect from an independent set of experiments.

If the ionic medium (*e.g.*, NaCl) is present in large excess, $[\text{Na}^+]$ is determined only by the total ionic strength and is essentially fixed. Since $[\text{NaCO}_3^-]$ and $[\text{CO}_3^{2-}]$, or $[\text{NaHCO}_3]$ and $[\text{HCO}_3^-]$ are indistinguishable by the usual pH methods and are measured *in toto*, we have

$$([\text{HCO}_3^-] + [\text{NaHCO}_3]) = K_1[\text{H}^+]([\text{CO}_3^{2-}] + [\text{NaCO}_3^-]) \quad (16)$$

and hence

$$K_1 = K_1^0 \left(\frac{\gamma_{\text{H}}\gamma_{\text{CO}_3}}{\gamma_{\text{HCO}_3}} \right) \left(\frac{1 + K_1''[\text{Na}^+]}{1 + K_1'[\text{Na}^+]} \right) \quad (17)$$

where K_1^0 is the acid-base equilibrium constant at zero ionic strength and the activity coefficients are hypothetical single-ion values for which only electrically neutral combinations (*e.g.*, γ_{Na} and γ_{HCO_3}) can be empirically determined. K_1' and K_1'' are formation constants determined in the medium of interest, such as we have given in Table V.

Similarly, we obtain

$$K_{12} = K_{12}^0 \left(\frac{\gamma_{\text{H}}\gamma_{\text{HCO}_3}}{\gamma_{\text{CO}_2}} \right) \left(\frac{1}{1 + K_1''[\text{Na}^+]} \right) \quad (18)$$

The curves drawn on Figure 4 were obtained by means of these equations using the accepted^{24,25} values for the zero ionic strength constants, the previously estimated activity coefficients,⁶ and the ion-pairing constants of Table V. The vertical bars indicate their estimated uncertainty. The contribution of ion pairing to the change in $\log K$ is approximately half that of the activity coefficient term for both K_1 and K_{12} over the whole

ionic strength range, with the exception of K_{12} at $I = 3$, where ion pairing is the principal contribution. The agreement with experimental values is excellent for K_{12} and certainly within the expected uncertainty for K_1 .

It appears that there is little specific effect of chloride since NaCl and NaClO_4 media give comparable values for both constants. Similarly, although K^+ has been assumed to give weaker ion pairs than Na^+ with the carbonate species⁵ this must be compensated for by association between H^+ and NO_3^- since KNO_3 gives the same values for K_{12} as does NaClO_4 or NaCl. Sea water gives a considerably smaller value for K_1 , which can be reasonably attributed to the formation of magnesium carbonate ion pairs,^{3,5,20} and the fact that there is little difference between K_{12} in sea water and NaCl indicates in turn that magnesium bicarbonate ion pairs are rather weak. Perhaps the most important gap in the present collection of data is a reliable set of experimental values for K_1 in NaCl over a wide range of ionic strength. Our experiments at $I = 1.0$ (Table IV) did not agree with the spectrophotometric data obtained by Brucenstein and Nelson,²⁷ and although values of K_1 higher than the curve are suggested by the low-ionic strength data, the NaClO_4 results¹⁹ are lower than ours. One possible explanation could lie in a specific effect of carbonate on the species of the thymol blue indicator used but this has not been investigated further.

As a final point, we should note that the ion-pairing constants of other workers^{4,5} quoted in Table V were in essence obtained from the ionic strength effect on the protonation equilibria. The value of the ion-pairing constants obtained from such an analysis is critically dependent on the assumptions used to calculate the activity coefficients of the ions. As we have seen, the activity coefficient contribution to the ionic strength effect is about twice as large as the ion-pairing effect. In particular, the activity coefficient term in K_1 involves γ_{CO_3} , and this is the major contribution to the uncertainty in values of K_1' calculated from the ionic strength dependence of K_1 . Garrels and coworkers^{5,20} obtained γ_{CO_3} from the paper by Walker, *et al.*,¹ and Nakayama⁴ estimated it from the extended Debye-Huckel equation. These two sets of values may in fact represent the extremes of the range which can be obtained with different activity coefficient assumptions. Our values fall well within this range and thus our model is as consistent as can be expected with previous estimates of ion pairing between Na^+ and HCO_3^- or CO_3^{2-} . It has the advantage of requiring a minimum of *ad hoc* assumptions.

Acknowledgment. This work was supported by the U. S. Department of the Interior, Office of Saline Water.

The Vapor Pressure of Ice between $+10^{-2}$ and -10^{+20} ^{1a}

by Gabor Jancso,^{1b} Jovan Pupezin,^{1c} and W. Alexander Van Hook^{1d}

Chemistry Department, University of Tennessee, Knoxville, Tennessee 37916 (Received January 16, 1970)

The vapor pressure of ice between the triple point and -100° has been reconsidered from two points of view. The results of a new thermodynamic calculation are expressed by the equation $\log P = -2481.604/T + 3.5721988 \log T - 3.097203 \times 10^{-3}T - 1.7649 \times 10^{-7}T^2 + 1.901973$. This equation is compared with our new experimental data and the agreement is found to be within experimental precision.

Introduction

The widespread use of the physical properties of water as reference standards makes it important that its physical properties be determined with the best possible precision and accuracy. Stimson^{2a} has recently reported vapor pressure measurements for the liquid at 25, 40, 50, 60, 70, 80, and 100° to a precision of about 1 part in 50,000 (40° and above). However, the data which are available in the ice range are much less precise. Even at the triple point where the temperature is unequivocally determined and experimentally can be controlled to 0.0001°K ^{2b} the vapor pressure is only determined to about 20 parts in 50,000. Furthermore one soon discovers that the standard compilations most commonly employed by chemists^{3,4} do not generally agree with the best available data within the experimental precision, contain a number of contradictions between themselves, and even make some outright errors. [For example, the tables in ref 3 all equate the vapor pressures of liquid and solid at 0° , the ice point, not, as is correct, at the triple point, 0.01° . The difference is small but readily detected experimentally.] Finally, no new measurements on the vapor pressure of ice have been reported since the 1909 work of Scheel and Heuse⁵ and the measurements of Weber⁶ and Drucker, Jimeno, and Kangro⁷ in 1915.

The standard reference tables^{3,4} are all based on thermodynamic computations rather than empirical fits to the vapor pressure data. Such computations are based on the enthalpy of vaporization at some reference temperature,⁸ the heat capacities of ice⁹⁻¹¹ and vapor,¹² the compressibility of the vapor,¹³ the density of the solid,¹⁴ and one value of the vapor pressure at a known temperature. This is generally taken as either the pressure at 0° (273.15°K) or at the triple point, 0.01° . There is no question that the high precision of the thermodynamic data allows the relative vapor pressure of ice, $P/P_{0.01}$, to be determined with a better precision than that with which it has been measured. This has been pointed out by a number of authors,¹⁵⁻²⁴ but in spite of this we observed that in the region above -20° the various calculations differ from each other by 2, 3, or even more microns. Therefore we concluded that it

would be useful to make a new accurate calculation and to test it with vapor pressure data.

Our interest in this problem originally stemmed from studies being made in this laboratory on aqueous vapor pressure isotope effects²⁵⁻²⁷ where the present results

(1) (a) Research supported by The United States Department of Interior, Office of Water Resources Research, Grant A-012-Tenn and The Petroleum Research Fund of the American Chemical Society; (b) Central Research Institute for Physics, Hungarian Academy of Sciences, Budapest; (c) Permanent address, Boris Kidrich Institute of Nuclear Sciences, Belgrade, Yugoslavia; (d) author to whom correspondence should be addressed.

(2) (a) H. F. Stimson, *J. Res. Nat. Bur. Stand., Sect. A*, **73**, 493 (1969); (b) C. R. Barber, *Metrologia*, **5**, 35 (1969).

(3) (a) N. A. Lange, "Handbook of Chemistry," 10th ed, McGraw-Hill, New York, N. Y., 1967, p 1474; (b) "Handbook Chemistry Physics," 46th ed, Chemical Rubber Publishing Co., Cleveland, Ohio, 1965, p D93; (c) "International Critical Tables," McGraw Hill, New York, N. Y., Vol. 3, 1928, p 210. All of these references reproduce a table based on the calculation of Washburn.¹⁵

(4) "Landolt-Börnstein, Tabellen," Zuhilwerte und Functionen, 6. Auflage, II. Bd-2-teil, Springer-Verlag, Berlin 1960, p 32. This reference reproduces a table based on the calculation of Kelley.¹⁶

(5) K. Scheel and W. Heuse, *Ann. Phys. (Leipzig)*, **29**, 723 (1909).

(6) S. Weber, *Commun. Phys. Lab. Univ. Leiden*, No. 150 (1915).

(7) C. Drucker, E. Jimeno, and W. Kangro, *Z. Phys. Chem. Steochiom. Verwandtschaftslehre.*, **90**, 513 (1915).

(8) (a) N. S. Osborne, *J. Res. Nat. Bur. Stand.*, **23**, 643 (1939); (b) N. S. Osborne, H. F. Stimson, and D. C. Ginnings, *ibid.*, **23**, 197 (1939).

(9) W. Nernst, F. Koref, and F. A. Lindemann, *Sitzber. Berlin Akad. Wiss.*, 247 (1910).

(10) W. F. Giaque and J. W. Stout, *J. Amer. Chem. Soc.*, **58**, 1144 (1936).

(11) P. Flubacher, A. J. Leadbetter, and J. A. Morrison, *J. Chem. Phys.*, **33**, 1751 (1960).

(12) A. S. Friedman and L. Haar, *ibid.*, **22**, 2051 (1954).

(13) F. G. Keyes, *ibid.*, **15**, 602 (1947).

(14) S. LaPlaca and B. Post, *Acta Crystallogr.*, **13**, 503 (1960).

(15) E. W. Washburn, *Mon. Weather Rev.*, **52**, 488 (1924).

(16) K. K. Kelley, *U. S. Bur. Mines, Rep. Invest.*, **383** (1935).

(17) O. Tetens, *Z. Geophys.*, **6**, 297 (1930).

(18) J. A. Goff, *Heat., Pip., Air Cond.*, **14**, 121 (1942).

(19) J. A. Goff, *Trans. Amer. Soc. Heat. Ventilation Eng.*, **48**, 299 (1942).

(20) J. A. Goff and S. Gratch, *ibid.*, **52**, 95 (1946).

(21) J. A. Goff, *ibid.*, **63**, 347 (1957).

(22) J. A. Goff, "Humidity and Moisture," Papers International Symposium, Vol. 3, Washington, D. C., 1963, p 289.

(23) G. A. Miller, *J. Chem. Eng. Data*, **7**, 353 (1962).

(24) F. W. Murray, *J. Appl. Meteorol.*, **6**, 203 (1967).

will be useful. Nonetheless, we feel that water is such an important reference substance that these new results and this new calculation will be of general interest.

In the article which follows we shall employ values of the fundamental constants and conversion factors as tabulated by Cohen.²⁸ These give $R = 82.055 \text{ cm}^3 \text{ atm mol}^{-1} \text{ deg}^{-1}$, and 1 thermochemical calorie = 4.184 J. Temperature is given on the International Practical Temperature Scale of 1948.

Experimental Section

The equipment employed in the present work was designed to measure isotopic vapor pressure differences with high precision and accuracy. Normally the two samples are held inside a common copper block which rests in a thermostated oil bath. The reference side of the apparatus was evacuated for the experiments described in this paper. The temperature of the bath is controlled to 0.001° (above -17°) by means of a solid state proportional controller using a platinum resistance sensor. The control circuitry was designed and built in our laboratory. For the best control (0.001°) it is necessary to circulate thermostated ($\pm 0.01^{\circ}$) cooling fluid at a carefully controlled constant flow so that proper proportional heating is maintained. The cooling fluid was kept approximately 2° below the main thermostat temperature. It in turn was cooled with a PolyScience Corp. KR-60 refrigerator. Below -17° various organic slush baths were employed. We found them to give satisfactory thermal stability (within 0.002° for 20 min).

The pressure transducer, a differential capacitance manometer (Datametrix, Waltham, Mass.), reads out four significant figures with a precision between 0.02 and 0.03% of full scale on any of its four ranges [10–100 mm, 1–10 mm, 0.1–1 mm, 0–0.1 mm]. This corresponds to 2 or 3 μ between -18 and 0° , about 0.3 μ below -18° . Calibration was made using mercury manometry ($\pm 0.01 \text{ mm}$) on the uppermost range. For the final adjustment the gauge was set to the best value of ice vapor pressure at the ice point, 4.581 mm (see below for discussion). The measurements reported here are then interpreted as relative to this fixed pressure. The two independent calibrations checked within the precision of the manometry. The temperature was measured with a Leeds and Northrup 4160 four-terminal platinum resistance thermometer of 25.5 ohms nominal resistance (0°). The resistance was read with a L and N G-1 Mueller Bridge which had been internally calibrated against a L and N 10-ohm standard resistor. Corrections for bridge temperature fluctuation are applied to all readings. The thermometer was calibrated in our laboratory at the ice and steam points. R_{100}/R_0 was found as 1.39267, quite satisfactory.²⁹ A check of the sodium sulfate transition temperature³⁰ yielded a value of 1.494 in the Callendar

equation³¹ in good agreement with the 1.492 calculated from the ice and steam points using the empirical correlation of Stimson.^{32,33} Below 0° we have chosen to employ the Callendar–Van Dusen equation³¹ with a value for β of 0.11 as calculated empirically.^{32,33} It would not appear that the present arbitrary value can be off by more than 5%. The 5% figure introduces an uncertainty which is less than 0.001° above -50° and even at -80° , the lowest experimental point, it amounts only to 0.005° . Since in this region the pressure is determined to only a little better than 0.1 μ , and the temperature coefficient of the vapor pressure is only 7.5 μ/deg (-80°), the temperature uncertainty introduced by the uncertainty in β is negligible in the present context. Above -50° temperature is measured with a precision within 0.001° . Around the ice point this corresponds to $\sim 0.4 \mu$, much less than the standard deviation for a given point. Over the entire range of the experiment then, the imprecision in temperature measurement does not contribute appreciably to the experimental scatter.

Results and Discussion

The experimental data are presented in Table I. We have fit these data by the method of nonlinear least squares using Lietzke's program³⁴ to two, three, four, and five-parameter equations of the proper theoretical form (see below). The data points were weighted according to our best estimate of the experimental precision. The five-parameter fit was chosen in strict analogy to our derived theoretical equation (eq 13). We noted, however, that the terms in $\log T$, T and T^2 were only of minor importance (since the heat capacity expansion, (eq 8), is nearly linear and ΔC_p itself is very small) and so also fit the data to four, three, and two-constant equations. Statistically there is very little reason to choose between the 2, 3, 4, and 5-parameter experimental fits and we are unwilling to ascribe physical meaning to the parameters in the longer equations. Therefore only the two-constant experimental fit (eq 1) is reported.

(25) W. A. Van Hook, *J. Phys. Chem.*, **72**, 1234 (1968).

(26) G. Jancso, J. Pupezin, and W. A. Van Hook, *Nature*, **225**, 723 (1970).

(27) J. Pupezin, G. Jancso, and W. A. Van Hook, in preparation.

(28) E. R. Cohen, *Rev. Mod. Phys.*, **37**, 537 (1965).

(29) H. F. Stimson, D. R. Lovejoy, and J. R. Clement, in "Experimental Thermodynamics," Vol. I, J. P. McCullough and D. W. Scott, Eds., I.U.P.A.C., Plenum Publishing Co., New York, N. Y., 1968.

(30) H. F. Stimson, *J. Res. Nat. Bur. Stand., Sect. A*, **65**, 139 (1961).

(31) D. Robertson and K. A. Welch in "Temperature, Its Measurement and Control," C. M. Herzfeld, Ed., Reinhold, New York, N. Y., 1962, p 291.

(32) H. F. Stimson, *Process-Verb. Seances, Com. Int. Poids Mes.*, **23B**, T 104 (1952).

(33) R. J. Corruccini in "Temperature, Its Measurement and Control," C. M. Herzfeld, Ed., Reinhold, New York, N. Y., 1962, p 329.

(34) M. H. Lietzke, ORNL-3259.

Table I: Experimental Vapor Pressures of Ice

Temp, °C	P (int mmHg)	Temp, °C	P (int mmHg)
-1.474	4.050	-15.441	1.189
-1.477	4.050	-15.443	1.189
-2.475	3.725	-15.751	1.154
-2.477	3.724	-25.080	0.4698
-2.971	3.573	-25.147	0.4668
-2.978	3.572	-25.225	0.4629
-2.982	3.572	-25.277	0.4607
-3.468	3.426	-25.333	0.4584
-3.469	3.430	-25.417	0.4550
-3.471	3.226	-35.470	0.1603
-3.474	3.429	-35.553	0.1589
-3.930	3.299	-35.616	0.1580
-3.931	3.299	-35.669	0.1572
-4.990	3.009	-35.821	0.1526
-5.002	3.007	-35.825	0.1526
-5.009	3.006	-36.203	0.1486
-5.012	3.005	-36.206	0.1484
-5.014	3.011	-36.223	0.1482
-5.016	3.010	-36.230	0.1482
-6.011	2.763	-45.626	0.05146
-6.011	2.763	-45.627	0.05149
-7.011	2.531	-45.628	0.05154
-7.012	2.531	-45.631	0.05135
-7.998	2.322	-45.636	0.05154
-8.002	2.321	-45.637	0.05165
-8.086	2.309	-45.640	0.05167
-9.012	2.129	-45.642	0.05168
-9.014	2.129	-63.758	0.00544
-9.028	2.125	-63.761	0.00533
-9.030	2.125	-63.765	0.00528
-10.016	1.948	-63.767	0.00531
-10.026	1.946	-78.496	0.00063
-11.014	1.780	-78.501	0.00062
-11.015	1.780	-78.504	0.00054
-12.020	1.628	-78.509	0.00060
-12.032	1.627		
-13.010	1.488		
-13.012	1.487		
-13.985	1.360		
-13.986	1.360		
-14.949	1.245		
-14.952	1.245		

$$\log P = -2668.726/T + 10.43112 \quad (1)$$

The Reference Pressure

The value of the vapor pressure at the ice point, P_0 , has been determined by only two groups of workers. Thiesen and Scheel³⁵ in 1900 gave $4.579_2 \pm 0.001$ with a spread of 0.0036, while Scheel and Heuse⁵ got $4.578_8 \pm 0.0006$ with a spread of 0.0030. The latter measurements were reported in 1909. Both sets of measurements appear to have been made on supercooled water and the values corrected to the triple point, P_{01} , become 4.582_5 and 4.582_1 , respectively. A posthumous paper of Prytz³⁶ in 1931 reported three measurements of P_{01} with a mean of 4.5867 mm and a spread of 0.0014. These data have been critically considered by at least two authors. Osborne³⁷ chooses to take the un-

weighted mean, $4.584_2 \pm 0.001$, while Veinberg³⁸ prefers a weighted mean, 4.585 ± 0.002 . We are in agreement with Veinberg that the more reasonable value is 4.585 mm. The most recent U. S. revision of the steam tables³⁹ quotes P_{01} as 4.585 but the latest United Kingdom table⁴⁰ gives $P_{01}(\text{liq}) = 4.584$.

It is clear that a definitive redetermination of either P_{01} or P_{00} is called for. This would be particularly useful as a pressure standard because the temperature is unambiguously defined at P_{01} and intercomparison between laboratories is facilitated. In this regard it is worth noting that direct comparison between the data which we report in the present paper and the bulk of the earlier work⁵⁻⁷ is made difficult because of ambiguities connected with the old temperature measurements. This is of course not true for the measurements made at the ice point or the triple point. [Note that the theoretical equation which is developed later in this paper will still be valid following a redetermination of P_{01} , subject only to modification of the constant of integration, I .]

The Calculation from Thermodynamic Data

The vaporization of a molecular substance to an essentially monomeric vapor phase is generally considered in terms of the Clapeyron equation

$$\frac{dP}{dT} = \frac{\Delta H}{T\Delta V} \quad (2)$$

where ΔH is the enthalpy of vaporization and ΔV the volume increase. ΔH and ΔV are dependent on the temperature and on gas imperfection and corrections can be applied so that exact integration of eq 2 is possible.¹⁸⁻²² We, however, choose to write the vaporization as a reaction whose equilibrium constant is the ratio of the vapor fugacity, f_g , to the condensed phase activity, a_c ⁴¹

$$\frac{d \ln (f_g/a_c)}{dT} = \frac{\Delta_{sv}H^\circ_T}{RT^2} \quad (3)$$

Here all gas imperfection effects are included in the f_g/P ratio for the gas, the effect of the condensed phase volume is incorporated in a_c . Thus $\Delta_{sv}H^\circ_T$ is the heat of sublimation (at temperature T) to the ideal gas in its standard state from the solid in its standard state (des-

(35) M. Thiesen, K. Scheel, *Wiss. Abh. Phys.-Tech. Reichsanst.*, **3**, 71 (1900).

(36) K. Prytz, *Math. Fys. Meddeleisen Danske Vidensk. Selskab*, **2**, No. 2, 1 (1931).

(37) N. S. Osborne, personal communication to F. G. Keyes, 1934, as quoted in ref 13, p 608.

(38) B. R. Veinberg, *J. Exptl. Theoret. Phys. (U.S.S.R.)*, **9**, 106 (1939).

(39) J. H. Kennan, F. G. Keyes, P. G. Hill, and J. G. Moore, "Steam Tables (International Edition)," Wiley, New York, N. Y., 1969.

(40) R. W. Bain, "Steam Tables 1964," Her Majesty's Stationery Office, Edinburgh, 1964.

(41) G. N. Lewis and M. Randall, "Thermodynamics," as revised by K. S. Pitzer and L. B. Brewer, McGraw-Hill, New York, N. Y., 1961, pp 532-533.

ignated by the superscript degree). Both standard states are taken at one atmosphere.

It is first necessary to find $\Delta_{sv}H^{\circ}_T$ from the available thermodynamic data. We begin by defining the enthalpy of the liquid at the ice point and its equilibrium vapor pressure, $H_{273.15}(\text{liq}, P_{\text{eq}})$, as zero—the reference level for the relative enthalpies, L_T , [$L_T(\text{phase}, P) = H_T(\text{phase}, P) - H_{273.15}(\text{liq}, P_{\text{eq}})$; $\Delta_{ij}L_T(P) = L_T(\text{phase } j, P) - L_T(\text{phase } i, P)$]. Data are available for the enthalpy of vaporization of the liquid^{8b} (at the equilibrium pressure) and for the enthalpy of fusion^{8a} (at one atmosphere) at 0° . In order to find $L_{273.15}(\text{solid}, 1 \text{ atm}) = L^{\circ}_{273.15}(\text{solid})$ we subtract the measured heat of fusion, $\Delta_{1s}H^{\circ}_{273.15}$ from the standard state liquid relative enthalpy, $L^{\circ}_{273.15}(\text{liq})$. This latter may be obtained by correcting the enthalpy of the liquid under its own vapor pressures to one atmosphere with eq 4.

$$\left(\frac{dH}{dP}\right)_T = V - T\left(\frac{dV}{dT}\right)_P \quad (4)$$

For purposes of the correction the density and thermal expansion data of Kell⁴² were employed. We found $L^{\circ}_{273.15}(\text{liq}) = 0.44 \text{ cal/mol}$ in agreement with earlier workers,^{8b} and thus obtain $L^{\circ}_{273.15}(\text{solid}) = -1435.7 \text{ cal/mol}$.

It is next necessary to calculate the enthalpy of the ideal vapor at one atmosphere and 0° . This entails application of the real gas correction to the measured heat of evaporation [since $\Delta_{1v}L_{273.15}(\text{meas}) = L_{273.15}(\text{real vapor}, P_{\text{eq}})$]. For this purpose we employed the second virial coefficients of Keyes¹³ as given by Eisenberg and Kauzmann.⁴³ The corrective term amounts to only 1.8 cal/mol; and $L^{\circ}_{273.15}(\text{ideal vapor}) = 10,765.1$ so $\Delta_{sv}L^{\circ}_{273.15} = 12,200.8 \text{ cal/mol}$. [$\Delta_{sv}L^{\circ}_{273.16}$ may be taken as identical to $\Delta_{sv}L^{\circ}_{273.15}$ with an accuracy which is well within the experimental precision involved in the enthalpy determinations.]

Equation 3 can then be integrated by introducing the temperature dependence of $\Delta_{sv}L^{\circ}_T$. This was taken in standard fashion as

$$\Delta L^{\circ}_T = \Delta L^{\circ}_{273.16} + \int_{273.16}^T \Delta C_p^{\circ} dT \quad (5)$$

where ΔC_p° was determined from the heat capacity data of Friedman and Haar¹² for the ideal vapor and those Giaque and Stout¹⁰ for the crystal. These data were fitted by least squares over the temperature region of interest.⁴⁴ Integration from the triple point, $T_{273.16}$, to temperature T , gives

$$R \ln (f_g/a) = \frac{-\Delta L^*}{T} + \Delta a \ln T + \frac{\Delta b}{2}T + \frac{\Delta c}{6}T^2 + I \quad (6)$$

where

$$-\Delta L^* = \left[-\Delta_{sv}L^{\circ}_{273.16} + \Delta a T_{273.16} + \frac{\Delta b}{2}T_{273.16}^2 + \frac{\Delta c}{3}T_{273.16}^3 \right] \quad (7)$$

Δa , Δb , and Δc come from the heat capacity expansion

$$\Delta c_p = \Delta a + \Delta b T + \Delta c T^2 \quad (8)$$

and I is the constant of integration

$$I = -\Delta a(1 + \ln T_{273.16}) - \Delta b T_{273.16} - \frac{\Delta c}{2}T_{273.16}^2 + \frac{\Delta_{sv}L^{\circ}_{273.16}}{T_{273.16}} + R \ln (f_{273.16}/a_{273.16}) \quad (9)$$

The real gas correction is given to sufficient accuracy by the second virial correction, so we may write

$$\ln P = \frac{1}{R} \left(-\frac{\Delta L^*}{T} + \Delta a \ln T + \frac{\Delta b}{2}T + \frac{\Delta b}{6}T^2 + I \right) - \frac{B(T)P}{RT} + \ln a \quad (10)$$

B is obtained from the equations given by Eisenberg and Kauzmann⁴³ and P (right-hand side) from eq 6 assuming $f/a = P$. The corrections we are evaluating are very small and a second iteration will not be necessary. The term, $\ln a$, was evaluated from the integral

$$\ln a = \int_1^P \frac{V}{RT} dP \quad (11)$$

where V , the molar volume of ice, was taken from LaPlaca and Post¹⁴ following Eisenberg and Kauzmann.⁴⁵ I is then evaluated from eq 10 by substituting in the triple point pressure $P_{273.16} = 4.585 \text{ mm}$.

The corrective terms in eq 10, $-BP/RT$ and $\ln a$, are small and we evaluated them numerically at different temperatures and fit the results by least squares. For example at 0° $-BP/RT$ corresponds to 2.3×10^{-3} mm and $\ln a$ to -4.0×10^{-3} mm. At -20° the figures are 0.11×10^{-3} mm and -0.72×10^{-3} mm. The least-square polynomial fit to the sum is

$$\left[\frac{-BP}{RT} + \ln a \right] \frac{1}{\ln 10} = 1.717 \times 10^{-3} - 2.2574 \times 10^{-5}T + 5.714 \times 10^{-8}T^2 \quad (12)$$

(42) G. S. Kell, *J. Chem. Eng. Data*, **12**, 66 (1967).

(43) D. Eisenberg and W. Kauzmann, "The Structure and Properties of Water," Oxford University Press, London, 1969, p 48.

(44) This was 0° to -100° . Note that shortly below -100° a ripple appears in the otherwise smooth heat capacity reported for the solid.¹⁰ This region is not included in our fitting procedure and for this reason extrapolation of our calculations below -100° is not warranted.

(45) Reference 41, p 104.

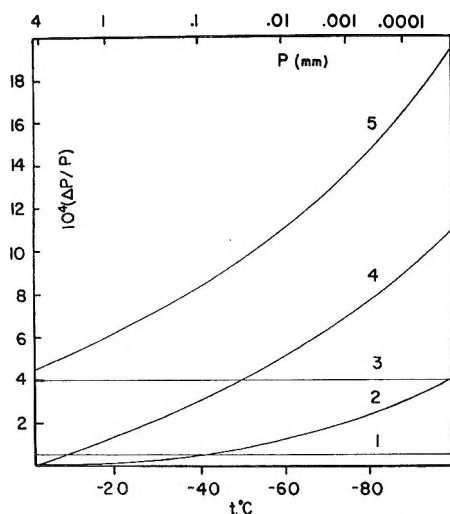


Figure 1. Estimated errors in pressures calculated by eq 13: 1, from fits to vapor fugacity and solid activity; 2, from uncertainty in ΔC_p ; 3, from uncertainty in the reference pressure; 4, from uncertainty in $\Delta_{sv}L^\circ_{273.15}$; 5, total estimated error (sum of 1, 2, 3, and 4).

and, collecting terms, and evaluating constants, eq 10 becomes

$$\log P = \frac{-2481.604}{T} + 3.5721988 \log T - 3.097203 \times 10^{-3}T - 1.7649 \times 10^{-7}T^2 + 1.901973 \quad (13)$$

At the triple point the uncertainty in eq 13 is mainly determined by the uncertainty in the assignment of the reference pressure. This we have taken as $\pm 2 \mu$ so $\Delta p/p \approx 2/4585 \approx 4 \times 10^{-4}$. As the temperature is lowered, contributions from the experimental uncertainties in the enthalpy (~ 1 cal/mol) and the heat capacity determinations become important. We have assessed these errors and plot the results in Figure 1.

Earlier Equations. The most important earlier calculations are those of Washburn,¹⁵ Kelley,¹⁶ Tetens,¹⁷ Goff,¹⁸⁻²² Miller,²³ and Goff, as expressed by Murray.²⁴

The Washburn calculation is the most familiar to chemists as it is the results of this calculation which are reported in the "International Critical Tables" and in turn reproduced in many editions of Lange's "Handbook of Chemistry," and in the "Handbook of Chemistry and Physics."²³ This calculation is the one reproduced by Keenan and Keyes⁴⁶ in their 1936 steam tables and even the new 1969 tables³⁹ seem only to update this calculation by multiplying each and every entry by the ratio of the new and old reference pressures. The original Washburn calculation incorrectly equates the solid and liquid vapor pressures at 0° , not, as would be proper, at the triple point. Kelley¹⁶ derived an equation for the free energy difference, $\Delta_{sv}G$. Subsequent authors⁴ have converted Kelley's equation to an ex-

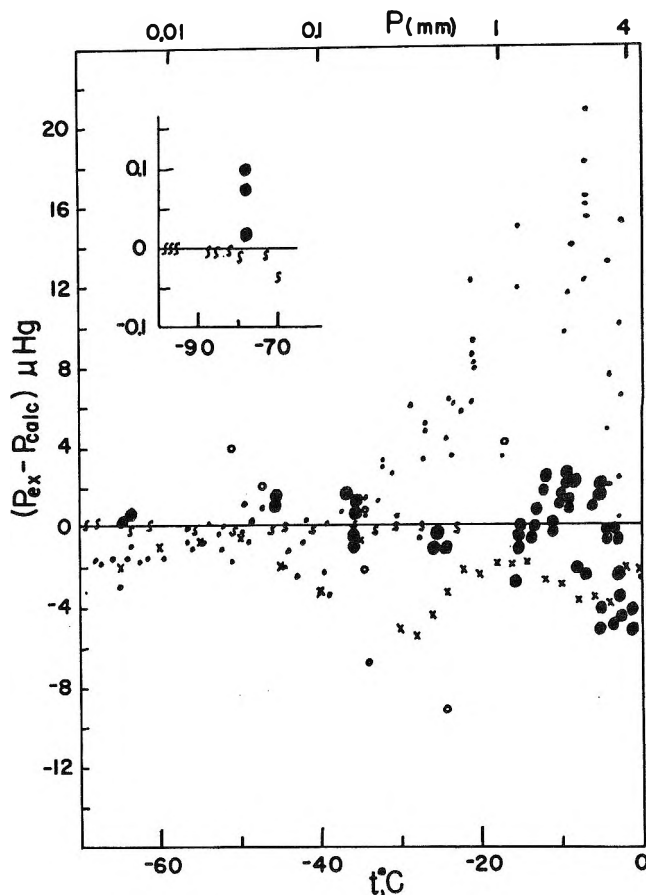


Figure 2. The available experimental data compared with eq 13: ●, present work; ·, Scheel and Heuse,⁶ ×, Warmetabellen;⁴⁴ √, Weber,⁸ ○, Drucker, Jimeno, and Kangro.⁷

PLICIT expression for $\log P$. From Kelley's original equation we conclude that at pressures above 1 mm the predicted vapor pressures should be good only to the nearest 0.01 mm. Unfortunately, the Landolt-Bornstein⁴ tabulated values have been forced to the nearest 0.001 mm, and in addition there appears to be a difference between the equation which they give and their tabulated values. Thus as far as the tables commonly employed by chemists and physicists are concerned the situation was unacceptable.

Among the equations which we will label as "less available" are a very old empirical fit due to Tetens¹⁷ and a newer calculation of Miller.²³ The latter is claimed to be highly accurate but an explicit equation is not quoted, and also, in our opinion, an inordinately low reference pressure, $P_{01} = 4.579$, was chosen.

A very careful calculation is that due to Goff.¹⁸⁻²² The original Goff and Gratch 1946 calculation²⁰ has been subsequently modified^{21,22} to allow for the changes made in the definition of the temperature scale, etc. Goff's most recent choice of $P_{01} = 4.584$ (to the nearest

(46) J. H. Keenan and F. G. Keyes, "Steam Tables," Wiley, New York, N. Y., 1936.

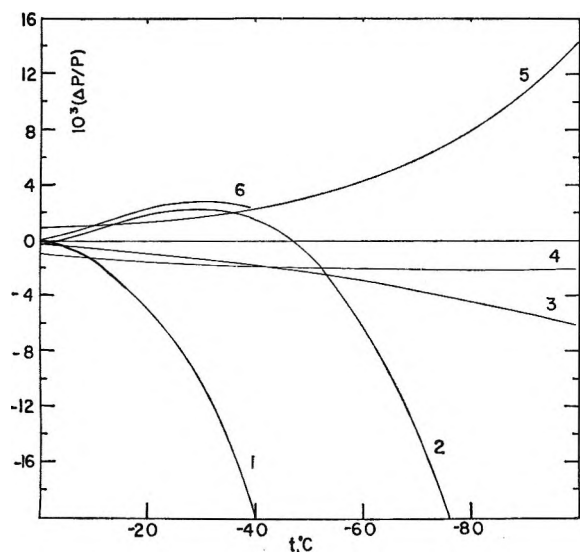


Figure 3. Comparison between eq 13 and other calculations: 1, Tetens;¹⁷ 2, Washburn;¹⁶ 3, Goff;¹⁸⁻²² 4, Miller;²³ 5, Kelley;¹⁶ 6, steam tables.³⁹

micron) is reasonable. The agreement between Goff's calculation and the present one is satisfactory. Quite recently, Murray²⁴ claims to have modified the Goff-Gratch equations to a more convenient algebraic form. Unfortunately he seems to have made an error in the transposition of the temperature scales.

Intercomparisons. A difference plot between eq 13 and the available measurements is shown in Figure 2. The maximum difference between the least-square fit (eq 1) and eq 13 is -0.8μ at -5° . The present data appear to be about two times more precise than the early German work. The graph shows both the points as originally reported and again as corrected by Holborn, Scheel, and Henning.⁴⁷ The lower temperature data of Weber⁶ are in very good agreement with the cal-

culated line. The present data show just about the scatter which was anticipated from the specifications of the pressure transducer. The variance of the raw data about the theoretical line is very nearly the same as that about the least-square fits, and thus within our experimental criteria the thermodynamic calculation is a proper one. However, it is interesting to notice that both our data and those of Holborn, Scheel, and Henning⁴⁷ are consistently low above -5° .

Difference plots between eq 13 and the various earlier calculations are shown in Figure 3. Differences as large as 6μ are found.

Conclusions

A new calculation and new measurements of the vapor pressure of ice between -100° and the triple point have been reported. Good agreement was found. It does not appear useful to make further experimental measurements or thermodynamic calculations of the type we describe until after a definitive redetermination of the triple-point pressure has been obtained. The precision of the calculations is such that it would be useful to have P_{01} determined to within 0.1μ .

Acknowledgment. This work was supported by the U. S. Department of the Interior, Office of Water Resources Research, A-012 Tennessee, and The Petroleum Research Fund, American Chemical Society. Grateful acknowledgment is made to the donors. Thanks are also extended to the University of Tennessee Computing Center for a generous donation of computing time. We should like to thank Dr. M. H. Lietzke for helpful discussions concerning the fitting of the data.

(47) L. Holborn, K. Scheel, and F. Henning, "Warmetabellen der Physikalisch-Technischen Reichsanstalt," F. Vieweg und Sohn, Braunschweig, 1919.

A Near-Infrared Spectroscopic Method for Investigating the Hydration of a Solute in Aqueous Solution^{1a}

by William C. McCabe^{1b} and Harvey F. Fisher

Department of Biochemistry, University of Kansas Medical Center, Kansas City, Kansas, and Veterans Administration Hospital, Kansas City, Missouri 64128 (Received February 9, 1970)

Near-infrared difference spectra of aqueous solutions of some alkali halides measured *vs.* water were resolved into two components, one representing the hydration of the solute, and the other, the volume of the hydrated solute. For each salt studied, a number of hydration parameters were determined from these two spectral components: (1) the molar excluded volume of the hydrated solute, V_{excl} ; (2) the molar hydration volume, nV_0 ; (3) the hydration number, n ; (4) the electrostriction; (5) the variation of n and of electrostriction with concentration and with anion or cation; and (6) the nature of the interaction of anions and cations with water. The results reported here are correlated with results obtained from measurements of the compressibility of aqueous solutions of alkali halides.

I. Introduction

McCabe and Fisher^{2a} have shown that near-infrared difference spectra of aqueous solutions measured *vs.* water consist of three components: (1) a negative component, consisting of an absolute spectrum of the amount of water excluded by the hydrated solute; (2) a positive component, contributed by the water of hydration of the solute; and (3) an additional component consisting of the absorption (if any) by the solute itself. We show here that resolutions of such difference spectra permit the quantitative evaluation of a number of parameters related to the hydration of solutes in aqueous solution.

We have chosen the alkali halides as the solutes in this study for several reasons: their difference spectra show relatively large hydration components; they have no significant absorption in this region of the spectrum; and there is a substantial amount of information in the literature concerning their hydration. The 1.45- μ band of water, assigned^{2b} to $\nu_1 + \nu_3$, was chosen for this investigation.

II. Experimental Section

NaCl, NaBr, NaI, KCl, KBr, and KI were analytical reagents obtained from Mallinckrodt Chemical Works. The CsCl and RbCl were 99.9% pure reagents obtained from K and K Laboratories, Inc. The solvent was deionized tap water.

Spectra were obtained using a modified Cary Model 14 double-beam recording spectrophotometer equipped with either a 0.0–0.1 or a 0.0–1.0 slide wire. Absorption cells were of the insert type with pathlengths of 0.1000 \pm 0.0001 cm.

In each experiment, the sample cell contained an aqueous salt solution and the reference cell contained water alone. The cells were thermostated by circulating water at 20° through metallic cell holders which

were in direct contact with over 50% of the cell surface. Temperature variations constitute the major source of error in the spectra obtained. The temperature was controlled to 20 \pm 0.01°.

An absorption base line, obtained by recording the spectrum of water *vs.* water under the same experimental conditions for solution difference spectra, was used to calculate the differential absorbance of solution *vs.* water. This base line was constant with time, indicating the absence of significant temperature fluctuations between the sample and reference absorption cells. The precision of the absorbance measurements is approximately \pm 2%.

III. Terminology and Equations

A. Definition of Terms. V_{in} is the intrinsic molar volume of the solute. ϕ_v is the apparent molar volume of the solute. V_{el} , the electrostriction volume, is the reduction in the volume of the solvent due to the interaction of the solvent with the solute. nV_0 , the hydration volume, is the volume of that portion of the solvent which interacts with the solute. The term V_0 represents the molar volume of this portion of the solvent and n represents the number of moles solvated. V_{excl} , the molar excluded volume of the hydrated solute, is that volume of the solution which is not accessible to the noninteracting solvent.

B. Equations which Show the Relationship between These Terms. Equation 1 is derived from the definition of electrostriction.

(1) (a) This work was supported in part by a Public Health Service research grant (GM 15188) from the National Institutes of Health and a National Science Foundation grant (GB 3915); (b) supported by a predoctoral fellowship from the National Institutes of Health (5-F1-GM-34,000).

(2) (a) W. C. McCabe and H. F. Fisher, *Nature*, **207**, 1274 (1965); (b) G. Herzberg, "Infrared and Raman Spectra of Polyatomic Molecules," D. Van Nostrand, New York, N. Y., 1945, p 281.

$$V_{el} = V_{in} - \phi_v \quad (1)$$

An expression which is equivalent to eq 1 has been introduced by Goto.³ Rearranging eq 1 gives eq 1a.

$$\phi_v = V_{in} - V_{el} \quad (1a)$$

Equation 2 is derived from the definition of the term V_{excl} .

$$V_{excl} = V_{in} + nV_h \quad (2)$$

Equation 3 is derived from the definition of the terms nV_h and V_{el} .

$$nV_0 = nV_h + V_{el} \quad (3)$$

In eq 3, V_0 is the molar volume of water at a given temperature and pressure. Equation 4 is derived from eq 1a and 2.

$$V_{excl} - \phi_v = (V_{in} + nV_h) - (V_{in} - V_{el}) = nV_h + V_{el} \quad (4)$$

Equation 5 is derived from eq 3 and 4.

$$nV_0 = V_{excl} - \phi_v \quad (5)$$

Equation 6 was introduced by Padova.⁴

$$\phi_s = V_{in} + nV_h = \phi_v + nV_0 \quad (6)$$

where ϕ_s is the molar solvated volume.

Rearranging eq 6 gives eq 6a.

$$nV_0 = \phi_s - \phi_v \quad (6a)$$

It is apparent from a comparison of eq 2 and 5 with those worked out by Padova, *i.e.*, eq 6 and 6a, that V_{excl} is equivalent to ϕ_s . Equation 7 was derived by Padova;⁴ it is included here for reference.

$$\begin{aligned} \phi_s &= 10^3/C - (10^3d - CM - nCM_0)/Cd_0 \\ &= 10^3(d_0 - d)/Cd_0 + M_2/d_0 + nM/d_0 \end{aligned} \quad (7)$$

Equation 8 is commonly used to express ϕ_v in terms of density.

$$\phi_v = 10^3(d_0 - d)/Cd_0 + M_2/d_0 \quad (8)$$

In both eq 7 and 8, C is the molar concentration of solute; d_0 is the density of the solvent; d is the density of the solution; M_0 is the molecular weight of the solvent; M is the molecular weight of the solute. Equation 9 is derived from eq 7 and 8 and the definition of nV_0 (see eq 3).

$$\phi_s - \phi_v = nM/d_0 = nV_0 \quad (9)$$

This relationship was introduced above in eq 6 and 6a. Here, d_0 is the density of normal water (water at 20°).

The variation of electrostriction with hydration can be expressed by an electrostriction factor (EF) defined in eq 10. Equation 11 is derived from eq 2 and 5.

$$EF = V_{el}/nV_0 \quad (10)$$

$$EF = (V_{in} - \phi_v)/(V_{excl} - \phi_v) \quad (11)$$

Tamura and Sasaki⁵ derived an expression, eq 12, from the empirical equation of Tait to represent electrostriction associated with salts at infinite dilution.

$$(\Delta V)/V_E = 0.4343(c)/V_1^{P_0} = 0.1338 \quad (12)$$

Electrostriction is calculated from compressibility data using eq 12. Equation 12 is equivalent to eq 10 in that, by definition, ΔV equals V_{el} and V_H equals nV_0 . This equation, which indicates that ΔV varies directly with V_H , was verified for a large variety of salts at infinite dilution.⁵ It was shown to be independent of temperature.⁵ The average value for $0.4343C/V_1^{(P_0)}$ and hence $\Delta V/V_E$ (0.1338)⁵ differs from those obtained by Carl⁶ (0.1243) and by Gibson⁷ (0.1368). The average of these three values is 0.1316.

IV. Determination of the Hydration of Solutes in Aqueous Solution

A. Excluded Volume Method. According to eq 5, the amount of hydration per mole of solute, nV_0 , equals $V_{excl} - \phi_v$. The quantity ϕ_v can be obtained from eq 8. The density data used in eq 8 to calculate ϕ_v for many salts is available in the literature. The quantity V_{excl} is calculated from near-infrared difference spectra of aqueous solutions measured *vs.* water as described below.

Description of a Typical Difference Spectrum. Curve A in Figure 1 is the near-infrared difference spectrum of an aqueous 3 M NaCl solution (sample cell) measured *vs.* water (reference cell). This spectrum represents absorption which is entirely due to various forms of water only since the solute, NaCl, has no significant absorption in this region of the spectrum. The recorded difference spectrum, curve A, is negative because the reference-cell absorption is greater than the sample-cell absorption at all wavelengths.

The difference spectrum, curve A, can be resolved into two arbitrary component spectra, one (curve B) representing the net contribution of the absorption by the water in the reference absorption cell, and the other (curve C) representing the net contribution of the absorption by the water in the sample absorption cell. Thus, curve A equals curve C minus curve B.

A schematic representation of this system is presented in Figure 2. The contents of the sample and reference absorption cells as well as the differences between the contents of the two cells are diagrammed in the upper row of figures. The corresponding spectral contributions as well as a summary of the differences between them are presented in the lower row of figures. The relationship between the different volume ele-

(3) S. Goto, *Bull. Chem. Soc. Jap.*, **37**, 1685 (1964).

(4) J. Padova, *J. Chem. Phys.*, **40**, 691 (1964).

(5) K. Tamura and T. Sasaki, *Bull. Chem. Soc. Jap.*, **36**, 975 (1963).

(6) H. Carl, *Z. Phys. Chem.*, **101**, 238 (1922).

(7) H. S. Harned and B. B. Owen, "The Physical Chemistry of Electrolytic Solutions," 3rd ed, Reinhold, New York, N. Y., 1958, p 380.

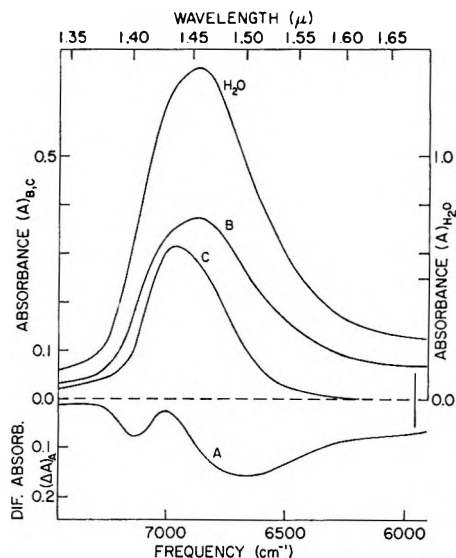


Figure 1. Determination of the hydration and excluded volume spectra for 3 M NaCl. Curve A is the difference spectrum for 3 M NaCl measured *vs.* water; the absorption pathlength was 0.1 cm; the absorption cells were thermostated at 20°. Curve B is the normalized water spectrum; it was determined by normalizing the spectrum for water measured *vs.* absorption cell (curve H₂O) to curve A at 1.68 μ . Curve C is the hydration spectrum for 3 M NaCl; it was obtained by adding curve B to curve A. Curve H₂O is the absorption spectrum for water measured *vs.* absorption cell; the absorption cell path length was 0.1 cm; the absorption cells were thermostated at 20°.

ments of the solutions in the two absorption cells and their corresponding absorption spectra is apparent from this figure.⁸

Resolution of Curve B from the Difference Spectrum. Curve B can be determined from curve A and curve H₂O. Both these curves are presented in Figure 1. Curve H₂O is the absorption spectrum of normal water (water at 20°). Since the reference absorption cell contains only normal water, curve B (the reference cell contribution) must have the same shape as the spectrum of normal water, *i.e.*, curve H₂O in Figure 1.

A minimum magnitude for the size of curve B can be determined from the difference spectrum, curve A. The procedure for determining this minimum magnitude must satisfy two criteria. (1) All of the negative character of the recorded difference spectrum (curve A) results from the absorption by the excess water in the reference absorption cell, *i.e.*, curve B. Therefore, the minimum contribution of curve B to curve A is that amount which, when added to curve A, will cancel all of the negative character of curve A. The resultant spectrum (curve C) must, therefore, be either positive or zero at all wavelengths. (2) Curve B can be determined by "normalizing"⁹ the recorded absorbance of a water spectrum (curve H₂O) to curve A at a particular frequency. The frequency which is chosen for normalization should be such that criterion (1) for the sum of curve B and curve A is satisfied.¹⁰ This

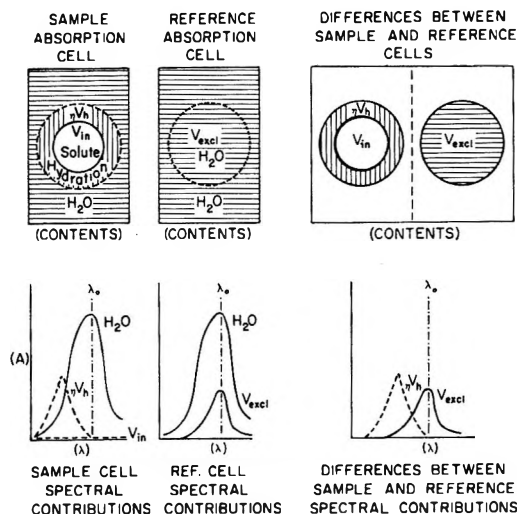


Figure 2. Schematic representation of the solution and spectral components of a typical difference spectrum system. The upper row of figures represent both the contents and the differences between the contents of the sample and reference cells. The lower row of figures represent the corresponding spectral contributions to the difference spectrum.

normalized water spectrum is shown in Figure 1 (curve B) in the positive sense. It represents the minimum net contribution from the absorption by the water in the reference absorption cell to the recorded difference spectrum, curve A.

Resolution of Curve C from the Difference Spectrum. Curve C can be determined directly from curves A and B. Curve C equals curve A plus curve B. The determination of curve C is based on the original, arbitrary definition of curves B and C, *i.e.*, curve A equals curve C minus curve B.

Errors in Curves B and C. The magnitudes of the absorbance at each frequency for curves B and C, as determined, are both minimal values. The only indeterminate error which is possible in these curves would be a normal water spectrum of some unknown magnitude, since we have added the spectrum of the minimal amount of water required to satisfy criterion (1). Curves B and C are directly dependent on one another

(8) This representation of the different volume elements in an aqueous solution is purely schematic and not meant to imply that there need be any similarity between the elements represented in Figure 2 and the actual physical state of these components in solution.

(9) The "normalization factor" is calculated at a given frequency as the ratio of the absolute value for the differential absorbance for curve A to the absorbance at the same frequency for curve H₂O. Then curve B is obtained by multiplying the recorded absorbance of water at each frequency by the "normalization factor." Thus, curve B will retain the shape of curve H₂O but will be of reduced magnitude. For the curves represented in Figure 1, the frequency chosen is 5952 cm⁻¹ (1.68 μ) and the normalization factor is 0.273.

(10) This argument is valid only for a single absorption band region, *e.g.*, the 1.45- μ absorption band. The absorption band region can be defined arbitrarily as the region of the absorption spectrum between two minima, *e.g.*, from approximately 1.26 μ to 1.69 μ for the 1.45- μ absorption band.

and the error in one must be the same as that in the other.

Relationship between the Absorption Represented by Curve C and the Hydration. Curve C and curve H₂O represent the absorption by different types of water. This is apparent from a comparison of the shapes of the two absorption curves. Water, with absorption properties which differ from those of normal water, is assumed to be "hydrated water."¹¹ Since water interacting with the solute is hydration by definition, curve C must represent the hydration spectrum.

Relationship between the Absorption Represented by Curve B and the Volume of the Hydrated Solute. The absorption represented by curve B results from an "excess" of normal water in the reference cell over that in the sample absorption cell (see Figure 2, component V_{excl}). This apparent excess of water in the reference cell is due to a decrease in the concentration of the normal water in the sample cell which occurs because part of the volume of the solution is occupied by the hydrated solute. The volume which is occupied by the hydrated solute is that volume which is excluded to the solvent (normal water). Thus, curve B is the spectrum of normal water occupying a volume equivalent to V_{excl} .

Determination of V_{excl} from Curve B. The molar excluded volume of the hydrated solute, V_{excl} , can be calculated from curve B and curve H₂O. If the magnitude of curve B represents that portion of the solution which is occupied by the hydrated solute, and if the magnitude of the curve H₂O represents the total volume of the solution, then the ratio of the magnitudes of curve B to curve H₂O, taken at any frequency, is equal to the fractional volume (FV) which is occupied by the hydrated solute. The molar excluded volume, V_{excl} , is defined experimentally in relation to this fractional volume term in eq 13.

$$V_{\text{excl}} = 1000(\text{FV})/C \quad (13)$$

Equation 13 can be compared to the equivalent expression by Padova⁴ which is represented as eq 14.

$$\phi_s = 1000(\beta_0 - \beta)/C\beta_0 = 1000[(\beta_0 - \beta)/\beta_0]/C \quad (14)$$

The term (FV) in eq 13 and the term $(\beta_0 - \beta)/\beta_0$ in eq 14 both refer to the fraction of the volume of the solution occupied by the hydrated solute. In eq 13 and 14, C is the molar concentration of solute. In eq 14 β and β_0 are the coefficients of compressibility of the solution and solvent (water), respectively. The coefficient of compressibility, β , is determined either from the velocity of sound in the solution under atmospheric pressure or by the direct measurement of the change in volume of the solution with change in pressure at pressures of about 1000 bars.

Although the quantities V_{excl} and ϕ_s are theoretically equivalent according to eq 5 and 6a, experimentally they depend on quite different properties of the solu-

tion. The quantity V_{excl} is determined from the near-infrared absorption of the solution, whereas the quantity ϕ_s is obtained from measurements of the velocity of sound in the solution. Therefore, the demonstration of a correlation between the values of the hydration number, n , calculated from the quantities V_{excl} and ϕ_s should be a critical test of the validity of both methods.

The value for V_{excl} which is obtained from eq 13 can be used in eq 5 to calculate nV_0 , the amount of hydration per mole of solute.

In the experiments described in this paper, the minimum value for the magnitude of curve B was calculated, but in the interpretation of the data this minimum value was assumed equal to the absolute value. This is a valid assumption for cases in which the absorption by the hydration is negligible at some frequency within the 1.45- μ absorption band region. Because of this assumption, both V_{excl} and nV_0 , which were calculated by this procedure, must be considered as minimum values and hence V_{excl} and nV_0 are listed in the following sections as $(V_{\text{excl}})_{\text{min}}$ and $(nV_0)_{\text{min}}$.

B. Integrated Absorption Method. The integrated absorption method for calculating the hydration of a solute in aqueous solution depends on an assumption which may not always be valid. It will be shown in the Results section, however, that useful information can be obtained despite this limitation.

The integrated absorption, (B), for a given salt can be determined from the area under the absorption curve representing the hydration spectrum, e.g., curve C in Figure 1. Assuming the value for the apparent integrated extinction to be equal for all similar salts, the amount of hydration for each of the alkali halides can be calculated from the respective hydration spectrum using the corresponding values for (B). It must be recognized as a limitation of this procedure that the integrated absorption coefficient for the OH stretching fundamental increases dramatically with an increase in H bonding of the OH. The extent of such changes in combination bands ($\nu_1 + \nu_3$) studied here is not well understood. In the absence of specific knowledge about this, it is risky to draw conclusions about hydration from integrated absorption data. However, in our study we have used anions which are known to disrupt water-water H bonds in the order $\text{I}^- > \text{Br}^- > \text{Cl}^-$. Besides the anions from H bonds with water molecules, the strength of such bonds varying in the order¹² $\text{I}^- > \text{Br}^- > \text{Cl}^-$. So, in effect, the differences in relative changes in H bonding of OH in water in

(11) It is assumed that any change in the absorption properties of water is caused directly or indirectly, e.g., structure breaking, by the presence of the solute in solution. All changes in the properties of water due to the presence of a solute are considered as effects of hydration.

(12) L. J. Bellamy and R. J. Pace, *Spectrochim. Acta*, **25A**, 319 (1969).

these solutions may not be significant enough to result in widely varying integrated absorption coefficients, as seen from the close concordance between hydration numbers obtained from excluded volume measurements and integrated absorption data (see Table IV). Despite this, it is more useful to regard hydration numbers from integrated absorption method as a verification for excluded volume measurements than as absolute values.

An illustration of the application of both the excluded volume method and the integrated absorption method is given in Table I. The calculation of the hydration

Table I: The Hydration of a Solute Calculated by the Excluded Volume Method and the Integrated Absorption Method

Hydration (3 M NaCl) calcd from $(V_{\text{excl}})_{\text{min}}$	Apparent integrated extinction for NaCl hydration	Hydration (3 M KCl) calcd from (B)
$(V_{\text{excl}})_{\text{min}}^a = 91.2$ ml/mol	$(B)_{\text{NaCl}}^e = 143$	$(B)_{\text{KCl}} = 123$
$\phi_v^b = 19.8$ ml/mol	$(C)_{\text{NaCl}}^f = 11.9 M$	$(C)_{\text{KCl}}^h = 10.3 M$
$(nV_0)_{\text{min}}^c = 71.4$ ml/mol	$(L)_{\text{NaCl}}^g = 0.1$ cm	$(L)_{\text{KCl}} = 0.1$ cm
$n^d = 3.96$ mol H ₂ O/mol	$(B)/(C)(L) = 120$	$n^i = 3.43$ mol H ₂ O/mol

^a $(V_{\text{excl}})_{\text{min}}$ was determined from the respective excluded volume spectrum using eq 13. ^b ϕ_v was calculated from eq 8 using density data taken from the "International Critical Tables." ^c $(nV_0)_{\text{min}}$ was calculated from eq 5. ^d The hydration number n equals $(nV_0)_{\text{min}} d/M$; d equals the density of water at 20° and M equals the molecular weight of water. ^e Values for (B) were determined from the hydration spectra and are tabulated in Table III. ^f $(C)_{\text{NaCl}}$ equals the molar concentration of the hydration in a 3 M NaCl solution. It was calculated from the hydration number, n , listed in column one of this table; $(C)_{\text{NaCl}}$ equals $n(3.0)$. ^g (L) is the path length of the absorption cells. ^h $(C)_{\text{KCl}}$ equals the molar concentration of the hydration in a 3 M KCl solution. It was calculated from the apparent integrated extinction for NaCl listed in column two of this table using the relationship, $(C)_{\text{KCl}} = (C)_{\text{NaCl}}(L)_{\text{NaCl}}(B)_{\text{KCl}}/(B)_{\text{NaCl}}(L)_{\text{KCl}}$. ⁱ The hydration number, n , for KCl in a 3 M solution. It was calculated directly from $(C)_{\text{KCl}}$; $n = (C)_{\text{KCl}}/3.0$.

number, n , by the two methods serves as a means of comparing the hydration represented by the excluded volume spectrum with the hydration represented by the respective hydration spectrum, e.g., curves B and C in Figure 1.

V. Results and Discussion

A. Variation of Hydration with Concentration. The hydration spectra for different concentrations of NaCl are presented in Figure 3. The variation of hydration with concentration is indicated in Table II. It can be seen from these data that this variation is approximately the same whether compared on the basis of the absorption at a given frequency, A_v , or the integrated absorption, (B) , of the hydration spectrum.

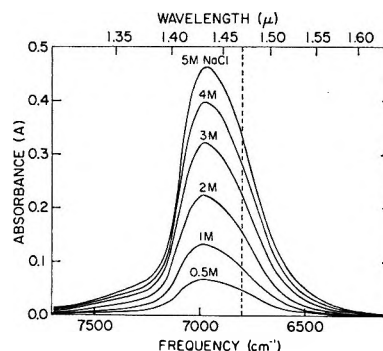


Figure 3. The variation of the hydration spectrum for NaCl with concentration. The hydration spectra were calculated from the corresponding NaCl solution measured *vs.* water difference spectra as indicated in Figure 1. The concentration ranged from 0.5 M to 5.0 M. The dashed vertical line at 6800 cm⁻¹ corresponds to the position of cation hydrate component.

Values for the hydration numbers, n , which were calculated from the respective values for V_{excl} and (B) are presented in Table II. The variation of n with concentration is the same whether calculated from V_{excl} or (B) . The value of n increases with decreasing concentration and approaches the range of literature values of n for NaCl at infinite dilution.

Values for the electrostriction, V_{el} , at each concentration were calculated from eq 1 and 8. These values and the corresponding values for the electrostriction factor (EF) are presented in Table II. Both the amount of hydration, n , and the amount of electrostriction, V_{el} , increase as the concentration of NaCl decreases while the electrostriction factor (EF) is almost independent of concentration. The range of literature values for (EF) at infinite dilution, is indicated in Table II for reference.

Both the shape of the hydration spectrum and the electrostriction factor (EF) should be sensitive to the interaction between the solute and water. These two hydration parameters are reasonably constant over the concentration range from 0.5 M NaCl to 5.0 M NaCl.

B. Characteristics of Anion and Cation Hydration. The hydration spectra for a series of cations with chloride anions are presented in Figure 4. The absorption maxima for all the hydration spectra are between 6950 and 7000 cm⁻¹ (approximately 1.43 μ). This indicates that all of these salts interact with water in a similar manner. For the chloride anion, the integrated absorption, (B) , [Table III] varies inversely with the size of the cation.

$$B_{(\text{Na}^+)} > B_{(\text{K}^+)} > B_{(\text{Rb}^+)} > B_{(\text{Cs}^+)}$$

The hydration spectra for a series of anions with sodium and potassium cations are presented in Figures 5 and 6. Here too, the absorption maxima for all of the hydration spectra are between 6950 and 7000 cm⁻¹ again

Table II: The Variation of the Hydration of NaCl with Concentration in Terms of Several Different Hydration Parameters

Hydration parameters	Concn of NaCl, <i>M</i>					
	0.5	1.0	2.0	3.0	4.0	5.0
A_{ν}^a	0.636	0.1298	0.2189	0.3164	0.3945	0.4612
A_{ν}/concn	0.1272	0.1298	0.1095	0.1055	0.0986	0.0922
% Max	98.0	100	84.4	81.3	76.0	71.0
(<i>B</i>)	29.4	58.0	97.8	143	178	208
(<i>B</i>)/concn	58.8	58.0	48.9	47.7	44.5	41.6
% Max	100	98.6	83.2	81.1	79.7	74.6
Density, g/ml ^b	1.01864	1.03854	1.07701	1.11416	1.15035	1.18574
ϕ_v , ml/mol	17.66	18.17	19.09	19.84	20.46	20.99
Fract vol (FV)	0.0523	0.106	0.184	0.273	0.352	0.422
V_{exol} , ml/mol	105	106	91.9	91.2	88.0	84.3
<i>n</i> , mol H ₂ O/mol calcd from						
V_{exol}	4.82	4.85	4.03	3.96	3.74	3.51
(<i>B</i>)	4.90	4.83	4.07	3.96	3.71	3.47
<i>c</i>		(5.91-6.41)		(av 6.2)		
V_{el} , ml/mol ^d	9.4	8.9	8.0	7.3	6.6	6.1
(EF)	0.108	0.102	0.110	0.102	0.098	0.096
(EF) ^e		(0.1243-0.1368)		(av 0.1316)		

^a The absorbance recorded at the frequency ν ; ν equals 6944 cm⁻¹. ^b The density data were obtained from the "International Critical Tables." ^c These values for the hydration number, *n*, at infinite dilution were taken from the literature. They were calculated from compressibility measurements by Padova,⁴ Tamura and Sasaki,⁵ and E. B. Freyer, *J. Amer. Chem. Soc.*, **53**, 1313 (1931). ^d V_{el} was calculated from eq 1 and 8. The value for V_{in} (27.1 ml/mol NaCl) used in eq 1 was taken from the literature.⁴ ^e These values for the electrostriction factor (EF) at infinite dilution were taken from the literature.⁵⁻⁷

Table III: A Summary of the Integrated Absorption Data

Solute	Concn (C), ^a <i>M</i>	Path length (L), cm	(<i>B</i>)	(<i>B</i>)/(<i>C</i>)(L), ^b cm ² mol ⁻¹	(ΔB)
Water ^c	55.40	0.1	955	172	
NaCl (3 <i>M</i>)	11.9	0.1	143	120	0.0
NaBr (3 <i>M</i>)	13.2	0.1	164	124	19
NaI (3 <i>M</i>)	13.7	0.1	178	130	35
KCl (3 <i>M</i>)	10.4	0.1	123	118	0.0
KBr (3 <i>M</i>)	12.6	0.1	152	121	29
KI (3 <i>M</i>)	12.9	0.1	165	128	42
NaCl (3 <i>M</i>)	11.9	0.1	143	120	0.0
KCl (3 <i>M</i>)	10.4	0.1	123	118	-20
RbCl (3 <i>M</i>)	10.4	0.1	119	115	-24
CsCl (3 <i>M</i>)	9.3	0.1	101	109	-42

^a The term (*C*) represents the molar concentration of "hydrated water" in the solution. It was calculated from the data in column eight of Table IV. ^b The quantity (*B*)/(*C*)(L) represents the apparent integrated extinction of the "hydrated water" for each hydration spectrum. ^c Water is included in this table for reference.

indicating that all of these salts interact with water in a similar manner. For both the sodium and potassium cations, the integrated absorption, (*B*), [Table III] varies directly with the size of the anion.

$$B_{(I^-)} > B_{(Br^-)} > B_{(Cl^-)}$$

The data presented in Figures 4, 5, and 6 indicate further that the hydration of the anions and cations is of the same order of magnitude.

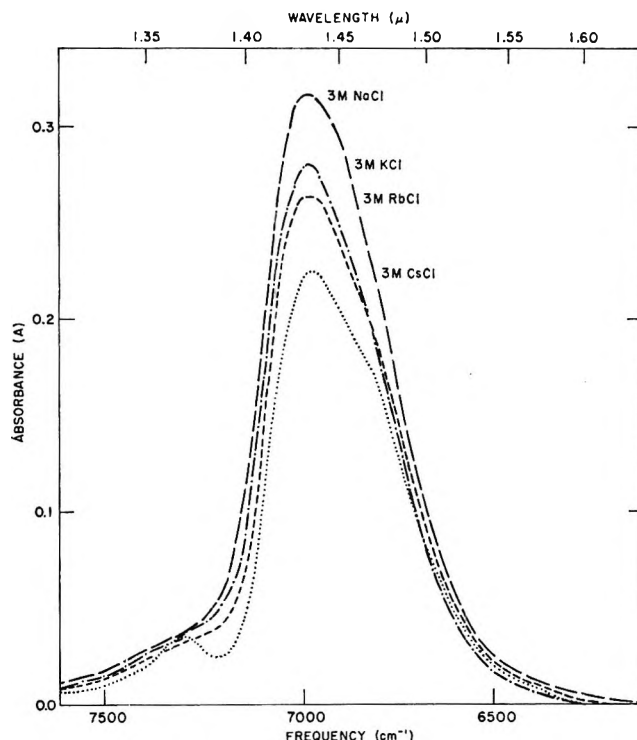


Figure 4. Variation of the hydration spectrum with changes in the cation for different chloride salts. The spectra are labeled using the symbol for the corresponding solute. Each of these hydration spectra was obtained as indicated in Figure 1. The concentration of each salt solution was 3 *M*.

The difference between the hydration spectra for NaI and NaCl is represented by curve A in Figure 7. If it is assumed that the contribution from the absorp-

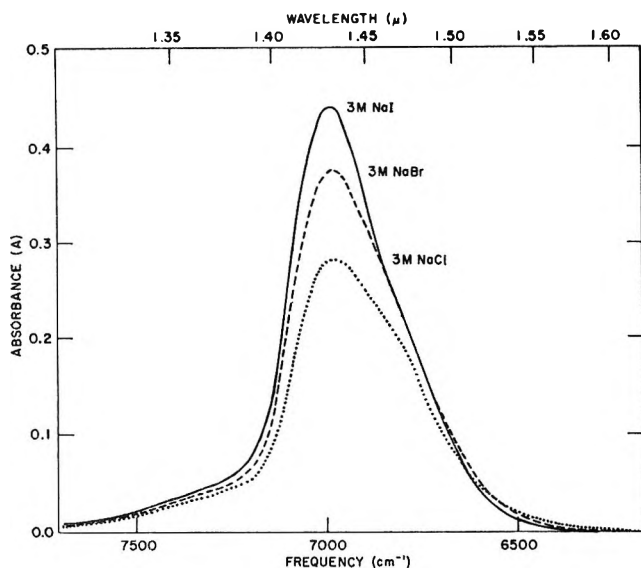


Figure 5. Variation of the hydration spectrum with changes in the anion for different sodium salts. The spectra are labeled using the symbol for the corresponding solute. Each of these hydration spectra was obtained as indicated in Figure 1. The concentration of each salt solution was 3 *M*.

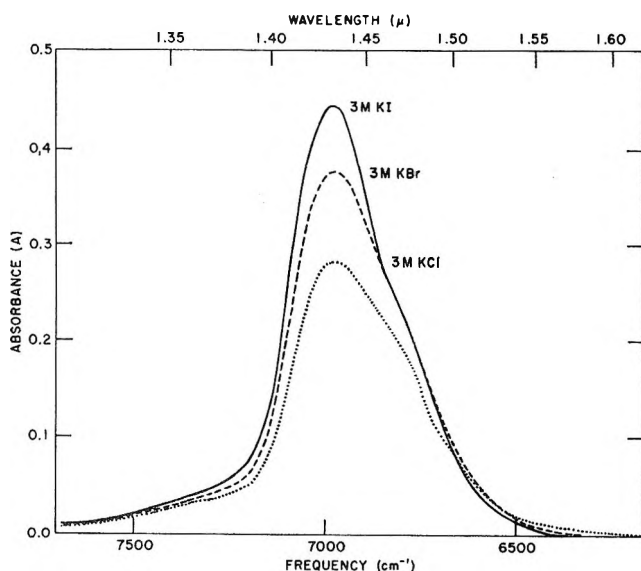


Figure 6. Variation of the hydration spectrum with changes in the anion for different potassium salts. The spectra are labeled using the symbol for the corresponding solute. Each of these hydration spectra was obtained as indicated in Figure 1. The concentration of each salt solution was 3 *M*.

tion by the sodium ion "hydrate" is canceled, then curve A would represent the difference between the absorption by the iodide and chloride "hydrates." Curve A is symmetrical and can be represented by a Gaussian distribution function^{13,14} (curve B) with the following absorption parameters: (1) absorption maximum, ν_0 , equal to $6997 \pm 3 \text{ cm}^{-1}$; (2) absorbance at ν_0 , A_{ν_0} , equal to 0.1708; and (3) half-band width, $\Delta\nu_{1/2}$, equal to $212 \pm 10 \text{ cm}^{-1}$. Absorption peaks

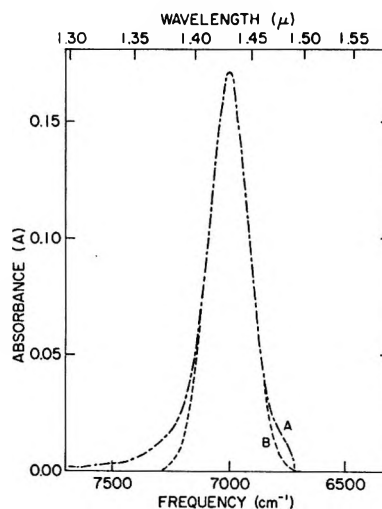


Figure 7. The hydration difference spectra representing the difference in hydration between the iodide and chloride anions. Curve A is the spectrum representing the difference between the hydration spectra for 3 *M* NaI, curve 3 *M* NaI in Figure 5, and 3 *M* NaCl, curve 3 *M* NaCl in Figure 5. Curve B is the appropriate Gaussian distribution of absorption; it is superimposed on curve A. The absorption distribution parameters for curve B used in calculating the Gaussian distribution of absorption are listed in the text.

which can be calculated from symmetrical distribution functions probably represent the absorption by a single, homogeneous molecular species. Thus, curve A in Figure 7 should represent the absorption by a single "species" of water molecule; *i.e.*, the anion hydrate.¹⁵ If so, the hydration spectrum for a given solute should represent the summation of a number of component absorption peaks each representing discrete H_2O molecules with different environments. The unambiguous resolution of the hydration spectrum into these component peaks would be the first step toward obtaining some understanding of the strength and nature of the interaction between the solute and water.

Curve A in Figure 8 is the hydration spectrum for 3 *M* NaI solution. Curves B and C are derived from curve A. They correspond to absorption by the different types of water molecules which comprise the hydration represented by curve A. Both curves B and

(13) The Gaussian error function,¹⁴ $A_{\nu} = A_{\nu_0} \exp(-\ln 2[(\nu_0 - \nu)/(\Delta\nu_{1/2})]^2)$, was used to calculate the absorbance at a given frequency, A_{ν} , for an absorption peak with its frequency of maximum absorbance at ν_0 , and with a half-band width equal to $\Delta\nu_{1/2}$.

(14) R. D. B. Fraser, "Infrared Spectra," in "A Laboratory Manual of Analytical Methods of Protein Chemistry (Including Polypeptides)," P. Alexander and R. J. Block, Ed., Pergamon Press, New York, N. Y., 1960, p 291.

(15) Any symmetrical absorption peak which can be represented by a Gaussian distribution of absorption can always be resolved into at least two component Gaussian peaks within experimental error. This does not, however, invalidate the statement concerning the relationship between the Gaussian peak resolved and the absorption by a single species of water molecule. The data obtained do suggest that there is only one species of water molecule contributing to this absorption peak; they do not, however, constitute proof of this relationship.

Table IV: A Summary of the Hydration Parameters Calculated from the Hydration and Excluded Volume Spectra

Salt soln	Density, ^a g/ml, 20°	ϕ_v , ml/mol	V_{in} , ^b ml/mol	(FV) ^c	V_{excl} , ml/mol	(EF)	Hydration no., n , calcd from—		(Δn)
							V_{excl} mol H ₂ O/mol salt	(B)	
3 M NaCl	1.11416	19.84	27.1	0.273	91.2	0.102	3.96	3.96	0.00
3 M KCl	1.13116	30.30	36.0	0.278	92.7	0.091	3.46	3.42	-0.04
3 M RbCl	1.25501	35.41	40.1	0.294	98.1	0.075	3.47	3.31	-0.16
3 M CsCl	1.37556	42.67	46.2	0.296	98.7	0.063	3.10	2.81	-0.29
3 M NaBr	1.22882	26.09	33.7	0.317	105.5	0.096	4.40	4.56	+0.16
3 M KBr	1.24523	36.74	42.6	0.337	112.4	0.078	4.19	4.22	+0.03
3 M NaI	1.33717	37.00	43.5	0.359	119.6	0.079	4.58	4.94	+0.36
3 M KI	1.35348	47.68	52.4	0.376	125.4	0.061	4.30	4.58	+0.28

^a The density data were obtained from the "International Critical Tables." ^b The values for V_{in} were taken from a paper by Padova.⁴ ^c The fractional volume, (FV), is used in eq 13 to calculate V_{excl} . The values for (FV) were determined directly from the respective excluded volume spectra.

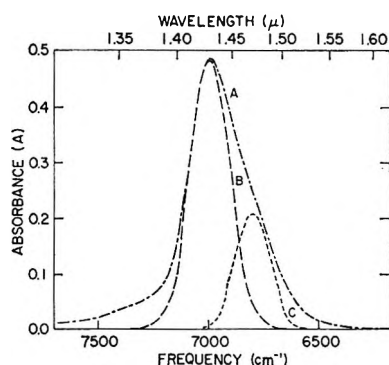


Figure 8. The resolution of the hydration spectrum for 3 M NaI into two component curves. Curve A is the hydration spectrum for 3 M NaI; it was obtained as indicated in Figure 1. Curve B is similar to curve B in Figure 7. The appropriate Gaussian distributions of absorption parameters are listed in the text. Curve C was obtained by subtracting curve B from curve A.

C represent Gaussian distributions of absorption. Curve B in Figure 8 is similar to curve B in Figure 7. It has the following absorption distribution parameters: (1) ν_0 equal to 6997 cm^{-1} , (2) $\Delta\nu_{1/2}$, equal to 212 cm^{-1} , and (3) A_{ν_0} equal to 0.484. Curve C is obtained by subtracting curve B from curve A. The absorption distribution parameters for curve C are as follows: (1) ν_0 equal to 6800 cm^{-1} , (2) $\Delta\nu_{1/2}$ equal to 200 cm^{-1} , and (3) A_{ν_0} equal to 0.206. If, as suggested above, curve B in Figure 8 represents the absorption by the anion (iodide) hydrate, then curve C should represent the absorption by the cation (sodium) hydrate. A further indication of the occurrence of the hydration component represented by curve C is seen in curve 3 M CsCl (Figure 4) and in curves 0.5 M to 5.0 M NaCl (Figure 3). In both cases a rather distinct shoulder occurs at 6800 cm^{-1} . More extensive studies should be made, however, before this resolution is considered as established.

C. Summary of Results. A summary of the integrated absorption data for all of the hydration spectra

is presented in Table III. A general summary of the data is presented in Table IV.

The internal consistency of the values for n , which were calculated from V_{excl} data, can be determined by comparing the differences between the values for n for different anions and cations with the same counterion. This test is presented in Table V. It can be

Table V: The Determination of the Internal Consistency of the Values for n Calculated from V_{excl}

Salt	n^a	n^b (cation) ^b	n^b (anion), ^b mol H ₂ O/ mol salt	$(n)^c$	Δn
NaCl	3.96	(3)	(3)	(0.99 M; 5.15)	0.00
KCl	3.46	(2)	(3)	(1.00 M; 4.25)	-0.50
RbCl	3.47	(2)	(3)	(0.42 M; 4.95)	
CsCl	3.10	(1)	(3)	(1.00 M; 3.50)	
NaBr	4.40	(3)	(2)		0.00
KBr	4.19	(2)	(2)		-0.21
NaI	4.58	(3)	(0)		0.00
KI	4.30	(2)	(0)		-0.28
NaCl	3.96	(3)	(3)		0.00
NaBr	4.40	(3)	(2)		+0.44
NaI	4.58	(3)	(0)		+0.62
KCl	3.46	(2)	(3)		0.00
KBr	4.19	(2)	(2)		+0.73
KI	4.30	(2)	(0)		+0.84

^a The hydration number, n , was calculated from V_{excl} data (Table IV) according to the procedure outlined in Table I. The salt concentration was 3 M. ^b These are the values for n at infinite dilution (n^0) of the salt. They were determined by the method of compressibility by Padova.⁴ They are included here for reference. ^c These are values for the hydration number, n , at the concentration indicated. They were determined by the method of compressibility by T. Isemura and S. Goto, *Bull. Chem. Soc. Jap.*, **37**, 1690 (1964).

inferred from the data in Table V that the anions and cations of a given salt are not being hydrated independently of one another at this concentration (3 M). It is not possible to state at this time whether the effect of

one ion on its respective counterion is direct or mediated through its effect on the solvent. It should be emphasized, however, that this effect is also observed when the values for the apparent molar volumes, ϕ_v , of these salts are compared (Table IV). Thus, the effect is real although its cause is unknown.

The differences between the values for n calculated from V_{exc1} and (B) data are presented in Tables II and IV. The value for Δn is approximately 0 wherever the shape of the hydration spectrum remains constant (Table II and Figure 3) and deviates from zero where the shape of the hydration spectrum changes.

The values for n calculated from the compressibility method, *i.e.*, from ϕ_s , and those calculated from V_{exc1} are tabulated in Table V for comparison. In the cation series NaCl, KCl, RbCl, and CsCl, the agreement between the two methods is quite good considering the differences in concentration for the two sets of data. In Table II the data for the variation of n with concentration of NaCl suggest that at infinite dilution the values for n calculated in this paper should approach, within experimental error, those obtained from compressibility measurements. The agreement for the anion series NaCl, NaBr, and NaI or KCl, KBr, and KI is less satisfactory. The values for n appear to be of the right order of magnitude and the sequence is the same in both, *i.e.*, Br⁻ between Cl⁻ and I⁻. The relative magnitudes of the values of n for Cl⁻, Br⁻, and I⁻ are reversed. The data in this paper indicate that the order should be $(n)_{\text{I}^-} > (n)_{\text{Br}^-} > (n)_{\text{Cl}^-}$, whereas the results obtained by Padova (quoted in Table V) give the order as $(n)_{\text{Cl}^-} > (n)_{\text{Br}^-} > (n)_{\text{I}^-} = 0$. Several Raman studies¹⁶⁻¹⁹ of aqueous solutions of various halides, however, indicate that the increase in intensity follows the sequence I⁻ > Br⁻ > Cl⁻. It is likely that structure-breaking propensities of these anions are responsible for reversing the order of hydration relative to the infinite dilution values of Padova.

In connection with the data presented in this paper, two points should be emphasized. (1) The hydration spectra presented in this paper appear to contain a

definite signal for the hydration of the anions, *e.g.*, Figures 7 and 8. All of these signals are significantly different from zero and appear to vary in the order I⁻ > Br⁻ > Cl⁻. (2) The data presented in this paper contain (or represent) two discrete and different (if not completely independent) signals corresponding to the hydration of a given salt. These are the excluded volume spectrum and the hydration spectrum, *e.g.*, curves B and C, respectively, in Figure 1. A comparison of the hydration numbers, n , calculated from these two parameters is shown in Table IV. Although this comparison is somewhat arbitrary, as pointed out above, the general trend of the agreement is significant.

The agreement between these two methods tends to demonstrate the general validity of both methods for measuring hydration. This agreement does not rule out the possibility that both methods are complementarily insensitive to some type of hydration; it should, however, put certain restrictions on the nature of any such solute-solvent interaction.

VI. Conclusion

The near-infrared, spectroscopic method for measuring hydration in electrolyte solutions presented here appears to be accurate and reasonably free of assumptions. The method is capable of delineating both the amount of water interacting with the solute and the gross characteristics of the interaction between the solute and water. In theory, this method should be applicable to all types of solutes. In practice, however, the method could be difficult to apply, especially for cases in which the interaction between the solute and water is similar to that of water with water. In all cases the near-infrared absorption of the solute itself must be known.

(16) W. R. Busing and D. F. Hornig, *J. Phys. Chem.*, **65**, 284 (1961).

(17) J. W. Schultz and D. F. Hornig, *ibid.*, **65**, 2137 (1961).

(18) H. A. Lauwers and G. P. Van der Kelen, *Bull. Soc. Chim. Belg.*, **72**, 477 (1963).

(19) Z. Kecki, J. Witanowski, K. Akst-Lipszyc, and S. Minc, *Rocz. Chem.*, **40**, 919 (1966).

Crystal Lattice Effects in the Nuclear Quadrupole Resonance Spectra of Some Hexachlorostannate(IV) Salts^{1a}

by T. B. Brill,^{1b} Z. Z. Hugus, Jr., and A. F. Schreiner

Department of Chemistry, North Carolina State University, Raleigh, North Carolina 27607 (Received February 2, 1970)

The ³⁵Cl and some ³⁷Cl nqr spectra in ten different salts of SnCl₆²⁻ have been recorded and the resonance frequency trends due to the lattice interpreted. When the anion-cation covalency was expected to be variable, the electrostatic point charge model failed to explain the observed trends. In compounds containing nearly constant-anion cation covalency, explanation of the trends using the point-charge model was reasonably successful. Differences in the crystal lattice induced up to a 10% variation in the ³⁵Cl resonance frequency. Use of an empirical lattice Sternheimer antishielding factor of 10 for chlorine is consistent with the results. Semiempirical LCAO-MO calculations were carried out on SnCl₆²⁻ and TeCl₆²⁻, and computational verification for the "inert pair effect" was obtained.

Introduction

An important problem in nqr spectroscopy is the understanding of how much the nqr frequency of an atom in a chemical moiety can be affected by the crystal lattice surrounding it. It is the purpose of this paper to report the effects of a variety of cations on the ³⁵Cl and some ³⁷Cl resonance frequencies in the hexachlorostannate(IV) ion, SnCl₆²⁻. In the absence of good crystal wave functions, approximate models were used in order to interpret the results. An attempt is therefore made to account for the trends rather than the absolute frequencies.

Experimental Section

Chloride salts of the cations (AR Grade) were added stoichiometrically to dilute HCl solutions containing known amounts of SnCl₄·5H₂O (AR Grade). The solutions were allowed to evaporate from one to four weeks. In most cases, large well-formed crystals grew. For several compounds, notably the Rb⁺, Cs⁺, and (CH₃)₄N⁺ salts, only small crystals were obtained. The nqr spectra reported in Table I were recorded using a Wilks Scientific NQR-1A nuclear quadrupole resonance spectrometer. A Hewlett-Packard 5245L electronic counter was used for frequency measurements. Only one ³⁵Cl resonance frequency was found in each compound studied but because a superregenerative oscillator-detector was used, the possibility of two very closely spaced resonances cannot be ruled out. Attempts were made to record the resonance frequencies of about twenty additional compounds, but their spectra could not be detected at room temperature using our spectrometer.

Calculations

Lattice electric field gradient (EFG) was computed using a general point charge lattice summation computer program. The elements, q_{ij} , of the symmetric

tensor at a point, such as at a nucleus, due to a charge, e_k , a distance r away are given by²

$$q_{ij} = \left(\frac{\partial^2 V}{\partial x_i \partial x_j} \right)_{r=0} = \sum_k e_k \sum_i \sum_j \frac{(3x_i x_j - \delta_{ij} r^2)}{r^5} \quad (1)$$

V is the electrostatic potential at the nucleus, and x_i , x_j are the cartesian coordinates x , y , and z . $\delta_{ij} = 1$ if $i = j$ and 0 otherwise. By scanning all charges in a spherical volume of a chosen radius and by computing six of the nine q_{ij} 's for each, the lattice EFG tensor was generated. Diagonalization of the tensor yields the eigenvalues of the principal axes, which are converted to MHz, along with their eigenvectors relative to the initial axes. The eigenvalues must be corrected for the Sternheimer antishielding effect.³ Burns and Wikner⁴ have suggested an empirical multiplicative factor of 10 for ³⁵Cl.⁵ This value appears to be very reasonable based on the results presented herein and will be discussed.

In order to obtain the self-consistent charges and intramolecular EFG in the SnCl₆²⁻ ion, an LCAO-MO calculation was carried out. The same type of calculation was also performed on TeCl₆²⁻ for purposes of comparison. An extensively modified SCCC-MO-like program based on Hoffmann's⁶ was used. In this

(1) (a) Abstracted from the thesis of T. B. B. submitted to the Graduate School of the University of Minnesota in partial fulfillment of a Doctor of Philosophy degree. (b) NDEA predoctoral fellow at the University of Minnesota, 1966-1969. Address inquiries to Department of Chemistry, University of Delaware, Newark, Del. 19711.

(2) A. Abragam, "The Principles of Nuclear Magnetism," Oxford University Press, New York, N. Y., 1961.

(3) R. M. Sternheimer and H. M. Foley, *Phys. Rev.*, **102**, 731 (1956), and references therein.

(4) G. Burns and E. G. Wikner, *ibid.*, **121**, 155 (1961).

(5) The Sternheimer antishielding factor is defined as $(1 - \gamma_\infty)$. We have thus chosen $\gamma_\infty = -9$.

(6) R. Hoffmann and W. N. Lipscomb, *J. Chem. Phys.*, **36**, 2179 (1962).

Table I: ^{35}Cl and ^{37}Cl Nqr Frequencies (MHz) for SnCl_6^{2-} Salts of Various Cations^a

Cation	$\nu(^{35}\text{Cl})$	S/N	$\nu(^{37}\text{Cl})$	S/N	e^2Qq/h (^{35}Cl) ^c
K ⁺ ^b	15.064 ± 0.003	12:1	11.870 ± 0.003	6:1	30.128 ± 0.006
Rb ⁺ ^b	15.60 ± 0.02	2:1	31.20 ± 0.04
Cs ⁺	16.05 ± 0.05	2:1	32.10 ± 0.10
Mg(H ₂ O) ₆ ²⁺	15.835 ± 0.003	9:1	12.478 ± 0.003	3:1	31.670 ± 0.006
Co(H ₂ O) ₆ ²⁺	15.752 ± 0.003	5:1	12.411 ± 0.003	2:1	31.504 ± 0.006
Ni(H ₂ O) ₆ ²⁺	15.708 ± 0.003	30:1	12.380 ± 0.003	7:1	31.416 ± 0.006
NH ₄ ⁺ ^b	15.475 ± 0.003	3:1	30.950 ± 0.006
CH ₃ NH ₃ ⁺	15.811 ± 0.003	25:1	12.460 ± 0.003	6:1	31.622 ± 0.006
(CH ₃) ₃ NH ⁺	16.635 ± 0.003	15:1	13.109 ± 0.003	5:1	33.270 ± 0.006
(CH ₃) ₄ N ⁺	16.663 ± 0.003	4:1	13.127 ± 0.003	2:1	33.326 ± 0.006

^a All resonance frequencies were recorded at 23°. ^b D. Nakamura, *Bull. Chem. Soc. Jap.*, **36**, 1162 (1963) (^{37}Cl resonance only.)
^c The coupling constant was taken to be twice the resonance frequency. In the cases of the K⁺, Rb⁺, Cs⁺, NH₄⁺, and (CH₃)₄N⁺ salts, this is exactly correct based on crystallographic data. In the others the lattice will probably generate a small asymmetry parameter in the EFG. However, even in the unlikely circumstance that the asymmetry parameter is as large as 0.1, this approximation still represents less than 0.2% error in the coupling constant.

computational procedure the diagonal Hamiltonian matrix elements, H_{ii} , of the metal were approximated as valence orbital ionization potentials⁷ with all orbital energies derived from atomic spectral data in Moore's tables.⁸ They were charge adjusted by -3.5 eV per unit charge. The analytical, single term, Slater-type metal orbital exponents were derived by fitting their shape in the overlap region to Herman-Skillman self-consistent field (SCF) wave functions.⁹ Clementi-Raimondi¹⁰ functions were used for chlorine. Bond distances of 2.43 Å in SnCl_6^{2-} and 2.54 Å in TeCl_6^{2-} were employed for these overlap integral calculations.^{11,12}

It became apparent that the metal 4d orbital is not very important in bonding, since it is very contracted, of low energy, and therefore completely filled in these complexes. In fact, the valence bond approach suggests the use of metal 5d orbitals by forming sp^3d^2 hybrids. Therefore, the tin 5d orbitals were employed. The exponents were generated by determining the maximum overlap with the chlorine orbitals and then contracting them due to the atom positive charge by 0.2(Sn) and 0.3(Te) unit. The magnitude of these contractions is in line with similar results obtained by Richardson, *et al.*¹³ The 4d orbital was then neglected.

Off-diagonal Hamiltonian matrix elements, H_{ij} , were calculated by the Wolfsberg-Helmholz method¹⁴

$$H_{ij} = 0.5KS_{ij}(H_{ii} + H_{jj}) \quad (2)$$

where S_{ij} is the overlap integral between the i^{th} and j^{th} functions. K is a constant set equal to 1.75. Cusachs' method¹⁵ for computing H_{ij} was also investigated. It led to substantially the same EFG as (2) but slightly larger charges resulted on the metal and chlorine atoms. The approximation was abandoned since small, but not negligible, negative orbital occupations resulted in the metal e_g orbitals.

Input orbital exponents and Coulomb integrals are listed in Table II. Self-consistent output charges and

orbital occupations are listed in Table III. Substitution of chlorine p orbital "holes", U (obtained from 2-orbital occupations) into the following equation yields the ^{35}Cl nuclear quadrupole coupling constant for the molecular ion in MHz. The approach that Cotton

$$(e^2Qq/h) = -109.7 \left(U_{p_x} - \frac{U_{p_z} + U_{p_y}}{2} \right)$$

Table II: Input Molecular Orbital Parameters for SnCl_6^{2-} and TeCl_6^{2-}

Orbital type	Slater-type orbital exponents, ^a α	H_{ii} , eV	
Sn {	5s	2.15	-13.10
	5p	1.65	-8.35
	5d	1.38	-1.31
Te {	5s	2.25	-16.30
	5p	1.89	-10.25
	5d	1.50	-2.31
Cl {	2s	2.356	-23.10
	3p	2.039	-13.94

^a $\alpha = (Z - s)/n$, where Z is the atomic number, s is the screening constant, and n is the principal quantum number.

- (7) H. Basch, A. Viste, and H. B. Gray, *J. Chem. Phys.*, **44**, 10 (1965).
(8) C. E. Moore, "Atomic Energy Levels," National Bureau of Standards Circular 467, 1958.
(9) F. Herman and S. Skillman, "Atomic Structure Calculations," Prentice-Hall, Englewood Cliffs, N. J., 1963.
(10) E. Clementi and D. L. Raimondi, *J. Chem. Phys.*, **38**, 2686 (1963).
(11) R. W. G. Wyckoff, "The Structure of Crystals," The Chemical Catalog Company, Inc., New York, N. Y., 1931.
(12) A. C. Hazell, *Acta Chem. Scand.*, **20**, 165 (1966).
(13) J. W. Richardson, W. C. Nieuwpoort, R. R. Powell, and W. F. Edgell, *J. Chem. Phys.*, **38**, 796 (1963).
(14) M. Wolfsberg and L. Helmholz, *ibid.*, **20**, 837 (1952).
(15) L. C. Cusachs and B. B. Cusachs, *J. Phys. Chem.*, **71**, 1061 (1967).

Table III: Self-Consistent Charges and Orbital Occupations in SnCl_6^{2-} and TeCl_6^{2-}

Atom	Charge	Orbital type	Orbital occupation
SnCl_6^{2-}			
Sn	+0.99	5d (e_g)	0.056
		5d (t_{2g})	0.070
		5p	0.562
		5s	1.000
Cl	-0.498	3p (σ)	1.713
		3p (π)	1.963
		3p (π)	1.963
		3s	1.860
TeCl_6^{2-}			
Te	+1.03	5d (e_g)	0.143
		5d (t_{2g})	0.118
		5p	0.777
		5s	2.000
Cl	-0.505	3p (σ)	1.706
		3p (π)	1.951
		3p (π)	1.951
		3s	1.897

and Harris¹⁶ used in their computational studies of hexachloro transition metal ions appears to be similar.

The calculated and observed coupling constants in isostructural $(\text{NH}_4)_2\text{SnCl}_6$ and $(\text{NH}_4)_2\text{TeCl}_6$ based on this method are -27.50 and -26.90 MHz, respectively. These values compare reasonably well with the experimental ones of 30.95 and 29.99 MHz.¹⁷

Results and Discussion

Regarding the electronic structures of the SnCl_6^{2-} and TeCl_6^{2-} ions, one most interesting observation can be made. The two additional electrons in TeCl_6^{2-} compared to SnCl_6^{2-} go into an MO of α_{1g}^* symmetry which is largely Te(5s) in character

$$\psi(\alpha_{1g}^*) = 0.87\phi_{5s}(\text{Te}) -$$

$$0.158\phi_{3s}(\text{Cl}) \pm 0.391\phi_{3p_i}(\text{Cl}) \pm \dots$$

where $\pm\phi_{3p_i}$ is the $3p_x$, $3p_y$, or $3p_z$ chlorine orbital depending on the axis chosen. This appears to be computational verification of what has long been referred to as the "inert pair effect."¹⁸

A. $M_2\text{SnCl}_6$ Salts, $M = \text{K}^+$, Rb^+ , and Cs^+ . These three isostructural salts are known to crystallize in the cubic antiferroite K_2PtCl_6 structure.¹⁹ The unit cell dimensions for each of the three lattices are, respectively: $a = 9.983 \text{ \AA}$, $a = 10.099 \text{ \AA}$, and $a = 10.347 \text{ \AA}$. The intramolecular EFG is assumed to remain constant within the series of compounds, although surely there are some small variations in the anion as the lattice is changed.

Table IV shows that the point charge model does not account for the resonance frequency difference. The reason for this is the fact that, contrary to reality, K^+ , Rb^+ , and Cs^+ are indistinguishable in the point charge model. Therefore, a method which will permit con-

Table IV: Lattice Coupling Constants (MHz) for $M_2\text{SnCl}_6$ Salts Using the Point Charge Model Compared to the Observed Shifts

M	e^2Qq_{ax}/h calcd	$\Delta e^2Qq/h^a$	
		Calcd	Obsd
K^+	-2.13	0	0
Rb^+	-2.09	-0.04	1.07
Cs^+	-1.91	-0.22	1.97

^a $\Delta e^2Qq/h = (e^2Qq/h)_{\text{K}^+, \text{Rb}^+, \text{Cs}^+} - (e^2Qq/h)_{\text{K}^+}$. K_2SnCl_6 is the reference compound.

sideration of the cation sizes or, in effect, take into account crystal lattice covalency²⁰ must be used. To evaluate this, the orbital overlap integrals were calculated between the cation and chlorine atom using an average interaction distance of 3.55 \AA .¹⁹ The cation was assumed to carry a +1 charge as a result of the removal of an ns electron. The size of the orbital overlap of the remaining $(n-1)p$ orbitals with the chlorine orbitals was then used as an indication of the relative extent of covalency in these compounds. Table V

Table V: Absolute Value of the Overlap Integrals, S_{ij} , for Cation-Chlorine Atom Pairs Compared to Some Sn-Cl Overlap Integrals in SnCl_6^{2-}

Orbitals	K-Cl	Rb-Cl	Cs-Cl	Sn-Cl
(metal) p_z -Cl(3s)	0.0187	0.0249	0.0295	0.3442
(metal) p_x -Cl(3p _x)	0.0385	0.0502	0.0610	0.2907
(metal) p_x, p_y -Cl(3p _{x, 3p_y})	0.0050	0.0070	0.0088	0.1270

shows that the Cs-Cl overlap integrals are significantly greater than those of K-Cl and are not negligible compared to similar Sn-Cl overlap integrals. This trend in the difference of lattice covalency may be related to the variation in resonance frequencies, but in view of the obvious approximations of this model, it would be unreasonable to attempt to predict quantitative frequency shifts.

B. $M(\text{H}_2\text{O})_6\text{SnCl}_6$ Salts, $M = \text{Mg}^{2+}$, Co^{2+} , and Ni^{2+} . The structure of $\text{Ni}(\text{H}_2\text{O})_6\text{SnCl}_6$ has been found to be a rhombohedrally distorted CsCl structure containing $\text{Ni}(\text{H}_2\text{O})_6^{2+}$ and SnCl_6^{2-} ions.²¹ Its cell constants are $a = 7.09 \text{ \AA}$ and $\alpha = 96^\circ 45'$. $\text{Mg}(\text{H}_2\text{O})_6\text{SnCl}_6$ and $\text{Co}(\text{H}_2\text{O})_6\text{SnCl}_6$ are isostructural with the nickel salt.²¹ The positions of the protons can be inferred from those

(16) F. A. Cotton and C. B. Harris, *Inorg. Chem.*, **6**, 376 (1967).

(17) D. Nakamura, K. Ito, and M. Kubo, *J. Amer. Chem. Soc.*, **84**, 163 (1962).

(18) N. V. Sidgwick, *Ann. Rept. Chem. Soc., (London)*, **30**, 110 (1933).

(19) G. Engel, *Z. Kristallogr.*, **90**, 341 (1935).

(20) R. Bersohn and R. G. Shulman, *J. Chem. Phys.*, **45**, 2296 (1966).

(21) L. Pauling, *Z. Kristallogr.*, **72**, 482 (1930).

in the isostructural $\text{Fe}(\text{H}_2\text{O})_6\text{SiF}_6$ salt which has been studied by neutron diffraction.²² Since the compounds are isostructural, hydrogen-bonding effects are nearly constant, and the primary source of variation in the nqr frequencies is probably related to the variation in charge distribution among atoms in the three aquo cations. The effective Mg^{2+} , Co^{2+} , and Ni^{2+} charges were assumed to be +1.0, +0.6, and +0.5, respectively; the relative difference in the charges is more important here than the absolute charges. Since there is some question as to the oxygen and hydrogen charges, several distributions were investigated. The lattice summations were carried out to a radius of 60 Å, and the results are listed in Table VI. The calculated

C. (Amine)₂SnCl₆ Salts, Amine = NH_4^+ , CH_3NH_3^+ , $(\text{CH}_3)_3\text{NH}^+$, and $(\text{CH}_3)_4\text{N}^+$. The obvious qualitative trend in the resonance frequencies in the compounds is this: as the extent of substitution of the nitrogen increases, the resonance frequency increases. The potential increase in the amount of hydrogen-chlorine interaction or perhaps the increase in the bulk of the easily distorted cation may be related to the increase in the EFG at the chlorine atom. Some X-ray crystallographic data are available on all these compounds,¹¹ but in every case the atomic parameters of the protons are unknown. In most cases the nitrogen and carbon atom positions are not definitely known. Without this knowledge, it would be unreasonable to speculate further on the source of the observed variations in the resonance frequencies. Neutron diffraction data will be needed before this problem can be investigated in detail.

Conclusions

(1) The results of this work indicate that the crystal lattice is important in the interpretation of moderate shifts in nqr frequencies in ionic compounds. Variations of more than three MHz in the coupling constants appear to have been induced by differences in the lattice. In SnCl_6^{2-} this represents about 10% of the total EFG at the ³⁵Cl nucleus. The compounds representing the two extremes (K^+ and $(\text{CH}_3)_4\text{N}^+$ salts) are basically isostructural. It would seem reasonable that the interpretation of intramolecular effects, which might rise to frequency shifts of about this amount or less, could be complicated by lattice effects.

(2) Use of a lattice Sternheimer antishielding factor, of about 10 for ³⁵Cl is consistent with the present results. The lattice EFG contribution causes frequency variations of several MHz. The calculated lattice EFG's should, therefore, be of the order of several MHz if they are to be considered reasonable. An empirical value of 10 leads to this approximate agreement.

(3) The general failure of the point charge lattice model in accounting for lattice EFG's is probably because it neglects crystal lattice covalency effects.²⁰ In cases where lattice covalency effects are nearly constant, the point charge model does account for variations in the EFG.

Acknowledgment. We wish to acknowledge the support of the North Carolina Board of Science and Technology toward the purchase of the nqr spectrometer.

(22) W. C. Hamilton, *Acta Crystallogr.*, **15**, 353 (1962).

Table VI: Point Charge Model Interpretation of the Variation of Nqr Coupling Constants in $\text{M}(\text{H}_2\text{O})_6\text{SnCl}_6$ Salts Compared to the Observed Shifts

M	Atom charges			e^2Qq/h , calcd, MHz	$\Delta e^2Qq/h^a$	
	Metal	Oxygen	Hydrogen		Calcd	Obad
Mg	+1.0	-0.20	+0.183	2.76	0.15	0.165
Co	+0.6	-0.16	+0.197	2.61	0	0
Ni	+0.5	-0.15	+0.20	2.58	-0.03	-0.088
Mg	+1.0	-0.05	+0.11	2.87	0.15	0.165
Co	+0.6	-0.03	+0.13	2.72	0	0
Ni	+0.5	-0.02	+0.135	2.67	-0.05	-0.088

^a $\Delta e^2Qq/h = (e^2Qq/h)_{\text{Co}^{2+}} - (e^2Qq/h)_{\text{Mg}^{2+}, \text{Co}^{2+}, \text{Ni}^{2+}}$. $\text{Co}(\text{H}_2\text{O})_6\text{SnCl}_6$ is the reference compound.

trends in the EFG do not appear to depend very much on the oxygen and hydrogen charges as long as their ratios remain about the same.

The point charge model accounts reasonably well for the trend in resonance frequencies in this series, perhaps because the metal of the cation, which appears to be the source of the EFG variation, is not a nearest neighbor to the chlorine atoms. The H_2O sphere surrounding the metal remains constant in all three compounds and could act as a shield against any significant metal-chlorine covalency. The EFG variation might, therefore, be expected to be interpretable on the basis of an electrostatic effect. This contrasts with the alkali metal salts just discussed in which the primary source of EFG variation may have been direct cation-chlorine covalency.

The fact that $\text{Ni}(\text{H}_2\text{O})_6^{2+}$ and $\text{Co}(\text{H}_2\text{O})_6^{2+}$ ions are paramagnetic seems to have no different effect on the chlorine resonance than the diamagnetic $\text{Mg}(\text{H}_2\text{O})_6^{2+}$ ion.

Flash Photolysis of the Charge-Transfer Band of 1-Methylpyridinium, 1-Methylcollidinium and 1-Methylquinolinium Iodides^{1a}

by R. F. Cozzens^{1b} and Thomas A. Gover

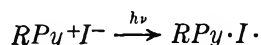
Department of Chemistry, University of Virginia, Charlottesville, Virginia 22903 (Received January 16, 1970)

The flash photolysis of the charge-transfer band of 1-methylpyridinium and 1-methylcollidinium iodide in degassed dichloromethane produced transient absorptions which were attributed to I_2^- . Both systems showed permanent loss of parent compound and growth of I_3^- absorptions. The rate of decay of I_2^- from 1-methylcollidinium iodide fit second-order kinetics. A $10^{-4} M$ solution of 1-methylquinolinium iodide in dichloromethane gave the same second-order transient but appeared to be completely reversible. In deoxygenated acetone the k/ϵ was observed to be *ca.* 10^5 at 6800 Å and decreased with increasing iodide concentration. Solutions of 1-methylquinolinium iodide in 1-propanol gave an additional transient absorption at *ca.* 5300 Å which may have been the 1-methylquinoline free radical.

Introduction

The role of the electron donor-acceptor complex in many chemical reactions has been a subject of intensive discussion over the past few decades.^{2a,b} Theoretical approaches to charge-transfer theory have been developed by Mulliken³ and more recently by Dewar,⁴ Murrell,⁵ and Flurry.⁶ With the exception of a recent note by Kosower and Lindqvist,⁷ experimental observation has been limited to studies of ground-state species.

The electronic absorption spectra of the N-alkyl halide salts of many nitrogen heterocyclic molecules have been observed to exhibit absorption bands which are not characteristic of the parent molecules.^{8,9} These anomalous absorptions have been attributed by Kosower¹⁰ and by Mason¹¹ to result from the transitions of an electron from the negative halide ion to the positive heterocyclic nucleus within a solvated ion pair. For the N-alkylpyridinium iodides this charge-transfer transition may be represented by



In the present study attention is focused on this optical transition and the species resulting from the reaction of the diradical excited-state complex.

Experimental Technique

The flash-photolysis apparatus used throughout this work was similar in design to the flash photographic apparatus developed by Porter.¹² The sample cell was placed at the common focus of four intersecting elliptical aluminum reflectors while the lamps were at the other four foci. The quartz lamps were filled with xenon to 9 Torr and were connected to a high-voltage capacitor bank consisting of two General Electric 20-kV, 6-μF low-inductance clam shell capac-

itors. Each capacitor had a natural ringing frequency of 500 kcps.

A 2-m grating spectrograph was optically coupled through the cell to a quartz capillary analysis flash lamp operated at 100 J. The spectrum was photographically recorded and the film densities were measured with a recording microdensitometer. The flash output was monitored with a Type 929 phototube circuit and a Tektronix 535-A oscilloscope. The time delay trigger circuit within the oscilloscope supplied the trigger pulse controlling the time interval between the photolysis flash and the spectroscopic flash.

The sample cell was constructed of Pyrex and had a path length of 20 cm. Surrounding the sample container was an annular jacket 1-cm thick which could be filled with a liquid to serve as an optical filter for the photolysis flash. The cell was equipped with a side arm assembly for degassing.

(1) (a) This research was supported by a NASA Institution Grant to the University of Virginia. (b) Address inquiries to George Mason College of the University of Virginia, Fairfax, Virginia 22030.

(2) (a) L. J. Andrews and R. M. Keefer, "Molecular Complexes in Organic Chemistry," Holden-Day, Inc., San Francisco, 1964; (b) E. M. Kosower in "Progress in Physical Organic Chemistry," Vol. 3. S. Cohen, A. Streitwieser, Jr., and R. Taft, Ed., Interscience Publishers, New York, N. Y., 1965.

(3) R. S. Mulliken, *J. Amer. Chem. Soc.*, **72**, 600 (1950); *J. Phys. Chem.*, **56**, 801 (1952).

(4) M. J. S. Dewar and A. R. Lepley, *J. Amer. Chem. Soc.*, **83**, 4560 (1961).

(5) J. N. Murrell, *ibid.*, **81**, 5037 (1959); *Mol. Phys.*, **7**, 363 (1963).

(6) R. L. Flurry, Jr., *J. Phys. Chem.*, **69**, 1927 (1965).

(7) E. M. Kosower and Lars Lindqvist, *Tetrahedron Lett.*, **50**, 4481 (1965).

(8) A. Hantzsch, *Ber.*, **44**, 1783 (1911).

(9) E. M. Kosower, *J. Am. Chem. Soc.*, **80**, 3253, 3261, 3267 (1958).

(10) E. M. Kosower, *ibid.*, **82**, 2188 (1960).

(11) S. F. Mason, *J. Chem. Soc.*, 2437 (1960).

(12) G. Porter, *Discuss. Faraday Soc.*, **9**, 60 (1950).

The alkyl halide salts were prepared by direct reaction between stoichiometric amounts of methyl iodide and either pyridine, collidine, or quinoline. The salt was then recrystallized twice from ethanol and washed with spectroscopic grade isooctane. All solvents used in the preparation of sample solutions were reagent grade chemicals.

All sample solutions were thoroughly degassed by the freeze-pump-thaw technique except when acetone was used as a solvent. In this case the sample was deoxygenated by bubbling dry, oil-free nitrogen through the sample for 2 hr prior to flashing.

The spectrographic film was calibrated with a series of neutral density filters whose optical densities were determined with a Cary Model 11 recording spectrophotometer. Only reasonably linear portions of the γ curve, where compared with the spectrophotometer traces indicated an accuracy of better than 10%, were used.

Experimental Results

A sample of $5 \times 10^{-2} M$ 1-methylpyridinium iodide in dichloromethane was degassed and flashed at 1500 J using an acetone filter solution which allowed excitation of only the charge-transfer band and not the pyridine group itself. A continuous transient absorption below 4200 Å and another above 6200 Å was observed. Film cutoff at 7000 Å and solution cutoff at 3800 Å limited the spectral range of observation. The sample solution was distinctly yellowed after several flashes. Absorption spectra taken before flashing compared with those taken after indicated a new permanent species absorbing at 3625 Å, which was inferred to be triiodide, I_3^- .

A $6.1 \times 10^{-4} M$ 1-methylcollidinium iodide solution in dichloromethane also showed the characteristic I_3^- band at 3625 Å after several flashes. In spite of slow decomposition upon flashing, useful data on the rate of decay of the transient in this system could be obtained. A plot of reciprocal absorptivity due to the transient *vs.* time gave a straight line, indicating a second-order process.

A $4.37 \times 10^{-4} M$ solution of 1-methylquinolinium iodide in dichloromethane was degassed and flashed through a nitromethane filter jacket which prevented direct irradiation of the quinoline portion of the molecule but allowed irradiation of the charge-transfer band at 4215 Å. A transient species was observed which absorbed from 6600 Å to the film cutoff at 7000 and from the solution cutoff at 4000 Å to about 5500 Å. This transient decayed very rapidly, having disappeared at 100 μsec . Only a small absorption was observed after 50 μsec . In contrast to the previously mentioned 1-methylpyridinium and 1-methylcollidinium iodides, the 1-methylquinolinium iodide system was apparently reversible. The spectrophoto-

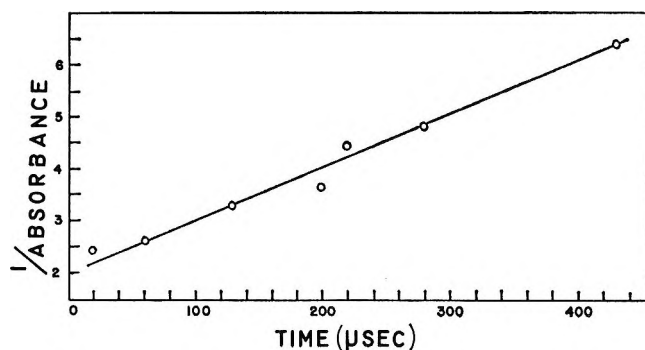


Figure 1. Second-order plot of the transient decay produced by flashing 1-methylquinolinium iodide in dichloromethane (6800 Å).

meter detected no change in the absorption spectrum of the solutions after several flashes.

Deoxygenated solutions of 1-methylquinolinium iodide at various concentrations in acetone were flashed using a nitromethane filter jacket. The transient absorptions were found to be longer lived than when dichloromethane was used as a solvent, and a kinetic study produced a second-order plot (see Figure 1). The values of k/ϵ , the ratio of the second-order rate constant to the extinction coefficient at 6800 Å, at various concentrations are given in Table I. Although the transient disappeared much more quickly in dichloromethane than in acetone, addition of 5% dichloromethane to an acetone solution did not noticeably increase the rate of disappearance of the transient.

Table I: The Rate of Decay of Transient in Acetone at Various Iodide Concentrations and the Peak Absorptivity Observed in Each Case

Quinolinium iodide, M	k/ϵ 6800Å, cm/sec	Peak absorptivity at $T = 0$
2.29×10^{-3}	5.2×10^4	0.65
1.14×10^{-3}	1.92×10^5	0.405
9.4×10^{-4}	7.8×10^5	0.19
1.14×10^{-3}	$<10^4$	0.8
+		
1.6×10^{-3}		

A solution of $1.14 \times 10^{-3} M$ 1-methylquinolinium iodide was doped with $1.6 \times 10^{-3} M$ NaI. The peak transient optical density was doubled to about 0.8 and the ratio of k/ϵ was decreased to less than 10^4 .

A degassed solution of 8.34×10^{-4} 1-methylquinolinium iodide in 1-propanol was flashed through a nitromethane filter solution. Flash spectra taken during the photolysis flash revealed a weak transient absorption between 5200 Å and 5500 Å as well as the absorptions which had been seen in dichloromethane and acetone (see Figure 2). At all time delays other than zero, no absorption in the 5200–5500-Å region

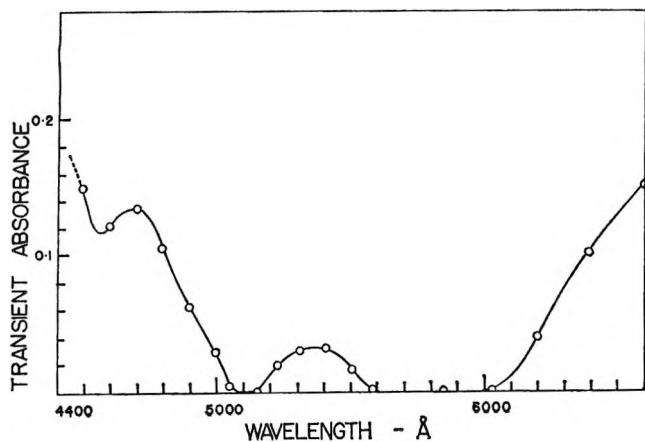


Figure 2. Transient absorption spectrum observed when 1-methylquinolinium iodide in 1-propanol was flashed. The absorption about 5100 Å and below 5600 Å occurred only in 1-propanol. The remainder of the absorption was seen in the other solvents also.

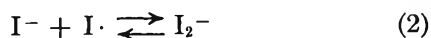
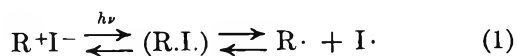
was detected. However, the system seemed to be reversible, and repeated flashing produced no permanent optical changes.

Flash photolysis of a 10^{-4} M NaI₃ solution in acetone using an acetone filter gave transient absorptions which appeared to be identical with those observed when the 1-methylpyridinium, 1-methylcollidinium, and 1-methylquinolinium iodides in acetone were flashed. The transient spectrum is thus assigned to the I₂⁻ ion which was observed by Stottleyer¹³ by flashing I₃⁻ and by Dobson and Grossweiner¹⁴ and by Grossweiner and Matheson,¹⁵ who flashed I⁻.

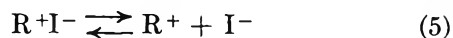
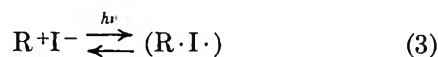
Discussion of Results

The transients observed below 5000 Å and above 6500 Å upon flashing the charge-transfer band of 1-methylpyridinium, 1-methylcollidium, or 1-methylquinolinium iodide were attributed to the diiodide ion, I₂⁻, on the basis of the similarity of the absorptions seen here to those reported elsewhere^{10,11} for this ion and of the similarity to absorptions produced upon flashing solutions of I₃⁻, which is known to result in the production of the diiodide ion. Since I₂⁻ was observed in all three of our cases, it is quite possible that at least part of the absorption at 3930 Å which Kosower and Lindqvist observed on flashing 1-ethyl-4-carbomethoxypyridinium iodide and which they attributed to the pyridinyl free radical may have been due to I₂⁻. The lower concentrations used by these workers reduces the possibility of I₂⁻ formation. The ion I₂⁻ in water has been reported¹⁶ to have a band maximum at 3850 Å with an extinction coefficient of 15,600 l. mol⁻¹ cm⁻¹.

The diiodide ion is apparently formed by the process



Reaction 2 has been discussed by Grossweiner and Matheson,¹⁶ who report for this reaction in water an equilibrium constant of 1.2×10^4 l. mol⁻¹ cm⁻¹. The first step in reaction 1 is the transfer of an electron from the iodide donor to an unfilled orbital of the organic cation producing a radical pair in the same solvent cage. The second step of reaction 1 indicates escape of the radicals from the cage. An alternate reaction sequence would be



Reaction 3 can be followed by cage escape with the same result as the former sequence. Reaction 5 represents the dissociation of the short-lived diiodide salt.

Flashing solutions of the pyridine or collidine salts produced permanent changes as shown by the formation of triiodide, I₃⁻. Thus the radicals produced from these salts appear to be removed permanently either by dimerization or by reaction with the solvent. The 1-methylquinolinium iodide, on the other hand, was completely reversible with no change observed in the solution absorption spectrum even after many flashes. It may be that delocalization of the unpaired electron due to contributing resonance structures is responsible for the apparent stability of the 1-methylquinoline free radical.

Kinetic data for the rate of disappearance of the I₂⁻ species produced from the quinoline salt gave a good second-order plot. As the concentration of the iodide species increased, either by increasing the concentration of 1-methylquinolinium iodide or by adding NaI, the second-order rate constant decreased (see Table I). Such concentration dependence can be shown to be due to an equilibrium such as (2) or (4) above.¹⁴

Unless there is a large change in the extinction coefficient of I₂⁻ in changing solvents from dichloromethane to acetone, the I₂⁻ species is much longer-lived in acetone. By analogy with I₃⁻ the extinction coefficient is not expected to change appreciably and the change in rate constant seems anomalous. The viscosities of the two solvents are very similar so at least in acetone the rate is not diffusion controlled. The addition of about 5% dichloromethane to a solution of 1-methylquinolinium iodide in acetone gave the same k/ϵ as had been observed for pure acetone. Thus,

(13) O. R. Stottleyer, Thesis, California Institute of Technology, 1954.

(14) G. Dobson and L. I. Grossweiner, *Radiat. Res.*, **23**, 290 (1964).

(15) L. I. Grossweiner and M. S. Matheson, *J. Chem. Phys.*, **23**, 2443 (1955).

(16) L. I. Grossweiner and M. S. Matheson, *ibid.*, **61**, 1089 (1957).

this increase in observed lifetime seems to be due to properties of the bulk solvent and also eliminates the possibility of reaction with the chlorinated solvent.

A new, weak absorption at 5200–5500 Å was observed when a solution of 1-methylquinolinium iodide in 1-propanol was flashed. This absorption may be due to the 1-methylquinoline free radical. The rate of decay of the transient was too fast for measurement and its identity is speculative. However, the 1-propanol should not give rise to species absorbing in this spectral region and the iodine atom–1-propanol charge-transfer complex should lie at much lower wavelengths.^{10,17} The reversible nature of the system suggests that the absorption was not due to a reaction intermediate. The possibility that this absorption was due to the $R^+I_2^-$ species shown in reactions 4 and 5 was eliminated on the basis that the apparent lifetime of this species was much less than that for the I_2^-

with which it was in equilibrium [reaction 5]. Since phosphorescence has been seen from excited charge-transfer complexes,¹⁸ the possibility also exists that a triplet–triplet transition was observed. It should be noted that the rapid decay of the observed transient does not imply anything about the rate constant. What is measured is k/ϵ ; thus k may be large or small depending on the value of the extinction coefficient.

Acknowledgment. This work was supported by a NASA Institution Grant to the University of Virginia. RFC wishes to thank NASA for a predoctoral fellowship.

(17) T. A. Gover and G. Porter, F. R. S., *Proc. Roy. Soc., Ser. A*, **262**, 476 (1961).

(18) Von J. Czekalla, G. Briegleb, W. Herre, and H. J. Vahlensieck, *Z. Elektrochem.*, **63**, 715 (1959).

Photoconductive and Photovoltaic Effects in Dibenzothiophene and Its Molecular Complexes¹

by Tapan K. Mukherjee

Energetics Branch, Air Force Cambridge Research Laboratories, Bedford, Massachusetts 01730 (Received August 22, 1969)

The photoconductivity of dibenzothiophene crystals was measured in the sandwich and surface type cells. The photocurrent spectral response and the suppression of photocurrent by small amount of fluorescence quencher tetracene demonstrate that optical excitation in the 340–230-m μ region generates carriers by a mechanism involving singlet exciton states. Mobile holes are majority carriers. Hole trapping, which modifies the conductivity type, can be accomplished by doping with electron acceptors. The photo emf consists of two stages; the fast rising positive emf in the region of low optical absorption changes sign in the stationary state. From the rise and decay characteristics of the short-circuit current in the regions of high and low optical absorption it is concluded that part of the total photo emf is diffusion controlled. The magnitude of the photovoltage in dibenzothiophene can be sensitized by doping with 2,7-dinitrofluoren- $\Delta^{\alpha\alpha}$ -malononitrile (DDF), 1,3,5-trinitrobenzene (TNB), and 2,4,5,7-tetranitrofluorenone (T₄NF). A number of new 1:1 charge-transfer complexes have been synthesized. The surface photocurrent peaks of these complexes, although considerably red shifted from the corresponding CT absorption peaks, are within the absorption edges. Dibenzothiophene–T₄NF complex, the best photoconductor of this series, was investigated in some detail. Electrons are found to be the majority carriers in this complex. A comparison of the photoconductivity and fluorescence of dibenzothiophene with anthracene did not yield any meaningful correlation between the two phenomena. In the case of dibenzothiophene crystal, the photoconductivity seems to be independent of the self-quenching process.

Introduction

The majority of the organic photoconductors are fluorescent materials. It has also been known that doping with small concentrations of fluorescent quenchers results in the suppression of photoconductivity of the host molecules.² Chaiken and Kearns have shown

that the long-wavelength photocurrents in anthracene³

(1) Part of this work was presented by T. K. Mukherjee, Abstracts, 156th National Meeting of the American Chemical Society, Atlantic City, N. J., Sept 1968, No. PHYS 23.

(2) D. O. Northrop and O. Simpson, *Proc. Roy. Soc., Ser. A*, **244**, 377 (1958).

(3) R. F. Chaiken and D. R. Kearns, *J. Chem. Phys.*, **45**, 3966 (1966).

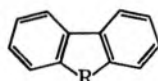
Table I: Elemental Analyses of Dibenzothiophene Charge-Transfer Complexes (1:1)

Acceptor ^a	Crystal- lization solvent	Dec. °C	Calcd %				Found %			
			C	H	N	S	C	H	N	S
TNF	CHCl ₃	205	60.11	2.62	8.41	6.41	59.92	2.75	8.29	6.28
T ₄ NF	CHCl ₃	237	55.14	2.22	10.29	5.88	55.43	2.28	10.17	5.93
DDF	CH ₃ CN	228	66.92	2.80	11.15	6.38	66.72	2.65	10.95	6.36
DTF	CH ₃ CN	249	61.42	2.39	12.79	5.85	61.17	2.19	12.80	6.01
TFM	CHCl ₃ + CH ₃ CN	280	56.75	2.04	14.18	5.41	56.59	1.81	14.09	5.57

^a See text for abbreviations.

and pyrene⁴ are substantially reduced by tetracene and acridine. These authors suggested that this behavior can be used as a test for the extrinsic process of charge carrier generation. In order to find a possible relationship between the photoconduction efficiency and the radiative properties associated with the optically excited states of photoconductive molecules, a number of structurally related fluorescent compounds were selected for investigation.

In the case of the annellated derivatives of some five-membered ring compounds (I), the fluorescence quantum yield decreases as fluorene (0.50) > carbazole (0.35) >



I

	-R-	Compound
(a)	-CH ₂ -	Fluorene
(b)	-NH-	Carbazole
(c)	-O-	Dibenzofuran
(d)	-S-	Dibenzothiophene

dibenzofuran (0.29) > dibenzothiophene (0.03).⁵ An evaluation of the photoconduction properties revealed that, among these compounds, only dibenzothiophene is photoconductive. Since very little information about the photoconductivity of sulfur-containing heterocyclic compounds is available, a detailed investigation of this compound was undertaken. A number of new stoichiometric complexes were synthesized and their photoelectrical properties studied.⁶

Experimental Section

1. Materials. Dibenzothiophene (Eastman Kodak, White Label) was crystallized first from glacial acetic acid followed by two crystallizations from acetonitrile. The electron acceptors were chosen so that the resulting complexes were fairly insoluble and they could be recrystallized without appreciable dissociation to the components. 2,4,7-Trinitrofluorenone (TNF) and 2,4,5,7-tetranitrofluorenone (T₄NF) were crystallized from glacial acetic acid. 2,7-Dinitro-(DDF), 2,4,7-trinitro-(DTF), and 2,4,5,7-tetranitro-(TFM) fluoren-Δ^{9α}-malononitrile were obtained from previous work.⁷

Spectrograde methylene chloride was used as solvent. The complexes were prepared by mixing hot solutions of equimolar quantities of dibenzothiophene and the acceptor. The precipitates were filtered, washed with the solvent, and recrystallized. In Table I, the elemental analyses and the final decomposition temperatures of the complexes are recorded.

2. Absorption Spectra. All spectra were measured on a Cary Model 14 spectrophotometer. The solid spectrum of dibenzothiophene was taken on a vacuum sublimed layer, as well as on a cluster of single crystals obtained by cooling the melt between two tin oxide coated (NESSA) plates. The charge-transfer complex was ground up with one drop of Cargille's nondrying immersion oil (*n*^{25D} 1.5150) and smeared on a quartz plate. The spectrum of the smear was taken against a blank quartz plate placed in the reference beam. Cargille's oil was found to be superior to a Nujol mull and this procedure avoids the troublesome KBr disk technique.

3. Photocells. Crystal sections, cut from zone-refined⁸ water-white ingots, were polished successively with fine emory paper, ethyl acetate-soaked lens paper, washed with benzene, and finally dried at 50° under vacuum. Single crystals were oriented with the long axis parallel to the cleavage plane.

For surface cells, epoxy-based silver electrodes were painted across the long axis on a single-crystal region which was selected by examining the section under a polarizing microscope. Alternatively, few crystals of zone-refined dibenzothiophene were melted on an Inconel grid deposited on quartz. A small piece of thin quartz plate placed on the solid helped the formation of an even layer of the melt. As the melt cooled, a cluster of randomly oriented needles was formed.

(4) R. F. Chaiken and D. R. Kearns, *J. Chem. Phys.*, **49**, 2846 (1968).

(5) D. W. Ellis and B. S. Solomon, *ibid.*, **46**, 3497 (1967).

(6) The solution spectroscopic properties of the charge-transfer complexes of dibenzothiophene and the related donors (I) have been reported; T. K. Mukherjee, *J. Phys. Chem.*, **73**, 3442 (1969).

(7) T. K. Mukherjee, *ibid.*, **70**, 3848 (1966).

(8) The zone refinement was carried out at the Franklin Institute Research Laboratories, Philadelphia, Pa., under Contract F19628-69-C-0129.

The single crystal of dibenzothiophene invariably cracked when it was pressed between two semitransparent NESSA electrodes. The low melting point of this compound (98°) precluded vacuum deposition of metallic electrodes on the surface of a pressed pellet. The photoconductivity action spectrum of a cracked crystal was identical with the spectrum obtained from the cell prepared by cooling a melt between two NESSA plates. All bulk conductivity experiments were performed on melt-cooled crystals.

The deeply colored CT complexes were deposited on the grid by slowly evaporating a hexane suspension of the powdered solid. Before the electrical measurements, the chemical homogeneity of each cell was visually examined under the microscope. Only those cells which did not show the presence of crystals of separate components were used. Evaporation from ethyl acetate and other polar solvents resulted in visible dissociation of the complexes.

4. *Measurements.* The apparatus for measuring the dc conductivity consisted of a Keithley Model 610A electrometer, a Keithley Model 241 voltage power supply, Bausch and Lomb Model 33-86-45 grating monochromator, and a 1000-W xenon light source equipped with "Schoeffel" power supply. The light intensity was measured by a calibrated thermopile.⁹ For the normalization of the bulk current data, the absorption and reflection loss due to the NESSA plates was compensated by using a blank plate as the thermopile window. For recording, an EAI Variplotter Model 1100 X-Y recorder was used. In the case of the molecular complexes, the harmonics from the lower wavelengths were removed by appropriate filters. Surface conductivity measurements were performed under vacuum.

Results and Discussions

The absorption spectra of dibenzothiophene, in the solid and solution states are shown in Figure 1. The bands in the 250–340- $m\mu$ region are red shifted in the solid by approximately 10 $m\mu$. Similar red shifts were also observed in the spectra of sublimed films of aromatic hydrocarbons.¹⁰ The surface photocurrent peaks (Figure 2) closely follow the optical absorption maxima of dibenzothiophene.

In addition to the strong peak at ~ 230 - $m\mu$ region, there is substantial photocurrent activity around 250 $m\mu$, which was not detected by Chiorobili and co-workers.¹¹ We saw no evidence of current saturation at higher fields. On the other hand, the solution grown or sublimed single crystals showed considerable imperfections and the current inclined to saturate rather rapidly. Since the photocurrent maximum around 230 $m\mu$ (5.93 eV) is well within the photoemission threshold of many organic compounds,¹² it is possible that the charge carriers at 230 $m\mu$ are generated by a direct ionization process rather than by an exciton dis-

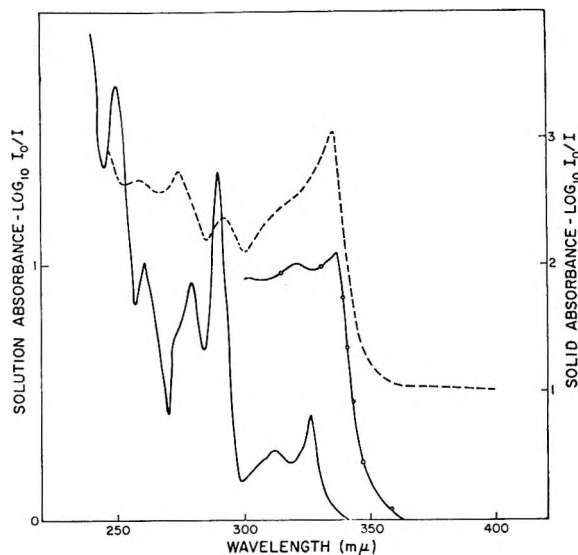


Figure 1. Absorption spectrum of dibenzothiophene: —, 10^{-4} M solution in methycyclohexane; - - - - -, sublimed layer on quartz plate; - · - · - ·, melt cooled crystals held between NESSA plates.

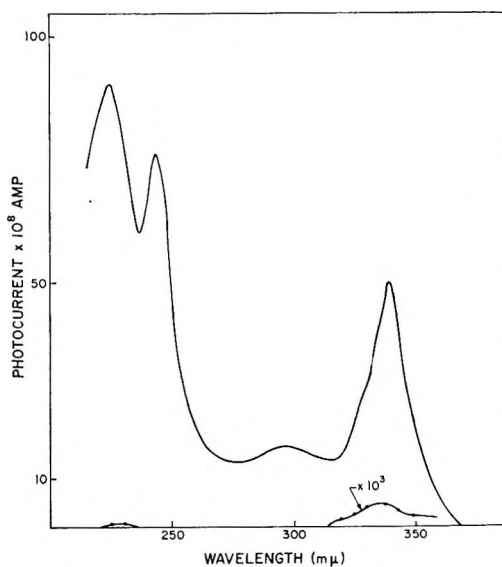


Figure 2. Spectral dependence of surface photocurrent in zone refined dibenzothiophene (—) corrected to $I_0 = 5 \times 10^{15}$ photons/sec, 200-V dc applied field; - · - · - ·, tetracene doped (uncorrected).

sociation mechanism. When the interelectrode space was coated with a very dilute solution of tetracene the photocurrent nearly disappeared from the entire spread of the spectrum (Figure 2). Similar suppression of photocurrent was observed in the grid configuration as well. The direct relationship between the photocurrent

(9) We are thankful to Dr. A. K. Ghose for the calibration.

(10) H. H. Perkampus, *Z. Phys. Chem.* (Frankfurt am Main), **19**, 791 (1959).

(11) P. Chiorobili, S. Peitra, and V. Passalacqua, *Ric. Sci.*, **38**, 796 (1968).

(12) F. Gutmann and L. E. Lyons, "Organic Semiconductors," Wiley, New York, N. Y., 1967, Table 6.7, p 693.

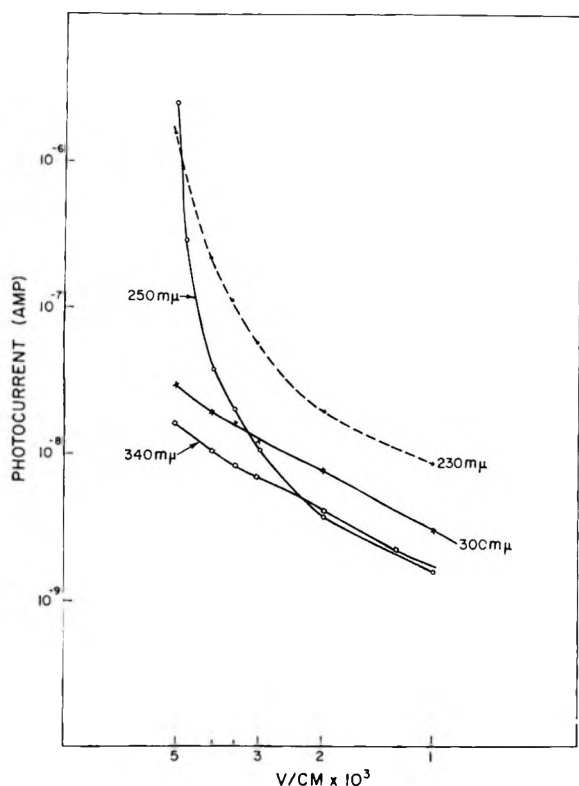


Figure 3. Voltage dependence of surface photocurrent in zone refined dibenzothiophene; photocurrent normalized to 5×10^{16} photons/sec.

and absorption maxima, in conjunction with the quenching phenomenon, support the view that exciton dissociation rather than photoemission from the contacts is the important step in the optical generation of charge carriers in dibenzothiophene. In our previous work³ we have shown that dibenzothiophene behaves more like a polycyclic aromatic hydrocarbon than a heterocyclic compound. It seems possible that the actual crystal photoemission threshold is situated at a higher energy level than the common heterocyclic compounds.

The field dependence of the surface photocurrent at 4.95 eV (250 $m\mu$) and 5.39 eV (230 $m\mu$) incident photon energies shows that the currents rise sharply at high fields (Figure 3). Although the trend towards superlinearity is faintly detectable for 300 $m\mu$, dielectric breakdown resulting in permanent short circuit prevented further measurements at these wavelengths.

The sharp rise in the I - V plots in Figure 3 show the characteristics of space-charge limited behavior; however, additional experiments are needed to confirm this point.

The surface photocurrent was found to be sensitive to the electrical contacts. The ratio $I_{340\ m\mu}/I_{230\ m\mu}$ in the grid cell (Figure 4) was reverse to that found in the single crystal cell (Figure 2). Illumination from the back caused enhancement of the current at 240 $m\mu$ without any significant rise in the 230-250- $m\mu$ region. The shift in the long wavelength peak in Figure 4 can be explained on the basis of light penetration and carrier

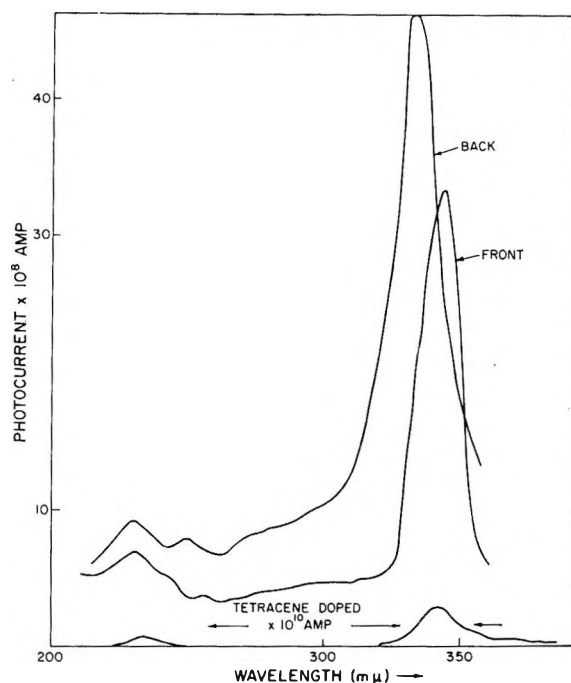


Figure 4. Spectral dependence of surface photocurrent in pure and tetracene doped, melt cooled dibenzothiophene (zone refined), deposited on grid electrodes; corrected to $I_0 = 5 \times 10^{16}$ photons/sec; 200 V dc.

removal rate. In the case of backside illumination, the surface-generated carriers are rapidly removed by the electrodes. On the other hand, carriers generated on the top of the surface (front illumination) are required to penetrate the bulk of the photoconductor before reaching the electrodes. Meanwhile, some weakly absorbed photons penetrate to some depth and generate carriers close to the electrodes. However, the range of shift was within the band width of the absorption peak. Since similar shifts have been observed in numerous other cases, it is not considered significant to the overall mechanism of conduction.

Since the transmission of light through the NESSA electrodes is limited to about 290 $m\mu$, the volume photoconductivity measurements were restricted to the long wavelength regions only. The magnitude of the photocurrent was 5 to 7 times greater when the positive electrode was illuminated. The dependence of the photocurrent on the incident light intensity ($I \propto L^n$) was determined with a 1.5×10^4 V cm field. At 10-100% relative light intensity, both hole and electron currents were linear ($n = 1.05$ and 1.07 , respectively). At lower photon flux, n dropped below 1.

The dark and photocurrent-voltage characteristics of SnO-dibenzothiophene-SnO system are shown in Figure 5. Except for the interesting phenomenon of sign inversion (Figure 5b), the curves are typical of an electrically neutral organic solid containing a single type of traps of equal energy. At very low fields, injection of carriers from the electrode and the removal of carriers from the crystal are usually negligible. The

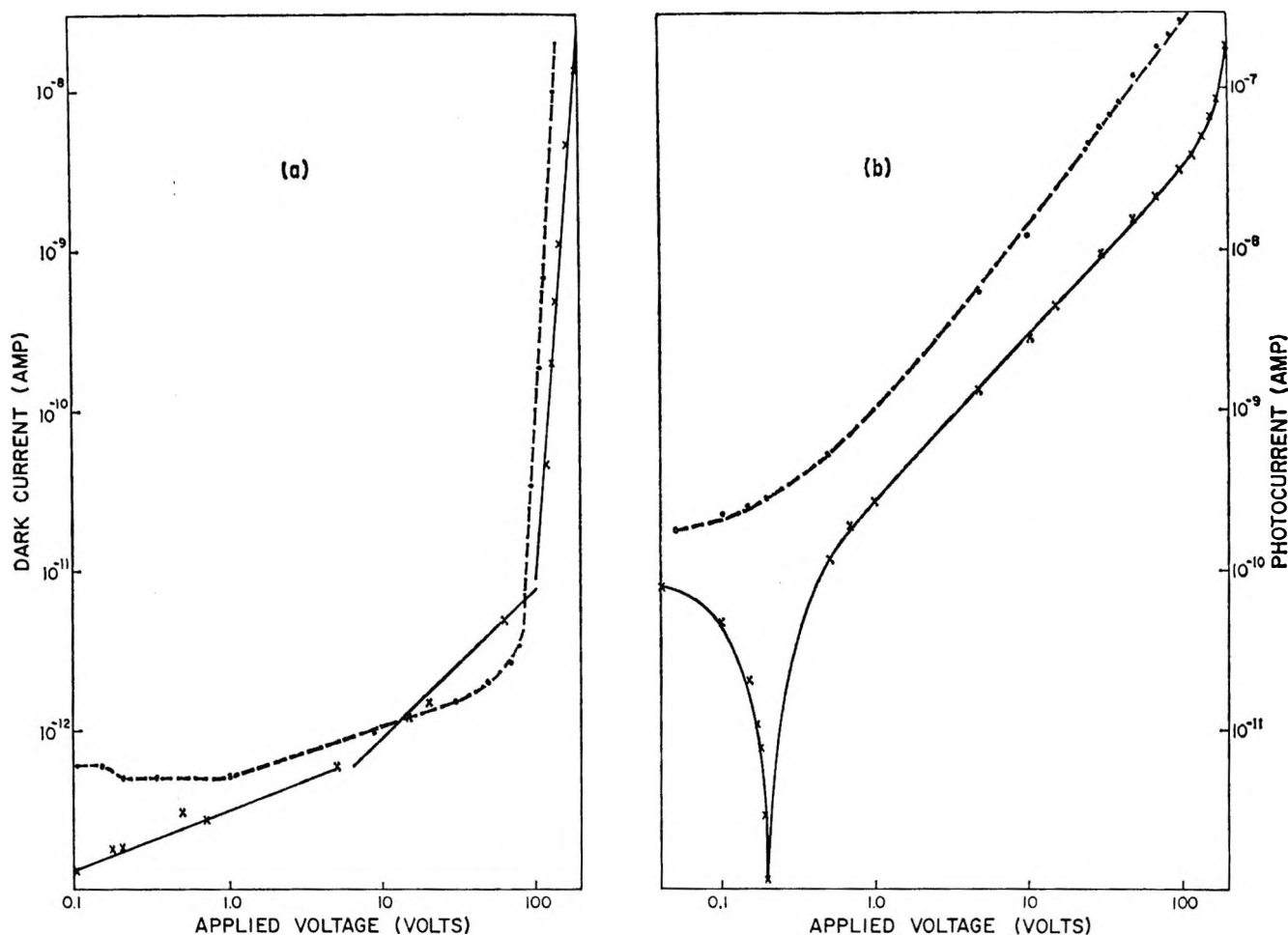


Figure 5. (a) Voltage dependence of bulk dark conductivity in dibenzothiophene: -----, before illumination of positive electrode; $\times-\times-\times$, before illumination of negative electrode. (b) Voltage dependence of bulk photoconductivity in dibenzothiophene: -----, positive electrode illuminated; $\times-\times-\times$, negative electrode illuminated; wavelength of exciting radiation, $340\text{ m}\mu$.

Table II: Effect of Doping ($10^{-3} M/M$) on the Photocurrent and Photovoltage of Dibenzothiophene

Dopant	Quantum efficiency of hole current, ϕ^+	Quantum efficiency of electron current, ϕ^-	Equilibrium photo emf, -mV	Photovoltaic current, amp	ϕ^+/ϕ^-
None	1.8×10^{-7}	4.8×10^{-8}	220	1.7×10^{-10}	3.7
Tetracene	1.7×10^{-12}	2.0×10^{-12}	240	3×10^{-10}	0.85
DDF	1.49×10^{-7}	1.49×10^{-7}	305	2.5×10^{-11}	1.0
TNB ^a	5.78×10^{-9}	2.38×10^{-8}	360	1.6×10^{-11}	0.24
T ₄ NF	4.08×10^{-8}	1.22×10^{-7}	340	2.4×10^{-10}	0.33
TCNE ^b	8.6×10^{-8}	7.6×10^{-9}	160	2×10^{-10}	11.0
Indigo	3.97×10^{-9}	2.24×10^{-9}	150	3×10^{-10}	1.77
Dicyanine	6.21×10^{-9}	3.97×10^{-9}	180	2.9×10^{-11}	1.56

^a Abbreviation: 1,3,5-trinitrobenzene (TNB). ^b Tetracyanoethylene (TCNE); for others, see Experimental Section.

inversion of sign seems to be the consequence of an opposite photovoltaic voltage developed within the cell. A study of the nature of this photo emf will be presented after the following section.

1. *Effect of Doping.* In Table II, the results are summarized in terms of relative quantum efficiency,¹³ defined as the ratio of the number of electrons in the

external circuit to the number of quanta absorbed at an applied field of 1 V/cm. There was no evidence of any significant sensitization of the wavelength of dibenzothiophene photocurrent peak. In several cases new

(13) Since the photocurrent did not saturate, absolute quantum efficiency was unobtainable.

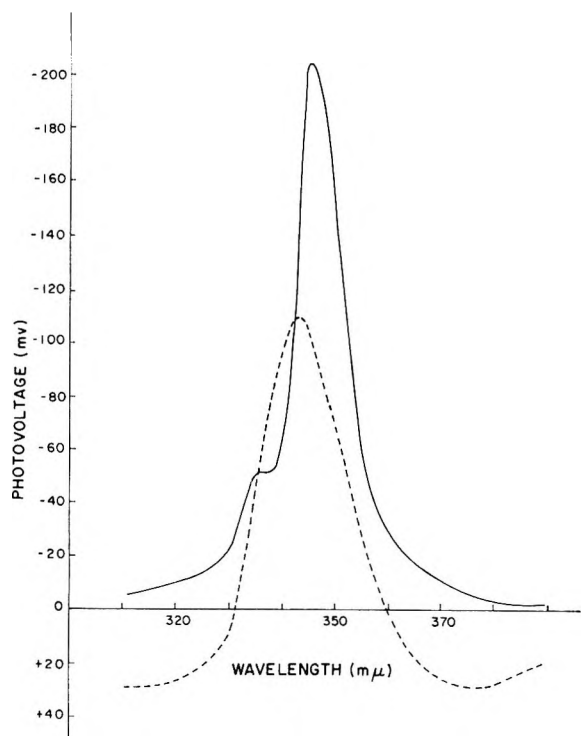


Figure 6. Photovoltaic spectral response in dibenzothiophene: ---, after 30 sec; —, after 5 min corrected to $I_0 = 2.8 \times 10^{16}$ photons/sec; cell short-circuited between readings.

tails were observed beyond the photocurrent peak at $\sim 340 \text{ m}\mu$. Although the origin of the photoconductivity corresponding to these long wavelength regions was not investigated, it seems reasonable to assume that they are due to the photoresponse of the free dopants (e.g., tetracene) or the corresponding CT complexes (e.g., $T_4\text{NF-dibenzothiophene}$). Doping with tetracyanoethylene (TCNE) enhanced the dark current. Since this acceptor is readily converted to an anion-radical, it is suspected that some ionic species, formed by electron-transfer reaction with dibenzothiophene, are responsible for the enhanced dark conductivity. The predominance of the hole current in dibenzothiophene was significantly reduced by the electron acceptors. In the case of trinitrobenzene (TNB) and tetranitrofluorenone ($T_4\text{NF}$), the electron currents superseded the hole current, suggesting that these acceptors create trapping sites for the mobile holes.

2. Photovoltaic Effect. The photovoltage spectral response (Figure 6) was characterized by a strong peak near the crystal absorption edge. The initial photo emf near the low-absorption region was positive but changed sign as the equilibrium state was approached. There were no measurable short-circuit photocurrents at the 320 and 370- $\text{m}\mu$ regions. The fast decay of the photovoltaic current (Figure 7a) at 335 $\text{m}\mu$ clearly demonstrates the contribution of Dember type voltage (diffusion emf) in the overall photo emf in dibenzothiophene. The photovoltaic current at 345 $\text{m}\mu$, corre-

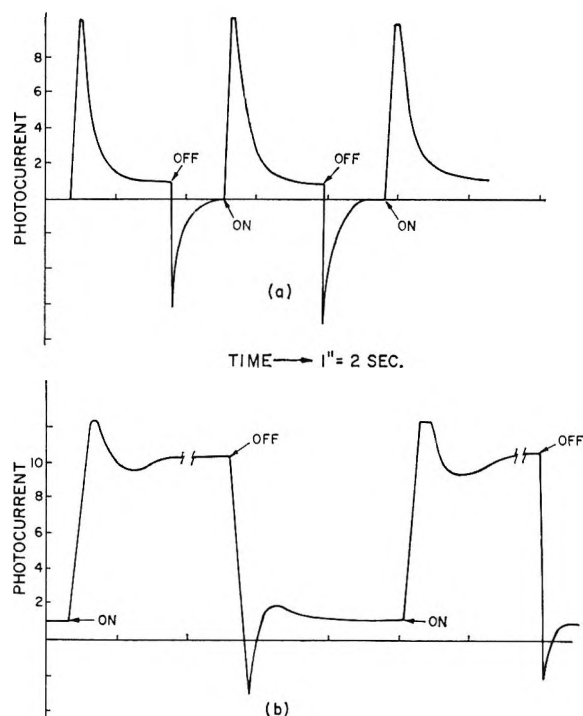


Figure 7. Rise and decay of photovoltaic current in dibenzothiophene; (a) excitation at 335 $\text{m}\mu$; (b) excitation at 345 $\text{m}\mu$.

sponding to the wavelength for maximum photovoltage, remained stable after initially suffering a small decay (Figure 7b). The transient surge in the opposite direction is considered due to the capacitive discharge of the photocell. Sign inversion of photo emf has been reported in anthracene¹⁴ and tetracene¹⁵ crystals. The phenomenon in these compounds was associated with the equilibrium states and was explained on the basis of field gradients set up by the filled and unfilled traps. In the present case, the origin of the non-stationary positive emf in the region of low optical absorption seems to be related to the potential difference at the electrode-semiconductor junction. A complete understanding of the mechanism will require the determination of the contact potential¹⁶ and work functions of the dibenzothiophene-SnO system.

3. Charge-Transfer Complexes. The appearance of long wavelength photocurrent in the acceptor doped cells has been mentioned earlier. This observation indicated that the 1:1 charge-transfer complexes might show photoconduction which could be related to the corresponding energies of the donor-acceptor interactions. Although the dark conductivities¹⁷ and spec-

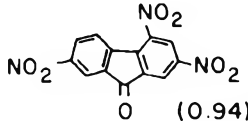
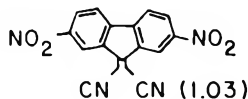
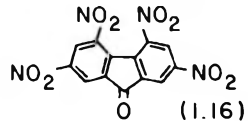
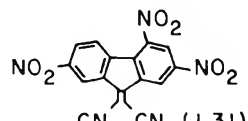
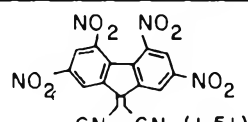
(14) V. V. Vladimirov, M. V. Kuri, and Yu. P. Pityatinskii, *Sov. Phys.-Dokl.*, **13**, 789 (1969).

(15) P. J. Reucroft, P. L. Kronick, and E. E. Hillnan, *Mol. Cryst. Liq. Cryst.*, **6**, 247 (1969).

(16) See Table 8.17 in ref 12; ref 1419 in this table could not be traced. Apparently this paper was not published (private communication from L. E. Lyons).

(17) See ref 12, Tables 8.5 and 8.6.

Table III: Surface Conductivity and Optical Absorption of Charge-Transfer Complexes; Donor Dibenzothiophene

ACCEPTOR (EA) ^a	ROOM TEMP. RESISTIVITY ρ , ohm cm	PHOTO CURRENT DARK CURRENT $\left(\frac{i_l}{i_d}\right)^b$	PHOTOCURRENT MAX. $m\mu$ (ev)	CT MAX. $m\mu$ (ev) $\pm 10 m\mu$	CT ABSORPTION EDGE $m\mu$ (ev) $\pm 20 m\mu$
 (0.94)	8×10^{11}	7.6	520 (2.38)	450 (2.75)	550 (2.25)
 CN CN (1.03)	8×10^{11}	71	575 (2.15)	490 (2.53)	585 (2.11)
 (1.16)	4.76×10^{11}	121	620 (2.00)	550 (2.25)	630 (1.96)
 CN CN (1.31)	4.54×10^8	10.2	642 (1.93)	550 (2.25)	635 (1.95)
 CN CN (1.51)	2×10^5	0.41	690 (1.79)	610 (2.03)	705 (1.75)

^a Electron affinity (EA) determined by polarography. T. K. Mukherjee, *Tetrahedron*, **24**, 721 (1968). ^b Photocurrent ($I = i_l - i_d$, where i_l = light current and i_d = dark current) normalized for equal intensity of illumination of 1 mW/cm².

trosopic characteristics¹⁸ of CT complexes have been extensively investigated, relatively little information concerning their photoconductive properties is available. Lardon and coworkers¹⁹ stated that the charge-transfer band corresponding to the polyvinylcarbazole (PVK)-TNF complex is efficient at exciting xerographic response in TNF-doped PVK films. On the other hand, the spectral response of the "primary" photocurrent in pyrene charge-transfer complexes²⁰ closely resemble the photocurrent spectrum of the free pyrene molecule.²¹ Similarly, the photocurrent in N-isopropylcarbazole-picryl chloride complex seemed to originate from the higher excitation levels of N-isopropylcarbazole alone.²² In the perylene-fluoranil single crystal,²³ the assignment of the photocurrent maxima was complicated due to the broad spectral response which extended into the infrared region.

A series of stoichiometric complexes of dibenzothiophene were synthesized and their dark and photoconductive properties were evaluated. The surface conductivities and optical absorption features of the photoconductive complexes are compared in Table III. A monotonic relationship between the photocurrent-dark current ratios (column 3) and the electronic affinities of the acceptors (column 1) is maintained up to the

T₄NF complex. Beyond this, the photoconductivity drops rather sharply. It may be mentioned that the complexes derived from TCNE, TCNQ, DDQ, and chloranil (EA = 1.95, 1.7, 1.95, and 1.37, respectively) did not show any photoresponse. In addition, the room temperature resistivities of the latter complexes were in the range of 10⁸-10⁶ ohm cm. It will be noted in Table III that the photocurrent maxima were consistently red-shifted from their CT absorption maxima. However, excepting the deviation of the DTF complex, the photoresponse peaks were located well within the absorption edges. The photocurrent maxima vs. CT absorption maxima, as well as the photocurrent maxima

(18) G. Briegleb, "Elektronen-Donator-Acceptor-Komplexe," Springer Verlag, West Berlin, 1961.

(19) M. Lardon, E. Lell-Döller, and J. W. Weigl, *Mol. Cryst.*, **2**, 241 (1967).

(20) H. Akamatu and H. Kuroda, *J. Chem. Phys.*, **39**, 3334 (1963). These authors prepared the photocells by cooling the melts of the charge-transfer complexes. We have found that on cooling most of these complexes deposited crystals of uncomplexed pyrene. Partial sublimation of TCNE was observed in the case of pyrene-TCNE complex.

(21) B. J. Mulder, *Rec. Trav. Chem.*, **84**, 713 (1965).

(22) J. H. Shapr, *J. Phys. Chem.*, **71**, 2587 (1967).

(23) H. Kokado, K. Hasegawa, and W. G. Schneider, *Can. J. Chem.*, **42**, 1084 (1964).

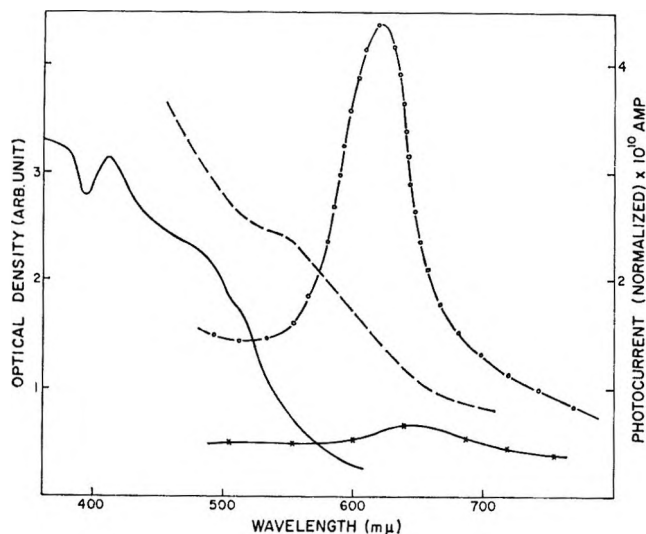


Figure 8. Spectral response of bulk photocurrent in dibenzothiophene- T_4NF charge-transfer complex: - - - - -, electron current; -X-X-X-X; hole current; —, absorption spectrum (CH_2Cl_2); ·····, oil smear.

vs. CT absorption edges (Table III) yielded straight-line plots. This finding indicates that the photocarrier generation process, at least qualitatively, is initiated by the photons which cause optical excitation of the CT complexes. This point was further examined with the T_4NF complex.

Dibenzothiophene- T_4NF complex crystallized as bright red silken needles. In methylene dichloride solution, it showed CT absorption band at $480\text{ m}\mu$ ($\log E = 2.75$).²⁴ It is estimated that 99.9% of the light incident on the solid surface is absorbed within a depth of $65\text{ }\mu$.²⁵ The spectral dependence of the volume photoconductivity, in the compressed disk form, is shown in Figure 8. The electron current in this complex predominates over the hole current. The photocurrents dropped significantly when the electrodes were blocked with mylar film. However, the electron current still superseded the hole current by a factor of three. Further, the photocurrent peak at $\sim 620\text{ m}\mu$ of the comb type surface cell (sedimentation layer) dropped by a factor of 5 when oxygen was passed through the evacuated chamber. These results strongly suggest that electrons are majority carriers in a dibenzothiophene- T_4NF complex. Thus, while holes are majority carriers in pure dibenzothiophene, they are converted to minority carriers in the T_4NF complex. Similar reversal was observed in the case of anthracene²⁶ where hole current was suppressed by the formation of 1,3,5-trinitrobenzene CT complex at the surface.

Although the exact locations of the CT maxima as well as the photocurrent maxima in polycrystalline forms are subjected to several experimental uncertainties, any attempt to correlate the two must exclude the role of unknown sensitizing impurities. Routine analytical experiments eliminated the possibility of the presence

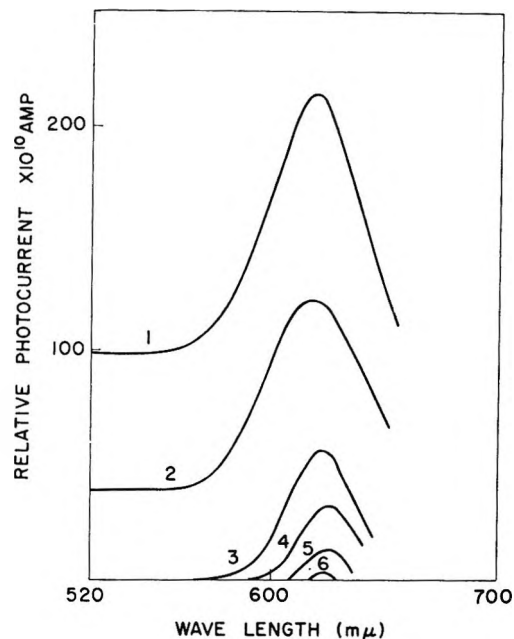


Figure 9. Concentration dependence of CT complex on the surface photoconductivity of DBT- T_4NF system: (1) 100% complex; (2) 80% complex; (3) 60% complex; (4) 50% complex; (5) 46% complex; and (6) 40% complex.

of detectable impurities of by-products in the present system. Reucroft and coworkers²⁷ have shown that the impurity sensitized long wavelength photocurrent in chloranil crystal is substantially decreased at high field strengths. In dibenzothiophene- T_4NF complex, however, the photocurrent at $620\text{ m}\mu$ increased linearly with the applied field and followed the relationship $I \propto V^n$ ($n = 1$ at 2×10^3 to $1.6 \times 10^4\text{ V cm}$; $n = 2.4$ at 1.6×10^4 to $2.4 \times 10^4\text{ V cm}$, and $n > 4$ above $3 \times 10^4\text{ V cm}$). In addition, the peak at $620\text{ m}\mu$ did not undergo any shift at higher fields.

Addition of incremental amounts of dibenzothiophene to nonphotoconductive T_4NF results in the appearance of a photocurrent band around $620\text{ m}\mu$.²⁸ The change in the magnitude of the photocurrent was compared in the surface cells of fixed interelectrode distance (comb cell). The results, shown in Figure 9, demonstrate that dibenzothiophene- T_4NF complex, by itself, is photoconductive and the photocarriers in this complex are generated within the energy range of the excited CT states.

(24) The $\log E$ values were calculated from Benesi-Hildebrand (*J. Amer. Chem. Soc.*, **71**, 2703 (1949)) procedure. The peak positions were estimated by half band width technique.

(25) It was not possible to directly determine the molar absorption coefficient. The average density value (1.5) of organic crystals was used in the approximation of the light absorption depth.

(26) D. C. Hoesterey, *J. Chem. Phys.*, **36**, 557 (1962).

(27) P. J. Reucroft, O. N. Rudijj, R. E. Salomon, and M. M. Labes, *ibid.*, **43**, 767 (1965).

(28) Weighed amounts of the powdered components were thoroughly mixed with 5 ml of chloroform, the solvent was evaporated, and the photocells were prepared with the fixed weight of dry residue. Dibenzothiophene is assumed to be completely complexed in all these cells.

Conclusion

The photocurrent quantum efficiency of dibenzothiophene, determined from 14 sandwich cells, varies between 10^{-7} and 10^{-8} electrons/quantum. Under similar experimental conditions, highly photoconductive anthracene gave values ranging between 10^{-6} and 10^{-8} electrons/quantum. This comparison must be considered tentative primarily due to the inherent uncertainty in the measurement of the photoconductivity data. Furthermore, the melt-cooled anthracene photocells are more uniform and show better electrical contacts. The solution fluorescence quantum efficiency of dibenzothiophene ($\phi_F = 0.025$) is about $1/10$ th of anthracene ($\phi_F = 0.23$).²⁹ From the relationship $\tau_n = \tau_e/\phi_F$ where τ_n is the mean lifetime in the absence of all other competitive process and τ_e is the actual lifetime, one can estimate $\tau_e = 0.2$ nsec for dibenzothiophene³⁰ which is an order of magnitude smaller than anthracene ($\tau_e = 4.5$ nsec).³¹ Thus the differential significance of the crystal photoconductivity and

the fluorescence lifetime or efficiency of the solution is not obvious.

On the other hand, the lack of fluorescence in the crystal of zone-refined dibenzothiophene implies that the photoconduction is not severely influenced by the fluorescence quenching features present in the solid state. Since there was no detectable photocurrent in the 410–500-m μ region, the involvement of triplet states in the carrier generation process may also be eliminated. In this respect dibenzothiophene resembles rubrene, which although an excellent photoconductor does not fluoresce in the crystal form.³²

(29) Measured in ethanol. We are indebted to Dr. S. Ness for these values.

(30) Calculations based on ethanolic solution: $\tau_n = 3.47 \times 10^8 \nu^2 n^2 \int \epsilon d\nu$.

(31) A. S. Cherkasov, V. A. Molchanov, T. M. Vember, and K. G. Voldaikina, *Sov. Phys.-Dokl.*, **1**, 427 (1956).

(32) M. Kleinerman, L. Azarraga, and S. P. McGlynn, *J. Chem. Phys.*, **37**, 1825 (1962).

The Effect of Pressure on the Density and Dielectric

Constant of Polar Solvents

by L. G. Schornack and C. A. Eckert

Department of Chemistry and Chemical Engineering, University of Illinois, Urbana, Illinois 61801
(Received February 25, 1970)

A technique has been developed for the simultaneous determination of density and dielectric constants of liquids at high pressure. This employs a bellows dilatometer attached to a linear differential transformer and containing the guarded capacitor of a heterodyne beat dielectric device. Data are reported for five polar solvents—chlorobenzene, ethyl acetate, isopropyl ether, tetrahydrofuran, and dichloromethane—at 30 and 50° and at pressures up to 5000 atm. The results are fit to various correlating equations.

The effect of pressure on the properties of solvents is important not only as a clue to the structure of the liquid state but is also invaluable in the interpretation of solvent interactions with various solute molecules. For example, high-pressure kinetic studies provide a formidable tool for the study of chemical reactions in solution, but interpretation of the results requires a knowledge of the variation of density and dielectric constant with pressure. Then the results can be used for mechanistic interpretations,¹ the determination of the structure and properties of the transition state,² and for the prediction of solvent effects on reaction rates.^{3,4} In this work we report an experimental technique for

the simultaneous determination of density and dielectric constant of liquids at pressures up to 5000 atm. New results for these quantities are reported for five polar solvents, and these data are compared with several analytical expressions proposed in the literature.

The classical relationship for expressing the pressure dependence of the molar volume v , is the Tait equa-

(1) R. A. Grieger and C. A. Eckert, *J. Amer. Chem. Soc.*, **92**, 2918 (1970).

(2) K. F. Wong and C. A. Eckert, *Trans. Faraday Soc.*, in press.

(3) C. A. Eckert, *Ind. Eng. Chem.*, **59**, 20 (1967).

(4) K. F. Wong and C. A. Eckert, *Ind. Eng. Chem. Process Des. Develop.*, **8**, 568 (1969).

tion,⁵ usually written in terms of the compression k as

$$k = \frac{v_1 - v_P}{v_1} = C \log \left(\frac{B + P}{B + 1} \right) \quad (1)$$

where v_1 and v_P are the molar volumes at 1 atm and at pressure P , respectively, and B and C are constants. The constant B is a function of the substance and of temperature, but not of pressure. Attempts have been made to relate it to internal pressure.⁶ For many substances, the same value of C has been found, invariant with both pressure and temperature. Recently, new derivations of the Tait equation have been worked out⁷ which indicate that it may have some basis in theory.

The dielectric constant ϵ has also been correlated by a Tait-like expression⁸

$$1 - \frac{\epsilon_1}{\epsilon_P} = A \log \left(\frac{B + P}{B + 1} \right) \quad (2)$$

where B is the Tait constant for density and A is a pressure-independent constant. If both eq 1 and 2 are valid, then the compression is linear in the reciprocal of dielectric constant.

$$k = \frac{C}{A} \left(1 - \frac{\epsilon_1}{\epsilon_P} \right) \quad (3)$$

Other authors⁹ have used eq 2 as a two-parameter expression, determining both constants A' and B' empirically

$$1 - \frac{\epsilon_1}{\epsilon_P} = A' \log \left(\frac{B' + P}{B' + 1} \right) \quad (4)$$

Skinner, Cussler, and Fuoss^{9b} proposed a similar expression, substituting dielectric susceptibility for dielectric constant

$$1 - \left(\frac{\epsilon_1 - 1}{\epsilon_P - 1} \right) = A'' \log \left(\frac{B'' + P}{B'' + 1} \right) \quad (5)$$

where A'' and B'' are constants to be fit. Recent comparisons of the results of using various expressions have been presented by Hartmann, *et al.*,^{9a} and Schadow and Steiner.¹⁰

The need to determine the effect of pressure on both density and dielectric constant has become more apparent recently, especially in terms of the above relationships. Some authors have determined both, but not simultaneously.^{9b,11} One example of a simultaneous determination was that of Brown,¹² but at pressures only up to a few hundred atmospheres. A similar apparatus was used by Mopsik¹³ to 2000 atm. In this work we describe a somewhat different type of apparatus which has been used up to 5000 atm.

Apparatus

The experimental apparatus consisted of a variable-volume high-pressure sample cell, containing a dielectric constant cell, all of which fit inside the cavity of a

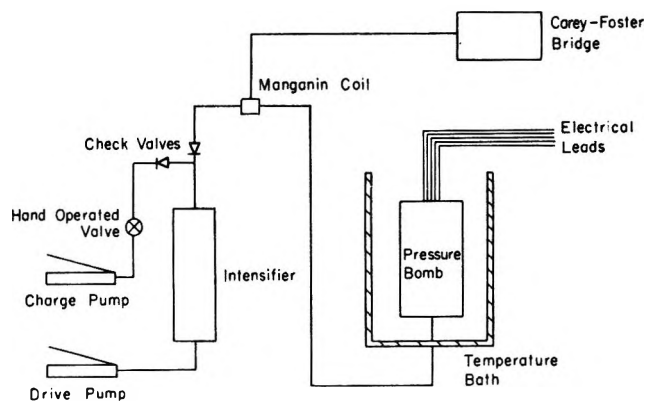


Figure 1. High-pressure system and thermostat.

thermostated high-pressure bomb. Electrical leads into the bomb permitted simultaneous measurement of dielectric constant, by a heterodyne beat technique, and of sample density, by electrical determination of the displacement of an iron core in a transformer inside the bomb.

A. High-Pressure System. A schematic diagram of the high-pressure rig is shown in Figure 1. The pressure generating system consisted of hand pumps, intensifier, and a manganin coil pressure gauge, all constructed by Harwood Engineering Co. The system was rated at 200,000 psi and a Carey-Foster bridge was used to measure pressures, with a resolution of 25 psi up to 100,000 psi. The pressure bomb, also by Harwood, was constructed of two concentric, shrink-fitted, autofrettaged Martinsitic steel cylinders, with an overall diameter of 10 in. and a length of 16 in. The available working space was 1.5 in. in diameter by 6 in. long. The pressure transmitting fluid was a 5:1 mixture of white gas and di-(α ethyl hexyl) sebacate (Esso's Univis P-38).

The entire bomb was mounted in a 25 gallon temperature bath (containing Wesson oil plus 1% hydroquinone as antioxidant) controlled and measured to $\pm 0.02^\circ$ by thermometers with calibration traceable to

(5) P. G. Tait, "Physics and Chemistry of the Voyage of the H. M. S. Challenger," Vol. II, Part, IV, 1888.

(6) (a) R. E. Gibson and J. T. Kincaid, *J. Amer. Chem. Soc.*, **60**, 511 (1938); (b) R. E. Gibson and O. H. Loeffler, *J. Phys. Chem.*, **43**, 207 (1939).

(7) (a) R. Ginell, *J. Chem. Phys.*, **34**, 1249 (1961); (b) G. A. Neece and D. R. Squire, *J. Phys. Chem.*, **72**, 128 (1968).

(8) (a) B. B. Owen and S. R. Brinkley, *Phys. Rev.*, **64**, 32 (1943); (b) B. B. Owen and S. R. Brinkley, *J. Chem. Educ.*, **21**, 59 (1944).

(9) (a) H. Hartmann, A. Neumann, and G. Rinck, *Z. Phys. Chem. (Frankfurt am Main)*, **44**, 218 (1965); (b) J. F. Skinner, E. L. Cussler, and R. M. Fuoss, *J. Phys. Chem.*, **72**, 1057 (1968).

(10) E. Schadow and R. Steiner, *Z. Phys. Chem. (Frankfurt am Main)*, **66**, 105 (1969).

(11) D. W. Brazier and G. R. Freeman, *Can. J. Chem.*, **47**, 893 (1969).

(12) R. F. Brown, Jr., *J. Res. Nat. Bur. Std., Sect. C*, **67**, 33 (1963).

(13) (a) F. I. Mopsik, *ibid.*, *Sect. A*, **71**, 287 (1967); (b) F. I. Mopsik, *J. Chem. Phys.*, **50**, 2559 (1969).

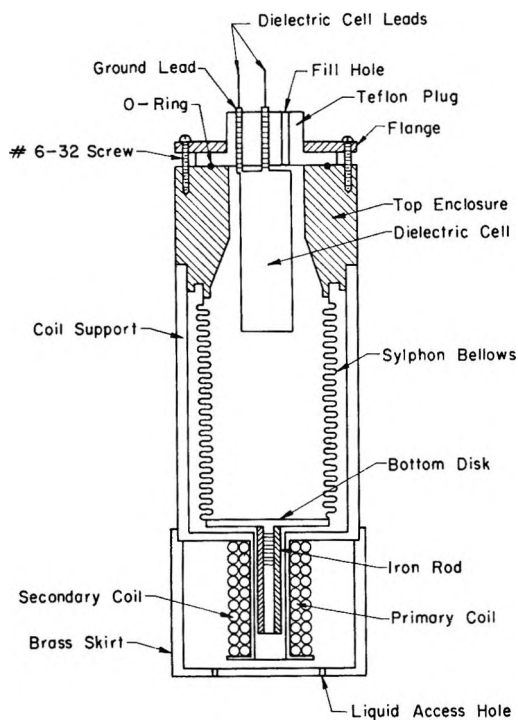


Figure 2. High-pressure density and dielectric constant cell.

the National Bureau of Standards. Further details of the high-pressure system are given elsewhere.¹⁴

B. High-Pressure Cell. The high-pressure cell, shown in Figure 2, had an internal volume of about 27 cm³, variable by the expansion of a Sylphon bellows. Attached rigidly to the base of the bellows was a 1½ in. long piece of ¼-in. soft iron rod, as a core for the transformer. The 1⅛-in. phosphorbronze bellows had an inside diameter of ⅝ in. and a length of 2⅔ in. With 22 active corrugations it was rated for a maximum compression of 1-1⅛ in. This bellows was soldered to the top enclosure, which was drilled out to provide space for the dielectric cell, well away from the moving end of the bellows. The sample chamber was closed by a Teflon plug, sealed by a CNR-nitroso rubber O-ring, and covered by a coating of epoxy glue.

Integral with the high-pressure cell shown at the bottom of Figure 2 was a variable transformer for determination of the position of the bellows. The coils were wound on a thin brass cylinder, slit to reduce eddy current losses. The primary coil was wound first with five layers of No. 32 Formvar-coated copper wire. The secondary coil was wound directly over the primary coil, again with five layers of the same wire. Both coils were wound at 80 turns per inch per layer. The dc resistance of the primary coil was 14.5 ohms; that of the secondary coil was 14.7 ohms. Before winding the coils the central shaft was coated with Teflon tape to reduce the possibility of rubbing the insulation off the wires. Each coil when completed was lightly covered with glue. This was sufficient to hold the wires in place and prevent unwinding. A protective brass skirt

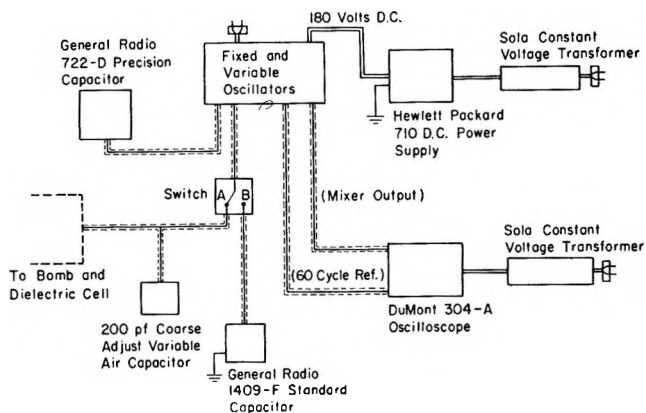


Figure 3. Heterodyne beat apparatus for dielectric constants.

was soldered to the coil support to form a rigid unit.

The dielectric cell was mounted inside the high-pressure cell by means of a threaded spindle on the inner cylinder screwed into the Teflon plug. The spindle served as the "hot" electrical lead to the dielectric cell, and a threaded rod placed through the plug was the ground lead.

This cell consisted of two precision-machined (± 0.0002 in.) concentric brass cylinders, both rigidly supported by and electrically insulated by two high-strength ceramic rings, made from McDanel ⅜-in. (Av 30) high-temperature alumina, with a compressive strength of 400,000 psi. The working dielectric gap was 0.3008 in. i.d. and 0.3550 in. o.d. by about 2 in. long. To protect against spurious effects from the movement of the bellows, the bottom of the dielectric cell was protected by a brass guard skirt.

C. Dielectric Constant Apparatus. The dielectric constants were measured by the heterodyne beat technique,¹⁵ which compares the frequency of a fixed, crystal-controlled reference oscillator with that of a variable oscillator. A schematic of the apparatus is shown in Figure 3.

The oscillator unit was that described by Gerteis.¹⁶ The 180-V power supply for it was a Hewlett-Packard Model 710 dc power supply. The oscilloscope used was a DuMont 304-A model. The output from the mixer circuit was placed in the Y axis of the scope while a 60 cps reference frequency was put into the X axis. The line voltage to both the dc generator and oscilloscope was stabilized against voltage fluctuations by Sola constant voltage transformers. The precision measuring capacitor was a General Radio 722-D variable air capacitor. The high range (200–1150 pF) used could be read directly to ± 0.1 pF and estimated to ± 0.02 pF. The high range was calibrated by the University of Illinois Physics-Betatron Laboratory to better than

(14) S. P. Sawin, M.S. Thesis, University of Illinois, Urbana, 1968.

(15) L. Hartshorn and W. H. Ward, *J. Inst. Elect. Engr. (London)*, **79**, 597 (1936).

(16) R. L. Gerteis, Ph.D. Thesis, University of Illinois, Urbana, 1963.

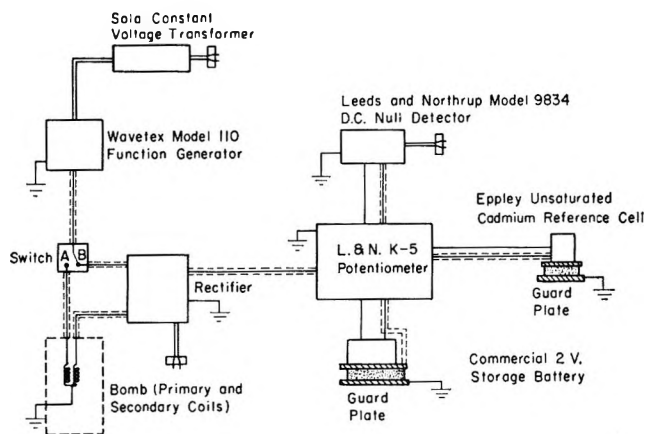


Figure 4. Schematic of apparatus for density measurements.

$\pm 0.01\%$. To eliminate inaccuracies due to frequency drift a low-capacity switch was placed in the probe line to permit checking with a General Radio 1409-F standard capacitor, which had a thermal- and time-insensitive 1000 pF rating.

All electronic equipment was properly grounded and thermally protected by surrounding with $\frac{1}{2}$ -in. styrofoam sheeting. All cables were coaxial (as indicated by dotted lines in the drawings) and were connected with UHF connectors. The lead into the pressure bomb was quite rigid to prevent geometrical changes, and completely shielded.

D. Density Measuring Apparatus. The technique used to measure density changes under pressure is related in part to that developed by Doolittle, Simon, and Cornish.¹⁷ The motion of a ferromagnetic rod inside a cylindrical transformer due to compression of the material within the cell produced a changing voltage in the secondary coil. *A priori* calibration of the coils then allowed one to translate the voltage change into a linear displacement and subsequently into volume and density changes. A schematic of the apparatus for density measurements is shown in Figure 4.

The signal source was a Wavetek Model 110 function generator. The operating conditions were set to maximize voltage amplitude and frequency stability as well as the sensitivity of the coil assembly, while the current flux through the coils was sufficiently small to minimize heating. The signal used was a 3000-cps sine wave with amplitude 3.3 V. A constant voltage transformer and thermal insulation held the amplitude stability to better than $\pm 0.05\%$ for short term usage (10 min) and $\pm 0.25\%$ for long term usage (24 hr). The dc offset control was periodically adjusted to ensure zero dc voltage through the primary coil.

For better accuracy, the ac output voltage was rectified and measured potentiometrically. The rectifier, based on two balanced Nexus operational amplifiers in a linearizing circuit, provided an output of sufficient stability to introduce no additional uncertainties into the signal.

The dc measuring device used was a Leeds and Northrup 7555 Type K-5 potentiometer. On the high (0–1.6 V) range used, the input signals could be read to $\pm 5 \mu\text{V}$ with an accuracy of 0.003%. Auxiliary equipment for the potentiometer included a Leeds and Northrup Model 9834 guarded dc null detector, an Eppley unsaturated cadmium constant voltage reference cell, and a 2 V dc power supply.

In Figure 4 the solid lines enclosed by two dashed lines represent coaxially shielded cable. All connections were of the BNC type except for binding posts on the potentiometer circuits. The two "hot" leads from coils within the bomb were soldered to BNC connectors which were rigidly fastened to a grounded plate held directly above the bomb. There were no visible effects due to any type of stray voltage pickup.

The null detector, reference cell, and power supply were all guarded against leakage voltage by using coaxial cable for the (+) lines, with the outer shielding of the cable connected to the guard post of the potentiometer. The reference cell and power supply were rested on guard plates consisting of aluminum-plexiglass-aluminum sandwiches. The other end of the guard plate was attached to the top aluminum sheet, and the bottom sheet was connected to an earth ground.

Since the function generator unit did have a slight variation of output amplitude, both the voltages to the primary coil and from the secondary coil were monitored, and the quantity measured was the voltage ratio ($V_{\text{sec}}/V_{\text{pri}}$) by the switching arrangement shown in Figure 4. The voltage ratio was time invariant and depended only upon the geometrical configuration of the coil-rod assembly.

Further details of the apparatus are given elsewhere.¹⁸

Procedure

Fischer reagent grade chlorobenzene was treated with 5% potassium carbonate solution to remove acids. It was then washed twice and fractionally distilled from Linde 4-A molecular sieves in a 1-in. column 36 in. long packed with glass helices. The boiling range was 131.4–131.6°.

Atmospheric densities were measured at 30 and 50° in a constant-temperature water bath using modified Sprengel pycnometers. The pycnometers were calibrated against water and had volumes of approximately 10 cm³. Weighings with and without liquid samples were made on a Mettler H-6 balance. Duplicate runs were made on each material and the results were reproducible to within $\pm 0.0001 \text{ g/cm}^3$.

The dielectric cell was calibrated by measuring its capacity when filled with a series of materials of varying dielectric constant, and the edge effects were found to be

(17) A. K. Doolittle, I. Simon, and R. M. Cornish, *AIChE J.*, **6**, 153 (1960).

(18) L. G. Schornack, M.S. Thesis, University of Illinois, Urbana, 1969.

quite small.¹⁸ The initial dielectric constants at 30° were measured relative to dry nitrogen, and the initial dielectric constants at 50° were calculated from the change in cell capacity with temperature.

The high-pressure cell was carefully cleaned and dried before each run. The dielectric liquid was weighed into the cell to an accuracy better than 0.05%, and the cell was sealed. The initial atmospheric point was taken after allowing the cell to reach equilibrium over a 3–4–

highest pressures used.¹⁴ Thus under the worst possible conditions, the residual temperature error due to the heat of compression would be of order 10⁻⁵°. In every case equilibrium was further assured by the constancy of both the density and dielectric measurements for at least 30 min before a data point was recorded.

Most data points were taken during the cycle of increasing pressure. The pressure was increased at the rate of about 1000 psi/min. Data points were taken

Table I: Experimental Results for Dielectric Constant and Density

Solvent	Data at 30°			Data at 50°		
	<i>P</i> , atm	ϵ	ρ , g/cm ³	<i>P</i> , atm	ϵ	ρ , g/cm ³
Chlorobenzene	1	5.552	1.0960	1	5.216	1.0630
	461	5.798	1.1280	1135	5.648	1.1362
	1355	6.050	1.1733	2407	5.946	1.1977
	1933	6.175	1.1978	3701	6.173	1.2441
	2955	6.445	1.2358	5029	6.363	1.2831
	4046	6.561	1.2715			
Ethyl acetate	1	5.984	0.8883	1	5.422	0.8642
	508	6.297	0.9271	624	5.792	0.9124
	1031	6.522	0.9634	1111	5.991	0.9444
	2075	6.884	1.0151	2075	6.308	0.9951
	3054	7.152	1.0508	3010	6.559	1.0315
	4070	7.392	1.0811	4026	6.828	1.0618
	5029	7.598	1.1048	5060	7.027	1.0881
Isopropyl ether	1	3.805	0.7129	1	3.519	0.6924
	524	4.216	0.7606	451	3.884	0.7349
	1054	4.515	0.7957	1007	4.176	0.7760
	2044	4.916	0.8418	1923	4.528	0.8230
	3020	5.229	0.8747	3034	4.858	0.8637
	4009	5.508	0.8998	4036	5.105	0.8919
	5016	5.767	0.9241	5046	5.339	0.9163
Tetrahydrofuran	1	7.261	0.8730	1	6.272	0.8320
	461	7.605	0.9021	612	6.614	0.8765
	1054	7.941	0.9345	1250	6.917	0.9148
	1566	8.195	0.9592	2512	7.473	0.9686
	2095	8.414	0.9814	3674	7.920	1.0033
	2965	8.750	1.0126	5102	8.419	1.0368
	3995	9.153	1.0376			
	5057	9.461	1.0632			
Dichloromethane	1	8.649	1.3078	40	7.757	1.2587
	178	8.860	1.3325	205	7.939	1.2716
	697	9.298	1.3886	502	8.239	1.3087
	959	9.524	1.4103	747	8.451	1.3279
	1342	9.770	1.4387	1057	8.673	1.3506
	2048	10.171	1.4893	1446	8.923	1.3852
	3074	10.708	1.5505	1963	9.198	1.4219
	4063	11.159	1.5963	2685	9.550	1.4658
	4883	11.545	1.6276	3491	9.878	1.5064
				4280	10.167	1.5401
			5121	10.439	1.5725	

hr period. For each succeeding point approximately 1.5 hr equilibrium time was allowed for each 500-atm pressure increase. The thermal time constant (temperature half-life) of the contents of a similar cell within the same bomb had been found previously to be about 3 min at atmospheric pressure and about 5 min at the

after equilibration at approximate values of 1, 500, 1000, 2000, 3000, 4000, and 5000 atm at each temperature. In addition, several points were taken during the cycle of decreasing pressure, the 1-atm point always being repeated. The pressure was dropped as slowly as possible to prevent cracking of the epoxy coating on the

seal and subsequent leaking. The pressure cycle at 30° was run first, followed by the 50° pressure cycle on the same sample of liquid.

Results and Discussion

The density and dielectric constants of five polar solvents—chlorobenzene, ethyl acetate, isopropyl ether, tetrahydrofuran, and dichloromethane—were measured at pressures up to 5000 atm at 30 and 50°. The experimental results are given in Table I, and the chlorobenzene data are compared with previously reported literature values in Figures 5 and 6. The densities are in excellent agreement with those reported by Skinner, *et al.*,^{9b} and the dielectric constant values lie very close to both those of Skinner, *et al.*,^{9b} and Hartmann, *et al.*,¹⁹

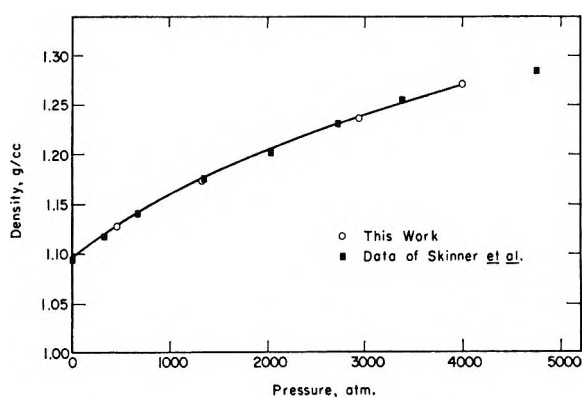


Figure 5. Density of chlorobenzene as a function of pressure at 30°.

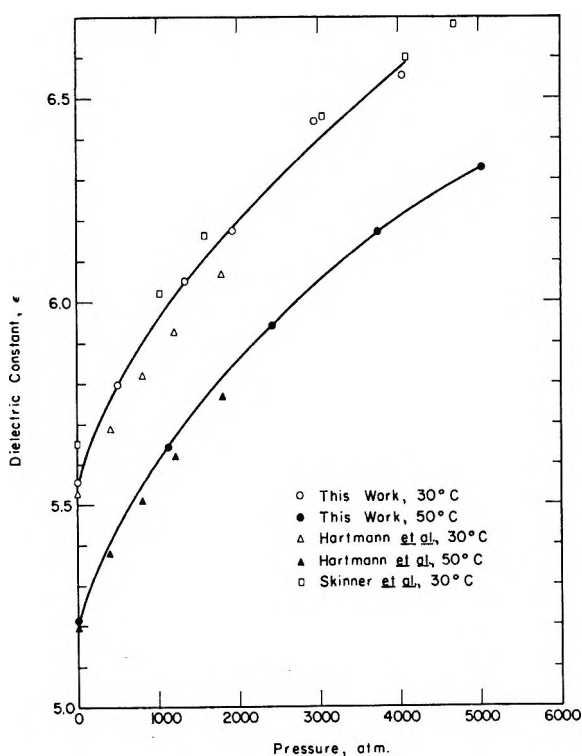


Figure 6. Dielectric constant of chlorobenzene as a function of pressure.

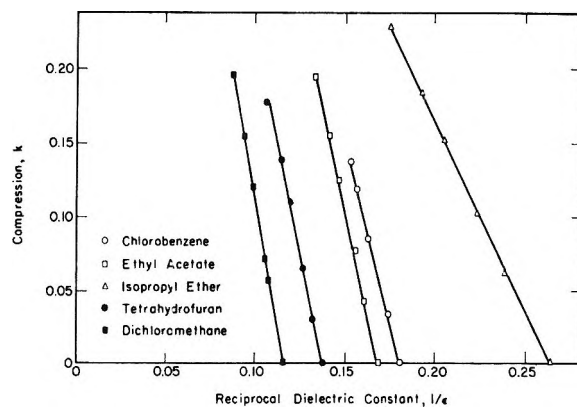


Figure 7. Compression as a function of reciprocal dielectric constant at 30°.

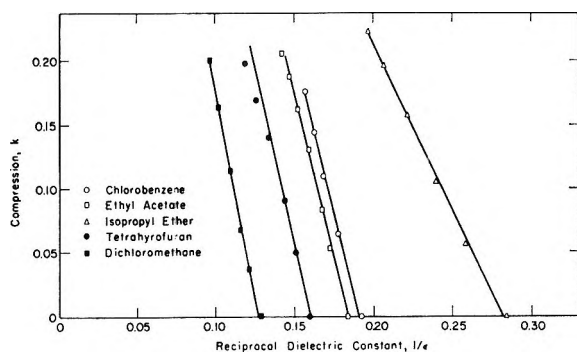


Figure 8. Compression as a function of reciprocal dielectric constant at 50°.

and lie between the two sets. The variation with pressure is quite similar; the major difference seems to be small discrepancies in the dielectric constant at one atmosphere. Also the dielectric constant of dichloromethane at 30° agrees to better than 0.15% with the results of Hartmann and Schmidt²⁰ up to 600 atm.

In order to check the validity of the assumption of Tait-type expressions to fit both density and dielectric constant with a common parameter B , plots of the type shown by eq 3 have been constructed (Figures 7 and 8). Except for one case the compression is linear in reciprocal dielectric constant, thus serving as another internal check on the data. The 50° tetrahydrofuran data curve slightly at the higher pressures. After this set of measurements, there appeared to be a small amount of polymer present, and this probably accounts for these deviations. Such an effect has been noted previously.²¹

The density data have been fit to the Tait expression (eq 1) and the dielectric constant to eq 2, 4, and 5. The resulting parameters, along with the average per

(19) H. Hartmann, A. Neumann, and G. Rinck, *Z. Phys. Chem. (Frankfurt am Main)*, **44**, 204 (1965).

(20) H. Hartmann and A. P. Schmidt, *Ber. Bunsenges. Phys. Chem.*, **72**, 879 (1968).

(21) K. E. Weale and S. A. Mehdi, "Conférence Internationale sur les Hautes Pressions," le Creusot, France, 1965.

Table II: Comparison of Experimental Results with Correlating Equations

Solvent	Temp. °C	Density			Dielectric constant								
		Equation 1			Equation 2		Equation 4			Equation 5			
		C	B ^a	% dev	A	% dev	A'	B'	% dev	A''	B''	% dev	
Chlorobenzene	30	0.2604	1705	0.12	0.1332	0.52	0.2035	842	0.40	0.2303	770	0.33	
	50	0.2740	1548	0.08	0.1275	0.33	0.2292	984	0.02	0.2593	885	0.01	
Ethyl acetate	30	0.2542	1010	0.12	0.1181	0.10	0.2742	1026	0.09	0.3014	925	0.08	
	50	0.2676	1015	0.18	0.1276	0.15	0.2894	986	0.12	0.3190	870	0.14	
Isopropyl ether	30	0.2352	596	0.09	0.1519	0.14	0.3391	557	0.09	0.3727	428	0.06	
	50	0.2852	780	0.30	0.1738	0.89	0.3178	471	0.11	0.3535	352	0.03	
Tetrahydrofuran	30	0.2618	1301	0.15	0.1456	0.18	0.3517	1414	0.14	0.3749	1285	0.13	
	50	0.2494	959	0.16	0.1310	0.97	0.4993	2279	0.08	0.5246	1992	0.08	
Dichloromethane	30	0.2681	1098	0.10	0.1455	0.22	0.3519	1198	0.18	0.3704	1104	0.16	
	50	0.2916	1245	0.17	0.1660	0.68	0.2964	773	0.04	0.3165	709	0.05	

^a Units of B, B', and B'' are atmospheres.

cent deviation of the data from the correlating curve are all given in Table II. It should be noted that the exact values of the parameters are not highly significant, in that for the two-parameter equations there are many sets of parameters which will give fits almost as good as those shown. Further, Hartmann *et al.*,^{9a} have remarked on the sensitivity of the parameters to the number of points used in the fit or even to the particular values of the pressure at which data were taken.

The Tait C has generally been found to be in the range 0.21–0.22 and fairly insensitive to material. The C's here are relatively constant but 0.04–0.05 higher. All density data are fit to 0.3% or better and the average deviation is less than 0.15%.

The one-parameter fit (eq 2) of the dielectric constant data, using the Tait B, is really quite good. The largest average deviation, for tetrahydrofuran at 50°, is still less than 1% and the average for all points is about 0.4%. This result, along with the linearity of the plots in Figures 7 and 8, seems to indicate that except for the most exacting work, a one-parameter equation is sufficient.

When the same expression is used with two adjustable parameters (eq 4), the average fit is improved to 0.13%, and the dielectric susceptibility approach (eq 5) gives an average deviation of 0.11%. In general B'' is lower than B' (or B) and the A'' is higher than A'.

To gain some insight into the effect of structure on the variation of dielectric constant with pressure, in Figure 9 are compared the results for four ethers—ethyl, *n*-propyl, isopropyl, and tetrahydrofuran. The effect of pressure on dielectric constant is least for the cyclic tetrahydrofuran and greatest for the branched isopropyl ether. The two straight chain ethers are intermediate with the effect being greater on the shorter of the two. These structural effects may be contrasted with those for hydrocarbons.¹¹ For six hydrocarbons—*n*-pentane, *n*-hexane, *n*-octane, cyclopentane, methylcyclohexane, and 2,2-dimethylbutane, the total change in dielectric constant at 4 kbars ranged only from 11 to 16%, with the maximum effect on *n*-pentane and the

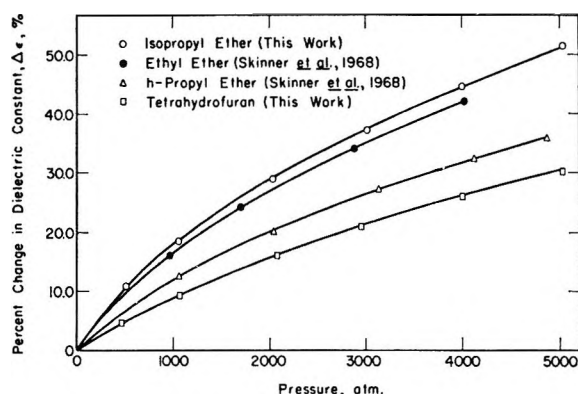


Figure 9. The effect of pressure on the dielectric constant of four ethers at 30°.

minimum for *n*-octane. The cyclic and branched species were intermediate.

Conclusions

A new technique for the simultaneous determination of the effect of pressure on both density and dielectric constant has been developed and tested. Results are reported for five solvents at two temperatures and at pressures to 5000 atm.

Acknowledgment. The authors gratefully acknowledge financial support from the Petroleum Research Fund of the American Chemical Society and from the United States Army Research Office, Durham. They are also indebted to Professor T. L. Brown for the use of the heterodyne beat apparatus.

Nomenclature

A, B, C	Empirical constants in correlating equations
k	Compression
P	Pressure
v	Molar volume
V	Voltage
ε	Dielectric constant
ρ	Density

Subscripts

1	At 1 atm
P	At pressure P

NOTES

Locations of Cations in Alkaline Earth Hydrogen Y Zeolites

by John W. Ward

Union Oil Company of California, Union Research Center, Brea, California 92621 (Received March 4, 1970)

The locations of cations in some synthetic-faujasite type zeolites have been reported. In particular, calcium, cerium, lanthanum, and hydrogen cation exchanged into sodium zeolites have received much attention.¹⁻⁵ However, although several studies of catalytic activity of cation-hydrogen zeolites have been reported, no information on the locations of the cations has been given.⁶⁻¹⁰ A study of the calcium-hydrogen and magnesium-hydrogen Y zeolite system is reported here.

Angell and Schaffer¹¹ have shown that carbon monoxide interacts with cations to give a cation specific infrared absorption band. This band can be used to locate cation positions, for example, the positions of Ca, Ni, and Co ions, in cation-sodium Y zeolites. Pyridine also interacts with cations to give a specific absorption band.¹²⁻¹⁴ Because of its size, pyridine will interact only with cations located in the supercage portions of the structure. In this study, the variations of the intensity of the hydroxyl group bands and the pyridine-cation band as a function of the cation content are examined.

Experimental Section

The cation-ammonium forms were prepared by ion exchange of the parent ammonium Y zeolite with suitable amounts of calcium and magnesium nitrate solutions. The ammonium Y zeolite was prepared by ion exchange of sodium Y zeolite $[\text{Na}_{55}\text{H}_2(\text{SiO}_2)_{135}(\text{AlO}_2)_{57}]$ until it contained 1.0% Na. The sodium Y was 98% crystalline relative to a well-characterized standard. The ammonium Y was 115% crystalline relative to the standard. The samples were all of high crystallinity and surface area. Samples suitable for spectroscopic examination were prepared by compacting approximately 0.05 g of the powdered zeolite in a 1 in. diameter die. The resulting wafers were calcined in an infrared cell under vacuum at 450° and their spectra recorded. Pyridine at a pressure of 5 Torr was adsorbed for 1 hr, the excess removed by evacuation at 250°, and the spectra recorded. Spectra were obtained with a Cary-White 90 infrared spectrometer as had been reported previously.¹²

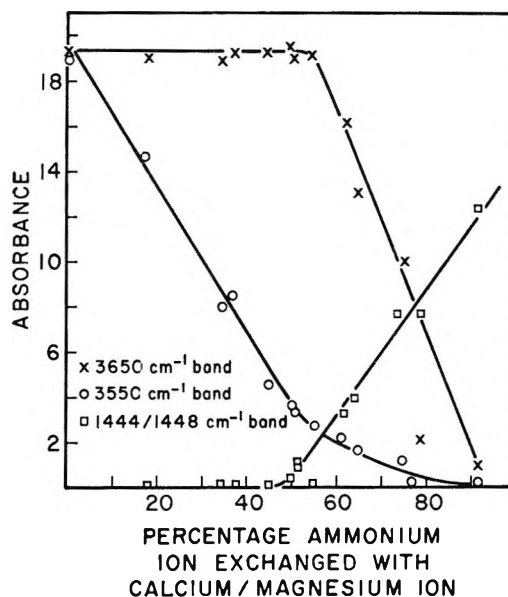


Figure 1. Absorbance of the 3650, 3550, and 1444 (1448)- cm^{-1} bands as a function of divalent cation content.

Results and Discussion

Table I lists the degree of exchange of the samples, the absorbance per unit mass of the hydroxyl bands (3650, 3550 cm^{-1}) and of the pyridine-cation band (1444-1448 cm^{-1}). The variations of the three bands with the percentage cation exchange are plotted in Figure 1.

It is seen that the absorbance of the 3550- cm^{-1} band starts to decrease as soon as calcium ions are introduced

- (1) J. M. Bennett and J. V. Smith, *Mater. Res. Bull.*, **3**, 633, 856, 933 (1968); **4**, 7, 77, 343 (1969).
- (2) J. V. Smith, J. M. Bennett, and E. M. Flanigen, *Nature*, **215**, 241 (1967).
- (3) D. H. Olson and E. Dempsey, *J. Catal.*, **13**, 221 (1969).
- (4) D. H. Olson, G. T. Kokotailo, and J. F. Charnell, *J. Colloid Interface Sci.*, **28**, 305 (1968).
- (5) D. H. Olson, *J. Phys. Chem.*, **72**, 4366 (1968).
- (6) D. A. Hickson and S. M. Csicsery, *J. Catal.*, **10**, 27 (1968).
- (7) M. A. Lanewala and A. P. Bolton, *J. Org. Chem.*, **34**, 3107 (1969).
- (8) J. W. Ward, *J. Catal.*, **11**, 251 (1968).
- (9) J. N. Miale, N. Y. Chen, and P. B. Weisz, *ibid.*, **6**, 278 (1966).
- (10) S. M. Csicsery, *J. Org. Chem.*, **34**, 3338 (1969).
- (11) C. L. Angell and P. C. Schaffer, *J. Phys. Chem.*, **70**, 1413 (1966).
- (12) J. W. Ward, *J. Catal.*, **10**, 34 (1968).
- (13) Y. Watanabe and H. W. Habgood, *J. Phys. Chem.*, **72**, 3066 (1968).
- (14) L. G. Christner, B. V. Liengme, and W. K. Hall, *Trans. Faraday Soc.*, **64**, 1679 (1968).

Table I: Physical Properties and Spectral Band Intensities of Zeolites

% Ammonium Y exchanged to M ²⁺ form	Calcium hydrogen Y			Magnesium hydrogen Y					
	Surface area, m ² g ⁻¹	Absorbance 3650-cm ⁻¹ band	Absorbance 3550-cm ⁻¹ band	Absorbance 1444-cm ⁻¹ band	% Ammonium Y exchanged to M ²⁺ form	Surface area, m ² g ⁻¹	Absorbance 3650-cm ⁻¹ band	Absorbance 3550-cm ⁻¹ band	Absorbance 1448-cm ⁻¹ band
92	842	1.0	0.1	12.3	79	891	2.0	0.1	7.8
74	860	10.0	1.3	7.8	83	863	16.1	2.2	3.3
65	890	13.0	1.6	4.0	52	861	19.0	3.2	1.1
56	900	19.1	2.9	0.2	50	868	19.3	3.7	0.4
51	908	19.4	3.7	0.9	45	884	19.3	4.8	0.1
37	924	19.2	8.6	0.0	35	948	18.9	8.0	0.0
18	920	19.0	14.8	0.0					

into the structure and continues to decrease as more divalent ions are added. The absorbance of the 3650-cm⁻¹ band remains constant until 55% exchange with calcium is reached and then it declines rapidly until at 90% exchange, only traces of the band are detected. Conversely, as the cation content is increased beyond the 55% level, the absorption band due to cation-pyridine interaction appears. The results for the magnesium system are analogous.

Olson and Dempsey³ have shown that the 3550-cm⁻¹ absorption band represents hydrogen atoms associated with the O₃ atoms located inside the hexagonal prism and that the 3650-cm⁻¹ band represents hydrogen associated with the O₁ atoms located in the supercages. The calcium dependence of the hydroxyl group band intensities indicates that in the initial stages of exchange, the calcium ions must replace ammonium ions in the small pore system of the structure. These ions could be located either in the hexagonal prisms or the sodalite cages since the calcium ions in the sodium Y system are known to migrate as the state of hydration changes. Infrared studies of adsorbed molecules do not allow distinction between the two locations.

In the Ca-NaY system, calcium ions appear in accessible positions in the structure after 16-18 calcium ions per unit cell have been added. In the Ca-HY system, the intensity of the 3650-cm⁻¹ band remains approximately constant until 15-17 ions per unit cell have been added; it then decreases rapidly as more calcium ions are added indicating the replacement of ammonium ions in accessible positions by calcium ions. Simultaneously, the absorption band at 1444 cm⁻¹ (1448 cm⁻¹ for Mg) due to calcium-pyridine interaction is observed, confirming the presence of calcium ions in accessible positions.

The intensity of the 3550-cm⁻¹ band does not reach zero near 55% exchange, but it still has a positive value which decreases on further exchange. This suggests that the occupancy of the inaccessible positions is not complete before the onset of occupancy of the accessible positions. However, the residual band intensity at 55% exchange is equivalent to about 1-2 residual hydroxyl groups while at 65% exchange, the band in-

tensity is equivalent to less than one hydroxyl group out of the original sixteen.

Hence it can be concluded that the distribution of calcium and magnesium in the ammonium Y zeolite system is the same as in the sodium system. Although it is not possible to be specific from the infrared results, the behavior of the 3550 cm⁻¹ band suggests that approximately the first 16 calcium and magnesium ions are located in the hexagonal prisms at least after dehydration at 450°. It is possible that the calcium and magnesium ions may change locations depending on the degree of hydration, similar to that reported for the calcium-sodium Y system.¹ Other measurements will be necessary to determine the specific locations of the inaccessible cations and whether migration occurs with changes in hydration level.

Interpretations of Nuclear Quadrupole Resonance Data in Some *trans*-Dichlorobis-(ethylenediamine)cobalt(III) Salts^{1a}

by T. B. Brill^{1b} and Z. Z. Hugus, Jr.

Department of Chemistry, North Carolina State University, Raleigh, North Carolina 27607 (Received January 13, 1970)

There exists an unusually large variation in the ⁵⁹Co nuclear quadrupole resonance frequencies in *trans*-dihalobis(ethylenediamine)cobalt(III)⁺ salts as the nature of the anions is changed. For example, in going from *trans*-(Coen₂Cl₂)Cl to *trans*-(Coen₂Cl₂)Cl·HCl·2H₂O, the ⁵⁹Co resonance frequency increases by about 15%. In going from *trans*-(Coen₂Br₂)ClO₄ to *trans*-(Coen₂Br₂)Br·HBr·2H₂O, there is a 25% increase in the resonance frequency. Understanding the possible sources of these variations is an interesting problem and one of importance to nqr spectroscopy.

(1) (a) Abstracted from the thesis of T. B. B. submitted to the University of Minnesota in partial fulfillment of a Doctor of Philosophy degree. (b) NDEA Fellow at the University of Minnesota, 1966-1969.

Table I: Nqr Frequencies^{a,b,c} and Coupling Constants in MHz and Asymmetry Parameters at 23°

Compounds	⁵⁹ Co			$\eta(\text{Co})$	$\nu(^{35}\text{Cl})$	$\nu(^{37}\text{Cl})$	$\frac{e^2qQ}{h(^{59}\text{Co})}$	Ref
	$\nu(7/2 \leftrightarrow 5/2)$	$\nu(5/2 \leftrightarrow 3/2)$	$\nu(3/2 \leftrightarrow 1/2)$					
(Coen ₂ Cl ₂) ⁺								
(Cl·HCl·2H ₂ O) ⁻	15.296 (70)	10.001 (80)	5.973 (5)	0.222	16.058 (15)	12.656 (4)	71.73	2, 3
Cl ⁻	12.892 (2)	[8.368]	[5.367]	0.272	60.63	4
NO ₃ ⁻	13.426 (8)	8.877 (6)	[4.777]	0.132	62.78	4
ClO ₄ ⁻	12.888 (11)	8.512 (5)	...	0.149	60.22	This work
	12.816 (10)	8.467 (5)	...	0.149	59.92	This work
SCN ⁻	12.870 (6)	8.395 (2)	...	0.245	60.43	This work
BrO ₃ ⁻	13.880 (8)	9.057 (4)	...	0.238	65.15	This work
(Coen ₂ Br ₂) ⁺								
					$\nu(^{79}\text{Br})$	$\nu(^{81}\text{Br})$		
(Br·HBr·2H ₂ O) ⁻	15.503 (65)	10.104 (70)	...	0.244	127.34 (20)	106.38 (20)	72.80	3
Br ⁻	12.860 (2)	[8.392]	...	0.235	60.36	4
ClO ₄ ⁻	12.264 (5)	8.096 (3)	...	0.149	57.38	This work

^a Resonances in brackets were reported in reference 4 but could not be found in this study. ^b Parenthetical numbers are signal to noise ratios. ^c Frequencies listed are good to within 3 kHz.

Table I²⁻⁴ shows that in general, the resonance frequencies fall into two classes: those of the acid halide double salts and those of the simple salts. It is the purpose of this note to investigate the source of this difference.

Self-consistent charge and configuration LCAO-MO calculations⁵ with all 27 atoms and 65 valence orbitals in *trans*-(Coen₂Cl₂)⁺ were carried out and indicate that the converged atom charges are: Co (+0.60), Cl (-0.50), N (-0.35), C (-0.35), H(N) (+0.34), H(C) (+0.18). Coulomb integrals for cobalt were computed using quadratically charge-adjusted valence orbital ionization potentials.⁶ Analytical single-term Slater-type valence orbital exponents for all atoms except cobalt were taken from Clementi and Raimondi's tables.⁷ Those for cobalt were based on data of Schreiner and Brown.⁸ The same calculation was carried out on *trans*-(Coen₂Br₂)⁺. The ring charges in the bromo compound were found to be about the same but the cobalt and bromine charges were +0.58 and -0.37, respectively. However, since the *trans*-(Coen₂Cl₂)⁺ cation remains essentially the same within experimental error in all of the compounds which have been studied by X-ray crystallography,⁹⁻¹⁴ the importance of differences in the lattice must be investigated.

A good comparison may be made between the acid double salt, *trans*-(Coen₂Cl₂)Cl·HCl·2H₂O, and the simple salt, *trans*-(Coen₂Cl₂)Cl. The lattice electric field gradient (EFG) was computed using the electrostatic point charge model¹⁵ with the atomic coordinates being obtained from the crystal structure data,⁹⁻¹⁴ and the atomic charges from the self-consistent charges in the MO calculation. The computer programs used have been described before.¹⁶ The electrostatic contributions to the EFG from atoms within the ion containing the nucleus at $r = 0$ were neglected since these are taken into account as part of the intramolecular EFG.

Summation was carried out to $r = 60 \text{ \AA}$ to ensure convergence. The eigenvalues of the resulting tensor must be corrected by the Sternheimer antishielding factor,¹⁷ $1 - \gamma_\infty$. A multiplicative factor of 12 for $1 - \gamma_\infty$ for ⁵⁹Co was used by Watanabe and Yamagata.⁴ Scott and Bernheim¹⁸ reasoned that the value could not be much larger than 8.

Table II lists the computed lattice coupling constants for several values of $1 - \gamma_\infty$ compared to the observed coupling constants. It must be kept in mind that the models used are approximate ones, but the lattice EFG difference computed from the point charge model is about the same as the experimental difference in the

(2) H. Hartmann, M. Fleissner, and H. Sillescu, *Naturwissenschaften*, **50**, 591 (1963).

(3) H. Hartmann, M. Fleissner, and H. Sillescu, *Theor. Chim. Acta*, **2**, 63 (1964).

(4) I. Watanabe and Y. Yamagata, *J. Chem. Phys.*, **46**, 407 (1967).

(5) R. Hoffmann and W. N. Lipscomb, *ibid.*, **36**, 2179 (1962).

(6) H. Basch, A. Viste, and H. B. Gray, *Theor. Chim. Acta*, **3**, 458 (1965).

(7) E. Clementi and D. L. Raimondi, *J. Chem. Phys.*, **38**, 2686 (1963).

(8) A. F. Schreiner and T. L. Brown, *J. Amer. Chem. Soc.*, **90**, 3366 (1968).

(9) A. Nakahara, Y. Saito, and H. Kuroya, *Bull. Chem. Soc. Jap.*, **25**, 331 (1952).

(10) J. M. Williams, *Inorg. Nucl. Chem. Lett.*, **3**, 297 (1967).

(11) S. Ooi, Y. Komiyama, Y. Saito, and H. Kuroya, *Bull. Chem. Soc. Jap.*, **32**, 263 (1959).

(12) K. A. Becker, G. Grosse, and K. Pleith, *Z. Kristallogr.*, **112**, 375 (1959).

(13) S. Ooi and H. Kuroya, *Bull. Chem. Soc. Jap.*, **36**, 1083 (1963).

(14) S. Ooi, Y. Komiyama, and H. Kuroya, *ibid.*, **33**, 354 (1959).

(15) R. Bersohn, *J. Chem. Phys.*, **29**, 326 (1958).

(16) T. B. Brill, Z. Z. Hugas, Jr., and A. F. Schreiner, *J. Phys. Chem.*, **74**, 469 (1970).

(17) R. M. Sternheimer and H. M. Foley, *Phys. Rev.*, **102**, 731 (1956), and references therein.

(18) B. A. Scott and R. A. Bernheim, *J. Chem. Phys.*, **44**, 2004 (1966).

Table II: Lattice Coupling Constants for Various Values of $1 - \gamma_\infty$ Compared to the Experimental Coupling Constants

Compounds	$(e^2Qq/h)_{\text{exptl.}}^a$ MHz	$(e^2Qq/h)_{\text{lat.}}$, MHz		
		$1 - \gamma_\infty = 8$	10	12
<i>trans</i> -(Coen ₂ Cl ₂)Cl· HCl·2H ₂ O ^b	71.73	-13.1	-16.8	-20.2
<i>trans</i> -(Coen ₂ Cl ₂)Cl	60.63	-2.0	-2.5	-3.0

^a The sign of the coupling constant cannot be determined in pure nqr spectroscopy. ^b In reference 3, the lattice EFG for *trans*-(Coen₂Cl₂)Cl·HCl·2H₂O was computed in esu/cm³. Our values are in substantial agreement with this in view of the fact that a different charge distribution and several more atoms were included in this study.

resonance frequencies, and it appears that the crystal lattice is the source of the variation. It must be presumed that the intramolecular coupling constant has the same sign as the lattice coupling constant. Scott and Bernheim's value of 8 for $1 - \gamma_\infty$ appears to be the right magnitude for cobalt.

X-Ray data are not available for many of the other salts but several comments may be made. The most strikingly different compound is that of *trans*-(Coen₂-Cl₂)ClO₄. Two ⁵⁹Co resonances of approximately equal intensity were found. The unit cell appears to contain at least two (or an even number if more than two) formula units such that the principal components of their EFG tensor differ in magnitude. This salt does not appear to be isostructural with *trans*-(Coen₂Br₂)-ClO₄.

trans-(Coen₂Cl₂)Cl and *trans*-(Coen₂Br₂)Br appear to be isostructural since both their asymmetry parameters and coupling constants are similar.

Acknowledgments. We wish to thank Dr. A. F. Schreiner for the use of the SCCM-MO program. The support of the North Carolina Board of Science and Technology toward the purchase of a Wilks NQR-1A nqr spectrometer is gratefully acknowledged.

A Comparison of the Gibbs Energy and Entropy of Interfaces Water-*n*-Hexane and Water-Perfluorotributylamine

by R. G. Linford, R. J. Powell, and J. H. Hildebrand

Department of Chemistry, University of California,
Berkeley, California 94720 (Received March 30, 1970)

Miller and Hildebrand¹ showed in 1968 that losses of entropy which accompany solution of nonreacting gases in water to the same mole fraction, 10⁻⁵, vary linearly with the total surface area per mole of the solute molecules, from Ne to *n*-C₁H₁₀. The losses agree, moreover, in order of magnitude, with values calculated

from the decrease in entropy per cm² that occurs when an alkane liquid flows over a surface of water. They discovered, further, that a corresponding line for the gases NF₃, CF₄, and SF₆ lies several calories per degree lower than the line for other gases. It has seemed worthwhile, therefore, to find out whether a fluorochemical liquid is more effective than an alkane in diminishing the entropy of a surface of water.

We availed ourselves of a supply of perfluorotributylamine, (C₄F₉)₃N, "FC43," of adequate purity kindly furnished by the Minnesota Mining and Manufacturing Co. Its density, not degassed, conformed, between 20 and 45°, with the expression: $\rho = 1.9335 - 0.00218t$. Its surface energy, determined by capillary rise between 15 and 35°, is given by the expression: $\gamma = 17.15 - 0.080(t - 15)$ erg/cm².

Water completely wets glass in the presence of this liquid making it possible to determine their interfacial tension from the hydrostatic pressure that can be sustained by a hemispherical drop of FC43 of maximum curvature projecting into water from a glass capillary of known radius. The FC43 was contained in a U tube, one arm of which was the capillary. The internal radius of the tip was 0.0299 cm.

Designating the height of FC43 in the broad arm of the U tube above the level of the drop in the capillary as Δh_t , and the corresponding level of water above the top of the drop as Δh_w , and using the relation between hydrostatic pressure, surface tension, and drop radius, $2\gamma = Pr$, we calculate interfacial Gibbs energy (in erg/cm²) by the equation

$$\gamma = \frac{980}{2}(\rho_t \Delta h_t - \rho_w \Delta h_w)$$

We obtained values of γ between 15 and 45°; they conform closely to the expression: $\gamma = 39.85 + 0.086(t - 15) \pm 0.1$ erg/cm². Its value at 25° is 40.7 erg/cm² and the interfacial entropy is -0.086 erg/deg cm².

We select for comparison the corresponding values for normal hexane: surface tension by Jasper and King,² interfacial tension with water by Aveyard and Hayden. We take values for pure water from a handbook.³

The data are summarized in Table I and plotted in Figure 1 to give a clearer view of the effects of temperature.

The most striking comparison revealed is the increase with temperature of the free energy of the interface water-(C₄F₉)₃N. The entropy of the surface of water

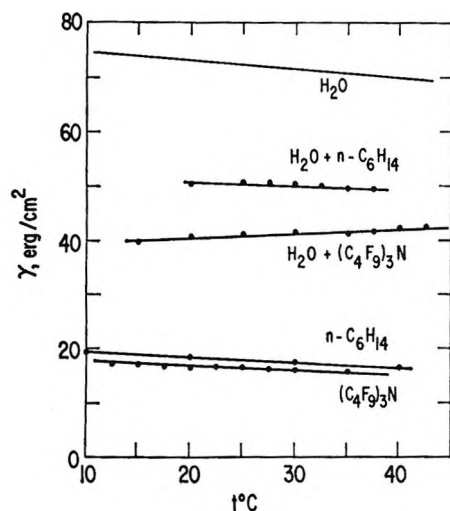
(1) K. W. Miller and J. H. Hildebrand, *J. Amer. Chem. Soc.*, **90**, 3001 (1968).

(2) J. J. Jasper and E. V. King, *J. Phys. Chem.*, **59**, 1019 (1955); R. Aveyard and D. A. Hayden, *Trans. Faraday Soc.*, **61**, 2255 (1965).

(3) "American Institute of Physics Handbook," McGraw-Hill, New York, N. Y., 1957.

Table I: Values of Surface Gibbs Energy, γ , at 25° (in ergs/cm²), and of Entropy, $-(\partial\gamma/\partial T)_p$

	H ₂ O	(C ₄ F ₉) ₃ N	Inter- face	n-C ₆ H ₁₄	Inter- face
γ	72.0	16.35	40.7	17.9	50.4
$-\partial\gamma/\partial T$	0.155	0.080	-0.086	0.105	0.089

Figure 1. Surface tensions of H₂O, n-C₆H₁₄, and (C₄F₉)₃N and interfacial tensions with H₂O.

changes from 0.155 to 0.089 when covered by n-C₆H₁₄, a loss of 0.050 erg/deg cm²; but the loss when covered by

(C₄F₉)₃N is much larger: 0.155 - (-0.086) = 0.241 erg/deg cm². This accords qualitatively with the larger negative entropy of solution of fluorochemical gases in water than that of alkane gases.

The "work of adhesion" is also larger in forming the water-FC43 interface: 72.0 + 16.35 - 40.7 = 47.7 than the water-hexane interface: 72.0 + 17.9 - 50.4 = 39.5 erg/cm². The larger attraction and larger loss of entropy in the former system seem consistent with our view that a fluorochemical, either liquid or gas, is especially effective in destroying hydrogen bonds and setting up stronger dispersion forces in their place.

That the results here reported can be regarded as typical for fluorochemical liquids can be inferred from the almost identical solubility of iodine⁴ in four of them; values in mole per cent at 25° are; (C₄F₉)₃N, 0.0232; c-C₆F₁₁CF₃, 0.0210; C₈F₁₆O, 0.0208; C₇F₁₆, 0.0180. The amine has no basic character; the color of the solution in each liquid is pure violet. We had a small amount of C₇F₁₆ with which we determined the interfacial energy against water at 25, 30, and 35°. The line was parallel to and 1.0 erg/cm² below the line for the FC43-water interface.

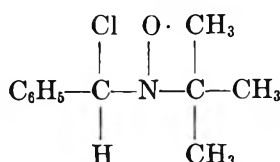
Acknowledgment. We express our thanks to the 3M Co. for FC43. This work was supported by the National Science Foundation.

(4) J. H. Hildebrand and R. L. Scott, "Regular Solutions," Prentice-Hall, New York, N. Y., 1962, p 164.

COMMUNICATIONS TO THE EDITOR

Electron Spin Resonance of β -Chloroalkyl Nitroxides. Angular Dependence of β -Chlorine Hyperfine Coupling¹

Sir: Recent work on the angular dependence of β -fluorine hyperfine coupling²⁻⁶ has prompted an investigation into the factors influencing β -chlorine hyperfine coupling. The esr spectrum of α -chlorobenzyl *t*-butyl nitroxide in benzene solution at room



temperature is shown in Figure 1. The smallest doublets are due to the single β -hydrogen. The over-

lapping quartets are due to coupling from chlorine-35 (75.4%, $\mu = 0.82089$)⁷ and chlorine-37 (24.6%, $\mu = 0.68329$).⁷ It is clear from the spectrum that the isotope of lower abundance has the smaller coupling constant.

(1) This work is being supported by AFOSR(SRC)-OAR USAF Grant No. 1069-66.

(2) E. T. Strom and A. L. Bluhm, *J. Phys. Chem.*, **74**, 2036 (1970); E. G. Janzen, B. R. Knauer, J. L. Gerlock, and K. J. Klabunde, *ibid.*, **74**, 2037 (1970).

(3) J. L. Gerlock, E. G. Janzen, and J. K. Ruff, *J. Amer. Chem. Soc.*, **92**, 2558 (1970).

(4) D. Kosman and L. M. Stock, *ibid.*, **92**, 409 (1970).

(5) K. J. Klabunde, *ibid.*, **92**, 2427 (1970); G. R. Underwood, V. L. Vogel, and I. Krefting, unpublished results; we acknowledge with appreciation the receipt of a preprint of this work.

(6) J. L. Gerlock and E. G. Janzen, *J. Phys. Chem.*, **72**, 1832 (1968).

(7) J. A. Pople, W. G. Schneider, and H. J. Bernstein, "High-Resolution Nuclear Magnetic Resonance," McGraw-Hill Book Co., Inc., New York, N. Y., 1959, p 481.

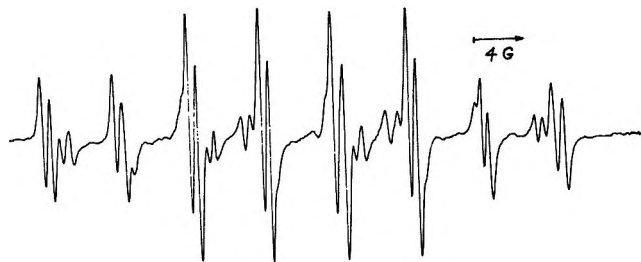


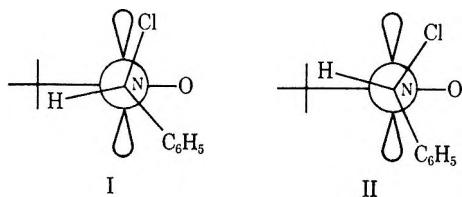
Figure 1. Electron spin resonance spectrum of α -chlorobenzyl *t*-butyl nitroxide in benzene solution.

The spectrum in Figure 1 was obtained in connection with spin trapping experiments⁸ wherein *t*-butyl hypochlorite was added to phenyl *t*-butylnitron (PBN)⁸ in the absence of oxygen. The same spectrum was obtained from benzene solutions of trichlorosilane or trimethylchlorosilane containing PBN to which *t*-butylperoxalate⁹ was added. Although it is probable that in the latter system *t*-butyl hypochlorite is also responsible for the reaction, the mechanism of production of the monochloro nitroxide derivative is not understood at this time. The addition of chlorine to PBN, for example, only produces benzoyl *t*-butyl nitroxide.⁸

The spectrum of a monochlorobenzyl nitroxide is particularly useful for the investigation of the angular dependence of β -chlorine coupling because the magnitude of the β -hydrogen coupling is related to the dihedral angle θ_H , *i.e.*, the angle between the β -hydrogen-carbon-nitrogen plane and the carbon-nitrogen-p-orbital plane, from which the dihedral angle θ_{Cl} can be obtained. From the Heller-McConnell equation¹⁰

$$A_{\beta}^H = (B_1 + B_2 \cos^2 \theta) \rho_N$$

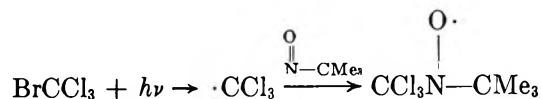
where $B_1 \cong 0$,¹¹ $B_0 \sim 50$,¹¹ $\rho_N = 0.37$,¹² θ_H is calculated to be 78° . The calculated θ_{Cl} is thus either 18° as in I or 42° as in II.



Temperature variation has very little effect on either the β -hydrogen or β -chlorine coupling. Thus the chlorine coupling increases by 0.15 G and the hydrogen coupling increases by 0.13 G with increase in temperature in the range 35 – 90° . At temperatures below 35° the line width increases substantially with no appreciable change in spacing between the lines. These findings strongly suggest that the α -chlorobenzyl *t*-butyl nitroxide is essentially locked in a conformation where $\theta_{Cl} \cong 18$ or 42° .

The spectrum of trichloromethyl *t*-butyl nitroxide is of interest because the freely rotating trichloromethyl

group with $\theta_{Cl} = 45^\circ$ should permit selection of the correct choice of θ_{Cl} for the monochloronitroxide radical. The spectrum of trichloromethyl *t*-butyl nitroxide was obtained by photolysis of BrCCl_3 at room temperature in benzene containing 2-methyl-2-nitrosopropane, a method previously used for the preparation of perfluoroalkyl *t*-butyl nitroxides.^{5,13} The nitrogen



coupling is almost the same as for the monochloro derivative (Table I) but the β -chlorine coupling is 2.29 G. This indicates that I is probably the preferred conformation for the monochloro derivative.

Table I: Nitrogen and Chlorine Hyperfine Coupling in Chloroalkyl *t*-Butyl Nitroxides^a

Radical	A_N	A_{Cl}	A_H	$T, ^\circ\text{C}$	$\theta_{Cl}, ^\circ$
	12.12	6.05, 4.88	0.75	35	18°
	12.2	6.1	0.86	63	
	12.1	6.2	0.88	90	
	13.2	3.3		35	30°
	12.4	2.3		35	45°
	11.8	1.25			45°

^a In gauss with an error (average deviation) $\pm \sim 0.1$ G. ^b Apparent dihedral angle. ^c Reference 14.

The spectrum of a third nitroxide of interest has been obtained by dissolving PBN previously exposed to *t*-butyl hypochlorite in the gas phase¹⁴ in carbon tetrachloride. The spectrum consists of 15 lines with some additional partially resolved splitting which can be assigned to α, α -dichlorobenzyl *t*-butyl nitroxide.

(8) E. G. Janzen and B. J. Blackburn, *J. Amer. Chem. Soc.*, **91**, 4481 (1969).

(9) P. D. Bartlett, E. P. Benzing, and R. E. Pincock, *ibid.*, **82**, 1762 (1960).

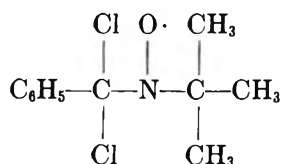
(10) C. Heller and H. M. McConnell, *J. Chem. Phys.*, **32**, 1535 (1960).

(11) M. D. Sevilla and G. Vincow, *J. Phys. Chem.*, **72**, 3647 (1968), and references therein.

(12) Assuming $A_N = 35.61 \rho_N + 0.93 \rho_O$; P. B. Ayscough and F. P. Sargent, *J. Chem. Soc., Sect. B*, 907 (1966); E. G. Janzen and J. W. Happ, *J. Phys. Chem.*, **73**, 2335 (1969).

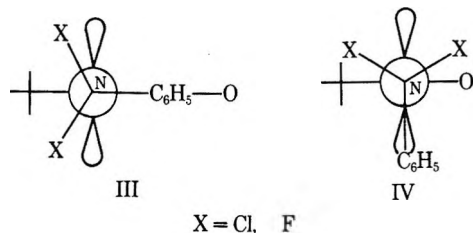
(13) After the completion of this work a previous report on the trichloromethyl *t*-butyl nitroxide spectrum became available: I. H. Leaver, G. C. Ramsay, and E. Suzuki, *Aust. J. Chem.*, **22**, 1891 (1969); $A_N = 12.73$, $A_{Cl} = 2.41$ G. The radical was produced by photolysis of indole in carbon tetrachloride containing 2-methyl-2-nitrosopropane.

(14) E. G. Janzen and J. L. Gerlock, *Nature*, **222**, 867 (1969).



The chlorine coupling is 3.3 G.

In a previous paper,² an argument was made for a conformational preference of III over IV in α, α -difluorobenzyl *t*-butyl nitroxide on the basis of steric and dipole-dipole interactions. Space-filling models show that for the dichloro derivative, III is clearly favored



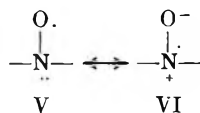
over IV for steric reasons. The eclipsing of the phenyl and oxygen in III is strongly offset by the greater freedom of motion possible for the two chlorine atoms. In III, $\theta_{\text{Cl}} = 30^\circ$.

The data for the three chloro-substituted nitroxides described shows that the β -chlorine coupling increases with a decrease in dihedral angle from 45° to near 0° very much like hydrogen and fluorine as recently pointed out.^{2,3} Examples of β -chloroalkyl radicals where the dihedral angle is greater than 45° are not available at this time.

In bis(trichloromethyl) nitroxide¹⁵ the β -chlorine coupling is considerably lower than in trichloromethyl *t*-butyl nitroxide (1.25 vs. 2.3 G). Although, this may be due in part to a smaller spin density on nitrogen in the bis(trichloromethyl) nitroxide,¹⁶ the nitrogen coupling does not decrease enough to account for the decrease in β -chlorine coupling. Small differences in planarity of the nitroxide function induced by different steric interactions in the two radicals may also produce differences in the nitrogen as well as the chlorine couplings.

(15) H. Sutcliffe and H. W. Wardale, *J. Amer. Chem. Soc.*, **89**, 5487 (1967).

(16) Since the trichloromethyl group is more electron withdrawing than the *t*-butyl group, V would be favored over VI (see E. G. Janzen, *Accounts Chem. Res.*, **2**, 279 (1969), for discussion and examples).



DEPARTMENT OF CHEMISTRY
THE UNIVERSITY OF GEORGIA
ATHENS, GEORGIA 30601

EDWARD G. JANZEN
BRUCE R. KNAUER
LEWIS T. WILLIAMS
W. B. HARRISON

RECEIVED MARCH 5, 1970

Water Structure Promotion by Large Organic Anions

Sir: Large organic cations such as tetraalkylammonium ions have been shown to promote structure, or increase the hydrogen bonding of water.¹⁻³ The special interaction between these ions and water has been referred to as "hydration of the second kind."⁴ It has been pointed out,^{5,6} for example, that the *B* coefficient of the Jones-Dole viscosity equation has large positive values for these "hydrophobic" ions, and the larger the cation the more positive the *B* coefficient. This is in

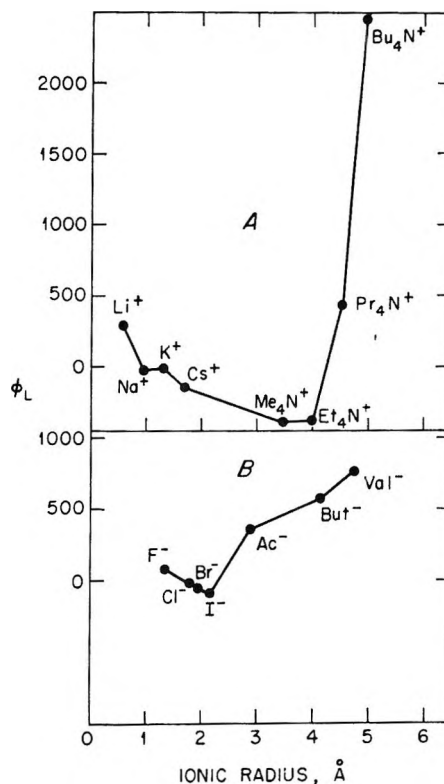


Figure 1. Apparent molal heat contents of 1 *m* aqueous solutions at 25°: A, chloride salts; B, sodium salts. Ionic radii for acetate, butyrate, and valerate were estimated from molecular models. Other ionic radii are taken from tables in R. A. Robinson and R. H. Stokes, "Electrolyte Solutions," 2nd ed, Academic Press, New York, N. Y., 1959. ϕ_L values of sodium fluoride, chloride, bromide, iodide and acetate, and lithium, sodium, potassium, and cesium chloride taken from V. B. Parker, "Thermal Properties of Aqueous Uni-univalent Electrolytes," NSRDS-NBS2, National Bureau of Standards, Washington, D. C., 1965.

- (1) H. S. Frank, *Z. Phys. Chem.*, (Leipzig), **228**, 364 (1965).
- (2) S. Lindenbaum, *J. Phys. Chem.*, **70**, 814 (1966).
- (3) A. H. Narten and S. Lindenbaum, *J. Chem. Phys.*, **51**, 1108 (1969).
- (4) H. G. Hertz and M. D. Zeidler, *Ber. Bunsenges. Phys. Chem.*, **68**, 82 (1964).
- (5) R. L. Kay, T. Vituccio, C. Zawoyski, and D. F. Evans, *J. Phys. Chem.*, **70**, 2336 (1966).
- (6) R. A. Horne and R. P. Young, *J. Phys. Chem.*, **72**, 1763 (1968).

contrast to the behavior of alkali metal ions which show decreasing B values with increasing crystallographic cation size. A similar comparison may be made with heat of dilution data. These are given in Figure 1A as apparent molal heat contents, ϕ_L , for alkali metal chlorides and tetra- n -alkylammonium chlorides. For the alkali metal ions ϕ_L decreases with increasing cation size whereas for the large organic ions ϕ_L increases markedly with increasing cation size. Many physical measurements have been reported all of which demonstrate this remarkable difference between the properties of large organic cations and those of inorganic cations. The purpose of this communication is to point out that this difference also exists between inorganic anions and large organic anions. We have measured heats of dilution of aqueous solutions of sodium salts of butyric (NaBut) and valeric acids (NaVal). These are given in Figure 1B together with ϕ_L values of sodium fluoride, chloride, bromide, iodide, and acetate in 1 m solutions. The inorganic salts show the expected dependence on ion size, *i.e.*, the larger the anion the smaller the value for ϕ_L . The sodium salts of the carboxylate anions gave large values of ϕ_L , increasing with anion size, suggesting that these anions too promote water structure, or increase hydrogen bonding in the solvent. The same dependence on ion size is also observed at other concentrations.

Low values of osmotic and activity coefficients⁷ of tetraalkylammonium iodide in aqueous solution have led to the suggestion^{7,8} that large cations and large anions are extensively ion paired by a special non-coulombic mechanism. In order to shed more light on this problem, heats of dilution have been measured for aqueous solutions of tetrabutylammonium butyrate (Bu₄NBut). The results are compared in Table I with

heats of dilution of tetrabutylammonium chloride (Bu₄NCl), NaBut, and NaCl. The ϕ_L of Bu₄NBut is seen to be larger than the sum of the ϕ_L values of NaBut

Table I: Apparent Molal Heat Contents (cal/mol) of 1 m Aqueous Solutions at 25°

Salt	ϕ_L
Bu ₄ NBut	5266
NaBut	565
Bu ₄ NCl	2455
NaCl	-23

and Bu₄NCl, suggesting that both the cation and anion are causing increased solvent hydrogen bonding. Osmotic coefficients of aqueous solution of tetra- n -butylammonium butyrate and tetra- n -butylammonium valerate were measured by the gravimetric isopiestic vapor pressure comparison method.⁹ In both cases the osmotic coefficients were greater than 1.0 for all concentrations greater than 0.3 m . This is strong evidence that ion pairing does not occur in these solutions. Further thermodynamic studies of these and other carboxylate solutions are in progress and will be reported in the near future.

(7) S. Lindenbaum and G. E. Boyd, *J. Phys. Chem.*, **68**, 911 (1964).

(8) R. M. Diamond, *ibid.*, **67**, 2513 (1963).

(9) Experimental methods for the determination of heats of dilution and osmotic coefficients are described in ref 2 and 7, respectively.

(10) Research sponsored by the U. S. Atomic Energy Commission under contract with the Union Carbide Corp.

CHEMISTRY DIVISION
OAK RIDGE NATIONAL LABORATORY¹⁰
OAK RIDGE, TENNESSEE 37830

SIEGFRIED LINDENBAUM

RECEIVED APRIL 14, 1970